# UNDERSTANDING THE SPATIAL AND TEMPORAL HETEROGENEITY OF PERMAFROST AT A RANGE OF SCALES ACROSS THE WESTERN CANADIAN ARCTIC AND SUBARCTIC

**MADELEINE C. GARIBALDI**
**Master of Science, University of Lethbridge, 2018**

A Thesis
Submitted to the School of Graduate Studies
of the University of Lethbridge
in Partial Fulfilment of the
Requirements of the Degree

**DOCTOR OF PHILOSOPHY**

Department of Geography and Environment, University of Lethbridge

LETHBRIDGE, ALBERTA, CANADA



UNDERSTANDING THE SPATIAL AND TEMPORAL HETEROGENEITY OF

PERMAFROST AT A RANGE OF SCALES ACROSS THE WESTERN CANADIAN ARCTIC AND SUBARCTIC

MADELEINE GARIBALDI

Date of Defense: July 17, 2023

| | | |
|---|---|---|
| Dr. Philip P. Bonnaventure<br>Supervisor | Associate Professor | Ph.D. |
| Dr. Hester Jiskoot<br>Thesis Examination Committee Member | Professor | Ph.D. |
| Dr. Robert Way<br>Thesis Examination Committee Member<br>Queen's University | Assistant Professor | Ph.D. |
| Dr. Craig Coburn<br>Internal External Examiner | Professor | Ph.D. |
| Dr. Stephen Wolfe<br>External Examiner<br>Natural Resources Canada | Research Scientist | Ph.D. |
| Dr. Dan Johnson<br>Chair, Thesis Examination | Professor | Ph.D. |

**Abstract**

Permafrost and active layer thickness (ALT) vary considerably spatially and in response and sensitivity to warming. Understanding the driving influences behind local scale variability and sensitivity is important to guide regional studies. Heterogeneity in the thermal state of permafrost (TSP), ALT and the most important influences on each were analyzed across the western Canadian Arctic and Subarctic. Spatial differences in ALT were related to ecoregional characteristics with increasing average ALT by ecoregion moving south (68 cm to 126 cm) and high variability in ALT for shrub dominated ecoregions (up to 145 cm). The sensitivity of the permafrost model varied between regions, highlighting the importance of winter conditions with less than 60 % of observations remaining within 1 ºC of the original value compared to 72 % for the thawing conditions. Local models of permafrost presence compared to regional models both under current (33% compared to 77%) and future climates (71% compared to 10%) demonstrated the unreliability of regional models in locations where the underlying model assumptions were not valid. Ultimately, the importance of using locally measured data to characterize and adjust regional assumptions was demonstrated. Finally, differential magnitudes of thermal responses to warming (up to 5 ºC), based on the connectivity of the air and ground thermal regime across the analysis, underscores the potential for permafrost resilience and the need to account for variable surface offsets when predicting future permafrost distribution maps.

**Statement of co-authorship**

The four papers comprising Chapters 3-6 of this thesis were prepared as separate manuscripts with the aim of publication in peer-reviewed journals. Chapter 3 was submitted for publication in 2021 and accepted in 2022. Chapters 4-6 were prepared as paper-based thesis chapters but some of the additional analysis will be removed and figures combined before final submission. I was the first author of all four chapters and was responsible for the methodological approach, data analysis, interpretation, and writing with guidance from the co-authors. Dr. Philip Bonnaventure was the second co-author on all of the papers giving guidance on the conceptualization, methodology, interpretation and writing. The additional co-authors and their contributions are discussed below.

Chapter 3 was submitted and accepted in Arctic, Antarctic, and Alpine Research with four co-authors. The first co-author was Dr. P. Bonnaventure who supervised and provided the most guidance for the data analysis and writing. The second co-author was Dr. S. Smith (Geological Survey of Canada, who provided the data used in the analysis, guidance during the writing process, and funding. Lastly, the third co-author was Mrs. C. Duchesne (Geological Survey of Canada) whose previous publication provided the rationale and guide for this paper and who provided figures and editorial support. The full reference and publication details for this paper is as follows

Garibaldi, M. C., Bonnaventure, P. P., Smith, S. L., & Duchesne, C. Active layer variability and change in the Mackenzie Valley, Northwest Territories between 1991-2014: An ecoregional assessment. *Arctic, Antarctic, and Alpine Research.* 2022;54(1); 274-293.

Chapter 4 is planned to be submitted to Permafrost and Periglacial Processes with six co-authors. The first co-author will be Dr. P. Bonnaventure who supervised and guided the

methodological approach, interpretation, and writing. The next co-author, Dr. R. Way (Queen's University) provided methodological and writing guidance. The third co-author will be Mr. A. Bevington (British Columbia Ministry of Forests) whose previous publication provided the rational and partial methodology of this paper. He additionally provided data to be used in this paper. Lastly, the remaining co-authors, Dr. S. Smith (Geological Survey of Canada), Dr. S. Lamoureux (Queen's University), and Dr. A. Lewkowicz (University of Ottawa) provided data for this study. All co-authors will provide editing and writing guidance. Aside from Dr. P. Bonnaventure and Dr. R. Way, none of the future co-authors had any input in the development or writing of the thesis chapter.

Chapter 5 will be submitted to The Cryosphere with three co-authors. The first co-author is Dr. P. Bonnaventure who supervised and guided all aspects of the paper. The second co-author will be Mr. N. Noad (University of Lethbridge) whose previous publication aided in the production of this paper and who provided field assistance and writing guidance. The last co-author is Dr. W. Kochtitzky (University of New England) who provided data access and editorial suggestions. Dr. W. Kochtitzky did not have any input in the development or writing of the thesis chapter.

Chapter 6 will be submitted to Arctic Science with three co-authors. The first co-author is Dr. P. Bonnaventure who supervised and guided all aspects of the paper. The second co-author will be Mr. N. Noad (University of Lethbridge) whose previous publication aided in the production of this paper and who provided field assistance and writing guidance. The last co-author is Dr. W. Kochtitzky (University of New England) who provided data access and editorial suggestions. Dr. W. Kochtitzky did not have any input in the development or writing of the thesis chapter.

**Acknowledgements**

This thesis would not have been possible without the help and support of so many people. First, I would like to thank my committee Dr. Laura Chasmer, Dr. Hester Jiskoot, and Dr. Robert Way for their advice and guidance throughout this process. Additionally, I would like to thank Dr. Craig Coburn and Dr. Stephen Wolfe for their roles on the thesis examination committee. Acknowledgements for the individual papers are as follows.

For Paper 1 (Chapter 3) I would like to thank Dr. Sharon Smith and Caroline Duchesne for their guidance through the development, writing and review stages of this paper. I would also like to thank Natural Resources Canada who funded this research and the Polar Continental Shelf Program and Inuvik Research Institute who provided logistical support. I am also thankful for the support and assistance provided by communities in the Northwest Territories. Additionally, I would like to acknowledge A. Leblanc who provided a review prior to submission and J Chartrand for data management and processing support.

For Paper 2 (Chapter 4), I would like to thank Dr. Scott Lamoureux, Dr. Toni Lewkowicz and Dr. Sharon Smith who provided data to be used in this study. I would also like to thank Alex Bevington for allow me to expand upon his previous work and providing additional guidance and data. Lastly, I would like to thank Dr. Robert Way for his guidance in methodology and writing.

For Papers 3 and 4 (Chapters 5 and 6) I would like to thank all of the fellow graduate students and assistants including Nick Noad, Oliver Kienzle, Scott Vegter, and Aidan Musk who have helped with fieldwork. Digging for loggers and dealing with Persephone and the weather would not have been as much fun without them. Additionally, I would like to thank Nick Noad

for his editorial revisions. Lastly, thank you to Dr. Will Kochtitzky for providing the high-resolution digital elevation models used in these studies.

Aside from the scientific acknowledgements, the five years dedicated to this thesis would not have been the same without my fellow graduate students, friends and family. First, thank you to all members of the Bonnaventure Lab for Permafrost Science both past and present including Nick Noad, Nick Hassink, Scott Vegter, Rabecca Thiessen, Ria Nicholson, and Lizzy Nnaji. The laughs, conversions and support from you all (even if virtual for a time) provided some much needed levity. I would like to especially thank Rabecca Thiessen for all the rides to and from campus and for the great time curling. We may not have been the best and got a few bruises, but we never fell. I would also like to thank my supervisor Dr. Philip Bonnaventure, for all of his guidance and support over the past seven years. Over this time, he has provided me numerous opportunities to expand my research skills and become a better scientist. He has also been there through my transition from a resident of perpetual summer to a seasoned winterer, complete with a Canadian accent. A special thank you also to Jeremy Benson for all of the support even if from afar. Your phone calls and texts always made the day better. Lastly, I would like to thank my parents and sister for all of the love and support and for sending doggy pictures just when I needed them the most.

The research in this thesis was generously supported by funding from Natural Resources Canada and the Northern Scientific Training Program and as well as grants held by Dr. Philip Bonnaventure from NSERC. Lastly sites used in these studies are located in Inuvialuit, Tr'ondëk Hwëch'in, Gwich'in, Ta'an Kwach'an, Sahtu, Acho Dene, Tagish and DehCho First Nations settlement regions and traditional territories.

## Table of Contents

## List of Figures

## List of Tables

## List of Equations

## Abbreviations List

| | |
|---|---|
| ALT | Active Layer Thickness |
| AMAT | Annual Mean Air Temperature (non-climate normal) |
| AMGST | Annual Mean Ground Surface Temperature (non-climate normal) |
| AMGT | Annual Mean Ground Temperature (non-climate normal) |
| ANOVA | Analysis of Variance |
| BTS | Basal Temperature of Snow |
| CALM | Circumpolar Active Layer Monitoring |
| DD | Degree Days |
| DEM | Digital Elevation Model |
| EBK | Empirical Bayesian Kriging |
| EDW | Elevation Dependent Warming |
| FDD | Freezing Degree Days |
| $FDD_a$ | Freezing Degree Days Air |
| $FDD_s$ | Freezing Degree Days Surface |
| GTN | Ground Temperature Node |
| HS | High Subarctic |
| LAI | Leaf Area Index |
| LA*n* | Low Arctic North |
| LS | Low Subarctic |
| MAAT | Mean Annual Air Temperature (climate normal) |
| MAGST | Mean Annual Ground Surface Temperature (climate normal) |
| MAGT | Mean Annual Ground Temperature (climate normal) |
| MB | Mid Boreal |
| MSE | Mean Square Error |
| MTS | Macmillan Transect South |
| MVLR | Multivariable Linear Regression |
| NEST | Northern Ecosystem Soil Temperature |

| | |
|---|---|
| $n_f$ | Freezing n-factor |
| NSP | Near Surface Permafrost |
| $n_t$ | Thawing n-factor |
| NVO | Nival Offset |
| PISR | Potential Incoming Solar Radiation |
| rk | Differential Thermal Conductivity |
| RMSE | Root Mean Square Error |
| SLR | Surface Lapse Rate |
| SO | Surface Offset |
| $T_a$ | Daily Average Air Temperature |
| TDD | Thawing Degree Days |
| $TDD_a$ | Thawing Degree Days Air |
| $TDD_s$ | Thawing Degree Days Surface |
| TO | Thermal Offset |
| TPI | Topographic Position Index |
| $T_s$ | Daily Average Ground Surface Temperature |
| TSO | Thawing Surface Offset |
| TSP | Thermal State of Permafrost |
| TTOP | Temperature at Top of Permafrost |
| TWI | Topographic Wetness Index |

# Chapter 1 Thesis Introduction

## 1.1 Introduction and Motivation

Permafrost is defined as perennially frozen or cryotic ground, remaining in a frozen state of below 0 ºC for at least two consecutive years (French, 2007). Permafrost is an important component of the cryosphere that can impact terrain stability (Harris et al., 2001; Lantz & Kokelj, 2008; Patton et al., 2019), hydrology (Woo et al., 2008), carbon storage (Schuur et al., 2008), and solute movement (Kokelj & Burn, 2003, 2005; Roberts et al., 2017; Lafrenière & Lamoureux, 2019). Additionally, permafrost is the only component of the cryosphere that is inhabited year-round, with major infrastructure such as communities, roads and pipelines built overtop.

Understanding the spatial distribution and thermal regime of permafrost, and characteristics such as active layer thickness (ALT), is difficult as it cannot be directly observed from the surface through remote sensing like other elements of the cryosphere (e.g. glaciers and sea ice) (Kääb, 2008). Therefore, modelling remains one of the main methods of evaluating the thermal state and occurrence of permafrost (Riseborough et al., 2008). However, permafrost modelling is complicated by the spatial and temporal variability, present at both regional and local scales, in permafrost occurrence, important influences, and characteristics such as active layer thickness.

Understanding the heterogeneity at a local scale is important for modelling permafrost at any spatial scale and assessing how well this heterogeneity may be represented by regional models. Additionally, as general permafrost models are used across a wide variety of permafrost environments on a wide range of scales, it is important to assess their performance and determine

parameter sensitivity to ensure accuracy and highlight sources of uncertainty. Lastly, using local models to assess the reliability of regional models is key to better representation of permafrost conditions currently, and to establish more authentic representations of permafrost conditions under warming climate. Therefore, using local heterogeneity and models to guide assumptions made in regional models is essential for accurate predictions of the thermal state of permafrost currently and in the future. This is especially important in locations where generalized assumptions of permafrost influences and conditions do not hold true.

### 1.2 Objectives

The main goal of this thesis is to assess how variability in permafrost conditions and active layer thickness (ALT), that are dependent on local environmental and climatic characteristics, can be related to regional trends. Understanding this variability will help improve smaller scale models of permafrost probability and thermal state. This was accomplished through four papers each with distinct research objectives presented as follows:

Paper 1. Examine local spatial and temporal variability in active layer thickness in relation to ecoregion in the Mackenzie Valley, NWT, Canada.

Paper 2. Determine the relative importance of temperature parameters for regional and territorial scale permafrost environments using the Temperature at the Top of Permafrost (TTOP) model and random forest variable importance rankings, and assess the performance of the TTOP model regionally.

Paper 3. Model air, ground surface, and ground temperatures at a fine spatial resolution in four dissimilar valleys in Yukon and compare local permafrost presence predictions to a regional permafrost probability model with differing assumptions of temperature inversion presence and strength.

Paper 4. Theoretically test elevation dependent warming (EDW), theorized for low latitude high elevations mountains in high-latitude, continental mountain valleys in Yukon subject to different relations between the thermal regime and elevation.

### 1.3 Thesis Structure

This thesis consists of eight chapters. Chapter 1 provides a brief introductory background on the rationale behind the thesis, the objectives of the overall thesis, and the individual chapters. Chapter 2 is a literature review, giving background information on the active layer, permafrost modelling and highlights the research gaps this thesis is attempting to fill. Chapters 3-6 are individual manuscripts written for publication in peer-reviewed journals. Chapter 3 relates active layer thickness to ecoregional characteristics in the Mackenzie Valley, and the work has been published (Garibaldi et al., 2022: AAAR). Chapter 4 analyzes the sensitivity of a widely used permafrost model to changes in parameter values across western Canada and determines variable importance through a random forest analysis. Chapter 5 utilizes spatial relations between a permafrost model parameters and topographic and vegetation characteristics to model the air and ground thermal regime in four high-latitude continental mountains in Yukon. Chapter 6 employs a scenario-based approach to alter the spatial models generated in Chapter 5 to assess the concept of elevation dependent warming in high-latitude continental mountains. Chapter 7 provides an overall summary of the thesis and the major conclusions for the four paper chapters (3-6). Lastly, Chapter 8 provides supplemental figures, methodology, and results for Chapters 3-6.

As each of the main chapters (3-6) are constructed as publications for submission to peer reviewed journals there is overlap between the individual chapter introductions and the background material presented in Chapter 2. Additionally, as Chapters 4-6 utilize the same

permafrost model there is overlap in the equations used and included in the equations list. Lastly, as the research conducted in Chapters 5-6 was in same study area there is repetition in the study area sections for these chapters.

# Chapter 2 Literature Review

## 2.1 Introduction and Background

The spatial distribution of permafrost and permafrost temperatures depends on a combination of macro and microscale environmental factors that may vary over small distances. In mountain environments, the spatial heterogeneity is extremely complex as permafrost-influencing characteristics can vary rapidly in this environment. This is further complicated by the presence of persistent temperature inversions in high-latitude, continental mountain settings, which disrupts the continuity permafrost probability at elevations. As permafrost impacts terrain stability, hydrology, and nutrient cycling, understanding the spatial distribution of permafrost and permafrost temperatures at a microscale in mountain environments is important to predicting local impacts of permafrost degradation. Additionally, the relative importance of each individual, physical factor on permafrost presence or temperature varies widely in different permafrost environments. Consequently, not all permafrost environments may respond equally to similar changes in climate or disturbance. To predict potential permafrost response to climate warming, it is therefore vital to identify the most important local factors and understand how these may evolve with climate change.

## 2.2 Influences on Ground Surface and Permafrost Temperatures

Permafrost is defined as earth material, which remains at or below 0 °C for at least two consecutive years (French, 2007). Permafrost is the only element of the cryosphere that people live on year round and is important on both local and global scales for hydrology (Woo, 1986; Woo et al., 2008), terrain stability (Harris et al., 2001; Lantz & Kokelj, 2008), and carbon storage (Schuur et al., 2008). It can be described by extent as continuous (90-100%), extensive

discontinuous (50-90%), sporadic (10-50%), and isolated patches (0-10%) based on the percentage of land underlain by permafrost (Heginbottom, 1995; French, 2007) (Figure 2-1).

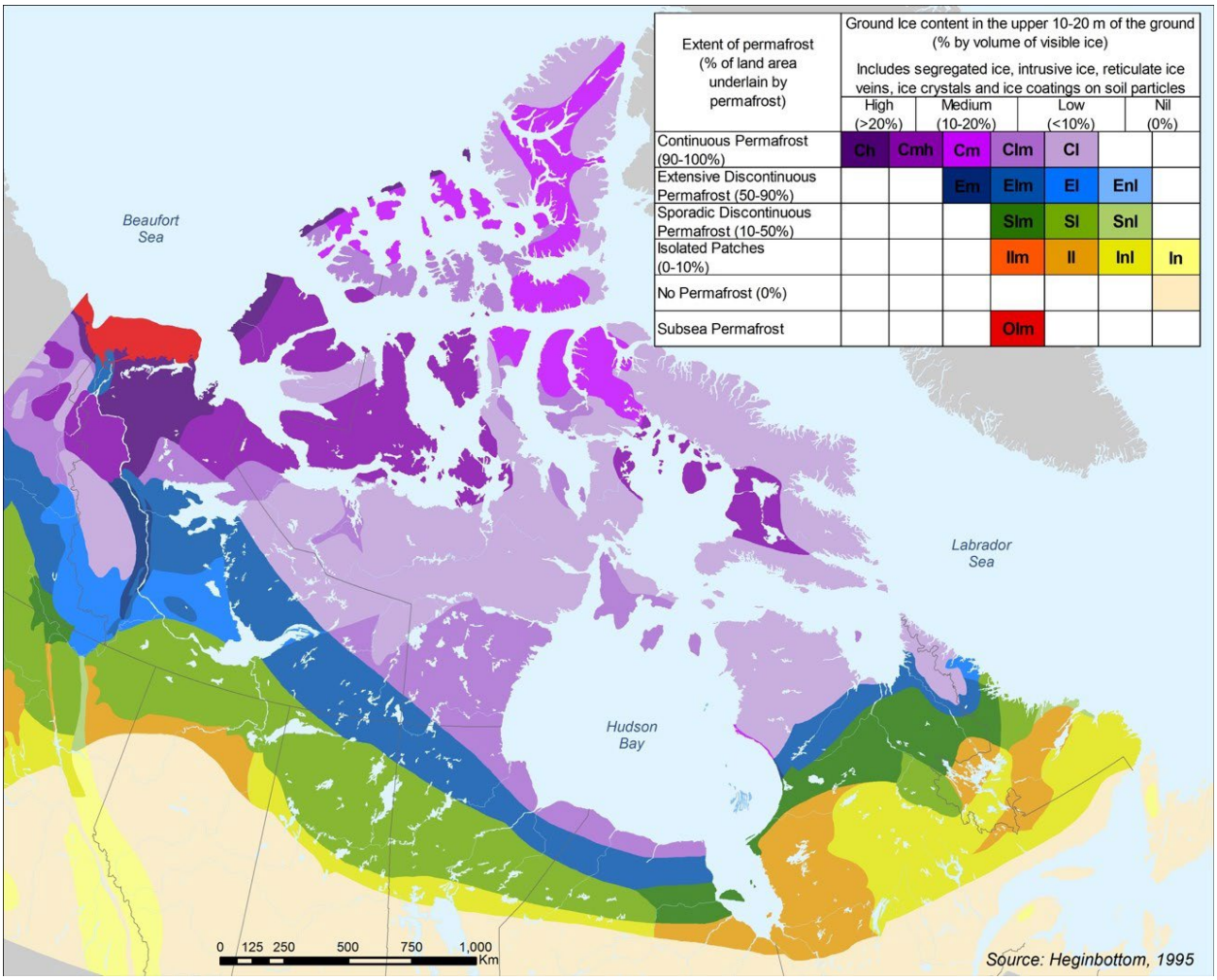


**Figure 2-1.** Permafrost map of Canada with zonation and ground ice content (Heginbottom et al., 1995).

Geographically, permafrost can be found in both northern lowland environments (lowland permafrost) and high elevation alpine regions (mountain permafrost).

Generally, mean annual air temperature (MAAT) has the most significant influence on permafrost temperatures and distribution at a regional scale (Etzelmüller et al., 1998; Juliussen & Humlum, 2007; Shur & Jorgenson, 2007). On local scales, other environmental factors such as snow cover, vegetation, and sediment thermal conductivity impact both the distribution and

thermal state of permafrost (TSP) by moderating the transfer of heat in and out of the ground (Williams & Smith, 1989; Smith & Riseborough, 1996; French, 2007; Juliussen & Humlum, 2007). The vertical profile in permafrost environments is typically conceptualized using three distinct temperature fields, air, ground surface, and temperature at the top of permafrost (TTOP) (Smith & Riseborough, 1996; Henry & Smith, 2001) (Figure 2-2).

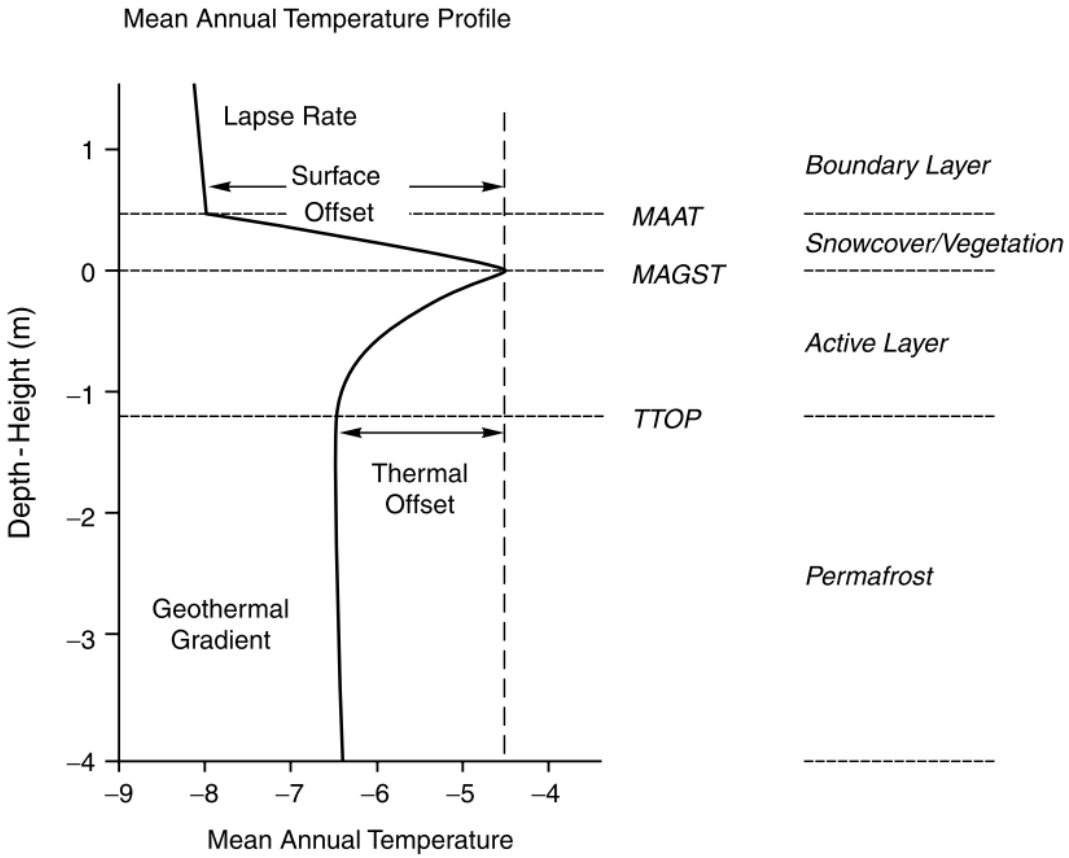


**Figure 2-2.** Mean annual temperature profiles through the lower atmosphere and into the subsurface for permafrost-underlain terrain (Henry and Smith, 2001).

The magnitude of the surface offset (temperature difference between the MAAT and the mean annual ground surface temperature (MAGST)) is largely dependent upon surface cover, namely vegetation and snow cover (Henry & Smith, 2001; Smith & Riseborough, 2002). During winter, the low thermal conductivity of snow causes it to act as an insulator, limiting winter heat loss (Zhang, 2005). As a result, increased snow cover generally results in higher winter (nival)

offsets and warmer ground surface and permafrost temperatures (Smith, 1975; Henry & Smith, 2001; Smith & Riseborough, 2002; Zhang, 2005). In areas of continuous permafrost, seasonal snow cover can increase ground surface and permafrost temperatures by several degrees and in discontinuous or sporadic permafrost may inhibit the development of permafrost (Zhang, 2005). Spatially, the distribution of snow contributes to the heterogeneity of ground and permafrost temperatures on both large and small scales (Smith, 1975; Young et al., 1997; Zhang, 2005). In the absence of vegetation, topography is the main control on snow redistribution, as it is scoured from locations of topographic prominence (ridges, hilltops) and deposited in low-lying areas (Young et al., 1997). Where vegetation is present, snow can either be trapped by shrubs or intercepted by taller vegetation (trees) leading to thicker snowpacks and warmer winter temperatures in shrub cover than in treed locations (Smith, 1975; Sturm et al., 2001; Duchesne et al., 2015).

In summer, the surface offset and ground surface temperatures are largely dependent on net radiation (Smith, 1975; Smith & Riseborough, 2002). Spatial variation in net radiation results largely from differences in vegetation, which can restrict incoming solar radiation through shading resulting in cooler ground temperatures beneath trees (Smith, 1975; Smith & Riseborough, 2002). Due to the brevity of the summer season in permafrost environments, ground surface and permafrost temperatures, are primarily dependent on winter cooling rather than summer heating (Smith, 1975; Smith & Riseborough, 2002). Snow cover is the controlling factor in determining the southern limit of continuous permafrost (Smith & Riseborough, 2002). Additionally, sites with high snow cover may also respond less to warming air temperatures, especially winter warming, than sites with little to no snow cover (Garibaldi et al., 2021).

The magnitude of the thermal offset (temperature difference between the ground surface and TTOP) is largely influenced by the thermal conductivity of the sediment, specifically the difference in thermal conductivity between the frozen and thawed state (Goodrich, 1982; Smith & Riseborough, 1996, 2002; Westermann et al., 2015; Way & Lewkowicz, 2016). Differential thermal conductivity is dependent on moisture content, which is controlled by texture and the presence of an organic or moss layer (Smith & Riseborough, 2002). Dry sediments and mineral soils have small seasonal variation in thermal conductivity, as the conduction is similar when frozen and thawed (Riseborough & Smith, 1998). Conversely, wet and organic soils or thick moss layers are more conductive when frozen than thawed leading to a large seasonal difference in conductivity (Burn & Smith, 1988; Bonnaventure & Lamoureux, 2013). This thermal conductivity differential allows more heat to escape during winter than can penetrate during summer resulting in cooler ground temperatures (Brown, 1970; Smith & Riseborough, 2002). As a result, thermal conductivity is a defining factor in the presence of isolated patched of permafrost at the southern climatological limit (Smith & Riseborough, 2002).

By combining climate characteristics with ecological processes (specifically thermal conductivity) permafrost can also be classified into five patterns of formation: climate driven, climate driven ecosystem modified, climate driven ecosystem protected, ecosystem driven, and ecosystem protected (Figure 2-3) (Shur & Jorgenson, 2007).

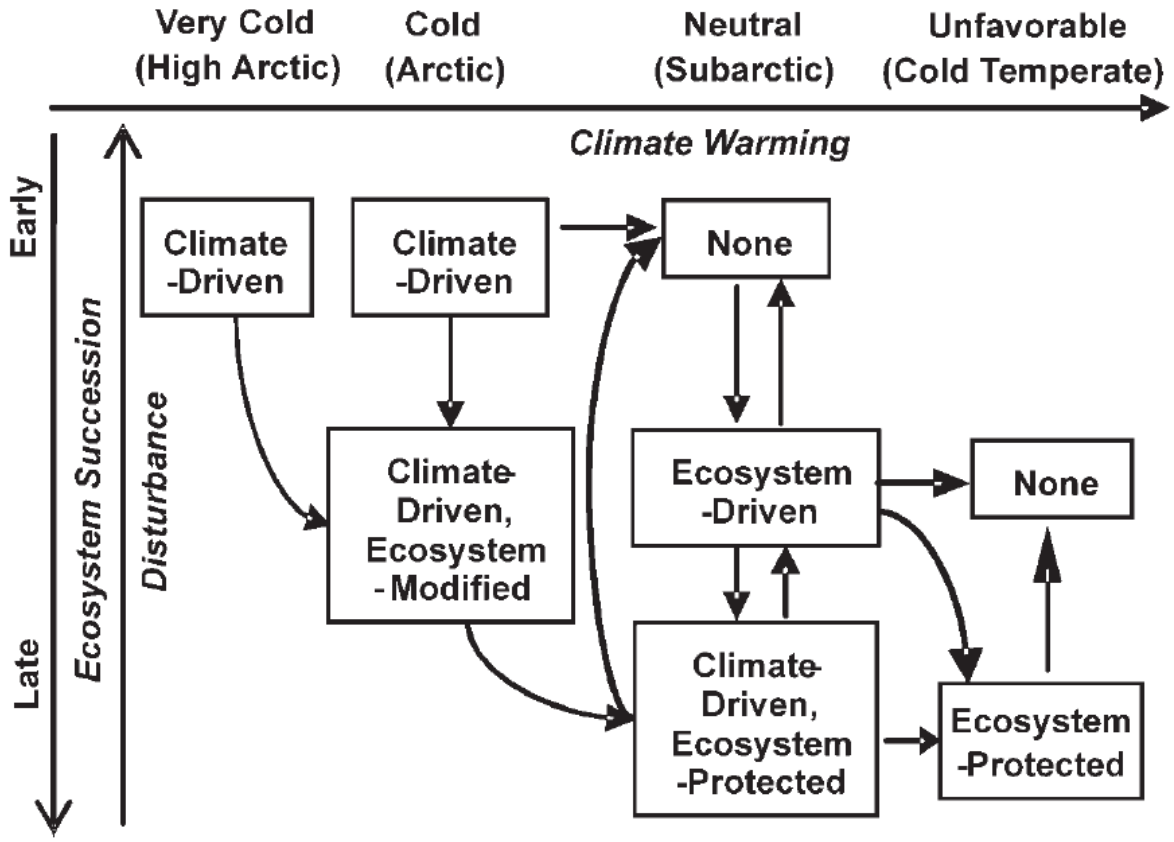


**Figure 2-3.** Diagram relating permafrost condition to climate and ecological succession (Shur & Jorgenson, 2007).

Climate driven permafrost is found in areas of continuous permafrost where the climate is favourable to permafrost formation, generally in the High Arctic and newly exposed ground in the Low Arctic. This class of permafrost is the most vulnerable to rapid climate change although there is little potential for thaw settlement due to the limited ground ice. In the Low Arctic, climate driven permafrost may be impacted by vegetation development leading to climate driven ecosystem modified permafrost. As vegetation develops and peat accumulates thaw depth begins to thin due to the differential thermal conductivity making it less dependent on climate. This thinning also leads to the formation of aggregational ice at the top of the permafrost. As a result, this class of permafrost is less sensitive to climate change but is very sensitive to disturbance and has a high potential for thaw settlement and thermokarst.

Permafrost that formed under favorable climatic conditions, but survives under a warmer climate through protection from ecosystem properties, is classified as climate driven ecosystem protected permafrost. This class of permafrost commonly contains massive relict ice wedges formed under antecedent climate conditions. This type of permafrost is less dependent on climate but more sensitive to disturbance. However, in this case once this permafrost has degraded, due to removal of vegetation and organic soil, it cannot be re-established with the original permafrost characteristics. Degraded climate driven ecosystem protected permafrost may re-establish as ecosystem driven permafrost under certain conditions. This ecosystem driven permafrost may transition to ecosystem-protected permafrost if climate conditions continue to warm. Understanding the variation in permafrost response, (warming or thermokarst) to thermal perturbation or disturbance is important for regional assessment of permafrost hazards and degradation with climate change. These interactions become increasingly complex in mountainous topography due to the increased spatial heterogeneity.

### 2.3 Mountain Permafrost

Mountain or alpine permafrost is perennially frozen ground located in mountainous environments (Gruber & Haeberli, 2009). Due to the extreme spatial variability in surface and near surface characteristics, including incoming solar radiation, elevation, slope, snow cover, and vegetation, and soil moisture, mountain permafrost is particularly spatially heterogeneous (Gruber & Haeberli, 2009). Additionally, the dominate influence on mountain permafrost can change depending on the nature of the mountain range, with elevation, incoming solar radiation, aspect, snow cover, substrate and cold air circulation all cited as the dominant influence on mountain permafrost presence or temperature (Bonnaventure & Lewkowicz, 2008; Gądek & Kędzia, 2008; Luetschg et al., 2008; Gruber & Haeberli, 2009; Apaloo et al., 2012).

*2.3.1 Permafrost in Mountains Subject to Annually Normal Surface Lapse Rates*

In maritime and low latitude mountain environments surface lapse rates or the relation between temperature and elevation are normal on an annual scale leading to decreasing MAAT with increasing elevation (Figure 2-4). As a result, permafrost in these environments is present at higher elevations and absent at lower elevations (Guglielmin et al., 2003; Boeckli et al., 2012; Bonnaventure et al., 2012). This creates a linear distribution of permafrost in these environments. Due to this distribution pattern, it is hypothesized that with climate change the lower elevation limit of permafrost will move upslope as higher elevations are more prone to warming (Bonnaventure et al., 2012; Pepin et al., 2015a; Rangecroft et al., 2016).

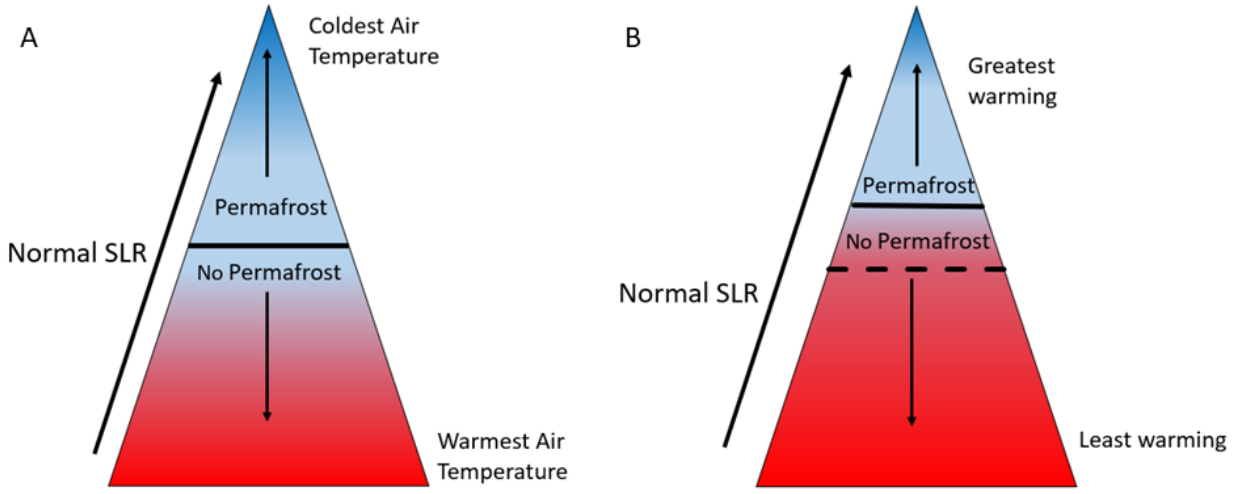


**Figure 2-4.** Elevation distribution of air temperature and permafrost in mountain environments subject to annually normal surface lapse rates (SLRs) A) Currently and B) with climate warming.

*2.3.2 Permafrost in Mountains Subject to Annually Inverted Surface Lapse Rates*

In high-latitude, continental mountains low solar angles during winter result in large negative surface radiation balances and limited turbulent mixing (Malingowski et al., 2014). This radiative cooling results in colder air temperatures at low elevations in the valley bottoms than at mid to high elevations, leading to an air temperature inversion (increasing temperature with

increasing elevation) (Figure 2-5). As these negative surface energy balances can persisted for extending time periods (days to weeks), the annual SLR for valleys in these regions is inverted. Additionally, the high continentally of these regions also contributes to the stability of these inversions due to limited wind compared to maritime environments and the potential for topographic obstruction (Pichugina et al., 2019; Noad & Bonnaventure, 2022). This prevents or limits inversion breakup through turbulent mixing initiated by wind. This annually inverted SLRs result in non-linear permafrost distribution with a high probability of permafrost at both low and high elevations while permafrost is generally absent around treeline (Bonnaventure et al., 2012).

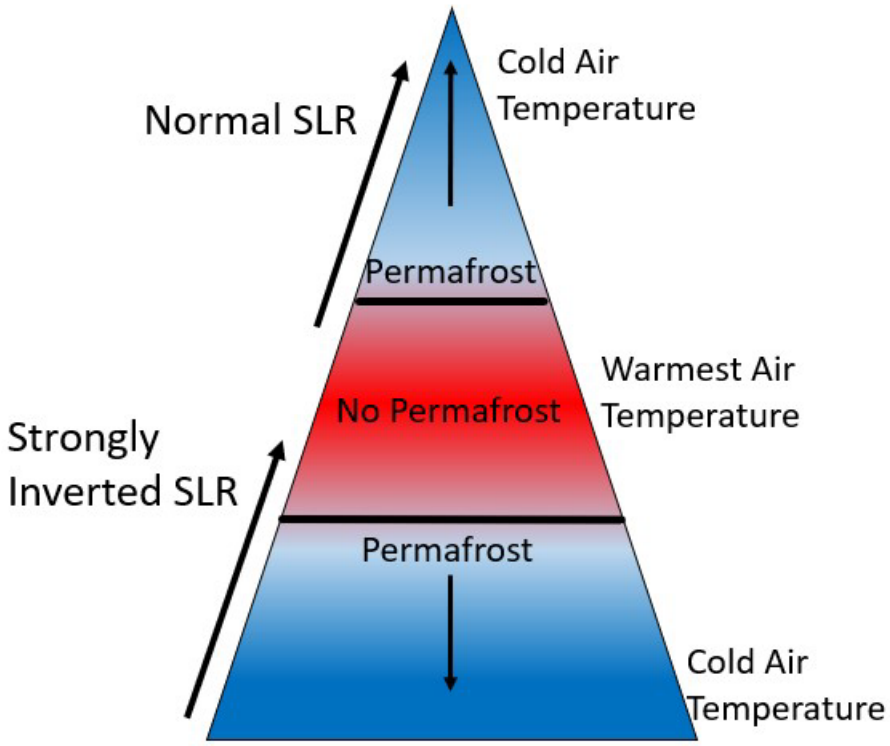


**Figure 2-5.** Elevation distribution of air temperature and permafrost in mountain environments subject to annually inverted surface lapse rates (SLRs).

Moving northward due to the increased radiation deficit these inversions become stronger, however, little is known about the ground thermal regimes in the presence of these "hyper-inversions" as previous studies mainly focused on permafrost probability (Bonnaventure et al., 2012; Noad, 2021). Additionally, previous studies in Yukon have focused mainly on a regional scale in the southern portion of the territory (south of Dawson) and little has been done to investigate how local conditions such as vegetation and snow may modify the impact of the inversion on the temperature of the ground (Lewkowicz & Ednie, 2004; Lewkowicz & Bonnaventure, 2011; Bonnaventure et al., 2012).

With climate warming the strength the of annual inverted SLRs in these regions are likely to be altered due to changes in sea ice and warmer ground temperatures which leads to greater, more prolonged atmospheric mixing (Ruman et al., 2022). As a result, the spatial distribution of warming may be different in these regions than in areas with annually normal SLRs. Additionally, the non-linear elevation distribution of permafrost may leave valley bottoms more susceptible to thaw than higher elevations. However, this relation is complicated by the presence of vegetation and organic material, which are more commonly found in valley bottoms, and may offer some protection to the underlying permafrost (Shur & Jorgenson, 2007). Understanding both the impact of inversions and the subsequent modification by surface characteristics on the ground thermal regimes in these high-latitude, continental mountains is critical to accurate prediction of permafrost response to climate change and potential related hazards.

### 2.4 Active Layer

Within permafrost terrain, the layer of earth material above permafrost, which is subject to annual freezing and thawing, is known as the active layer (Burn, 1998). In permafrost environments, the vast majority of subsurface biological process occur in the active layer

(Hinzman et al., 1991). Most studies concerning the active layer focus on the metric is active layer thickness (ALT) which is defined as the depth of the active layer (top of the soil to the top of the permafrost) during maximum thaw.

### *2.4.1 Influences on ALT*

ALT is dependent on a combination of macro- and micro-scale controls that results in ALT variability on a variety of scales (Bonnaventure & Lamoureux, 2013). On a macro-scale, ALT is influenced by climate with colder climates resulting in thinner active layers (Bonnaventure & Lamoureux, 2013). This results in broad general distribution patterns of ALT with relatively thin active layers found in high-latitudes, underlain by continuous permafrost and relatively thick active layers found in lower latitude environments and areas of mountain permafrost (Bonnaventure & Lamoureux, 2013). Previous studies focus particularly on the influence of summer temperatures on active layer thickness concluding that warmer summers contribute to thicker active layers (Brown et al., 2000; Woo et al., 2007; Smith et al., 2009b). However, antecedent winter meteorological conditions may also contribute to ALT especially in topographically complex terrain (Brown et al., 2000; Duchesne et al., 2015). On a micro-scale, the impact of climate is moderated by local conditions including snow cover, vegetation, and substrate properties (soil moisture, texture, etc…) (Smith, 1975; Romanovsky & Osterkamp, 1995; Zhang et al., 1997; Duchesne et al., 2015; Fisher et al., 2016).

The relation between snow cover and ALT is complex as the impact depends on the timing, thickness, and density of the snow cover. Additionally, there is some disagreement about whether increased snow thickness inhibits or facilitates changes in ALT and depth of thaw penetration or has no impact (Zhang et al., 1997; Woo et al., 2007; Lafrenière et al., 2013; Duchesne et al., 2015; Atchley et al., 2016). In the High Arctic, the relation between ALT and

snow depth was more apparent in locations of thin snow cover with a small increase in snow resulting in a decrease in ALT (Lafrenière et al., 2013). In this case, the largest impact of snow accumulation on ALT was the length of the thaw season, with increased snow persisting longer into the thaw season limiting thaw penetration (Lafrenière et al., 2013). However, other studies have found that increased snowfall is positively correlated with ALT as increased snow depth prohibits extremely cold winter soil temperatures allowing for deeper thaw penetration in summer (Duchesne et al., 2015; Atchley et al., 2016).

Vegetation has also been shown to affect ALT through snow entrapment and interception, shading, evapotranspiration, and insulation (Duchesne et al., 2015; Fisher et al., 2016; Loranty et al., 2018). As previously discussed, shrubs readily trap windblown snow leading to greater snow depths in shrub sites than sites without shrub cover (Smith, 1975) (Figure 2-6). As a result, active layers are commonly thicker under shrub cover than those with no shrubs (Duchesne et al., 2015). In forested environments, leaf area index (LAI) is inversely correlated to ALT with thinner active layers present in forests with higher LAI, potentially because of greater snow interception (Fisher et al., 2016). However, more likely this relation is a product of greater evapotranspiration and shading during summer which results in drier soils (reducing thermal conductivity) and lowering the downward heat flux (Fisher et al., 2016). Surface vegetation cover, specifically a moss layer has also been shown to impact ALT. Moss layer thickness and ALT are inversely related where a thicker moss layer results in a thinner active layer due to the insulating properties of dry moss slowing thaw during summer (Fisher et al., 2016).

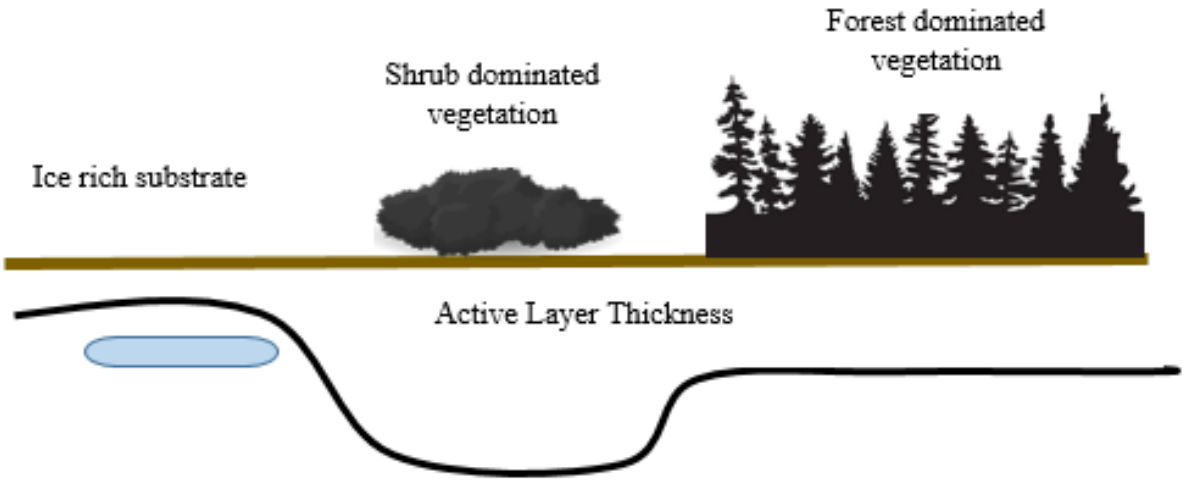


**Figure 2-6.** Illustration of relative active layer thickness (ALT) for ice-rich substrate, shrub vegetation cover and forested vegetation cover.

Moving into the subsurface, soil composition, specifically ice content, substrate type and organic layer thickness, influence ALT by reducing thawing in summer and enhancing freezing during winter (Romanovsky & Osterkamp, 1995; Woo et al., 2007). The most important soil properties are the ice content, and seasonal difference in thermal conductivity within the active layer (Romanovsky & Osterkamp, 1995). Ice content within the active layer is largely a product of antecedent conditions (proximity to past glacial margins and potential for relict ground ice) and substrate (formation of segregated ice in fine grained, frost susceptible soils) (O'Neill et al., 2019a). Ice content delays thawing during summer as a greater amount of energy is consumed as latent heat within the active layer (Romanovsky & Osterkamp, 1995). Thickness of organic layer is inversely related to ALT, as the organic matter is more thermally conductive in winter when frozen than when thawed in summer (Fisher et al., 2016). As a result, thaw penetration in ice rich organic soils is inhibited compared to ice poor mineral soils (Woo et al., 2007).

The combination of differential snow cover, vegetation, and soil properties results in spatial and temporal heterogeneity in ALT conditions and in active layer response to changes in climate.

Active layers are generally thinner in tundra environments (north of treeline) than forested locations (south of treeline) but have larger spatial variability due to differences in vegetation, specifically the presence of shrubs (Duchesne et al., 2015). Within vegetation classes, difference in substrate can create spatial differences in ALT as mineral soil sites typically have deeper thaw depths than sites with organic cover (Smith et al., 2009b). Temporally, snow cover, vegetation and soil properties influence the impact of annual differences in air temperature on active layer thickness and thaw penetration.

Active layers at tundra sites with little organic cover typically have a more direct connection to air temperatures and therefore often have greater interannual variability in response to fluctuations in air temperatures (Smith et al., 2009a; Duchesne et al., 2015). In the boreal forest, ALT response to variations in air temperatures is dampened and show less interannual variability as a result of the forest vegetation, snow cover, and less favourable soil conditions (higher ice contents and thicker organic layers) (Nixon & Taylor, 1998; Brown et al., 2000; Smith et al., 2009b; Duchesne et al., 2015). This indicates that ALT is more dependent on forest canopy, snow cover, and ground cover than summer air temperatures in these environments (Brown et al., 2000). Additionally, this disconnect between the air and ground surface means that warmer summer air temperatures are required to achieve similar ALT in the boreal forest compared to the tundra (Nixon & Taylor, 1998). As a result, active layers in the tundra show a greater response to climate change than those in boreal environments, which are more likely show a greater response to disturbance (Smith et al., 2009b; Smith et al., 2015).

### *2.4.2 Monitoring ALT*

Most ALT studies involve in situ measurement and monitoring of ALT over several thaw seasons to establish spatial patterns of thickness and assess trends in thickness through time. The

two main techniques used for this are thaw tubes and probing (Bonnaventure & Lamoureux, 2013). Physical probing involves forcing a metallic rod into the ground until it is met with considerable resistance, indicating the depth of the frost table (Bonnaventure & Lamoureux, 2013). Several variables impact the accuracy and comparability of these measurements year to year, the most important being timing of the measurement, substrate type and strength of the prober. Timing of probing is important, as it must be done in late summer to ensure measurements are taken at the time of maximum thaw, generally late August to early September in the Northern Hemisphere (Bonnaventure & Lamoureux, 2013). Determining ALT through probing is most simplistic in fine-grained sediment as the resistance can solely be attributed to reaching the frost table. However, in areas with varying soil density with depth or large clasts it becomes more difficult to determine whether the resistance is the end of the active layer. In this case, physical probing can be paired with a temperature sensor to determine temperature at the depth of probing.

Thaw tubes determine the depth of maximum thaw penetration through the position of a glass bead, which sits on the frozen surface and descends to the point of maximum thaw each year during the thaw season (Figure 2-7) (Nixon & Taylor, 1994). They can also be used to determine the position of the ground surface at the time of maximum heave and ground surface subsidence (Mackay, 1973). ALTs can then be determined using the depth of maximum thaw penetration and the position of the ground surface at the time of maximum thaw. Thaw tubes are considered a superior technique compared to probing for determining active layer thickness as they do not require personnel to be present on the specific day of maximum thaw which varies annually (Smith et al., 2009b; Bonnaventure & Lamoureux, 2013). However, the thaw tubes still need to be visited annually as the record is destroyed the subsequent year. These methods have

been used extensively to yield long-term ALT records across the Arctic including in the Mackenzie Valley.

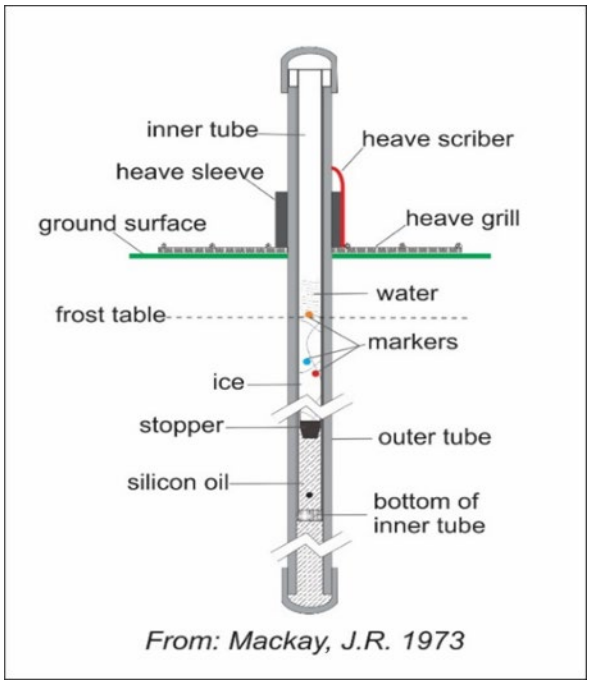


**Figure 2-7.** Diagram of a thaw tube (Mackay, 1973).

*2.4.3 Active Layer Studies in the Mackenzie Valley, NWT*

In the Mackenzie Valley, an ALT monitoring network spanning the length of the valley has been maintained for over a decade with studies used to assess temporal and spatial relations between climate ALT variability as well as the evolution of ALT after disturbance (Tarnocai et al., 2004). Thirteen of the sites in this network have been selected as a part of the circumpolar active layer monitoring (CALM) network which aims to archive ALT throughout polar regions through time (Tarnocai et al., 2004).

The data from these sites has been used to evaluate ALT and surface subsidence as well as explore change in ALT within three ecoclimatic zones (Arctic, Subarctic and Boreal) (Tarnocai et al., 2004). Results from this study indicate that despite warmer ground surface

conditions at the Boreal sites, most sites showed similar patterns of thaw penetration. Additionally, it was concluded that warmer conditions are required in Subarctic and Boreal environments to achieve similar ALTs indicting that surface and soil conditions in these locations are less favorable to thaw development than in the Arctic. However, this study did not evaluate longer trends in ALT compared to warming air temperatures in each ecoclimatic zone but rather focused more on short-term interannual variability. Additionally, this study was completed using data from 1991-2001 using only thirteen sites, which did not allow for a more detailed conclusions and comparisons of ALT in each ecoclimatic zone (Tarnocai et al., 2004).

Other studies of ALT in the Mackenzie Valley focused on differences based on local site characteristics including air temperature, vegetation, and substrate (Duchesne et al., 2015). The Mackenzie Valley CALM sites were also used to assess the response of ALT to thermal forcing and seasonal climate variability in various settings (Smith et al., 2009b). Similar to the previous study Smith et al. (2009a) found that boreal sites experience much warmer air temperatures than more northern sites but the impact on ALT was limited due to a well-developed organic layer. Additionally, there was greater correlation between late season thaw temperatures and ALT at Southern Arctic sites, although these could be further divided into organic soils with shallow to intermediate thaw depths and mineral soils that have deep thaw depths. Greater interannual variability in response to seasonal climate was observed for arctic sites with no organic layer compared to forested sites or those with some organic cover. However, once again this study was limited in the number of sites (8 total and 1-3 sites per ecozone), which makes it difficult to fully characterize the active layer for each ecological region.

The Geological Survey of Canada has maintained an active layer monitoring network since the early 1990s consisting of 66 sites, which have been utilized to assess differences in

ALT spatially and temporally (Duchesne et al., 2015). The results of this study largely reported variation in ALT based on vegetation type, concluding that active layers were generally thinner above treeline than below treeline and the thickest active layers were measured at sites with high shrubs. Greater temporal variability in ALT was associated with sites with low ice content and summer temperatures were shown to have a greater influence on ALT at tundra sites compared to forested sites. Although this study provides necessary baseline information on ALT spanning the valley and the potential impact of climate change it focuses more on site specific and local ALT rather than trends and impacts on a broader regional scale, which may be more useful when attempting to create adaptation strategies.

Active layer monitoring sites in the Mackenzie Valley were used to study local ground thermal conditions following fire (Smith et al., 2015). Following a burn in 1994, ground temperatures and ALT increased likely due to increased snow accumulation (lack of interception by trees as pre-fire) and decreased summer albedo and evapotranspiration. After the re-establishment of aspen, willow, and tamarack, ground surface temperatures cooled; however, because the aspen forest did not have the same micrometeorological properties as the original spruce forest and lacked the thick organic layer, permafrost recovery was likely limited in the short to medium term. As a result, with predicted climate warming, the authors concluded that the permafrost was unlikely to redevelop even after the ecosystem reaches equilibrium. This study highlights the importance of the ecosystem on ALT and permafrost preservation in the southern portion of the valley. Due to the protection of the ecosystem, active layers in boreal forest environments are likely to respond differently to climate change then those in tundra environments. This demonstrates the need for assessment of ALT based on regional ecosystems to better predict active layer response on a broader scale.

### *2.4.4 Research Gaps in Active Layer Processes*

Many studies on ALT in the Mackenzie Valley, NWT have focused on characterizing ALT based on air temperature, vegetation, and substrate both temporally and spatially (Smith et al., 2009b; Duchesne et al., 2015). Additionally, research is also focused on ALT response to disturbance (primarily fire) over small local areas (Smith et al., 2015). Previous studies have demonstrated that regional patterns in ALT can be inferred using average values from extensive field measurements in representative conditions (Nelson et al., 1997). This allows for mapping of ALT across larger areas to better predict general response of ALT to warming more broadly. As ecological regions are defined based on similar factors to those that influence ALT (climate, physiography, vegetation, and geology) they provide a predefined geographical context with which to relate broad patterns of ALT attributes both spatially and temporally.

In the Mackenzie Valley, an extensive ecoregional approach to ALT variability has not been conducted despite longer data records and additional monitoring sites outside of the CALM network (Tarnocai et al., 2004). Exploring the spatial variability in ALT both within and between ecoregions in the Mackenzie Valley will assist in understanding broad scale patterns in ALT and may assist in future regional scale ALT modelling as ecoregions in the Northwest Territories have currently defined extents and characteristics (Group, 2007 (rev. 2009), 2010, 2012). Understanding temporal changes in ALT by ecoregion will help also to further define regions more susceptible to either disturbance driven or climate driven active layer thickening which can potentially be used in future studies to better assess the associated hazards and their timing in the Mackenzie Valley.

## 2.5 Permafrost Modelling

A model is an idealized representation of reality, which uses conceptual, physical, or mathematical terms to express the essential elements of a system (Inkpen, 2005). Modelling is one of the most commonly used methods to study permafrost since it cannot be directly observed from the surface by remote sensing like other elements of the cryosphere (e.g. glaciers and sea ice) (Kääb, 2008). Since permafrost distribution is the result of complex environmental interactions, several different techniques for modelling permafrost-climate relations have emerged in the literature (Riseborough et al., 2008; Bonnaventure & Lamoureux, 2013). One technique is a process based numerical approach that models the energy balance directly to identify ground temperature conditions. Another technique is through empirical or statistical models that associate topographic and/or climate variables to permafrost distribution or attributes (Riseborough et al., 2008; Bonnaventure & Lamoureux, 2013; Etzelmüller, 2013). Finally, a third technique is using process based analytical models that make simplifying assumptions regarding surface and subsurface characteristics and thermal properties (Riseborough, 2008). Permafrost models also vary based on their use. Due to the nature of each model and the associated uncertainties transient models are more often used to model transient or changing permafrost conditions through time while equilibrium models are used to model permafrost which is in equilibrium with current climate conditions (Riseborough et al., 2008).

### *2.5.1 Numerical Models*

Numerical models are process-based models that directly estimate the ground-atmosphere energy exchange using theories of heat transfer and flow to create an energy balance equation (Sazonova & Romanovsky, 2003; Zhang et al., 2003; Bonnaventure & Lamoureux, 2013; Kurylyk & Hayashi, 2016; Yin et al., 2016). These models perform best in areas with known boundary conditions and forcing parameters, as they require large amounts of site-specific data

(Oelke et al., 2003; Riseborough et al., 2008). Since these types of models require a large amount of input data and have high calculation requirements, their use in modelling studies is limited especially in remote locations and areas of complex terrain (Riseborough et al., 2008; Bonnaventure & Lamoureux, 2013). As a result, these studies are primarily used as point source models in lowland permafrost environments and are rarely used for spatial studies (Sazonova & Romanovsky, 2003; Riseborough et al., 2008; Bonnaventure & Lamoureux, 2013; Kurylyk et al., 2014) (Sazonova & Romanovsky, 2003; Riseborough et al., 2008; Bonnaventure & Lamoureux, 2013; Kurylyk et al., 2014). One numerical model that has been used to model permafrost spatially is the Northern Ecosystem Soil Temperature (NEST) model.

#### 2.5.1.1 Northern Ecosystem Soil Temperature (NEST) Model

The NEST model was developed to assess the impact of climate warming, specifically the increase in summer thaw depth and permafrost degradation, on northern ecosystem functions and dynamics (Zhang et al., 2003). The NEST model treats soil, vegetation, and the atmosphere as an integrated system through a combination of soil-vegetation-atmosphere systems and strengths from existing permafrost models. A series of one-dimensional heat conduction and energy balance equations are used to determine thermal dynamics of the ground and snow layers in the model (Figure 2-8).

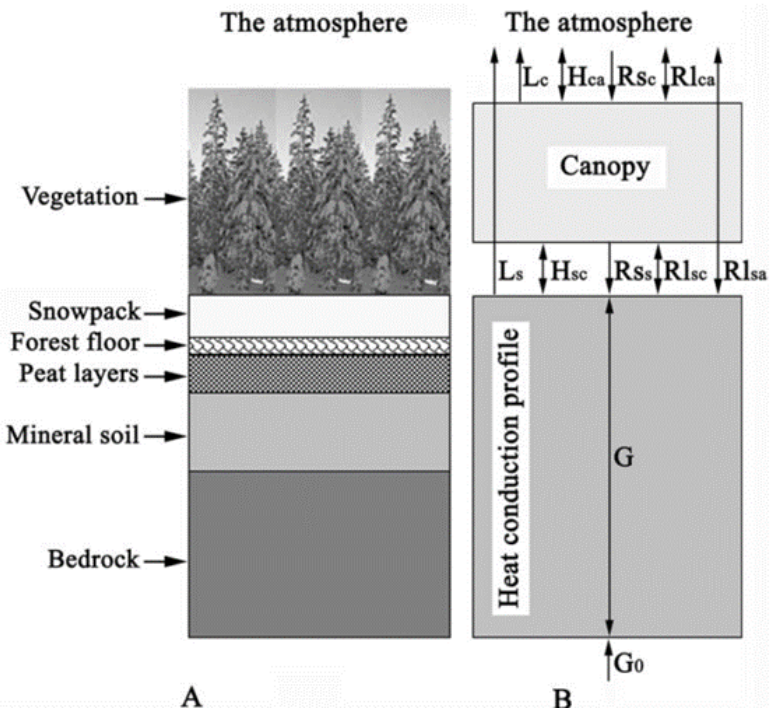


**Figure 2-8.** A) The environmental components used in the NEST model. B) Exchange of energy between soil, vegetation, and atmosphere accounted for in the NEST model. The energy balance equation created for the model includes the sensible heat (H), the latent heat (L), solar radiation (Rs), long-wave radiation (Rl), and the convective heat flux (G) exchange between the ground surface (s), the vegetation canopy (c), and the atmosphere (a). Zhang et al. (2003).

The NEST model is able to simulate the transient impacts of climate change on northern ecosystems as it can account for the impact of altered soil thermal regimes and permafrost degradation on ecosystems and biogeochemical cycles across a variety of vegetation and ground conditions (Zhang et al., 2003). As a numerical model one of the main drawbacks to the NEST model is large quantity of site-specific data related to vegetation, ground conditions, and atmospheric climate to run the model affectively (Zhang et al., 2003; Riseborough et al., 2008). The NEST model was initially developed for lowland permafrost and has yet to be utilized in mountain permafrost environments, as the spatial resolution of the input data may not accurately capture the complex heterogeneity.

*2.5.2 Empirical Models*

Empirical models are statistical models that use computed or measured topoclimatic variables to determine permafrost probability, rather than explicitly calculating the energy balance directly (Hoelzle et al., 2001; Riseborough et al., 2008; Bonnaventure & Lamoureux, 2013). Permafrost occurrence is usually linked to basal temperature of snow (BTS), geophysical investigations, or the existence of specific periglacial landforms such as rock glaciers (Riseborough et al., 2008). As the influential variables may vary between locations, the number of required input parameters is limited and empirical models can be run without the direct climate data (Hoelzle et al., 2001; Bonnaventure & Lamoureux, 2013). For these reasons, empirical models are more frequently used to model permafrost spatially than numerical models (Henry & Smith, 2001; Riseborough et al., 2008; Westermann et al., 2015; Way & Lewkowicz, 2016). Additionally, empirical models are best suited for modelling in remote locations and mountains, since there is often sparse or temporally limited or disjointed data in these areas (Etzelmüller et al., 2006; Riseborough et al., 2008). Finally, these types of models are well suited for examining impacts of climate change on permafrost since their inputs are easy to manipulate in platforms such as GIS; however, they may not be the best option to study the transient development or changes of permafrost (Etzelmüller et al., 1998; Wright et al., 2003; Juliussen & Humlum, 2007; Gisnås et al., 2013).

#### 2.5.2.1 Basal Temperature of Snow (BTS)

The BTS model relies on statistical relations between a variety of environmental factors, including MAAT, incoming solar radiation, and BTS measurements to determine the probability of permafrost occurrence (Riseborough et al., 2008). The method was first developed to detect permafrost in the Alps but has since been used in a variety of mountain environments including Yukon (Haeberli, 1973; Lewkowicz & Ednie, 2004). The underlying principle of the BTS model

is the insulation of the ground from short-term energy balance variations by deep snow due to its low heat transfer capacity (Hoelzle, 1993; Lewkowicz & Ednie, 2004). This allows for equilibrium temperatures at the snow ground interface in late winter to reflect the thermal conditions within the ground (Lewkowicz & Ednie, 2004). In this case low ground temperatures indicate the presence of permafrost while higher values indicated seasonally frozen ground.

One of the main advantages of the BTS model is that field measurements from a relatively limited number of sites can be used to generate spatial models for larger areas (Bonnaventure & Lewkowicz, 2008). This is possible since the explanatory variables can be derived from digital elevation models (DEM). This makes it practical for modelling the spatial distribution of mountain permafrost. However, as BTS values may vary annually due to changes in snow depth, one main drawback is that measurements need to be taken under at least 80 cm of snow during late winter or early spring (Lewkowicz & Ednie, 2004; Riseborough et al., 2008). As this model required physical validation during the coldest time of year, its use may be limited in very remote locations that cannot be accessed during winter. Additionally, physical sampling is biased towards locations with deep snow (>80 cm) which prevents sampling at sites with little snow cover (mountaintop and ridges) potentially leading to discrepancies in the spatial permafrost distribution in these locations. Lastly, the model also needs to be recalibrated for different environments, although this is not always necessary if the model equation is created with robust physical validation and used within 200 km (Bonnaventure & Lewkowicz, 2008).

### *2.5.3 Analytical Models*

Analytical models are process-based models that have a closed form solution and make simplifying assumptions of real word conditions rather than calculating energy balance directly (Riseborough, 2008). These types of models are commonly used to model permafrost

temperature and movement of the freezing (or thaw) front (Smith & Riseborough, 2002; Riseborough et al, 2008; Kurylyk et al., 2014; Kurylyk & Hayashi, 2016). These attributes are modelled using defined equations and temperatures measured with data loggers and/or simplified assumptions regarding vegetation, snow cover and substrate characteristics (Juliussen & Humlum, 2007; Gisnås et al., 2013; Williams et al., 2015; Obu et al., 2019; Garibaldi et al, 2021). Additionally, the analytical equations used in these types of models are often simpler than numerical solutions but can become complex when describing more complicated systems (Riseborough et al., 2008). Finally, the analytical models are transferable between regions and do not always require recalibration before use (Riseborough et al, 2008). For these reasons as with empirical models, analytical models are more frequently used to model permafrost spatially than numerical models (Henry & Smith, 2001; Riseborough et al., 2008; Westermann et al., 2015; Way & Lewkowicz, 2016). Additionally, these models are better suited for modelling in remote locations (depending on the complexity of the system) and mountains, since there is often limited or disjointed data in these areas (Etzelmüller et al., 2006; Riseborough et al., 2008). Finally, these types of models are also well suited for examining impacts of changing environmental factor on permafrost since their inputs are easy to manipulate in platforms such as GIS; however, they also are not well suited to model the transient evolution of permafrost (Etzelmüller et al., 1998; Wright et al., 2003; Juliussen & Humlum, 2007; Gisnås et al., 2013).

#### 2.5.2.2 N-factors

N-factors are transfer functions or ratios comparing air and ground surface temperature, which act as an analytically alternative to numerical solutions for surface energy balance (Equation 2-1) (Riseborough et al., 2008).

$$n = \frac{DD_{\mathrm{s}}}{DD_{\mathrm{a}}} \tag{2-1}$$

Where N-factors are calculated using degree-days (DD), which for this calculation are the absolute value of the sum of the average daily temperatures. The subscripts s and a denote ground surface and air, respectively.

Since the surface offset is influenced by surface properties which differ during summer and winter, N-factors are often split into freezing ($n_f$) and thawing ($n_t$) (Equation 2-2) (Smith & Riseborough, 2002).

$$n_{\mathrm{f}} = \frac{FDD_{\mathrm{s}}}{FDD_{\mathrm{a}}} \qquad \text{and} \qquad n_t = \frac{TDD_{\mathrm{s}}}{TDD_{\mathrm{a}}} \tag{2-2}$$

$FDD_a$ and $FDD_s$ are freezing degree-days in the air and ground surface, respectively and $TDD_a$ and $TDD_s$ are thawing degree-days in the air and ground surface. FDD and TDD are the absolute value of the sum of the daily average temperature above or below 0 ºC for a period (P) (generally 365 days) (Equation 2-3) (Smith & Riseborough, 2002).

$$FDD = |\Sigma_1^P T|, T < 0$$
$$TDD = |\Sigma_1^P T|, T > 0 \tag{2-3}$$

As the surface offset is largely determined by vegetation during summer, the magnitude of $n_t$ depends on vegetation (Smith & Riseborough, 2002). Greater amounts of vegetation lower $n_t$ as a result of shading and transpiration keeping the ground surface cooler than the air (Smith & Riseborough, 2002). In areas with little to no vegetation, $n_t$ may exceed 1.0 as the ground becomes warmer than the air during summer (Garibaldi et al., 2021).

The value of $n_f$ is influenced by snow cover, with areas of higher snow cover producing smaller $n_f$ values as a result of the insulation of the ground surface from the coldest winter air

temperatures (Smith & Riseborough, 2002). However, even the relation between $n_f$ and snow depth is complex as the value of $n_f$ differ between regions even at the same snow depth (Way & Lewkowicz, 2016). For example, an $n_f$ of 0.3 requires a much deeper snow pack in the High Arctic than in a boreal forest due to the difference in the thermal conductivity of the snow (Zhang, 2005).

Additionally, the value of $n_f$ has been shown to also be a function of MAAT, with colder temperatures yielding larger N-factors than warmer temperatures given the same snow depths (Figure 2-9) (Smith & Riseborough, 2002). MAAT also provides a theoretical minimum for $n_f$, which is higher for colder MAAT. This is a product of the underlying permafrost since as the active layer freezes, energy is used as latent heat, delaying the temperature change of the sediment and releasing heat into the surrounding ground, known as the zero-curtain effect (Smith & Riseborough, 2002). In permafrost terrain, there is a limit to the freezing depth and eventually the active layer freezes to the permafrost. Once this happens, the latent heat pump keeping the ground surface warm, stops and the ground begins to cool. The shallower the active layer the sooner this process stops yielding colder ground surface temperatures and subsequently larger values of $n_f$ (Figure 2-9). If the air and the ground are in perfect connection, the $n_f$ is one.

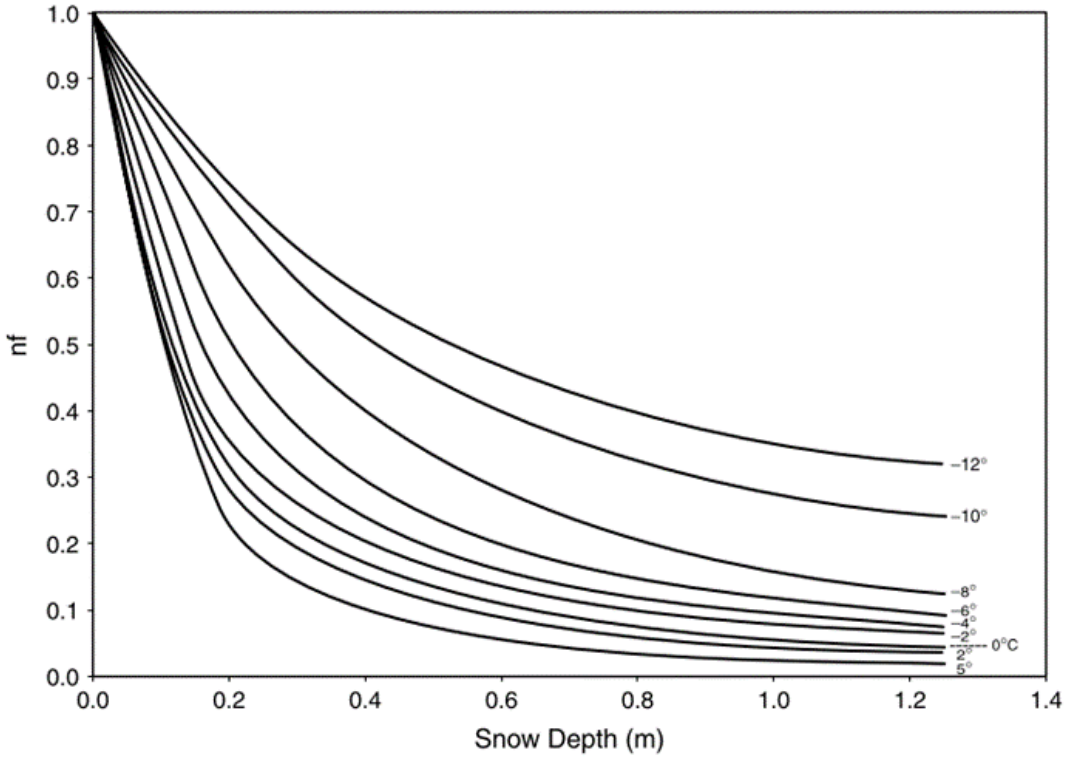


**Figure 2-9.** Theoretical curves showing $n_f$ as a function of MAAT and snow depth (Smith & Riseborough, 2002)**.**

2.5.2.3 TTOP Model

The TTOP model uses analytically derived N-factors and differential thermal conductivity to estimate average permafrost temperatures at the base of the active layer (Smith & Riseborough, 1996; Henry & Smith, 2001; Smith & Riseborough, 2002; Riseborough et al., 2008; Bonnaventure & Lamoureux, 2013; Bonnaventure et al., 2016) (Equation 2-4).

$$TTOP = \frac{(n_t * \lambda_T * TDD_a) - (n_f * \lambda_F * FDD_a)}{\lambda_F * P} \quad (2\text{-}4)$$

Where $n_t$ and $n_f$ are the thawing and freezing N-factors, $\lambda_T$ and $\lambda_F$ are the thawing and freezing thermal conductivities of the sediment, $FDD_a$ and $TDD_a$ are the freezing and thawing degree-days of the air, and P is the annual period (365 days). $\lambda_T$ and $\lambda_F$ are usually assigned based on substrate and/or vegetation and estimations based on values from the literature.

As per Smith and Riseborough (2002), the TTOP model for permafrost terrain (TTOP < 0 ºC) can be simplified by combining the thermal conductivity terms (Equation 2-5).

$$TTOP = \frac{(n_t * TDD_a * rk) - (n_f * FDD_a)}{P} \quad (2\text{-}5)$$

Where rk is the ratio of thawed to frozen thermal conductivity of the sediment. In seasonal thaw environments (TTOP > 0 ºC) a TTOP model for seasonal thaw should be utilized to limit errors (Equation 2-6) (Smith & Riseborough, 1996).

$$TTOP = \frac{(n_t * TDD_a) - (\frac{1}{rk} * n_f * FDD_a)}{P} \quad (2\text{-}6)$$

The TTOP model estimates permafrost temperature and presence at a variety of scales ranging from continental to local (Gisnås et al., 2013; Obu et al., 2019; Garibaldi et al., 2021) and in a variety of permafrost environments including High Arctic and alpine (Bevington & Lewkowicz, 2015). Additionally, TTOP has been used to predict permafrost temperature currently and in the future in response to climate warming (Smith & Riseborough, 1996; Riseborough, 2002; Juliussen & Humlum, 2007; Bonnaventure & Lewkowicz, 2013). One of the main reasons the TTOP model is widely used is because it is simple, only requiring data such as thermal offsets and air temperature, which are commonly measured by meteorological stations (Juliussen & Humlum, 2007). However, the TTOP model does not perform well as a transient model (or with a short-term record) at permafrost temperatures close to 0 °C. Errors associated with this can be lessened by averaging a longer data record (Riseborough, 2007). Additional errors may result from the model assumption of a single value for the thermal conductivity of frozen sediment (mineral and organic sediment), which due to its dependence on the sediment's unfrozen water content, may not hold true for all sediments (Riseborough, 2002). Similarly, the

TTOP model may result in errors in soils with significant freezing characteristics; however, a simple parameterization may help to minimize these errors (Riseborough et al., 2008).

One of the main challenges of using the TTOP model is determining the values of the scaling factors (N-factors and the ratio of thermal conductivity) (Juliussen & Humlum, 2007). When modelling using the TTOP model these scaling factors are assigned based on vegetation class or topographic class using field measurements or values presented in the literature (Riseborough et al., 2008; Gisnås et al., 2013; Obu et al., 2019). In southern Yukon variability in measured n-factor values were statistically differentiated best using vegetation classes rather than topography and region (Lewkowicz et al., 2012). However, another study highlighted the significant importance of both landcover and elevation (Bevington & Lewkowicz, 2015).

In the High Arctic due to the absence of well-developed vegetation, N-factors were statistically related to topographic position due to its impact on snow redistribution (Garibaldi et al., 2021). To map permafrost distribution across Norway, Gisnås et al. (2013) utilized a modified TTOP model known as CryoGrid and classified the landscape by vegetation and substrate to assign the scaling factors. To determine the values of $n_f$ spatially, a combination of vegetation and substrate classes was used. Values for forest, shrub, and mire vegetation classes were held constant at 0.35, 0.3, and 0.6, respectively while for bare ground the value was determined using snow depth. Values of $n_t$ were fixed by vegetation class and were calculated using air and ground stations. Values ranged from 0.85 for mires and 1.0 for barren ground, which was lower, compared to values observed in Canada that can be greater than 1.0. Lastly, thermal conductivity was estimated using known values for substrate types and estimated water content ranging from 1-5%.

On a broader scale, Westermann et al. (2015) utilized the TTOP model to map permafrost temperature distribution across the North Atlantic. Similar to Gisnås et al. (2013), $n_f$ values were estimated using snow depth and upper and lower limits that were set based on landcover class. However, unlike the previous study, $n_t$ values were set to one across the entire study area regardless of landcover class. For this study, a range of rk values (0.7-1.0) was used for all landcover classes. Similarly, in their attempt to map the spatial distribution of permafrost temperature over the northern hemisphere, Obu et al. (2019) used $n_t$ values of 1.0 over the entire area despite differences in vegetation classes. They also used functional relations based on snow depth and MAAT to estimate $n_f$ values and assigned rk values based on landcover and soil moisture classes ranging from 0.55 for wetlands and 0.95 for bare ground and deciduous forest. This estimation of N-factors and rk although necessary can lead to uncertainties in modelled permafrost temperatures and little is known about the magnitude of potential error based on the environment.

2.5.2.4 Research Gaps Using the TTOP Model

A few studies have examined the impact of the value of the TTOP model parameters on the permafrost temperature output. While modelling the spatial distribution of permafrost in Labrador-Ungava, Way and Lewkowicz (2016), demonstrated the uncertainties introduced when importing measured $n_f$ values from one region to another. When using four unique parameterization techniques the resulting ground surface temperature models had modal frequency differences of up to 2 °C. The resulting ground surface temperature (GST) surfaces differed both in the southernmost extent of extensive discontinuous permafrost and in areas with predicted GSTs of 0-2 °C, where the thermal offset determines the presence of permafrost. The largest differences occurred in forested regions especially when using Alaska-Yukon $n_f$ values.

This stems from forests in these locations, which are typically cold with permafrost while in Labrador-Ugava forests are warm and commonly lack permafrost. This demonstrates the potential errors resulting from the direct transfer of $n_f$ values from different environments in one location; however, the impacts in other environments are still unknown.

In their assessment of the relations between climate and permafrost limits in Canada, Smith and Riseborough (2002) make several theoretical assumptions based on the nature of the TTOP model equation. The first two assumptions focus on $FDD_a$ and $TDD_a$, the first stating that TTOP should decrease with an increase in $FDD_a$ and a decrease in $TDD_a$. In areas where $FDD_a$ is much greater than $TDD_a$, TTOP is likely negative (indicating permafrost) everywhere regardless of the value of $n_f$, $n_t$, and rk. Based on latitude the authors suggest that moving north $n_f$ is a more important influence than rk while the opposite is true moving south where rk reduces the impact of the warmer thawing season. These conclusions and assumptions were derived using climate data and theoretical values for rk and have yet to be widely tested using site measured data in a variety of different permafrost environments.

The first attempt utilizing measured data to assess model response to change in parameters was completed for areas including the southern Yukon and Northern BC (Bevington & Lewkowicz, 2015). As a part of their study assessing the feasibility of a landcover driven TTOP model in Southern Yukon and Northern BC, Bevington and Lewkowicz (2015), looked to use field data to determine the sensitivity of the TTOP model to changes in each parameter. Their results showed that in this environment, the TTOP model is more sensitive to changes in $n_f$ than $n_t$, due in part to greater $FDD_a$ than $TDD_a$ at all study sites. Additionally, the model was more sensitive to changes in $TDD_a$ compared to $FDD_a$ attributed to the dampening impact of snow cover on changes in $FDD_a$. Results also indicated moderate sensitivity to changes in rk.

As the parameterization of the scaling factors and rk remain one of the main challenges in utilizing the TTOP model, understanding the relative importance and sensitivity of the model to the parameters is essential. Currently, there is limited understanding of this in the literature and thus far no usable field data from a variety of permafrost environments. Therefore, quantifying the impact of changing values of input parameters and determining the relative importance of each variable in unique permafrost environments will aid in guiding future modelling studies by highlighting the relative value to place on characterizing individual variables.

#### 2.5.2.5 Random Forest

Another method that may aid in variable importance ranking for permafrost temperature is random forest. Random forest is an ensemble classifier which combines randomized decision trees with bagging and aggregates their predictions though averaging or majority vote (Figure 2-10) (Breiman, 2001; Biau & Scornet, 2016). Individual decisions trees within the random forest are computed using a small subset of features selected for splitting at each node in addition to a small random subset of training data with replacement (Breiman, 2001; Biau & Scornet, 2016). This ensures low correlation among the decision trees.

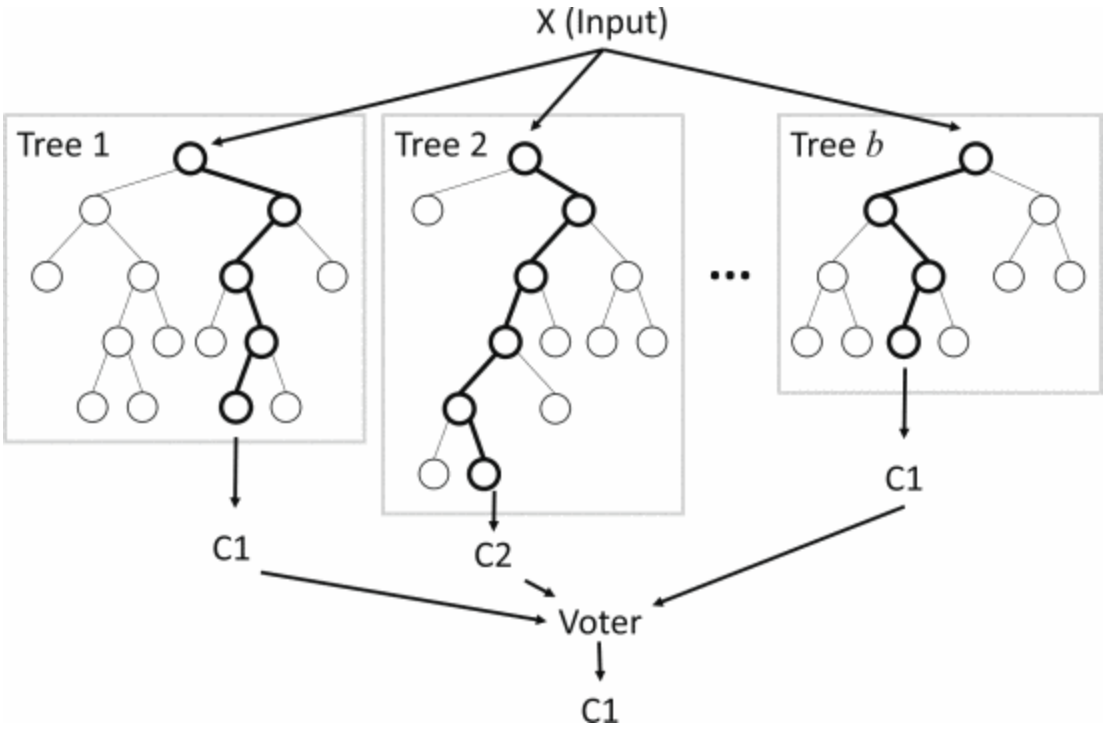


**Figure 2-10.** Example of diagram of random forest (Nakahara et al., 2017).

Random forest has been successfully used in general-purpose classification and regression problems including when the number of variables is much larger than the number of observations. One advantage of random forest is its versatility allowing for its use in a variety of prediction problems and adaptation to various *ad hoc* learning tasks. Random forest is generally recognized for its accuracy and can be run in parallel giving it the ability to deal with large real-life systems. Another advantage is it only has a few parameters to tune, which include the number of randomized regression trees, number of sample points in each tree and the number of variables randomly sampled as candidates at each split. Lastly, an important aspect of random forest is the ability to save the trees to be run with additional datasets. One drawback to random forest is it considered a black box algorithm, as the processes and rulemaking is unknown to the user, and the motivation behind the model's prediction is not comprehensible without additional rule extraction (Moeyersoms et al., 2015; Biau & Scornet, 2016; Ahmed & Sadiq, 2018).

Random forest has been used in studies of air quality (Yu et al., 2016; Pendergrass et al., 2022), chemoinfomatics (Mitchell, 2014), ecology (Cutler et al., 2007; Brieuc et al., 2018), and remote sensing (Belgiu & Drăgu, 2016) to name a few (Biau & Scornet, 2016). However, until recently its use in mapping permafrost distribution studies has been limited. For the northeastern region of the Himalayas, permafrost probability distribution maps were generated using random forest and three other machine-learning algorithms (Baral & Haq, 2020). The authors have determined the reliability in using these machine-learning models due to the congruence of the outputs of permafrost distribution (Baral & Haq, 2020). Random forest has also been used to map permafrost distribution in alpine locations. Deluigi et al. (2017) utilized random forest in addition to several other statistical and machine learning classification algorithms to predict permafrost occurrence in the western Swiss Alps. All of the outputs from the machine learning algorithms matched well with ground truthing once again demonstrating the reliability of these methods (Deluigi et al., 2017). To date random forest has yet to be widely used as a permafrost prediction method in Canada but has been used to predict interannual and seasonal thaw characteristics (Liu et al., 2022).

Another important use of random forest is variable importance rankings. Random forest provides variable importance rankings through two methods, permutation accuracy importance (mean square error (MSE) reduction) or Gini importance (Strobl et al., 2008). Gini importance uses the total decrease in node impurity (averaged acrross all trees) from splitting the variaible to determine the importance ranking (Baiu & Scornet, 2016). Reduction in MSE involves the random permutation of each variable individually to simulate its absence in the model prediction. Variable importance is then determined based on the difference in prediction accuracy before and after the permutation. Of these two methods, reduction in MSE has been more widely used

in variable importance studies due to Gini importance biases when predictor parameters vary in number and scale (Díaz-Uriarte & Alvarez de Andrés, 2006; Strobl et al., 2008; Grömping, 2009; Genuer et al., 2010). Once variable importance rankings are established, these results are then used either to identify important variables for explanatory or interpolation purposes or to identify a small number of variables that provide a good prediction (Díaz-Uriarte & Alvarez de Andrés, 2006; Grömping, 2009; Genuer et al., 2010). As a result, random forest variable importance rankings may allow for unique parameterization of permafrost models in a variety of different environment and focus data collection efforts. The expanded use of machine learning parameterization in conjunction with process-based models may be an important next step for permafrost modelling studies.

### *2.5.3 Alpine Permafrost Modelling*

One of the most common models used in mountain permafrost studies in Yukon is the BTS model. Models using BTS previously focused on assigning a three-fold classification or testing said classification with a small number of ground truthing points; however extensive ground truthing in mountains of Yukon allowed for the development of quantative probability maps of mountain permafrost using logistic regression (Lewkowicz & Ednie, 2004; Bonnaventure & Lewkowicz, 2008). This was expanded upon by Bonnaventure and Lewkowicz (2008), demonstrating the transferability of the methodology to other mountainous areas of Southern Yukon. They found the methodological approach and use of logistic regression to predict permafrost probability were able to provide a reasonable prediction of extent and spatial distribution of mountain permafrost for up to 200 km away from the initial study region (Bonnaventure & Lewkowicz, 2008). This resulted from a combination of physical validation, an increased number of validation sites, and the use of unique predictor variables used in the logistic

regression for each region. However, they caution that ground truthing is still and important method for validation.

The BTS model was also used to predict permafrost probability in two climatically dissimilar regions of Southern Yukon and Northern BC (Bonnaventure & Lewkowicz, 2008). One potential source of error was that most of the BTS sample points were located above treeline, as sites below treeline did not always have the required snow depth. To remedy this Bonnaventure and Lewkowicz (2011), took BTS measurements at five new study sites in Yukon focusing particularly on sites below treeline. During this work, it was discovered that due to the presence of substantial inversions particularly in the more continental regions of Yukon, permafrost probability was not always statistically related to elevation. To cope with this, (Lewkowicz & Bonnaventure, 2011), proposed a new variable, equivalent elevation. Equivalent elevation reflects the measured differences between surface air temperature lapse rates both above and below treeline, particularly in areas prone to inversions. The inclusion of equivalent elevation rather than elevation increased the statistical significance of permafrost probability models in several locations in Yukon as it better represented the non-linear relation between permafrost probability and elevation in this environment. These models were then used to create a regional map of permafrost probability throughout southern Yukon (Bonnaventure et al., 2012).

The TTOP model has also been proven to create reasonably accurate spatial permafrost distribution maps in mountainous regions of Southern Yukon and Northern BC (Bevington & Lewkowicz, 2015). When compared to measured permafrost and ground temperature at depth, TTOP model outputs were shown to be reasonably successful (within 1 ºC) when parameters were derived based on land cover and other topographic variables (Bevington & Lewkowicz,

2015). This is due to the permafrost existing in equilibrium with the current climate and the derivation of input parameters from locally measured data.

#### 2.5.3.1 Research Gaps in Alpine Permafrost

Although the relation between inversions and permafrost probability has been well studied, little is known about the impact of surface air temperature inversion on the spatial distribution of ground surface and permafrost temperatures in alpine environments. While these permafrost probability studies focused on the southern portion of Yukon where moderate inversions have been observed, recent studies have shown that the magnitude of inversions increases substantially moving north (Noad & Bonnaventure, 2022). Additionally, previous studies assume a lack of surface air temperature inversions in treeless valleys as lapse rates in treed valleys typically become normal above treeline (Bonnaventure et al., 2012). However, recent research has shown the presence of these strongly inverted lapse rates in valleys even in the absence of trees (Noad, 2021). Lastly, most of the previous work mapping permafrost probability in Yukon was conducted on a regional scale and did not account for site-specific factors, which may dampen or enhance the impact of air temperature on ground surface and permafrost temperatures.

Much like the concept of Arctic amplification, the rate of warming is expected to be magnified at higher latitudes due to a variety of mechanisms including changes in albedo, changes in water vapor and latent heat release and aerosols (Pepin et al., 2015a). This is referred to as elevation dependent warming (EDW) and has been supported by observations and climate modelling studies in the Andes, Rocky Mountains, and Alps (Minder et al., 2018; Aguilar-Lome et al., 2019; Palazzi et al., 2019; Li et al., 2020). However, all these regions maintain normal, linear relations between air temperature and elevation. The concept of EDW may break down for

areas of the Tibetan Plateau likely due to the lack of elevation dependent temperature trends (You et al., 2010; Li et al., 2020). Similarly, EDW may not hold true in the high-latitude, continental mountains of Yukon due to the presence of persistent inverted SLRs complicating the relation between temperature and elevation. Current predictions of mountain permafrost distribution and its response to climate change assume a linear distribution of permafrost related to elevation (Bonnaventure & Lewkowicz, 2011; Rangecroft et al., 2016; Deluigi et al., 2017). Applying the concept of EDW to these predictions leads to greater change in permafrost distributions at higher elevations leading to an upward shift in the lower elevation limit of permafrost. However, due to inverted SLRs and the non-linear nature of permafrost distribution in Yukon mountains, changes in air temperature and permafrost distribution may not follow patterns typical of EDW. Therefore, understanding the relations between the SLR and the spatial distribution of the ground thermal regime in Yukon mountains is key to accurate prediction of permafrost response to climate change and the associated hazards.

# Chapter 3 Active layer variability and change in the Mackenzie Valley, Northwest Territories between 1991-2014: an ecoregional assessment

Garibaldi, M. C., Bonnaventure, P. P., Smith, S. L., & Duchesne, C. Active layer variability and change in the Mackenzie Valley, Northwest Territories between 1991-2014: An ecoregional assessment. *Arctic, Antarctic, and Alpine Research.* 2022;54(1); 274-293.

**Authors:** Madeleine C. Garibaldi[1], Philip P. Bonnaventure[1], Sharon L. Smith[2], Caroline Duchesne[2]

[1] Department of Geography and Environment, University of Lethbridge

[2] Geological Survey of Canada, Natural Resource Canada

**Key Words:** Permafrost, Active layer, Ecoregion, Mackenzie Valley.

## 3.1 Abstract

Active layer thicknesses (ALT) from sites along a transect through the Mackenzie Valley, NT, Canada were analyzed to explore variation in thickness within and between ecoregions. At an ecoregional scale the relation between ALT, latitude, freezing and thawing degree-days, and snowfall were examined to determine the presence of trends. Site-specific variables including dominant vegetation and substrate were explored to explain spatial variability in ALT within ecoregions. Generally, average ALT increases moving southward through the comprising ecoregions (68 cm to 126 cm), following the increase in air temperature. Spatial variability in ALT within ecoregions was greater than between ecoregions (up to 145 cm) which may be attributed to site-specific conditions (vegetation and snow cover). Most notably sites with shrubs had thicker than average active layers likely because of increased snow retention leading to warmer overall ground conditions. Despite a warming trend in air temperatures, only one northern ecoregion showed a corresponding thickening trend in ALT. Sites located in southern ecoregions with mature forests showed limited response to changes in air temperature. For these

locations, disturbance, specifically changes in thermally protective vegetation cover, rather than changing air temperature could potentially have a larger impact on ALT into the future.

### 3.2 Introduction

The active layer refers to the layer of ground in areas underlain by permafrost, which is subject to annual freezing and thawing and is the location where most subsurface ecosystem processes occur in the permafrost landscape. The nature of this layer is dynamic, responding to temporal climatic shifts showing only subtle connection to atmospheric inter-annual variability (Shur et al., 2005). Although the most common metric used to describe the nature of the active layer is thickness at the time of maximum thaw, the predictability of this value is not universally tied to latitude or even mean annual air temperature (Bonnaventure & Lamoureux, 2013). Active layer thicknesses (ALT) are dependent on several factors, including latitude, elevation, solar insolation patterns, albedo, proximity to glaciers and/or warm maritime ocean currents as well as site specific factors including soil texture and moisture content (Bockheim & Hall, 2002). Some factors including vegetation and snow distribution can vary substantially within climatic zones due to topography, hydrology and dominant wind patterns (Garibaldi et al., 2021; Evans et al., 1989; Young et al., 1997). Vegetation has been shown to influence ALT through snow entrapment and interception, shading, evapotranspiration, and insulation depending on the vegetation type (Duchesne et al., 2015; Fisher et al., 2016; Loranty et al., 2018). Previous studies of ALT have primarily considered the impact of summer (thawing degree-days) conditions on ALT, however antecedent winter conditions including snow cover and freezing degree-days may also substantially impact ALT (Mazhitova et al., 2004). Seasonal snow cover insulates the surface from cold winter conditions, leading to warmer winter ground conditions and potentially thicker active layers (Zhang, 2005). Snow cover also alters the timing of freeze-back in the

autumn, the progression of the ground freezing front and the nature of the spring thaw (Zhang, 2005; Morse et al., 2012). Thicker snow covers can also have considerable impact on the ground surface temperature by trapping latent heat expelled from the subsurface that cannot be freely dispersed to the atmosphere (Bonnaventure & Lewkowicz, 2008; Zhang, 2005).

The complexities of the active layer are further complicated by conflicting definitions of the active layer itself (Burn & Smith, 1988). Thermally, the base of this layer ideally exists at the idealized freezing/melting point of water in nature (0 °C); however, this may not match the base of the physical active layer. Much of this discrepancy is attributed to the intricacy and diversity of active layer materials, which can contain variable levels of moisture and substrate composition including mineral sediment, ions in solution and organic layers (Hinkel et al., 2001; Shiklomanov et al., 2010). Additionally, the active layer is morphologically linked to the environment and can be influenced by the adjacency to water bodies or mass movement debris (Hinkel & Nelson, 2003).

Because the active layer can be spatially heterogeneous on multiple scales, assessing variability is challenging, but necessary to better understand the impact of change in cold regions (Bonnaventure et al., 2017; Garibaldi et al., 2021). Understanding this variability helps to recognize the range and complexity that goes with trying to ascertain how permafrost environments will be impacted by warming (Bonnaventure & Lamoureux, 2013). The goal of this study is to examine the temporal and spatial variability in active layer thickness using an ecoregional approach. Recent studies have focused on the impact of vegetation and ecosystem characteristics on ALT largely focusing on tundra and boreal forests (Loranty et al., 2018; Fisher et al., 2016, Duchesne et al., 2015). Expanding these regional ALT assessments specifically in the Mackenzie Valley on an ecoregional scale will aid in small-scale (circumpolar, national

scale) modelling studies which utilize regional data (e.g. Obu et al., 2019) and may allow for the creation of ALT models in this region (e.g. Yi et al., 2018). This study updates previous work in the Mackenzie Valley relating ALT to ecoclimatic zone and further analyzes an ALT dataset used in previous work (Tarnocai et al., 2004 & Duchesne et al., 2015) building to explore the relation between active layer thickness, broad climate, and vegetation characteristics. The different ecoregions in the Mackenzie Valley have shown variable attributes with respect to the nature and timing of ground freeze-back in the autumn (Smith et al., 2016). Therefore, it is possible that active layer thickness also varies within and between these ecoregions. In order to conduct this analysis multiple years of data must be examined and compared. This study utilizes data collected since 1991 from an active layer monitoring network in the Mackenzie Valley and Delta region, to document ALT through time. Sites are representative of the range of vegetation and surficial material conditions throughout the region. The Mackenzie Valley is well suited for this type of study as both permafrost and vegetation are heterogeneous across the study transect, which passes through discontinuous (underlying <90%) to continuous (underlying 90-100 %) permafrost zones and from boreal forested to tundra vegetation ecoregions. This study compares regional and temporal ALT patterns between ecoregions spanning the valley, expanding on work previously conducted by Duchesne et al. (2015) by further examining these data and conditions according to ecoregions.

### 3.3 Study Area

The Geological Survey of Canada active layer monitoring transect spans the length of the Mackenzie Valley and Delta, with sites from the Delta and Tuktoyaktuk Peninsula to the southern Northwest Territories (Figure 3-1). Sites are in Inuvialuit, Gwich'in, Sahtu, and DehCho First Nations settlement regions and traditional territories. The transect (Figure 3-1,

Table 3-1) is comprised of multiple monitoring sites, and extends from the zone of discontinuous to continuous permafrost and from the boreal forest near Fort Simpson to the Beaufort Sea coast (Smith et al., 2009a).

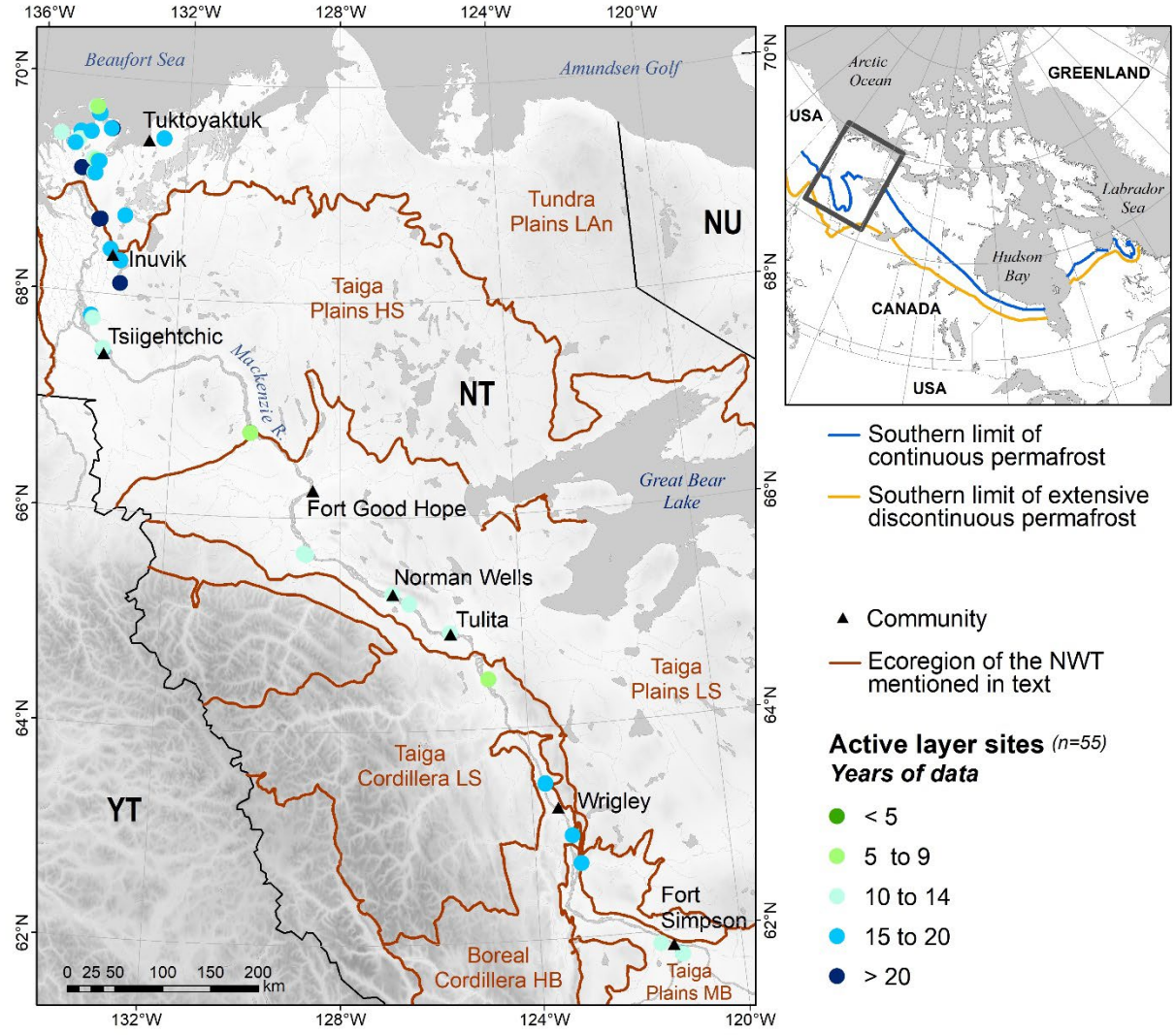


**Figure 3-1.** Site map with active layer monitoring sites. Sites are located both above and below treeline and monitor active layer thickness over both continuous and discontinuous permafrost. Sites with the longest records are located in the Northern and Southern end of the delta. Permafrost zones from Heginbottom et al. (1995) and ecoregion boundaries from Ecosystem Classification Group (2009, 2010, 2012).

**Table 3-1.** Summary table of characteristics of each ecoregion with active layer monitoring sites (Ecoregions Working Group 1989, Ecosystem Classification Group, 2007, 2010 & 2012; Atlas of Canada, 3rd edition; Environment Canada, 2017). AMAT is the annual mean air temperature (Ecosystem Classification Group, 2007, 2010 & 2012).

| Ecoregion | Lat (°N) | Long (°W) | AMAT (°C) | Precipitation (mm) | Characteristic Vegetation | Permafrost Condition | Community |
|---|---|---|---|---|---|---|---|
| **Tundra Plains LA*n*** | 66-70 | 118-130 | -11 | 130-190<br>50 % falling as snow | low shrubs, sedge, and mosses | Continuous | Tuktoyaktuk |
| **Taiga Plains HS** | 65-69 | 118-135 | -5 to -11 | 250-340<br>50 % falling as snow | White spruce (*picea glauca*) (Krummholz) | Continuous and extensive discontinuous | Inuvik |
| **Taiga Plains LS** | 62-66 | 117.9-132.8 | -3.5 to -9 | 230-350<br>50 % falling as snow | open canopy white *(picea glauca*) and black spruce forests (*picea mariana*) | Extensive discontinuous | Norman Wells<br>Fort Good Hope |
| **Taiga Cordillera LS** | 62-64 | 123.7-130 | -7 | 280-350<br>40 % falling as snow | open spruce woodlands and Jack Pine (*pinus banksiana*) | Continuous in the northern half of the ecoregion to extensive discontinuous in the southern portion | None |
| **Boreal Cordillera HB** | 61-62 | 123-126 | -4 to -5 | 340-400<br>40 % falling as snow | lodge pole pine (*pinus contorta*) | Extensive discontinuous | Wrigley |
| **Taiga Plains MB** | 60-62 | 112-123.5 | -2 to -5.5 | 310-410<br>45 % falling as snow | mixed wood forests of aspen (*populous tremuloides*) and white spruce | Extensive to sporadic discontinuous | Fort Simpson |

Substrate along the transect is variable but consists of mainly moraine, lacustrine, fluvial, and deltaic deposits which can be ice-rich although ice content varies from site to site (Aylsworth et al., 2000a, b, Heginbottom et al., 1995). Extensive peatlands and fens consisting of sedges, mosses, and stunted black spruce are particularly prevalent in the Southern portion of the valley (Aylsworth et al., 2000a, b, Ecosystem Classification Group, 2009). The sites in the transect are representative of the various ecoregions in Northwest Territories which are generally defined based on unique regional climatic gradients and major changes in physiography (Ecosystem Classification Group, 2010). Ecoregions are classified further in (Level II) ecoregional classification. This Level II classification adds an additional level of complexity based on macroclimate, vegetation, soil, geology, and physiographic features, which is the subdivision basis of permafrost and vegetation characteristics. These Level II ecoregions combined with climatic parameters create the Level III ecosystem classifications (Ecosystem Classification Group, 2012). Level III ecoregions, that contain active layer monitoring sites in the Mackenzie Valley along this transect, include Tundra Plains Low Arctic *north* (LA*n*), Taiga Plains High Subarctic (HS), Low Subarctic (LS), and Mid Boreal (MB), Boreal Cordillera High Boreal (HB), and Taiga Cordillera Low Subarctic (LS), encompassing seven of the nineteen possible Level III ecoregions found in the Northwest Territories (Figure 3-2 and Table 3-1). Throughout the valley, air temperature, annual precipitation, and snowfall increases moving north to south (Table 3-2).

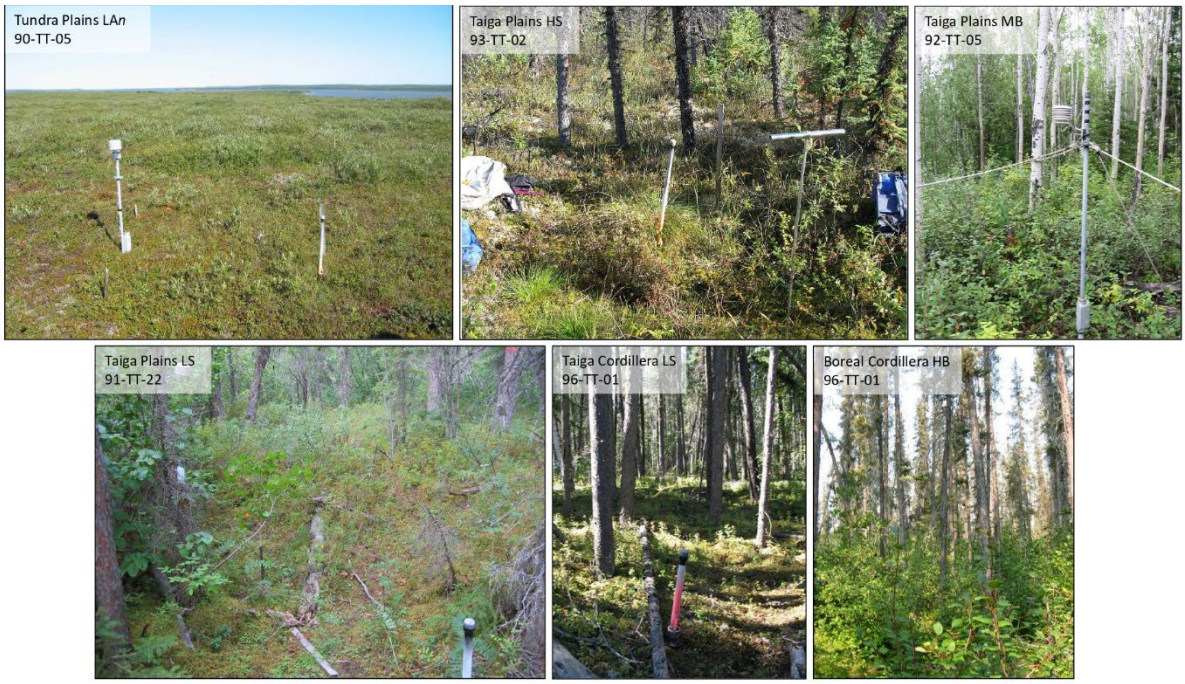


**Figure 3-2.** Site photos with representative vegetation cover for each ecoregion sampled. More site details can be found in the Supplementary Material Table S3-1 (Smith et al., 2009; Duchesne et al., 2014).

**Table 3-2.** Climate Normals (1981-2010) for 4 of the Environment Canada climate stations located in the Mackenzie Valley. MAAT indicates the use of the climate normal to calculate the mean annual air temperature.

| Climate Station | MAAT (°C) | Annual Precipitation (mm) | Annual Snowfall (cm) |
|---|---|---|---|
| **Tuktoyaktuk** | -10.1 | 160.7 | 103.1 |
| **Inuvik** | -8.2 | 240.6 | 158.6 |
| **Norman Wells** | -5.1 | 294.4 | 161.5 |
| **Fort Simpson** | -2.8 | 387.6 | 187.0 |

### 3.4 Methods

Active layer monitoring sites throughout the study area were established to represent variable terrain conditions including surficial material, and vegetation characteristics of the Mackenzie Valley (Nixon & Taylor, 1994; Duchesne et al., 2014; Duchesne et al., 2015). Thaw tubes (e.g., Mackay, 1973; Smith et al., 2009a, b) were used to measure maximum annual thaw

penetration, the position of the ground surface at the time of maximum heave, and ground surface subsidence. Maximum thaw depth is determined by the position of a glass bead that sits on the frozen surface and descends to the point of maximum thaw each year during the thaw season (Nixon & Taylor, 1994). Measurements are made to 1 mm precision and are considered accurate to about 2 cm (Nixon & Taylor, 1998). Thaw tubes are considered a superior technique compared to probing for determining active layer thickness, as they do not require personnel to be present on the specific day of maximum thaw, which varies annually (Bonnaventure & Lamoureux, 2013). Maximum thaw penetration and ground surface position at time of maximum thaw were used to calculate active layer thickness. At some sites (n= 20) air and ground surface temperatures were recorded using single channel data loggers (Onset HOBO accuracy ± 0.4 °C or Vemco accuracy ± 0.3 °C) with air temperature sensors housed in radiation shields 1.5 m above the ground surface and ground surface temperature sensors buried at a depth of 3-7 cm (Duchesne et al., 2014).

Sites were classified by ecoregion by plotting the site location using the specified coordinates on a location ecoregion map from Northwest Territories Environment and Natural Resources to assess classification. Of the 55 sites, 30 are in the tundra plains LA*n* ecoregion, 11 in the Taiga Plains HS ecoregion, 6 in the Taiga Plains LS ecoregion, 4 in the Taiga Plains MB ecoregion and 4 in the Boreal and Taiga Cordillera (Table S3-1). Sites are not evenly distributed throughout the ecoregions partly due to logistical and accessibility issues.

Temporal gaps in the record were identified for each site. Most notably there was a lack of recent data in the central portion of the valley, with most of the station records ending between 2008-2010. For each ecoregion, the annual minimum, maximum, and average of annual maximum ALTs were calculated. If there was only a record for one site in a given year for an

ecoregion, no statistics were calculated, as it may have been misrepresentative of the ALT trends for that ecoregion.

Historical climate data and the Canadian monthly climate summaries for the nearest climate station (Environment Canada, 2017) were used to determine monthly and yearly air temperature averages from 1990 to 2015 (the length of the monitoring record). At Tuktoyaktuk and Inuvik, multiple EC stations (n = 2 in close proximity, <400 m, with similar elevations, < 0.3 m difference) were used to create a more continuous temperature record over the study period. A regression analysis was run for periods with data from both stations for comparison (Tuktoyaktuk $R^2 = 0.67$ and Inuvik $R^2 = 0.99$). Freezing and thawing degree-days were calculated for each year (September 1$^{st}$ to August 31$^{st}$) of the study period at each climate station through the summation of all the average daily temperatures below ($FDD_a$) and above ($TDD_a$) 0 °C. $FDD_a$ and $TDD_a$ provide an indication of the duration and magnitude of freezing or thawing temperatures. At sites with on-site air and ground temperature measurements, FDD and TDD for the air (a) and ground surface (g) were calculated. Snowfall over the study period was compiled from the climate stations with data taken from several neighboring stations for Inuvik and Fort Good Hope. A regression analysis was done to compare the difference between the two stations (Inuvik $R^2 = 0.57$ and Fort Good Hope 0.79). The regression analysis for Fort Good Hope was only used to infill missing snowfall data for April 2006. Missing snowfall values for the months of May – September were assumed to be 0 cm based on analysis of snowfall during this period over the entire 1990-2015 record and measurements of snowfall at other stations during the same month.

Air and ground surface FDD and TDD, were used to calculate seasonal N-factors (ratio of surface temperature to air temperature) (Smith & Riseborough, 2002) for sites having on-site

temperature data. N-factors are transfer functions representing the energy fluxes at a single location, which can be used to estimate the surface offset (Smith & Riseborough, 1996; Klene et al., 2001). Since the surface offset is influenced by vegetation and snow cover which vary throughout the year, N-factors (ratios of air and surface temperature) are typically divided into freezing ($n_f$) and thawing ($n_t$) N-factors, with $n_f$ largely determined by snow cover in winter, and the $n_t$ characterizing vegetation cover in summer (Smith & Riseborough, 2002). Values of $n_f$ and $n_t$ were calculated using ground surface and air temperature data from October 1st of the previous year to April 30th of the current year and May 1st to September 30th of the current year respectively (Equation 3-1) (Duchesne et al., 2014, Smith & Riseborough, 2002).

$$n_{\mathrm{f}} = \frac{FDD_{\mathrm{g}}}{FDD_{\mathrm{a}}} \quad \text{and} \quad n_{\mathrm{t}} = \frac{\mathrm{TDD_g}}{TDD_{\mathrm{a}}} \tag{3-1}$$

Climatic data were examined using the downscaling program ClimateNA (Wang et al., 2016). This climatic data for each of the active layer monitoring sites were used to compare annual and seasonal air temperature trends over the study period. This allowed for the assessment of generalized climatic changes for each specific ecoregion to assess the relation between air temperature and ALT. Additionally, a simple random forest and multivariable linear regression (MVLR) analyses were conducted to determine the relative importance of winter ($FDD_a$ and $FDD_g$) and summer ($TDD_a$ and $TDD_g$) conditions on ALT at sites with both ALT and temperature records. Random forest (R studio, randomForest) was run to determine variable importance ranking while MVLR (Excel, Analysis ToolPak) was completed to test each variable for statistical significance for all sites. Only MVLR was done for each ecoregion individually. These were selected as the produce for their variable importance rankings or statistical significance, which can be used to infer the relative influence of these variables on ALT.

## 3.5 Results

### *3.5.1 Climate Analysis*

Records of air temperature from Environment Canada stations indicate a warming trend during the study period (1990-2015) (Figure 3-3). At the northernmost station, Tuktoyaktuk, (Figure 3-1) annual mean air temperature (AMAT) increased by 3.1 °C from 1990 to 2015 while at the southernmost station, Fort Simpson AMAT increased by 2.7 °C. This equates to warming trends of 0.12 °C/decade and 0.10 °C/decade at Tuktoyaktuk and Fort Simpson respectively. The greatest warming (0.24 °C/decade) occurred at Fort Good Hope. These values are all comparable to that estimated for the Mackenzie region in the most recent Arctic assessment (AMAP, 2017). Results of the ClimateNA reanalysis data indicated warming was seasonally asymmetric, with warming trends observed in autumn and winter (warming 0.8-1.3 and 1.0-2.0 °C/decade with slope errors of 0.03 and 0.05, respectively), but no trend evident in spring and summer for all ecoregions (cooling 0.1-0.3 °C/decade and warming 0-0.3 °C/decade with slope errors of 0.05 and 0.03, respectively).

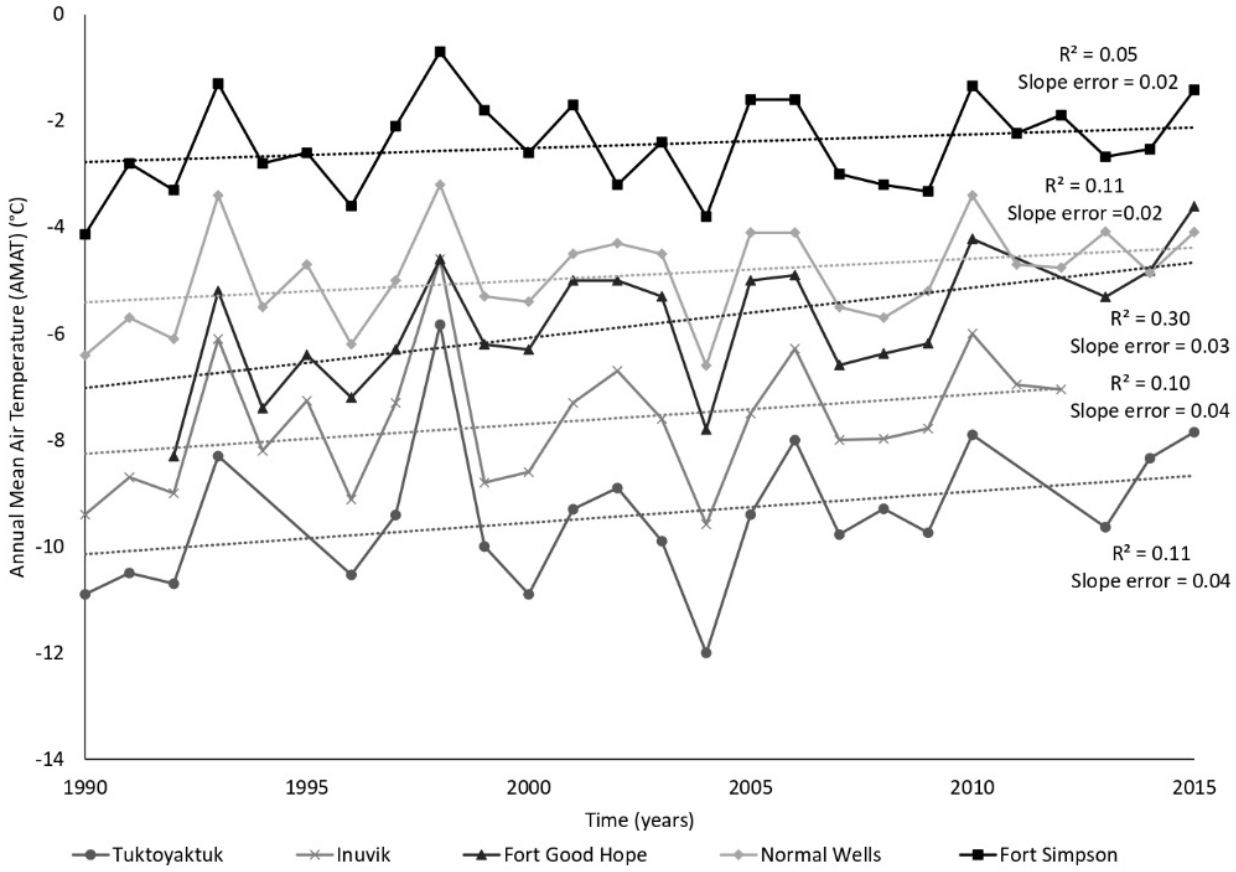


**Figure 3-3.** Annual mean air temperature (AMAT) with the trendlines for Environment Canada climate stations (see Figure 3-1 for location) closest to active layer monitoring sites in the Mackenzie Valley (from Environment Canada, 2017).

Spatially, the average annual $FDD_a$ decreased southward while the average annual $TDD_a$ increased, with the Tuktoyaktuk station recording the highest $FDD_a$ and lowest value of $TDD_a$ and Fort Simpson station recording the lowest $FDD_a$ and the highest $TDD_a$ (Figure 3-4). Temporally, there was a slight decrease in $FDD_a$ at each of the EC stations; however, the fit in each case was very weak ($R^2 < 0.1$ slope errors ranging from 8.7-28.5 °C $yr^{-1}$). The greatest temporal range in $FDD_a$ occurred at the Wrigley station while the lowest occurred at the Tuktoyaktuk station (Figure 3-4).

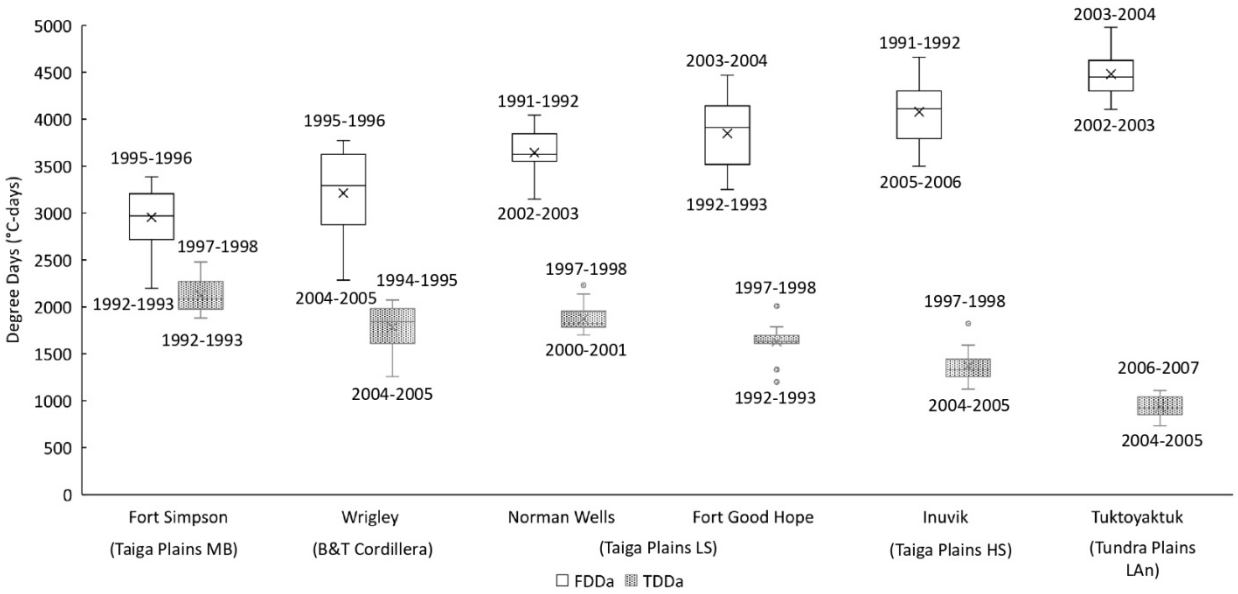


**Figure 3-4**. $FDD_a$ and $TDD_a$ for the EC stations in the Mackenzie Valley. Mean $FDD_a$ and $TDD_a$ for all years with data are represented by an X. For most stations, the maximum and minimum $FDD_a$ and $TDD_a$ are shown by the ends of the whiskers. However, for some sites, outliers are shown as circles after the whiskers and the ends of the whiskers instead show the value for one and a half times the interquartile range. The ends of the box show the first (25%) and third (75 %) quartiles while the black line within the box shows the median. The years with the highest and lowest $FDD_a$ and $TDD_a$ are written respectively above and below the marker.

There was a slight but weak ($R^2 < 0.1$ slope errors ranging from 4.9-15.0) increase in $TDD_a$ over the monitoring period at all EC stations. Over the monitoring period, the greatest range in $TDD_a$ was observed at the Wrigley station while the lowest occurred at the Inuvik station (Figure 3-5). Across every ecoregion with active layer monitoring sites, $FDD_a$ varied more inter-annually than $TDD_a$ (Figure 3-5).

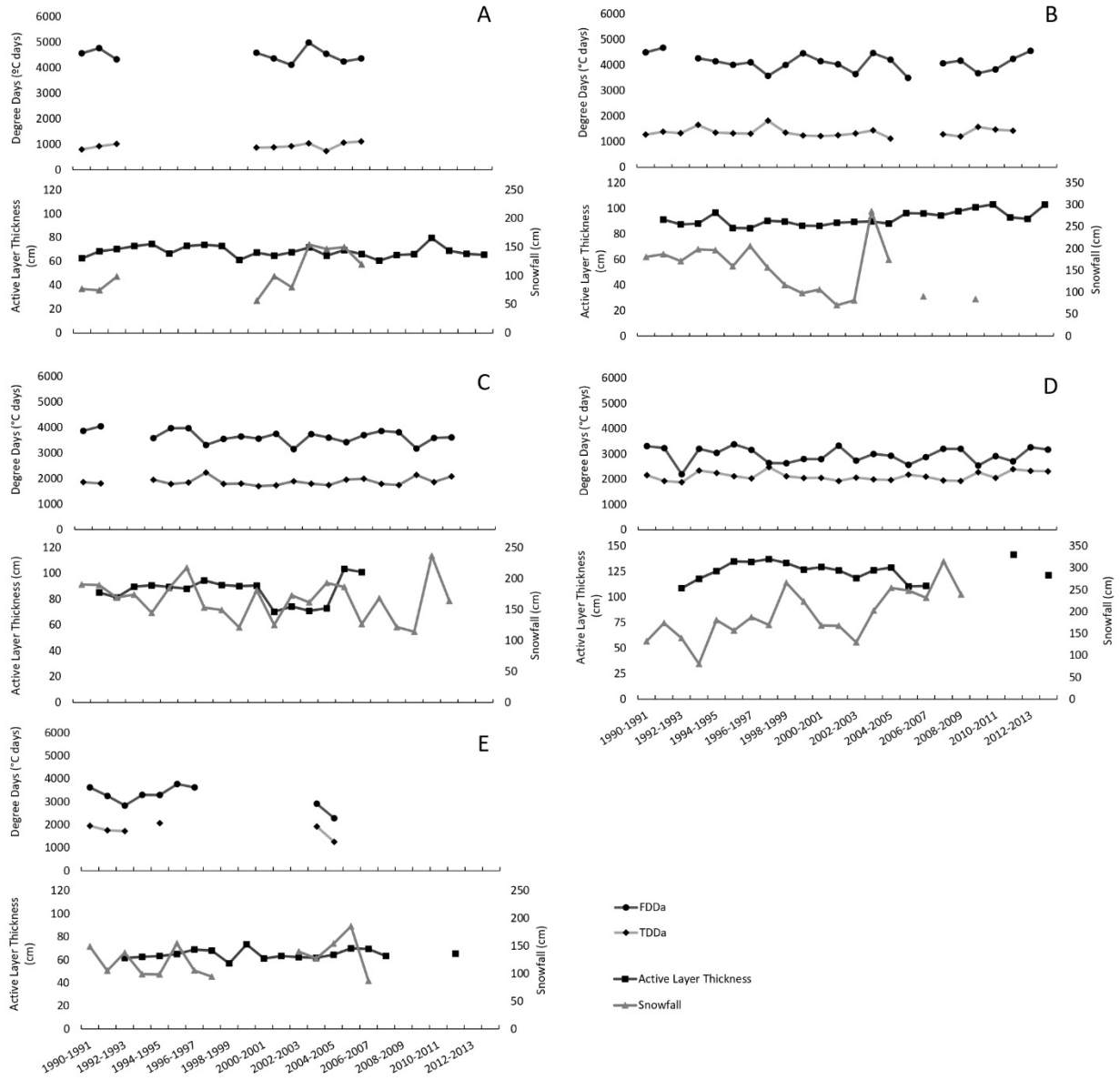


**Figure 3-5**. Average active layer thickness (ALT) for each ecoregion plotted with $FDD_a/TDD_a$ and snowfall from the nearest EC station. A) Tundra Plains LA*n* average ALT with $FDD_a/TDD_a$ and snowfall from the Tuktoyaktuk EC station, B) Taiga Plains HS average ALT with $FDD_a/TDD_a$ and snowfall from the Inuvik EC station, C) Taiga Plains LS average ALT with $FDD_a/TDD_a$ and snowfall from the Norman Wells EC station, D) Taiga Plains MB average ALT with $FDD_a/TDD_a$ snowfall from the Fort Simpson EC station, E) Boreal and Taiga Cordillera average ALT with $FDD_a/TDD_a$ snowfall from the Fort Simpson EC station.

Spatial range in $FDD_a$ within the ecoregions was greatest in the two northernmost ecoregions and smallest for the southern ecoregions (Figure 3-6). The same spatial pattern in variability was also observed for $TDD_a$ although the variation within each ecoregion was smaller than for $FDD_a$.

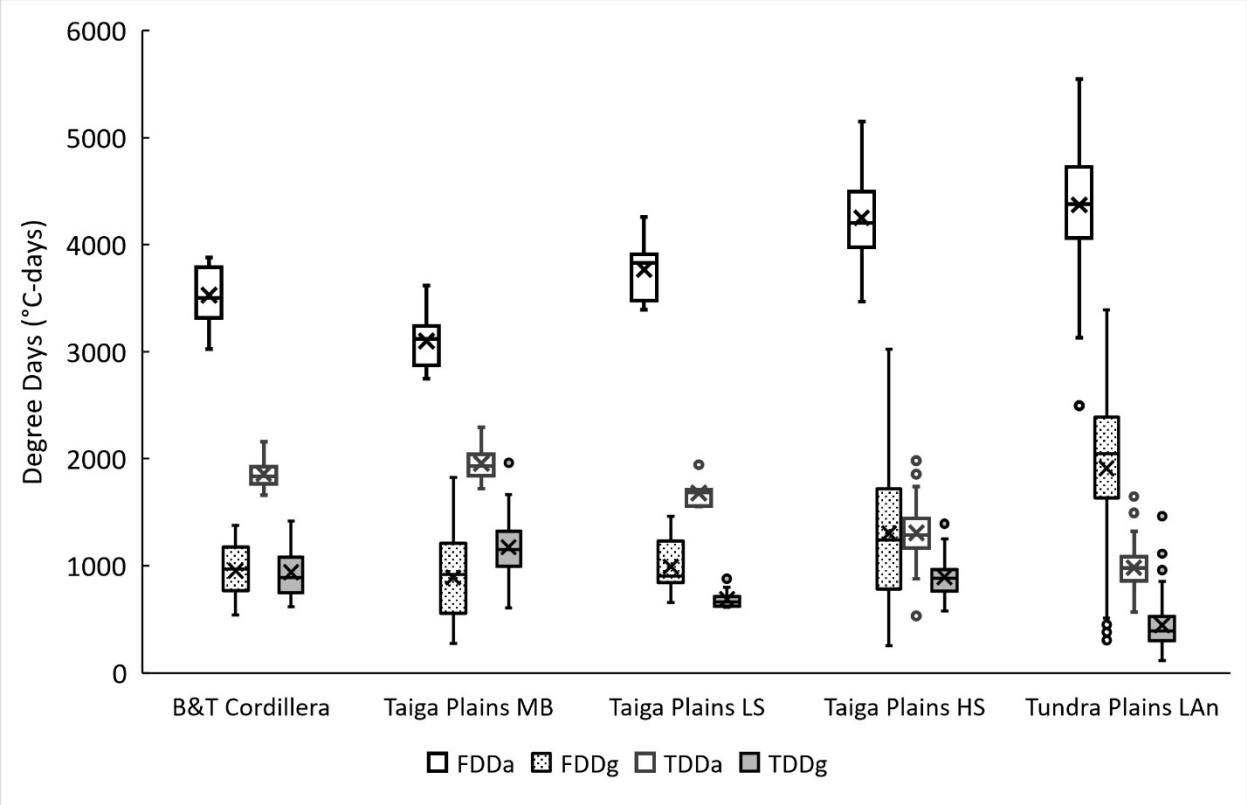


**Figure 3-6.** Box and whiskers plot for $FDD_a$, $TDD_a$, $FDD_g$ and $TDD_g$ measured at sites for each ecoregion. "g" is ground and "a" is air. X represents the mean while the circle indicates the value of outliers, which are points outside one and a half times the interquartile range.

Snowfall in the valley varies substantially annually and these fluctuations are not consistent between stations (Figure 3-7). For the study period (1990-2015), the lowest snowfall was recorded at Tuktoyaktuk (annual average 106 cm) with limited inter-annual variability (range 97 cm) whereas the most snowfall was recorded at Fort Simpson (annual average 199 cm) which also exhibited the largest inter-annual variability (range 234 cm). Over the monitoring period trends in snowfall varied by station. At Tuktoyaktuk and Fort Simpson snowfall exhibited

a positive temporal trend ($R^2$ = 0.37 and 0.31 with slope errors of 1.6 and 1.5 cm $yr^{-1}$, respectively). Snowfall seemed to decrease through time at Fort Good Hope ($R^2$ = 0.67 slope error of 1.3). Although there appeared to be trends in snowfall at Inuvik, Norman Wells, and Wrigley, the correlation was very weak ($R^2$ < 0.1 with slope errors of 2.5, 0.94, and 1.5 cm $yr^{-1}$, respectively).

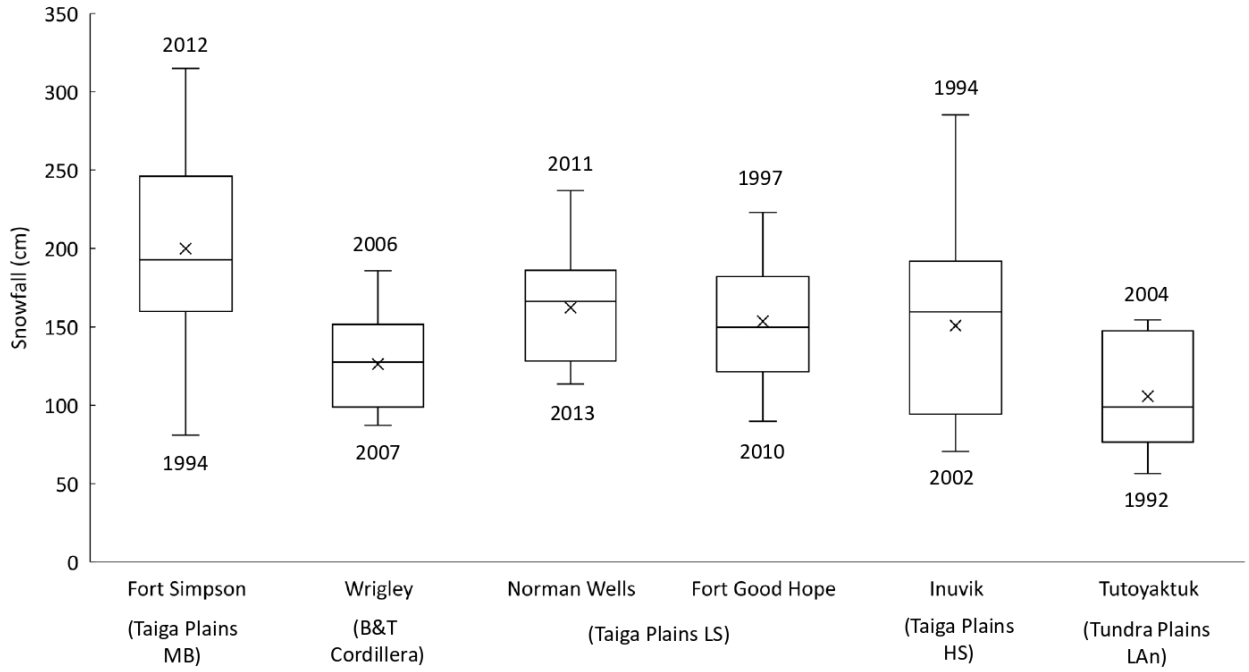


**Figure 3-7.** Annual total snowfall data for Environment Canada stations in the Mackenzie Valley from 1990-2015 (Environment Canada, 2017). Mean snowfall for all years with data is represented by an X. The maximum and minimum yearly snowfall at each station is represented by the whiskers. The black line within the box shows the median yearly snowfall at each station, while the ends of the box show the first (25%) and third (75%) quartiles. The years with maximum and minimum annual snowfall at each station are written above and below the marker respectively.

*3.5.2 Active Layer Monitoring*

3.5.2.1 Regional

The average ALT for 1991 to 2014 ranged from less than 50 cm in the northern portion of the Mackenzie Valley in the Tundra Plains LA*n* ecoregion to greater than 160 cm in the southernmost part of the valley in the Taiga Plains MB ecoregion (Figure 3-8).

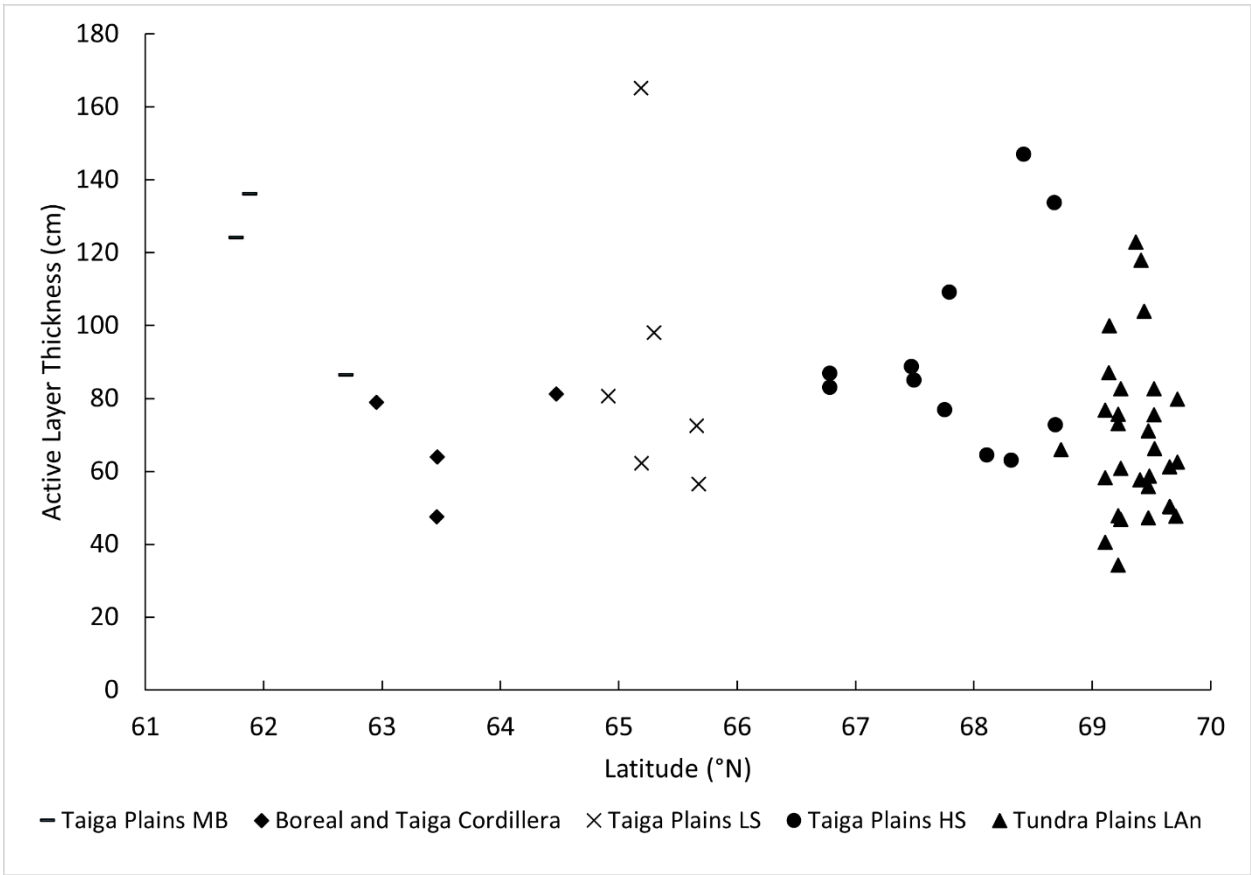


**Figure 3-8.** Mean active layer thickness for all years and sites classified by ecoregion. 30 monitoring sites are in the Tundra Plains LA*n* ecoregion, 11 are within the Taiga Plains HS ecoregion, 6 in the Taiga Plains LS ecoregion, 4 in the Taiga Plains MB ecoregion, and 3 in the Boreal and Taiga Cordillera.

Generally, the active layer is thinnest in the Tundra Plains LA*n* ecoregion and thickest in the Taiga Plains MB increasing moving south (Table 3-3 and Figure 3-9). However, this does not hold true for the Taiga Plains LS and Boreal and Taiga Cordillera ecoregions. Spatial range in ALT was greatest for the northern ecoregions and Taiga Plains MB. The spatial range in ALT for the Taiga Plains LS ecoregion is largely due to one outlier sites with a relatively thick active layer. The spatial range in ALT for the remaining sites is 42 cm.

**Table 3-3.** Active layer thickness (ALT) metrics for each ecoregion. Spatial range refers to the difference in the maximum and minimum ALT across all years and sites. Minimum and maximum refer to the thickest and thinnest active layers across all sites and years. Average temporal range refers to the average of the individual sites temporal range over the monitoring period.

| Ecoregion | Average ALT (cm) | Spatial ALT Range (cm) | Average Temporal ALT Range (cm) | Minimum ALT (cm) | Maximum ALT (cm) |
|---|---|---|---|---|---|
| **Tundra Plains LA*n*** | 67 | 145 | 22 | 26 | 171 |
| **Taiga Plains HS** | 92 | 132 | 27 | 49 | 181 |
| **Taiga Plain LS** | 86 | 128 (*60) | 19 | 48 | 176 |
| **Taiga Plains MB** | 129 | 121 | 35 | 79 | 199 |
| **Boreal and Taiga Cordillera** | 65 | 54 | 22 | 42 | 96 |

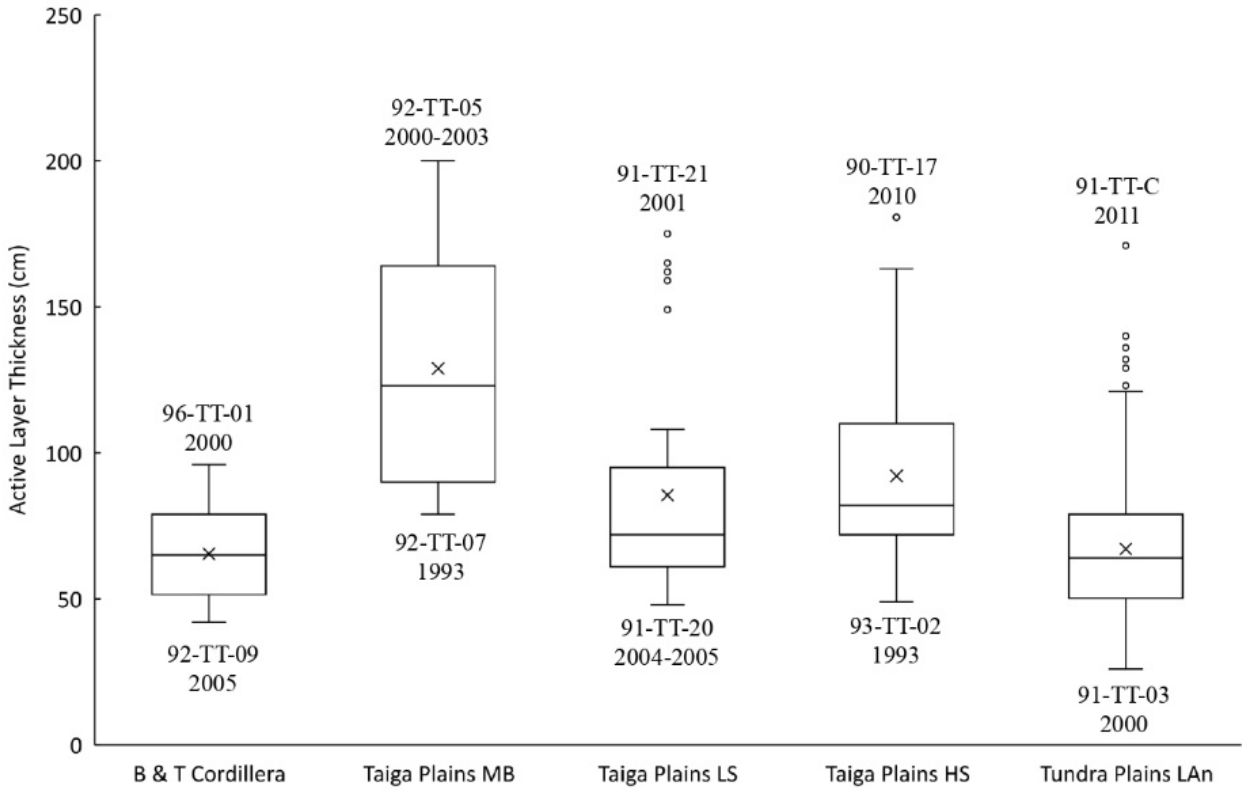


**Figure 3-9.** Mean and ranges of ALT by ecoregion along the Mackenzie Valley transect. Mean ALT for all years with data is represented by an X. The maximum and minimum ALT for all years and sites within an ecoregion is represented by the ends of the lines except for those with outliers (circles past the ends of the whiskers) in which case the ends of the whiskers represent the value one and a half times the interquartile range. The black line within the box shows the median annual ALT for each ecoregion, while the ends of the box show the first (25%) and third (75%) quartiles. The year and site with the thickest and thinnest active layer are written respectively above and below the marker. Some sites maintained the thickest or thinnest active layer for multiple years and for these sites, the years indicate this duration. More details on the individual stations can be found in the supplementary material in table S3-1.

Temporally, sites with thinnest active layers generally remained thin throughout the monitoring period. Similarly, sites with the thickest active layers remained the thickest. Over the monitoring period ALTs in the Taiga Plains HS and MB ecoregions varied the most through time while ALTs in the Tundra Plains LA*n*, Taiga Plains LS, and Boreal and Taiga Cordillera showed the least variability.

Air-ground surface connectivity also varied spatially and temporally between ecoregions. Average $n_f$ values for each ecoregion decreased from north to south with the highest mean $n_f$

(0.43) in the Tundra Plains LA*n* ecoregion and the lowest value (0.27) in both the Taiga Plains MB and Boreal and Taiga Cordillera ecoregions (Table 3-4 and Figure 3-10). The two northernmost ecoregions (Tundra Plains LA*n* and Taiga Plains HS) had the largest spatial range in $n_f$, while the Taiga Plains MB and Boreal and Taiga Cordillera had the smallest range. Temporally, variability in $n_f$ over the monitoring period was similar for each ecoregion (0.02-0.12) but was lowest for the two northern ecoregions and highest for the Taiga Plains MB and Boreal and Taiga Cordillera ecoregions. Within each ecoregion $n_f$ showed more temporal variation at sites with higher $n_f$ values. Average $n_t$ was more similar between ecoregions than $n_f$. Like $n_f$, the spatial range in $n_t$ was highest for the northern ecoregions (Tundra Plains LA*n* and Taiga Plains HS) and smallest for the Taiga Plains MB and Boreal and Taiga Cordillera ecoregions (Table 3-4 and Figure 3-10). The range in $n_t$ interannually was greatest for the Tundra Plains LA*n* and Boreal and Taiga Cordillera and smallest for the Taiga Plains MB ecoregion.

**Table 3-4.** Average $n_f$ and $n_t$ values and ALT for sites with data. *For site 92-TT-04, the air temperature data from site 92-TT-05 was used due to the proximity of the two stations.

| Site | Ecoregion | Average $n_f$ | Average $n_t$ | Average ALT (cm) | $FDD_g$ (°C days) | $TDD_g$ (°C days) |
|---|---|---|---|---|---|---|
| **90-TT-04** | Tundra Plains LA*n* | 0.45 | 0.33 | 87 | 2033 | 428 |
| **90-TT-05** | Tundra Plains LA*n* | 0.57 | 0.53 | 75 | 4411 | 524 |
| **90-TT-06** | Tundra Plains LA*n* | 0.37 | 0.28 | 48 | 1697 | 325 |
| **90-TT-13** | Tundra Plains LA*n* | 0.64 | 0.58 | 63 | 2616 | 386 |
| **91-TT-C** | Tundra Plains LA*n* | 0.09 | 0.98 | 125 | 403 | 801 |
| **92-TT-01** | Tundra Plains LA*n* | 0.49 | 0.29 | 47 | 2215 | 311 |
| **92-TT-02** | Tundra Plains LA*n* | 0.37 | 0.47 | 56 | 1693 | 415 |
| **90-TT-17** | Taiga Plains HS | 0.09 | 0.71 | 147 | 421 | 997 |
| **91-TT-12** | Taiga Plains HS | 0.55 | 0.70 | 73 | 2288 | 771 |
| **91-TT-13** | Taiga Plains HS | 0.24 | 0.89 | 134 | 997 | 1085 |
| **91-TT-14** | Taiga Plains HS | 0.29 | 0.59 | 109 | 1277 | 782 |
| **91-TT-15** | Taiga Plains HS | 0.32 | 0.57 | 77 | 1482 | 890 |
| **91-TT-16** | Taiga Plains HS | 0.30 | 0.57 | 89 | 1332 | 863 |
| **91-TT-22** | Taiga Plains LS | 0.25 | 0.41 | 62 | 992 | 688 |
| **92-TT-04*** | Taiga Plains MB | 0.29 | 0.61 | 124 | 1001 | 1202 |
| **92-TT-05** | Taiga Plains MB | 0.22 | 0.55 | 184 | 816 | 1102 |
| **92-TT-06** | Taiga Plains MB | 0.22 | 0.50 | 137 | 654 | 978 |
| **92-TT-07** | Taiga Plains MB | 0.34 | 0.73 | 86 | 1191 | 1455 |
| **92-TT-08** | B&T Cordillera | 0.24 | 0.49 | 79 | 916 | 913 |
| **92-TT-10** | B&T Cordillera | 0.29 | 0.50 | 64 | 995 | 961 |

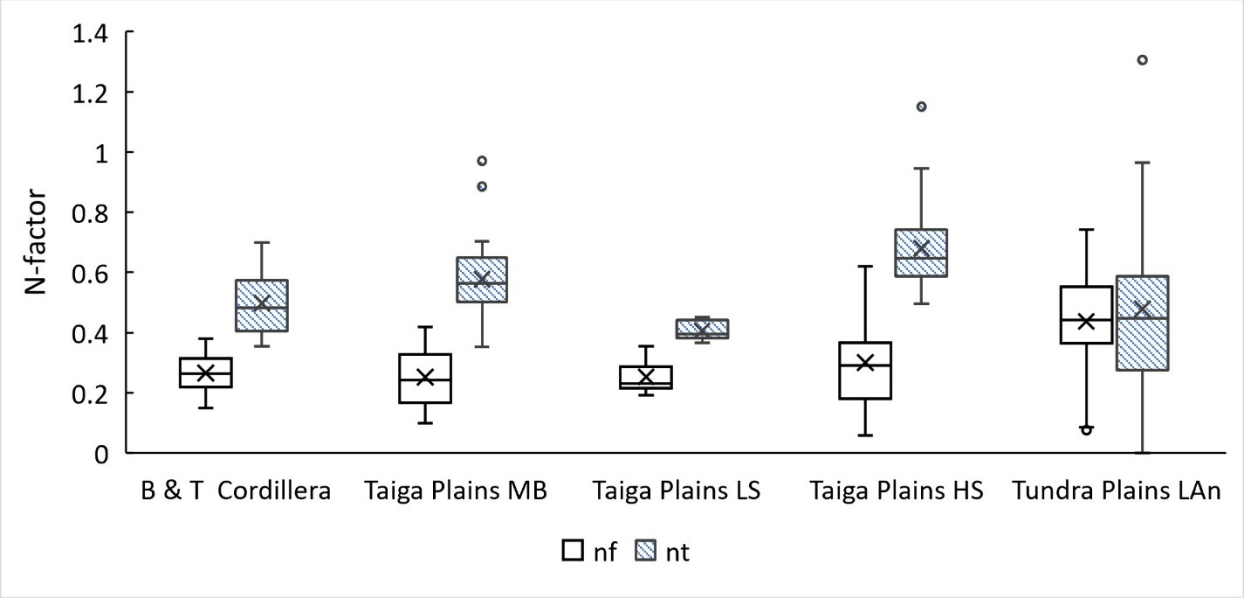


**Figure 3-10.** Box and whiskers plot for the freezing n-factor (nf) and the thawing n-factor (nt) for each ecoregion. X represents the mean while the circle indicates the value of outliers (one and a half times the interquartile range).

Spatial and temporal variability in $FDD_g$ and $TDD_g$ was also observed between ecoregions. $FDD_g$ generally decreased from north to south (Figure 3-6). Northern ecoregions also had the largest spatial variability in $FDD_g$ between sites. Interannually, the greatest range in $FDD_g$ occurred in the Taiga Plains HS ecoregion while the lowest was in the Taiga Plains MB ecoregion. Average $TDD_g$ exhibited a positive spatial trend from the northern ecoregions to the southern except for the Taiga Plains LS ecoregion, which only had one site. Temporally, the Boreal and Taiga Cordillera ecoregion showed the greatest variability in $TDD_g$ while the Taiga Plains MB showed the least over the study period. Temporal trends for $n_f$, $n_t$, $FDD_g$ and $TDD_g$ were difficult to determine due to data gaps and limited years with data.

Variable importance ranking in the random forest analysis identified $FDD_g$, $n_f$, and $TDD_g$ as the three most important factors determining ALT (in this order) followed by $FDD_a$, $n_t$, and lastly $TDD_a$ (Figure S3-1). For overall average ALT the MVLR analysis produced an $R^2$ of 0.61 indicating that only $FDD_g$ was significant ($p = 0.032$). Using all measurements across all sites

and years, $FDD_g$, $TDD_g$, and $TDD_a$ were all significant ($p < 0.001$ for $FDD_g$ and $TDD_g$ and $p = 0.006$ for $TDD_a$) with an $R^2$ of 0.45. When divided by ecoregion the MVLR analysis showed variability in significant variables between ecoregions. For the Tundra Plains LA*n* ecoregion only $TDD_g$ was significant ($p = 0.001$, $R^2 = 0.55$) while for the Taiga Plains MB ecoregion only $FDD_g$ was significant ($p = 0.03$, $R^2 = 0.46$). The Taiga Plains HS and Boreal and Taiga Cordillera MVLR analysis showed $FDD_g$ and $TDD_g$ to be significant with $p < 0.001$ and $p = 0.001$ ($R^2 = 0.83$) for Taiga Plains HS and $p = 0.001$ and 0.047 ($R^2 = 0.46$) for the Boreal and Taiga Cordillera. The results indicate the importance of considering antecedent winter conditions when analyzing ALT especially in the southern portion of the valley where they are shown to have a higher level of significance.

3.5.2.2 Site Specific

Site-specific changes in ALT and measured temperature parameters showed unique temporal changes over the duration of the study. At sites 91-TT-13 (Taiga Plains HS), 91-TT-22 (Taiga Plains LS), 92-TT-04 (Taiga Plains MB), and 92-TT-10 (B&T Cordillera), $FDD_g$ and $n_f$ showed a degree of variability through time (Figure 3-11). Of these sites, 91-TT-13, 92-TT-04, and 92-TT-10 also showed increasing ALT through time (0.5, 1.7, and 0.5 cm $yr^{-1}$, respectively). At site 92-TT-04 the increase in ALT over the study period corresponded with a drop in $FDD_g$ and $n_f$ as well as an apparent increase in $n_t$ and a large degree of interannual variation in $TDD_g$. Sites 91-TT-22 and 92-TT-10 had limited ALT response and showed contrasting warming winter and cooling summer ground surface temperature trends.

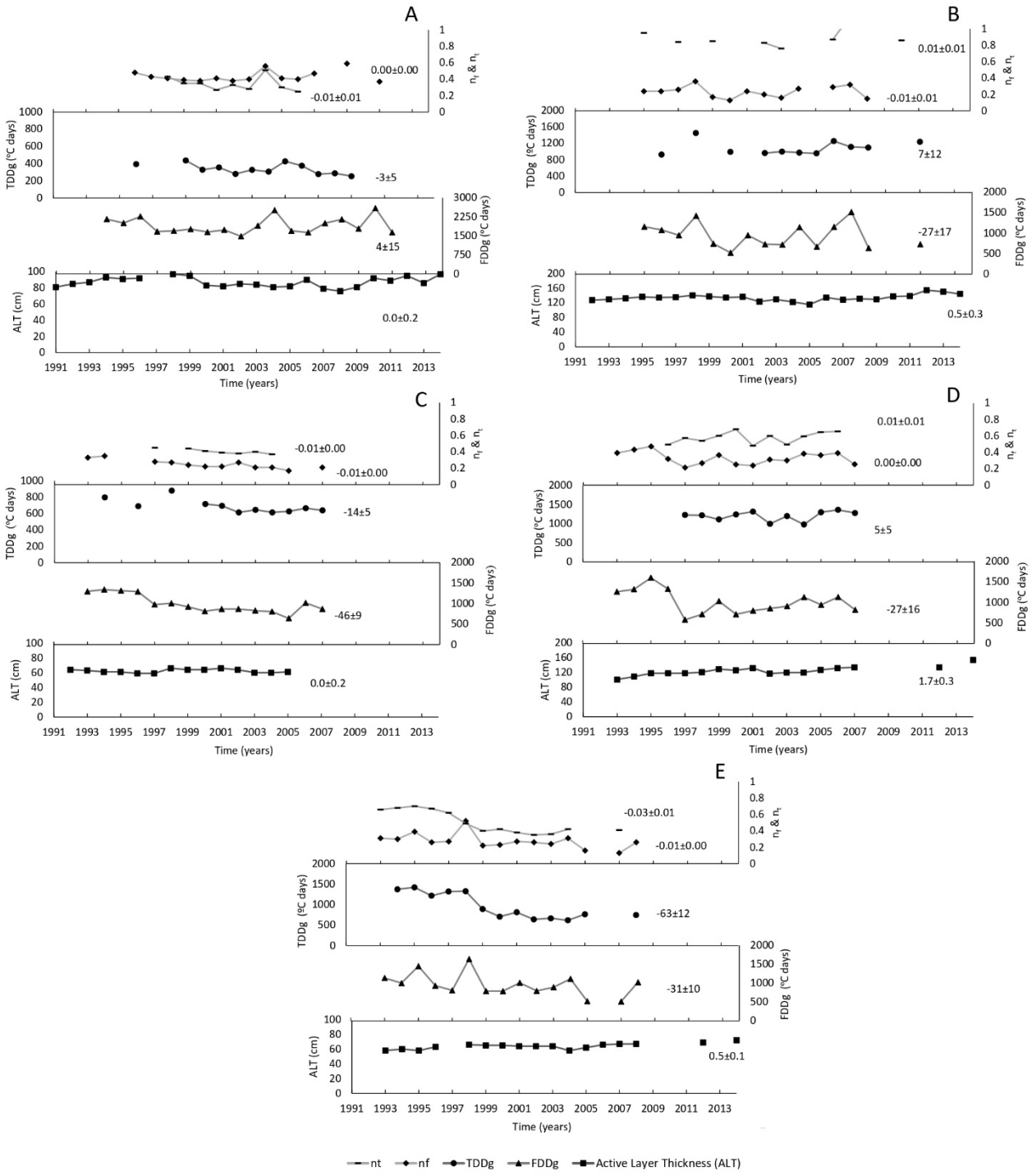


**Figure 3-11.** Average active layer thickness (ALT), $TDD_g$, and $n_t$ and $FDD_g$ and $n_f$ for the preceding year. Slope and slope error for each series are given. A) Site 90-TT-04 in the Tundra Plains LA*n* ecoregion B) Site 91-TT-13 in the Taiga Plains HS ecoregion C) Site 91-TT-22 in the Taiga Plains LS ecoregion D) Site 92-TT-04 in the Taiga Plains MB ecoregion E) Site 92-TT-10 Boreal and Taiga Cordillera.

## 3.6 Discussion

It is important to note that the spatial variability was greater within ecoregions than between ecoregions likely due to the variations in snow cover, vegetation, and substrate within each ecoregion, which control ALT on a sub ecoregional scale (Bonnaventure & Lamoureux, 2013). This highlights the difficulty in using general bioclimatic variables to broadly characterize ALT, particularly in areas dominated by shrubs. Given the high degree of spatial variability in shrub dominated environments, an ecoregional approach may be inappropriate especially at a local scale. However, for broad scale modelling studies of ALT, the ecoregional approach may still be advantageous as unique spatial and temporal patterns can still be discerned. This is largely a product of variation in the dominant influence on ALT between each ecoregion and will be explored further in the following sections.

### *3.6.1 FDD and TDD*

The random forest and MVLR highlighted the importance of both winter and summer conditions on ALT. In previous studies, the impact of winter conditions has been largely overlooked with an emphasis placed on using summer conditions, primarily $TDD_a$, to infer the state of the active layer (Shiklomanov & Nelson, 2002; Mazhitova et al., 2004). However, in recent years, the importance of antecedent winter conditions has been documented (Grünberg et al., 2020; Wilcox et al., 2019). This analysis reaffirms the importance of considering antecedent winter ground conditions in regional ALT studies especially in more southern environments where those were shown to be most important.

Moving north to south, average ALT for ecoregions generally increases corresponding to a decrease in $FDD_a$ and increase in $TDD_a$ (Figures 3-5 and 3-9). The exception to this trend is

average ALT in the Boreal and Taiga Cordillera (68 cm), which was similar to that of the Tundra Plains LA*n* (67 cm), despite the difference in $FDD_a$ (2954 °C days in the Cordillera compared to 4480 °C days in the Tundra Plains) and $TDD_a$ (2132 °C days in the Cordillera compared to 934 °C days in the Tundra Plains). However, the ground surface thermal conditions for each ecoregion show some similarity during the freezing ($FDD_g$ of 955 °C days for the Cordillera and 1880 °C days in the Tundra Plains) and thawing seasons ($TDD_g$ of 937 °C days in the Cordillera and 456 °C days for the Tundra Plains). The similarity in ALTs and the ground thermal regime (particularly the summer conditions) despite large differences in the air thermal regime is likely indicative of an influence of protective vegetation cover or organic material (Shur & Jorgenson, 2007). Despite similar air thermal conditions, the difference in the average ALT (58 cm) for the two southernmost ecoregions (Boreal and Taiga Cordillera and Taiga Plains MB) was greater than the difference between the Boreal and Taiga Cordillera and the Tundra Plain LA*n* ecoregions (1 cm). This difference between the ALT of the two southernmost ecoregions is likely the result of mosses and organic material at sites in the Boreal and Taiga Cordillera, which allow for the thin active layer despite less favorable air temperature (Bonnaventure & Lamoureux, 2013). However, there are only a small number of sites with data in the Boreal and Taiga ecoregion, which may not be representative of the entire ecoregion.

### *3.6.2 Vegetation and Snow Cover Dynamics*

The impact of snow cover on the active layer and permafrost on a yearly scale is dependent on the timing, duration, thickness, structure, and physical and thermal properties of the snowpack (Hinkel & Nelson, 2003; Ling & Zhang, 2003; Zhang et al., 2005; O'Neill & Burn, 2017a; O'Neill & Burn, 2017b; Uhlemann et al., 2021). The accumulation of snow cover in autumn and early winter has a strong influence on ground temperature by insulating the

ground from the low winter air temperatures, resulting in warmer ground surface temperatures compared to locations with thin or no snow cover (Gold, 1963; Goodrich, 1982; Zhang, 2005). Additionally, the insulating effect of snow cover reaches a maximum when snow depth is about 40 cm, although this depth depends on snow morphology and water content (Zhang, 2005; Wilson et al., 2020). $FDD_g$ and $n_f$ values are commonly used to show air-ground surface winter connectivity, which is largely influenced by snow conditions at a site. Inter-site variability in vegetation characteristics is one of the likely reasons for variability in active layer thickness within the ecoregions and is consistent with other local studies (Fisher et al., 2016; Smith et al., 2016). Based on the variability in $n_t$ both within and between ecoregions appears to partly explain the spatial variability in ALT.

A previous ecoregional assessment of $n_f$ in the Mackenzie Valley found that $n_f$ generally increased moving northward, largely indicating an increased connectivity between the air and ground surface at northern sites representing less and more dense snow cover (Smith et al., 2016). Additionally, this may also be influenced by the presence of permafrost or the generally lower ALT in more northern environments, which influence $n_f$ (Smith & Riseborough, 2002). When comparing ecoregions, the same trend is apparent with the northern-most Tundra Plains LA*n* ecoregion having the highest mean $n_f$ and the southernmost Taiga Plains MB and Boreal Cordillera ecoregions having the lowest mean $n_f$ (Figure 3-10). Within ecoregions, lower $n_f$ values are associated with greater ALT as these sites experience warmer winter ground surface conditions than sites with high $n_f$. Additionally, the variability in $n_f$ was highest in the Tundra Plains LA*n* ecoregion (Figure 3-6), which was attributed to highly variable spatial snow cover within the ecoregion, likely due to the presence of shrubs at some sites trapping and retaining

blowing snow (Sturm et al., 2001, Palmer et al., 2012, Yang & Woo, 1999; Zhang, 2005; Bonnaventure et al., 2017; Garibaldi et al, 2021).

This combination of vegetation and snow cover may also explain why shrub dominated ecoregions (Tundra Plains LA*n* and Taiga Plains HS) showed the greatest variability in ALT within ecoregions. Forest dominated ecoregions likely show less inter-ecoregional variability due to more uniform snow conditions. The greatest observed ALT, $n_f$ and $n_t$ variability in the Tundra Plains LA*n* ecoregion may also just be a result of a higher level of sampling sites (n = 30) compared to any other ecoregion. This allowed for a wider range of site characteristics to be sampled giving this ecoregion the most robust variability of sites. Changes in site specific ALT may also reflect changes in vegetation and snow cover dynamics.

Summer temperatures, represented by $TDD_a$, $TDD_g$, and the thawing N-factor, $n_t$, were also shown to influence ALT. Between ecoregions, $n_t$ decreased from the northern ecoregions to the southern ecoregions in response to changing vegetation conditions. Average $n_t$ is highest for the Tundra Plains LAn ecoregions due to the lack of shading during summer as a result of no tree cover and limited vegetation or topographic shadowing. This results in less uniform heating between the ground and the air, which can be amplified when darker surface soils are present. In the southern forested ecoregions, $n_t$ is low due to shading effects of vegetation and thicker organic layers, muting the response of the ground temperatures to air temperatures through increased evaporation and differential thermal conductivity (Fisher et al., 2016; Shur & Jorgenson, 2007).

At the northernmost sites, especially those in the Tundra Plains LA*n* ecoregion including 90-TT-04, there appears to be more of a direct link between $FDD_g$ and ALT as changes in some

years (2007-2009) closely follow each other (Figure 3-11). Additionally, there was no apparent negative trend in ALT despite a decrease in $TDD_g$ (Figure 3-11). The influence of increases in $TDD_g$ was amplified moving southward as ALT responded more to changes in $TDD_g$ alone and in conjunction with changes in $FDD_g$ such as at sites 91-TT-22 and 92-TT-04 (Figure 3-11). Additionally, the warming of the ground surface in winter at sites (decrease in $FDD_g$) in the Taiga Plains MB ecoregion may reflect the increase in the overall snowfall of the area as the Fort Simpson climate station indicates about a 7 cm increase in snowfall per year over the study period (Chapin et al., 2005).

Since ALT is influenced by snow accumulation and vegetation, a disturbance or change in vegetation may result in changes to ALT through changes to snow entrapment or loss of shading, transpiration, and organic matter (Shur & Jorgenson, 2007; Fisher et al., 2016; Way & Lapalme, 2021). This was observed at site 92-TT-12 in the Taiga Plains LS ecoregion, which burned in a fire in 1995. In the 12 years following the fire, ALT increased by approximately 44 cm. This magnitude of change during this timeframe is consistent with other studies examining active layer changes post fire (Smith et al., 2015; Holloway & Lewkowicz, 2020; Holloway et al., 2020). At this site, the active layer thickening is likely the result of surface modification during the fire since no other site nearby or in the ecoregion shows this trend. An additional contributing factor to active layer development could be the presence of surface water that does not freeze to the ground surface, which can substantially keep the ground warm during winter, resulting in an overall warming effect (Harris, 2002; Smith et al., 2009b). This is likely the case at site 91-TT-C, which has been observed to occasionally flood.

### *3.6.3 Substrate*

Substrate, particularly grain size, moisture and ice content moderate ALT through latent heat exchanges and the differential thermal conductivity between the frozen and thawed state (Smith et al., 2001; Shur & Jorgenson, 2007; O'Donnell et al., 2009; Bonnaventure & Lamoureux, 2013). Surface subsidence (downward vertical movement of the surface) results as thaw progresses deeper into ice-rich ground. Seasonal freeze-thaw of the active layer results in latent heat exchanges and seasonal heave and settlement. However, ongoing settlement can occur as the thaw progresses deeper over time, thawing new ice rich material (O'Neill et al. 2019a). Therefore, at sites with high excess ice content, ALT can remain relatively stable as melting of ground ice results in surface subsidence (Duchesne et al., 2015; O'Neill et al. 2019a). Sites with thin active layers and very little annual variability are typically associated with ice-rich material susceptible to thaw settlement.

The results indicate that of the sites sampled, sites with frost susceptible substrate such as ice-rich silts and clay were more commonly associated with higher subsidence than variability in ALT than sites with more ice poor sand or gravel (Figure 3-12) (Shur et al., 2005). These ice-poor sites often showed less subsidence compared to variability in ALT over the study period (Shur et al., 2005). There was no pattern relating subsidence and ecoregion as the type of substrate and ice content varies widely within ecoregions likely contributing to the intra-ecoregion ALT variability.

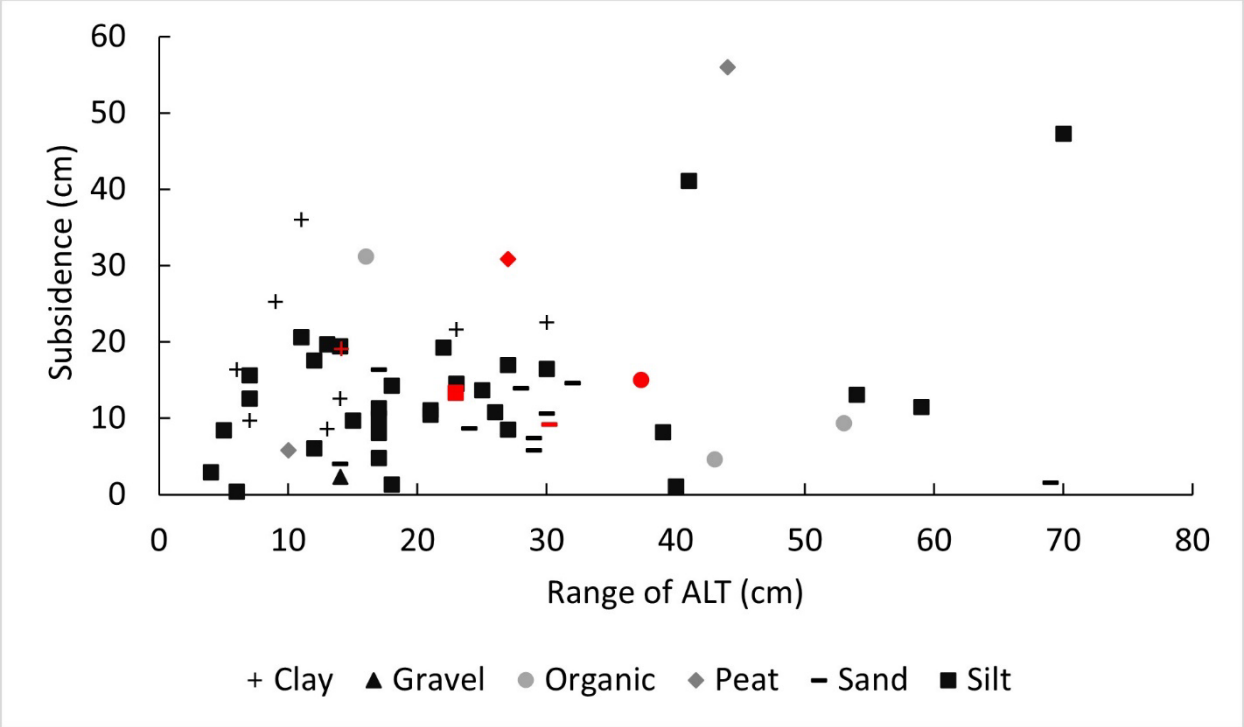


**Figure 3-12.** Comparison of ALT range and subsidence for each site classified based on substrate texture (GSC datafiles updated from Smith et al., 2009a). Subsidence was measured cumulatively over all years of observations. Range of ALT refers to the difference between the maximum and minimum ALT for all years at a site. Red symbols indicate the average subsidence for that substrate.

Some of the sites can be divided into four classes based on the range in ALT and subsidence (low ALT range high subsidence, low ALT range low subsidence, high ALT range low subsidence, and high ALT range high subsidence). Examples of low ALT variability and high subsidence include site 91-TT-11, which has a thin active layer (66 cm) with very little annual variability, but with a surface subsidence of 25 cm (over 19 years), and site 91-TT-02, which has similar active layer conditions and surface subsidence of 36 cm over 17 years (GSC datafiles updated from Smith et al., 2009a). These sites both have fine-grained clay substrate, are low elevation, flat and are located in an area which has a medium potential for segregated ground ice content according to recent ground ice maps (O'Neill et al., 2019b). At these sites, the high subsidence and consolidation of the thaw layer, results in smaller changes in ALT.

Sites with low ALT variation and low subsidence include 90-TT-01 and 90-TT-12 both have fine grained, silt substrate with high ground ice content limiting the progression of thaw (O'Neill et al., 2019b). These sites are two of the northernmost sites with two of the thinnest active layers. Therefore, it is possible that the low subsidence at these sites is a result of limited thaw penetration into the ice rich layers of the substrate. A high range in ALT with low subsidence occurs at sites 90-TT-06, 91-TT-13, and 92-TT-05 likely due to limited ground ice. Site 90-TT-06 shows 6 cm subsidence over 20 years with a 30 cm range in ALT. While this site has a small average ALT (48 cm) it has a sand substrate in which excess ice is unlikely to be present. Site 91-TT-13 is ice-poor silt, which may explain the limited subsidence (8 cm), large variation in ALT (39 cm over 22 years) and thick average active layer (134 cm).

Lastly, sites with both high ALT variation and high subsidence such as 92-TT-03 and 92-TT-12 are likely in places where ice-rich material may have already thawed and consolidated early in the record. At 92-TT-03 little change in ALT (11 cm) and substantial subsidence (26 cm) occurs from 1994-2004 followed by larger changes in ALT (34 cm) and minimal subsidence from 2004-2014. This site is classified as ice-rich silt. A similar pattern occurs at 92-TT-12 with limited variation in ALT (28 cm) and substantial subsidence (43 cm) during the initial part of the record (1993-2001) followed by higher variability in ALT (up to 10 cm fluctuations between years) and minimal subsidence (8 cm). This site is classified as ice-rich peat. Higher ice contents are commonly found at the top of the permafrost (Shur et al., 2005) and the larger subsidence observed earlier in the record is likely the result of thawing of this ice-rich material. As thaw progresses into material containing less ice, less subsidence occurs and larger variation in ALT is observed. Latent heat effects also decrease as thaw progresses into the lower ice-content material (Shur et al., 2005).

*3.6.4 Temporal Trends in ALT*

A key rationale for utilizing an ecoregional approach is the ability to assess broad temporal trends in ALT based on bioclimatic variables hypothesized to impact the response of permafrost to climate change (Shur & Jorgenson, 2007). Using the three-year running means for all annual ALT in each ecoregion over the study period, only the Taiga Plains HS showed a strong positive trend in average ALT ($R^2 = 0.8$) despite the positive air temperature trend in all regions (Figure 3-13).

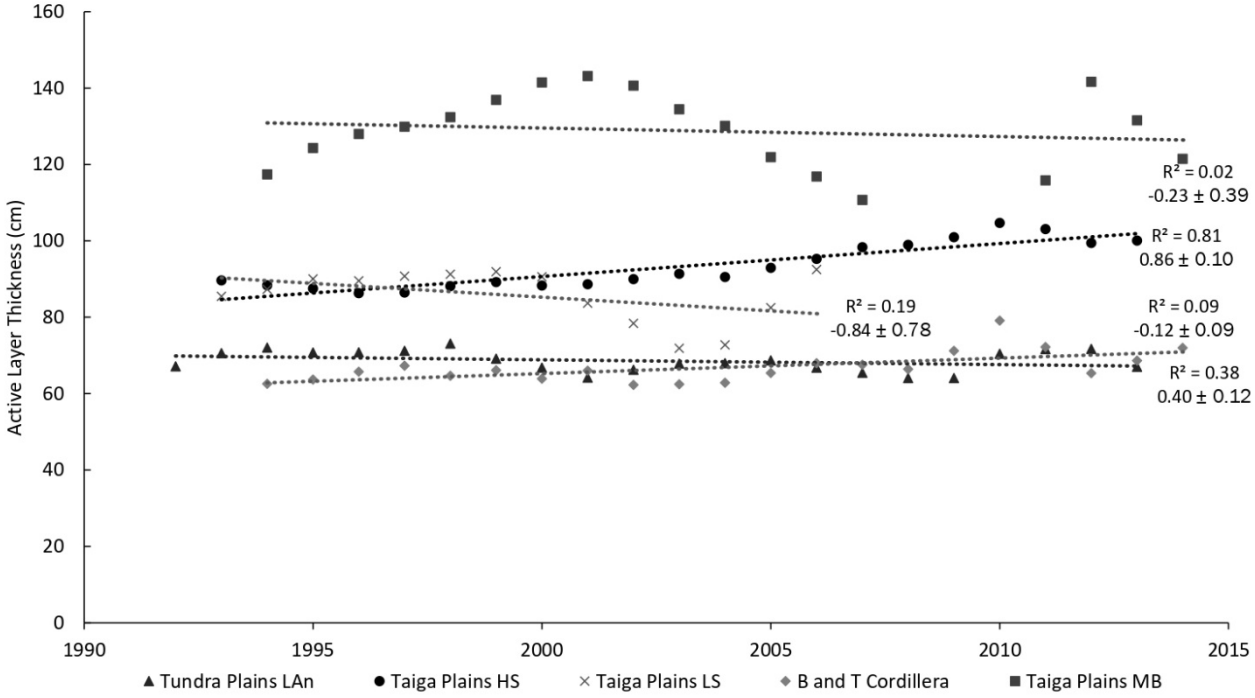


**Figure 3-13.** Three-year running means for average active layer thickness for each ecoregion. $R^2$, slope and slope error are given for each series.

ALT for the Tundra Plains LA*n* and Boreal and Taiga Cordillera showed a slight positive trend with low $R^2$ values of 0.1 and 0.4, respectively. The Taiga Plains LS and Taiga Plains MB ecoregions showed a negative trend or no trend with low $R^2$ values of 0.2 and 0.0, respectively. The trends may be impacted by the number of sites per ecoregion, as an ecoregion with a smaller number of sites is more influenced by changes in individual sites than an ecoregion with a larger

number of sites. In this case, the trend or lack thereof would not be representative of the entire ecoregion. This is more likely to be the case in the Taiga Plains LS and MB ecoregions as they have fewer sites than the Taiga Plains HS and Tundra Plains LA*n* ecoregions and have one site with a substantially different ALT than the other sites in the ecoregion.

The variation in ALT responses to similar warming throughout the valley may demonstrate the variable sensitivity to climatological or ecological disturbances depending on the ecoregion. For example, permafrost in most tundra environments is considered to be climate driven (e.g., Shur & Jorgenson, 2007) and ALT in these ecoregions is a product of low air temperatures and is thus particularly susceptible to long-term changes in climate. This is due to a limited ecological buffer shielding the ground from the direct impacts of increasing air temperatures. The thickening of the active layer in the Taiga Plains HS ecoregion may demonstrate this; however, the Tundra Plains LAn ecoregion did not show this same thickening possibly as a result of higher ground ice or due to the lack of a warming trend in air temperature over the monitoring period (O'Neill et al., 2019b).

Other forested ecoregions with well-developed organic surface layers including those in the Boreal Cordillera can be classified as climate driven, ecosystem modified, and ecosystem protected permafrost. Thus, the active layer is potentially less sensitive to short- or medium-term changes in air temperature but is more sensitive to vegetation disturbance including fire, hydrological and anthropogenic changes (Fisher et al., 2016; Shur & Jorgenson, 2007). Therefore, it is unlikely that even on the time frame of this study or into the short-term future that these locations will display a substantial response to climatic change through active layer thickening unless paired with substantial vegetation disturbance or pond or wetland expansion (Holloway & Lewkowicz, 2020). This may explain why the ecoregions with more developed

vegetation cover did not on average show a response over the monitoring period. As a result, the variability in response of the active layer depends on the type of disturbance, and thus it is important to understand in order to properly conceptualize the timing of associated landscape hazards, which may result from permafrost degradation.

### 3.7 Conclusion

ALT at monitoring sites throughout the Mackenzie Valley exhibit a great deal of spatial and temporal variability within and across ecoregions as ALT is a product of complex interactions between climate, vegetation, snow cover, and soil type. The Tundra Plains LA*n* ecoregion showed the largest spatial range in ALT, while the Taiga Plains MB ecoregion has the greatest average ALT. Thick active layers at certain sites in the Tundra Plains LA*n* and Taiga Plains HS ecoregions likely result from the increased accumulation of snow by willow shrubs, resulting in warmer ground conditions than tundra upland sites, which are wind scoured and have thin active layers. This causes large ranges in ALT in these ecoregions. Generally, air temperature, including winter conditions, is the major influence as average ALT increases moving southward, a result of air temperature increase and greater ALT occurring in years with warmer winters and summers. However, the relative importance of winter and summer thermal conditions on ALT depends on the ecoregion. The characteristic vegetation type of an ecoregion may also be used as an explanation for the average ALT; however, this is more difficult to use as dominant vegetation may vary between sites within an ecoregion. Overall, winter conditions can have significant influence on ALT.

ALT at some sites was less responsive to shorter-term variation in air temperature potentially due to the moderating effect of vegetation, organic layer, and snow. For these

locations, disturbance, rather than changing air temperature may have a larger impact on ALT due to the surface modification. Where ice-rich permafrost is present, increases in summer thaw due to warming and increased disturbance, will likely result in increased ground subsidence. This subsidence may result in landscape changes, which impact hydrology and drainage as well as ecosystems throughout the valley potentially causing further changes in ALT and increase permafrost degradation with increased ponding. Understanding the relation between ALT, climate, dominant vegetation type, and ecoregion is essential to assess how ALT will respond to changing air temperatures, snowfall, and vegetation under climate warming.

# Chapter 4 Determining TTOP model parameter importance and TTOP model performance across western Canada

**Authors:** Madeleine C. Garibaldi[1], Philip P. Bonnaventure[1], Robert G. Way[2], Alexandre Bevington[3], Sharon L. Smith[4], Scott F. Lamoureux[2], Antoni G. Lewkowicz[5]

[1] Department of Geography and Environment, University of Lethbridge
[2] Department of Geography and Planning, Queen's University
[3] Ministry of Forests, Lands, and Natural Resource Operations
[4] Geological Survey of Canada, Natural Resources Canada
[5] Department of Geography, Environment and Geomatics, University of Ottawa

**Key Words:** TTOP model, random forest, permafrost, Sensitivity, High Arctic, Subarctic

## 4.1 Abstract

TTOP model sensitivity and parameter importance using random forest was tested across western Canada using in situ data. The TTOP model was most sensitive to changes in freezing parameters $n_f$ and $FDD_a$, and least sensitive to changes in thawing parameters $TDD_a$, $n_t$ and rk. However, the importance of specific parameters varied regionally. Where the magnitude of $FDD_a$ was similar to $TDD_a$, the model was most sensitive to changes in freezing parameters and had minimal response to changes in thawing parameters. However, as $TDD_a$ became comparable to $FDD_a$ the sensitivity to thawing parameters increased. These findings were supported by the random forest variable importance rankings, however, additional parameters including the thermal offset and annual air and ground surface temperatures were also shown to be important. When tested against measured annual mean ground temperature (AMGT), the TTOP model performed well overall and especially in areas of cold climate driven permafrost while breaking down in areas of warm potentially ecosystem protected or modified permafrost. The sensitivity and variable importance results using in situ data both supported and refined findings of previous studies, which were based only on theoretical inputs. Lastly, findings from this study can aid in parameterization efforts and parameter selection based on modelling location and scale.

## 4.2 Introduction

Permafrost is an important element of the cryosphere as it impacts terrain stability (Harris et al., 2001; Lantz & Kokelj, 2008; Patton et al., 2019), hydrology (Woo et al., 2008), carbon storage (Schuur et al., 2008), and solute movement (Kokelj & Burn, 2003, 2005; Roberts et al., 2017; Lafrenière & Lamoureux, 2019). Modelling is one of the most commonly used methods to study permafrost temperature and distributions as direct observation, used for other elements of the cryosphere, (e.g., glaciers and sea ice) remains challenging (Kääb, 2008). A commonly utilized permafrost model is the temperature at top of permafrost (TTOP model) having been used to estimate permafrost temperature and presence at a variety of scales ranging from continental to local (Gisnås et al., 2013; Obu et al., 2019; Garibaldi et al., 2021) and in a variety of permafrost environments including High Arctic and alpine (Bevington & Lewkowicz, 2015). The TTOP model is widely used because it is simple, only requiring data that are commonly measured by meteorological stations or assigned based on surface and subsurface characteristics. It is also applicable to a variety of permafrost environments without the need for recalibration (Juliussen & Humlum, 2007).

One of the primary challenges of using the TTOP model is determining the values of the scaling factors (N-factors) and soil thermal conductivities (Juliussen & Humlum, 2007). In modelling studies these scaling factors are typically assigned based on landcover class or topographic class using field measurements or values presented in the literature (Riseborough et al., 2008; Gisnås et al., 2013; Obu et al., 2019). However, few studies have examined the uncertainties, which arise from mischaracterization of the value of the TTOP model parameters on the TTOP model output or the relative importance of each parameter in different permafrost environments.

Way and Lewkowicz (2016) demonstrated that utilizing freezing N-factors ($n_f$) from different environments when running the TTOP model for Labrador-Ungava introduced uncertainties in the model output especially in forested environments. Theoretical and field data have both been used to assess TTOP model variable importance (Smith & Riseborough, 2002; Bevington & Lewkowicz, 2015). Both studies conclude the importance of $n_f$, especially in northern environments and highlight the increasing influence of differential thermal conductivity (rk) moving south. However, these studies rely either on calculated or theoretical inputs or on measured data covering only a relatively small area limiting the applicability of the conclusions to other locations or broader scales. As the parameterization of the scaling factors and rk remain one of the main challenges in utilizing the TTOP model, understanding the relative importance and sensitivity of the model to the parameters is essential. Therefore, quantifying the impact of changing values of input parameters and determining the relative importance of each variable in unique permafrost environments will aid in guiding future modelling studies by highlighting the relative value to place on characterizing individual variables.

Another method that may aid in understanding the influence of certain parameters on permafrost temperature in different environments is random forest. Random forest is an ensemble classifier, which combines randomized decision trees with bagging and aggregates their predictions though averaging or majority vote (Breiman,2001; Biau & Scornet, 2016). Random forest has been used in studies of air quality (Yu et al., 2016; Pendergrass et al., 2022), chemoinfomatics (Mitchell, 2014), ecology (Cutler et al., 2007; Brieuc et al., 2018) and remote sensing (Belgiu & Drăgu, 2016). However, until recently, in mapping permafrost distribution studies its use remains limited but effective (Deluigi et al., 2017; Baral & Haq, 2020).

Random forest also provides variable importance rankings through two methods, permutation accuracy importance (mean square error (MSE) reduction) or Gini importance (Strobl et al., 2008). However, the reduction in MSE has been more widely used in variable importance studies due to Gini importance biases when predictor parameters vary in number and scale (Díaz-Uriarte & Alvarez de Andrés, 2006; Strobl et al., 2008; Grömping, 2009; Genuer et al., 2010). Generally, the variable importance results are then used either to identify important variables for explanatory or interpolation purposes or to identify a small number of variables that provide a good prediction (Díaz-Uriarte & Alvarez de Andrés, 2006; Grömping, 2009; Genuer et al., 2010). As a result, random forest variable importance rankings may allow for unique parameterization of permafrost models in a variety of different environment and focus data collection efforts. The expanded use of machine learning parameterization in conjunction with process-based models may be an important next step for permafrost modelling studies.

The objectives of this study were to 1) analyze the sensitivity of TTOP model parameters and permafrost temperature output, 2) compare this sensitivity to a variable importance ranking produced through random forest and 3) compare TTOP model outputs to measured ground temperatures for several permafrost environments. The results of this study should guide effort placed on TTOP model parameter calculations and assess the performance of the TTOP model relative to the environment.

### 4.3 Study Area

To assess the sensitivity of the TTOP model and determine variable importance rankings, a variety of western Canadian permafrost environments ranging from High Arctic to Subarctic, lowland and alpine were sampled (Figure 4-1).

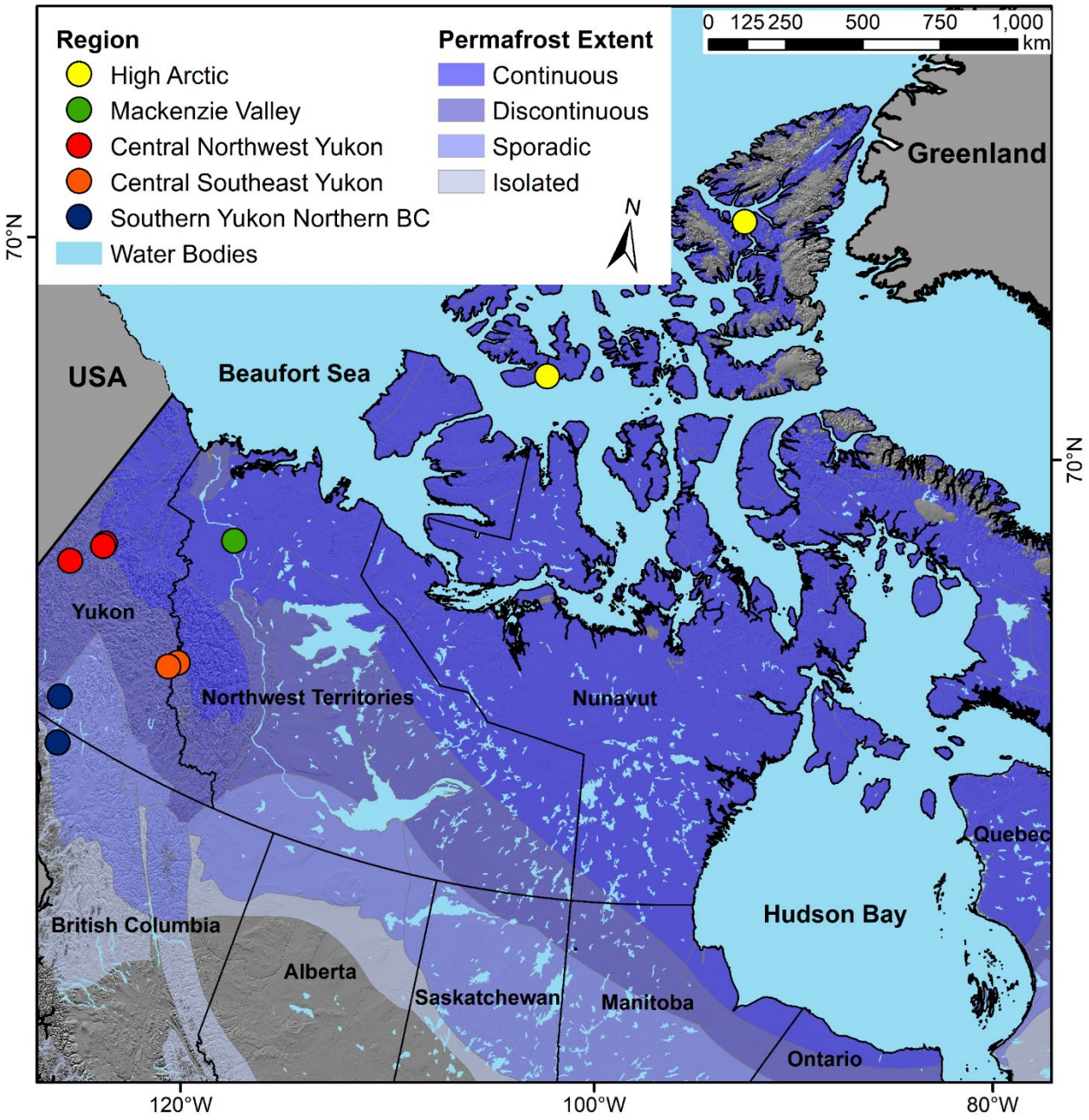


**Figure 4-1.** Study regions for TTOP sensitivity analysis and random forest.

The main study regions are Cape Bounty, Eureka, and sections of the Mackenzie Valley, Dawson, Southern Dempster, North Canol, Whitehorse and Atlin. The two High Arctic locations are Cape Bounty, located on the south-central coast of Melville Island, Nunavut and Eureka located on Ellesmere Island. Both locations are polar deserts with MAAT of -18.8 °C (1981-2010) in Eureka and an annual mean air temperature (AMAT) of -14.0 °C (2012-2017) at Cape

Bounty (Environment Canada, 2021). Both locations are underlain by continuous permafrost and have limited relief. Vegetation consisting of sparse polar desert tundra communities and the substrate is mostly composed of siltstone and sandstone bedrock overlain by unconsolidated glacial and marine sediment (Hodgson et al., 1984; Walker et al., 2002; Gregory, 2011; Lewis et al., 2012).

Moving southward, the Mackenzie Valley spans several climatic regions, dominant vegetation communities and permafrost conditions. The northern section of the valley is dominated by tundra vegetation and is underlain by continuous permafrost (Heginbottom, 1995; Smith et al., 2009b). Substrate in the north and delta region consists of broad alluvial plain with limited peatlands (Burn & Kokelj, 2009). MAAT for the northern section ranges from -10.1 °C in Tuktoyaktuk to -8.2 °C in Inuvik (1981-2010) (Environment Canada, 2017). The central and southern portion of the valley is underlain by discontinuous permafrost while vegetation in the central portion of the valley is predominantly boreal forest with extensive peatland present (Aylsworth & Kettles, 2000; Duchesne et al., 2015). MAAT ranges from -5.1 °C for Norman Wells to -2.8 °C for Fort Simpson (1981-2010) (Environment Canada, 2017). Throughout the valley, ice-rich lacustrine silt and clays are common. Sediments in the valley are mainly moraine, lacustrine, fluvial and deltaic in nature (Duchesne et al., 2015).

Central Yukon sites are located along the Dempster Highway running from Dawson City north to the Ogilvie Mountains. Permafrost conditions range from extensive discontinuous in Dawson City to continuous in the Ogilvie Mountains (Heginbottom, 1995) with permafrost commonly found below treeline even in Dawson City. The southern portion of the Dempster Highway experienced glaciation during the Wisconsinan period while the middle section has remained unglaciated (Burn et al., 2015). Surficial geology in this region is mainly comprised of

colluvium, till, and alluvium and topography transitions to narrower mountain valleys from Dawson to the Ogilvies (Burn et al., 2015). Measured AMAT over the monitoring period ranges from -4.2 °C near Dawson to -9.2 °C in the Ogilvie Mountains. This landscape is also characterized by strong wintertime inversions, which increase in strength moving northward (Noad & Bonnaventure, 2022). Vegetation consists of white (*picea glauca*) and black spruce (*picea mariana*) forests with alpine tundra vegetation present at higher elevations (Stanek et al., 1980).

In the Southern Yukon, sites are located near Whitehorse, Ross River and up the North Canol road to the Yukon-Northwest Territories boarder. The Whitehorse area is mountainous, with large U-shaped valleys stemming from previous glaciation (Bevington & Lewkowicz, 2015). Permafrost in this region is considered to be extensive discontinuous, although may be continuous above treeline (Bonnaventure et al., 2012). Vegetation is primarily boreal forest and MAAT is 0.2 °C (1981-2010) (Environment Canada, 2021). Along the North Canol road from Ross River to MacMillan Pass, permafrost is considered to be extensive discontinuous with MAAT ranging from -3.4 °C to -5.2 °C, respectively (1981-2010) (Environment Canada, 2021; Heginbottom, 1995). Vegetation is mainly boreal forest but transitions to alpine vegetation at higher elevations. On the N.W.T side of the MacMillan Pass, vegetation transitions from primarily forest to treeless and is dominated by dwarf birch shrub.

Finally, the southernmost sites in Northern British Columbia were centered around Atlin. Permafrost in this location is characterized as sporadic discontinuous with permafrost only present in the mountains where it can be extensive discontinuous or continuous above treeline (Bonnaventure et al., 2012; Bevington & Lewkowicz, 2015). MAAT is 1.1 °C (1981-2010) and vegetation is classified as boreal white and black spruce forests at lower elevations and spruce,

willow, and birch in the subalpine elevations (Government of British Columbia, 2018, Environment Canada, 2021). For the purpose of this study, sites were grouped based on proximity and similarity, resulting in five main study regions, High Arctic (Eureka and Cape Bounty), Mackenzie Valley, Central Northwest Yukon (Dawson and Dempster), Central Southeast Yukon (North Canol) and Southern Yukon Northern BC (Whitehorse and Atlin).

### 4.4 Methods

Air, ground surface and ground temperature at depth measurements were recorded hourly or bi-hourly (on even hours) at 193 sites (Table 4-1). Record lengths range from 2-16 years.

**Table 4-1.** Number of sites and length of monitoring period for each study region. TTOP sensitivity utilizes all sites while random forest analysis only includes sites with air, ground surface and ground depth temperatures. Total number of observations is the number of individual years of data for each site in the region.

| Region | Total Number of Sites | # Sites with Air, Ground Surface, and Ground Temperature | # Sites with only Air and Ground Surface Temperature | Monitoring Period | Number of Annual Observations |
|---|---|---|---|---|---|
| **Eureka** | 6 | 6 | 0 | 2009-2013 | 13 |
| **Cape Bounty** | 49 | 10 | 39 | 2011-2018 | 75 |
| **Mackenzie Valley** | 55 | 0 | 55 | 1994-2011 | 353 |
| **Dempster** | 13 | 13 | 0 | 2015-2021 | 30 |
| **Dawson** | 15 | 15 | 0 | 2008-2021 | 102 |
| **North Canol** | 21 | 21 | 0 | 2016-2021 | 48 |
| **Whitehorse** | 28 | 28 | 0 | 2007-2015 | 34 |
| **Atlin** | 6 | 6 | 0 | 2011-2019 | 28 |

Air temperature is measured about 1.5 meters above the ground surface with a Hobo U23-002 (± 0.25- 0.4 °C accuracy, 0.04 °C resolution) thermistor housed in a radiation shield (Onset RS1). At newer sites, a Hobo U23-001 (± 0.25 °C accuracy, 0.04 °C resolution) was housed in aradiation shield. Ground surface temperature was measured 2-5 cm below the ground surface

with the Hobo U23-002 internal thermistor while the external thermistor measures ground temperature at depth, which at most sites is the top of the frost table. Exceptions to this are mainly sites located on exposed rocky substrate or scree. The depth of the ground temperature measurements at these locations were not located at the top of the frost table due to restrictions based on substrate, which prevented measurements deeper.

*4.4.1 TTOP Model Sensitivity*

Baseline input parameters for the TTOP model and the reference TTOP value were calculated for each site (Table 4-2).

**Table 4-2.** Variables and equations used in the TTOP sensitivity and random forest analysis. Freezing (FDD) and thawing (TDD) degree-days were calculated for air (a), ground surface (s), and ground at a shallow depth (g). P is the period, usually 365 days.

| Variable | Abbreviation | Equation |
|---|---|---|
| **Freezing Degree Days** | FDD | $FDD = \lvert\Sigma_1^P T\rvert, T < 0$ |
| **Thawing Degree Days** | TDD | $TDD = \lvert\Sigma_1^P T\rvert, T > 0$ |
| **Freezing n factor** | $n_f$ | $n_\mathrm{f} = \frac{FDD_\mathrm{s}}{FDD_\mathrm{a}}$ |
| **Thawing n factor** | $n_t$ | $n_\mathrm{t} = \frac{TDD_\mathrm{s}}{TDD_\mathrm{a}}$ |
| **Temperature at Top of Permafrost** | TTOP | $TTOP = \frac{(n_\mathrm{t} * TDD_\mathrm{a} * rk) - (n_\mathrm{f} * FDD_\mathrm{a})}{P}$ |
| **Thermal Conductivity ratio** | rk | $rk = \frac{FDD_\mathrm{s} + (TDD_\mathrm{g} - FDD_\mathrm{g})}{TDD_\mathrm{s}}$ |
| **Nival Surface Offset** | NVO | $NVO = \frac{FDD_\mathrm{a} - FDD_\mathrm{s}}{P}$ |
| **Thawing Surface Offset** | TSO | $TSO = \frac{TDD_\mathrm{s} - TDD_\mathrm{a}}{P}$ |
| **Surface Offset** | SO | $SO = AMGST - AMAT$ |
| **Thermal Offset** | TO | $TO = AMGT - AMGST$ |

To allow for direct comparison of model sensitivity in all environments only the TTOP model equation for permafrost was utilized even for sites considered to be seasonally frozen. For each

year and each site, FDD and TDD were calculated using daily average air ($T_a$) and ground surface temperatures ($T_s$) from September 1st to August 31st of the subsequent year (Table 4-2). Following this, freezing and thawing N-factors, were calculated for each site (Table 4-2). The thermal conductivity (rk) for sites with a depth temperature measurement was calculated using FDD and TDD for both the ground surface (s) and shallow ground depth (g) (Table 4-2). For sites without a depth sensor, rk, was assigned based on vegetation class (n = 38). These sites were included even though rk needed to be assigned as they filled a substantial latitudinal gap in the dataset. It was assumed that thermal conductivity remained uniform with depth.

Once the parameters and reference TTOP value were calculated the sensitivity of the model to changes in each parameter was assessed using a method similar to leave one out cross validation, whereby each parameter was iteratively substituted to assess the changes in the output result. The four different methods were used for determining the value to substitute for perturbation (Table 4-3). The first method was the direct substitution of selected percentiles (minimum, $5^{th}$, $25^{th}$, $50^{th}$, $75^{th}$, $95^{th}$ and maximum) for each variable determined using he entire dataset. For this method, the tested parameter was assigned the same value at all sites. Additionally, the new value for each parameter was based on the range and values measured in the dataset. For the second method, the new parameter values were determined through a percentage change of the original parameter value. Therefore, for this method the parameter value at each individual site was altered by a magnitude proportional to the initial parameter value. Lastly, the final two methods involved a fixed magnitude of change for each parameter at each site, either by adding/subtracting the value of a percentile calculated from the entire dataset (3), or an assigned value (4). The results for the last two methods are presented in the supplemental data section for Paper 2.

**Table 4-3.** Description for each scenario used in the TTOP sensitivity analysis. The iteration indicates the amount one parameter in the TTOP model equation was altered. For each scenario each parameter (excluding period (P)) were changed to/by the iteration value.

| Trial | Description | 1st Iteration | 2nd Iteration | 3rd Iteration | 4th Iteration | 5th Iteration | 6th Iteration | 7th Iteration |
|---|---|---|---|---|---|---|---|---|
| **1** | Direct Substitution of percentile value | Min | 5th | 25th | 50th | 75th | 95th | Max |
| **2** | ± percentage | ± 5% | ± 10% | ± 25% | ± 50% | NA | NA | NA |
| **3** | ± percentile | ± min | ± 5th | ± 10th | ± 25th | ± 50th | NA | NA |
| **4** | ± fixed value | ± 0.05<br>± 100 | ± 0.1<br>±250 | ± 0.25<br>± 500 | ± 0.5<br>± 1000 | NA | NA | NA |

For scenarios 3 and 4, values for parameters were capped to preserve proper function of the model, (E.g. values were kept above zero). Additionally, $n_f$ and rk were capped at values below one and three, respectively to ensure these values remained realistic. For this analysis, each year of data for each site was treated as its own observation and run through the sensitivity analysis resulting in 683 observations. The resulting outputs were then compared to the reference TTOP value to assess the sensitivity of the model to changes in each parameter.

### *4.4.2 Random Forest Variable Importance Ranking*

Variable importance rankings were also obtained using random forest-based machine learning techniques and compared to TTOP model sensitivity results. For this study, reduction in MSE was used as the primary method for variable importance ranking. Reduction in MSE involves the random permutation of each variable individually to simulate its absence in the

model prediction. Variable importance is then determined based on the difference in prediction accuracy before and after the permutation. Algorithm inputs included all the TTOP model parameters, including $TDD_a$, $FDD_a$, $n_f$, $n_t$ and rk in addition to MAAT, MAGST, nival offset (NVO), thawing surface offset (TSO), surface offset (SO), thermal offset (TO), $TDD_s$ and $FDD_s$ (Table 4-2). Samples were split into testing and training data (40% and 60 % respectively. Random forest was run using individual years as unique observations and using only site averages; however, only the methodology and results for the individual years are reported as these models performed the best for the testing dataset. Two random forest models were created, one using all the input variables and the other using only the TTOP model parameters (Table 4-4). The random forests were generated in R Studio and run using the default settings for the number of variables sampled for splitting at each node (mtry) and with 500 trees.). For each iteration, the same training and test dataset was used.

**Table 4-4.** Random forest trials including a description of variable selection, and variables used.

| Random Forest Iteration | Description | Variables used |
|---|---|---|
| **1** | All Variables | $FDD_a$ $TDD_a$ $n_f$ $n_t$ rk MAAT MAGST NVO TSO SO TO $FDD_s$ $TDD_s$ |
| **2** | TTOP model variables | $FDD_a$ $TDD_a$ $n_f$ $n_t$ rk |

Variable importance plots were created for each random forest both for the entire dataset and for each region individually. For some sites, measured MAGT may not correspond to the temperature at the top of the frost table due to limitations for the depth of the sensor. However, these sites are generally confined to coarse grained, rocky sediment. Therefore, it can be assumed that the difference between the temperature and the monitoring depth and the true

TTOP value is likely at most 0.5 °C due to the naturally small thermal gradient at these locations (Lewkowicz et al., 2012).

## 4.5 Results

### *4.5.1 TTOP Model Parameter Sensitivity*

#### 4.5.1.1 Summary of Input Parameters

Average values for each of the input parameters varied both between parameters and between regions (Figure 4-2). On average the highest values for the freezing parameters were measured in the more Northern regions with $FDD_a$ over three times greater in the High Arctic compared to Southern Yukon and Northern BC and $n_f$ on average decreasing moving south. Conversely, the highest values for $TDD_a$ were measured at southern sites with a general decreasing trend moving north. Values of $n_t$ were highest for the sparsely vegetated High Arctic and a large number of rocky, un-vegetated sites in Southern Yukon and Northern BC. Of the offset parameters, rk, showed the greatest range amongst all measurements (2.28), followed by $n_t$ (1.44), and $n_f$ (0.97). $FDD_a$ had almost two times the variability than $TDD_a$ with measured values ranging by 6948.7 °C days compared to 3525.2 °C days. Understanding the values and variability of each parameter is crucial to interpreting the results of the sensitivity trials correctly, as the sensitivity output for each method may depend not only on the actual model sensitivity but also on the value of the perturbed parameter relative to the measured value.

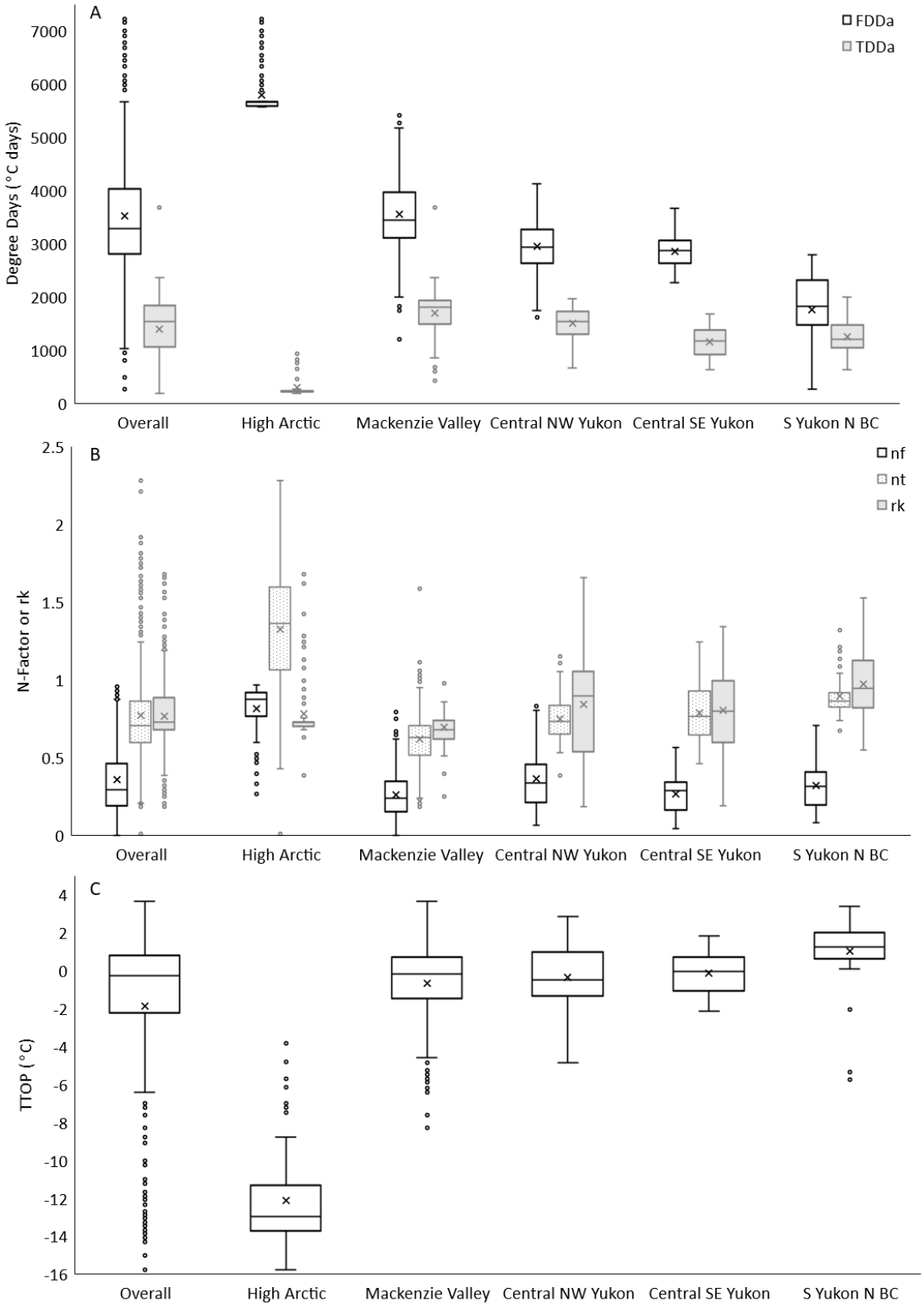


**Figure 4-2.** Boxplots for A) $FDD_a$ and $TDD_a$, B) $n_f$, $n_t$, and rk and C) TTOP overall and for individual regions.

4.5.1.2 Percentile Substitution

For the first trial to test TTOP model sensitivity, percentile values for each parameter were directly substituted for the measured parameter value (Table 4-5). As the range of measured values were different for each parameter, the values and range of the substituted percentiles were also different. The potential impact of this on the interpretation of the sensitivity will be discussed later.

**Table 4-5.** Substituted percentile values for each parameter replacing the measured parameter value for each iteration of this trial method.

| | **Minimum** | **5th Percentile** | **25th Percentile** | **50th Percentile** | **75th Percentile** | **95th Percentile** | **Maximum** |
|---|---|---|---|---|---|---|---|
| **$N_f$** | 0 | 0.08 | 0.19 | 0.30 | 0.47 | 0.90 | 0.97 |
| **$N_t$** | 0.01 | 0.38 | 0.60 | 0.71 | 0.87 | 1.47 | 2.28 |
| **rk** | 0.18 | 0.39 | 0.68 | 0.73 | 0.88 | 1.21 | 1.68 |
| **$FDD_a$** | 274.3 | 1801.1 | 2809.1 | 3278.9 | 4028.7 | 5670.4 | 7223.0 |
| **$TDD_a$** | 189.6 | 226.3 | 1066.0 | 1533.4 | 1835.7 | 2072.6 | 3714.8 |

For every iteration of quantile substitution across all regions, the TTOP model showed the most sensitivity to changes in $n_f$ and $FDD_a$ and overall, the least sensitivity to changes in rk, $n_t$ and $TDD_a$ (Figure 4-3).

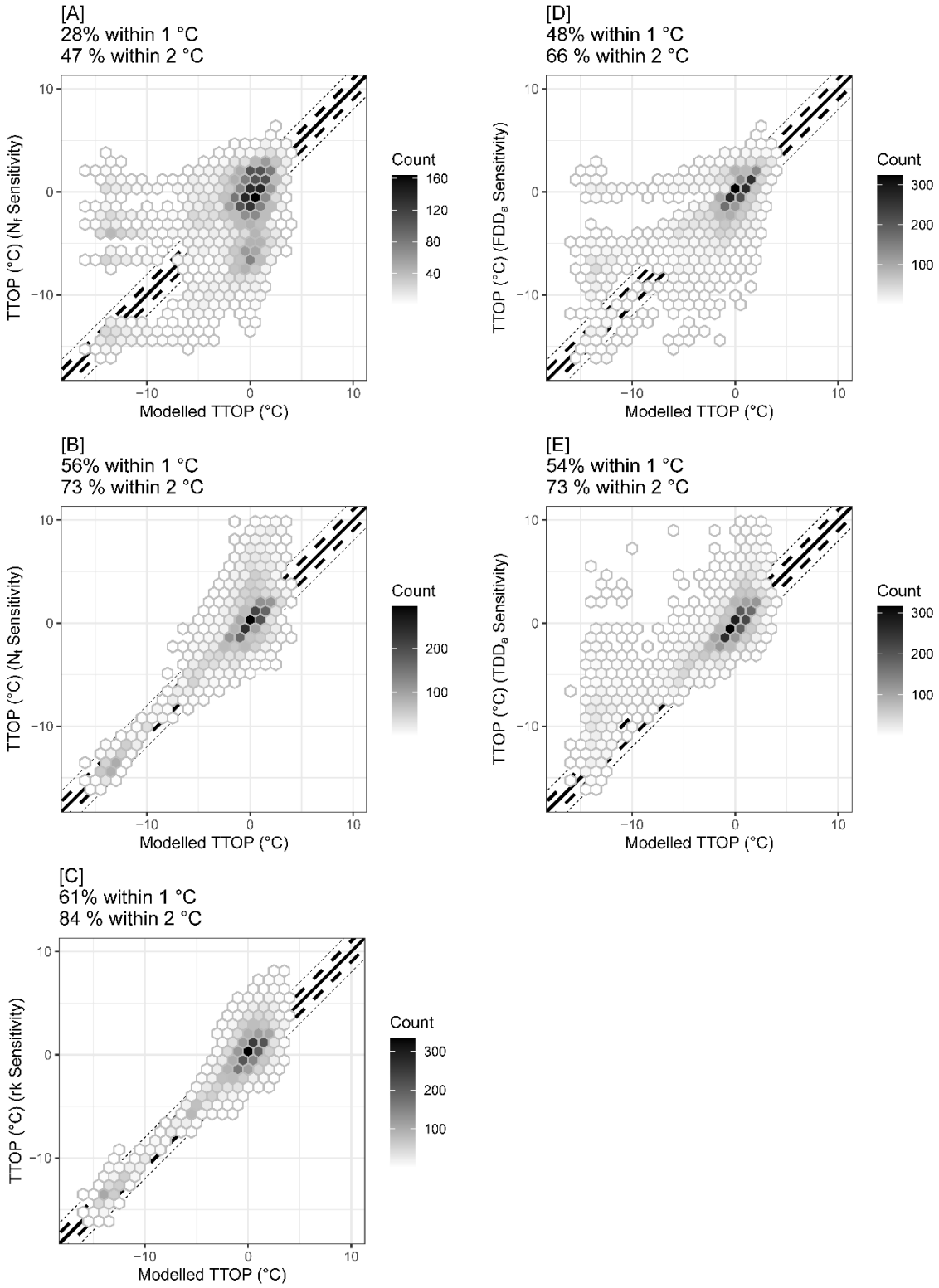


**Figure 4-3.** Reference TTOP model values compared to perturbed TTOP model values for the direct substitution of the minimum, 5$^{th}$, 25$^{th}$, 50$^{th}$, 75$^{th}$, 95$^{th}$, and maximum percentile value for [A] $n_f$, [B] $FDD_a$, [C] $n_t$, [D] $TDD_a$, and [E] rk. Large dashes indicate a ± 1 °C difference while small dashes indicated a ± 2 °C difference.

For a majority (>54 %) of sample points, changes to rk, $TDD_a$, and $n_t$ result in less than 1 ºC difference between the reference and perturbed TTOP output. However, for $n_f$ and $FDD_a$ only a minority of sample points (< 48 %) remained within 1 ºC of the initial TTOP value. When divided into iterations substituting the maximum and minimum value for each parameter resulted in the greatest number of samples with a difference greater than 1 ºC, as these were the largest magnitude changes for most of the sample points.

Latitudinal trends in sensitivity were observed with the locations with the coldest permafrost showing a greater response to changes in winter parameters ($n_f$ and $FDD_a$) and muted response to changes in summer parameters ($n_t$) and the thermal conductivity (rk). The latitudinal differences in the magnitude of response of the TTOP model output to changes in each parameter was apparent by region. The High Arctic showed the most overall sensitivity to changes in $n_f$, $FDD_a$, and $TDD_a$, while the Southern Yukon and Northern BC showed decreasing sensitivity to changes in $n_f$ (Figure 4-4).

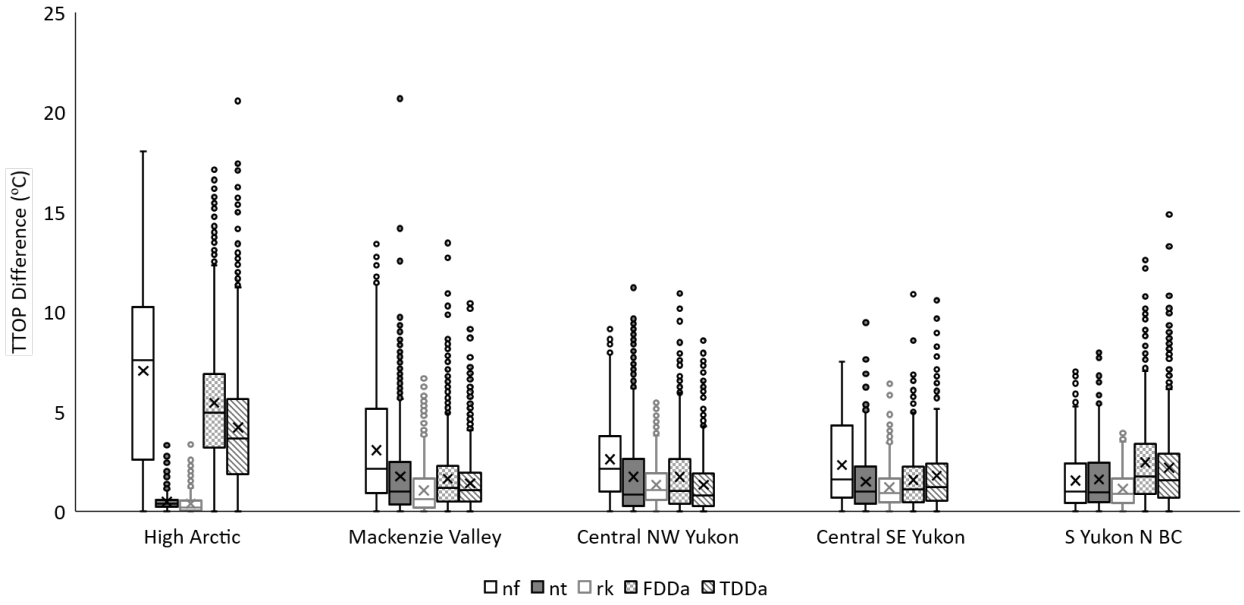


**Figure 4-4.** Boxplots for the regional absolute difference between the reference TTOP and the TTOP calculated when parameters were directly substituted to a percentile value.

The High Arctic region showed the least overall sensitivity to changes in $n_t$ and rk with only 8 % of observations across all substitutions changing by more than 1 °C. Moving southward observations in the Mackenzie Valley, Central Southeast Yukon, and Southern Yukon Northern BC showed the least sensitivity to changes in rk, with less than 46 % of observations changing by more than 1 ºC. The Central Northwest Yukon showed the least overall sensitivity to changes in $TDD_a$ (only 42 % changed by more than 1 °C).

Looking at each region individually, all regions had the largest response for changes in freezing parameters. Both the High Arctic and Southern Yukon Northern BC had the largest response for changes in $FDD_a$, with 86 and 54 % of observations changing by more than 1 ºC, respectively. The Mackenzie Valley, Central Northwest Yukon and Central Southeast Yukon had the response to changes in $n_f$, with a majority of observations (>64 %) changing by more than 1 °C. For all but one region (Central NW Yukon), the least sensitive parameter by region was rk. The Central NW Yukon showed the least sensitivity to changes in $TDD_a$. However, there were latitudinal differences, with the northernmost regions (High Arctic, Mackenzie Valley, Central Northwest Yukon) showing overall less sensitivity to the summer parameters ($n_t$ and/or $TDD_a$) relative to the freezing parameters. Contrastingly, the two southernmost regions (Central Southeast Yukon and Southern Yukon Northern BC) showed increasing sensitivity to changes in the thawing parameters relative to the freezing.

The regions with the maximum and minimum discrepancies between the reference and perturbed TTOP value was concentrated between the High Arctic, the Mackenzie Valley, and Central Northwest and Southeast Yukon. Additionally, the quantile value which elicited the maximum and minimum response differed by region and parameter depending on the magnitude of change from the measured value. The largest difference between the reference and perturbed

TTOP for changes to $n_f$ (18.0 °C), $FDD_a$ (17.1 ºC) and $TDD_a$ (20.6 ºC) was found in the High Arctic region using the minimum values. The minimum difference for $n_t$ , rk , $FDD_a$ and $TDD_a$ (0.0 ºC for all) was also observed in the High Arctic using the minimum values for $n_t$ and $TDD_a$, the 5th and 50th percentile for rk, and the 95th percentile for $FDD_a$. The greatest difference for $n_t$ and rk was found in the Mackenzie region (20.7 °C and 10.6 ºC) using the maximums. Lastly, the smallest difference for $n_f$ (0 ºC) was modelled in Mackenzie region (Dempster) using the minimum value.

4.5.1.3 ± Percentage

The second TTOP sensitivity trial involved changing each individual observation by a percentage of the original value. This method involved only capping of $n_f$ and rk values to less than one and three respectively. Similar to the quantile substitution method, there was overall greater sensitivity to changes in $n_f$ and $FDD_a$ than to $n_t$, rk and $TDD_a$ for every iteration across all regions (Figure 4-5). Overall, the changes in $n_f$ and FDDa resulted in the smallest number of observations (76 and 75 %) within 1 °C of the original TTOP value, while change in nt, rk, and $TDD_a$ has the greatest number of observations (86 %). Unsurprisingly, the greatest percentage change resulted in the greatest difference in predicted TTOP resulting in the largest percentage of observations with a difference of at least 1 °C from the reference value for all parameters.

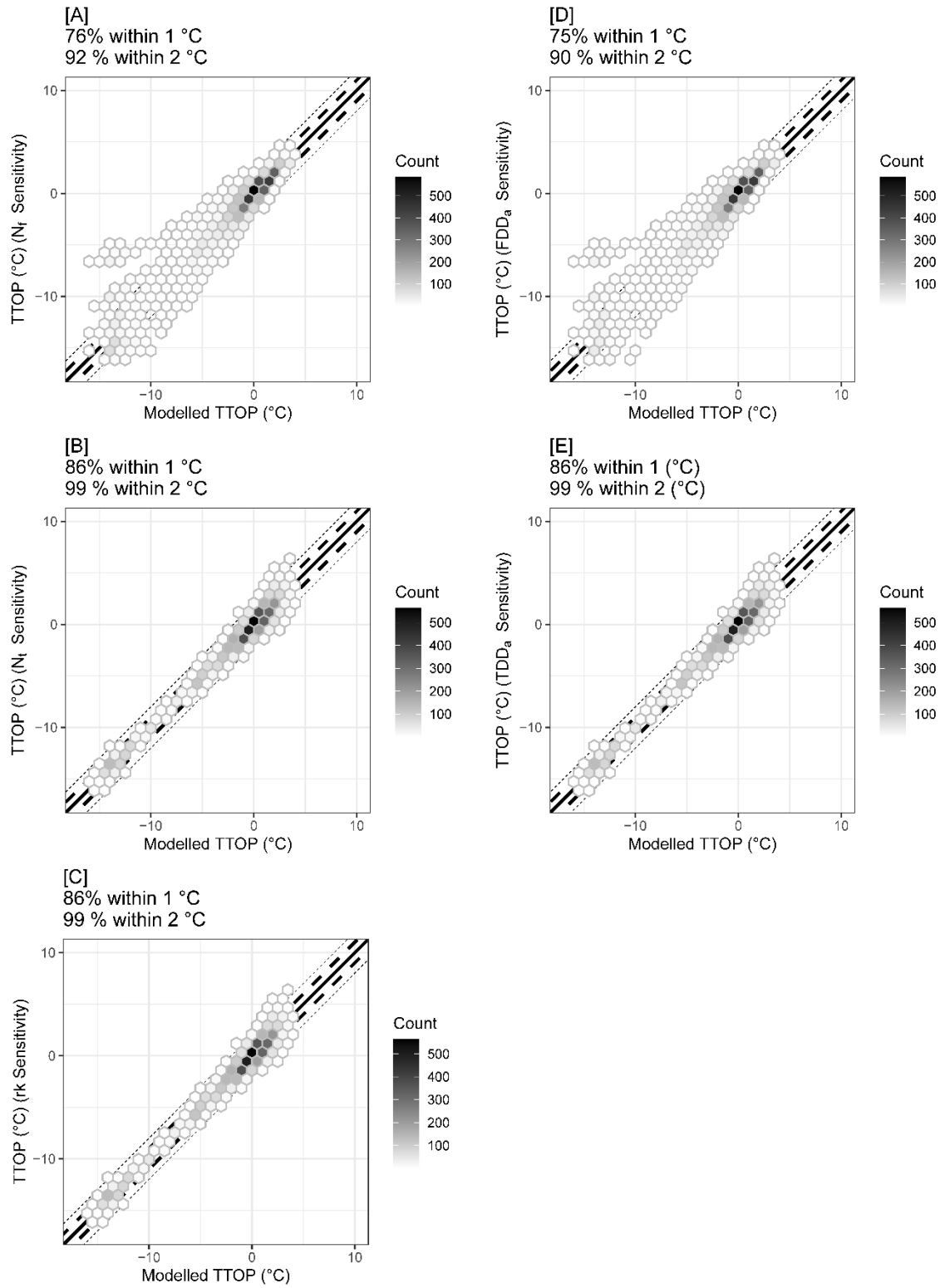


**Figure 4-5.** Reference temperature at top of permafrost (TTOP) model values compared to perturbed TTOP model values for the addition and subtraction of 5%, 10%, 25%, and 50% of the measured parameter value for [A] $n_f$, [B] $FDD_a$, [C] $n_t$, [D] $TDD_a$, and [E] rk. Large dashes indicate a ± 1 °C difference while small dashes indicated a ± 2 °C difference.

Locations with the coldest permafrost showed a greater response to changes in winter parameters ($n_f$ and FDDa) and minimal response to changes in summer parameters (nt) and the thermal conductivity (rk) with most sample points remaining within 1 °C of the reference value despite changes in these parameters by up to 50 %. At individual sites, the sensitivity of the TTOP model varied by parameter and region with the maximum and minimum overall discrepancies found in the High Arctic, Mackenzie Valley, and Central Northwest Yukon.

While the sensitivity was often proportional to the value of the measured parameter (i.e., a higher value will result in a greater discrepancy as the percentage change will be larger in magnitude), the observation with the highest and lowest differences were not always those with the highest and lowest value for that parameter. For example, the High Arctic sites had the highest measured $n_t$ values yet some of the smallest responses to changes in $n_t$ despite the larger magnitude of change compared to other regions. The largest difference between the reference and perturbed TTOP for $n_f$ and $FDD_a$ (9.0 °C) was found in the High Arctic altering the measured values by 50 %. For $n_t$, rk, and $TDD_a$ the greatest difference was observed in the Central Northwest Yukon (3.2 °C) again altering the measured values by 50 %. The smallest difference for changes in $n_f$ and $FDD_a$ was observed in the Mackenzie Valley (0 °C) across all iterations, as the $n_f$ value was zero. Similarly, at one site in the High Arctic region, a $n_t$ of zero also resulted in the smallest difference (0 °C) across all iterations for $n_t$, rk, and $TDD_a$.

Regionally, there was a difference in the most sensitive parameters by latitude with the High Arctic showing the greatest sensitivity to changes in the winter parameters, $n_f$ and $FDD_a$ (2.3 and 3.2 °C, respectively) and the least sensitivity to the summer parameters, $n_t$, rk, and $TDD_a$ (0.3 °C difference). Conversely, the southernmost region, Southern Yukon Northern BC

showed the greatest sensitivity to changes in the summer parameters (0.6 °C) and the least sensitivity to changes in the winter parameters (0.3 °C) (Figure 4-6).

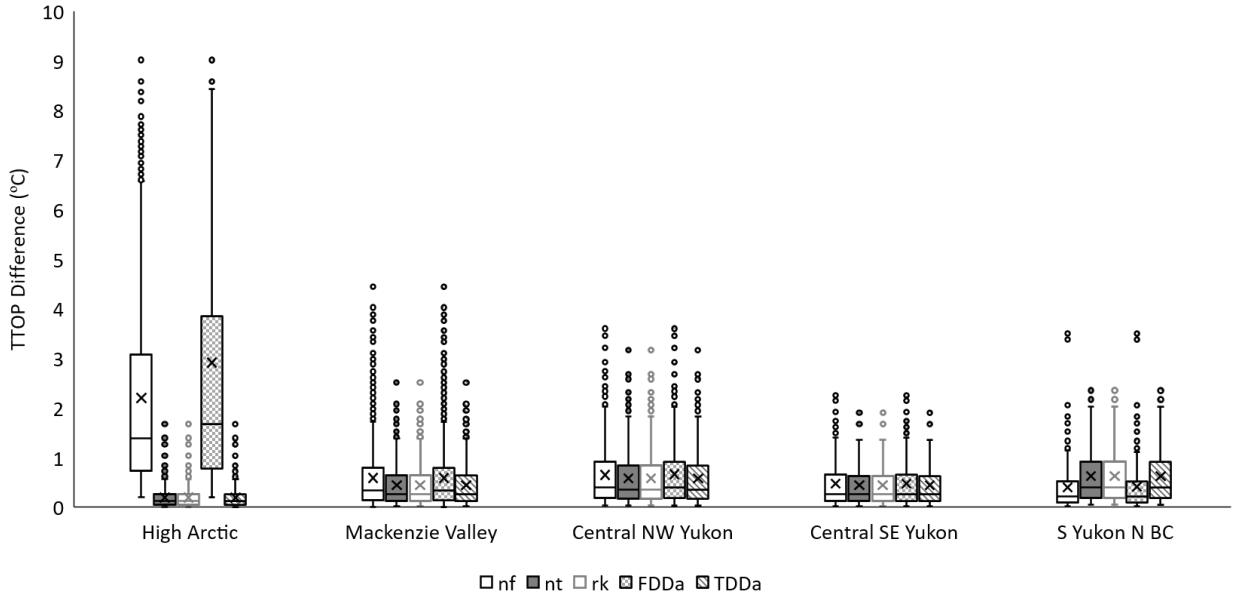


**Figure 4-6.** Boxplots for the regional absolute difference between the reference TTOP and the TTOP calculated when parameters were increased or decreased by a percentage.

Looking at each region individually, the High Arctic showed the greatest sensitivity to changes in $n_f$ and $FDD_a$ with 64 % of perturbed TTOP having a greater than 1 °C difference from the reference value. The High Arctic also showed the least sensitivity to changes in $n_t$, rk and $TDD_a$ with only 2 % of observations changing by more than 1 °C. Likewise, the Mackenzie Valley also showed the same sensitivity pattern (greatest for $n_f$ and $FDD_a$, least for $n_t$, rk, and $TDD_a$), albeit with much less variation (average difference of 0.6 and 0.4 °C, respectively). The Central Northwest and Southeast Yukon also displayed the same sensitivity. Only in the Southern Yukon Northern BC region was sensitivity greater for the summer parameters (0.6 °C and 23 %) compared to the winter parameters (0.4 °C and 7 %).

4.5.1.4 Summary of TTOP Model Sensitivity

Across all methods of testing TTOP model sensitivity, several patterns were observed for the sensitivity of the TTOP model to changes in specific parameters overall and regionally. Overall, based on the number of observations remaining within 1 and 2 ºC from the reference value, the model was most sensitive to changes in $n_f$ followed by $FDD_a$, while the model was least sensitive to changes in rk (Figure 4-7). Based on average difference between the perturbed and reference, TTOP the model across all observations and regions was most sensitive to changes in $n_f$, with an average difference of 1.9 °C from the reference TTOP value followed by $FDD_a$ (1.4 °C), $TDD_a$, (1.0 ºC), $n_t$ (1.0 °C), and rk (0.7 ºC). For every sensitivity trial, the model was most sensitive to changes in the freezing parameters, $n_f$ (Trials 1-3) and $FDD_a$ (Trial 2 and 4). For all but one trial, the model was least sensitive to changes in the thawing parameters, $n_t$ (Trial 2), rk (Trials 1-2) and $TDD_a$ (Trials 2 and 4). The only trial for which the model was least sensitive to a freezing parameter $FDD_a$ was Trial 3 (assigned fixed change) and some potential explanations for this will be discussed in the supplemental section (S4). Additional figures for Trials 1 and 2, and results for Trails 3 and 4 are also presented in the supplemental section for this chapter.

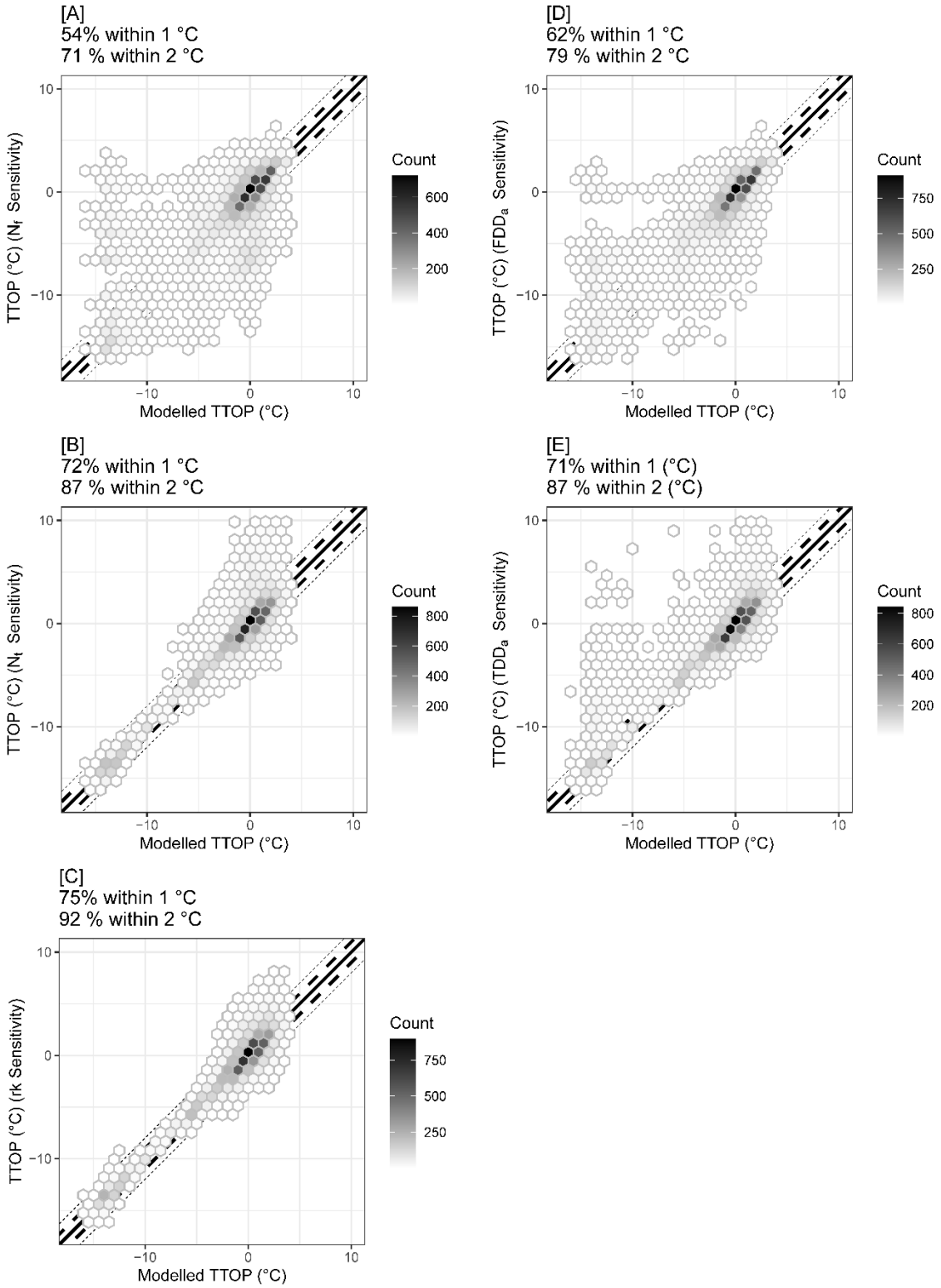


**Figure 4-7.** Reference temperature at top of permafrost (TTOP) model values compared to perturbed TTOP model values for all TTOP sensitivity trials for [A] $n_f$, [B] $FDD_a$, [C] $n_t$, [D] $TDD_a$, and [E] rk. Large dashes indicate a ± 1 °C difference while small dashes indicated a ± 2 °C difference.

Regionally the sensitivity of the model varied with the freezing parameters shown to cause the greatest discrepancy between the reference and perturbed TTOP values at the more northern regions and a general increase in the impact of the changes to the thawing parameters moving south (Figure 4-8).

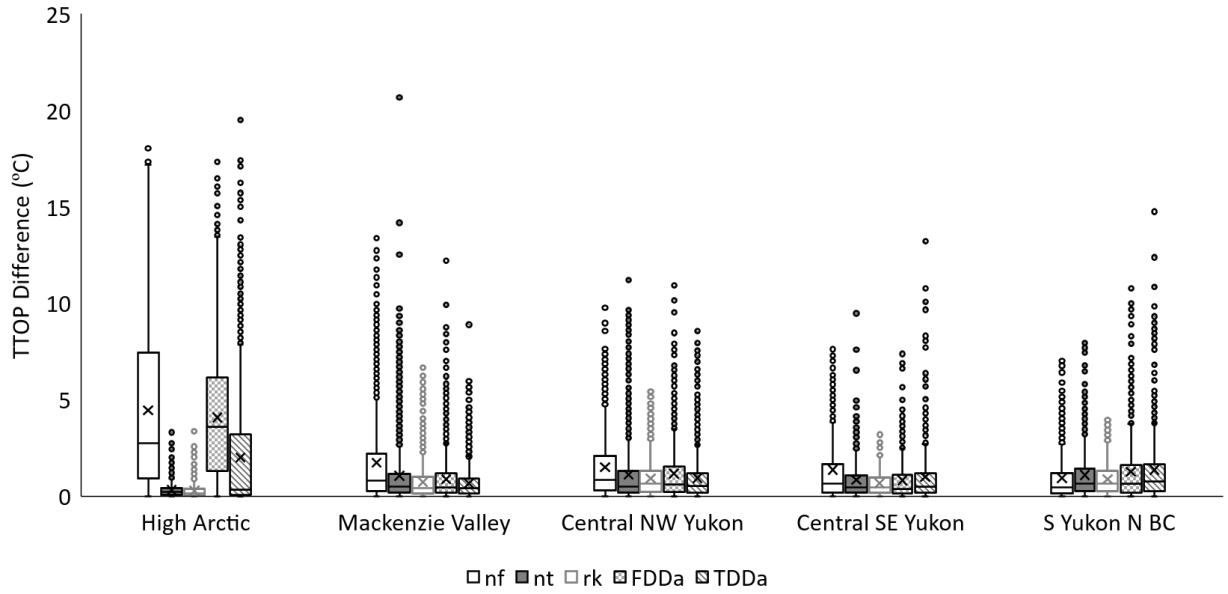


**Figure 4-8.** Boxplots for the regional absolute difference between the reference TTOP and the TTOP calculated when parameters were increased or decreased by an assigned amount.

The High Arctic was shown to be the most sensitive to changes in $n_f$ as it resulted in the largest response in all but one of the trials (Trial 4), and the least sensitivity to changes in rk and $n_t$ as they resulted in the smallest response across all trials. $FDD_a$ showed the greatest average magnitude of change in TTOP for the four trials followed closely by $n_f$ in the High Arctic, while rk and $n_t$ showed the lowest. Similar to the High Arctic, the freezing parameters resulted in the greatest difference in TTOP for the Mackenzie Valley, with $n_f$ showing the greatest sensitivity for three trials and $FDD_a$ for one. There was more variability in the parameter with the least sensitivity for the Mackenzie Valley with $TDD_a$ (Trial 2 and 4), $FDD_a$ (Trial 3), and rk (Trial 1 and 2) as the least sensitive parameter for at least one trial. However, the TTOP model was least

sensitive generally to changes in the thawing parameters in the Mackenzie Valley. For every trial the TTOP model for Central Northwest Yukon was most sensitive to changes in the freezing parameters, $n_f$ (Trials 1-3) and $FDD_a$ (Trials 2 and 4) and overall showed the greatest magnitude of change for variations in $n_f$. For this region the parameter which resulted in the lowest discrepancy from the reference TTOP value for all but one trial was a thawing parameter, $TDD_a$ (Trials 2, 3, and 4) and rk (Trial 1 and 2). The model was the least sensitive to changes in $FDD_a$ once (Trial 3). In Central Southeast Yukon, the TTOP model had the greatest response to changes in, $n_f$ (Trials 1-3) and $FDD_a$ (Trial 2 and 4). However, there was an increased response to changes in $TDD_a$ for this region compared to the previous three more northern regions. In this region, the model showed the least sensitivity to a variety of parameters, with $FDD_a$, $n_f$, and $TDD_a$, $n_t$, and rk as the least sensitive parameter in at least one trial. This is also shown in the average magnitude of difference with the greatest average difference between the perturbed and reference TTOP resulting from changes in $n_f$ followed by $TDD_a$. Lastly, Southern Yukon Northern BC was the only region for which the TTOP model for every trial was least sensitive to changes in the freezing parameters, $n_f$ (Trials 2, 3, and 4) and $FDD_a$ (Trials 2-3). This region also showed the greatest variability in the parameter with the greatest sensitivity, with $TDD_a$ and $FDD_a$ the most frequent (Trials 2-3 for $TDD_a$ and 1 and 4 for $FDD_a$) followed by $n_t$ and rk (Trial 2). This was the only region for which the model was most sensitive to changes a parameter other than $n_f$ for at least one trial.

### *4.5.2 Random Forest*

#### 4.5.2.1 Summary of Input Parameters

A wide range of ground temperature conditions and climatological parameter values across the four study regions were used in both the testing and training of the random forest (Figure 4-9).

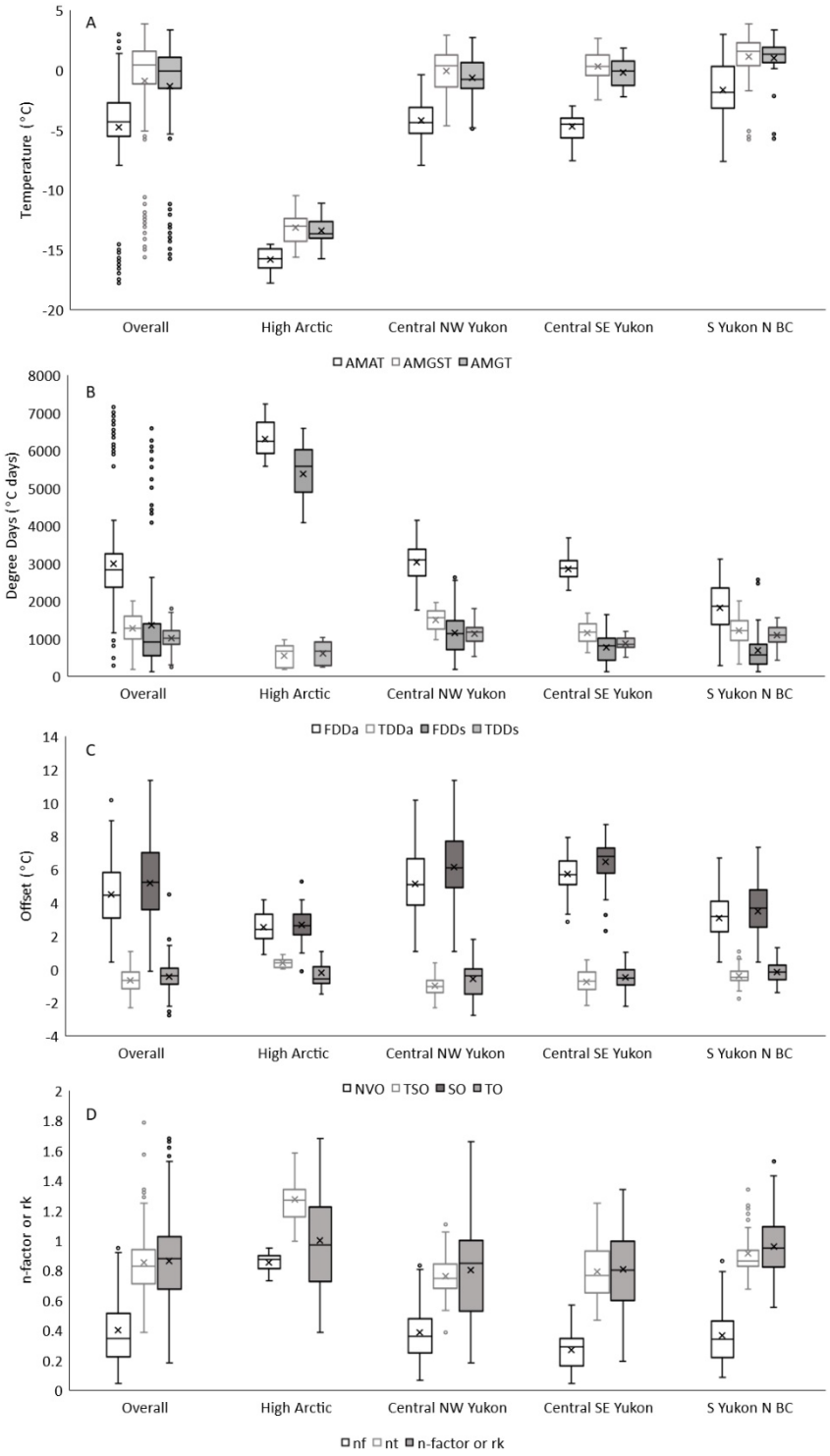


**Figure 4-9.** Overall and regional boxplots for A) annual mean air temperature (AMAT), annual mean ground surface temperature (AMGST) and annual mean ground temperature (AMGT), B) freezing degree day for air ($FDD_a$) and ground surface ($FDD_s$) and thawing degree days for air ($TDD_a$) and ground surface ($TDD_s$), C) Nival offset (NVO), thawing surface offset (TSO), surface offset (SO) and thermal offset (TO), and D) $n_f$, $n_t$, and rk.

Parameter values for the High Arctic region sites showed the greatest difference from the remaining regions and had the lowest number of both training and testing points. By comparison, the remaining three regions had relatively similar values across all parameters and a substantially higher number of both training and testing points. For each region, the relative proportion of training and testing data remained about the same (~ 60 and 40%, respectively). The average values for each parameter in both the testing and training data remained similar overall and within each region for both random forest datasets (individual years and site averages).

A few interesting observations became apparent through the data. First, rk values greater than 1 were calculated, indicating higher thermal conductivity during the thawing season than the freezing season. For 68 individual years and 23 site averages in all regions, rk values were greater than 1.0 were observed with a maximum rk of 1.7. The second observation was the presence of positive thermal offsets (TO) indicating warmer annual average temperatures in the ground at depth than those in the ground surface (AMGT > AMGST). This was also observed in all regions and for 62 individual years and 19 site averages. A majority of sites with positive TOs also had an rk value greater than 1. Most of these sites have rocky or bedrock substrate with limited vegetation cover and soil moisture, which may contribute to these phenomena.

#### 4.5.2.2 Random Forest Variable Importance

For the random forest iterations, using all of the variables and only the TTOP model parameters for the entire dataset and those for individual regions a number of parameters were consistently ranked as the most and least important by virtue of the percent increase in MSE (Figure 4-10). When all variables for the entire dataset were used, TO and the freezing and annual parameters in both the air and the ground surface were deemed to be the most important. The least important were the thawing parameters. Looking at the individual regions, freezing

parameters were most important in the High Arctic and the importance of annual and thawing parameters increased moving south. The least important parameters were more variable between regions but generally consisted of the thawing parameters.

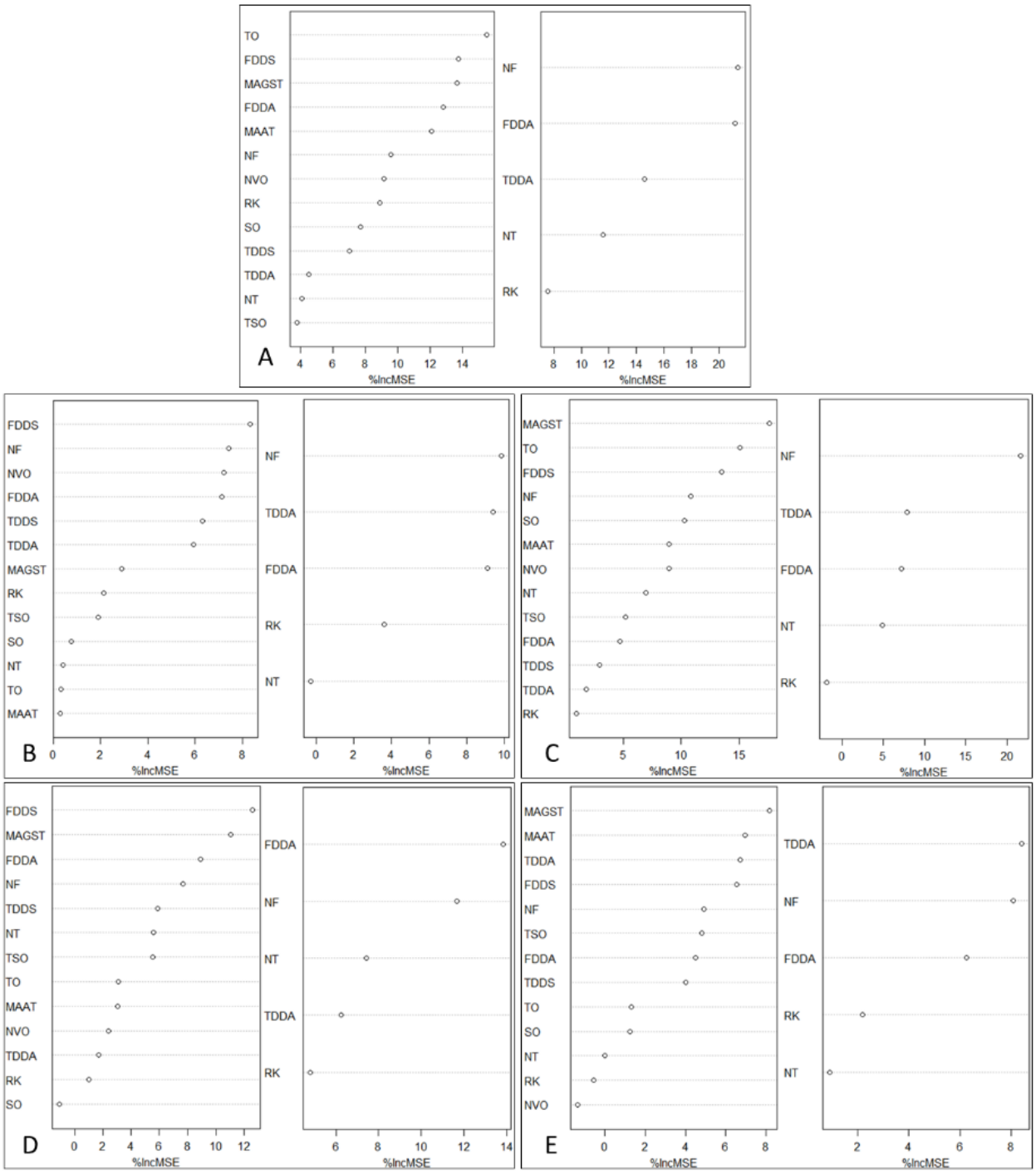


**Figure 4-10.** Variable importance plots for random forest models run using all of the variables or only parameters used in the standard form of the TTOP model for A) the entire dataset, B) High Arctic, C) Central Northwest Yukon, D) Central Southeast Yukon and E) Southern Yukon Northern BC.

When using only the TTOP model parameters, $n_f$ and $FDD_a$ were ranked as the most important for the total dataset, while $n_t$ and rk were ranked as the least important. Regionally $n_f$ was the second most important parameter for three regions and the most important parameter for the Central Northwest Yukon. Surprisingly, $TDD_a$ was ranked as the most important parameter for the High Arctic, although there was little difference in the increased MSE between the top three. $TDD_a$ was also deemed the most important parameter in the Southern Yukon Northern BC region. Finally, $FDD_a$ was the most important parameter in the Central Southeast Yukon. The $n_t$ and rk parameters were least important in three of the four regions with rk being the second most important parameter in the Central Northwest Yukon and $n_t$ the third in the Central Southeast Yukon. Overall, the variable importance rankings once again highlight the importance of freezing season conditions compared the thawing.

### *4.5.3 Random Forest Variable Importance Rankings Compared to TTOP Sensitivity Results*

Although the variable importance conclusions from the TTOP sensitivity and random forest using only the TTOP parameters did not match perfectly, there were still common findings of the importance of certain parameters. Using the entire dataset both the TTOP sensitivity results and the random forest have the same general ranking of variable importance with $n_f$, $FDD_a$, and $TDD_a$ as the most important. Additionally, the TTOP sensitivity and random forest rank rk as the least important parameter. Regionally, there were more prominent differences in the variable importance rankings. For the High Arctic, the TTOP sensitivity and random forest both ranked $n_f$ as the most important parameter. However, the in TTOP sensitivity analysis $FDD_a$ is ranked as the second most important parameter (followed by $TDD_a$), while the random forest $TDD_a$ is ranked as the second most important variable (followed by $FDD_a$). However, compared to the other northern regions $TDD_a$ was disproportionately important in the High Arctic in the

sensitivity analysis as well. Additionally, $n_f$, FDDa, and $TDD_a$ had similar percent increases in MSE. In both, rk was the second least important followed by $n_t$. In the Central Northwest Yukon, both ranked $n_f$ as the most important variable. However, $TDD_a$ was ranked as the second most important in the random forest but the second to least most important in the TTOP sensitivity analysis. In the Central Southeast Yukon and Southern Yukon Northern BC, both methods showed the increasing importance of the thawing parameters. Both methods captured trends in the overall and regional differences in parameter importance.

*4.5.4. TTOP Model Performance*

The TTOP model performed well compared to the measured AMGT overall with and RMSE of 0.2 ºC. However, there were regional differences in the model performance (Figure 4-11). Generally, the model produced lower errors in the northern regions with RMSEs of 0.1 and Central NW Yukon, respectively. RMSE was highest for the High Arctic (0.6 ºC) and the southern regions, Central SE Yukon (0.2 ºC) and Southern Yukon Northern BC (0.2 ºC). However, in the High Arctic only 7 out of 22 observations contributed to the high RMSE as when these were removed, the RMSE dropped to 0.1 ºC. The lowest absolute difference between the measured and modelled ground temperature was in the Central NW Yukon (0.0 ºC). The highest absolute difference between the measured and modeled ground temperatures occurred in the High Arctic (1.4 ºC) and the Southern Yukon Northern BC (1.1 ºC). These regions also had large ranges of absolute differences between the modelled and measured ground temperature showing the variability of model performance between sites. Again, if the 7 observations were removed the largest absolute difference in the High Arctic is reduced to (0.1 ºC). These regions also had large ranges of absolute differences between the modelled and measured ground temperature showing the variability of model performance between sites.

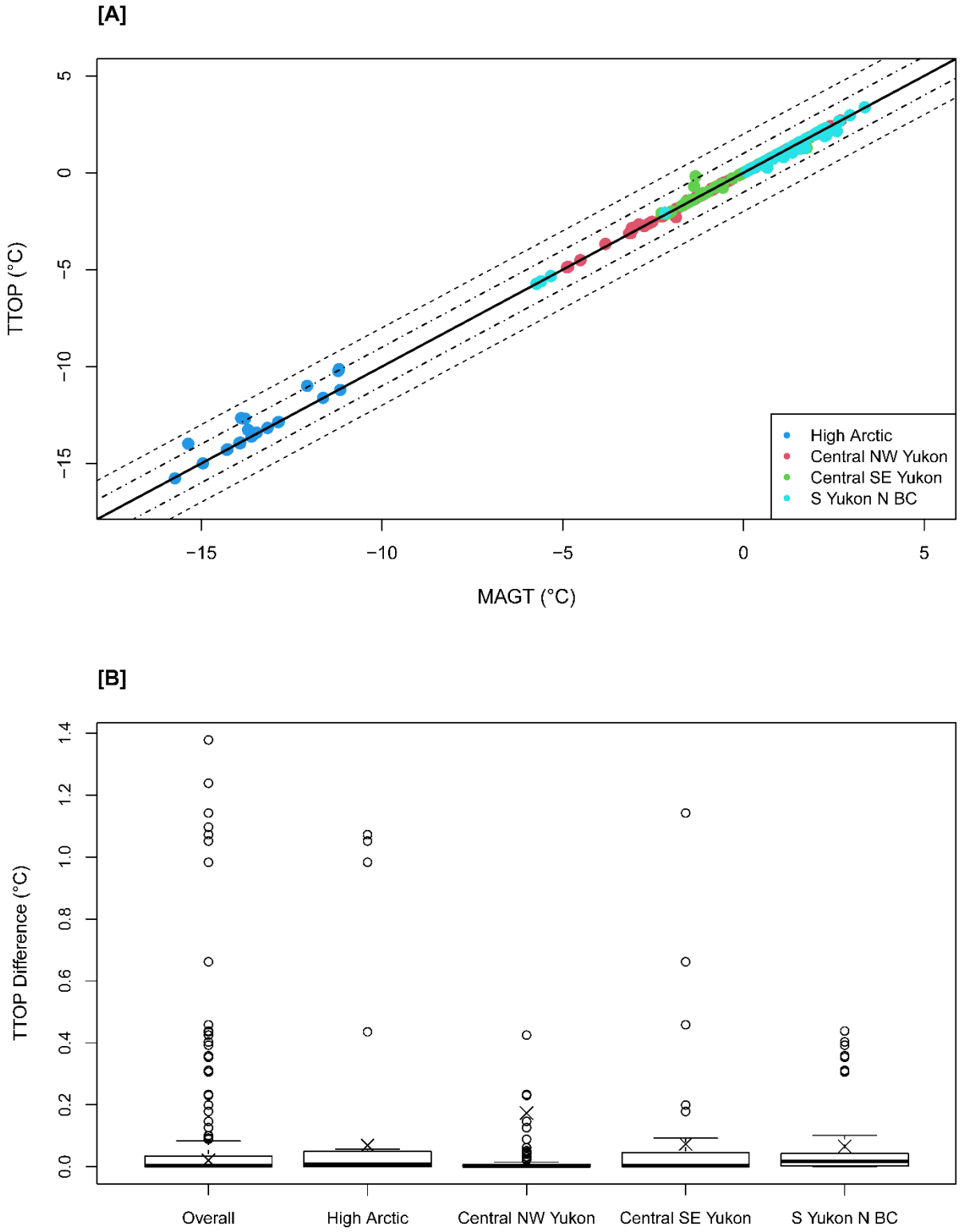


**Figure 4-11.** A) Comparison of TTOP model outputs to the measured annual mean ground temperature (AMGT) and B) boxplots for the absolute difference between the modelled TTOP and the measured AMGT across the entire study area and for individual regions.

## 4.6 Discussion

### *4.6.1 TTOP Sensitivity*

#### 4.6.1.1 Advantages and Disadvantages of Each TTOP Sensitivity Testing Method

Each method used to test the TTOP model sensitivity to changes in parameter values had advantages and disadvantages, which may influence the relative response of the model and the interpretation of the results. For Trial 1 no capping was required for any parameter as the percentile values which were directly substituted were all measured parameter values and therefore realistic. Since there was no capping, none of the model sensitivity results were artificially limited, reducing the apparent sensitivity to the capped parameters. Additionally, this method allows for a direct comparison of sensitivity to each parameter across regions as the parameters at all sites were changed to the same value. The main disadvantage of this sensitivity testing method is that the values of the percentile are directly dependent on the range and spread of the data. As a result, the direct comparison of parameter sensitivity may not be possible, the step change for the individual observations were not the same. Therefore, the corresponding difference in the perturbed and reference TTOP may be higher for one parameter due to a larger change in value rather than an increased model sensitivity. However, this is likely not the case for this analysis as each TTOP model parameter had a large range of values since sites from a wide range of climatological and environmental conditions were sampled. Additionally, this method does not allow for the direct comparison of sensitivity for each individual percentile change within a parameter, as the magnitude of change will be different depending on the initial value. For example, the model will show less sensitivity to a change to the $95^{th}$ percentile of $n_t$ in the High Arctic than in the Mackenzie Valley since the initial $n_t$ value in the High Arctic is likely to be closer to the new perturbed value.

Moving to Trial 2, one advantage of this trial's method (changing each parameter by a percentage of the original value) was the limited amount of capping required as only $n_f$ values needed to be restricted to remain below 1.0. Once again, this limits the possibility of artificially reducing the model's overall sensitivity to changes in this parameter. This was observed for this trial as the average difference between the perturbed and reference TTOP was 0.2 ºC higher for $FDD_a$ than $n_f$ for + 25% and 0.5 ºC higher for + 50% solely due to the capping of $n_f$ rather than an increased sensitivity to changes in $FDD_a$. Additionally, the changes applied for this trial were not dependent on the range of parameter values in the dataset. However, one major limitation of this method is since the perturbed value is based on the initial measured parameter value, certain parameters overall and at individual sites or regions may change more than others might. For example, a higher $n_f$ value would have a larger absolute magnitude change than a lower $n_f$ if reduced or increased by 5% of the initial value. This may result in a perceived increase in sensitivity for sites, regions, or parameter with larger starting values. However, despite this, it is not always the case as the High Arctic region had the highest average $n_t$ values, but the model still showed a lower response to changes in this parameter than other regions. Another disadvantage of this method originates from the nature of the TTOP model whereby changing one parameter by a percentage results in the same percentage change across the other multiplicative factors (i.e. changing $n_f$ by 5% changes the entire $n_f$*$FDD_a$ term by 5 percent). This can mask the sensitivity of the model to changes in individual parameters, but the overall sensitivity to the specific parameter groupings can still be determined.

#### 4.6.1.2 Overall and Regional TTOP Model Parameter Sensitivity

The sensitivity of the TTOP model to changes in specific parameters was dependent on the structure of the model and the values of the parameters. The model across all regions was

most sensitive to changes in $FDD_a$ and $n_f$, due to the higher number of $FDD_a$, which amplified the response to changes in these parameters. Regionally, the sensitivity of the model to changes in the thawing parameters, especially $TDD_a$ and $n_t$ increased moving south following a reduction in the difference between $FDD_a$ and $TDD_a$. The exception to this was the High Arctic, where the model was disproportionately sensitive to changes in $TDD_a$ compared to the other northern regions. The sensitivity to $TDD_a$ was also inordinately high given the large contrast in the number of $FDD_a$ and $TDD_a$ in this region (up to 5 times higher $FDD_a$ than $TDD_a$). The increased sensitivity to changes in $TDD_a$ likely results from the high values of $n_t$ and rk, with a majority of values approaching or exceeding 1.0. As a result, changes in $TDD_a$, which were then multiplied by $n_t$ an rk, were amplified in this region. This also highlights the vulnerability of this region to changes in climate.

The Southern Yukon Northern BC was the only region in which the model showed greater sensitivity to changes in $n_t$ than $n_f$. This results from the similar number of $FDD_a$ and $TDD_a$ in this region, which contributed to the comparable sensitivity for both N-factors. Additionally, the importance of $n_t$ was elevated above $n_f$ due to the higher $n_t$ values in this region. The sensitivity results of this study the importance of depends on accurate characterization of all input parameters to determine representative model response. This characterization may not be possible using theoretical data alone, highlighting the importance of utilizing measured field data in these types of studies.

### *4.6.2 Random Forest Variable Importance Ranking*

#### 4.6.2.1 Uncertainty in Variable Importance Rankings

Although random forest is able to cope with highly correlated variables for prediction (Boulesteix et al., 2012), there is conflicted conclusions on the reliability of variable importance

rankings (Strobl & Zeileis, 2008; Nicodemus et al., 2010; Tolosi & Lengauer, 2011; Gregorutti et al., 2017). For this study, a majority of the input parameters are highly correlated with at least one other parameter, which may lead the variable importance rankings to be unreliable. Additionally, although the random forest model using all of the variables performed relatively well (RMSE 0.54 % Variance explained 98%), the regional models using all of the variables had considerably lower percentages of variance explained (70 - 81 %) even though RMSE remained similar (0.5 – 0.7 °C). This may potentially impact the reliability of the variable importance rankings for these models, as they may not be accurately predicting ground temperature. When only using the TTOP model parameters the RMSE and percentage of variance explained decreased overall and in each individual region. Despite the possible errors and uncertainty in the results of this, the variable importance analysis generally agreed with the results of the TTOP sensitivity analysis and matched findings from previous studies.

#### 4.6.2.2 Overall and Regional Variable Importance Rankings

The variable importance rankings for the overall and regional datasets were a product of differences in values of the measured field inputs. When all variables were used TO was ranked as the most important parameter, but it was only ranked as an important parameter regionally in the Central NW Yukon. The high ranking of this parameter overall may result from the high number of sites in the Central NW Yukon, elevating its importance for the entire dataset. Additionally, TO had lower correlation than the other parameters, which may have artificially elevated its importance. AMGST was also ranked as important overall and for all regions except for the High Arctic. This may have resulted from the greater importance of annual parameters in regions where the number of freezing and thawing degree days in the air and ground surface were similar. As a result, the importance of AMGST in the High Arctic, where the number of

freezing degree days are substantially higher than the thawing degree days, is reduced.

Differences in variable importance ranking for the TTOP model parameters between the TTOP sensitivity analysis and the random forest may have resulted from the calculation method and the desired output. As the TTOP model utilized multiplicative factors, the importance of the parameters was elevated by nature of the model equation. The random forest variable importance ranking did not utilize this equation. As a result, the importance of parameters was potentially difference based on the predictive method alone. Additionally, the TTOP model sensitivity analysis was determined through perturbation of the model parameters, thereby ranking the parameters importance based on the response. Contrastingly, the random forest variable importance ranking was determined based on the current thermal conditions. This may also have resulted in some discrepancy in the rankings. Finally, the TTOP sensitivity analysis used calculated TTOP based on the unperturbed measured parameters, while the random forest variable importance ranking used AMGT as the dependent variable. This difference in output variable may also have contributed to some of the discrepancy. However, overall both methods showed similar rankings and trends.

### *4.6.3 Comparison to Other Variable Importance Studies*

#### 4.6.3.1 TTOP Model Parameters

The results from the TTOP sensitivity analysis and random forest generally support the conclusions from previous studies regarding the overall and regional importance of specific TTOP model parameters and their sensitivity (Smith & Riseborough, 1996, 2002; Bevington & Lewkowicz, 2015; Way & Lewkowicz, 2018). First, the importance of $n_f$, $n_t$ and rk was thought to be relative to the magnitude of $FDD_a$ and $TDD_a$ with a greater importance of freezing parameters in locations with high $FDD_a$ and greater importance of the thawing parameters with

high $TDD_a$ (Smith & Riseborough, 2002). The results of this analysis support this, showing increased sensitivity to changes in $n_f$ corresponding to higher numbers of $FDD_a$ and increased sensitivity to changes in $n_t$ and rk with higher $TDD_a$. Generally, these followed a latitudinal trend with the exception of the Central Southeast Yukon which showed lower sensitivity to changes in $n_t$ despite being farther south than the Central Northwest Yukon sites. However, this region also has a lower number of $TDD_a$ than the Central Northwest Yukon despite being farther south, likely due to increased elevation. Similarly, in parts of Yukon and Northern BC, the TTOP model was found to be more sensitive to change in $n_f$ than $n_t$ due to higher numbers of $FDD_a$ compared to $TDD_a$ (Bevington & Lewkowicz, 2015). The same relation was observed in Labrador and Ungava (Way & Lewkowicz, 2018). This was supported by the results of this study except in the Southern Yukon Northern BC region where the model was more sensitive to changes in $n_t$. This may result from the similar number of both freezing and thawing degree-days in this region coupled with high $n_t$ values and low $n_f$ values, which may have been disproportionately prone to capping at zero. Additionally, for this study the range of $n_t$ was larger than that of $n_f$, differing from the previous study, potentially resulting in greater changes to $n_t$ even for methods, which did not require capping (Bevington & Lewkowicz, 2015).

Regionally, previous studies noted that $n_f$ and rk were a more important influence on TTOP than $n_t$ (Smith & Riseborough, 1996, 2002). This was partially supported by the findings of this study; there was greater sensitivity to $n_f$ than $n_t$ overall and in all regions except the Southern Yukon Northern BC (for reasons discussed previously). However, the model was only slightly more sensitive to changes $n_t$ than rk showing only moderate sensitivity to both parameters similar to a previous sensitivity study in the area (Bevington & Lewkowicz, 2015). Additionally, as reported in previous studies, in regions with high $FDD_a$ and low $TDD_a$ the model

was more sensitive to changes in $n_f$ than rk, as evident in the High Arctic region (Smith & Riseborough, 1996, 2002). However, in both the TTOP model and the random forest, the sensitivity to and importance of $TDD_a$ was disproportionately high in the High Arctic compared to the other regions. This is likely due to the lack of vegetation in this region increasing the importance and influence of MAAT on the ground thermal regime compared to other regions with more well developed surface cover (Shur & Jorgenson, 2007). Lastly, in this study, the TTOP model was shown to be more sensitive to changes in $FDD_a$ compared to $TDD_a$ overall and in every region except the Central Southeast Yukon, contradicting previous conclusions (Bevington & Lewkowicz, 2015). This potential discrepancy may have resulted from the limited number of regions in Yukon sampled with only sites in Atlin, Dawson, and Whitehorse used in the previous study. In the Central Southeast Yukon, the number of freezing and thawing degree days were relatively similar, which coupled with the low $n_f$ values, dampened in impact of $FDD_a$ while high $n_t$ values strengthened the impact of $TDD_a$. This likely resulted in an increased sensitivity to changes in $TDD_a$ similar to the previous findings (Bevington & Lewkowicz, 2015).

Finally, when comparing permafrost to seasonal frost environments, FDD has been show as the most important predictor of MAGT in permafrost terrain, while TDD was most important for seasonal frost environments, with soil properties having a minimal impact in both environments (Karjalainen et al., 2019). The minimal importance of soil properties in both permafrost and seasonal frost was supported, as there was limited sensitivity to rk overall and in the individual regions. Additionally, for this study, while the sensitivity to $TDD_a$ was high for the two southern regions, $FDD_a$ still had larger response than $TDD_a$ even in the southernmost region. This may be a product of combining both permafrost and seasonal frost sites into the sensitivity analysis, which does not allow for comparison and potentially dampens the sensitivity produced

by one or the other. This may also be a product of sites not located far enough within the seasonal frost zone for the importance of $TDD_a$ to become apparent as sites sampled in the previous study were well outside of the permafrost margins (Karjalainen et al., 2019).

#### 4.6.3.2 All Parameters

In addition to the TTOP model parameters discussed above, three other variables were regularly ranked as important according to the random forest. TO has previously been suggested as the most important parameter for determining the southern extent of permafrost as a high TO can protect permafrost from warmer air temperatures (Smith & Riseborough, 2002). NVO has also been shown to be an important parameter, determining the northern limit of discontinuous permafrost (Smith & Riseborough, 2002). For the random forest run using the entire dataset, TO was ranked as the most important variable while NVO was the most important variable in the High Arctic. The higher ranking of TO was likely due to the location of sample points with a majority located farther south closer to the southern extent of permafrost. Similarly, the importance of NVO only in the High Arctic may be a product of the limited number of sample points near the northern limit of discontinuous permafrost. Both overall and regionally, MAGST was deemed an important variable for accurate predictions of MAGT. This is also supported by previous studies, which highlighted the reliability of using MAGST as a proxy for the thermal state of permafrost (Luo et al., 2019). Overall, the findings of this study generally supported those of the previous literature despite the use of field data and the increased range of climatological and ecological conditions sampled. Understanding the relative importance and sensitivity of different TTOP model parameters regionally may help guide the allocation of effort to parameter classification and assess locations of potential increased errors in previous model predictions.

*4.6.4 Parameter Classification Recommendations and Sources of Uncertainty*

Since the TTOP model was deemed more sensitive to certain model parameters overall and in certain regions, accurate parameterization of the most important variables for the study location is vital. Overall, the freezing season parameters were deemed the most important generally; therefore, accurate characterization is essential to correct predictions of MAGT at national or small scales. For the air temperature parameters, this would entail utilizing climate data that are more representative of freezing conditions than thawing. As such, simply using a MAAT, which is similar to the climate normal, may yield errors in the predicted MAGT, as years with an abnormally warm freezing season paired with an abnormally cool thawing season may have a representative MAAT but not $FDD_a$. Additionally, $n_f$ is typically the most difficult to parameterize since it is dependent on a wide range of conditions including timing, depth, and morphology of snow and surface soil moisture and is not necessarily transferable between regions (Smith & Riseborough, 2002; Zhang, 2005; Way & Lewkowicz, 2016). However, as outputs from the TTOP model showed sensitivity to changes in $n_f$ across all regions studied, increasing uncertainty in modelled MAGT may arise from incorrect parametrization.

Regionally, in locations where $FDD_a$ is much greater than $TDD_a$, the impact of incorrect classification of $n_t$, rk, and $TDD_a$ was shown to be minimal. Therefore, more general assumptions and classifications will not result in a substantial increase in uncertainty. Additionally, for these locations, using representative freezing conditions is more important than representative thawing or annual air temperatures. However, this is only applicable in locations where the magnitude of $FDD_a$ is considerably greater than $TDD_a$. Due to the importance of $TDD_a$ in locations of similar $FDD_a$ and $TDD_a$, the data record used should be typical for both freezing and thawing season air temperatures. In areas where $FDD_a >> TDD_a$, due to the elevated

importance of $n_f$, incorrect parameterization may result in cold bias if $n_f$ used values were higher than existing conditions or warm bias if values were lower (Obu et al., 2019). As $FDD_a$ and $TDD_a$ become more similar, generally at locations farther south, the sensitivity of the model to changes in thawing parameters is elevated and accurate classification of $n_t$ and rk become more important. For several continental and circumpolar modelling studies, a uniform value of 1.0 was utilized as the input for $n_t$ across the study area (Henry & Smith, 2001; Obu et al., 2019). While this assumption is unlikely to increase uncertainty in the High Arctic and more northern locations (where $FDD_a >> TDD_a$) it is likely to result in errors farther south in these MAGT maps. Additionally many mapping MAGT studies characterize rk-using vegetation, assigning values between 0.0 and 1.0 and may not adequately account for lower rk values due to organic material and soil moisture (Smith & Riseborough, 1996; Riseborough & Smith, 1998; Way & Lewkowicz, 2016; Obu et al., 2019; Garibaldi et al., 2021). Additionally, recent studies have shown rk values exceeding 1.0 (Bevington & Lewkowicz, 2015; Lin et al., 2015; Zou et al., 2017). Utilizing rk values lower than the existing conditions will result in a cold bias and overestimation of permafrost, while using rk values higher than existing conditions will result in a warm bias and an underestimation of permafrost (Obu et al., 2019). As misclassifying rk results in higher errors in locations where $TDD_a$ and $FDD_a$ are similar in magnitude, accurate parameterization at lower latitudes is essential. Conversely, when modelling High Arctic MAGT, the impact of inaccurate parameterization of rk is minimal, and therefore assumptions based on vegetation classes, or the use of uniform values is acceptable. Finally, the varying sensitivity of the TTOP model to specific parameters in different environments demonstrates the need for accurate parameterization and validation of TTOP model parameters to ensure valid outputs.

This highlights the need for in situ data parameter to increase the accuracy of future TTOP modelling studies to validate remotely derived parameter values.

### *4.6.5 Comparison of TTOP Model to Measured AMGT*

In this analysis, the TTOP model performed well resulting in minimal errors in predicted MAGT even in seasonal frost environments. The RMSE for the TTOP model for this study was generally lower than or similar to those from previous TTOP modelling studies in the same region (Obu et al., 2019; Garibaldi et al., 2021). This is likely a product of the use of directly measured and calculated input parameters rather than the characterization of parameters from environmental variables such as vegetation or spatial interpolation. This highlights the importance of in situ data for validation of parameters for accurate predictions of permafrost and ground temperatures.

The TTOP model performed best in the northern regions with relatively cold permafrost and performed worse in locations of warm, marginal permafrost or locations with seasonal frost. This is potentially due to the model's reduced performance at temperatures approaching 0 ºC, especially when a short temporal record is utilized (Riseborough, 2007). Additionally, this increase in error may result from disequilibrium of permafrost and climate. In these more southern regions, the permafrost is more likely to be ecosystem protected and less reliant on the climate to persist and may be out of equilibrium with the current climate (Shur & Jorgenson, 2007). As a result, while the climate may be suitable only for seasonal frost, permafrost may be present due to the protection of the vegetation, usually mature forest with thick moss or organic layers (Shur & Jorgenson, 2007). As the TTOP model assumes equilibrium conditions and is primarily driven by climate inputs, it likely predicts the ground thermal regime incorrectly in these types of locations (Vegter, 2023). Additionally, as the model was run using individual

years, errors may have resulted in the parameter value for the year that was not representative of the normal climate conditions (Riseborough, 2007).

Unexpectedly, the TTOP model did not perform well in the High Arctic for seven of the 22 observations. These observations were concentrated at five of the nine sites. Four of the sites were located at Cape Bounty and all of the large errors were from 2016-2017. At all of these sites, the AMGST during this year was substantially higher than those from the previous years. While the AMAT showed only a slight deviation, $n_f$ at these sites decreased substantially, indicating higher snow depths. As a result, the TTOP model parameters were out of equilibrium with TTOP for this year, yield a larger discrepancy.

*4.6.6 Thermal Offsets and rk*

Positive or reversed thermal offsets as well as calculated rk values greater than 1 (greater thermal conductivity in the unfrozen state than frozen) are not widely reported in North America, however have been observed at sites on the Qinghai-Tibet Plateau (Lin et al., 2015; Zou et al., 2017; Luo et al., 2018; Li et al., 2019). These sites usually have exceedingly dry fined grained material or unconsolidated bedrock material similar to the sites in this study with reversed thermal offsets and rk values greater than 1. It is hypothesized that this is a product of extremely dry sediment and a vapor deficit resulting in greater thermal conductivity in summer than in winter (Lin et al., 2015; Luo et al., 2018). In situ thermal conductivity measurements in this same region showed higher thermal conductivity in the unfrozen state for soils with a degree of saturation less than the critical point, while laboratory tests of four types of soil also showed greater unfrozen thermal conductivity than frozen for dry material (Kersten, 1949; Li et al., 2019). Greater thermal conductivities in the unfrozen state were also calculated for aridisols (dry arid ground) and entisols (unconsolidated bedrock) (Zou et al., 2017). The substrate and moisture

conditions from these sites are similar to those for this study. However, further investigation and validation of these calculated values is necessary.

### 4.7 Conclusion

The results of this analysis highlight the overall sensitivity of the TTOP model to changes in the freezing parameters ($n_f$ and $FDD_a$) compared to the response to changes in the thawing parameters ($n_t$, $TDD_a$, and rk). Across all sites, regions, and perturbation methods, the model was most sensitive to changes in $n_f$ with 49 % of TTOP outputs changing by at least 1 ºC from the original TTOP value followed by $FDD_a$ at 40 %. The model was least sensitive to changes in $TDD_a$ with only 28 % of TTOP model outputs exceeding 1 ºC difference from the reference TTOP value, followed by $n_t$ and rk at 35 %. Regionally, different sensitivity patterns emerged primarily showing the diminishing response to changes in $n_f$ and the increasing response to changes in $TDD_a$ moving south, although sensitivity to changes in $n_f$ remained high. The random forest variable importance rankings also highlighted the importance of the freezing parameters using both a wide variety of temperature parameters and only those used in the standard form of the TTOP model. The increasing importance of the thawing and annual parameters moving south was also shown. Although the random forest variable importance rankings did not perfectly match the TTOP sensitivity results, potentially due to high correlation between variables, it still captured similar regional trends in variable importance.

While the TTOP model performed well overall, there were regional differences in accuracy. The model most accurately predicted permafrost temperatures in regions of cold climate driven permafrost likely in equilibrium with the current climate due to relatively fast response times. The model did not perform well at southern locations in marginal permafrost or seasonal frost, where the ground temperature at depth was more influenced by surface and

subsurface characteristics and, as a result, may be out of equilibrium. However, even in these regions, the model still performed well in locations of limited vegetation cover. As a result, the TTOP model should be used with some discretion in areas of warm permafrost or seasonal frost, especially when covered by vegetation or organic material. Additionally results of circumpolar TTOP modelling studies are likely more inaccurate in these locations than those farther north.

The results of this study highlight the importance of correct parameterization, specifically of the freezing parameters in small-scale national or circumpolar modelling studies, and the increased importance of parameterization of the thawing parameters in locations where the magnitude of $FDD_a$ and $TDD_a$ are similar. Although these conclusions had been theorized previously the use of a robust network of in situ data to support these assumptions was necessary. Ultimately, the findings of this study help future modelling studies determine parametrization allocation effort based on location and scale and may help explain sources of error and uncertainty in modelled results.

# Chapter 5 Modelling air, ground surface and permafrost temperature variability across four dissimilar valleys, Yukon, Canada

**Authors:** Madeleine C. Garibaldi[1], Philip P. Bonnaventure[1], Nick C. Noad[1], Will Kochtitzky[2]

[1] Department of Geography and Environment, University of Lethbridge
[2] School of Marine and Environmental Programs, University of New England

**Key Words:** TTOP model, permafrost, Yukon, Surface Lapse Rate, Dempster Highway

## 5.1 Abstract

Spatial maps of the air and ground thermal regime were generated for four distinctively different Yukon valleys. The aim was to model the thermal regime (at fine spatial resolution) using locally measured inverted surface lapse rates (SLR), in order to better predict the elevation distribution of temperature. This provided a comparison to better ascertain uncertainty in a commonly used regional permafrost probability model, which utilizes general inversion assumptions and an inflection point at treeline, as well as models generated assuming no inversions. Overall, the permafrost probability in the regional model matched well with the local models where assumptions of treeline and inverted SLRs held true as permafrost was assumed to be present at high and low elevations. When normal surface lapse rates were assumed despite the presence of temperature inversions, permafrost presence was overestimated in each valley. This discrepancy was greatest at high elevations in the local models where permafrost was predicted to be the coldest and most widespread and at low elevations in the regional model where permafrost was predicted to be absent. However, the difference of this impact was dependent on surface and subsurface characteristics as valleys with higher snow cover, mature forest or thick organic layers showed a greater disassociation from the air temperature overall. Appropriate characterization of the SLR is essential for accurate predictions of the spatial distribution of the ground thermal regime and permafrost presence. These models also provide a starting point for

better predictions of warming with elevation in these valleys and other areas subject to inversions of similar magnitude.

## 5.2 Introduction

Mountain or alpine permafrost is classified as perennially frozen ground located in mountainous environments but absent from adjacent valleys and lowlands (French, 2008; Gruber & Haeberli, 2009). Permafrost here is especially spatially heterogeneous due to the extreme variability in surface and near surface characteristics, including incoming solar radiation, elevation, slope, snow cover, vegetation, and soil moisture (Gruber & Haeberli, 2009). Additionally, due to the wide variety of mountain range climatic characteristics, the dominant influence on mountain permafrost may differ depending on the mountain range, with elevation, incoming solar radiation, aspect, snow cover, substrate and cold air circulation all cited as the dominant influence on mountain permafrost presence or temperature in different studies (Bonnaventure & Lewkowicz, 2008; Gądek & Kędzia, 2008; Luetschg et al., 2008; Gruber & Haeberli, 2009; Apaloo et al., 2012). Thus, this generalized classification of mountain permafrost may oversimplify the distribution of permafrost in complex topography, especially where the spatial distribution of permafrost is influenced by the presence of temperature inversions. For example, it assumes that increased elevation controls air temperature and does not account for permafrost whose spatial distribution is highly influenced by the presence of temperature inversions (increasing air temperature with increasing elevation (e.g. Bonnaventure et al., 2012). This increases the complexity of spatially mapping permafrost in these locations. Previously it was widely assumed that in mountain environments permafrost was generally present at higher elevations while absent lower down due to the decreasing mean annual air temperature (MAAT) with elevation. This is generally observed in maritime and lower latitude mountain environments

and results in a linear distribution of permafrost (Guglielmin et al., 2003; Boeckli et al., 2012; Bonnaventure et al., 2012). However, in high-latitude, continental mountains, such as those in Yukon, the presence of persistent winter temperature inversions results in non-linear permafrost distribution with a high probability of permafrost at both low and high elevations while permafrost is generally absent around treeline (Bonnaventure et al., 2012). This permafrost distribution pattern has been modelled most extensively using the Basal Temperature of Snow (BTS) method allowing for the creation of permafrost probability surfaces over large portions of Yukon (Lewkowicz & Ednie, 2004; Bonnaventure & Lewkowicz, 2008, 2011; Bonnaventure et al., 2012).

Although the relation between inversions and permafrost probability has been well studied, little is known about the impact of surface air temperature inversion on the spatial distribution of ground surface and permafrost temperatures in these environments. While these permafrost probability studies focused on the southern portion of Yukon where moderate inversions have been observed, recent studies have shown that the magnitude of inversions increases substantially northward (Noad & Bonnaventure, 2022). Additionally, previous studies assume a lack of surface air temperature inversions in treeless valleys as lapse rates in treed valleys typically become normal above treeline (Bonnaventure et al., 2012). However, recent data has shown the presence of these strongly inverted lapse rates in valleys even in the absence of trees (Noad & Bonnaventure, 2022). Models in this area, also substantially underestimated the strength of the inverted SLRs. Lastly, most of the previous work mapping permafrost probability in Yukon was conducted on a regional scale, and did not account for site-specific factors, which may dampen or enhance the impact of air temperature on ground surface and permafrost temperatures.

The first objective of this study is to spatially model air, ground surface and ground depth temperatures at a fine resolution in four dissimilar valleys in Yukon. This will be done to assess the impact of both the persistent winter inversions and the potential modification by surface cover on the topographic distribution of the ground thermal regime. A second objective is to assess the performance of a regional model of permafrost probability with differing assumptions of treeline and inversion strength. The results of this study should guide not only current assessment of the ground thermal regime as it relates to elevation, but also present a starting point whereby the pattern of warming with elevation can be evaluated in mountain valleys subject to strong, persistent inversions.

### 5.3 Study Area

Four unique valleys in Yukon were sampled, two along the Dempster Highway and two along the North Canol Road in Yukon (Figure 5-1 and Table 5-1).

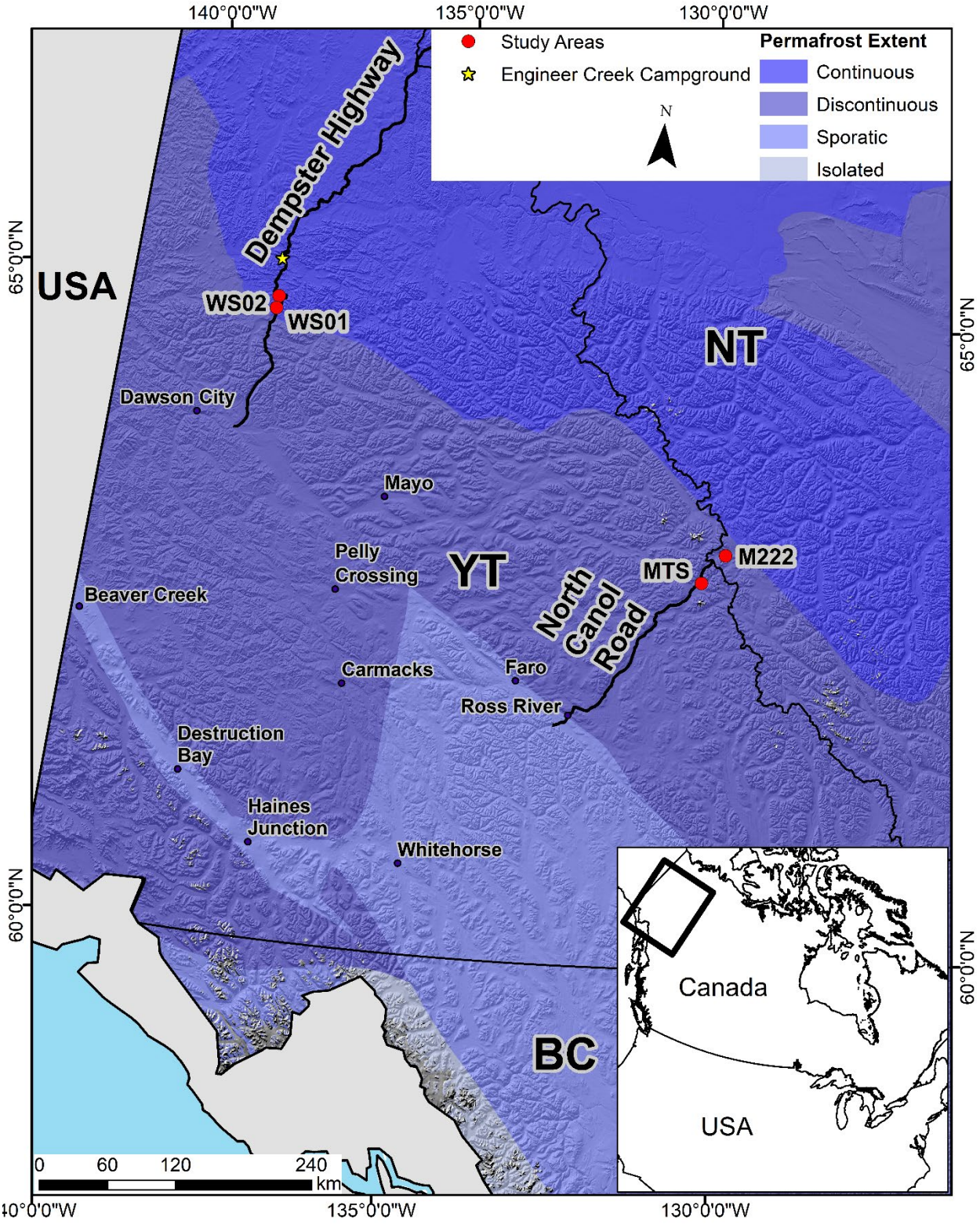


**Figure 5-1.** Map showing the locations of the four study area valleys. Permafrost layer from Brown et al. (2002).

**Table 5-1.** Coordinates for the four valleys used in the study.

| Valley | Latitude (ºN) | Longitude (ºE) |
|---|---|---|
| **Valley WS01** | 64.959 | -138.280 |
| **Valley WS02** | 65.050 | -138.263 |
| **Valley M222** | 63.298 | -129.837 |
| **Valley MTS** | 63.055 | -130.211 |

All four valleys are in mountainous terrain with a distinctive elevation range, latitude, vegetation cover, aspect, and valley geometry. The study areas along the Dempster Highway in the Ogilvie Mountains were called Valley WS01 and Valley WS02 while the sites along the North Canol in the Selwyn Mountains were named Mile 222 Valley (Valley M222) and MacMillan Transect South Valley (Valley MTS). These valleys were primarily selected based on their distinct characteristics, which would allow for an overall comparison of the range of inversions, ground surface temperatures and permafrost temperatures within the Ogilvie and Mackenzie mountains in the Yukon. Logistically, these sites were selected based on their accessibility from the road and the existing infrastructure in each location.

The Ogilvie Mountains were last glaciated during the Pre Reid Glaciation (0.25 myr B.P.) and have remained unglaciated during more recent glacial periods (Yukon Ecoregions Working Group, 2004). They are comprised of narrow valleys with surface deposits of colluvium and low to moderate segregated and wedge ice Yukon Ecoregions Working Group, 2004; Burn et al., 2015; O'Neill et al., 2019a). The climate is sub-arctic continental and the mountains have moderate relief (Burn Yukon working group). Precipitation amounts in this region are moderate (300-450 mm), with precipitation mainly falling as rain in summer (Yukon Ecoregions Working Group, 2004). Contrastingly the Selwyn Mountains have been extensively glaciated, most recently during the McConnell Glaciation (20,000 yr B.P), and still have local alpine glaciers (Bostock, 1996; Yukon Ecoregions Working Group, 2004). This recent glaciation results in the

high range of elevation in these mountains compared to the Ogilvie Mountains. Additionally, these mountains receive some of the highest amounts of precipitation in Yukon outside of the Pacific Maritime region (Yukon Ecoregions Working Group, 2004). This heavy amount of snowfall prevents the establishment of continuous permafrost in this region. Large accumulations of glacial sediments are only present in the bottoms of major valleys while the upper slopes and smaller valleys are composed of Holocene colluvium. Lastly, this region is expected to have low to moderate segregated ice and negligible wedge ice (O'Neill et al., 2019a).

Valley WS01 is the southernmost site in the Ogilvie Mountains located about 43 km south of the Engineer Creek Territorial Campground. It is an east-facing valley, which is treed on one slope (south facing) and treeless on the other slope (north facing) (Figure 5-2).

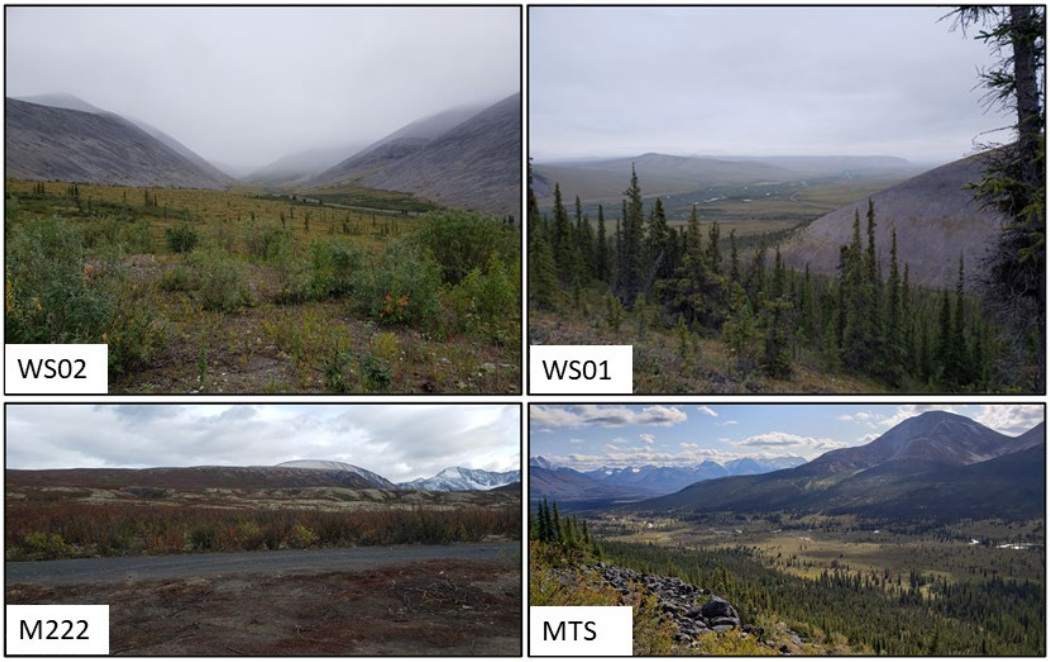


**Figure 5-2.** Site photos for each of the four valleys.

Valley WS01 has an elevation difference from the valley floor to the highest ridge of about 700 m and the annual mean air temperature (AMAT) measured at the valley floor was -6.2 °C from 2018-2021. Mean monthly SLRs in the valley are strongly inverted during the winter months and

normal during the summer months, resulting in an inverted annual SLR of 11.6 °C $km^{-1}$ on the treed side of the valley and 8.3 °C $km^{-1}$ on the treeless (Noad & Bonnaventure, 2022). The valley is considered to be underlain by continuous permafrost (Heginbottom, 1995).

Valley WS02 is the northernmost site and despite being only 10 km away from Valley WS01, is quite different in terms of vegetation. Valley WS02 is a treeless valley, with vegetation only consisting of moss and lichen on the valley floor with a few scattered shrubs and scree slopes (Figure 2). This valley has a north facing aspect. The elevation difference in this valley is 520 m with an AMAT of -4.4 °C (2018-2021) at the valley floor. As with Valley WS01, mean monthly SLRs are strongly inverted during winter months and normal during the summer months. The annual lapse rate in this valley is also inverted (4.7 °C $km^{-1}$ on the east facing slope and 1.7 °C $km^{-1}$ on the west-facing slope) but is not as strong as in Valley WS01 (Noad & Bonnaventure, 2022). This valley is also considered to be in the continuous permafrost zone (Heginbottom, 1995).

Mile 222 Valley is located on the North Canol Highway near the Yukon/ Northwest Territories boarder in a wide valley. The dominant vegetation is dwarf birch in the lower portions of the valley transitioning into predominately mosses and lichens at higher elevations (Figure 2). AMAT in the valley bottom is -6.5 °C and the valley has an elevation difference of about 570 m. Monthly SLRs (measured during this study) were generally inverted during winter months and normal during the summer; however, the annual SLR in this environment fluctuated between inverted and normal depending on the year. The average SLR in the lower portion of the valley (< 1361 m) is 10.8 °C $km^{-1}$ while the average SLR at higher elevations is -1.4 °C $km^{-1}$. This valley is considered to be underlain by extensive discontinuous permafrost (Heginbottom, 1995).

Mac T South Valley is located along the North Canol and is the southernmost site. This site has the largest elevation difference of the study areas (about 805 m) and is comprised of treed slopes one west facing and one south-east facing (Figure 2). Above treeline, vegetation is mainly alpine tundra consisting of moss and lichen and scree slopes. The AMAT for this site is -5.9 °C in the valley bottom and SLRs (measured during this study) were inverted below treeline at 10.4 °C $m^{-1}$ annually and is normal above treeline at -4.8 °C $m^{-1}$ annually. This valley is also deemed to be in the extensive discontinuous permafrost zone (Heginbottom, 1995).

## 5.4 Methods

### *5.4.1 Site Selection and Data Collection*

#### 5.4.1.1 Air Temperature Stations

Each valley was equipped with at least three air, ground surface and ground temperature at depth stations recording temperature bi-hourly (on even hours). Air temperature was measured about 1.5 meters above the ground surface in a radiation shield (Onset RS1) with a Hobo U23-002 (± 0.25 °C accuracy, 0.04 °C resolution) thermistor. At newer sites, a Hobo U23-001 (± 0.25 °C accuracy, 0.04 °C resolution) was used. Ground surface temperature was measured using a Hobo U23-002 internal thermistor buried 2-5 cm below the ground surface while ground temperature at depth was measured using the external thermistor located to the depth of the frost table at most sites. Exceptions to this were mainly sites located on exposed rocky substrate or scree. The three initial stations in Valley WS01 were installed in 2017 with one station located in the valley bottom and one located on each slope (Figure 5-3).

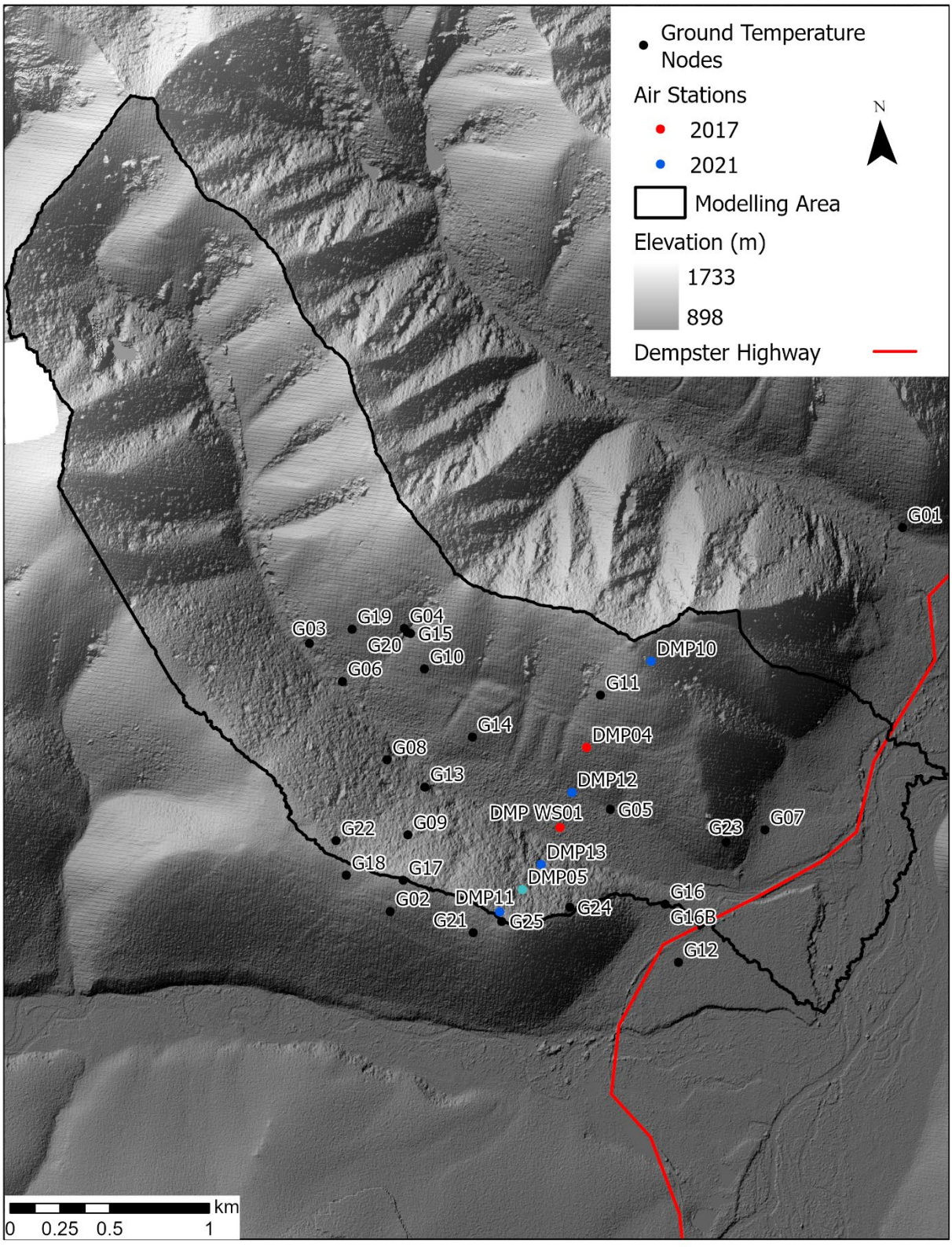


**Figure 5-3.** Locations of ground surface temperature stations, air temperature stations and the modelling area for Valley WS01. Colours for the air temperature stations indicate the year in which they were installed.

In Valley WS02 the air stations and on one of the slopes were installed in 2017 while the station on the other slope was installed in 2018 (Figure 5-4).

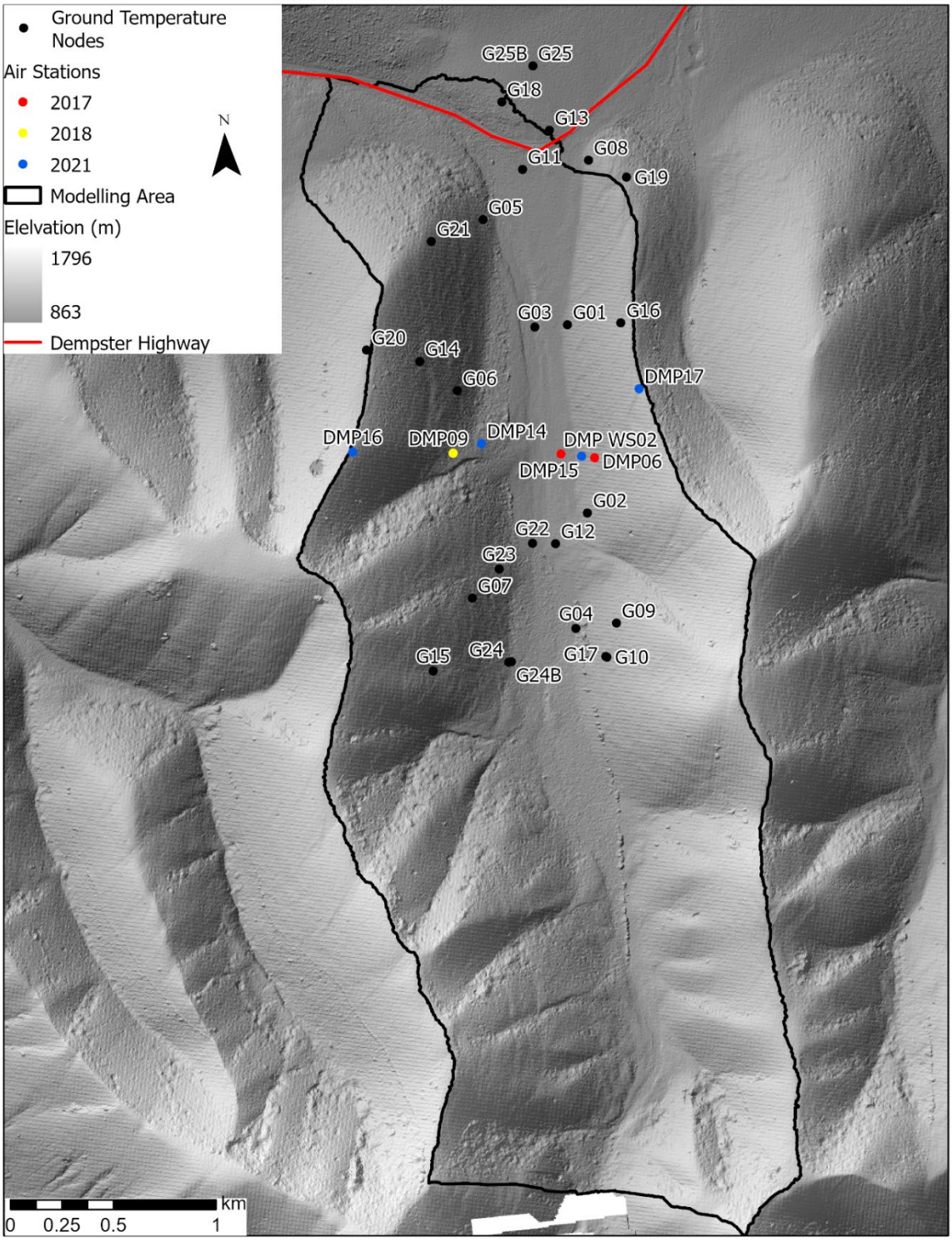


**Figure 5-4.** Locations of ground surface temperature stations, air temperature stations and the modelling area for Valley WS02. Colours for the air stations indicate the year in which they were installed.

In 2021 six additional stations were added in each valley, one on each ridge, one in between the ridge and the existing 2017 slope station, and one between the 2017 slope station and the station in the valley bottom. The three stations in Valley M222 were installed in 2016 and no additional stations have been added in this valley (Figure 5-5).

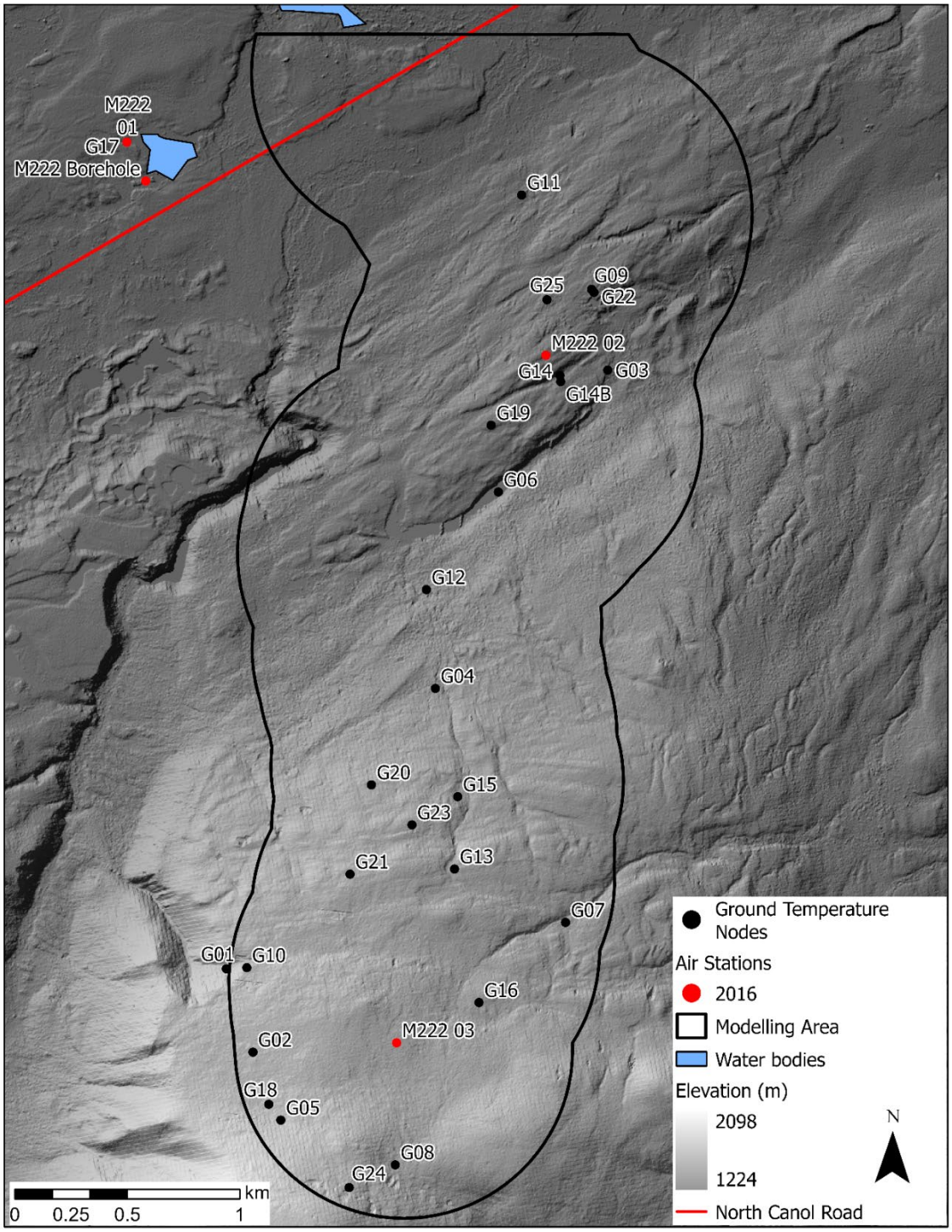


**Figure 5-5.** Locations of ground surface temperature stations, air temperature stations and the modelling area for Valley M222. Colours for the air temperature stations indicate the year in which they were installed.

The three original Valley MTS stations were installed in 2018 with and additional lower station installed in 2019 extending the transect to the true valley bottom (Figure 5-6).

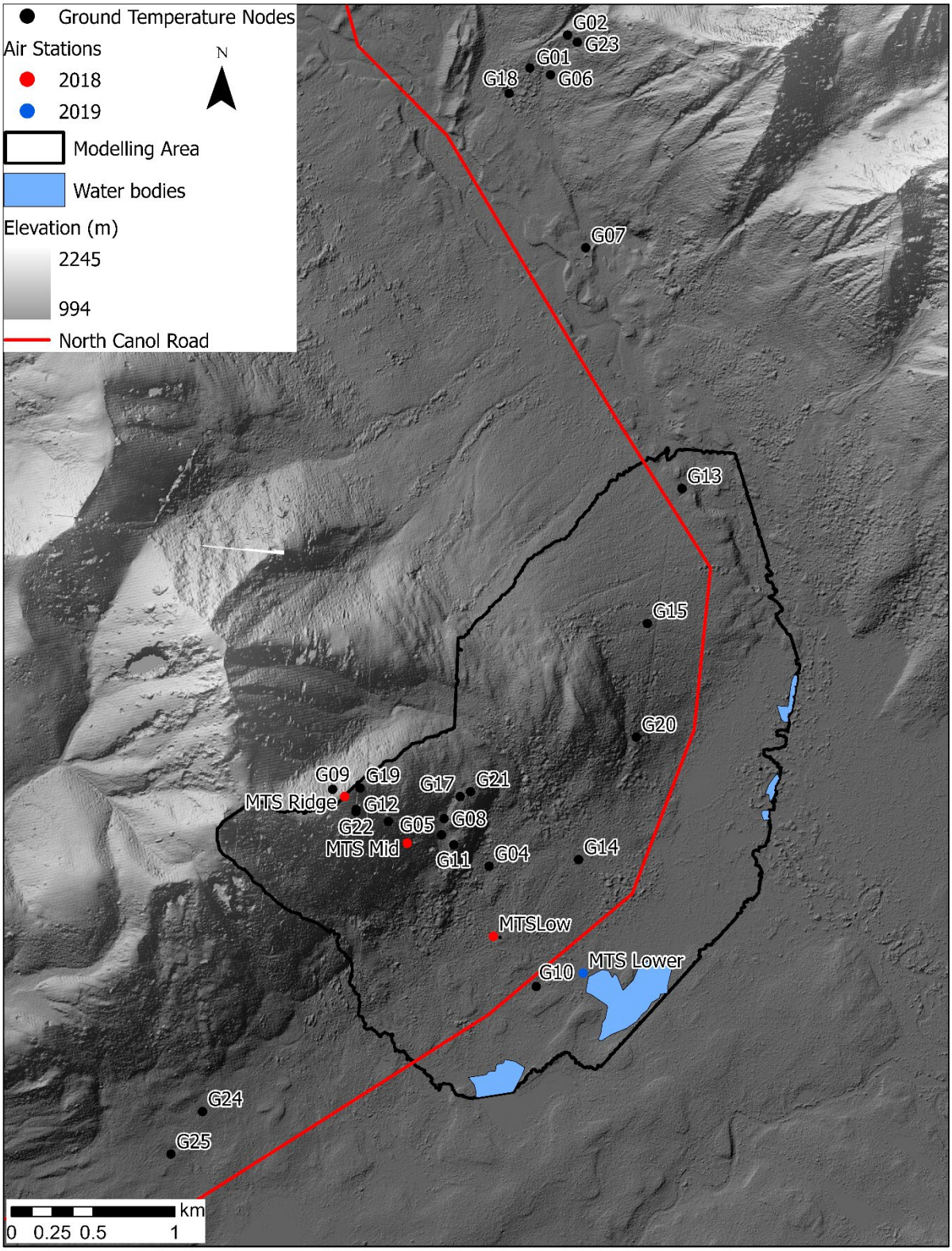


**Figure 5-6.** Locations of ground surface temperature stations, air temperature stations and the modelling area for Valley MTS. Colours for the air temperature stations indicate the year in which they were installed.

5.4.1.2 Ground Temperature Nodes

Sites in each valley were selected in an attempted to maximize the heterogeneity in ground surface temperature conditions sampled. To do this, variables derived from a Digital Elevation Model (DEM) in ArcGIS including Topographic Position Index (TPI), Potential Incoming Solar Radiation (PISR), aspect, slope and elevation were used. The 2m spatial resolution elevation models for each valley were derived from GeoEye optical imagery (Imagery © [2017] DigitalGlobe, Inc.). The Polar Geospatial Center at the University of Minnesota produced the surface model through surface extraction with TIN-based search and space minimization (SETSM) algorithm (Noh & Howat, 2017).The specifics of the site selection methodology can be found in the supplemental data section (S5.1). Twenty-five sites in each valley were then selected to sample the spread of topographic and vegetation heterogeneity in each valley accounting for accessibility, mainly proximity to the existing stations and the road. Some additional sites were added in the field based on in situ observations of the topographic conditions. For sampling, HOBO pendant loggers (± 0.53 °C accuracy, 0.14 °C resolution) were selected as they are relatively inexpensive, robust and have a good success and recovery rate in other locations (Garibaldi et al., 2021). Loggers were buried 2-5 cm below the ground surface, including any vegetation cover and recorded temperature at a one-hour interval.

*5.4.2 Data Analysis*

5.4.2.1 Ground Temperature Nodes

Annual mean ground surface temperature (AMGST) and daily average ground surface temperatures at each of the measured ground temperature node (GTN) locations were calculated over the monitoring period. The AMGST were calculated for August 1$^{st}$ to July 31$^{st}$ of the

subsequent year to minimize the number of missing days, keep the period for each valley the same and keeping freezing season intact. Annual and daily averages were calculated for both years of data (2019-2020 and 2020-2021) along with the overall average. $FDD_s$ and $TDD_s$ for each ground surface temperature point were also calculated for each year (Equation 5-1) (Smith & Riseborough, 2002).

$$FDD = |\Sigma_1^P T|, T < 0$$
$$TDD = |\Sigma_1^P T|, T > 0 \quad (5\text{-}1)$$

Where T is the daily average temperature and P is the period. Like the AMGST, the degree-days were calculated using a split calendar year (August 1st to July 31st). These degree days were then used to calculate N-factors for the spatial modelling of the ground thermal regime.

5.4.2.2 Air Temperature Spatial Modelling

In order to create spatial models for air temperature, surface lapse rates were calculated for each valley following the formula for the slope of a line to determine the linear relation between air temperature and elevation (Equation 5-2).

$$SLR = \frac{T_2 - T_1}{E_2 - E_1} \quad (5\text{-}2)$$

Where T is the temperature and E is the elevation. These were calculated for every day using the daily average temperatures between two of the air stations and the elevation difference. The daily averages for August 1st to July 31st of the subsequent year were then averaged to get the annual SLR. As with the ground surface temperature, the year was divided in this manner to minimize the number of missing days while also keeping the period for each valley the same and keeping

freezing season intact. For Valley WS01 and Valley WS02 SLRs in the valley bottom were calculated between the air station in the valley bottom and those at the mid slope for the years of study (Aug 2019- July 2021). As the air stations at the ridge were not installed until 2021 due to the Covid-19 pandemic, the lapse rates above the mid slope station were calculated for Aug 2021 to July 2022. Due to the lack of data for the mid slope to ridge SLRs during the monitoring period, the 2021-2022 SLRs were assumed to be the same and used in the model creation. Measured $FDD_a$ and $TDD_a$ were also calculated for each air temperature station (Equation 5-1). As with AMAT once $FDD_a$ and $TDD_a$ were determined for each station the relation between each degree day parameter and elevation was ascertained following the same method used to calculate the SLRs in each valley, replacing air temperature with the annual freezing or thawing degree days (Equation 5-2). These relations between degree days and elevation were then used to spatially model $FDD_a$ and $TDD_a$ for each valley in ArcGIS Pro.

Theoretical models were then created for AMAT, $FDD_a$ and $TDD_a$ assuming normal environmental SLR conditions (-6.5 ºC $km^{-1}$) from the measured temperature in the valley bottom for each study area. This normal environmental lapse rate is theoretical free air lapse rate of mixed (dry-wet) air. Normal surface lapse rate in mountains may differ (even without inversions) depending on air temperature, moisture content, and solar radiation (Barry, 2008). To determine the rate of change with elevation for $FDD_a$ and $TDD_a$ following the normal environmental SLR, daily average air temperatures measured in the valley bottoms were decreased by 6.5 ºC $km^{-1}$ to determine the theoretical temperature at the elevation of the middle station. Theoretical $FDD_a$ and $TDD_a$ were then calculated at the middle station (Equation 5-1). The elevation difference and the theoretical and measured $FDD_a$ and $TDD_a$ were then used to calculate the theoretical rate of change for $FDD_a$ and $TDD_a$ with elevation (Equation 5-2).

5.4.2.3 Ground Temperature Spatial Modelling

The temperature at top of permafrost (TTOP) model (Equation 5-3) was used to spatially model ground temperature at depth due to its simplicity and transferability between locations (Smith & Riseborough, 2002).

$$TTOP = \frac{(rk * n_{\mathrm{t}} * TDD_{\mathrm{a}}) - (n_{\mathrm{f}} * FDD_{\mathrm{a}})}{P} \quad for\ TTOP \leq 0$$
$$TTOP = \frac{(n_{\mathrm{t}} * TDD_{\mathrm{a}}) - \left(\frac{1}{rk} * n_{\mathrm{f}} * FDD_{\mathrm{a}}\right)}{P} \quad for\ TTOP > 0 \tag{5-3}$$

Since the TTOP model assumes equilibrium conditions, the typicality of each year in each valley were assessed against the 1981-2010 climate normal using ClimateNA (Wang et al., 2016) The TTOP model parameters for each ground surface temperature point were determined.

The spatial models for $FDD_a$ and $TDD_a$ for each valley were used to calculate N-factors using the modelled $FDD_a$ and $TDD_a$ and the measured $FDD_s$ and $TDD_s$ at each site (Equation 5-4).

$$n_{\mathrm{f}} = \frac{FDD_{\mathrm{s}}}{FDD_{\mathrm{a}}} \qquad \text{and} \qquad n_{\mathrm{t}} = \frac{TDD_{\mathrm{s}}}{TDD_{\mathrm{a}}} \tag{5-4}$$

To create a spatial map of N-factors, aspect and/or PISR, TPI and vegetation were utilized to relate the surface offset ratios to a topographic or spatial biological variables, as all have been shown to influence the distribution thawing and freezing surface offsets (Smith & Riseborough, 2002; Lacelle et al., 2016; Obu et al., 2019; Garibaldi et al., 2021; Garibaldi et al., 2022). PISR was derived using the Area Solar Radiation tool (ArcGIS Pro) for May 15 to September 30, 2018, with a sky size of 400 and 16 Zenith/ Azimuth division. The default was used for the remaining inputs. TPI compares elevation of each cell to the mean elevation of a user specified

neighborhood (Jenness, 2006). For each valley, a 200m x 200m window was utilized. Finally, a vegetation class was determined from a 30 m vegetation inventory feature layer (Government of Canada, 2015).

Empirical Bayesian Kriging (EBK) in ArcGIS Pro was used to create spatial n-factor models (validation and comparison to alternative methods in S5). EBK is a combination of ordinary least-squared regression and simple kriging, where the dependent variable is predicted through the sum of the average value and an error term. The average value is determined from the regression equation (weighted sum of the explanatory variables) and the error term is determined from a semivariogram or covariance model. The combination of regression and kriging in EBK allows for more accurate predictions than either method individually. Several iterations of EBK for each n-factor in each valley were run to determine the combination of input variables with the lowest error (Table S5-3). Predicted values for $n_f$ and $n_t$ were capped for each EBK model to limit unreasonable predictions. These capping values were determined for each valley and parameter based on the measured values and the known general limitation of each parameter. As a result, $n_f$ was capped between 0.0 and 1.0 while $n_t$ was capped between 0.0 and 2.0. Due to the narrower range, $n_f$ surfaces required more capping than $n_t$. For each valley, capping was only required for a small portion of the valley and generally was required in locations where TPI and PISR values were outside of the range sampled through the ground sensor network.

Lastly, spatial maps of rk were created for each valley using a combination of calculated values from the air stations and inferences based on topographic and landcover characteristics. For each valley, rk values for every air station were calculated using $FDD_s$, $TDD_s$, and freezing and thawing degree days in the ground at depth (Equation 5-5).

$$rk = \frac{FDD_s + (TDD_g - FDD_g)}{TDD_s} \quad (5\text{-}5)$$

Where $FDD_g$ and $TDD_g$ are the freezing and thawing degree days in the ground at depth. These calculated rk values were then assigned to the vegetation class in which the air station was located. Some air stations located in the same vegetation class had differing calculated rk values. To account for this elevation, slope and TWI were also used to map the spatial distribution of rk (Table S5-3). Slope was calculated using the DEM and ArcGIS Pro. TWI is an index that describes the tendency of an area to accumulate water and is derived using the upslope contributing area and slope. To determine the upslope contributing area several hydrology tools from the Spatial Analyst toolbox in ArcGIS Pro were utilized, including Flow Direction and Flow Accumulation.

The parameter surfaces were then combined using the TTOP model in raster calculator (ArcGIS Pro) (Equation 5-3). For pixels where TTOP was calculated to be greater than 0 ºC the TTOP model for seasonal frost was used (Equation 5-3) and the annual mean ground temperature (AMGT) surfaces were made through the combination of the areas calculated using the TTOP model and the seasonal frost model. The AMGT surfaces were then validated against the measured ground temperatures at depth recorded in each valley. In addition to AMGT, AMGST spatial maps were also created for each valley using the TTOP model equation but removing the thermal conductivity parameter.

## 5.5 Results

### *5.5.1 Measured Air Temperature*

The AMAT at the lowest station in all four valleys was similar ranging from -7.4 ºC in Valley WS01 to -5.9 ºC to Valley WS02. Valley M222 had an AMAT of -6.1 ºC while Valley MTS had an AMAT of -5.9 ºC. The air temperature during the two years were similar to that of the 1981-2010 climate normal (Wang et al., 2016). Both Valley M222 and Valley MTS had AMAT similar to those of the climate normal of -6.3 and -5.6 ºC, respectively. Valley WS01 and Valley WS02 had a greater difference in AMAT and that of the climate normal with the AMAT in Valley WS01 1.2 ºC colder than the climate normal (-6.2) and the AMAT of Valley WS02 1.6 ºC warmer than the climate normal. For these two valleys the greatest differences occurred during autumn and winter for Valley WS02 when the air temperature was 3.1 and 2.4 ºC warmer than the climate normal and spring and winter for Valley WS01 as the air was 1.6 and 2.4 ºC colder than expected. However due to the remote nature of these valleys and their complex topography it is possible that even the 1981 - 2010 MAAT may not be representative.

All four valleys experienced substantial winter inversions resulting in an inverted annual SLR in at least the lower portion of the valley (Table 5-2). In Valley WS01 and Valley WS02 the inverted annual SLRs on one slope extended above the mid elevation station to the ridge top, although they were substantially less inverted than those in the valley bottom. On the opposing slope in these valleys the SLR was marginally normal above the mid elevation station. During winter, however the inverted SLR on both sides of both valleys extended to the top of the ridge. In Valley M222 and Valley MTS the annual inverted SLRs were only present below the mid elevation station, with the annual SLR above reverting to normal. However, even in these valleys the inverted SLRs during the winter extended to the highest elevation station.

**Table 5-2.** Annual average surface lapse rates (SLR) and the elevation difference between air stations for each valley.

| Valley | Lower SLR (ºC km$^{-1}$) | Elevation Difference (m) | Upper SLR (ºC km$^{-1}$) | Elevation Difference (m) |
|---|---|---|---|---|
| **Valley WS01** | 11.7 (DMP04)<br>8.0 (DMP05) | 144 (DMP04)<br>146 (DMP05) | -0.9 (DMP10)<br>0.5 (DMP11) | 240 (DMP10)<br>80 (DMP11) |
| **Valley WS02** | 3.5 (DMP09)<br>7.1 (DMP06) | 93 (DMP 09)<br>60 (DMP06) | -0.1 (DMP16)<br>1.3 (DMP17) | 273 (DMP16)<br>139 (DMP17) |
| **Valley M222** | 5.9 | 76 | -2.7 | 350 |
| **Valley MTS** | 10.6 | 251 | -5.1 | 274 |

Similar to AMAT the four valleys had comparable numbers of $FDD_a$ at the lowest air station. $FDD_a$ ranged from 3782 ºC days in Valley WS01 to 3006 ºC days in Valley MTS. Valley WS02 had $FDD_a$ of 3176 ºC days while Valley M222 had 3243 ºC days. The strong persistent inversions were primarily present during winter in all four valleys lasting from the valley bottom to the ridge top, except at the upper slope of Valley M222 and Valley MTS. As a result, the lower portion of all four valleys had decreasing numbers of $FDD_a$ with increasing elevation (Table S5-4). This persisted to the top of the valley in all valleys except Valley M222 and Valley MTS where $FDD_a$ began increasing with elevation above the middle air station. $TDD_a$ at the lowest station in each valley was also similar as it ranged from 980 ºC days for Valley MTS to 1183 ºC days for Valley WS02. Valley WS01 and Valley M222 had 1130 and 1003 ºC days, respectively. For Valley WS02 and Valley M222 $TDD_a$ decreased with increasing elevation for the entire elevation range of the valley. For Valley WS01 the southwest facing lower slope showed an increase in $TDD_a$ with increasing elevation. This was also true for the lower portion of Valley MTS. For both of these valleys, $TDD_a$ then began to decrease with elevation above the mid elevation station at treeline. Although the air thermal regime in the valley bottoms were similar, there was considerable variability in the ground surface thermal regime both within and between valleys.

*5.5.2 Modelled Temperatures*

For all four valleys air, ground surface and ground temperatures showed considerable spatial variability. Air temperature in all four valleys was coldest in the valley bottom and warmest at either mid or high elevations due to the presence of the inverted SLRs during winter. In Valley WS02, the warmest air temperatures were predicted on the ridges and at high elevations while the coldest temperatures were predicted in the valley bottoms. In Valley WS01, the warmest temperatures were predicted at treeline on the southwest facing slope as the SLR above this elevation on this slope reverted to gently normal above treeline. In both Valley WS01 and Valley WS02, the SLRs were different on each side of the valley yielding asymmetrical air temperature distribution. This was especially true at high elevations in Valley WS01 where the southwest facing slope reverted to a normal SLR above treeline while at a similar elevation on the Northwest facing slope the SLR remained inverted. A similar pattern was predicted in Valley WS02 where at high elevations the SLR on the west facing slope became slightly normal while on the easting facing slope the SLR remained inverted although the difference between the two SLRs was much less. In both Valley M222 and Valley MTS mid elevations were predicted to have the warmest air temperatures as SLRs reverted to normal at mid elevations or around treeline. The coldest air temperatures were also predicted in the valley bottoms for these valleys. The topographic pattern of air temperature, however, was not always replicated in the ground surface temperature and ground temperature distribution. In all of the valleys, except Valley M222, the coldest AMGST and AMGT were modelled in the valley bottoms and at high elevations while the warmest temperatures were predicted at mid elevations highlighting the impact of inverted winter and average annual SLRs. When the inverted annual SLRs were not accounted for and the normal environmental SLR was assumed AMAT, AMGST, and AMGT

were all predicted to be colder than expected especially at high elevations. This assumption led to an over estimation of the area of each valley underlain by near surface permafrost. The spatial distribution of the air and ground thermal regime for each valley will be presented in detail in the following sections.

5.5.2.1 Valley WS01

Following the measured SLRs, the modelled air temperature in Valley WS01 ranged from -8.4 °C in the valley bottom to -5.7 °C at the ridges (Figure 5-7). Modelled AMAT for the whole valley was -6.4 °C. Using the normal environmental SLR (-6.5 °C $km^{-1}$) the AMAT over all of Valley WS01 was -8.8°C. The biggest differences between the AMAT using the normal environmental SLR and the measured inverted SLRs were at high elevations with differences of 4-6 °C. At these locations, the AMATs following the inverted SLRs were warmer than predicted using the normal SLR. Predicted AMAT in the valley bottom remained colder than expected if assuming the normal ELR. Modelled $FDD_a$, following the measured SLR for Valley WS01, ranged from 4103 °C days in the valley bottom to 2932 °C days at the highest elevations at the ridges (Figure S5-21). Average $FDD_a$ across the whole valley was modelled to be 3362 °C. Due to the winter inversions, the spatial pattern of $FDD_a$ based on elevation showed higher $FDD_a$ at low elevations and the lowest $FDD_a$ at the highest elevations, the opposite from the expected distribution if assuming a normal SLR. As a result, when comparing to the $FDD_a$ surface created using a SLR of -6.5 °C $km^{-1}$, $FDD_a$ was higher than expected in the valley bottom and the largest discrepancy occurred at high elevations (up to 1857 °C days) where $FDD_a$ was much lower than expected. Modelled $TDD_a$ ranged from 747 °C days at the highest elevations to 1185 °C days at mid to low elevations on the southwest facing slope (Figure S5-22). Average $TDD_a$ for Valley WS01 was modelled to be 1068 °C days. This spatial distribution shows the warmest summer

temperatures were found at mid elevations on the southwest facing slope rather than the valley bottom as expected. When compared to the modelled distribution of $TDD_a$ following the typical expected conditions, actual $TDD_a$ were higher than expected over most of the valley and especially at high elevations, and lower than expected in the valley bottom.

RMSEs for the EBK $n_f$ surface were 0.06 for training and 0.08 for testing, while for $n_t$ the RMSEs were 0.06 for training and 0.21 for testing. Modelled N-factors ranged from 0.04 to 1.00 for $n_f$ and 0.65 to 1.80 for $n_t$ (Figure S5-23). Average modelled $n_f$ for the entire valley was 0.53 while average $n_t$ was 1.16. Generally, both $n_f$ and $n_t$ increased with increasing elevation. Following the assigned values based on vegetation classes, rk was equal to 0.61 at lower elevations and in the coniferous forest class and 1.00 at higher elevations on the bare slopes. The spatial distribution of rk was related to the distribution of the vegetation classes and elevation. RMSE for modelled AMGST was 1.1 ºC. Modelled AMGST ranged from -8.4 to 3.7 with the coldest temperatures generally located at higher elevations on exposed ridges and in the valley bottom (Figure 5-8). The warmest temperatures were predicted to be at mid elevations especially on the southwest facing slope near treeline. Overall, the average AMGST for this valley was predicted to be -1.4 ºC. When modelling AMGST assuming a normal SLR, AMGST was predicted to be colder with an average AMGST across the valley of -3.3 ºC and a range from -10.9 to 3.0 ºC. The coldest temperatures were predicted to be at high elevations on exposed ridges while the warmest were predicted at mid elevations. Although the spatial pattern of AMGT was predicted to be similar, high elevations were much colder and the mid elevations were not as warm when the inversion was not considered. The largest difference between the two models were found at high elevations (up to 6.0 ºC), with warmer AMGST predicted when

the measured inverted SLRs were used than when using the standard ELR. The valley bottom was also colder than expected (up to 1.5 ºC) when the inverted SLRs were utilized.

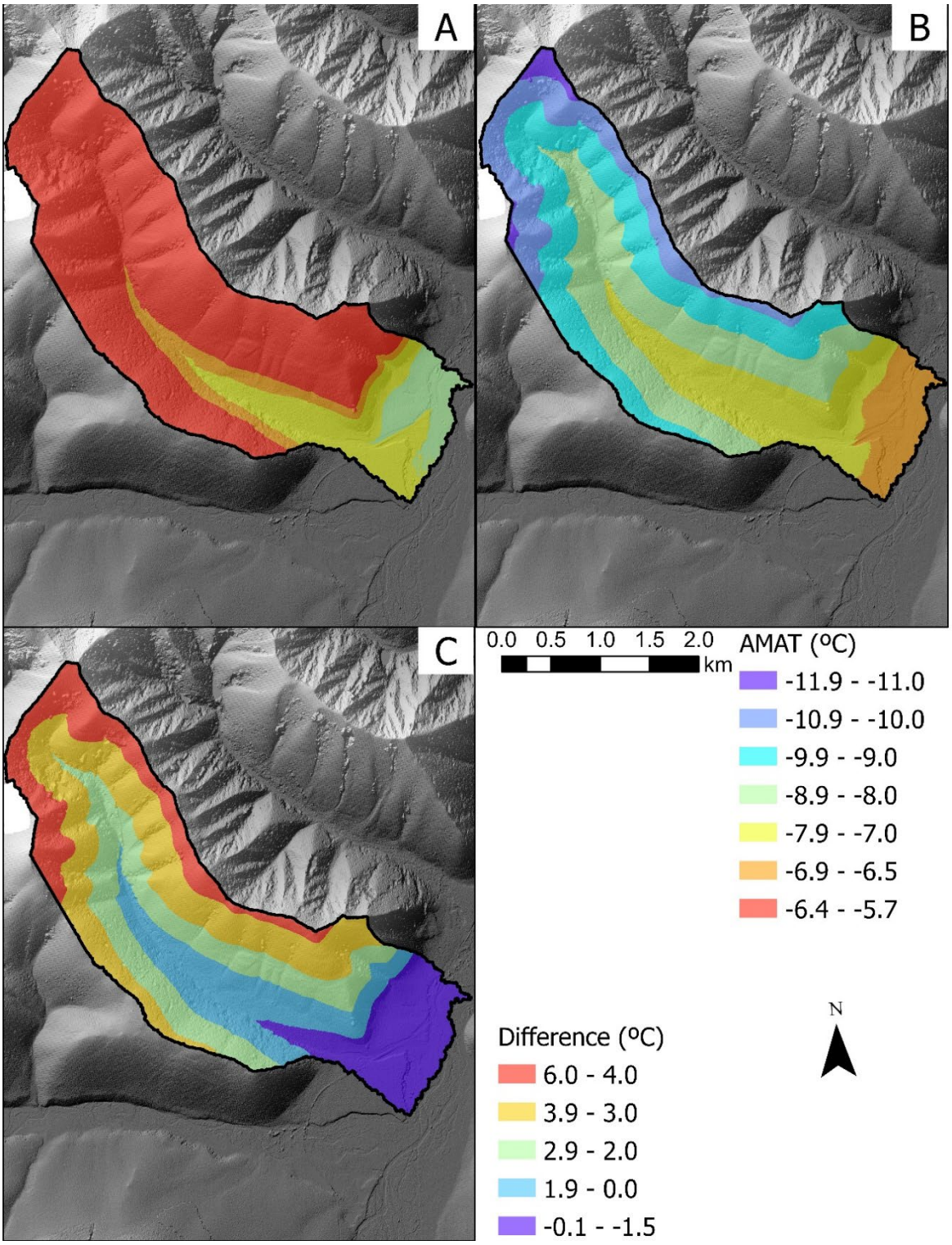


**Figure 5-7.** Annual mean air temperature (AMAT) models for Valley WS01 A) Calculated surface lapse rates (SLR), B) Normal environmental SLR (-6.5 °C $km^{-1}$), and C) the difference between the two models where negative values indicate actual AMAT (accounting for inverted SLRs) is colder and positive values indicate actual AMAT is warmer than expected if assuming the normal environmental SLR.

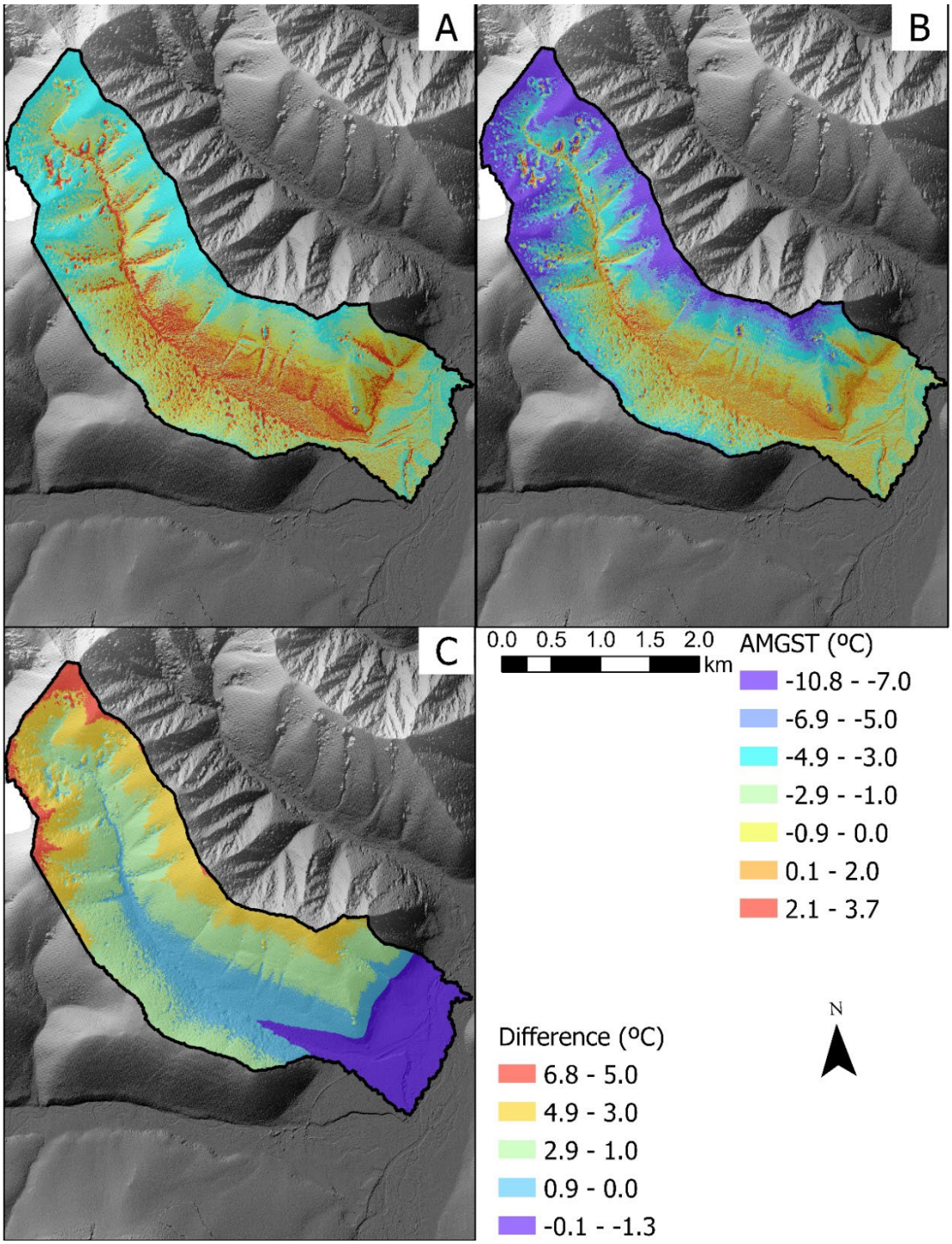


**Figure 5-8.** Annual mean ground surface temperature (AMGST) models for Valley WS01 A) calculated using freezing and thawing degree days accounting for inverted surface lapse rates (SLR), B) calculated using freezing and thawing degree days assuming the normal environmental SLR (-6.5 °C $km^{-1}$ ), and C) the difference between the two models where negative values indicate actual AMGST (accounting for inverted SLRs) is colder and positive values indicate actual AMGST is warmer than expected if assuming the normal environmental SLR.

Lastly, modelled AMGT had an RMSE of 0.9 ºC compared to measured temperatures at depth. The coldest AMGT, similar to AMGST, were predicted at both high and low elevations while the warmest AMGT were modelled at mid elevations, ranging from -9.4 to 3.7 ºC (Figure 5-9). Near surface permafrost was modelled to underlay 80% of this valley with an average AMGT of -1.6 ºC. Near surface permafrost was also predicted to be present mainly in the valley bottom and at high elevations, while absent in some locations at mid elevations. If the inversion was not considered, AMGTs were predicted to be much colder than expected, especially at high elevations, with the coldest AMGT predicted to be -10.9 ºC, a difference of 6.8 ºC from the actual AMGT. There was a smaller difference at low elevations (up to 1.2 ºC) however, AMGT were colder than predicted assuming a normal lapse rate. When the inversions were not accounted for, near surface permafrost was predicted to underlay 88% of the valley with a predicted average AMGT of -3.5 ºC. Generally, when the SLR in this valley was assumed to be normal, predictions of AMAT, AMGST and AMGT were colder than in reality due to the presence of the strong persistent winter inversion contributing to warmer than expected temperatures at higher elevations.

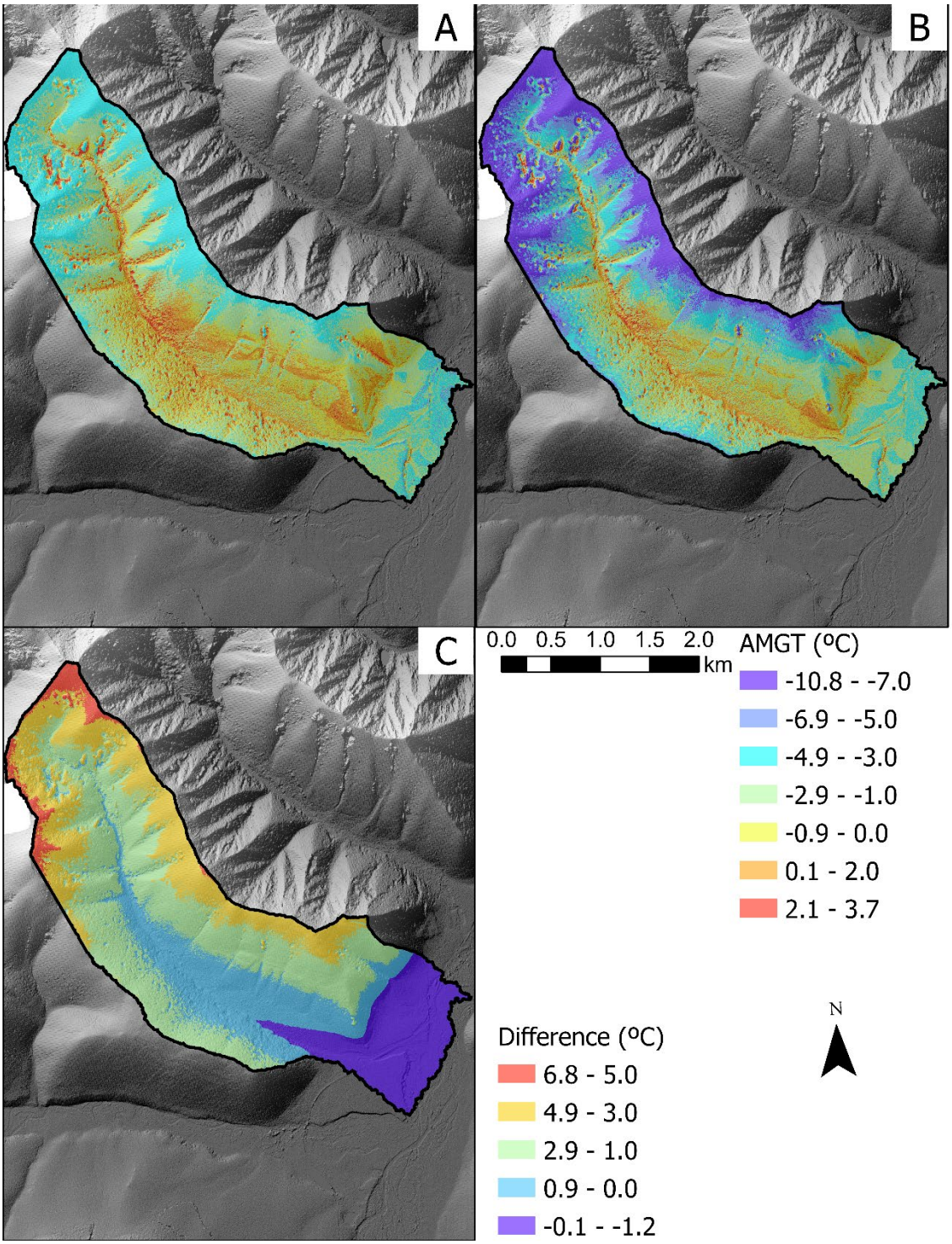


**Figure 5-9.** Annual mean ground temperature (AMGT) models for Valley WS01 A) calculated using freezing and thawing degree days accounting for inverted surface lapse rates (SLR), B) calculated using freezing and thawing degree days assuming the normal environmental SLR (-6.5 °C $km^{-1}$ ), and C) the difference between the two models where negative values indicate actual AMGT (accounting for inverted SLRs) is colder and positive values indicate actual AMGT is warmer than expected if assuming the normal environmental SLR.

5.5.2.2 Valley WS02

Following the measured SLRs in Valley WS02 modelled AMAT ranged from -6.1 to -4.3 ºC with the coldest air temperatures modelled at low elevations (valley bottom) and the warmest temperatures at the highest elevations (ridges) especially on the west facing slope (Figure 5-10). Average AMAT over the whole valley was predicted to be -5.1 ºC. When the inverted SLRs were not accounted for AMAT was predicted to be colder ranging from -9.3 to -4.9 ºC with an average of -6.7 ºC across the valley. The biggest discrepancy between the actual AMAT model (using the measured SLRs) and the normal SLR AMAT model was found at high elevations with the actual AMAT being up to 4.5 ºC warmer than expected. In the valley bottom, AMAT were colder than expected if the inverted SLRs were not considered. Modelled $FDD_a$ ranged from 2571 ºC days at the highest elevations to 3425 ºC days in the valley bottom (Figure S5-24). Average $FDD_a$ across the valley was modelled to be 2918 ºC days. When the inverted winter SLRs were not considered Valley WS02 was predicted to be much colder than in actuality with an average $FDD_a$ for the valley of 3455 ºC days. The spatial distribution of $FDD_a$ when not accounting for inversions was opposite of that when inversions were considered, with the least amount of $FDD_a$ predicted in the valley bottom (as few as 3047 ºC days) and the highest amount predicted at the highest elevations (up to 4006 ºC days). As a result, the greatest discrepancy was found at the highest elevations with a difference of up to 1434 ºC days fewer when inverted SLRs were included. In the valley bottom, more $FDD_a$ (up to 378 ºC days) were expected under an inverted SLR. Finally, as the inverted SLRs for this valley were only strongly present during winter, the spatial distribution for $TDD_a$ following the measured change with elevation was similar to that using the normal environmental SLR. Both models predicted more $TDD_a$ in the

valley bottom (up to 1270 ºC days) and fewer at the highest elevations (as few as 710 and 618 ºC days for the measured and normal environmental SLRs, respectively) (Figure S5-25).

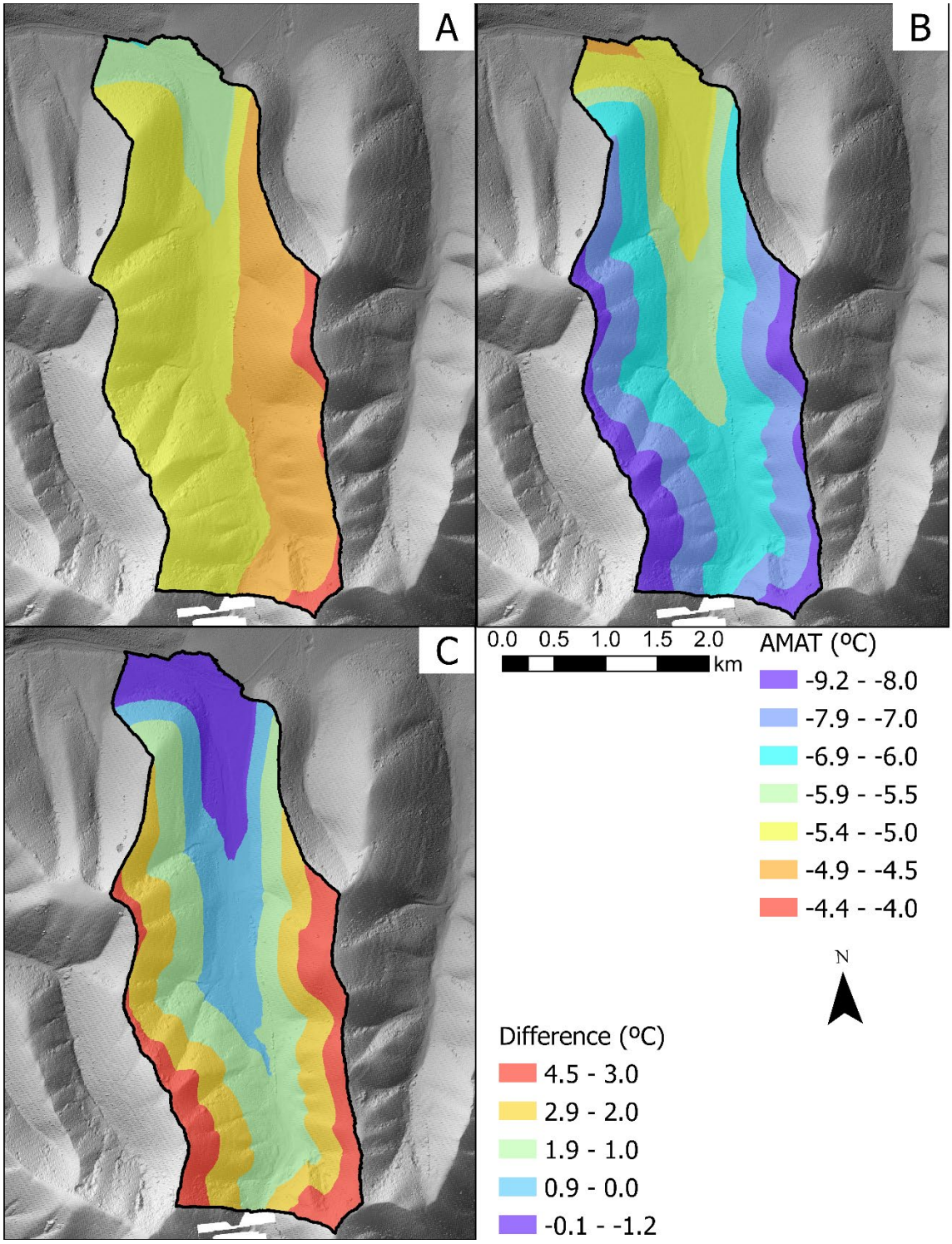


**Figure 5-10.** Annual mean air temperature (AMAT) models for Valley WS02 A) Calculated surface lapse rates (SLR), B) Normal environmental SLR (-6.5 °C $km^{-1}$), and C) the difference between the two models where negative values indicate actual AMAT (accounting for inverted SLRs) is colder and positive values indicate actual AMAT is warmer than expected if assuming the normal environmental SLR.

RMSE of the $n_f$ model created through EBK was 0.10 for the training dataset and 0.13 for the testing dataset. For $n_t$ RMSEs for the EBK $n_f$ surface were 0.06 for training and 0.08 for testing, while for $n_t$ the RMSEs were 0.13 for training and 0.20 for testing. Modelled N-factors ranged from 0.06 to 1.00 for $n_f$ and 0.23 to 1.54 for $n_t$ (Figure S5-26). Average modelled $n_f$ for the entire valley was 0.56 while average $n_t$ was 0.93. Generally, both $n_f$ and $n_t$ increased with increasing elevation however this was complicated by topography with the lowest $n_f$ and $n_t$ values modelled in incised topographic hollows regardless of elevation while the highest values were modelled in convex slope locations. Following the assigned values based on vegetation classes, elevation and slope, rk was equal to 0.64 in the valley bottom increasing to 0.78 in shrubbed locations with limited moss, and finally to 0.91 and 0.93 for the rock and herbaceous exposed slopes at higher elevations. RMSE for modelled AMGST was 0.4 ºC. Modelled AMGST ranged from -4.7 to 1.1 with the coldest temperatures generally located on the west-facing slope at higher elevations and on exposed ridges (Figure 5-11). The warmest temperatures were predicted to be in the valley bottom in a disturbance dominated by shrubs and in incised channels along the slopes. Overall, the average AMGST for this valley was predicted to be -1.8 ºC. When modelling AMGST assuming a normal SLR, AMGST was predicted to be colder with an average AMGST across the valley of -2.8 ºC and a range from -8.2 to 1.1 ºC. The coldest temperatures were also predicted to be on the west-facing slope and on exposed ridges, while the warmest were predicted in under shrubs and in incised channels. The largest difference between the two models were found at high elevations (up to 4.5 ºC) with the AMGST modelled with inversion warmer than the one without inverted SLRs. The valley bottom was also colder than expected (up to 0.8 ºC) when the inverted SLRs were utilized.

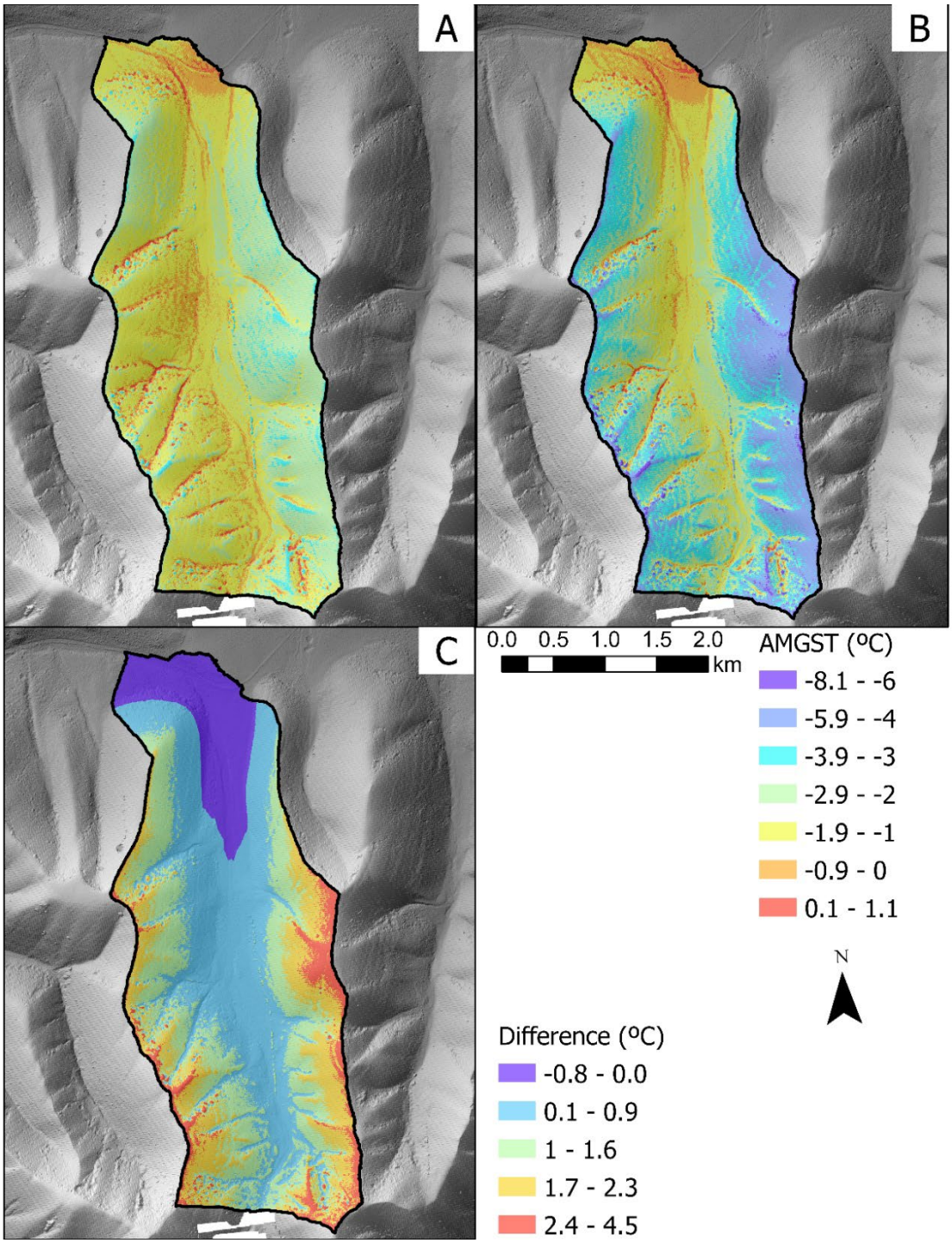


**Figure 5-11.** Annual mean ground surface temperature (AMGST) models for Valley WS02 A) calculated using freezing and thawing degree days accounting for inverted surface lapse rates (SLR), B) calculated using freezing and thawing degree days assuming the normal environmental SLR (-6.5°C km-1 ), and C) the difference between the two models where negative values indicate actual AMGST (accounting for inverted SLRs) is colder and positive values indicate actual AMGST is warmer than expected if assuming the normal environmental SLR.

Transitioning to the subsurface, the RMSE for AMGT was 0.7 ºC. Over the Valley WS02 valley, the average AMGT was modelled to be -2.1 ºC with ground temperatures ranging from -5.9 to 1.0 ºC. As with AMGST, the coldest AMGTs were predicted on the west facing exposed slope (Figure 5-12). In addition, some of the coldest AMGT were also modelled in the valley bottom. Near surface permafrost was modelled to underlay 99% of the valley. When a normal SLR was used, the AMGT was colder than that modelled using the measured SLRs with an average AMGT of -3.1 ºC. AMGT for this scenario ranged from -8.4 to 1.1 ºC with the coldest temperature predicted at the highest elevations and the warmest temperature predicted at low elevations and in incised channels. Near surface permafrost was also expected to underlay 100% (99.6 %) of this valley. The difference between the AMGT model created using the measured inverted SLRs and the one created using the normal environmental SLR was greatest at high elevations (up to 4.5 ºC) where AMGT was predicted to be colder than in actuality. In the valley bottom AMGT were colder than expected if using a normal SLR.

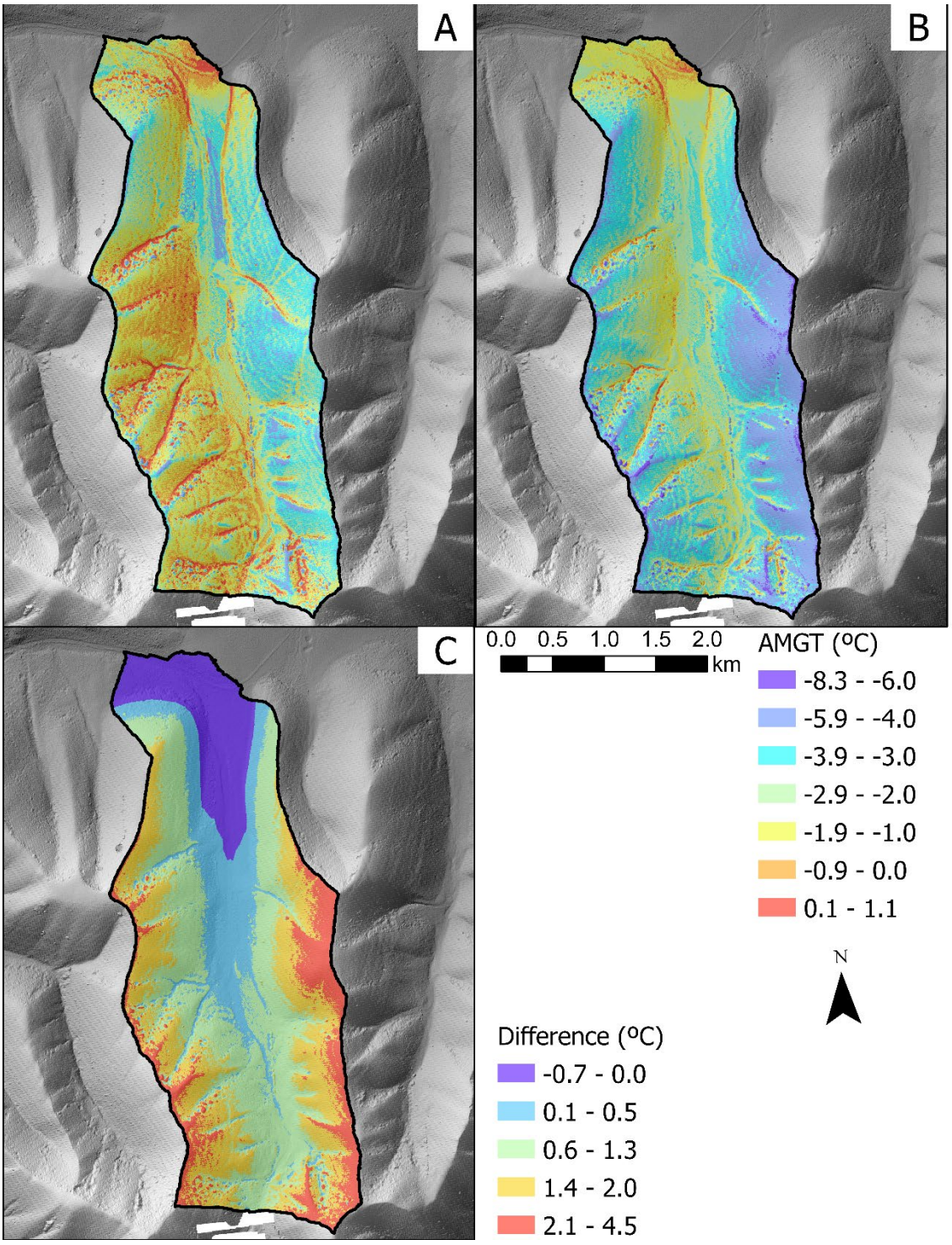


**Figure 5-12.** Annual mean ground temperature (AMGT) models for Valley WS02 A) calculated using freezing and thawing degree days accounting for inverted surface lapse rates (SLR), B) calculated using freezing and thawing degree days assuming the normal environmental SLR (-6.5 °C $km^{-1}$ ), and C) the difference between the two models where negative values indicate actual AMGT (accounting for inverted SLRs) is colder and positive values indicate actual AMGT is warmer than expected if assuming the normal environmental SLR.

5.5.2.3 Valley M222

In Valley M222 modelled AMAT ranged from -7.1 to -5.7 °C (Figure 5-13). The warmest air temperatures were predicted to be at mid elevations with relatively cold temperatures found in the valley bottom and at higher elevations. The overall average across the valley was -6.2 °C. Not accounting for the inversion, AMAT across the valley was generally colder with an average of -7.2 °C and predicted temperatures as low as -9.9 °C at the highest elevations. Due to the use of a normal environmental SLR temperature decreased with increasing elevation resulting in the warmest temperatures in the valley bottom and the coldest temperatures at high elevations in contrast to the spatial distribution modelled using the measured SLRs. As a result, the greatest difference between the two models was at the highest elevations where the actual AMAT was up to 2.8 °C warmer. The valley bottom was colder than expected when not considering the winter inversion with a difference up to -0.5 °C. The spatial distribution of modelled $FDD_a$ reflected the prevalence of the winter inversions with the most $FDD_a$ predicted at low elevations in the valley bottom (as many as 3286 °C days), decreasing to its minimum at mid elevations (3164 °C days) before increasing again to high elevations (Figure S5-27). The average $FDD_a$ for this valley was predicted to be 3207 °C days. Assuming a normal SLR $FDD_a$ was predicted to increase with elevation over the entire valley with the fewest $FDD_a$ predicted in the valley bottom (as few as 3177 °C days) and the most predicted for the highest elevation (4164 °C days). With no inversion, $FDD_a$ increased over the entire elevation range and the range in $FDD_a$ was greater than for surface created using the measured SLRs. Average $FDD_a$ across the valley was also greater (3497 °C days). The greatest difference between the two surfaces was at the higher elevations where the $FDD_a$ surface created using the measured change

with elevation was up to 946 °C days less. In the valley bottom, the actual number of $FDD_a$ was higher than following a normal SLR (up to 108 °C days more).

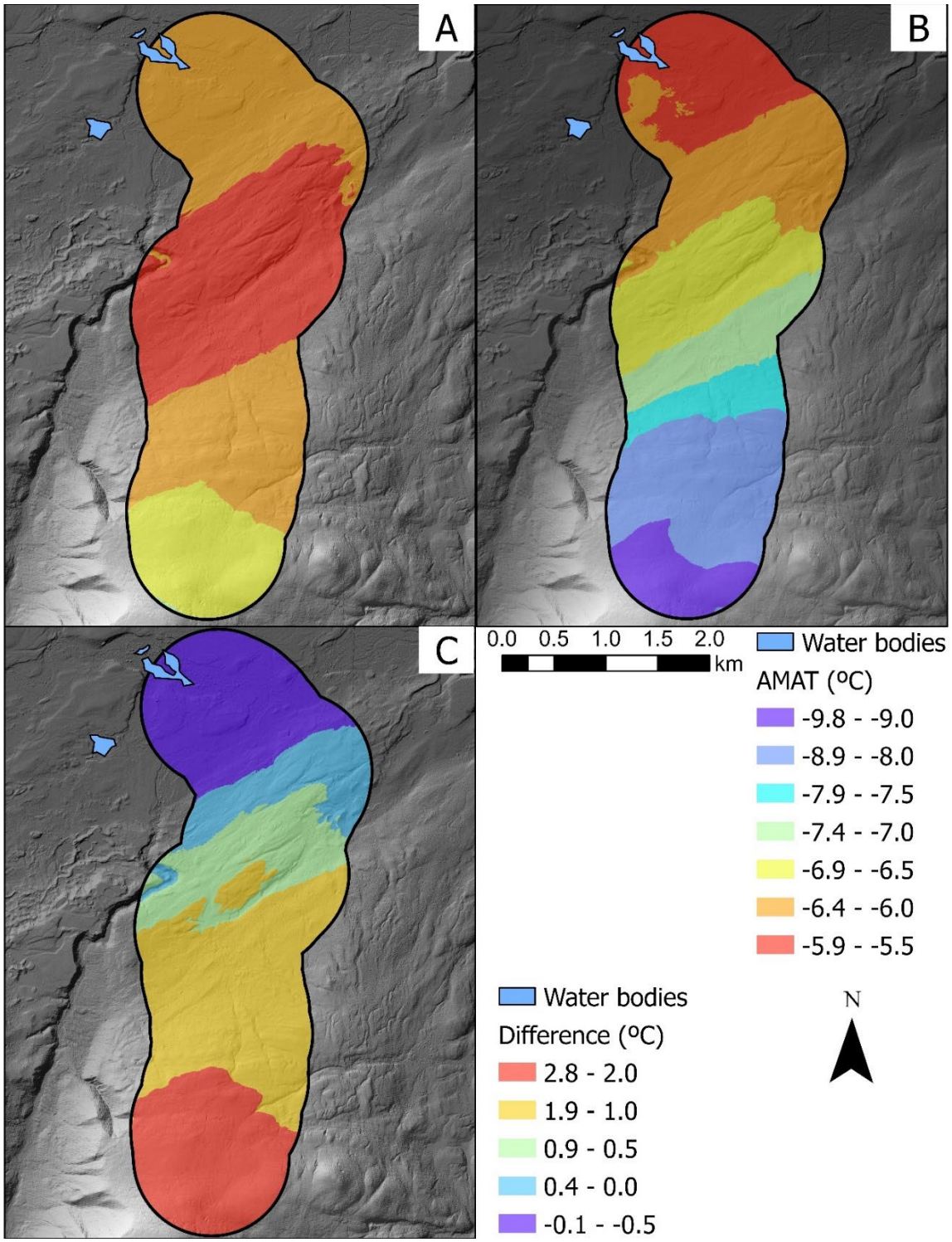


**Figure 5-13.** Annual mean air temperature (AMAT) models for Valley M222 A) Calculated surface lapse rates (SLR), B) Normal environmental SLR (-6.5 °C km$^{-1}$), and C) the difference between the two models where negative values indicate actual AMAT (accounting for inverted SLRs) is colder and positive values indicate actual AMAT is warmer than expected if assuming the normal environmental SLR.

The measured change in $TDD_a$ with elevation was close to that following the normal environmental SLR resulting in similar spatial distribution, values, and range (Figure S5-28). Following the measured change in $TDD_a$, values were modelled to range between 661 to 1040 °C days with an average of 899 °C days. With the change in $TDD_a$ following the normal environmental SLR, values ranged from 526 to 1037 °C days with an average of 871 °C days. For both models, $TDD_a$ decreased with increasing elevation.

RMSE for the $n_f$ surface created through EBK was 0.08 for the training dataset and 0.10 for the testing. For $n_t$, the RMSE was 0.13 for training and 0.15 for testing. Modelled N-factors ranged from 0.06 to 0.83 for $n_f$ and 0.51 to 1.25 for $n_t$ (Figure S5-29). Average modelled $n_f$ for the entire valley was 0.18 while average $n_t$ was 0.83. Generally, both $n_f$ and $n_t$ increased with increasing elevation however, this was complicated by topography. The lowest $n_f$ values were modelled in the valley bottom and in incised channels while the highest were predicted at high elevations on exposed slopes. The lowest $n_t$ values modelled in incised topographic hollows regardless of elevation while the highest values were modelled on convex slopes especially at high elevations. Based on topographic wetness, rk values were 0.73 and 1, with the lower value used at lower elevations and in topographic hollows, which were expected to be wetter, and the higher value on exposed dry slopes and at high elevations. RMSE for the ground surface temperature model was 1.1 ºC. Modelled AMGST ranged from -5.4 to 2.2 ºC with the warmest ground surface temperatures predicted to be at low elevations while the colder temperatures were predicted to be on exposed ridges and slopes particularly at high elevations (Figure 5-14). Average AMGST across the valley was predicted to be 0.4 °C. However, the relation between AMGST and elevation was not as directly apparent and clear as the relation between elevation and AMAT as shown in the spatial distribution of AMGST.

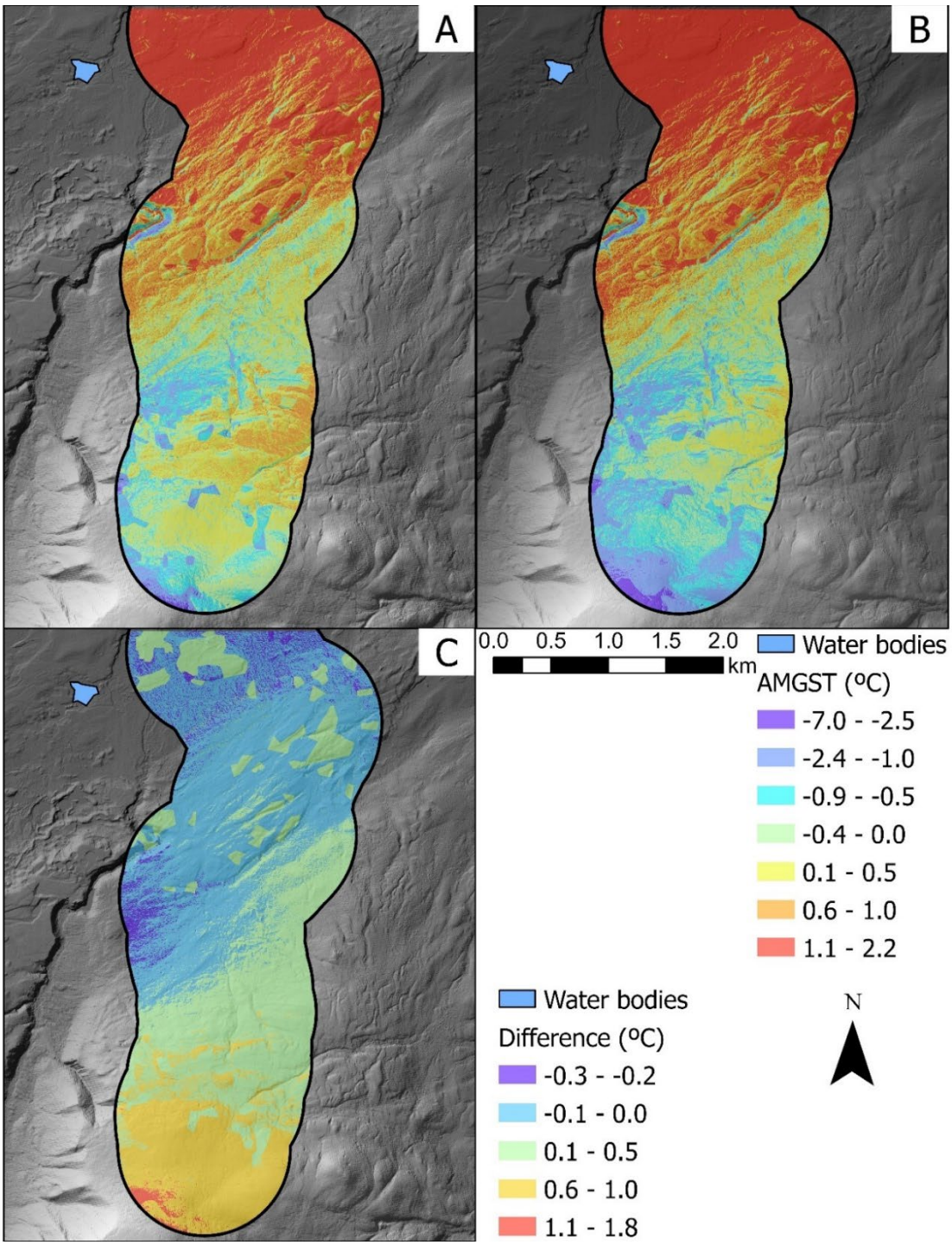


**Figure 5-14.** Annual mean ground surface temperature (AMGST) models for Valley M222 A) calculated using freezing and thawing degree days accounting for inverted surface lapse rates (SLR), B) calculated using freezing and thawing degree days assuming the normal environmental SLR (-6.5 °C $km^{-1}$ ), and C) the difference between the two models where negative values indicate actual AMGST (accounting for inverted SLRs) is colder and positive values indicate actual AMGST is warmer than expected if assuming the normal environmental SLR.

When a normal lapse rate was assumed AMGSTs were predicted to be slightly colder than in actuality, ranging from -7.1 to 2.2 ºC and an average of 0.24 °C. The relation between elevation and AMGST was also clearer under this assumption with relatively warm ground surface temperatures generally predicted at lower elevations and cooling moving upslope until the coldest temperatures at the highest elevations. However, there were still relatively cold AMGST predicted on exposed ridges even at lower elevations. If the inverted winter SLRs were not accounted for, the greatest discrepancy was found at high elevations where AMGST can be up to 1.8 ºC warmer than expected while at low elevations the AMGST was slightly colder than expected. However, the AMGST surface following both the measured SLRs and the normal environmental SLR were similar.

Moving into the subsurface, the RMSE for AMGT was 1.9 ºC. Over Valley M222, the average AMGT was modelled to be 0.3 ºC with ground temperatures ranging from -5.4 to 2.2 ºC. As with AMGST, the coldest AMGTs were predicted on exposed ridges, and steep slopes especially at high elevations (Figure 5-15). Near surface permafrost was modelled to underlay only 33 % of the valley. When a normal SLR was used, the AMGT was slightly colder than when modelled using the measured SLRs with an average AMGT of -0.3 ºC. AMGT for this scenario ranged from -7.9 to 2.0 ºC with the coldest temperatures generally predicted at the highest elevations and exposed ridges and the warmest temperature predicted at low elevations and in incised channels. Near surface permafrost was also expected to underlie 51 % of this valley. The difference between the AMGT model created using the measured inverted SLRs and the one created using the normal environmental SLR was greatest at high elevations (up to 2.6 ºC) where AMGT was predicted to be colder than in actuality. In the valley bottom AMGT were colder than expected if using a normal SLR. Once again, without accounting for the winter

inversions air, ground surface and ground temperatures would all be colder than in actuality although less pronounced in this valley due to the limited elevation change and limited depth and strength of the winter inversion.

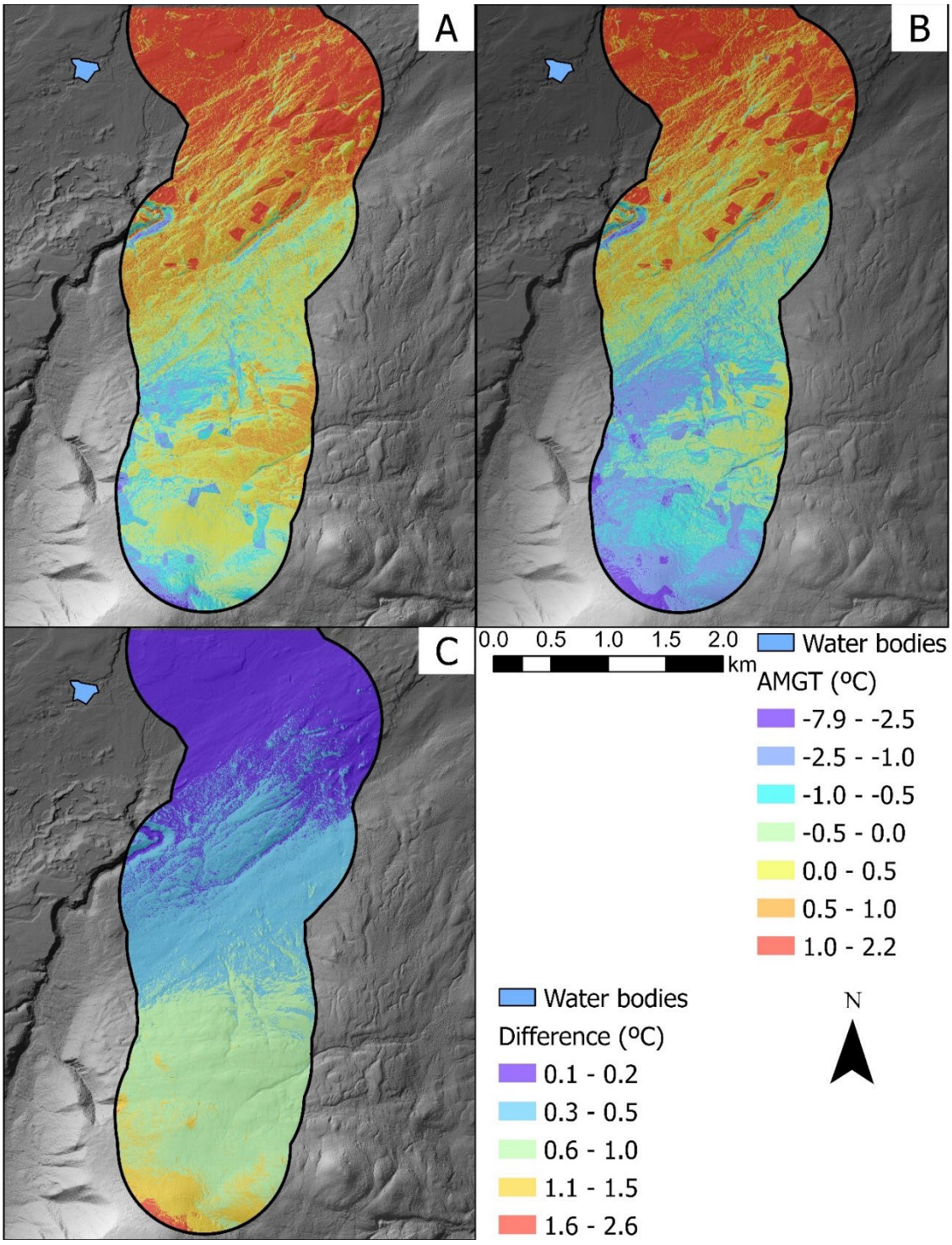


**Figure 5-15.** Annual mean ground temperature (AMGT) models for Valley M222 A) calculated using freezing and thawing degree days accounting for inverted surface lapse rates (SLR), B) calculated using freezing and thawing degree days assuming the normal environmental SLR (-6.5 °C $km^{-1}$ ), and C) the difference between the two models where negative values indicate actual AMGT (accounting for inverted SLRs) is colder and positive values indicate actual AMGT is warmer than expected if assuming the normal environmental SLR.

5.5.2.4 Valley MTS

In Valley MTS, modelled air temperature following the measured SLRs ranged from -6.0 to -3.2 °C with an average across the valley of -5.1 °C (Figure 5-16). Due to the inverted annual SLR below treeline air temperatures were predicted to be coldest in the valley bottom and warm moving upslope until reaching a maximum around treeline. Air temperatures were then predicted to cool from treeline to the highest elevations due to the measured normal lapse rate above treeline. If the inverted SLR was not accounted for, air temperatures would be predicted to be colder than in actuality with modelled AMAT ranging from -10.0 to -5.9 °C with an average of -6.6 °C. As the normal environmental SLR assumes uniform cooling with elevation, the spatial temperature distribution for this model predicts the warmest AMATs in the valley bottom and the coldest at the highest elevations. When comparing the two surfaces, the difference was largest at high elevations where assumption of normal environmental SLR results in an underestimation of AMAT by up to 4.8 °C. Modelled $FDD_a$ ranged from 3026 °C days in the valley bottom to 2358 °C days at mid elevations around treeline (Figure S5-30). Average $FDD_a$ was predicted to be 2795 °C days. Not accounting for the winter inversions resulted in substantially greater predictions of $FDD_a$ ranging from 2994 to 3912 °C days with and average for the valley of 3150 °C days. Following the normal environmental SLR, modelled $FDD_a$ was expected to increase with increasing elevation contrary to the spatial distribution using the measured SLRs. As a result, the greatest difference occurred at high elevations with up to 1197 °C days less than actually expected if a normal SLR was assumed.

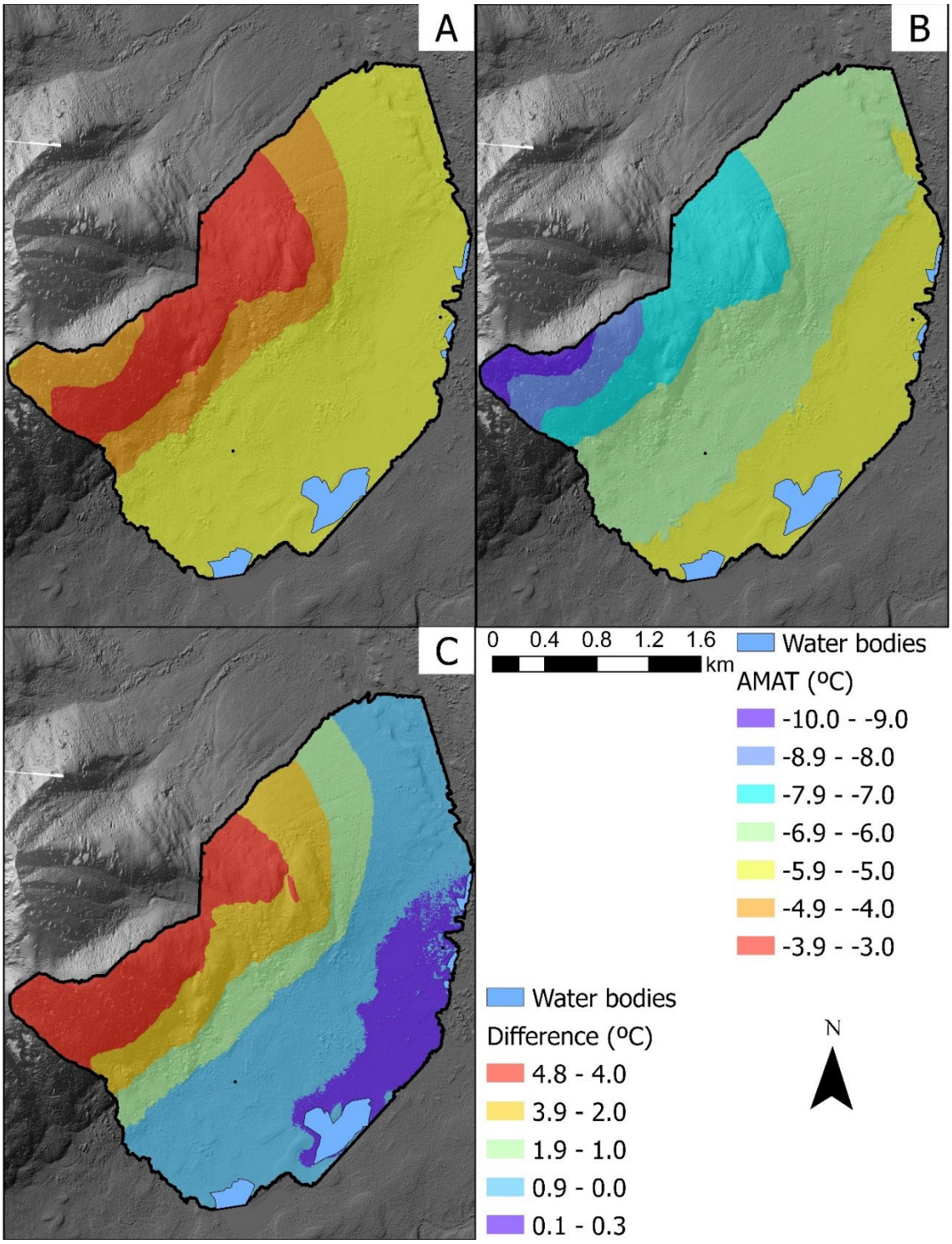


**Figure 5-16.** Annual mean air temperature (AMAT) models for Valley MTS A) Calculated surface lapse rates (SLR), B) Normal environmental SLR (-6.5 °C $km^{-1}$), and C) the difference between the two models where negative values indicate actual AMAT (accounting for inverted SLRs) is colder and positive values indicate actual AMAT is warmer than expected if assuming the normal environmental SLR.

Modelled $TDD_a$ ranged from 815 to 1175 °C days with an average of 1035 °C days (Figure S5-31). Due to the presence of inverted SLR even during the thawing season in this valley, $TDD_a$ was predicted to be highest around treeline (at mid to high elevations) and lowest in the valley bottom. $TDD_a$ at the highest elevations were modelled to be lower than at treeline but higher than those in the valley bottom. If the normal environmental SLR was assumed, average modelled $TDD_a$ was substantially lower than in actuality (883 °C days) with a range from 367 to 988 °C days. As the change in $TDD_a$ with elevation was assumed to be normal, the highest predicted values were in the valley bottom while the lowest were predicted at high elevations. The largest difference between the two models was once again at the highest elevations with actual $TDD_a$ up to 448 °C days higher than expected assuming normal SLR conditions.

RMSE for the $n_f$ model was 0.14 for the training dataset and 0.08 for the testing, while for $n_t$ the RMSE was 0.11 for training and 0.09 for testing. Modelled N-factors ranged from 0.01 to 0.48 for $n_f$ and 0.50 to 1.17 for $n_t$ (Figure S5-32). Average $n_f$ for the entire valley was 0.19 while average $n_t$ was 0.83. Average $n_f$ was highest generally at the higher elevations above treeline on the bare exposed slopes and lower at low to mid elevations especially in the coniferous forest class. Values of $n_t$ were generally highest at higher elevations above treeline and lower below treeline; however, the exact spatial distribution was complicated by topographic position and vegetation class. Rk varied based on vegetation class and elevation but generally increased with increasing elevation and decreasing vegetation cover.

Modelled AMGST had a RMSE of 0.5 °C for the testing sites and ranged from -1.3 to 2.9 °C. Average modelled AMGST was 0.9 °C. The coldest AMGSTs were predicted at the higher elevations while the warmest were predicted around treeline and at mid elevations (Figure 5-17). Despite having the coldest air temperatures, AMGST in the valley bottom remained

relatively warm and was only cold compared to the temperatures at high elevations in locations with high $n_f$ values. If the normal environmental SLR was used, AMGST would be slightly colder than in actuality with an average over the valley of 0.3 °C and range between -3.6 and 2.4 °C. Under this scenario, the coldest AMGSTs were predicted at the highest elevations above treeline while the warmer temperatures were found at low to mid elevations. The difference between the two surfaces was greatest at high elevations where the AMGST model using actual SLRs was up to 2.5 °C warmer than if the normal environmental SLR was used.

Lastly, the RMSE for AMGT was 0.5 °C. Modelled AMGT ranged from -2.8 to 2.7 °C with an average of -0.3 °C for the whole valley. Unlike AMGST, the coldest AMGTs were predicted in the valley bottom and relatively cool AMGT were also predicted at high elevations (Figure 5-18). The warmest AMGTs were predicted for mid elevations particularly exposed ridges in this elevation range. Near surface permafrost was modelled to underlay 61 % of the valley. When a normal SLR was used, the AMGT was slightly colder than that modelled using the measured SLRs with an average AMGT of -0.8 ºC. AMGT for this scenario ranged from -3.8 to 2.4 ºC with the coldest temperatures generally predicted at the highest elevations and relatively cool AMGTs predicted in the valley bottom. Near surface permafrost was also expected to underlay 96 % of this valley. The difference between the AMGT model created using the measured inverted SLRs and the one created using the normal environmental SLR was greatest at high elevations (up to 2.3 ºC) where AMGT was predicted to be colder than in actuality. In the valley bottom AMGT were colder than expected if using a normal SLR. Once again without accounting for the winter inversions air, ground surface and ground temperatures would all be colder than in actuality although less pronounced in this valley due to the low $n_f$, $n_t$ and rk values particularly at low elevations.

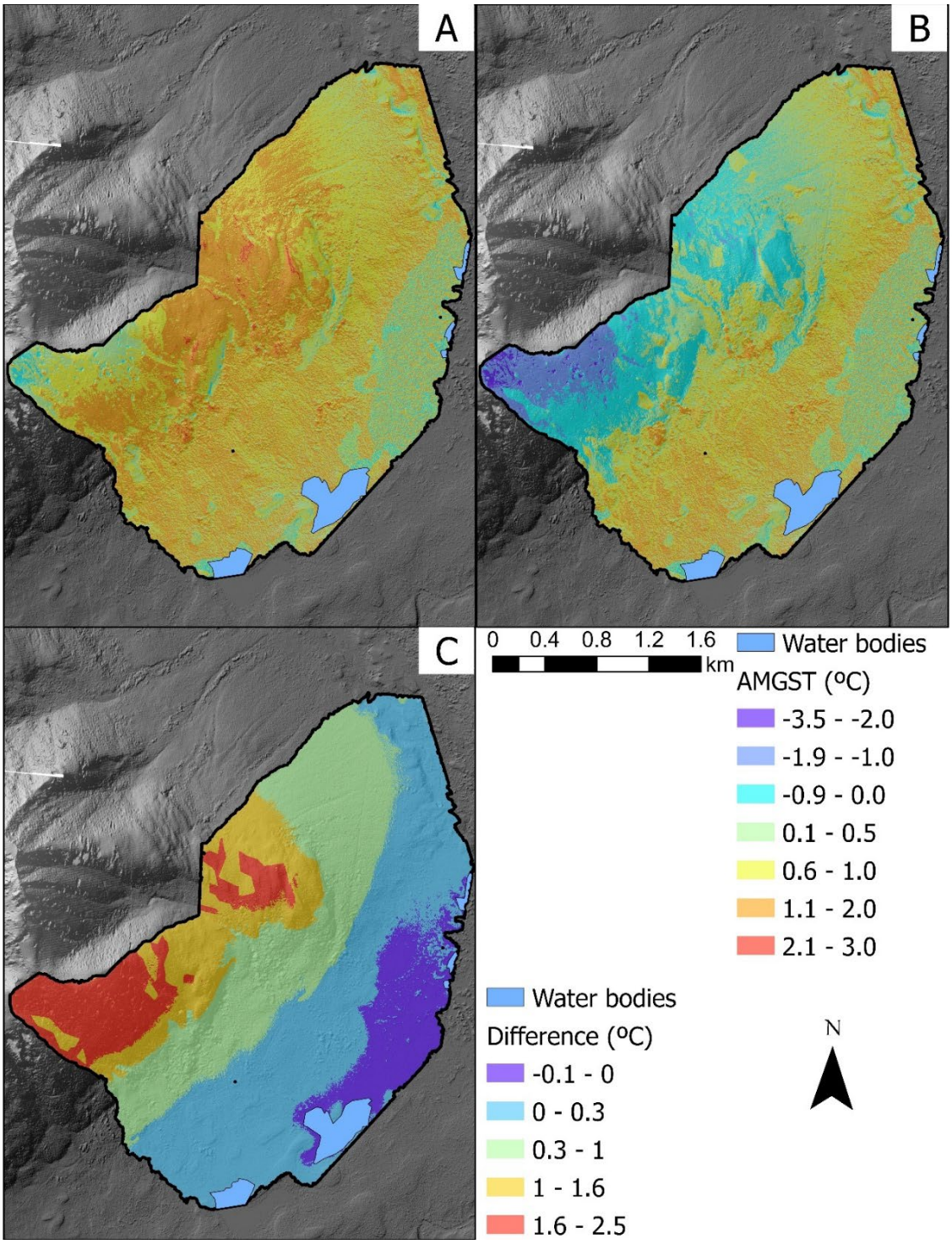


**Figure 5-17.** Annual mean ground surface temperature (AMGST) models for Valley MTS A) calculated using freezing and thawing degree days accounting for inverted surface lapse rates (SLR), B) calculated using freezing and thawing degree days assuming the normal environmental SLR (-6.5 °C $km^{-1}$), and C) the difference between the two models where negative values indicate actual AMGST (accounting for inverted SLRs) is colder and positive values indicate actual AMGST is warmer than expected if assuming the normal environmental SLR.

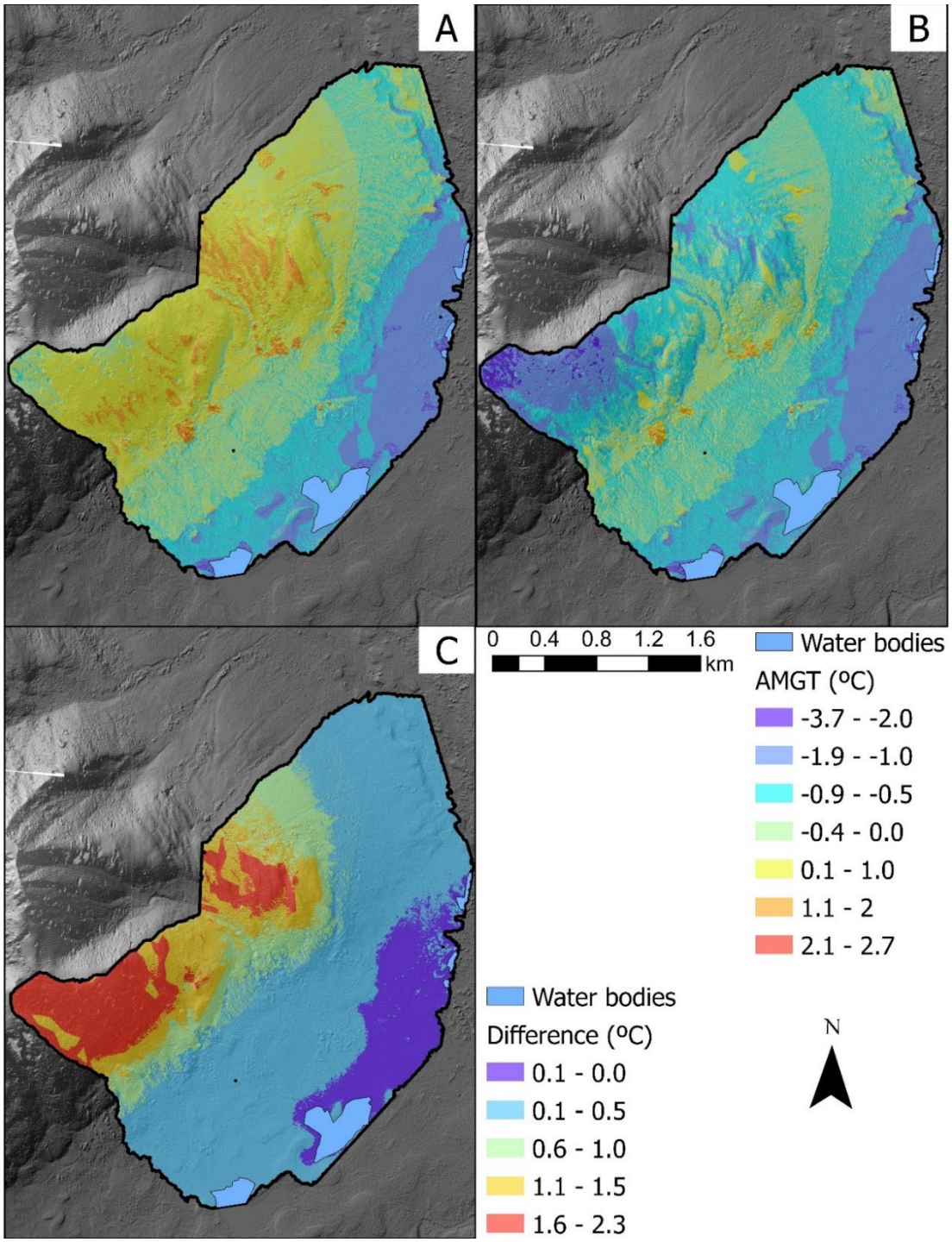


**Figure 5-18.** Annual mean ground surface temperature (AMGST) models for Valley WS02 A) calculated using freezing and thawing degree days accounting for inverted surface lapse rates (SLR), B) calculated using freezing and thawing degree days assuming the normal environmental SLR (-6.5 °C $km^{-1}$ ), and C) the difference between the two models where negative values indicate actual AMGT (accounting for inverted SLRs) is colder and positive values indicate actual AMGT is warmer than expected if assuming the normal environmental SLR.

### *5.5.3 Comparison to Regional Permafrost Probability Model*

The regional model (Bonnaventure et al., 2012) predicts permafrost probability while the models produced in this study represent AMGT, therefore direct comparison is challenging. To remedy this, the average permafrost probability for each valley was compared to the percentage of the valley underlain by permafrost and general visual comparison between permafrost presence (AMGT < 0 ºC) and permafrost probability were made. Although this comparison was not perfect, it allows for some conclusions to be made on the reliability of the regional model. The permafrost probability and permafrost presence were closest in Valley WS01 where average permafrost probability was 71% while near surface permafrost was expected to underlie 80% of the valley. Both models indicated high probability or presence of permafrost at high elevations and in the valley bottom (Figure 5-19 A and C). Both indicated the absence of permafrost or low probability around treeline especially on the southwest facing slope. Valley WS01 was the only valley in which the probability model predicted a lower percentage of permafrost than the local AMGT model. The regional model however did not agree as well in Valley WS02 where permafrost probability was low in the valley bottom despite near surface permafrost present (Figure 5-19 B and D). In this valley, average permafrost probability was 80% while 99% of the valley was predicted to be underlain by near surface permafrost.

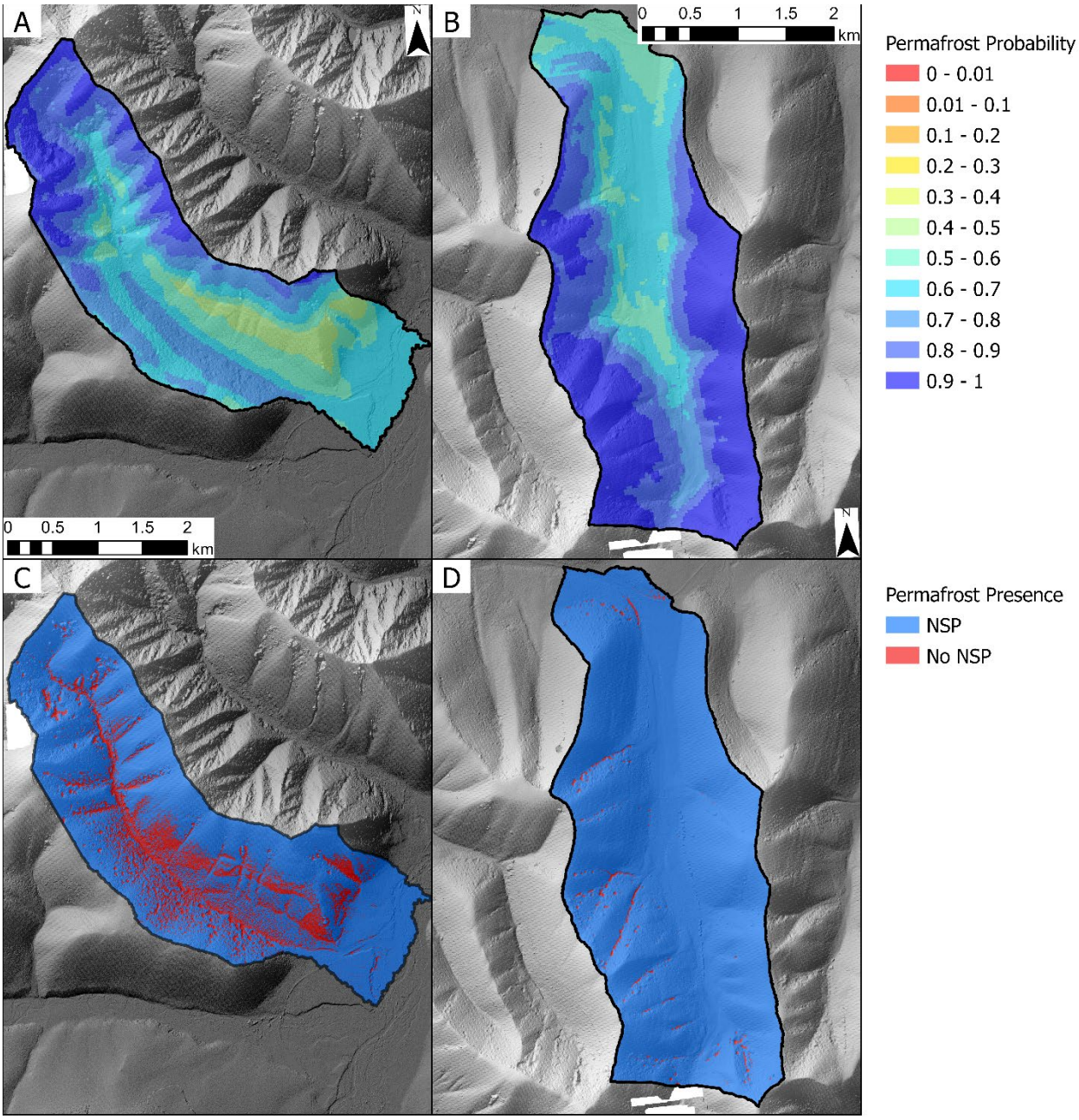


**Figure 5-19.** Permafrost probability from regional model (Bonnaventure et al., 2012) for A) Valley WS01 and B) Valley WS02 and permafrost presence and absence based on annual mean ground temperature (AMGT) for C) Valley WS01 and D) Valley WS02

The probability model had the largest discrepancy in Valley M222 where average probability was 77% while only 33% of the valley had predicted AMGT below 0 ºC. Permafrost probability was predicted to be high throughout the valley and only slightly lower at mid elevations, however permafrost was largely predicted to be absent in this valley (Figure 5-20 A

and C). Finally, in the Valley MTS valley both models captured the lack of or low probability around treeline and the presence or high probability in the valley bottom (Figure 5-20 B and D). In this valley, average permafrost probability was 80%. Overall, the regional model agreed with most of the local AMGT models capturing the general patterns of permafrost distribution.

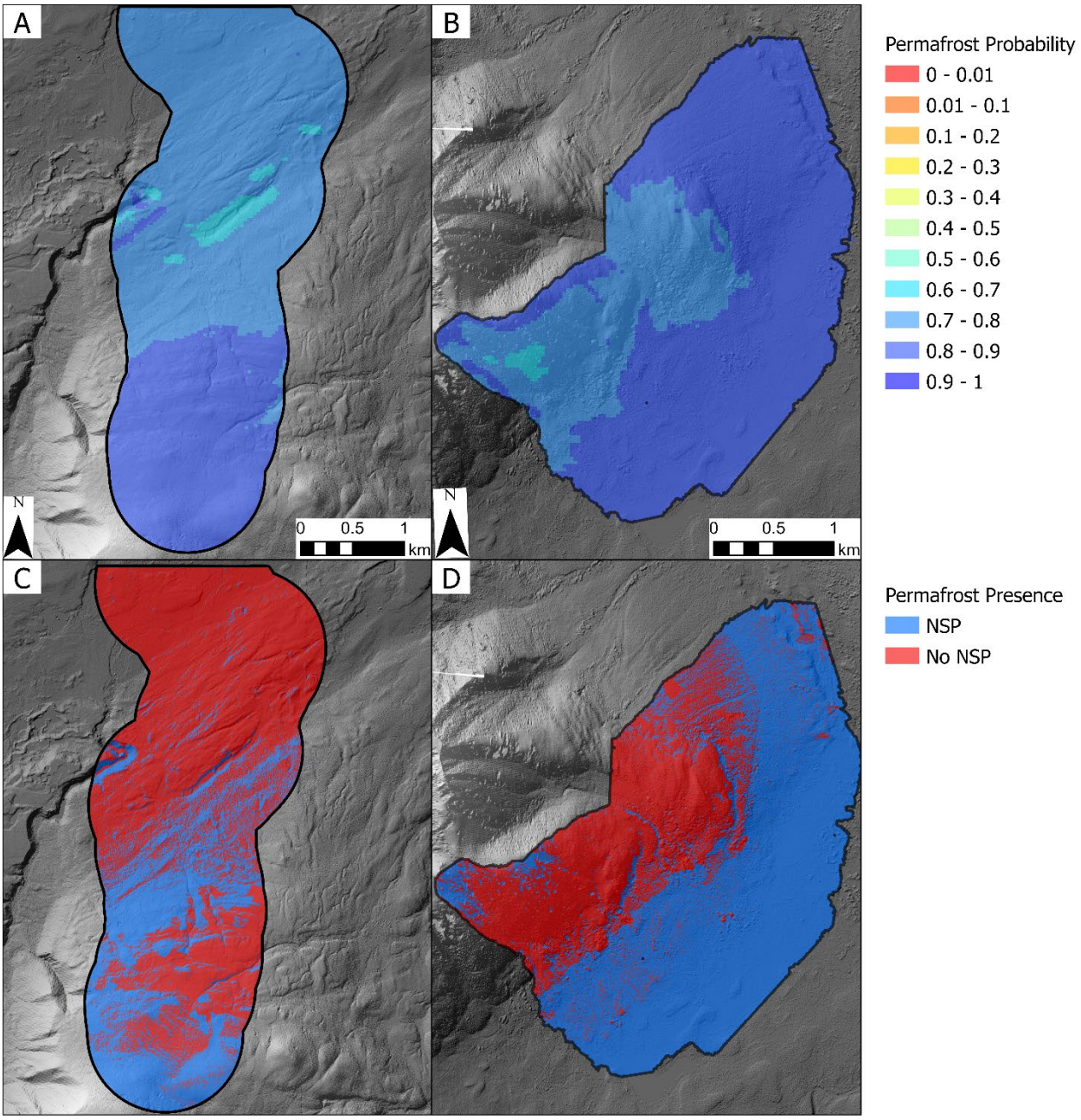


**Figure 5-20.** Permafrost probability from regional model (Bonnaventure et al., 2012) for A) Valley M222 and B) Valley MTS and permafrost presence and absence based on annual mean ground temperature (AMGT) for C) Valley M222 and D) Valley MTS.

## 5.6 Discussion

### *5.6.1 Errors and Locations of Uncertainty*

Although, the RMSE for the AMGST and AMGT surfaces are comparable to those from previous modelling studies (Obu et al., 2019; Garibaldi et al., 2021), there were a few locations within the valleys which may have larger errors. In Valley WS01 and Valley WS02, most of the ground surfaces sensors were located near the front of the valley. As a result, deeper parts of the valley were sampled and therefore were not included in the model creation or testing. This makes it difficult to assess the accuracy of the modelled temperatures in these locations. Additionally, since these parts of the valley were outside of the sampled area, they were modelled more through extrapolation than interpolation, which often lead to unrealistic predictions of $n_f$ and $n_t$. However, the capping of these unrealistic n-factor values likely limited the error in AMGST and AMGT in these locations.

Valley M222 had the largest RMSE for both AMGST and AMGT with the largest errors between the measured and modelled ground surface and ground temperatures found at M222 01 and M222 03 (in the valley bottom and at high elevations). While the model predicted the warmest AMGST and AMGT in the valley bottom and the coldest at high elevations, the measured values at these sites indicated the opposite, with colder AMGST and AMGT at Valley M222 01 than M222 03. One possible reason for this discrepancy is the assigned rk values. At M222 03, measured rk was calculated to be up to 2.0 for certain years. As rk, values in previous literature have been assumed to be equal to or less than 1.0, the maximum rk value used in this modelling was set at 1.0. This may explain why AMGTs were underestimated at this upper elevation site. Finally, another explanation could be the strength of the inverted SLR during the years used in the study. From August of 2016 to August of 2018 the annual SLRs between M222

01 and M222 02 were much more inverted than during the sampling years (up to 19 ºC $km^{-1}$). This likely resulted in colder AMGST and AMGT in the valley bottom during this time. As a result, these residual colder temperatures may have persisted into the sampling year resulting in the under estimation of ground surface and ground temperatures in the valley bottom. Additionally, although the model predicts no near surface permafrost in the valley bottom there is evidence of permafrost in this area as there is at least one palsa in the valley bottom. As the AMAT in the valley bottom during the sampling years was representative of the 1981-2010 climate normal it is therefore possible that the palsa is not in equilibrium with the current climate and is protected by the organic peat allowing it to persist (Seppälä, 1982; Shur & Jorgenson, 2007; Mamet et al., 2017). This may explain why the model does not predict permafrost at this location even though it is present.

Finally, in Valley MTS, the locations with the largest uncertainty in predicted AMGST and AMGT are located in portions of the valley bottom and in locations of burnt coniferous forest. First, there are a number of water bodies located in the valley bottom, which extend into the shrubs lining the shores. As a result, certain parts of the valley bottom classified as shrubs may have extremely wet terrain and be underwater for part of the year. This was attempted to be represented by applying the low rk (0.1) to large portions of the lowest elevations in this valley. The advective heat transfer and moderating impacts of the lakes are not directly accounted for in the model and may explain why $TDD_a$ in the lower portion of this valley increased with increasing elevation. Lastly, the vegetation classification did not have a class for burnt coniferous forest even though recently burned areas are present near the modelling area. Measured AMGST at the burned site were up to 3.5 ºC warmer than a comparable unburnt site (S5-19). As a result, any areas of burnt forest are not accounted for in this model. Although there

are limitations to the models in each valley, overall, they are likely representative of the ground thermal conditions in these valleys and show comparable error to other modelling studies with longer measurement records.

Additionally, since the TTOP model is an equilibrium permafrost model, input parameters should be within the climatological normal in order to accurately predict AMGST. For Valley WS02 and Valley M222, using the longer data record (5 years) resulted in AMAT with a greater discrepancy from the downscaled climate normal than the two-year record used in this study. For Valley M222, the difference between the 5-year record and the climate normal compared to the two-year record was minimal when accounting for the accuracy and precision of the sensors (0.24 to 0.17 ºC, respectively). For Valley WS02 increasing the record length resulted in a 0.6 ºC increase in difference from the climate normal meaning the AMAT in the valley bottom would have been overestimated by 2.2 º rather than 1.6 ºC. For Valley MTS, there were only two years with air temperature data in the lowest part of the valley, however since the AMAT for the two years was only 0.3 ºC different than the climate normal it is unlikely that an additional year or more of data would have improved the accuracy. For Valley WS01, using the 5-year data record would have decreased the difference from the climate normal by 0.7 ºC meaning the AMAT would have only been underestimated by 0.5 ºC rather than 1.2 ºC. Since the air temperatures were underestimated compared to the climate normal, near surface permafrost extent and AMGT may have been over and underestimated, respectively. However, as the purpose of the study was to assess the spatial distribution of the ground thermal regime, the resulting relative distribution of AMGT was likely to be accurate even if the exact magnitude of AMGT is underestimated. Furthermore, as these valleys are located in complex and remote topography there is little in situ data that can be used to validate the accuracy of the downscaled

climate reanalysis data. As a result, it is possible that even these data are not representative of the normal climatic conditions in these valleys.

*5.6.2 SLR Comparison*

The SLRs measured and modelled in Valley WS01 and Valley WS02 were a continuation of previous work in these valleys (Noad & Bonnaventure, 2022). The inversion characteristics in these valleys have previously been analyzed in great detail (Noad & Bonnaventure, 2022). The only new temperature inversion data presented in this study data shows the SLRs measured from the highest sensor in the previous work (the mid elevation sensor for this study) remained inverted to the ridge on the west facing slope of Valley WS02 and the northeast facing slope of Valley WS01. The SLRs on all of the slopes remained inverted to the ridge during the freezing season. As this was only shown during the one year of data collected, a longer record is necessary to determine if this is a regular occurrence. Further investigations and analysis of this phenomenon will be done in future work.

SLRs along the North Canol were more closely aligned with SLR measurements and models for southern Yukon and Northern BC, whereby SLRs were inverted below treeline and normal above (e.g. Bonnaventure et al., 2012). This was especially true for Valley MTS where the SLR was strongly inverted (10.6 °C $km^{-1}$) from the valley bottom to the mid station at treeline and then became strongly normal above treeline to the ridge station (Lewkowicz et al., 2012). However, as Valley M222 is above treeline since much like Valley WS02 trees are not present anywhere in the valley, it is likely that the inverted SLRs would have been mischaracterized and underestimated using the assumption of normal SLRs above treeline (Lewkowicz et al., 2012; Noad & Bonnaventure, 2022). Additionally, as the SLRs in the lower portion of Valley M222 showed substantial variability ranging from 19.4 ºC $km^{-1}$ in 2017-2018

to 5.9 ºC $km^{-1}$ during the year for this study, it is possible that large scale pressure changes and atmospheric conditions may be responsible for this variability. However, this also may be a product of the limited elevation difference between the two air temperature stations (76 m) and the extrapolation to an SLR measured over a kilometer of elevation change. It is also important to note that while SLRs in the lower portion of the valley were highly variable, SLRs in the upper portion of the valley remained normal and consistent throughout the record (difference of 0.5 ºC $km^{-1}$). The inversion characteristics and variability for this region is an area of future work.

### *5.6.3 Influences on Modelled AMGST and AMGT Within and Between Valleys*

The spatial models for AMGST and AMGT showed the impact of the temperature inversions especially when compared to models assuming normal SLRs. When a normal environmental SLR was assumed, AMGSTs at high elevations were expected to be much colder than those predicted using the measured SLR due to the assumed colder AMAT and the high $n_f$ values (low surface offsets) at these locations (Zhang, 2005; Lewkowicz et al., 2012; Bevington & Lewkowicz, 2015; Freudiger et al., 2017). This allowed for a more direct impact of the colder air temperatures on the ground surface. The interaction between AMAT and $n_f$ likely explains why Valley M222 and Valley MTS saw limited difference in AMGST between the measured SLR and normal SLR models. In both Valley M222 and Valley MTS, AMGST at high elevations in both models showed limited difference compared to Valley WS01 and Valley WS02 (1.8 and 2.5 ºC compared to 6.8 and 4.5 ºC, respectively). This may partially be explained by the reversal of the inverted SLR at mid elevations, which resulted in cooling of air temperatures above, limiting the difference in AMAT between the two models at this elevation. However, this may also result from the lower maximum $n_f$ values at high elevations in these valleys (0.83 and 0.85)

compared to those for Valley WS01 and Valley WS02 (1.00), limiting the impact of AMAT on AMGST resulting in similar predicted ground surface temperatures despite the difference in air temperature. The lower maximum $n_f$ values in the valleys with warmer AMGSTs aligns with theoretical values for $n_f$ based on both snow depth and MAAT and measured values in frozen and unfrozen terrain (Smith & Riseborough, 2002; Karunaratne & Burn, 2003; Karunaratne & Burn, 2004). The lower maximum $n_f$ is also likely a product of the increased snowfall and accumulation in the Selwyn Mountains compared to the Ogilvie Mountains (Yukon Ecoregions Working Group, 2004). However, at the highest elevations and most exposed terrain, where snow depth is likely to be relatively low, measured, and modelled $n_f$ for the North Canol valleys could be lower due to the warmer ground conditions resulting in the release of latent heat from the subsurface to the surface longer into the freezing season.

The importance of $n_f$ in moderating the impact of air temperatures can also be observed in the spatial distribution of AMGST in Valley WS02 where the coldest ground surface temperatures were measured and modelled on the west-facing slope. The AMAT model for this valley predicted the warmest air temperatures on the upper portions of the west-facing slope, due to the inverted SLR during winter. However, this was not replicated in the AMGST and AMGT as the west-facing slope was predicted to have a colder ground thermal regime than the rest of the valley. This is a product of the higher $n_f$ (lower surface offsets) on this side of the valley due to the convexity of the slope compared to the opposing side. This allows for the most freezing season cooling on this side of the valley, compensating for the warmer AMAT, highlighting the importance of winter, and freezing season conditions on the annual ground thermal regime.

Moving into the subsurface, accurately characterizing the SLRs in these valleys is essential to the correct estimation of near surface permafrost coverage as assuming a normal SLR

resulted in an overestimation of near surface permafrost extent. For all valleys, AMGT and near surface permafrost presence or absence was correctly determined for the valley bottom using the normal environmental SLR. This is likely a product of using the same starting air temperature measured in the valley bottoms. Due to the similarity in air temperature in the valley bottoms, the ground temperature at depth was also the most similar in these locations. However, due to the low rk values, it is also likely that given a larger discrepancy in air temperature between the two models in the valley bottom the AMGT should remain similar due to the low rk values buffering the ground at depth from the climate.

The rk values and the ground thermal conditions of each valley influence both the difference in AMGT and near surface permafrost extent predicted by both models. The Valley WS01 and Valley WS02 AMGT models showed fairly large differences in average AMGT between the models using measured SLR and using the normal environmental SLR, 1.9 and 1 ºC respectively. However, both had limited difference in the percentage of the valley predicted to be underlain by near surface permafrost (8 and 1 %, respectively). This is a result of the cold ground thermal conditions, whereby the increase in AMGT for the measured SLR model did not result in large portions of the valley transitioning from below 0 ºC to above. This however was not true for Valley MTS where the difference in average AMGT between the two models was the smallest (0.5 ºC), but the difference in the percentage of near surface permafrost was the greatest (35 %). This is a product of the marginal nature of this valley with AMGTs under both models predicted to be only slightly below freezing. Therefore, even a small difference in AMGT may result in a location transitioning from near surface permafrost to classified as seasonal frost. Lastly, in Valley M222 there was a large difference in average AMGT (2.2 ºC) but a smaller difference in near surface permafrost extent compared to Valley MTS (18 %). This is likely a

result of the warmer ground thermal conditions in this valley, whereby there is limited marginal permafrost in this valley.

### *5.6.4 Comparison to Previous Models*

Based on previous assessments of near surface permafrost in Canada the two Dempster valleys should be classified as continuous permafrost, whereby permafrost underlays 90-100% of the landscape, and the two North Canol Road valleys should be classified as discontinuous permafrost, 50-90% (Heginbottom, 1995). Valley WS02 was predicted to have 99% near surface permafrost matching the designation given in the circumpolar map. However, Valley WS01 does not fit the designation as only 80% of the valley is expected to be underlain by permafrost. This may result from difference scales used in the circumpolar map creation, as Valley WS01 is located on the margin of continuous to discontinuous permafrost. The classification of Valley MTS as discontinuous permafrost in the circumpolar map matches the results of the AMGT model in this study were 61 % of the valley is predicted to be underlain by permafrost. However, Valley M222 was predicted to be underlain by substantially less permafrost than in the circumpolar map with only 33 % classified as having near surface permafrost. This would instead classify Valley M222 as sporadic. This once again may be a product of differences in scale and the complex topography and remoteness of this region limiting data from this area in the circumpolar map creation. Additionally, as discussed earlier, it is also possible that this area is out of equilibrium with the current climate resulting in errors in permafrost prediction from this study. A previous comparison of this circumpolar map to regional models of permafrost probability in Yukon noted that the northern end was classified as discontinuous while the regional model classified this area as sporadic (Bonnaventure et al., 2012). This was attributed to the presence of strong inversions in these highly continental locations resulting in the absence of

permafrost around treeline. This may also explain why Valley WS01 and Valley M222 were assumed to have a greater permafrost extent in the circumpolar model compared to the predictions of this study. An updated, high spatial resolution circumpolar permafrost map also does not correctly classify all four valleys, with Valley M222 still classified as discontinuous and Valley MTS classified as either discontinuous or sporadic (Obu et al., 2019). This map does however match the classification of Valley WS01, mapping it as discontinuous, but also maps Valley WS02 as discontinuous when in this study it was predicted to be continuous.

The spatial distribution of AMGT closely matches those of previous studies in various parts of Yukon. Both the spatial AMGT models created for the four valleys in this study and larger regional modelling studies in Yukon predict permafrost to be present in both high elevations and in the valley bottom (Bonnaventure et al., 2012; Lewkowicz et al., 2012). This results in no lower elevation limit of permafrost in locations with inverted SLRs, which are generally found in continental mountain regions. However, due to the difference in scale, the distribution of permafrost and AMGT was more complex in each of the valleys than predicted in the regional model. Additionally, assumptions of treeline elevation and a weaker and uniform SLR assumed for all four valleys contributed to model discrepancies. First, the regional model of permafrost probability (Bonnaventure et al., 2012) assumed a 1 $^{o}$C km$^{-1}$ inverted SLR in all four valleys. Second, based on assumptions of treeline, Valley WS01, Valley MTS and Valley M222 were all considered to be partially below treeline while Valley WS02 was above treeline entirely. This impacted permafrost probability predictions as inverted SLR were only implemented in valleys with elevations below treeline. The SLRs were also assumed to be normal above treeline. As a result of these assumptions, the regional model's permafrost probability predictions matched each of the fine resolution models of AMGT for each valley differently.

In Valley WS01 the regional permafrost probability model (Bonnaventure et al., 2012) and the local AMGT model showed the best agreement both in terms of the spatial distribution of permafrost and the percentage of near surface permafrost likely present in the valley. This is likely due to this valley adhering to the model assumptions (treeline and forested) and its proximity to one of the training locations (Dawson). Additionally, this valley was the only one where the probability model predicted less permafrost than the local AMGT model. This could be a product of the slightly colder than average air temperature conditions in the creation of the local model. There was also good agreement between the regional and local model for Valley MTS in terms of the spatial distribution pattern and the area of the valley predicted to be underlain by permafrost. Again, this is likely a product of correct prediction of treeline for the valley. However, there was a larger difference for this valley than Valley WS01, possibly since it was farther away from the sampling locations. Although the SLR used in the regional model vastly underestimated the strength of the inversions present in these valleys it did not largely impact the permafrost probability prediction. This is potentially because of the mature ecosystem present in these valleys limiting the impact of air temperature on permafrost presence especially in the valley bottom (Shur & Jorgenson, 2007). Additionally, as the regional model assessed permafrost probability rather than strict presence or absence as in the local models there is more leeway for error, which may have limited the impact of the misclassification of the inversion strength. However, in Valley MTS, the underestimation of the inverted SLR likely contributed to higher probability of permafrost at treeline and at some higher elevations than in the local model as air temperatures were not expected to warm as rapidly with elevation.

The regional model did perform well in Valley WS02 and Valley M222 likely because these valleys did not conform to assumptions made in the model. First, Valley WS02 was

predicted to be above treeline in the regional model and therefore was assumed to have a normal SLR. This led to low permafrost probability predictions in the valley bottom compared to AMGT in the local model. As a result, the valley was classified as discontinuous rather than continuous as in the local model. This misclassification is more likely a product of assuming a normal SLR rather than a discrepancy in the magnitude of the inverted SLR used. However, as Valley WS02 was still close to a sampling area for the regional model it still largely captured the probability of permafrost overall better than in Valley M222. In Valley M222, the regional model predicted a high probability of permafrost throughout the valley except at a few areas at mid elevations, likely because it was misclassified as below treeline. Additionally, the closest sampled region for the regional model was farther from this valley than Valley WS02, which likely led to larger inaccuracies in this area. Some of the discrepancy between the two models in this valley may also be attributed to the more marginal permafrost in this valley as a small error in AMGT predictions may have led to the misclassification of permafrost absence. This may have resulted in the local model falling into sporadic permafrost while the regional model classifies it as discontinuous. The regional model, when compared to the local AMGT model overestimated the probability of permafrost at high elevations potentially due to the weaker predicted SLR resulting in limited warming with elevation. Additionally, the high amount of snowfall and shrub dominated landscape may have resulted in overall warmer ground conditions than would be predicted in the regional model if this valley was assumed to be partially below treeline (i.e. forested in the valley bottom). Overall, the regional model performed best in valleys where the elevation assumption of treeline, and therefore the spatial pattern of air and permafrost probability, held true. This was especially true at sites in relatively close proximity to a sampled

region. The model performed the worst in valley bottoms classified as above treeline due to the assumption of a normal SLR in these valleys.

The spatial distribution of AMGT for all four valleys were similar with a generally normal distribution (Figure 5-21). The distribution was the most skewed with a long tail of cold temperatures generally present at high elevations constituting a small portion of the landscape. Valley WS02, Valley M222 and Valley MTS had a narrow range of temperatures with a normal distribution generally due to the warmer AMAT at the exposed locations limiting how cold the ground can become during winter. The four valleys had a much different AMGT distribution than a similar size area at Cape Bounty, Melville Island, Nunavut (Garibaldi et al., 2021). The temperature distributions in Valley WS02, Valley M222, and Valley MTS appear similar to that at Cape Bounty under climate warming scenarios where the long tail of warm temperatures is reduced as larger portions of the landscape begin to warm. As such the distribution curve shape in these valleys likely result from limited cold AMGT due to warmer air temperatures at exposed locations, while warm locations are protected or moderated from AMAT through high thermal and surface offsets. As a result, the distribution of ground temperatures is limited on both ends producing a normal distribution.

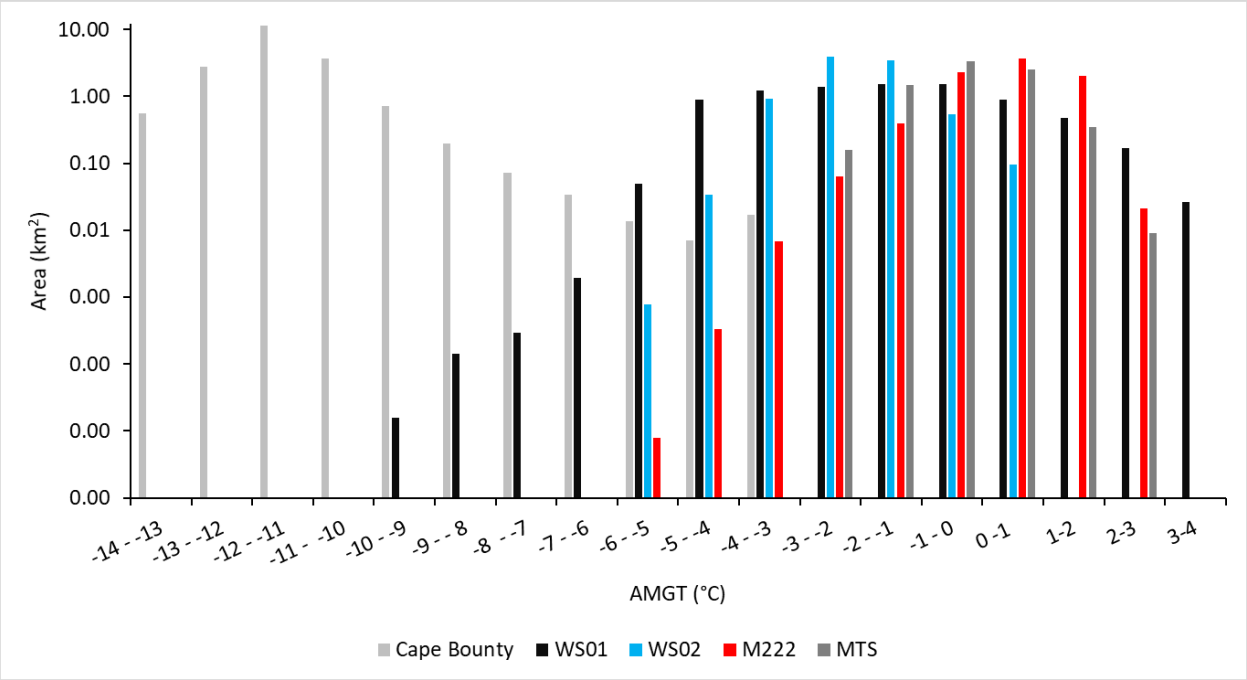


**Figure 5-21.** Histograms for AMGT in all four valleys and a High Arctic Site (Cape Bounty) taken from (Garibaldi et al., 2021).

## 5.7 Conclusion

Overall, the strong persistent winter inversions in these four valleys greatly impacted the spatial distribution of AMAT, AMGST and AMGT with elevation. As a result of the annually inverted SLR, air temperatures in each valley were predicted to be coldest in the valley bottom. Depending on the height of the inversions, the warmest air temperatures were either located at mid elevations (corresponding with treeline if present) or at the highest elevations if the inversion persistent until the ridgeline. This contradicts the typical assumption of air temperature distribution where the coldest temperatures were typically assumed to be present the highest elevations. The inversions present in these valleys also impacted the spatial distribution of the ground surface and ground thermal regimes with the coldest AMGST and AMGT predicted in the valley bottoms and at high elevations in all but one valley (Valley M222). This permafrost distribution pattern held true even for the valleys assumed to be underlain by discontinuous

permafrost where permafrost was predicted to be present in the valley bottoms and high elevations, while absent at mid elevations. However, the spatial distribution of the ground thermal regime was also dependent on snow cover, vegetation, and substrate properties, which limited the impact of the inverted SLRs in certain valleys and locations. As a result of the surface and subsurface characteristics ground temperatures were also predicted to be relatively cold even in locations with relatively warm winter air temperatures and relatively warm in locations with the coldest air temperatures due to differences in snow accumulation.

When a normal environmental SLR was assumed in all valleys AMAT, AMGST, and AMGT were all predicted to be colder than expected especially at high elevations. This assumption led to an over estimation of the area of each valley underlain by near surface permafrost in every valley. The discrepancy in permafrost coverage was especially high for valleys in discontinuous warm permafrost. However, the impact of the mischaracterization of the spatial distribution of the air temperature on the ground thermal regime was also dependent on surface and subsurface properties. In valleys with low surface and thermal offsets, which are more directly influenced by air temperatures, the difference in AMGT between the two SLR scenarios was up to 4.5 °C. However, in valleys with high surface offsets even at the most exposed locations, the difference in AMGT was small relative to the difference in AMAT at the same elevation (2.3 compared to 4.8 °C). Accurate representations and understanding of the current ground thermal distribution with elevation is key to realistic predictions of the spatial response to warming in these mountain environments.

The regional model of permafrost probability agreed with the local AMGT models in valleys meeting the assumptions made in the model creation, namely the position of treeline as an indicator of annually inverted SLRs. This was shown to be especially important as valleys

above treeline were assumed to have a normal SLR and therefore a low probability of permafrost in the valley bottom. However, all the valleys had inverted SLRs regardless of if they were above or below treeline. When the regional model correctly classified the SLR as inverted permafrost probability more closely matched the local AMGT model even if the strength of the inverted SLR was largely underestimated as permafrost was assumed to be present in the valley bottom and high elevations while absent at mid elevations at treeline. Overall, this analysis highlighted that regional models can be an adequate predictor of local conditions assuming the local areas conform to assumptions made in the regional model's creation. Additionally, since the regional model adequately represented conditions in some valleys it can likely be used to inform the spatial probability of permafrost with warming. This is important as spatial warming and permafrost thaw patterns predicted for other mountain regions may not hold true in parts of Yukon due to the atypical permafrost distribution patterns currently present.

In mountain regions with annually inverted SLRs, the spatial distribution of the air and ground thermal regime is different from mountains under normal SLR conditions annually. As a result, an assumption of normality in high-latitude continental mountains such as those in Yukon, results in an over prediction of permafrost presence based on measured air temperatures in the valley bottom and a misrepresentation of the spatial distribution of permafrost. The spatial patterns of AMGT in these four unique valleys, as well as the assessment of the variable impact of the inverted SLR in each valley, may help guide other assessments of current ground temperature distributions and provide a more accurate starting point for studies of future warming in mountain valleys.

# Chapter 6 Exploring the impact of surface lapse rate change scenarios on mountain permafrost distribution in four dissimilar valleys in Yukon, Canada

**Authors:** Madeleine C. Garibaldi[1], Philip P. Bonnaventure[1], Nick C. Noad[1], Will Kochtitzky[2]

[1] Department of Geography and Environment, University of Lethbridge
[2] School of Marine and Environmental Programs, University of New England

**Key words:** TTOP model, permafrost, Yukon, Surface Lapse Rate, Elevation Dependent Warming

## 6.1 Abstract

A scenario-based approach was used to test the air, ground surface and ground response to warming with and without changes to the inverted surface lapse rates (SLRs) in four dissimilar valleys in Yukon. Generally, climate warming coupled with weakening of temperature inversions resulted in the greatest increase at low elevations for air temperature. However, high elevations showed the greatest response to warming and variability between scenarios due to increased connectivity between the air and ground. Similarly, low elevations showed less of a response to warming and permafrost was largely preserved in these locations. Local models also predicted higher percentages of permafrost in each valley with warming than a regional permafrost probability model, due to the inclusion of differential surface and thermal offsets throughout the valleys. Results show that the spatial warming patterns in these mountains may not follow those predicted in other mountain environments according to elevation dependent warming (EDW). As a result, the concept of EDW should be expanded to become more inclusive of a wider range of possible spatial warming distributions. The purpose of this paper is not to provide exact estimations of warming but rather to provide hypothetical spatial warming patterns, based on logical predictions of changes to temperature inversion strength, which may not directly follow the distribution projected through EDW.

## 6.2 Introduction

The distribution of mountain permafrost is complex owing to the extreme spatial variability in surface and near surface characteristics, including incoming solar radiation, elevation, slope, snow cover, vegetation, and soil moisture (Shur & Jorgenson, 2007; Gruber & Haeberli, 2009). Generally, however, there are two main distribution patterns based on the change in mean annual air temperature (MAAT) with elevation. First, in low latitude or maritime mountain ranges, permafrost is generally assumed to be present at high elevations and absent at low elevations, following the spatial topographic distribution of MAAT cooling with increased elevation (Guglielmin et al., 2003; Boeckli et al., 2012; Bonnaventure et al., 2012). With warming climate, permafrost in these environments is expected to warm and thaw unidirectionally, with the lower elevation limit of permafrost moving upslope (Harris et al., 2009; Bonnaventure & Lewkowicz, 2013). In these environments, warming is also expected to be amplified at higher elevations due to a variety of mechanisms including changes in albedo, changes in water vapor and latent heat release and aerosols (Pepin et al., 2015a). This phenomenon is referred to as elevation dependent warming (EDW) and has been supported by observations and climate modelling studies in the Andes, Rocky Mountains, and Alps (Minder et al., 2018; Aguilar-Lome et al., 2019; Palazzi et al., 2019; Li et al., 2020; Williamson et al., 2020). However, this concept and observations have only been made in regions with normal, linear relations between air temperature and elevation (Bonnaventure & Lewkowicz, 2011; Rangecroft et al., 2016; Deluigi et al., 2017). As a result, the concept of EDW is already thought to be non-inclusive for certain mountain environments including areas of the Tibetan Plateau, likely due to the lack of elevation dependent temperature trends (You et al., 2010; Li et al., 2020).

A second mountain permafrost distribution pattern is more commonly found in high-latitude, continental mountains, where permafrost is present in both valley bottoms and high elevations as a result of persistent winter temperature inversions (Bonnaventure & Lewkowicz, 2011; Lewkowicz & Bonnaventure, 2011; Bonnaventure et al., 2012; Noad & Bonnaventure, 2022). These inversions produce warming air temperatures with increasing elevation up to treeline or higher, resulting in the warmest air temperatures at mid to high elevations. In such locations the surface lapse rate (SLR) or change in temperature with elevation, is said to be inverted. With warming MAAT, this permafrost distribution pattern and the complicated relation between temperature and elevation may not produce the same warming and thawing pattern as in locations with a linear permafrost distribution. As shown for portions of Yukon subject to inverted SLRs below treeline, warming results in a bidirectional loss of permafrost as thaw advances both up and downslope from treeline (Bonnaventure & Lewkowicz, 2013). However, previously only uniform changes in MAAT have been applied and potential changes in the strength of the inverted SLR were not considered (Bonnaventure & Lewkowicz, 2013). With climate change, winter inversions over larger portions of the Arctic are expected to weaken (become more normal) although there is limited consensus on how surface-based inversions (SBIs) might change (Koenigk et al., 2013; Hou & Wu, 2016; Ruman et al., 2022). This further complicates spatial and elevation warming distribution of both the air and the ground. As a result, EDW may not hold true in the high-latitude, continental mountains due to the presence of persistent inverted SLRs.

The objectives of this paper were to theoretically test potential alternatives to EDW in four dissimilar high-latitude, continental mountain valleys in Yukon through changes in inverted SLR strength and to evaluate the performance of a regional permafrost probability model. This

was done using a scenario-based approach to examine the logical possibilities for responses in warming in both the air and ground thermal regime, as the exact changes in SLR for this region remain undetermined. The results of this study should provide an evaluation of the reliability of EDW both in the high-latitude, continental mountains of Yukon, but also in other locations where the thermal regime is not linearly related to elevation. The results should also demonstrate the potential implications of changing SLRs on the distribution of regional uniform warming predictions.

### 6.3 Study Area

Four valleys with unique temperature inversions strengths, surface characteristics and spatial distributions of the air and ground thermal regimes in Yukon were selected, two along the Dempster Highway and two along the North Canol Road (Figure 6-1). The study areas along the Dempster Highway in the Ogilvie Mountains are called Valley WS01 and Valley WS02, while the sites along the North Canol in the Selwyn Mountains are named Mile 222 Valley (Valley M222) and MacMillan Transect South Valley (Valley MTS). These valleys were primarily selected based on their distinct characteristics and the existence of fine resolution models of the air and ground thermal regime in addition to spatial maps for each of the TTOP model parameters under current conditions. These would allow for scenario-based changes in air temperature and SLRs to assess the potential response in the air and ground thermal regime accounting for spatial differences in surface and thermal offsets.

The Ogilvie Mountains have remained unglaciated since the Pre Reid Glaciation and are mainly comprised of narrow valleys with moderate relief, surface deposits of colluvium and low to moderate segregated and wedge ice Yukon Ecoregions Working Group, 2004; Burn et al.,

2015; O'Neill et al., 2019a). The climate is considered to be Subarctic continental, with moderate precipitation amounts mainly falling as rain in the summer (Yukon Ecoregions Working Group, 2004). Contrastingly, the Selwyn Mountains have been extensively glaciated, resulting in a high elevation range compared to the Ogilvie Mountains, and still have local alpine glaciers Bostock, 1996; Yukon Ecoregions Working Group, 2004). Additionally, these mountains receive some of the highest precipitation amounts in Yukon outside of the Pacific Maritime region (Yukon Ecoregions Working Group, 2004). This heavy amount of snowfall prevents the establishment of continuous permafrost in this region. Large accumulations of glacial sediments are only present in the bottoms of major valleys while the upper slopes and smaller valleys are composed of Holocene colluvium (Yukon Ecoregions Working Group, 2004). Lastly, this region is expected to have low to moderate segregated ice and negligible wedge ice (O'Neill et al., 2019a).

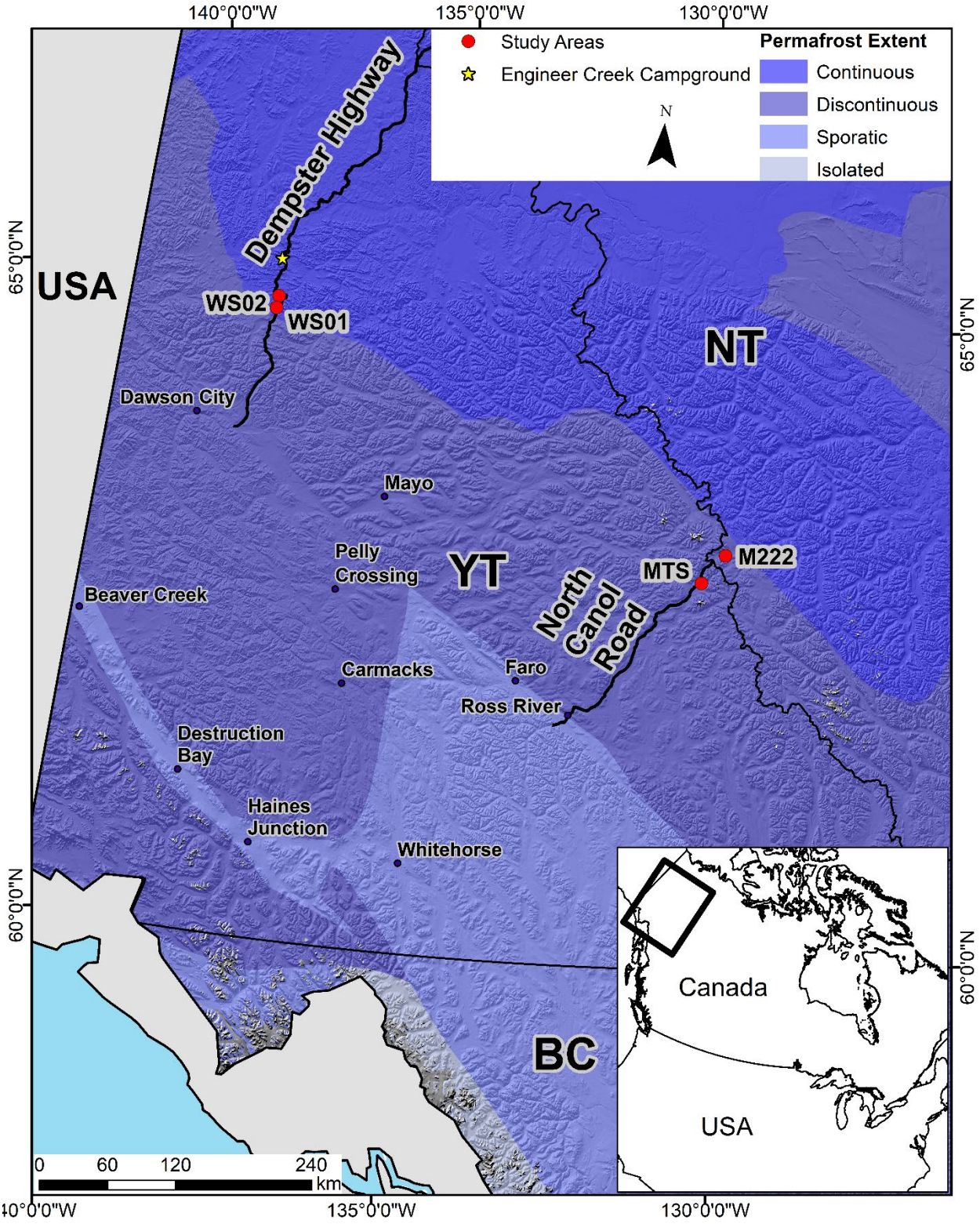


**Figure 6-1.** Map showing the locations of the four study area valleys. Permafrost layer from Brown et al. (2002).

Valley WS01 is the southernmost site in the Ogilvie Mountains, located about 43 km south of the Engineer Creek Territorial Campground. It is an east oriented valley, which is treed on one slope and treeless on the other slope (Figure 6-2).

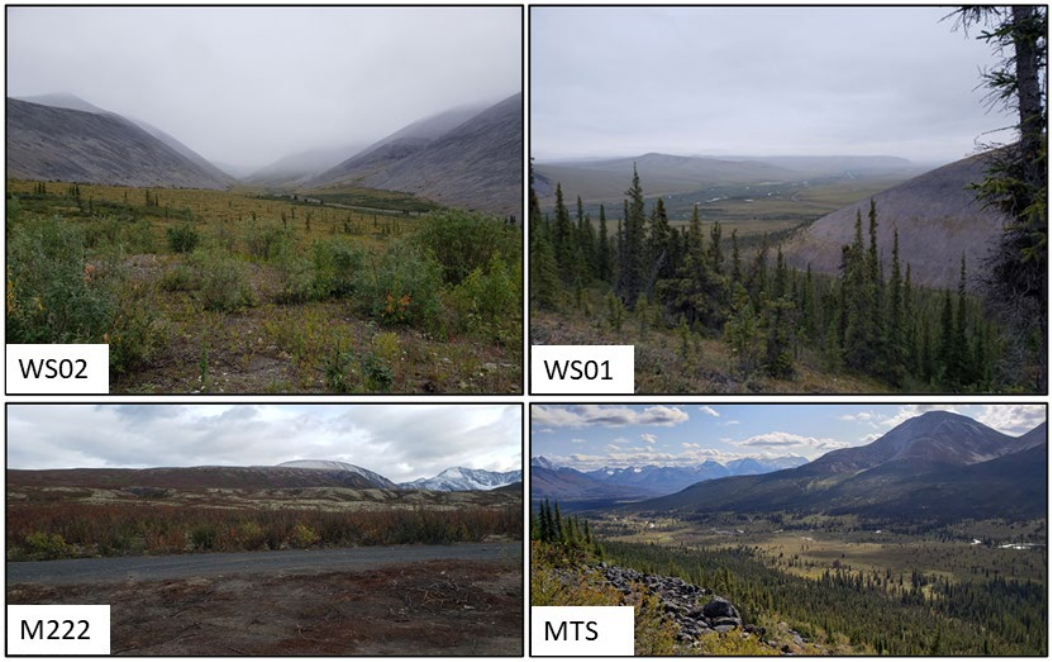


**Figure 6-2.** Site photos for each of the four valleys.

Valley WS01 has an elevation range of about 700 m. Based on previous models, the average AMAT over the valley is -6.4 ºC with the coldest temperatures found in the valley bottom and the warmest around treeline or high elevations (Chapter 5). The valley is considered to be underlain by continuous permafrost, however recent models have shown it is likely to have discontinuous permafrost (Heginbottom, 1995; Bonnaventure et al., 2012; Chapter 5). Additionally, average AMGT was modelled to be -1.6 ºC, with permafrost present in both the valley bottom and at high elevations (Chapter 5).

Valley WS02 is the northern most site and despite being only 10 km away from Valley WS01, is quite different in terms of vegetation. Valley WS02 is a treeless valley, with vegetation consisting of moss and lichen on the valley floor with a few scattered shrubs and scree slopes

(Figure 6-2). This valley has a north orientation. The elevation range in this valley is about 520 m. As in Valley WS01 the strong temperature inversions in this valley result in the coldest AMATs in the valley bottom while the warmest are at the highest elevations due to SLRs remaining inverted or only slightly normal to the ridgetops. Average AMAT over the valley was modelled to be -5.1 ºC (Chapter 5). This valley is also considered to be in the continuous permafrost zone, which is supported by recent local modelling (Heginbottom, 1995; Chapter 5). Average AMGT was modelled to be -2.1 ºC with permafrost only predicted to be absent in deeply incised channels at mid elevations on the east facing slope.

The Mile 222 Valley site is located on the North Canol Highway near the Yukon/ Northwest Territories border in a wide valley. The dominant vegetation is dwarf birch in the lower portions of the valley, transitioning to predominately mosses and lichens at higher elevations (Figure 6-2). AMAT was predicted to be -6.2 ºC over the valley, with the coldest temperatures also predicted in the valley bottoms and the warmest at mid elevations. Despite the comparably cold air temperatures, permafrost was modelled to underlay only a small portion of the valley, likely due to the high amount of snow and shrub dominant vegetation keeping the ground warm during winter. As a result, AMGT over the valley was modelled to be 0.3 ºC. This valley was considered to be underlain by extensive discontinuous permafrost in circumpolar models but was more likely to be underlain by sporadic discontinuous permafrost (Heginbottom, 1995; Chapter 5).

Lastly, Valley MTS is the southernmost site located on the North Canol and amongst the study areas overall. This site has the largest elevation range of the study areas (about 805 m) and is comprised of treed slopes that transition to alpine tundra, consisting of moss, lichen, and scree slopes at high elevations. AMAT was modelled to be -5.1 ºC with the coldest air temperatures in

the valley bottom and the warmest at treeline due to the annually inverted SLR. This valley is also deemed to be in the extensive discontinuous permafrost zone and local modelling predicted average AMGT to be -0.3 ºC (Heginbottom, 1995; Chapter 5).

## 6.4 Methods

### *6.4.1 Current Air and Ground Model Development*

The models for current air temperature metrics were created using in situ data from at least three air temperature stations in each valley and the associated elevations. SLRs were calculated and AMAT was spatially modelled using a 2m digital elevation model (DEM) (Imagery © [2017] DigitalGlobe, Inc.) (Equation 6-1).

$$SLR = \frac{T_2 - T_1}{E_2 - E_1} \tag{6-1}$$

Where T is the daily average air temperature and E is the elevation. AMGST and AMGT were spatially modelled using the temperature at top of permafrost (TTOP) model (Smith & Riseborough, 2002) (Equation 6-2).

$$TTOP = \frac{(rk * n_t * TDD_a) - (n_f * FDD_a)}{P} \quad for\ TTOP \leq 0$$
$$TTOP = \frac{(n_t * TDD_a) - (\frac{1}{rk} * n_f * FDD_a)}{P} \quad for\ TTOP > 0 \tag{6-2}$$

Where rk is the differential thermal conductivity of the substrate, $n_f$ and $n_t$ are freezing and thawing N-factors, $FDD_a$ and $TDD_a$ are freezing and thawing degree days in the air and P is the period (365 days). Each of the TTOP model parameters were calculated and related spatially to

topographical derived variables and vegetation classes. First $FDD_a$ and $TDD_a$ at each air temperature station were calculated (Equation 6-3).

$$DD = |\Sigma_1^P T|, T < 0 \tag{6-3}$$

Where DD are either $FDD_a$ or $TDD_a$, T is the daily average air temperature and P is the period (365 days). The change in $FDD_a$ and $TDD_a$ with elevation was then determined and the 2m DEM was used to spatially model this change (Equation 6-4).

$$\Delta DD = \frac{DD_2 - DD_1}{E_2 - E_1} \tag{6-4}$$

N-factors for 25 ground temperature nodes (GTN) were then calculated using the modelled $FDD_a$ and $TDD_a$ for each site and the measured freezing and thawing degree days at the ground surface ($FDD_s$ and $TDD_s$) (Equation 6-5).

$$n_f = \frac{FDD_s}{FDD_a} \quad \text{and} \quad n_t = \frac{TDD_s}{TDD_a} \tag{6-5}$$

The N-factors where then spatially modelled using Empirical Bayesian Kriging (EBK) and a variety of topographically derived variables. Lastly, rk was spatially assigned based on vegetation class, elevation and topographic wetness. The details for the model creation can be found in Chapter 5.

*6.4.2 Surface Lapse Rate Changes and Climate Change Scenarios*

To assess the potential outcomes of warming and evaluate alternative to EDW in this region, a number of different potential scenarios were run including both baseline warming coupled with current SLR conditions and weakening of the inverted SLRs in each valley. Using the location of the lowest air station, the baseline magnitude of warming was determined for the

shared socioeconomic pathways (SSP) 2-4.5 and 3-7.0 for the 2041-2070 and the 2071-2100 climate normal using ClimateNA (Wang et al., 2016; IPCC, 2022). To determine the magnitude of warming, the difference between MAAT for the downscaled current climate (1981-2010) and the predicted MAAT for each climate warming scenario was added to the measured AMAT for the valley (Table 6-1). This was done to account for discrepancies between the downscaled climate normal and the measured air temperatures in each valley. For the first warming scenario, only the uniform warming was applied and the SLRs were held at the measured current values. For the subsequent scenarios, the annual inverted SLRs were weakened by 1, 2.5, and 5 °C $km^{-1}$ in addition to the baseline warming. The baseline warming was applied in two different ways. First, the warming was applied to the measured AMAT at the lowest elevation air station in each valley and the change in SLR was applied from the same elevation. Second, the warming was applied to the air station at the mid elevation and the change in SLR was applied from this elevation. This was to prevent the overall warming in each valley from exceeding that predicted in each SSP scenario.

**Table 6-1.** Magnitude of the baseline change in MAAT, $FDD_a$ and $TDD_a$ for each valley for the shared socioeconomic pathway (SSP) 2-4.5 scenario 2041-2070 and 2071-2100 climate normal.

| | **ΔMAAT** | | **Δ FDDa** | | **ΔTDDa** | |
|---|---|---|---|---|---|---|
| | **2041-2070 (ºC)** | **2071-2100 (ºC)** | **2041-2070 (ºC days)** | **2071-2100 (ºC)** | **2041-2070 (ºC days)** | **2071-2100 (ºC)** |
| **Valley WS01** | + 2.1 | + 3.1 | - 443 | - 662 | + 240 | + 326 |
| **Valley WS02** | + 2.1 | + 3.1 | - 470 | - 687 | + 228 | + 312 |
| **Valley M222** | + 1.6 | + 2.4 | - 291 | - 478 | + 206 | + 297 |
| **Valley MTS** | + 1.6 | + 2.4 | - 286 | - 468 | + 223 | + 318 |

The TTOP model was used to determine the resulting changes in the ground thermal regime in response to warming air temperatures (Equation 6-2) (Smith & Riseborough, 2002).

For this study, spatial models of $n_f$, $n_t$, and rk developed for current conditions were utilized (Chapter 5). To determine the baseline magnitude of change in both $FDD_a$ and $TDD_a$, the same method as for MAAT was utilized, where the difference between the downscaled climate data for the 1981-2010 climate normal and the values from each climate change scenario from ClimateNA were added to the spatial models for the current climate. As only changes to the winter inverted SLRs are expected with climate change, only the change in $FDD_a$ with elevation was adjusted. To determine the change in $FDD_a$ with elevation that corresponds to the 1, 2.5 or 5 °C $km^{-1}$ change in the annual SLR, the proportion of daily average temperatures below 0 °C was determined for each valley. For each valley, this was about 60 % of the year. The change in freezing season SLR, which corresponded to a 1, 2.5, and 5 °C $km^{-1}$ change in the annual SLR, was then calculated. For each valley, this resulted in a 60 % increase to the proposed annual SLR change due to the proportion of the year below freezing. Theoretical $FDD_a$ for a specified elevation were then calculated using measured air temperatures in the valley bottom and the adjusted freezing season SLR (Equations 6-1, 6-3 and 6-4). Since the inversions are primarily a freezing season or winter phenomenon, only a uniform change in $TDD_a$ was used with no adjustment to the change in $TDD_a$ with elevation. For each scenario, only inverted SLRs were weakened. If the SLR was strongly normal (> 3.0 °C $km^{-1}$), the SLR and $FDD_a$ were kept the same and only the uniform warming was applied. The new $FDD_a$, and $TDD_a$ and SLRs were then used in conjunction with a 2m DEM (Imagery © [2017] DigitalGlobe, Inc.) to spatially model the new $FDD_a$ and $TDD_a$ distribution spatially. These surfaces, in addition to the original $n_f$, $n_t$ and rk surfaces, were then used as inputs in the TTOP model to determine the new spatial distribution of the ground thermal regime. Cells determined to be above 0 ºC were recalculated using the TTOP model equation for seasonal frost.

## 6.5 Results

Only results from the SSP2-4.5 scenario are presented, as the patterns of warming between the two climate change scenarios were the same and a radiative forcing of 4.5 rather than 7.0 is generally used in climate change studies (Nitzbon et al., 2020; Soong et al., 2020; Garibaldi et al., 2022; Ruman et al., 2022). Additionally, only the models with baseline warming initiated at the valley bottom are presented, as they provided average warming most similar to that predicted in the downscaled climate reanalysis data. When baseline warming was initiated at the mid elevation station coupled with changes in the inversion strength, the resulting model had an average predicted warming across the valley that exceeded the predictions of the downscaled climate data. As a result, these models are not shown. Additionally, only the figures for the 2071-2100 climate normal are presented.

### *6.5.1 Changes in Inversion Strength*

In valleys with highly inverted SLRs at lower elevations, even a 5 °C weakening still resulted in annual inverted SLRs in these portions of the valleys (Table 6-2). The only exception to this was the lower east facing side of Valley WS02, where the SLR became normal annually with a 5 °C $km^{-1}$. Additionally, as some of the upper SLRs were only slightly inverted, even small decreases in inversion strength resulted in a change from an annually inverted SLR to a normal SLR. For SLRs at high elevations, which are currently normal, decreasing winter inversions produced an even stronger normal annual SLR, resulting in decreasing air temperature with increasing elevation.

**Table 6-2.** Current and perturbed SLRs for each valley used in the different warming scenarios. Italicized values are the upper elevation SLRs

| | Slope | Current SLR (°C km$^{-1}$) | | - 1 SLR (°C km$^{-1}$) | | - 2.5 SLR (°C km$^{-1}$) | | - 5 SLR (°C km$^{-1}$) | |
|---|---|---|---|---|---|---|---|---|---|
| **Valley WS01** | NE Facing | 8.0 | *0.5* | 7.0 | *-0.5* | 5.5 | *-2.0* | 3.0 | *-4.5* |
| | SW Facing | 11.7 | *-0.9* | 10.7 | *-1.9* | 9.2 | *-3.4* | 6.7 | *-5.9* |
| **Valley WS02** | E Facing | 3.5 | *-0.1* | 2.5 | *-1.1* | 1.0 | *-2.6* | -1.5 | *-5.1* |
| | W Facing | 7.1 | *1.3* | 6.1 | *0.3* | 4.6 | *-1.2* | 2.1 | *-3.7* |
| **Valley M222** | NA | 5.9 | *-2.7* | 4.9 | *-2.7* | 3.4 | *-2.7* | 0.9 | *-2.7* |
| **Valley MTS** | NA | 10.6 | *-5.1* | 9.6 | *-5.1* | 8.1 | *-5.1* | 5.6 | *-5.1* |

This also held true for changes in $FDD_a$ with elevation as the strong winter inversions present in the lower portions of each valley resulted in a decrease in the number of $FDD_a$ with increasing elevation even with a 5 °C km $^{-1}$ weakening of the annual inverted SLR. Although the annual SLR for the lower portion of the east facing side of Valley WS02 became normal with changes to the inversion strength, FDDa continued to decrease with increasing elevation in all of the valley bottoms except Valley M222. Additionally, like the annual SLRs at higher elevations weakening of the inversions resulted in increasing $FDD_a$ with increasing elevation.

### *6.5.2 Potential Changes in the Spatial Distribution of Air Temperature*

In all four valleys a uniform warming scenario without changes in the SLR, MAAT was predicted to warm evenly maintaining the current spatial distribution pattern of air temperatures. As a result, under this warming scenario, the warmest air temperatures in Valley WS01 were still predicted at mid elevations around treeline on the southwest facing slope (Figure 6-3). At Valley

WS02, the warmest air temperatures were predicted at high elevations especially on the west-facing slope similar to the current spatial distribution (Figure 6-4). The warmest air temperatures at Valley M222 were still elevations with the coldest temperatures predicted at the highest elevations (Figure 6-5). Lastly, at Valley MTS, the warmest MAAT were also still predicted at mid elevations, corresponding to treeline (Figure 6-6). However, scenarios involving a uniform warming coupled with a change in SLR strength, altered the spatial distribution of air temperature with elevation, as high elevations became colder relative to temperatures at mid and low elevations. Additionally, due to the reduced warming at high elevations resulting from more weakly inverted SLRs or even a transition to normal SLRs, warming over the valleys was less than predicted in the downscaled climate reanalysis data. This reduction in overall warming increased with decreasing inverted SLR strength, becoming most pronounced for the 5 °C weakening scenario. The magnitude of this reduction was dependent on the strength of the lower inverted SLR and the magnitude and sign (normal or inverted) of the higher elevation SLR.

In Valley WS01, if no change in the SLR occurred, average MAAT across the valley was expected to increase from -6.4 to -3.3 ºC. However, if the strength of the inverted SLR weakened, average air temperatures were only predicted to increase by 2 to 2.9 °C depending on the magnitude. Similarly, for Valley WS02 the warming with no change in SLR scenario produced an average increase of 3 °C across the valley while scenarios involving a change in SLR produced average warming of 2 to 2.9 °C depending on the magnitude of change to the SLR. In Valley MTS, the same pattern was observed with a 2 to 2.3 °C warming with changing SLR compared to a 2.4 °C warming assuming the SLR remained the same. In all three of these valleys, SLR from low to mid elevations remained strongly inverted (SLR > 3.0 °C $km^{-1}$) even with a 5 °C reduction, while the SLR above the mid elevations switched from inverted to normal

(or remained normal), causing the largest change in temperature in the valley bottom and reducing warming at high elevations. At Valley M222 a similar trend was observed with a reduction in warming for scenarios with changes in the SLR, however, there was less of a difference than compared to the other valleys (2.2 – 2.4 °C). Additionally, in this valley under a 5 °C decrease in inverted SLR strength, the SLR remained only slightly inverted (< 1 °C $km^{-1}$). This resulted in air temperatures in the valley bottom remaining only slightly colder than those at mid elevations. Overall, the changes in the spatial distribution of warming and MAAT, specifically the disproportionate less warming at low elevations under reduced SLR strength, highlights how changes in SLR may offset warming at these locations.

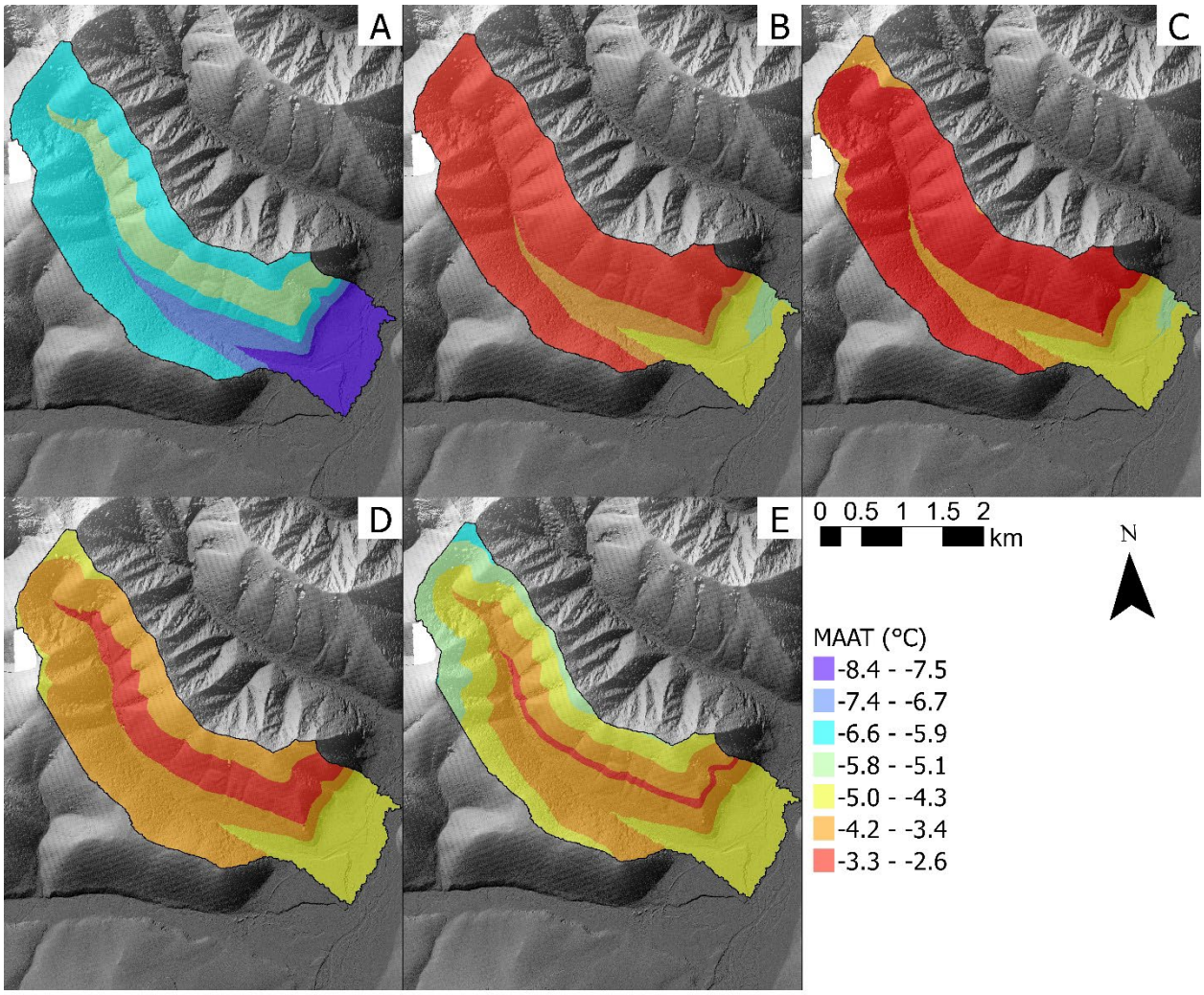


**Figure 6-3.** Spatial distribution of mean annual air temperature (MAAT) in Valley WS01 for A) current conditions, and for the SSP2-4.5 2071-2100 climate normal assuming B) no change in the surface lapse rate (SLR), C) 1 ºC $km^{-1}$ weakening of the SLR, D) 2.5 ºC $km^{-1}$ weakening of the SLR, E) 5 ºC km-1 weakening of the SLR.

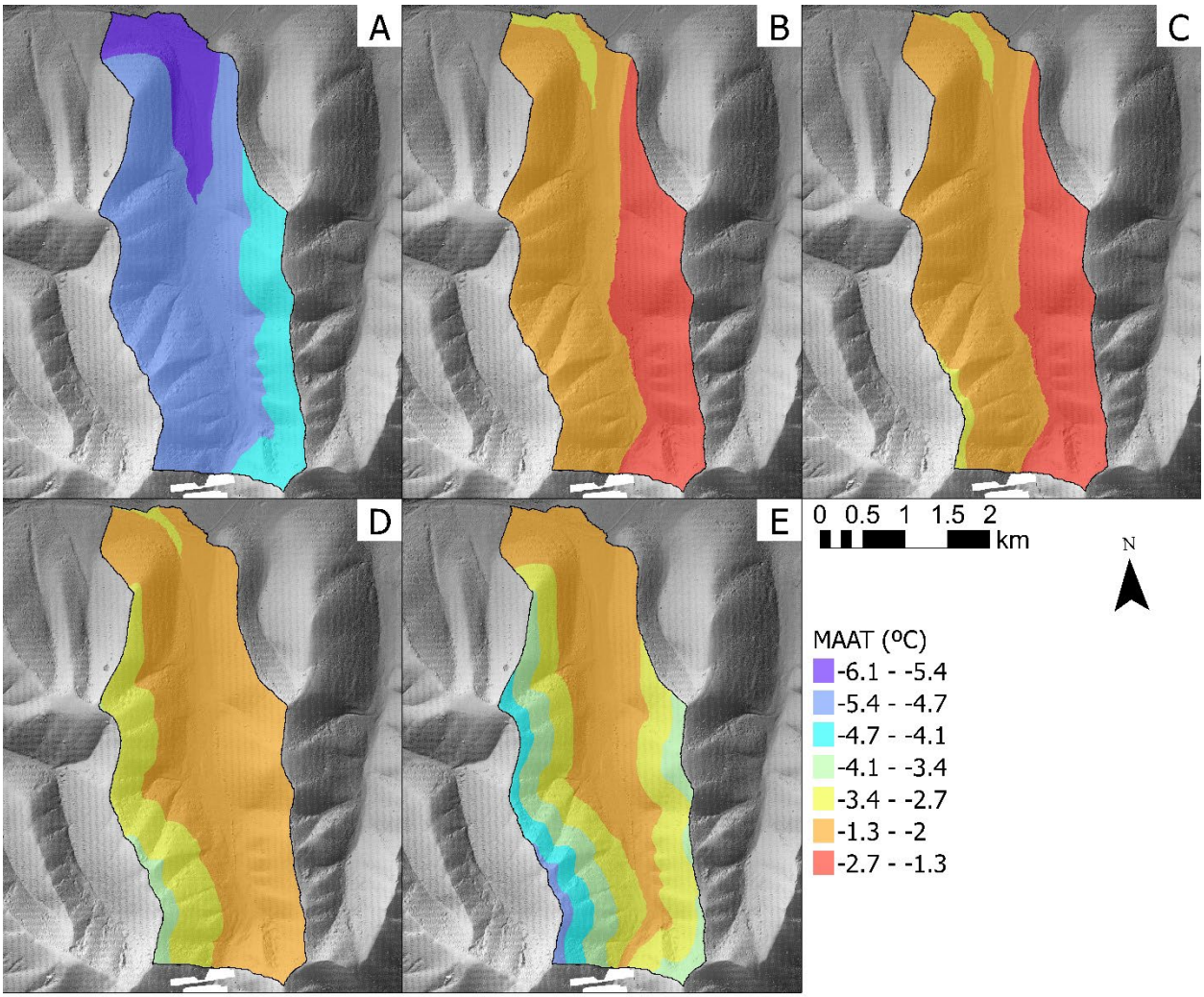


**Figure 6-4.** Spatial distribution of mean annual air temperature (MAAT) in Valley WS02 for A) current conditions, and for the SSP2-4.5 2071-2100 climate normal assuming B) no change in the surface lapse rate (SLR), C) 1 ºC km-1 weakening of the SLR, D) 2.5 ºC km-1 weakening of the SLR, E) 5 ºC km-1 weakening of the SLR.

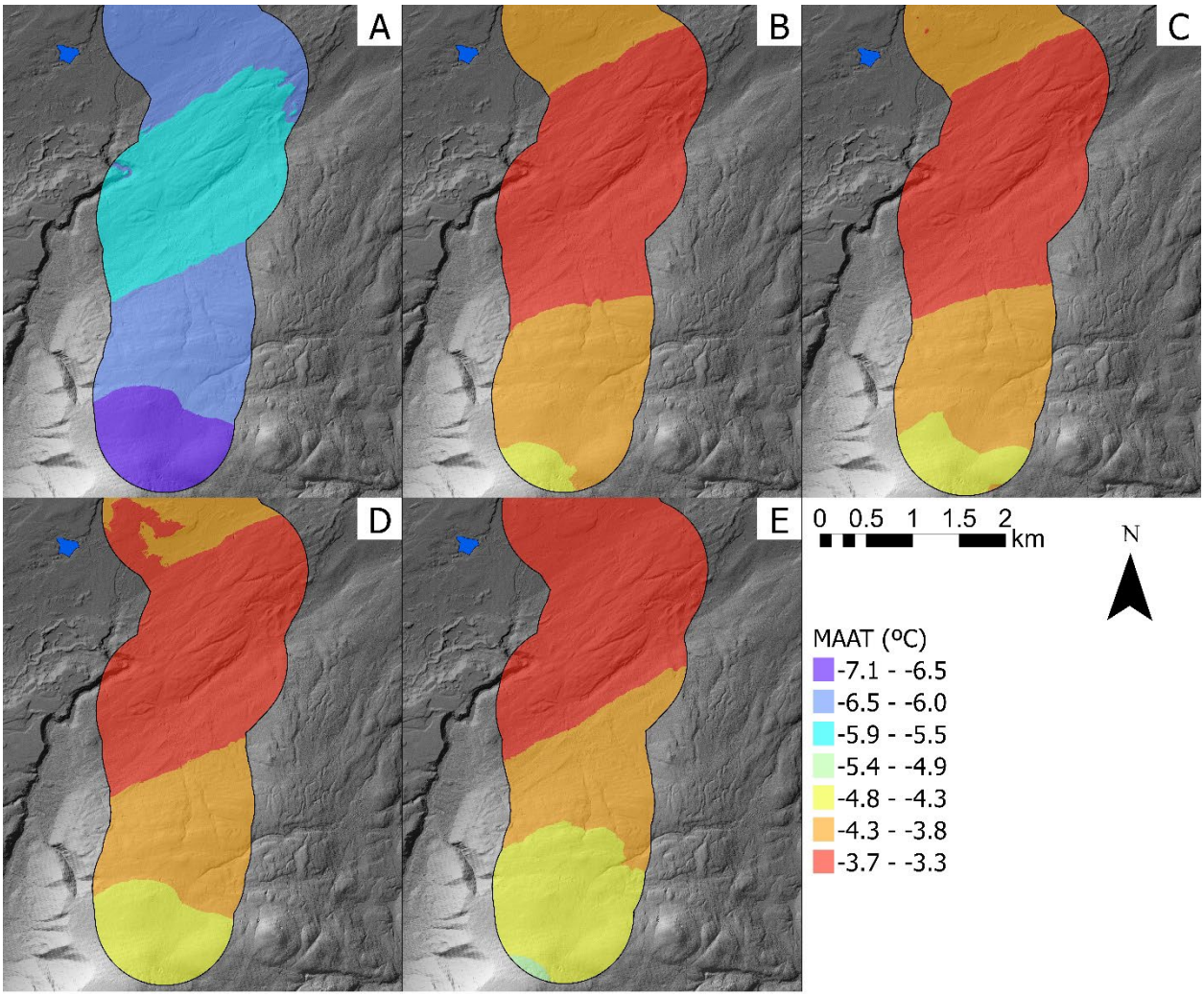


**Figure 6-5.** Spatial distribution of mean annual air temperature (MAAT) in Valley M222 for A) current conditions, and for the SSP2-4.5 2071-2100 climate normal assuming B) no change in the surface lapse rate (SLR), C) 1 ºC $km^{-1}$ weakening of the SLR, D) 2.5 ºC $km^{-1}$ weakening of the SLR, E) 5 ºC $km^{-1}$ weakening of the SLR.

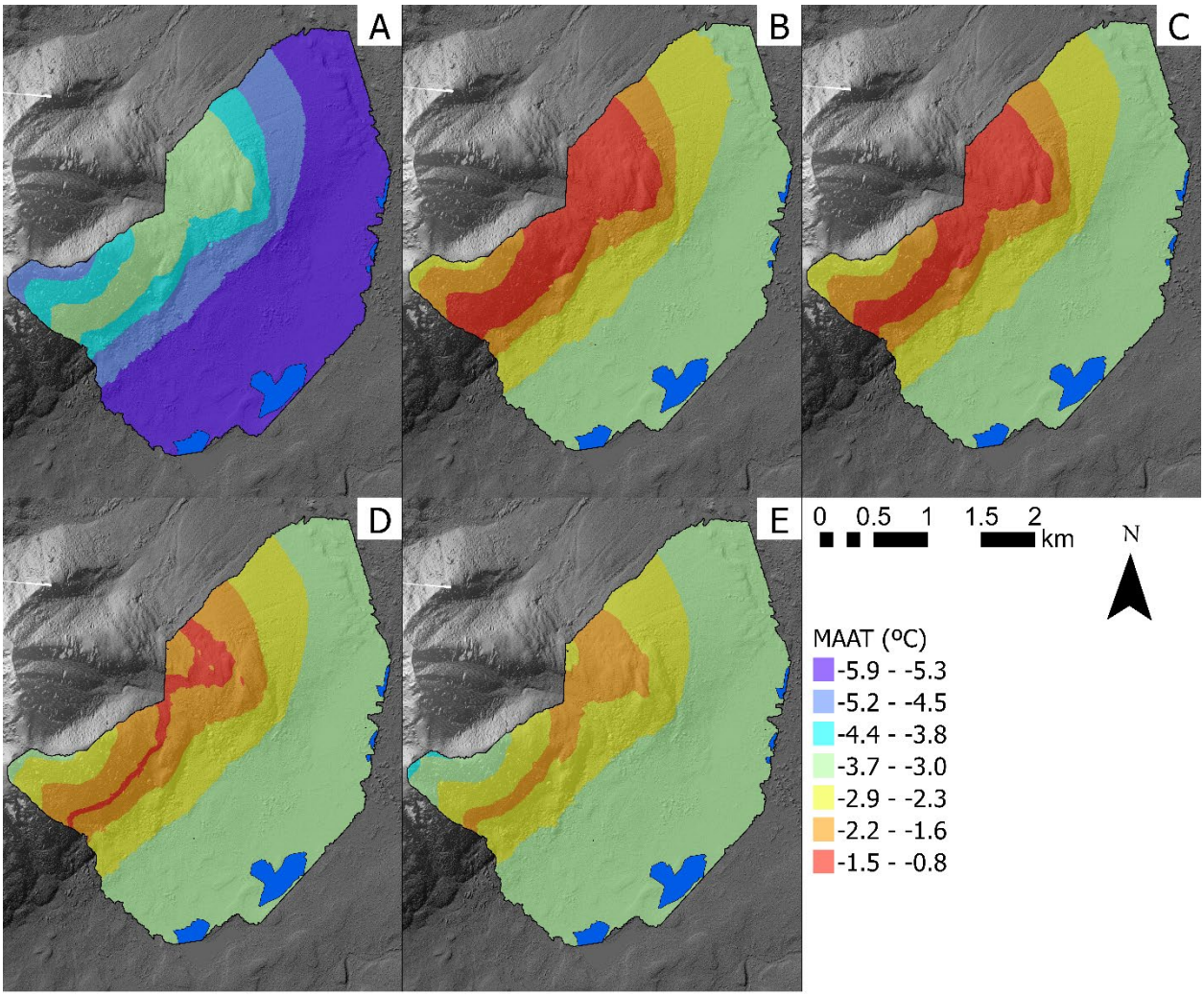


**Figure 6-6.** Spatial distribution of mean annual air temperature (MAAT) in Valley MTS for A) current conditions, and for the SSP2-4.5 2071-2100 climate normal assuming B) no change in the surface lapse rate (SLR), C) 1 ºC km-1 weakening of the SLR, D) 2.5 ºC km-1 weakening of the SLR, E) 5 ºC km-1 weakening of the SLR.

*6.5.3 Potential Changes in the Spatial Distribution of Ground Surface Temperature*

Despite uniform warming in air temperature with no changes in SLR and greater warming at low elevations with changes to the temperature inversion strength, MAGST warmed the most at high elevations for all but the 5 ºC reduction in inverted SLR strength. The exception to this was Valley M222, in which MAGST was predicted to warm the most at high elevations for all scenarios. Under this scenario, the MAGST at high elevations would be expected to warm

the least while ground surface temperatures in the valley bottom would warm the most. As a result, under this scenario the spatial distribution of MAGST would be expected to differ slightly from the current distribution in all valleys except Valley M222, with the coldest air temperatures now predicted to be at high elevations while temperatures in the valley bottoms become relatively warm. In these valleys, the coldest AMGST for all scenarios was predicted to remain at high elevations on the southwest and west-facing slope, respectively (Figure 6-7 and Figure 6-8). At Valley M222, however, MAGST was predicted to warm the most at high elevations for all scenarios, which would result in disproportionately warm AMGST at high elevations compared to the valley bottom (Figure 6-9). Finally, at Valley MTS, MAGST was predicted to remain the warmest at mid elevations around treeline, while temperatures in the valley bottom were predicted to become warmer relative to those at high elevations (Figure 6-10).

Under each warming scenario in all four valleys, the average MAGST warmed less than the average MAAT although the difference was greater with increased weakening of the inverted SLR. The magnitude of the difference was also dependent on the valley with MAGST in warming the least relative to the MAAT in Valley M222 and Valley MTS and warming the most in Valley WS01 and Valley WS02. In Valley WS01 and Valley WS02, average MAGST was predicted to increase by 1.3 to 1.9 ºC depending on the magnitude of weakening to the inverted SLR compared to a potential 2-3 ºC increase in average MAAT. However, for Valley M222 the difference in warming was 0.9 to 1.7 ºC compared to 2.2 to 2.4 ºC for MAGST and MAAT, respectively. For Valley MTS this difference was even greater with average warming of MAGST ranging from 0.9 to 1.0 ºC compared to 2.0 to 2.3 ºC for MAAT. Additionally, the difference in MAGST across the valley for each SLR and warming scenario was less than the difference in the

MAAT. This was especially true in Valley MTS were the average MAGST across the valley ranged from 1.8 to 1.9 between all scenarios.

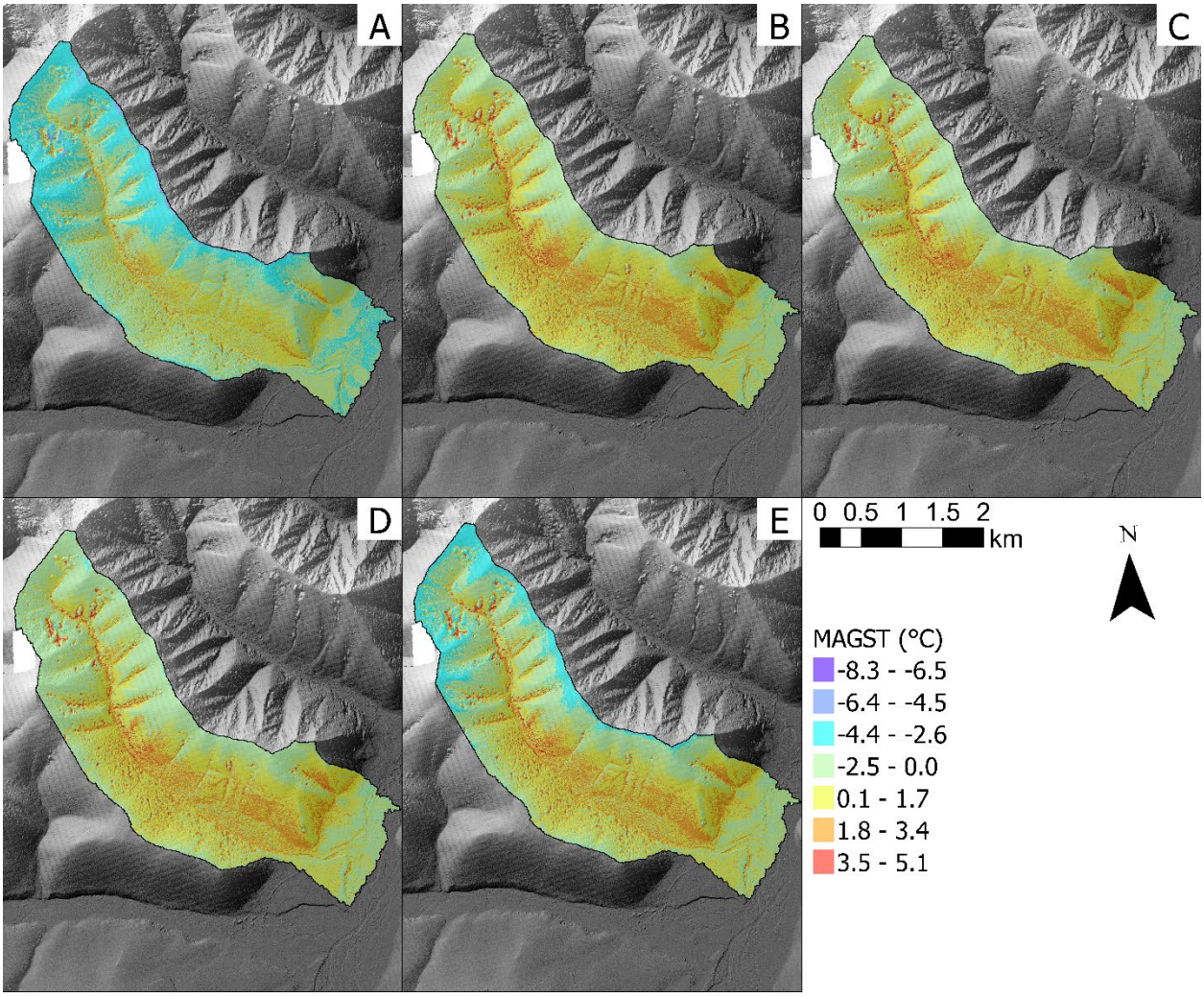


**Figure 6-7.** Spatial distribution of mean annual ground surface temperature (MAGST) in Valley WS01 for A) current conditions, and for the SSP2-4.5 2071-2100 climate normal assuming B) no change in the surface lapse rate (SLR), C) 1 ºC km-1 weakening of the SLR, D) 2.5 ºC km-1 weakening of the SLR, E) 5 ºC km-1 weakening of the SLR.

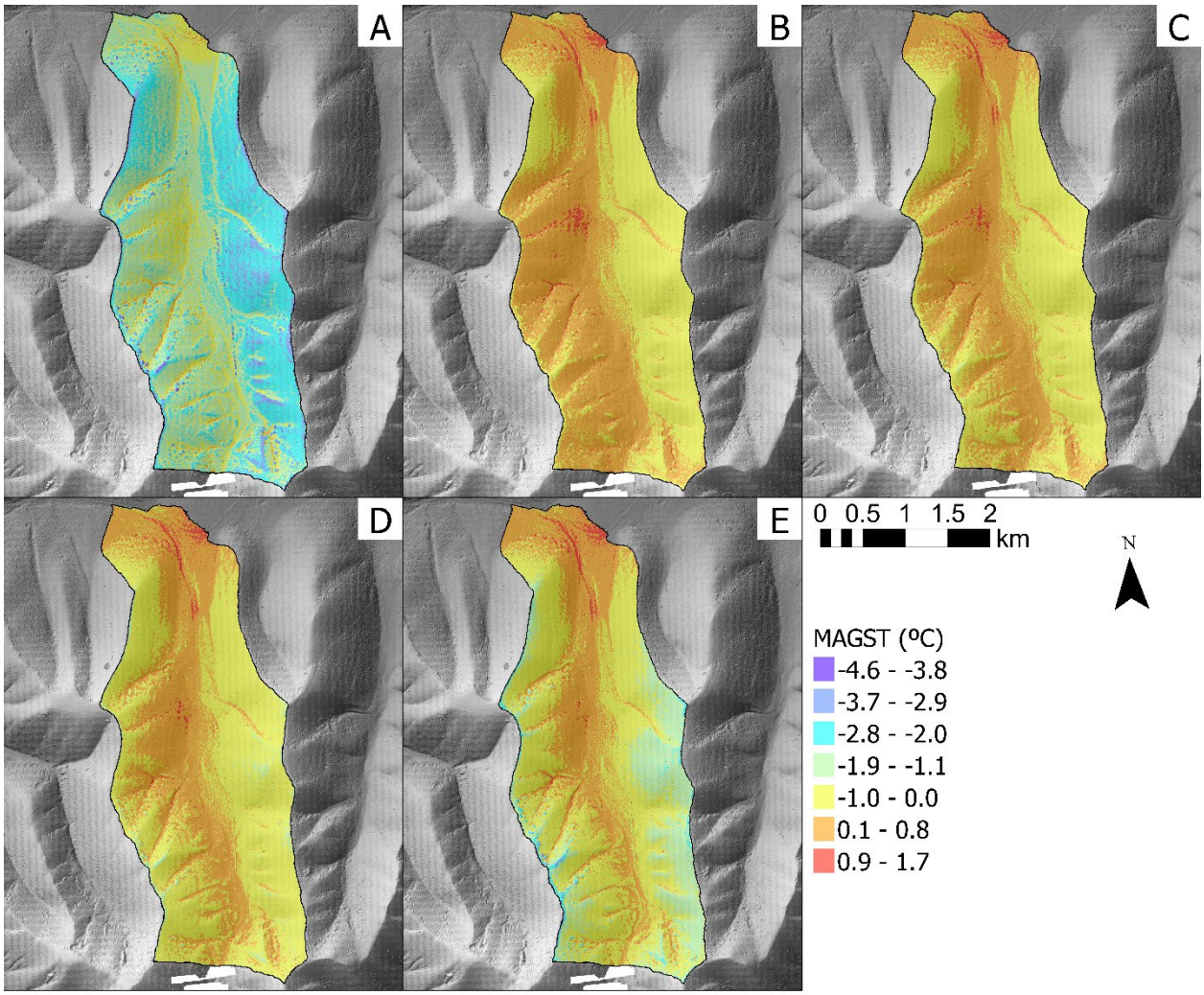


**Figure 6-8.** Spatial distribution of mean annual ground surface temperature (MAGST) in Valley WS02 for A) current conditions, and for the SSP2-4.5 2071-2100 climate normal assuming B) no change in the surface lapse rate (SLR), C) 1 ºC km-1 weakening of the SLR, D) 2.5 ºC km-1 weakening of the SLR, E) 5 ºC km-1 weakening of the SLR.

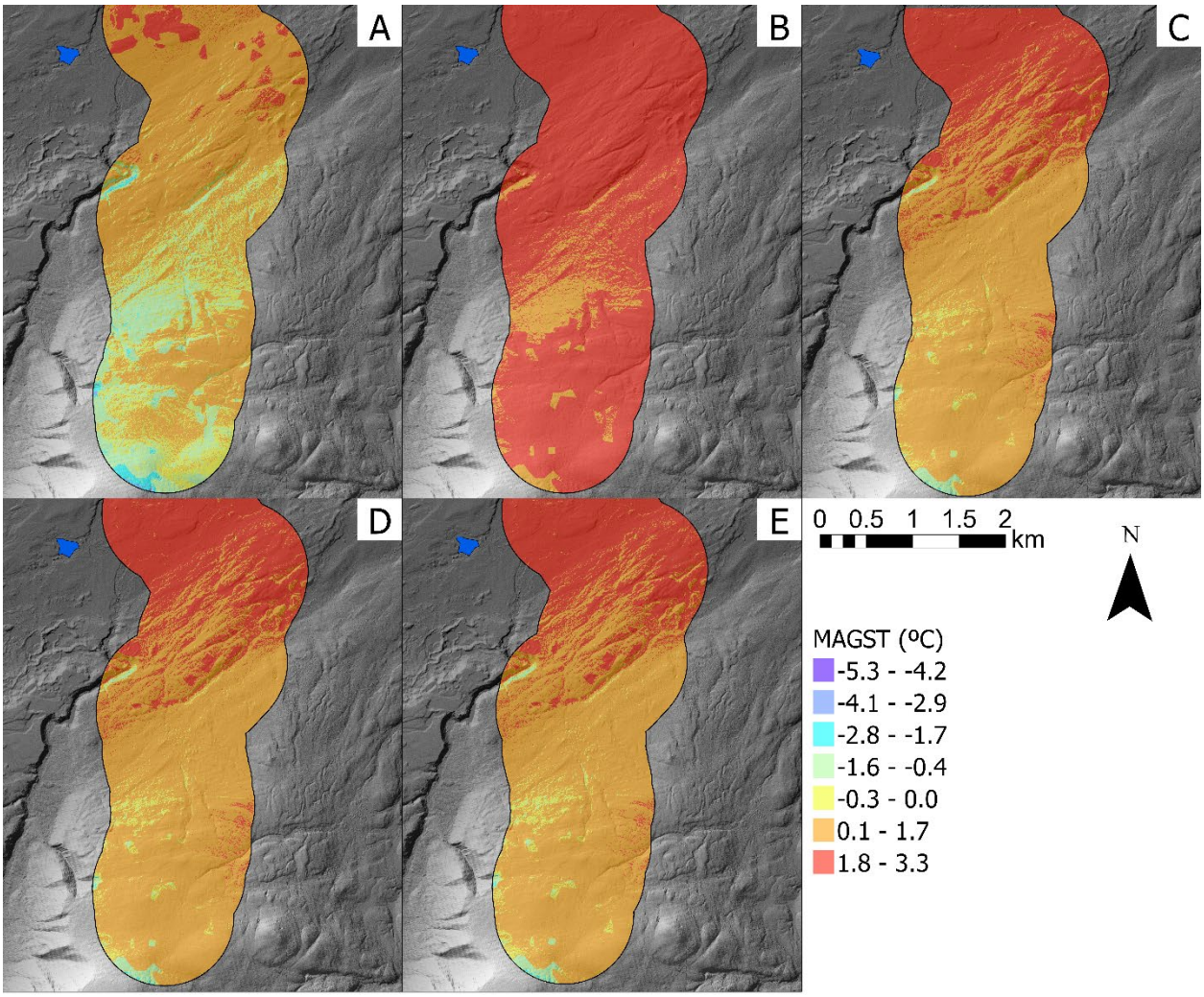


**Figure 6-9.** Spatial distribution of mean annual ground surface temperature (MAGST) in Valley M222 for A) current conditions, and for the SSP2-4.5 2071-2100 climate normal assuming B) no change in the surface lapse rate (SLR), C) 1 ºC km-1 weakening of the SLR, D) 2.5 ºC km-1 weakening of the SLR, E) 5 ºC km-1 weakening of the SLR.

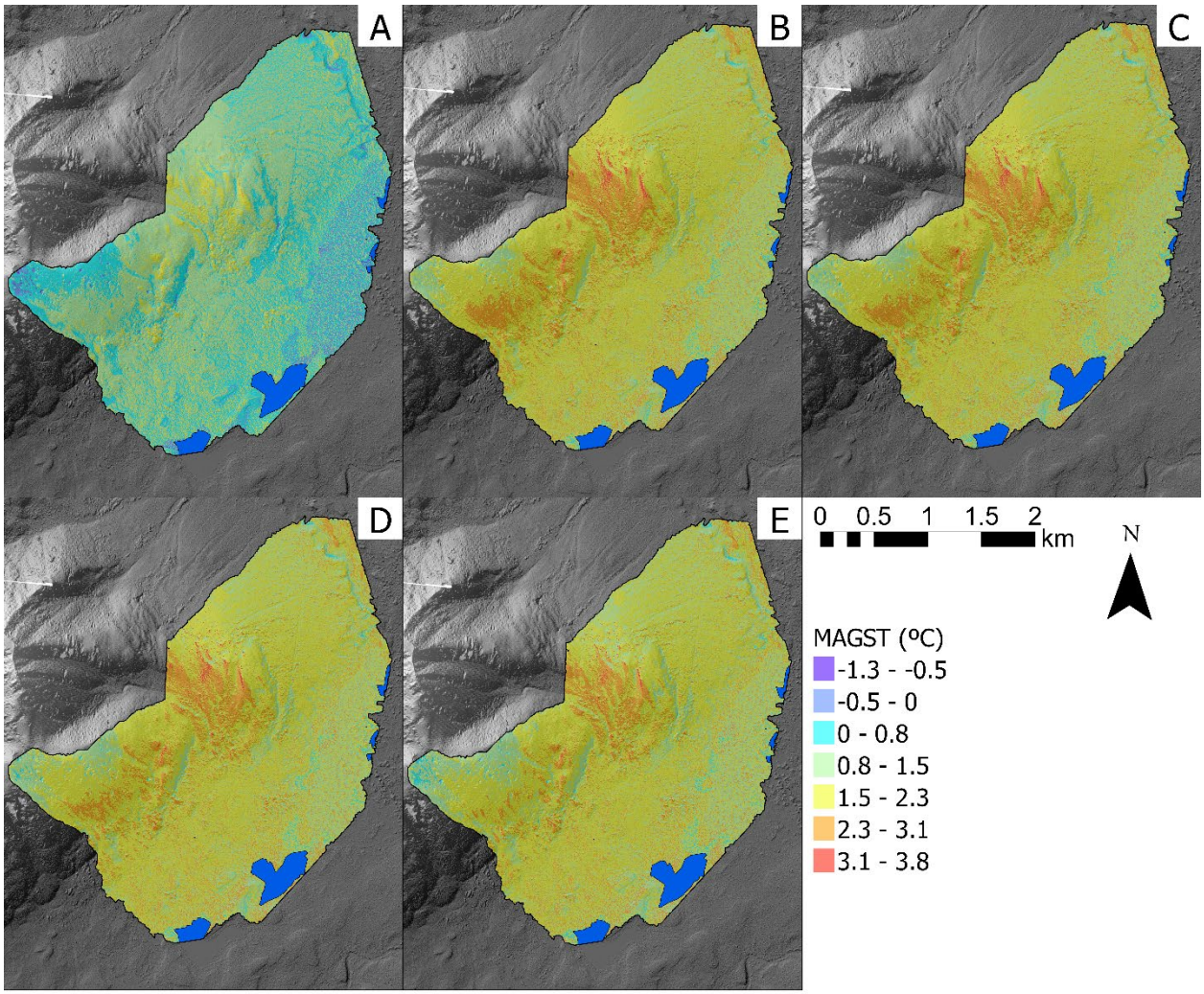


**Figure 6-10.** Spatial distribution of mean annual ground surface temperature (MAGST) in Valley MTS for A) current conditions, and for the SSP2-4.5 2071-2100 climate normal assuming B) no change in the surface lapse rate (SLR), C) 1 ºC km-1 weakening of the SLR, D) 2.5 ºC km-1 weakening of the SLR, E) 5 ºC km-1 weakening of the SLR.

*6.5.4 Potential Changes in the Distribution of Ground Temperature*

For all scenarios and valleys, the pattern of warming for MAGT was the same as MAGST, with the greatest warming at high elevations in Valley WS01, Valley WS02 and Valley MTS except for the 5 ºC decrease in temperature inversion strength scenario. Under this scenario, MAGT at high elevations warmed relatively little compared to temperatures in the

valley bottom (Valley WS01 and Valley WS02) or mid elevations (Valley MTS). In Valley M222, the warming pattern in MAGT was also the same as MAGST. However, there were differences in the spatial distribution of MAGT compared to MAGST and between the warming scenarios in each valley. In Valley WS01, the relatively cold MAGTs were predicted for all scenarios in the valley bottom and at high elevations (Figure 6-11). This was also true in Valley WS02, where the coldest temperatures were predicted on the west-facing slope and in a small portion of the valley bottom (Figure 6-12). In Valley M222, the spatial distribution of MAGTs was the most similar to that of MAGST with the coldest MAGT at high elevations and the warmest in the valley bottom (Figure 6-13). For these three valleys, the magnitude of warming in MAGST and MAGT were similar ranges of 1.2- 1.9, 1.3-1.8, and 0.9-1.8 ºC for Valley WS01, Valley WS02 and Valley M222, respectively. Lastly, in Valley MTS, MAGT in the valley bottom remained the coldest throughout each warming scenario (Figure 6-14). This valley also showed the largest difference in the spatial distribution and warming of MAGST and MAGT with a range of average warming of 0.7- 0.8 ºC for MAGT compared to 1.8 to 1.9 ºC for MAGST across all scenarios.

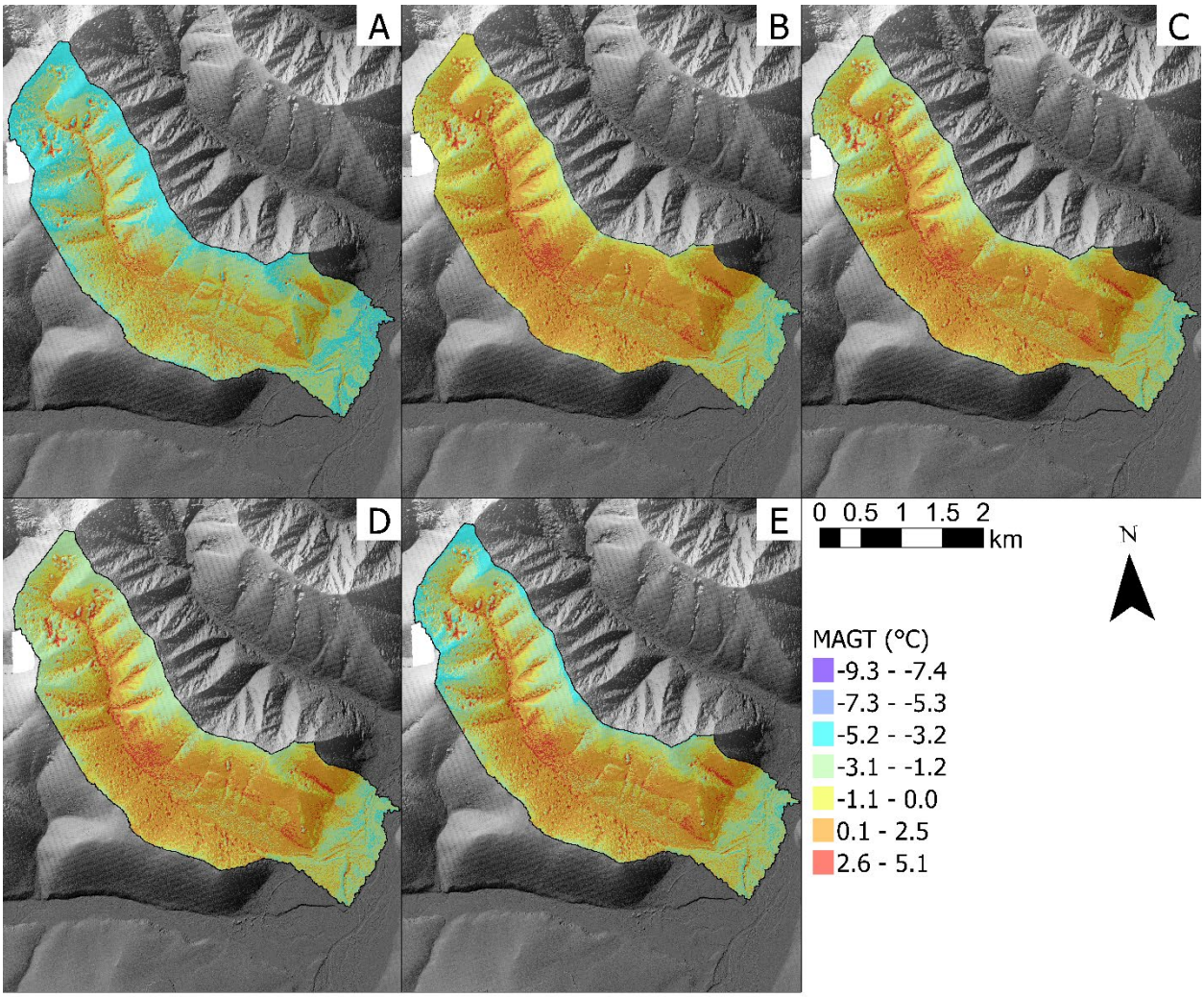


**Figure 6-11.** Spatial distribution of mean annual ground temperature (MAGT) in Valley WS01 for A) current conditions, and for the SSP2-4.5 2071-2100 climate normal assuming B) no change in the surface lapse rate (SLR), C) 1 ºC $km^{-1}$ weakening of the SLR, D) 2.5 ºC $km^{-1}$ weakening of the SLR, E) 5 ºC $km^{-1}$ weakening of the SLR.

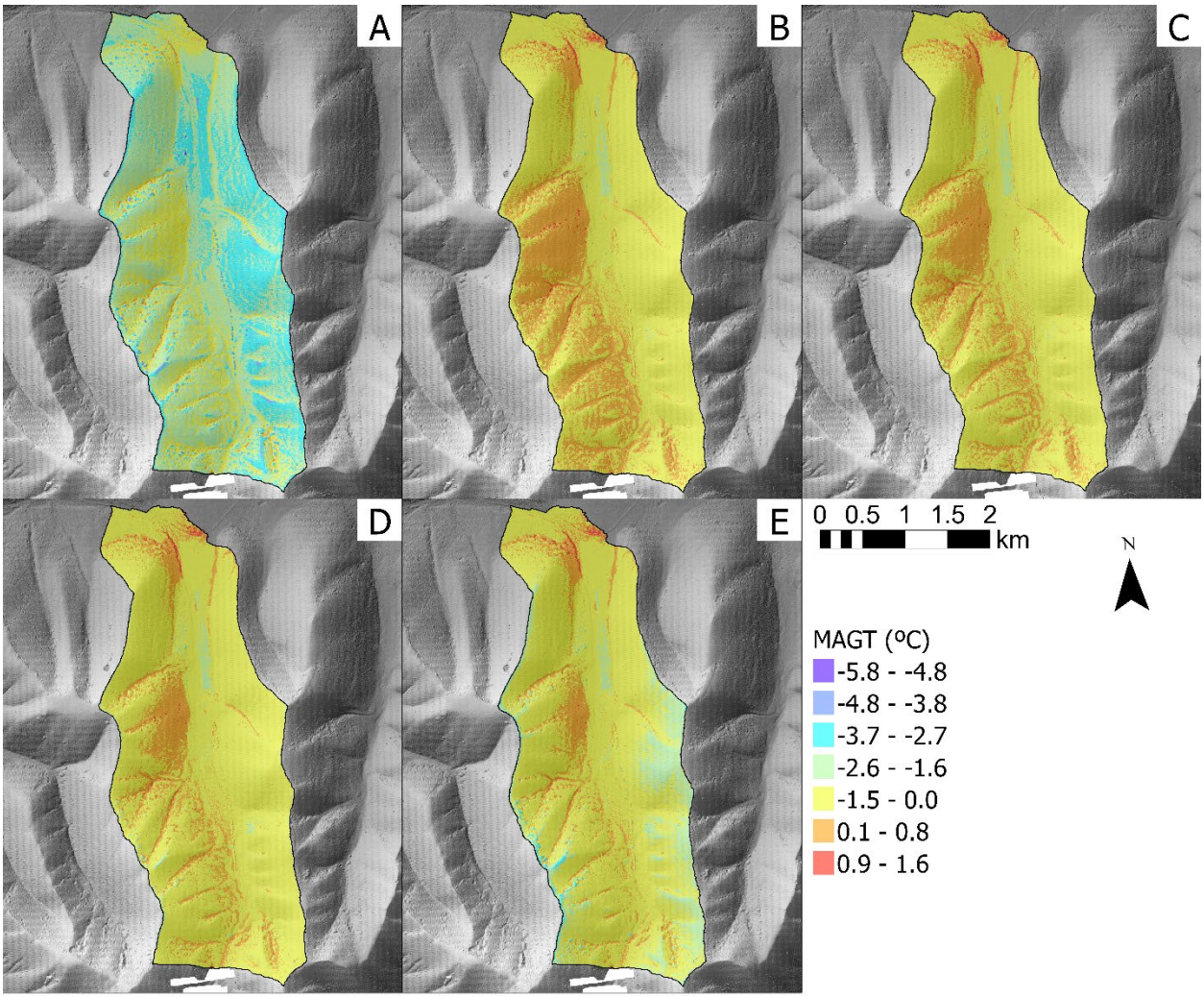


**Figure 6-12.** Spatial distribution of mean annual ground temperature (MAGT) in Valley WS02 for A) current conditions, and for the SSP2-4.5 2071-2100 climate normal assuming B) no change in the surface lapse rate (SLR), C) 1 ºC km-1 weakening of the SLR, D) 2.5 ºC km-1 weakening of the SLR, E) 5 ºC km-1 weakening of the SLR.

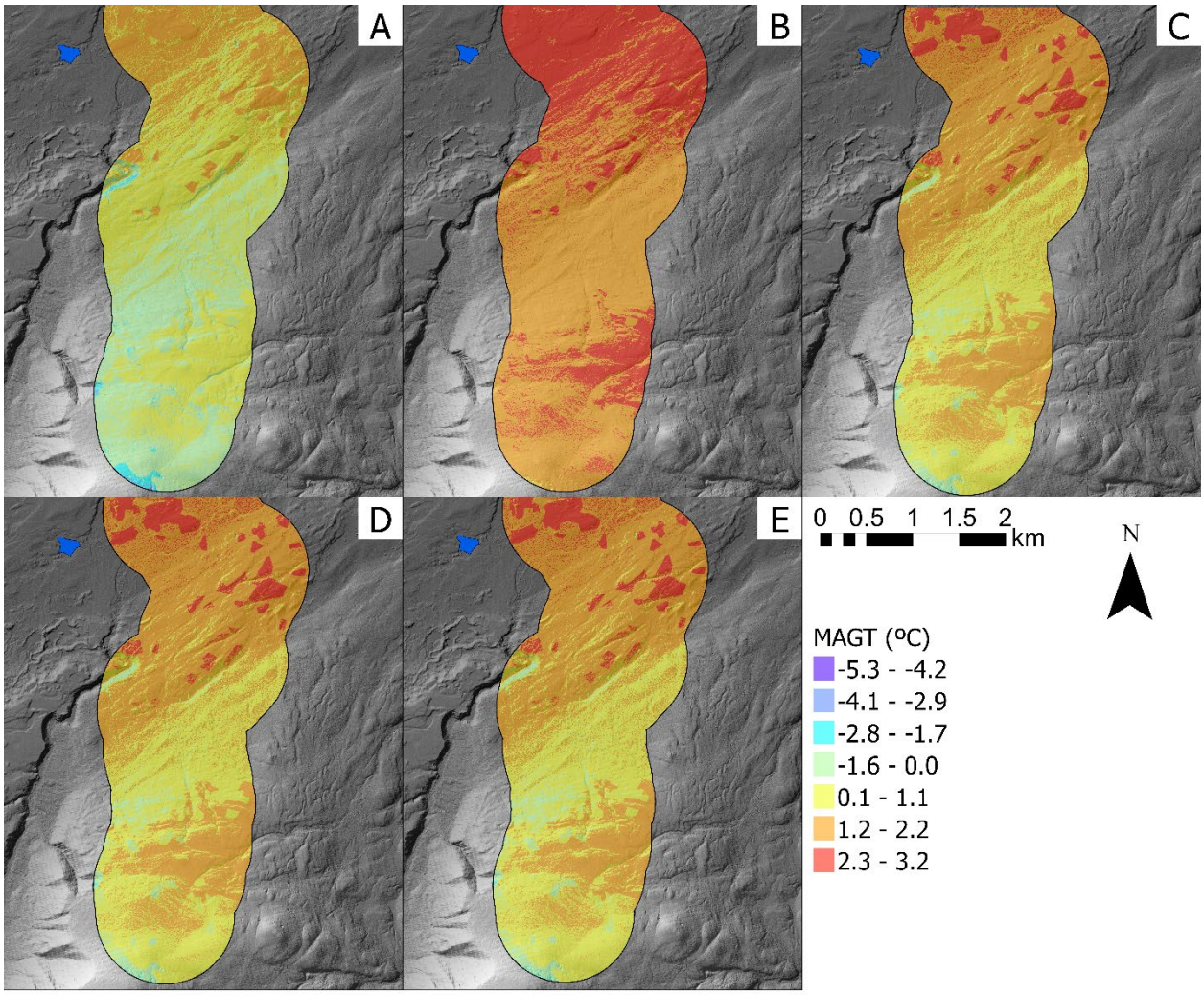


**Figure 6-13.** Spatial distribution of mean annual ground temperature (MAGT) in Valley M222 for A) current conditions, and for the SSP2-4.5 2071-2100 climate normal assuming B) no change in the surface lapse rate (SLR), C) 1 ºC km-1 weakening of the SLR, D) 2.5 ºC km-1 weakening of the SLR, E) 5 ºC km-1 weakening of the SLR.

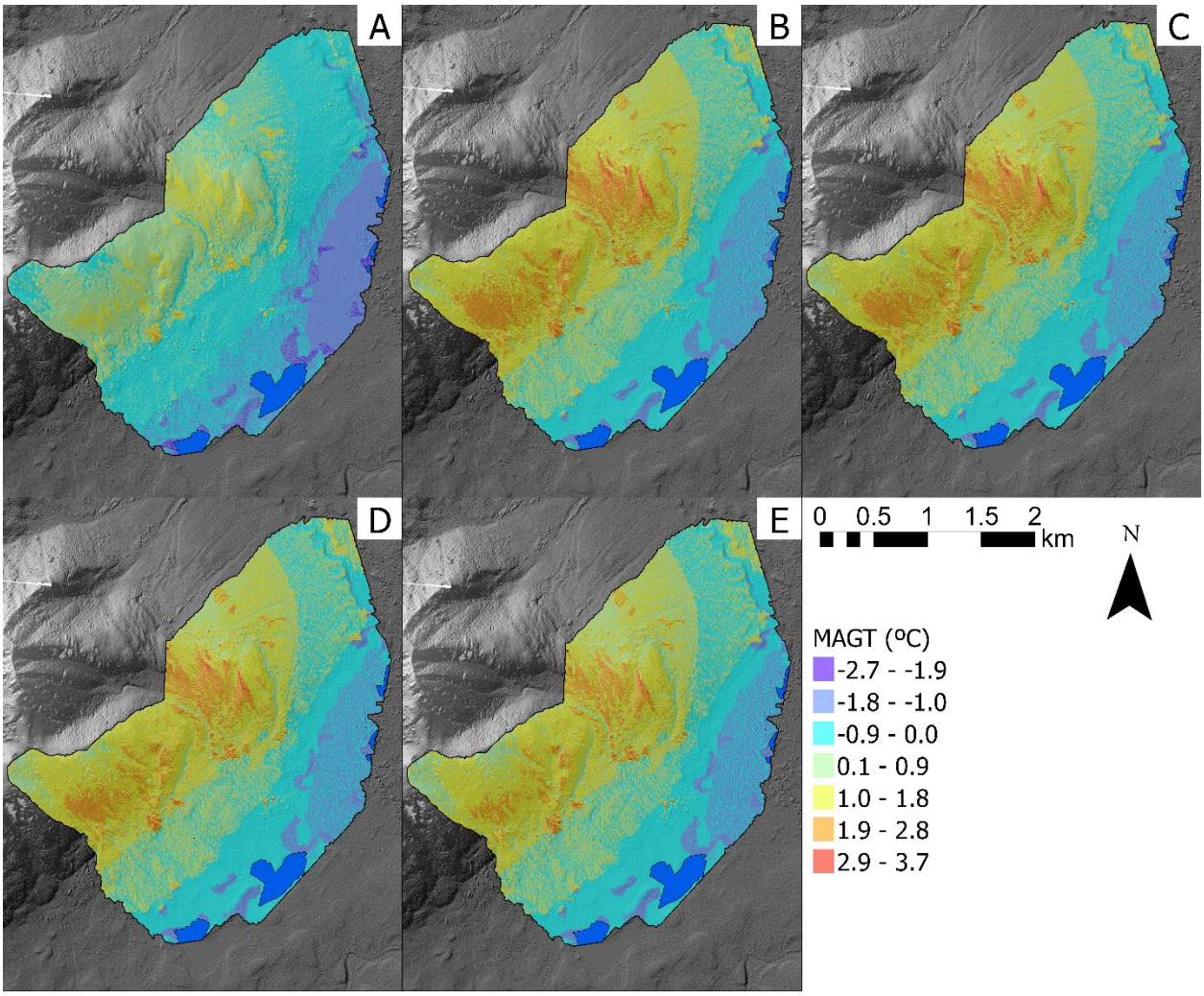


**Figure 6-14.** Spatial distribution of mean annual ground temperature (MAGT) in Valley MTS for A) current conditions, and for the SSP2-4.5 2071-2100 climate normal assuming B) no change in the surface lapse rate (SLR), C) 1 ºC km-1 weakening of the SLR, D) 2.5 ºC km-1 weakening of the SLR, E) 5 ºC km-1 weakening of the SLR.

Overall, MAGT in the valley bottom remained relatively cold for all scenarios while MAGT at high elevations varied depending on the warming scenario. As a result, the percentage of each valley underlain by near surface permafrost (NSP) was highest for the 5 ºC weakening of the inverted SLRs as it resulted in the least amount of warming at high elevations (Figure 6-15). Similarly, the warming scenario with no change in the SLR resulted in the lowest percentage of NSP in each valley due to the increased warming at high elevations (Figure 6-16). Additionally, this pattern of warming coupled with the original presence of permafrost at both high and low

elevations, even in discontinuous permafrost, resulted in the bidirectional spatial loss of NSP in three of the four valleys, Valley WS01, Valley WS02 and Valley MTS. In Valley M222, the loss of NSP was unidirectional as permafrost was only assumed to be present at high elevations under the current climate.

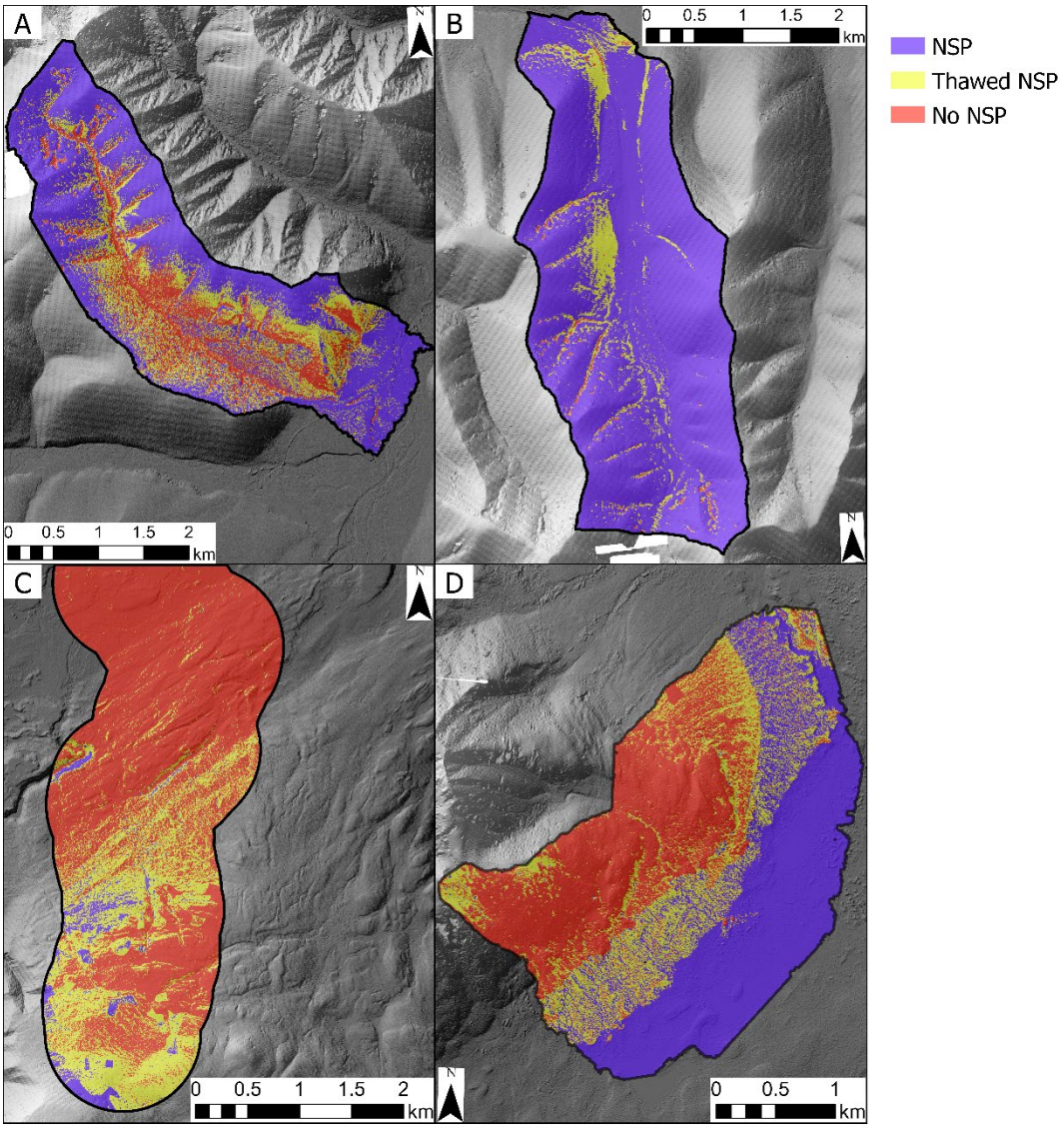


**Figure 6-15.** Near surface permafrost (NSP) presence and absence for each valley under the baseline warming with a 5 ºC $km^{-1}$ weakening of the inverted surface lapse rate (SLR) scenario. Thawed NSP indicates the NPS, which was predicted to thaw between this scenario and the modeled distribution under the current climate.

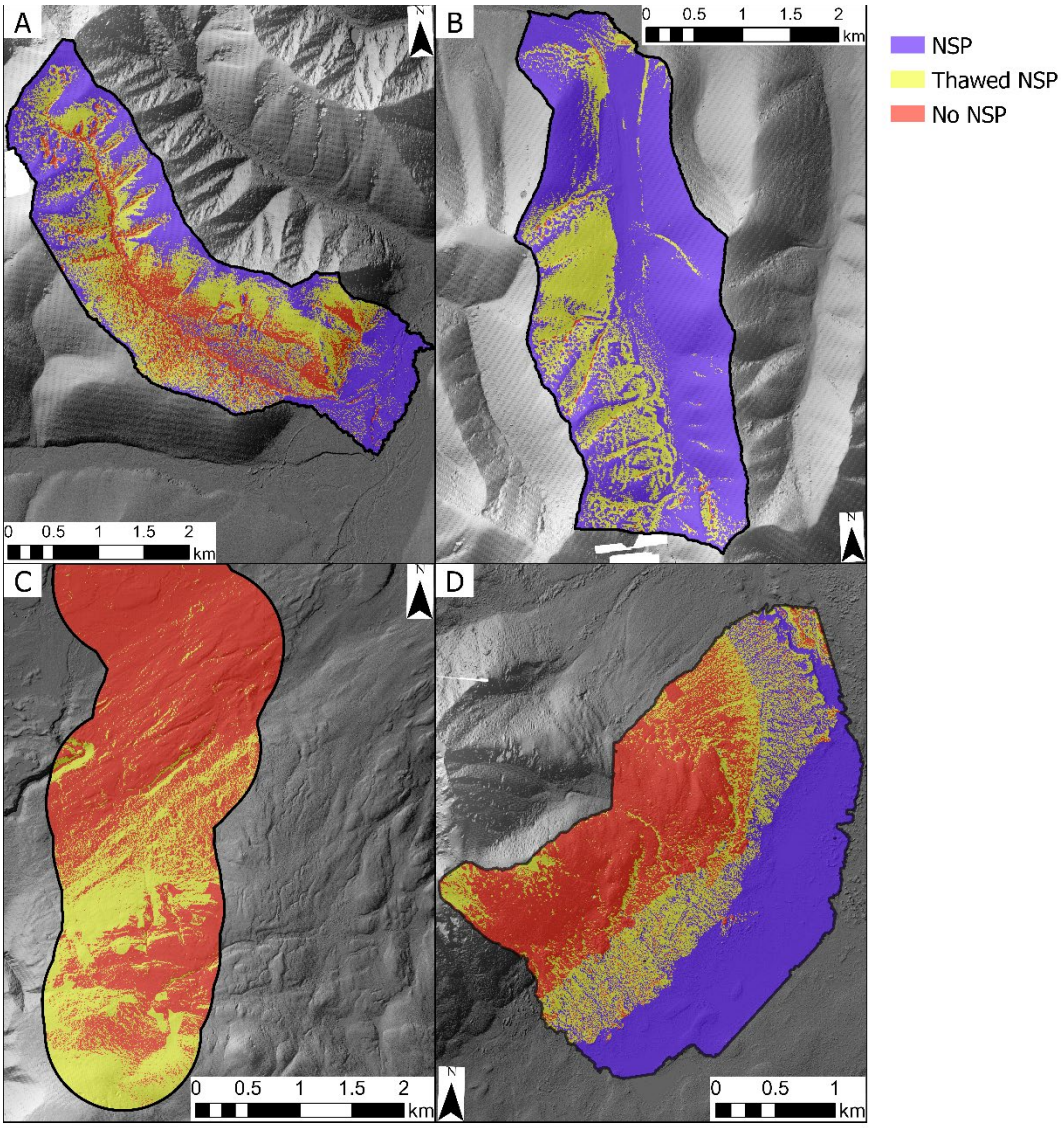


**Figure 6-16.** Near surface permafrost (NSP) presence and absence for each valley under the baseline warming with no change in the surface lapse rate (SLR) scenario. Thawed NSP indicates the NPS, which was predicted to thaw between this scenario and the modeled distribution under the current climate.

*6.5.5 Comparison to Regional Model*

When compared to a regional model of permafrost probability created for a uniform 3 ºC warming across southern Yukon (Bonnaventure & Lewkowicz, 2013), the local scenario models showed higher levels of permafrost occurrence based on the percentage of each valley predicted

to be underlain by permafrost (Table 6-3). This was true across all scenarios, even those which assumed a uniform warming of 2.4 -3 ºC (depending on the valley) and no change to the SLR.

**Table 6-3.** Percentage of near surface permafrost (NSP) underlying each valley for the current climate and under each warming scenario. Permafrost probability is from a regional model (Bonnaventure & Lewkowicz, 2013).

| | Current NSP (%) | Constant SLR (%) | - 1 º C km$^{-1}$ Δ SLR (%) | - 2.5 º C km$^{-1}$ Δ SLR (%) | -5 º C km$^{-1}$ Δ SLR (%) | Permafrost Probability (%) |
|---|---|---|---|---|---|---|
| **Valley WS01** | 80 | 42 | 46 | 51 | 56 | 5 |
| **Valley WS02** | 99 | 71 | 78 | 84 | 90 | 10 |
| **Valley M222** | 33 | 0 | 3 | 4 | 5 | 30 |
| **Valley MTS** | 61 | 40 | 40 | 41 | 42 | 31 |

Although the regional model largely disagreed with the local models, a few general trends were the same in both models when assumptions of the magnitude of warming were the same and the SLRs were not changed (Figure 6-17). First, in Valley WS01 both models showed the presence of NSP or higher permafrost probability at high elevations and absent at mid elevations on the slopes. However, the regional model does not indicate a higher probability of permafrost in the valley bottom, even though its presence was indicated in the local model. For Valley WS02, the regional model also does not predict the presence of permafrost in the valley bottom or widely distributed on the west-facing slope as in the local model. However, it does capture the limited probability of permafrost on the east-facing slope particularly in the incised channels. Valley M222 was the only valley where the regional model predicted a higher probability of permafrost than the local model, as it predicted a 50-70 % probability of permafrost at the highest elevations. This was not shown in the local model scenario assuming no change in SLR but was captured in the other scenarios. Lastly, the regional model in Valley MTS

did not indicate a high probability of permafrost in the valley and instead predicted a high probability of permafrost at the highest elevations. This was the opposite of the NSP distribution in the local model where permafrost was predicted to be widely present in the valley bottom and absent at high elevations. However, both models show the lowest probability or absence of NSP at mid elevations around treeline. Overall, however, the regional model did not agree well with the local models, even when similar warming assumptions were made, likely due to other assumptions made in the creation of both models.

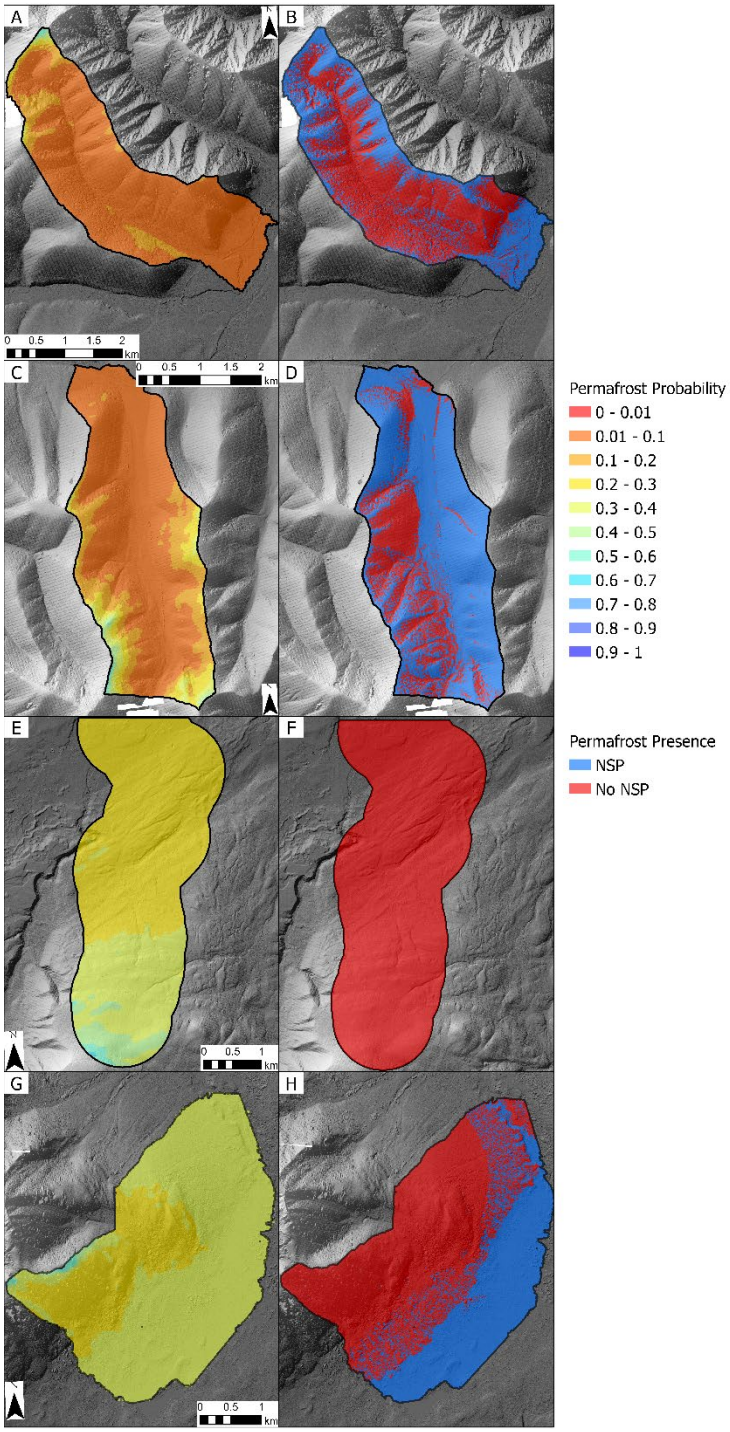


**Figure 6-17.** A) Permafrost probability for Valley WS01, B) Near surface permafrost (NSP) presence and absence for Valley WS01, C) Permafrost probability for Valley WS02, D) NSP presence and absence for Valley WS02, E) Permafrost probability for Valley M222, F) NSP presence and absence for Valley M222, G) Permafrost probability for Valley MTS, and H) Near surface permafrost presence and absence for Valley MTS. Both the regional permafrost probability model and the local NSP models assume a 3 ºC baseline warming (SSP2-4.5 2071-2100) with no change in surface lapse rate (SLR) (Bonnaventure & Lewkowicz, 2013).

## 6.6 Discussion

### *6.6.1 Errors and Uncertainties*

As the models of the future air and ground thermal regime were generated through a scenario-based approach, the exact magnitude of warming at each location is unknown. Additionally, the scenarios used in the study were also based on hypothetical magnitude changes or lack thereof to the strength of the inverted SLR. However, as theorized in several studies, the strength of winter temperature inversions in the Arctic is likely to decrease in a warmer climate due to reduced sea ice extent and increased cloud cover, which prevents the radiative surface cooling required for the formation of strong temperature inversions (Bourne et al., 2010; Screen et al., 2013; Ruman et al., 2022). These mechanisms are also generally responsible for asymmetric climate warming both latitudinally and seasonally whereby temperatures are expected to warm disproportionately at high-latitudes and during winter (Serreze & Barry, 2011; IPCC 2022). Although, the temperature inversions in these valleys are primarily radiation based (caused by a lack of solar radiation during winter) and the main factors influencing their presence are not going to change (winter solar radiation and valley geometry), winter air temperatures are expected to be warmer (Wang et al., 2016; Noad & Bonnaventure, 2022). Inverted SLRs in Valley WS01 and Valley WS02 were more frequently present with colder air temperatures, especially during cold air events ($T_a$ < -30 ºC) (Noad and Bonnaventure, *Submitted*). As a result, fewer winter cold air events due to generally warmer winter air temperatures result in less frequent and weaker temperature inversions, decreasing the magnitude of the inverted SLR annually. Therefore, the assumptions made in each scenario regarding changes in SLR strength only in winter (only changing $FDD_a$) are likely representative of the type of change even if the exact magnitudes used are not accurate. Consequently, although the

exact magnitude of warming in both the air and ground for each valley may not be completely certain, the spatial distribution of warming based on changes to the SLR are representative.

Some additional sources of uncertainty arise from assumptions of consistency in $n_f$, $n_t$ and rk values through time. As $n_f$ is linked not only to snow depth but also MAAT, changes in climate and the resulting warming of the ground contribute to lower $n_f$ values due to thicker active layers and increased latent heat release to the ground surface during winter (Smith & Riseborough, 2002). Future $n_f$ values are difficult to predict as a result of the large uncertainties in snowfall, depth and morphology with climate change, especially in these remote mountain environments (Callaghan et al., 2011; Kapnick & Delworth, 2013; Way & Lewkowicz, 2016). Additionally, $n_t$ and rk may vary between the current and future values due to changes in vegetation cover and soil moisture (Andresen et al., 2020; Heijmans et al., 2022). Though both $n_f$ and $n_t$ are generally expected to decrease due to changes in vegetation and snow capture, the corresponding response seasonally is expected to be different, with cooling during summer and warming during winter (Heijmans et al., 2022). Additionally, with only an increase in snowfall and a corresponding increase in $n_f$, ground temperatures are also expected to rise (Krasting et al., 2013). With permafrost thaw, hydrologic pathways and flows are expected to change leading to either drier or wetter surface conditions (Walvoord & Kurylyk, 2016; Andresen et al., 2020). Depending on which occurs, the rk value of a location may increase or decrease, with drier conditions resulting in a higher rk (lower differences between frozen and thawed) and wetter conditions decreasing rk values (Burn & Smith, 1988; Shiozawa & Campbell, 1990). Additionally, future removal of organic layers and moss with fire may increase rk, and result in deeper thaw penetration during the summer, further increasing warming in the ground at depth (Holloway et al., 2020). However, for this analysis $n_f$, $n_t$, and rk were assumed to remain the

same due to the increased complexity in determining the new values and limited knowledge of how they may change locally. Additionally, as previous studies have shown errors associated with incorrect parameterization of $n_f$ are likely to generate larger errors than $n_t$ and rk in these regions (Chapter 4). Therefore, because of limited knowledge and understanding of the possible changes to these parameters and the potential for increased errors in the resulting ground temperature surfaces, these values were held constant.

As the TTOP model does not directly use surface energy balance terms, variation in the surface energy balance resulting from changes in albedo and cloud cover were not considered, even though these are the main drivers behind EDW (Pepin et al., 2015b). However, as the results of this study were mainly to show potential alternatives to EDW based on changes in SLR in high-latitude, continental mountains, direct comparison is not strictly necessary. The inclusion of surface energy balance components to model changes in the air and ground thermal regimes in these regions is an important topic for future work. Finally, this study did not account for changes in precipitation, even though the Arctic is expected to become both warmer and wetter (Boisvert & Stroeve, 2015). Changes in precipitation type, timing, and amount will likely alter the effect of changes in air temperature on the ground thermal regime.

### *6.6.2 Differences in warming response between valleys*

For each scenario, there were different theoretical warming responses both within and between valleys due to ground cover and soil properties. At high elevations and on convex exposed slopes the surface offsets in all valleys were low due to limited vegetation and snow cover (Zhang, 2005; Freudiger et al., 2017). As a result, the variability between scenarios was relatively high due to the lack of surface cover, which allowed for a more direct impact of air

temperature on the ground thermal regime (Shur & Jorgenson, 2007). This shows that ground surface temperatures at these locations are more susceptible to changes in climate. Despite equal or greater warming of air temperatures in the valley bottom compared to higher elevations in each scenario, ground surface temperatures varied less between and within scenarios. This is a result of higher surface offsets due to greater increased snow retention and vegetation cover (Lewkowicz et al., 2012; Bevington & Lewkowicz, 2015; Freudiger et al., 2017). Additionally, increased soil moisture in the valley bottom also may have increased surface offsets (Famiglietti et al., 1998; Karunaratne & Burn, 2004; Vivoni et al., 2008). On average, Valley WS01 and Valley WS02 showed greater warming than Valley M222 and especially Valley MTS at the ground surface. This again results from differences in surface offsets, with higher average offsets at Valley M222 and Valley MTS even at the highest elevations that are most exposed due to increased snowfall in this region and warmer ground temperatures (Yukon Ecoregions Working Group, 2004). Additionally, Valley MTS showed the least amount of warming due to the presence of well-developed vegetation over most of the valley, limiting the ground surface response to changes in air temperature (Viereck, 1970; Shur & Jorgenson, 2007; Dashtseren et al., 2014; Ran et al., 2021). As a result, ground surface temperatures in this valley are likely to respond more to warming air temperatures coupled with disturbance rather than warming alone.

Differing thermal offsets in each valley also contributed to differences in warming of the ground at depth. In Valley WS02 and Valley M222, the magnitude and distribution pattern of warming in both the ground surface and ground at depth were similar, especially at high elevations. This results from the dry soil with limited ice content, organic material or moss cover, especially on the upper slopes, which allows for a more direct connection between the air and ground at depth due to high thermal conductivity during both the thawing and freezing season

(Smith & Riseborough, 2002; Shur & Jorgenson, 2007; Loranty et al., 2018). In contrast, MAGT in Valley MTS, especially in the valley bottom, did not have a similar spatial distribution pattern or magnitude of warming compared to both MAAT and MAGST. Additionally, the variability between scenarios was limited. The lower portion of Valley MTS is covered by mature forest with a thick moss layer and high soil moisture. This produces differential thermal conductivity seasonally and a high thermal offset, limiting the impact of changing air temperatures on the ground temperature at depth (Loranty et al., 2018). This is also shown in Valley WS01, where there is greater similarity in permafrost presence between scenarios than in Valley WS02 and Valley M222. However, it shows substantially more variability than Valley MTS as the ecosystem is less developed in this valley. As a result, high thermal offsets limit the consequences of both warming and changes in temperature inversion strength on the ground temperature at depth, preserving the underlying NSP (Oblogov et al., 2023).

### *6.6.3 Differential Consequences of Permafrost Thaw*

As a result of the differences in MAGT response to warming and subsurface properties, there are likely different consequences and drivers of permafrost thaw at different elevations in each valley. Permafrost present at high elevations is largely climate driven, due to the lack of complex ecosystem structure, and its temperature is largely influenced by changes in MAAT (Shur & Jorgenson, 2007). Permafrost at these locations is therefore more likely to respond quickly as a direct result of changes in climate. As permafrost at these locations is unlikely to be ice rich and is primarily composed of bedrock, its warming has the potential to result in isolated slope destabilization events (Gruber & Haeberli, 2007; Harris et al., 2009). However, as these valleys are remote and uninhabited this is unlikely to be a hazard or damage infrastructure as in the Alps (Fischer et al., 2006; Duvillard et al., 2021).

Due to the presence of mature ecosystems and well-developed organic layers, the permafrost in the valley bottoms, especially in Valley MTS, is likely to be climate driven ecosystem protected. Therefore, permafrost in the valley bottoms is more susceptible to disturbance coupled with warming rather than warming alone, as the permafrost remains protected by the ecosystem properties (Shur & Jorgenson, 2007; Daly et al., 2022; Vegter, 2023). With the warming projected in this region, it is also likely that this NSP may persist for an extended time beyond 2100, as average MAAT is expected to remain below 0 ºC and ecosystem properties have been known to protect permafrost even with MAAT up to + 2 ºC (Jorgenson et al., 2010). The permafrost in the valley bottoms also has the potential to be ice rich and contain organic material, resulting in different consequences with thaw. The greater potential for ice rich substrate in the valley bottom also yields a higher likelihood for surface disturbance resulting from permafrost thaw manifesting as ground instability including subsidence and thermokarst (Shur et al., 2005; Kokelj & Jorgenson, 2013). This likely poses a greater risk than the thaw of the high elevation permafrost due to the infrastructure present in valley bottoms including roadways and the recently constructed fibre optic line digitally connecting the strategically important location of Inuvik NT (Dempster Fibre Project, 2020). Additionally, permafrost thaw in the valley bottoms has a higher potential for carbon release due to the greater amount of organics stored in the soils compared to the bedrock high elevations (Hugelius et al., 2013; Pastick et al., 2014).

### *6.6.4 Comparison to regional model*

The local models created in this study help to both validate and calibrate a regional model of permafrost probability (Bonnaventure & Lewkowicz, 2013). The difference in permafrost presence between the models was much greater under a 3 ºC warming scenario with no change in

SLR strength than models for the current climate (Chapter 5). This is a product of the use of basal temperature of snow (BTS) in the creation of the regional model, which only accounted for aspect, elevation and changes in air temperature but did not consider surface and thermal offset (Bonnaventure & Lewkowicz, 2013). The local models, however, indirectly accounted for the protection of NSP from warmer air temperatures by snow cover and ecosystems through the use of N-factors and differential thermal conductivity. As a result, permafrost, especially in the valley bottom, was predicted to warm less, leading to higher estimations of NSP in the local models. This was also observed in a similar study in the High Arctic, where MAGT at locations of increased snow cover were modelled to warm less than snow free locations due to higher nival offsets decreasing the impact of the warmer winter air temperatures (Garibaldi et al., 2022). By not considering the impact of ecosystems and snow cover during warming, the regional model oversimplified the thermal response of the ground to warmer air temperatures and under predicted permafrost probability, especially in the valley bottom. This also highlights an advantage of using the TTOP model over BTS for modelling MAGT response to warming, as it can to some degree account for differential surface and thermal offsets.

Despite differences in permafrost presence estimates, the general pattern of NSP loss in both models is the same, with a bidirectional spatial thaw of permafrost predicted for the four valleys. Additionally, both models had some similar patterns of permafrost distribution. In Valley MTS, both the regional and local model predict no permafrost (or the lowest probability) at mid elevations around treeline. Additionally, in Valley WS01 both models predicted permafrost (or a higher probability) in portions of the valley bottom and at high elevations. The spatial distribution is most similar in these two valleys, likely since both the local and regional models for current permafrost distribution were the most similar (Chapter 5). However, in all

valleys except Valley M222, which was predicted to have no NSP, the regional model likely underestimated the probability of permafrost in the valley bottom due to the reasons discussed previously. Additionally, in the regional model the least sensitive permafrost was predicted at sites above treeline. However, in the local models, MAGT at high elevations showed the greatest warming and the largest variability between scenarios. Again, this is likely due to the low surface and thermal offsets in these locations, allowing for a more direct connection between the air and ground thermal regimes. Finally, although the regional model predicted permafrost probability and the local models showed potential NSP presence, general conclusions can be made about the performance of the regional model in these environments, which can provide insight about limitations of the regional model and areas for improvement.

### *6.6.5 Assessment of EDW in Mountains Subject to Strong Temperature Inversions*

The concept of EDW has been widely tested in low latitude, high elevation mountains dominated by glacial process (Pepin et al., 2015a; Palazzi et al., 2019). The logic and mechanisms behind EDW in these regions are sound, and greater magnitudes of warming at these elevations have been observed (Rangwala & Miller, 2010, 2012). A recent evaluation of EDW in the St. Elias Mountains in Yukon also produced evidence of EDW in these high-latitude, maritime mountains with strongly normal SLRs (Williamson et al., 2020). However, as shown through the various warming scenarios in this study, EDW may not be inclusive of all mountain environments. In lower elevation, high-latitude mountains subject to annually inverted SLRs, weakening of the SLR in combination with uniform warming potentially results in a greater increase in MAATs in the valley bottom than in high elevations. Additionally, depending on the magnitude of the weakened SLR, this distribution of warming may propagate to the ground surface and ground at depth. This was shown in a 5 ºC $km^{-1}$ SLR weakening scenario as

MAGST and MAGT were predicted to warm less at high elevations than mid to low elevations. The discrepancy in potential warming patterns is likely a result of the different relations between air temperature and elevation currently present in these valleys compared to those used in the development of EDW. As a result of warming, there are additional possible evolutions to the elevation-MAAT relation that are not present in these low latitude mountains, namely the potential for increasing normality due to warmer overall conditions (Ruman et al., 2022; Noad & Bonnaventure, *Submitted*). However, this study did not account for changes in energy balance and therefore did not consider changes in albedo, cloud cover, or latent heat release, all of which are expected to contribute to EDW (Rangwala & Miller, 2012; Pepin et al., 2015a). As a result, concrete conclusions about the validity of EDW in these high-latitude, continental mountain environments cannot be made. Instead, potential alternative elevation related warming patterns were demonstrated to allow for refinement of EDW to better represent a wider variety of mountain environments.

### 6.7 Conclusion

Under a number of potential warming scenarios, MAAT, MAGST, and MAGT showed a variety of responses based on the magnitude and distribution of warming in addition to surface and subsurface characteristics. In all four valleys, warming coupled with weakening inverted SLRs resulted in the greatest increase in MAAT predicted at low elevations. However, under the same scenarios, MAGST and MAGT showed the greatest warming at high elevations and limited change in the valley bottoms. This discrepancy in warming patterns likely results from variability in surface and thermal offset between the different topographic and vegetation characteristics at the various elevations. Lower elevations were more likely to have lower $n_f$, $n_t$, and rk values due to flatter and more incised topography, more mature and complex ecosystem structure and higher

soil moisture. Contrastingly, higher elevations had higher $n_f$, $n_t$, and rk values due to more exposed topography, limited to no vegetation, and drier bedrock substrate. As a result, between each scenario, there were larger differences at high elevations, and permafrost was more likely to be preserved in valley bottoms. Due to the prediction of permafrost in the valley bottom and high elevations under each warming scenario, the thaw in these valleys is likely to be bidirectional, with thawing fronts moving up and down from mid elevations rather than unidirectional. This generally supports the concept outlined in the regional permafrost model when subjected to warming conditions outlined by Bonnaventure and Lewkowicz (2013).

The local models produced in this study showed higher permafrost occurrence than a regional model of permafrost probability for the same area. This was especially true at low elevations, where permafrost probability was predicted to be low compared to high elevations in the regional model but was largely present in the local models. This resulted from the lack of consideration for permafrost resilience under well-developed ecosystems in the regional model, which was accounted for indirectly in the local models. Therefore, an understanding and inclusion of the spatial distribution of surface and thermal offsets is important for accurate predictions of differential MAGT warming rates and future permafrost distribution. Lastly, although the concept of EDW is sound for high elevation mountains with normal SLRs, it may not be entirely representative of the possible warming patterns present in high-latitude continental mountains with intensely inverted SLRs. As a result, EDW should be adjusted to become more inclusive of a wider range of possible spatial warming distributions in distinct mountain environments. This will provide better assessments of warming and potential permafrost thaw and therefore produce more accurate predictions of the subsequent hazards

(ground stability and thermokarst) and feedbacks (carbon dioxide and methane release) in environments that are not currently well represented.

# Chapter 7 Thesis Summary and Conclusions

## 7.1 Summary and Conclusions

In this thesis, local heterogeneity in ALT, TTOP model parameter importance, and permafrost presence and differential response to changes in MAAT and inverted SLR strength, were examined across the western Canadian Arctic and Subarctic. These local scale observations and models were then compared to regional environmental and climatic characteristics or models to assess how well they capture the local variability and their performance on this scale. Specific conclusions from each paper are given below, followed by overall conclusions form the thesis.

In Chapter 3 (Paper 1) spatial and temporal variability in ALT from 1991 to 2014 along a transect through the Mackenzie Valley, NWT were examined to explore the variation at an ecoregional and local scale. Spatial and temporal variability in ALT both between and within ecoregions was largely based on complex interactions between climate, surface characteristics (snow and vegetation), and subsurface characteristics. It was determined that the characteristic vegetation of an ecoregion could be used to explain average ALT trends spatially, however this may be difficult based on site specific differences in vegetation especially in shrub dominated ecoregions. Additionally, antecedent winter conditions were shown to have a significant influence on ALT, however the relative importance of winter and summer conditions varied by ecoregion. Lastly, temporal response of ALT to short-term changes in climate varied due to the moderating impact of vegetation, organic material, and snow cover. Generally, patterns of response can be linked to ecoregion with forest-dominated ecoregions showing less temporal variability. Overall, linking ALT to climate, dominant vegetation and other ecoregion characteristics is essential to assess broadly how ALT in different environments will respond to

changing MAAT, snowfall and vegetation, with some regions more climate driven and others more depending on the overlying ecosystem.

In Chapter 4 (Paper 2), TTOP model parameter sensitivity and random forest variable importance rankings were determined across the western Canadian Arctic and Subarctic using in situ data. The results of this study highlight the overall importance of freezing season parameters compared to thawing in both the TTOP model sensitivity and variable importance rankings. However, there was regional difference in both model sensitivity and variable importance, with thawing season and annual parameters increasing in importance and influence moving south. Additionally, although freezing season parameters remained important, there was a diminishing response to perturbation moving south. Lastly, the TTOP model performed well overall compared to measured ground temperatures at depth, however there were once again regional differences in performance. The TTOP model more closely matched the measured ground temperatures in regions with cold, more climate dependent permafrost. There were larger discrepancies between the modelled and measured temperatures in more southern regions with warm to marginal permafrost, as these sites were more likely to be protected by the ecosystem and may be out of equilibrium with the current climate. The findings of this study highlight the importance of correct parameterization of specific variable depending on location and scale and can be used to help future modelling studies allocate effort in parameterization.

In Chapter 5 (Paper 3), fine scale spatial models of the air and ground thermal regime were created for four dissimilar Yukon valleys subject to strong, persistent winter temperature inversions. Due to the inverted SLRs, the coldest AMATs were predicted at low elevations in the valley bottoms while the warmest temperatures were either at mid or high elevations depending on the height of the temperature inversion. This impacted the spatial distribution of AMGSTs

and AMGTs, with the coldest predicted at low and high elevations. As a result, permafrost was predicted to be present in both the valley bottom and at high elevations even in discontinuous permafrost. However, the impact of the inverted SLRs on the ground thermal regime was dependent on surface and subsurface characteristics including snow cover, vegetation, and soil moisture. The performance of a regional permafrost probability model in the valleys was dependent on model assumptions holding true locally. This highlights that regional models can and do perform well at a finer resolution in locations where assumptions are met but can break down in areas where they are not. The models from this study can help guide assessments of the current distribution of permafrost in other mountain regions subject to inverted SLRs, provide a more accurate starting point for future warming studies, and can be used to refine and calibrate regional models.

In Chapter 6 (Paper 4), a scenario-based approach was utilized to test air and ground thermal response to warming air temperatures with and without changes to temperature inversion strength in four dissimilar valleys in Yukon. The response in all valleys was dependent on the magnitude and distribution of warming in addition to surface and subsurface characteristics, which moderated the impact of changing air temperature on the ground at depth. As a result of higher surface and thermal offsets permafrost was most likely to be present and persist in the valley bottom compared to mid and high elevations though all scenarios. A regional model underestimated permafrost probability at low elevations, relative to high elevations, since it did not account for the resilience of permafrost due to the overlying ecosystem. Lastly, the potential spatial distributions of warming presented provide alternative possibilities to those assumed under EDW. This highlights the need to make EDW more inclusive of different mountain environments especially with different relations between elevation and air temperature.

The conclusions for this thesis overall, highlight the importance of using local measured data to inform and calibrate regional assumptions and models of permafrost and active layer characteristics now and under future warming scenarios. Of particular importance are local estimations of SLRs, parameterization of model inputs and influences on permafrost presence and temperature. This will allow for better estimation of permafrost presence and active layer thickness currently and improved predictions of responses to warming. This is especially true given the distinct reactions highlighted both locally and regionally throughout this thesis, specifically locations with direct responses to changes in climate compared to locations of muted response due to ecosystem protection. Locations with differential responses to warming were shown to vary both locally and regionally with more climate dependent sites found farther north regionally and at high exposed elevations locally. Contrastingly, ecosystem dependent sites were found farther south regionally and at low elevations locally, corresponding to more vegetation cover due to more well-developed ecosystems. As a result, better understanding of local heterogeneity in permafrost resilience or lack thereof, will provide regional models improved predictions of future permafrost distribution and potential predictions of permafrost related hazards. Additionally, better comprehension of the seasonal sensitivity of permafrost and ALT in a variety of permafrost environments across Canada will aid in predictions of permafrost and ALT on broader scales. In more northern locations, with limited snow cover and vegetation, winter conditions were shown to be the dominant influence. However, moving father south the influence of summer conditions on the ground thermal regime increases. This can be particularly important when looking at future conditions as warming is expected to be seasonally asymmetric, with disproportionally greater temperature increasing during winter. As a result, locations and regions largely influenced by winter conditions may warm more than locations

with a greater reliance on summer conditions given the same magnitude of warming. Overall, local understanding the heterogeneity spatially and temporally of permafrost and its corresponding attributes such as ALT, in relation to climate and environmental characteristics is important for accurate regional characterization and prediction currently and under future warming conditions.

### 7.2 Future Work

Future work from this thesis is mainly focused on the two valleys along the Dempster Highway in Chapters 5 and 6. In August 2022 an additional 44 GTNs were added in transects both up the individual valley slopes and farther toward the back of the valley along the valley floor to increase the spatial resolution sampled. Additionally, another 16 air temperature sensors were deployed in a line along the valley floor toward the back of the valley to measure temperature inversion characteristics spanning the length of the valley. This will be utilized in the future to better understand and model temperature inversion characteristics in each of these two valleys. Additionally, a surface energy balance model (NEST) will be used to spatially model the ground thermal regime in these valleys for comparison to the TTOP model. The local models produced in Chapters 5 and 6 in addition to site measurements in each of the valleys may be used to recalibrate the regional permafrost probability model for Southern Yukon to include more strongly inverted SLRs and adjust assumptions made about SLRs in areas above treeline. Lastly, the regional model of permafrost probability under future warming scenarios, should be recalibrated to account for the more strongly inverted SLRs and to included surface and thermal offsets to better predict permafrost probability in valley bottoms.

Expanding the findings of this thesis into other ecological and biological studies is also an area of future consideration. One potential way these results could contribute to work outside

of permafrost modelling is through investigations of hydrological pathways in the valleys used in this research, both under current and future permafrost conditions. This could also include the assessment of potential new subsurface pathways, which may emerge with permafrost degradation or the transition of surface to subsurface flow. This is important as the valleys along the Dempster Highway both have stream channels and Valley WS02 has several springs on the slopes. Finally, knowledge about the temperature inversion and the newly created air temperature maps for each of these valleys, may allow for studies documenting animal movement through these areas. Due to the presence of these strong winter temperature inversions, species of importance, such as caribou, may avoid the colder valley floor and instead remain at higher elevations. Understanding how the elevation air temperature distribution relates to animal movement is an important area of future study.

## List of References


Aguilar-Lome, J., Espinoza-Villar, R., Espinoza, J.-C., Rojas-Acuña, J., Willems, B. L., & Leyva-Molina, W.-M. Elevation-dependent warming of land surface temperatures in the Andes assessed using MODIS LST time series (2000–2017). *International Journal of Applied Earth Observation and Geoinformation.* 2019;77; 119-128.

Ahmed, N. S., & Sadiq, M. H. (2018, 9-11 Oct. 2018). *Clarify of the Random Forest Algorithm in an Educational Field.* Paper presented at the 2018 International Conference on Advanced Science and Engineering (ICOASE).

AMAP, 2017. Snow, Water, Ice and Permafrost in the Arctic (SWIPA) 2017. Arctic Monitoring and Assessment Programme (AMAP), Oslo, Norway. xiv + 269 pp

Andresen, C. G., Lawrence, D. M., Wilson, C. J., McGuire, A. D., Koven, C., Schaefer, K., . . . Zhang, W. Soil moisture and hydrology projections of the permafrost region – a model intercomparison. *The Cryosphere.* 2020;14(2); 445-459. doi:10.5194/tc-14-445-2020

Apaloo, J., Brenning, A., & Bodin, X. Interactions between Seasonal Snow Cover, Ground Surface Temperature and Topography (Andes of Santiago, Chile, 33.5°S). *Permafrost and Periglacial Processes.* 2012;23(4); 277-291. doi:https://doi.org/10.1002/ppp.1753

Atchley, A. L., Coon, E. T., Painter, S. L., Harp, D. R., & Wilson, C. J. Influences and interactions of inundation, peat, and snow on active layer thickness. *Geophysical Research Letters.* 2016;43(10); 5116-5123. doi:https://doi.org/10.1002/2016GL068550

Aylsworth, J., Burgess, M., Desrochers, D., Duk-Rodkin, A., Robertson, T., & Traynor, J. (2000). Surficial geology, subsurface materials, and thaw sensitivity of sediments. The physical environment of the Mackenzie Valley, Northwest Territories: a base line for the assessment of environmental change, 547, 41-48.

Aylsworth, J., & Kettles, I. Distribution of peatlands. *The Physical Environment of the Mackenzie Valley, Northwest Territories: A Base Line for the Assessment of Environmental Change, Geological Survey of Canada Bulletin.* 2000;547; 49-55.

Baral, P., & Haq, M. A. Spatial prediction of permafrost occurrence in Sikkim Himalayas using logistic regression, random forests, support vector machines and neural networks. *Geomorphology.* 2020;371; 107331.

Barry, R. G. (2008). Mountain weather and climate. Cambridge University Press

Bevington, A., & Lewkowicz, A. G. (2015). *Assessment of a land cover driven TTOP model for mountain and lowland permafrost using field data, southern Yukon and northern British Columbia, Canada.* Paper presented at the Proceedings of GéoQuebec: 68th Canadian Geotechnical Conference and 7th Canadian Permafrost Conference. Quebec City, Canada.

Biau, G., & Scornet, E. A random forest guided tour. *TEST.* 2016;25(2); 197-227. doi:10.1007/s11749-016-0481-7

Bockheim, J. G., & Hall, K. J. (2002). Permafrost, active-layer dynamics and periglacial environments of continental Antarctica: periglacial and permafrost research in the Southern Hemisphere. South African Journal of Science, 98(1-2), 82-90.

Boeckli, L., Brenning, A., Gruber, S., & Noetzli, J. Permafrost distribution in the European Alps: calculation and evaluation of an index map and summary statistics. *The Cryosphere.* 2012;6(4); 807-820. doi:10.5194/tc-6-807-2012

Boisvert, L. N., & Stroeve, J. C. (2015). The Arctic is becoming warmer and wetter as revealed by the Atmospheric Infrared Sounder. Geophysical Research Letters, 42(11), 4439-4446.

Bonnaventure, P. P., & Lamoureux, S. F. The active layer: A conceptual review of monitoring, modelling techniques and changes in a warming climate. *Progress in Physical Geography.* 2013;37(3); 352-376. doi:10.1177/0309133313478314

Bonnaventure, P. P., Lamoureux, S. F., & Favaro, E. A. Over-Winter Channel Bed Temperature Regimes Generated by Contrasting Snow Accumulation in a High Arctic River. *Permafrost and Periglacial Processes.* 2016. doi:10.1002/ppp.1902

Bonnaventure, P. P., & Lewkowicz, A. G. Mountain permafrost probability mapping using the BTS method in two climatically dissimilar locations, northwest Canada. *Canadian Journal of Earth Sciences.* 2008;45(4); 443-455. doi:10.1139/E08-013

Bonnaventure, P. P., & Lewkowicz, A. G. Modelling climate change effects on the spatial distribution of mountain permafrost at three sites in northwest Canada. *Climatic Change.* 2011;105(1); 293-312. doi:10.1007/s10584-010-9818-5

Bonnaventure, P. P., & Lewkowicz, A. G. Impacts of mean annual air temperature change on a regional permafrost probability model for the southern Yukon and northern British Columbia, Canada. *The Cryosphere.* 2013;7(3); 935-946. doi:10.5194/tc-7-935-2013

Bonnaventure, P. P., Lewkowicz, A. G., Kremer, M., & Sawada, M. C. A Permafrost Probability Model for the Southern Yukon and Northern British Columbia, Canada. *Permafrost and Periglacial Processes.* 2012;23(1); 52-68. doi:10.1002/ppp.1733

Bostock, H. S. (1966). *Notes on glaciation in central Yukon Territory* (Vol. 65): Ottawa, Department of Mines and Technical Surveys 1966.

Boulesteix, A.-L., Janitza, S., Kruppa, J., & König, I. R. Overview of random forest methodology and practical guidance with emphasis on computational biology and bioinformatics. *WIREs Data Mining and Knowledge Discovery.* 2012;2(6); 493-507. doi:https://doi.org/10.1002/widm.1072

Bourne, S. M., Bhatt, U. S., Zhang, J., & Thoman, R. Surface-based temperature inversions in Alaska from a climate perspective. *Atmospheric Research.* 2010;95(2); 353-366. doi:https://doi.org/10.1016/j.atmosres.2009.09.013

Breiman, L. Random Forests. Machine Learning. 2001;45(1); 5-32. doi:10.1023/A:1010933404324

Brieuc, M. S. O., Waters, C. D., Drinan, D. P., & Naish, K. A. A practical introduction to Random Forest for genetic association studies in ecology and evolution. *Molecular Ecology Resources.* 2018;18(4); 755-766. doi:https://doi.org/10.1111/1755-0998.12773

Brown, J., Ferrians, O., Heginbottom, J., & Melnikov, E. Circum-Arctic map of permafrost and ground-ice conditions, version 2. *Boulder, Colorado USA, National Snow and Ice Data Center.* 2002.

Brown, J., Hinkel, K. M., & Nelson, F. E. The circumpolar active layer monitoring (calm) program: Research designs and initial results. *Polar Geography.* 2000;24(3); 166-258. doi:10.1080/10889370009377698

Brown, R. J. E. (1970). *Permafrost in Canada: Its Influence on Northern Development*: University of Toronto Press, Scholarly Publishing Division.

Burn, C., Moore, J., O'Neill, B., Hayley, D., Trimble, J., Calmels, F., . . . Idrees, M. (2015). *Permafrost characterization of the Dempster Highway, Yukon and Northwest Territories.* Paper presented at the 7th Canadian Permafrost Conference.

Burn, C. R. The active layer: two contrasting definitions. *Permafrost and Periglacial Processes.* 1998;9(4); 411-416.

Burn, C. R., & Kokelj, S. V. The environment and permafrost of the Mackenzie Delta area. *Permafrost and Periglacial Processes.* 2009;20(2); 83-105. doi:10.1002/ppp.655

Burn, C. R., & Smith, C. A. S. Observations of the "Thermal Offset" in Near-Surface Mean Annual Ground Temperatures at Several Sites near Mayo, Yukon Territory, Canada. *Arctic.* 1988;41(2); 99-104.

Callaghan, T. V., Johansson, M., Brown, R. D., Groisman, P. Y., Labba, N., Radionov, V., . . . Yang, D. The Changing Face of Arctic Snow Cover: A Synthesis of Observed and Projected Changes. *Ambio.* 2011;40(Suppl 1); 17-31. doi:10.1007/s13280-011-0212-y

Canada, E. Historical Data. Retrieved 2021, from Government of Canada https://climate.weather.gc.ca/historical_data/search_historic_data_e.html

Chapin, F. S., Sturm, M., Serreze, M. C., McFadden, J. P., Key, J. R., Lloyd, A. H., . . . Welker, J. M. (2005). Role of Land-Surface Changes in Arctic Summer Warming. Science, 310(5748), 657-660. doi:10.1126/science.1117368

Cutler, D. R., Edwards Jr., T. C., Beard, K. H., Cutler, A., Hess, K. T., Gibson, J., & Lawler, J. J. RANDOM FORESTS FOR CLASSIFICATION IN ECOLOGY. *Ecology.* 2007;88(11); 2783-2792. doi:https://doi.org/10.1890/07-0539.1

Daly, S. V., Bonnaventure, P. P., & Kochtitzky, W. Influence of ecosystem and disturbance on near-surface permafrost distribution, Whatì, Northwest Territories, Canada. *Permafrost and Periglacial Processes.* 2022;33(4); 339-352. doi:https://doi.org/10.1002/ppp.2160

Dashtseren, A., Ishikawa, M., Iijima, Y., & Jambaljav, Y. Temperature Regimes of the Active Layer and Seasonally Frozen Ground under a Forest-Steppe Mosaic, Mongolia. *Permafrost and Periglacial Processes.* 2014;25(4); 295-306. doi:https://doi.org/10.1002/ppp.1824

Deluigi, N., Lambiel, C., & Kanevski, M. Data-driven mapping of the potential mountain permafrost distribution. *Science of The Total Environment.* 2017;590-591; 370-380. doi:https://doi.org/10.1016/j.scitotenv.2017.02.041

Díaz-Uriarte, R., & Alvarez de Andrés, S. Gene selection and classification of microarray data using random forest. *BMC Bioinformatics.* 2006;7(1); 3. doi:10.1186/1471-2105-7-3

Duchesne, C., Riseborough, D. W., & Smith, S. L. (2014). Air and near surface ground temperatures, indices, and summary statistics from 1993 to 2012 for the Mackenzie Valley Corridor, Northwest Territories. (Open File 7392). Natural Resources Canada.

Duchesne, C., Smith, S. L., Ednie, M., & Bonnaventure, P. P. (2015). *Active layer variability and change in the Mackenzie Valley, Northwest Territories.* Paper presented at the Proc. 68th Canadian Geotechnical Conf. and Seventh Canadian Conf. on Permafrost (GEOQuébec 2015).

Duvillard, P. A., Ravanel, L., Schoeneich, P., Deline, P., Marcer, M., & Magnin, F. Qualitative risk assessment and strategies for infrastructure on permafrost in the French Alps. *Cold Regions Science and Technology.* 2021;189; 103311. doi:https://doi.org/10.1016/j.coldregions.2021.103311

Ecoregions Working Group. 1989. Ecoclimatic Regions of Canada, first approximation. Environment
Canada, Canadian Wildlife Service, Sustainable Development Branch. Ecological Land Classification Series No. 23.

Ecosystem Classification Group. 2007 (rev. 2009). Ecological Regions of the Northwest Territories – Taiga
Plains. Department of Environment and Natural Resources, Government of the Northwest Territories, Yellowknife, NT, Canada. viii + 173 pp. + folded insert map

Ecosystem Classification Group. 2010. Ecological Regions of the Northwest Territories – Cordillera. Department of Environment and Natural Resources, Government of the

Northwest Territories, Yellowknife, NT, Canada. x + 245 pp. + insert map.

Ecosystem Classification Group. 2012. Ecological Regions of the Northwest Territories – Southern Arctic. Department of Environment and Natural Resources, Government of the Northwest Territories, Yellowknife, NT, Canada. x + 170 pp. + insert map

Environment Canada-Historical Data - Climate - Environment and Climate Change Canada. (2017). Government of Canada. https://climate.weather.gc.ca/historical_data/search_historic_data_e.html

Environment Canada-Historical Data - Climate - Environment and Climate Change Canada. (2021). Government of Canada. https://climate.weather.gc.ca/historical_data/search_historic_data_e.html

Etzelmüller, B. Recent Advances in Mountain Permafrost Research. *Permafrost and Periglacial Processes.* 2013;24(2); 99-107. doi:10.1002/ppp.1772

Etzelmüller, B., Berthling, I., & Sollid, J. L. (1998). *The distribution of permafrost in Southern Norway; a GIS approach.* Paper presented at the Seventh International Conference on Permafrost, Proceedings. Collection Nordicana. Centre d'Etudes Nordiques, Universite Laval, Quebec, PQ, Canada.

Etzelmüller, B., Heggem, E. S. F., Sharkhuu, N., Frauenfelder, R., Kääb, A., & Goulden, C. Mountain permafrost distribution modelling using a multi-criteria approach in the Hövsgöl area, northern Mongolia. *Permafrost and Periglacial Processes.* 2006;17(2); 91-104. doi:10.1002/ppp.554

Famiglietti, J. S., Rudnicki, J. W., & Rodell, M. Variability in surface moisture content along a hillslope transect: Rattlesnake Hill, Texas. *Journal of Hydrology.* 1998;210(1); 259-281. doi:https://doi.org/10.1016/S0022-1694(98)00187-5

Fischer, L., Kääb, A., Huggel, C., & Noetzli, J. Geology, glacier changes, permafrost and related slope instabilities in a high-mountain rock wall: Monte Rosa east face, Italian Alps. *Natural Hazards and Earth System Sciences.* 2006;6; 761-772.

Fisher, J. P., Estop-Aragonés, C., Thierry, A., Charman, D. J., Wolfe, S. A., Hartley, I. P., . . . Phoenix, G. K. The influence of vegetation and soil characteristics on active-layer thickness of permafrost soils in boreal forest. *Global Change Biology.* 2016;22(9); 3127-3140. doi:https://doi.org/10.1111/gcb.13248

French, H. M. (2007). *The Periglacial Environment* (third ed.). Chichester, England: John Wiley & Sons.

French, H. M. (2008). *The Periglacial Environment* (third ed.). Chichester, England: John Wiley & Sons.

Freudiger, D., Kohn, I., Seibert, J., Stahl, K., & Weiler, M. Snow redistribution for the hydrological modeling of alpine catchments. *WIREs Water.* 2017;4(5); e1232. doi:https://doi.org/10.1002/wat2.1232

Gądek, B., & Kędzia, S. Winter ground surface temperature regimes in the zone of sporadic discontinuous permafrost, Tatra Mountains (Poland and Slovakia). *Permafrost and Periglacial Processes.* 2008;19(3); 315-321. doi:https://doi.org/10.1002/ppp.623

Garibaldi, M. C., Bonnaventure, P. P., & Lamoureux, S. F. Utilizing the TTOP model to understand spatial permafrost temperature variability in a High Arctic landscape, Cape Bounty, Nunavut, Canada. *Permafrost and Periglacial Processes.* 2021;32(1); 19-34
.

Garibaldi, M. C., Bonnaventure, P. P., Smith, S. L., & Duchesne, C. Active layer variability and change in the Mackenzie Valley, Northwest Territories between 1991-2014: An ecoregional assessment. *Arctic, Antarctic, and Alpine Research.* 2022;54(1); 274-293.

Genuer, R., Poggi, J.-M., & Tuleau-Malot, C. Variable selection using random forests. *Pattern Recognition Letters.* 2010;31(14); 2225-2236. doi:https://doi.org/10.1016/j.patrec.2010.03.014

Gisnås, K., Etzelmüller, B., Farbrot, H., Schuler, T. V., & Westermann, S. CryoGRID 1.0: Permafrost Distribution in Norway estimated by a Spatial Numerical Model. *Permafrost and Periglacial Processes.* 2013;24(1); 2-19. doi:10.1002/ppp.1765

Gold, L. W. (1963). Influence of the snow cover on the average annual ground temperature at Ottawa, Canada: Division of Building Research, National Research Council.

Goodrich, L. The influence of snow cover on the ground thermal regime. *Canadian geotechnical journal.* 1982;19(4); 421-432.

Government of Canada. (2015). *Canadian Land Cover Circa 2000 (Vector)- Geobase Series, 1996-2005* [Dataset].Natural Resources Canada. https://open.canada.ca/data/en/dataset/97126362-5a85-4fe0-9dc2-915464cfdbb7

Gregorutti, B., Michel, B., & Saint-Pierre, P. Correlation and variable importance in random forests. *Statistics and Computing.* 2017;27(3); 659-678. doi:10.1007/s11222-016-9646-1

Gregory, F. M. (2011). *BIOPHYSICAL REMOTE SENSING AND TERRESTRIAL CO2 EXCHANGE AT CAPE BOUNTY, MELVILLE ISLAND.* (Master of Science), Queen's University, Kingston, Ontario, Canada
.

Grömping, U. Variable Importance Assessment in Regression: Linear Regression versus Random Forest. *The American Statistician.* 2009;63(4); 308-319. doi:10.1198/tast.2009.08199

Gruber, S., & Haeberli, W. Permafrost in steep bedrock slopes and its temperature-related destabilization following climate change. *Journal of Geophysical Research: Earth Surface.* 2007;112(F2). doi:https://doi.org/10.1029/2006JF000547

Gruber, S., & Haeberli, W. Mountain permafrost. *Permafrost soils.* 2009; 33-44.

Grünberg, I., Wilcox, E. J., Zwieback, S., Marsh, P., and Boike, J.: Linking tundra vegetation, snow, soil temperature, and permafrost, Biogeosciences, 17, 4261–4279, https://doi.org/10.5194/bg-17-4261-2020, 2020.

Guglielmin, M., Aldighieri, B., & Testa, B. PERMACLIM: a model for the distribution of mountain permafrost, based on climatic observations. *Geomorphology.* 2003;51(4); 245-257. doi:https://doi.org/10.1016/S0169-555X(02)00221-0

Haeberli, W. Die Basis-Temperatur der winter-lichen Schneedecke als moglicher Indikator fur die Verbreitung von Permafrost in den Alpen. *Zeitschrift fur Gletscherkunde und Glazialgeologie.* 1973;9; 221-227.

Harris, S. A. (2002). Causes and consequences of rapid thermokarst development in permafrost or glacial terrain. Permafrost and periglacial processes, 13(3), 237-242.

Harris, C., Arenson, L. U., Christiansen, H. H., Etzelmüller, B., Frauenfelder, R., Gruber, S., . . . Vonder Mühll, D. Permafrost and climate in Europe: Monitoring and modelling thermal, geomorphological and geotechnical responses. *Earth-Science Reviews.* 2009;92(3); 117-171. doi:https://doi.org/10.1016/j.earscirev.2008.12.002

Harris, C., Davies, M. C. R., & Etzelmüller, B. The assessment of potential geotechnical hazards associated with mountain permafrost in a warming global climate. *Permafrost and Periglacial Processes.* 2001;12(1); 145-156. doi:10.1002/ppp.376

Heginbottom, J. (1995). *Canada, permafrost*: Canada Map Office. Contains information licensed under the Open Government Licence – Canada.

Heijmans, M. M. P. D., Magnússon, R. Í., Lara, M. J., Frost, G. V., Myers-Smith, I. H., van Huissteden, J., . . . Limpens, J. Tundra vegetation change and impacts on permafrost. *Nature Reviews Earth & Environment.* 2022;3(1); 68-84. doi:10.1038/s43017-021-00233-0

Henry, K., & Smith, M. A model-based map of ground temperatures for the permafrost regions of Canada. *Permafrost and Periglacial Processes.* 2001;12(4); 389-398. doi:10.1002/ppp.399

Hinkel, K. M., & Nelson, F. E. (2003). Spatial and temporal patterns of active layer thickness at Circumpolar Active Layer Monitoring (CALM) sites in northern Alaska, 1995–2000. Journal of Geophysical Research: Atmospheres (1984–2012), 108(D2). doi:10.1029/2001JD000927

Hinkel, K. M., Paetzold, F., Nelson, F. E., & Bockheim, J. G. (2001). Patterns of soil temperature and moisture in the active layer and upper permafrost at Barrow, Alaska: 1993–1999. Global and Planetary Change, 29(3), 293-309. doi:https://doi.org/10.1016/S0921-8181(01)00096-0

Hinzman, L. D., Kane, D. L., Gieck, R. E., & Everett, K. R. Hydrologic and thermal properties of the active layer in the Alaskan Arctic. *Cold Regions Science and Technology.* 1991;19(2); 95-110. doi:https://doi.org/10.1016/0165-232X(91)90001-W

Hodgson, D. A., Vincent, J.-S., & Fyles, J. G. Quaternary geology of central Melville Island, Northwest Territories. *Paper/Canada. Geol. survey.* 1984.

Hoelzle, M. (1993). *Application of BTS-measurements for modeling mountain permafrost distribution.* Paper presented at the Proceedings of the Sixth International Conference on Permafrost, 1993.

Hoelzle, M., Mittaz, C., Etzelmüller, B., & Haeberli, W. Surface energy fluxes and distribution models of permafrost in European mountain areas: an overview of current developments. *Permafrost and Periglacial Processes.* 2001;12(1); 53-68. doi:10.1002/ppp.385

Holloway, J. E., & Lewkowicz, A. G. (2020). Half a century of discontinuous permafrost persistence and degradation in western Canada. Permafrost and Periglacial Processes, 31(1), 85-96. https://doi.org/10.1002/ppp.2017

Holloway, J. E., Lewkowicz, A. G., Douglas, T. A., Li, X., Turetsky, M. R., Baltzer, J. L., & Jin, H. Impact of wildfire on permafrost landscapes: A review of recent advances and future prospects. *Permafrost and Periglacial Processes.* 2020;31(3); 371-382. doi:https://doi.org/10.1002/ppp.2048

Hou, P., & Wu, S. Long-term changes in extreme air pollution meteorology and the implications for air quality. *Scientific Reports.* 2016;6(1); 1-9.

Hugelius, G., Tarnocai, C., Broll, G., Canadell, J. G., Kuhry, P., & Swanson, D. K. The Northern Circumpolar Soil Carbon Database: spatially distributed datasets of soil coverage and soil carbon storage in the northern permafrost regions. *Earth Syst. Sci. Data.* 2013;5(1); 3-13. doi:10.5194/essd-5-3-2013

Inkpen, R. (2005). *Science, Philosophy and Physical Geography*: Routledge.

IPCC, 2022: Climate Change 2022: Impacts, Adaptation and Vulnerability. Contribution of Working Group II to the Sixth Assessment Report of the Intergovernmental Panel on Climate Change [H.-O. Pörtner, D.C. Roberts, M. Tignor, E.S. Poloczanska, K. Mintenbeck, A. Alegría, M. Craig, S. Langsdorf, S. Löschke, V. Möller, A. Okem, B. Rama (eds.)]. Cambridge University Press. Cambridge University Press, Cambridge, UK and New York, NY, USA, 3056 pp., doi:10.1017/9781009325844.

Jenness, J. 2006. Topographic Position Index (tpi_jen.avx) extension for ArcView 3.x, v. 1.3a. Jenness Enterprises. Available at: http://www.jennessent.com/arcview/tpi.htm.

Jorgenson, M. T., Romanovsky, V., Harden, J., Shur, Y., O'Donnell, J., Schuur, E. A. G., . . . Marchenko, S. Resilience and vulnerability of permafrost to climate change. *Canadian Journal of Forest Research.* 2010;40(7); 1219-1236. doi:10.1139/X10-060

Juliussen, H., & Humlum, O. Towards a TTOP ground temperature model for mountainous terrain in central-eastern Norway. *Permafrost and Periglacial Processes.* 2007;18(2); 161-184. doi:10.1002/ppp.586

Kääb, A. Remote sensing of permafrost-related problems and hazards. *Permafrost and Periglacial Processes.* 2008;19(2); 107-136. doi:10.1002/ppp.619

Kapnick, S. B., & Delworth, T. L. Controls of global snow under a changed climate. *Journal of Climate.* 2013;26(15); 5537-5562.

Karjalainen, O., Luoto, M., Aalto, J., & Hjort, J. New insights into the environmental factors controlling the ground thermal regime across the Northern Hemisphere: a comparison between permafrost and non-permafrost areas. *The Cryosphere.* 2019;13(2); 693-707. doi:10.5194/tc-13-693-2019

Karunaratne, K., & Burn, C. (2003). *Freezing n-factors in discontinuous permafrost terrain, Takhini River, Yukon Territory, Canada.* Paper presented at the Proceedings of the 8th International Conference on Permafrost.

Karunaratne, K. C., & Burn, C. R. Relations between air and surface temperature in discontinuous permafrost terrain near Mayo, Yukon Territory. *Canadian Journal of Earth Sciences.* 2004;41(12); 1437-1451. doi:10.1139/e04-082

Kersten, M. S. (1949). *Laboratory research for the determination of thermal properties of soils*. Retrieved from Engineering Experiment Station Bulletins:

Klene, A. E., Nelson, F. E., Shiklomanov, N. I., & Hinkel, K. M. (2001). The N-Factor in Natural Landscapes: Variability of Air and Soil-Surface Temperatures, Kuparuk River Basin, Alaska, U.S.A. Arctic, Antarctic, and Alpine Research, 33(2), 140-148. doi:10.2307/1552214

Koenigk, T., Brodeau, L., Graversen, R. G., Karlsson, J., Svensson, G., Tjernström, M., . . . Wyser, K. Arctic climate change in 21st century CMIP5 simulations with EC-Earth. *Climate Dynamics.* 2013;40(11); 2719-2743. doi:10.1007/s00382-012-1505-y

Kokelj, S., Smith, C., & Burn, C. (2002). Physical and chemical characteristics of the active layer and permafrost, Herschel Island, western Arctic Coast, Canada. Permafrost and Periglacial Processes, 13(2), 171-185. https://doi.org/10.1002/ppp.417

Kokelj, S. V., & Burn, C. R. Ground ice and soluble cations in near-surface permafrost, Inuvik, Northwest Territories, Canada. *Permafrost and Periglacial Processes.* 2003;14(3); 275-289. doi:10.1002/ppp.458

Kokelj, S. V., & Burn, C. R. Geochemistry of the active layer and near-surface permafrost, Mackenzie delta region, Northwest Territories, Canada. *Canadian Journal of Earth Sciences.* 2005;42(1); 37-48. doi:10.1139/e04-089

Kokelj, S. V., & Jorgenson, M. T. Advances in Thermokarst Research. *Permafrost and Periglacial Processes.* 2013;24(2); 108-119. doi:10.1002/ppp.1779

Krasting, J. P., Broccoli, A. J., Dixon, K. W., & Lanzante, J. R. Future Changes in Northern Hemisphere Snowfall. *Journal of Climate.* 2013;26(20); 7813-7828. doi:https://doi.org/10.1175/JCLI-D-12-00832.1

Kurylyk, B. L., & Hayashi, M. Improved Stefan Equation Correction Factors to Accommodate Sensible Heat Storage during Soil Freezing or Thawing. *Permafrost and Periglacial Processes.* 2016;27(2); 189-203. doi:10.1002/ppp.1865

Kurylyk, B. L., McKenzie, J. M., MacQuarrie, K. T. B., & Voss, C. I. Analytical solutions for benchmarking cold regions subsurface water flow and energy transport models: One-dimensional soil thaw with conduction and advection. *Advances in Water Resources.* 2014a;70; 172-184. doi:http://dx.doi.org/10.1016/j.advwatres.2014.05.005

Lacelle, D., Lapalme, C., Davila, A. F., Pollard, W., Marinova, M., Heldmann, J., & McKay, C. P. Solar Radiation and Air and Ground Temperature Relations in the Cold and Hyper-Arid Quartermain Mountains, McMurdo Dry Valleys of Antarctica. *Permafrost and Periglacial Processes.* 2016;27(2); 163-176. doi:https://doi.org/10.1002/ppp.1859

Lafrenière, M. J., & Lamoureux, S. F. Effects of changing permafrost conditions on hydrological processes and fluvial fluxes. *Earth-Science Reviews.* 2019;191; 212-223. doi:https://doi.org/10.1016/j.earscirev.2019.02.018

Lafrenière, M. J., Laurin, E., & Lamoureux, S. F. The impact of snow accumulation on the active layer thermal regime in high Arctic soils. *Vadose Zone Journal.* 2013;12(1).

Lamhonwah, D., Lafrenière, M. J., Lamoureux, S. F., & Wolfe, B. B. (2016). Multi-year impacts of permafrost disturbance and thermal perturbation on High Arctic stream chemistry. Arctic Science, 3(2), 254-276. doi:10.1139/as-2016-0024

Lamhonwah, D., Lafrenière, M. J., Lamoureux, S. F., & Wolfe, B. B. (2017). Evaluating the hydrological and hydrochemical responses of a High Arctic catchment during an exceptionally warm summer. Hydrological Processes, 31(12), 2296-2313. doi:doi:10.1002/hyp.11191

Lantz, T. C., & Kokelj, S. V. Increasing rates of retrogressive thaw slump activity in the Mackenzie Delta region, N.W.T., Canada. *Geophysical Research Letters.* 2008;35(6). doi:10.1029/2007GL032433

Lewis, T., Lafrenière, M. J., & Lamoureux, S. F. Hydrochemical and sedimentary responses of paired High Arctic watersheds to unusual climate and permafrost disturbance, Cape Bounty, Melville Island, Canada. *Hydrological Processes.* 2012;26(13); 2003-2018. doi:10.1002/hyp.8335

Lewkowicz, A. G., & Bonnaventure, P. P. Equivalent Elevation: A New Method to Incorporate Variable Surface Lapse Rates into Mountain Permafrost Modelling. *Permafrost and Periglacial Processes.* 2011;22(2); 153-162. doi:10.1002/ppp.720

Lewkowicz, A. G., Bonnaventure, P. P., Smith, S. L., & Kuntz, Z. Spatial and thermal characteristics of mountain permafrost, northwest canada. *Geografiska Annaler: Series A, Physical Geography.* 2012;94(2); 195-213. doi:10.1111/j.1468-0459.2012.00462.x

Lewkowicz, A. G., & Ednie, M. Probability mapping of mountain permafrost using the BTS method, Wolf Creek, Yukon Territory, Canada. *Permafrost and Periglacial Processes.* 2004;15(1); 67-80. doi:10.1002/ppp.480

Li, B., Chen, Y., & Shi, X. Does elevation dependent warming exist in high mountain Asia? *Environmental Research Letters.* 2020;15(2); 024012. doi:10.1088/1748-9326/ab6d7f

Li, R., Zhao, L., Wu, T., Wang, Q., Ding, Y., Yao, J., . . . Shi, J. Soil thermal conductivity and its influencing factors at the Tanggula permafrost region on the Qinghai–Tibet Plateau. *Agricultural and Forest Meteorology.* 2019;264; 235-246. doi:https://doi.org/10.1016/j.agrformet.2018.10.011

Lin, Z., Burn, C. R., Niu, F., Luo, J., Liu, M., & Yin, G. The Thermal Regime, including a Reversed Thermal Offset, of Arid Permafrost Sites with Variations in Vegetation Cover Density, Wudaoliang Basin, Qinghai-Tibet Plateau. *Permafrost and Periglacial Processes.* 2015;26(2); 142-159. doi:https://doi.org/10.1002/ppp.1840

Ling, F., & Zhang, T. (2003). Impact of the timing and duration of seasonal snow cover on the active layer and permafrost in the Alaskan Arctic. Permafrost and Periglacial Processes, 14(2), 141-150. https://doi.org/10.1007/s11629-013-2893-0

Liu, Q., Niu, J., Lu, P., Dong, F., Zhou, F., Meng, X., . . . Hu, B. X. Interannual and seasonal variations of permafrost thaw depth on the Qinghai-Tibetan Plateau: A comparative study using long short-term memory, convolutional neural networks, and random forest. *Science of The Total Environment.* 2022;838; 155886. doi:https://doi.org/10.1016/j.scitotenv.2022.155886

Loranty, M. M., Abbott, B. W., Blok, D., Douglas, T. A., Epstein, H. E., Forbes, B. C., . . . Walker, D. A. Reviews and syntheses: Changing ecosystem influences on soil thermal

regimes in northern high-latitude permafrost regions. *Biogeosciences.* 2018;15(17); 5287-5313. doi:10.5194/bg-15-5287-2018

Luetschg, M., Lehning, M., & Haeberli, W. A sensitivity study of factors influencing warm/thin permafrost in the Swiss Alps. *Journal of Glaciology.* 2008;54(187); 696-704. doi:10.3189/002214308786570881

Luo, D., Jin, H., & Bense, V. F. Ground surface temperature and the detection of permafrost in the rugged topography on NE Qinghai-Tibet Plateau. *Geoderma.* 2019;333; 57-68. doi:https://doi.org/10.1016/j.geoderma.2018.07.011

Luo, D., Jin, H., Wu, Q., Bense, V. F., He, R., Ma, Q., . . . Lü, L. Thermal regime of warm-dry permafrost in relation to ground surface temperature in the Source Areas of the Yangtze and Yellow rivers on the Qinghai-Tibet Plateau, SW China. *Science of The Total Environment.* 2018;618; 1033-1045. doi:https://doi.org/10.1016/j.scitotenv.2017.09.083

Mackay, J. R. A Frost Tube for the Determination of Freezing in the Active Layer above Permafrost. *Canadian geotechnical journal.* 1973;10(3); 392-396. doi:10.1139/t73-033

Mamet, S. D., Chun, K. P., Kershaw, G. G. L., Loranty, M. M., & Peter Kershaw, G. Recent Increases in Permafrost Thaw Rates and Areal Loss of Palsas in the Western Northwest Territories, Canada. *Permafrost and Periglacial Processes.* 2017;28(4); 619-633. doi:https://doi.org/10.1002/ppp.1951

Mazhitova, G., Malkova, G., Chestnykh O., et al. (2004) Active layer spatial and temporal variability at European Russian circumpolar-active-layer-monitoring (CALM) sites. Permafrost and Periglacial Processes 15: 123–139. https://doi.org/10.1002/ppp.484

Minder, J. R., Letcher, T. W., & Liu, C. The character and causes of elevation-dependent warming in high-resolution simulations of Rocky Mountain climate change. *Journal of Climate.* 2018;31(6); 2093-2113.

Mitchell, J. B. Machine learning methods in chemoinformatics. *Wiley Interdisciplinary Reviews: Computational Molecular Science.* 2014;4(5); 468-481.

Moeyersoms, J., Junqué de Fortuny, E., Dejaeger, K., Baesens, B., & Martens, D. Comprehensible software fault and effort prediction: A data mining approach. *Journal of Systems and Software.* 2015;100; 80-90. doi:https://doi.org/10.1016/j.jss.2014.10.032

Morse, P. D., Burn, C. R., & Kokelj, S. V. (2012). Influence of snow on near-surface ground temperatures in upland and alluvial environments of the outer Mackenzie Delta, Northwest Territories1This article is one of a series of papers published in this CJES Special Issue on the theme of Fundamental and applied research on permafrost in Canada. Canadian Journal of Earth Sciences, 49(8), 895-913. doi:10.1139/e2012-012

Nakahara, H., Jinguji, A., Sato, S., & Sasao, T. (2017, 22-24 May 2017). *A Random Forest Using a Multi-valued Decision Diagram on an FPGA.* Paper presented at the 2017 IEEE 47th International Symposium on Multiple-Valued Logic (ISMVL).

Nelson, F. E., Shiklomanov, N. I., Mueller, G. R., Hinkel, K. M., Walker, D. A., & Bockheim, J. G. Estimating Active-Layer Thickness over a Large Region: Kuparuk River Basin, Alaska, U.S.A. *Arctic and Alpine Research.* 1997;29(4); 367-378. doi:10.2307/1551985

Nicodemus, K. K., Malley, J. D., Strobl, C., & Ziegler, A. The behaviour of random forest permutation-based variable importance measures under predictor correlation. *BMC Bioinformatics.* 2010;11(1); 110. doi:10.1186/1471-2105-11-110

Nitzbon, J., Westermann, S., Langer, M., Martin, L. C. P., Strauss, J., Laboor, S., & Boike, J. Fast response of cold ice-rich permafrost in northeast Siberia to a warming climate. *Nature Communications.* 2020;11(1); 2201. doi:10.1038/s41467-020-15725-8

Nixon, F., & Taylor, A. Active layer monitoring in natural environments, Mackenzie Valley, Northwest Territories. *Current Research, Geological Survey of Canada. Current Research.* 1994; 27-34.

Nixon, F. M., & Taylor, A. E. (1998). *Regional active layer monitoring across the sporadic, discontinuous and continuous permafrost zones, Mackenzie Valley, northwestern Canada.* Paper presented at the Proceedings of the Seventh International Conference on Permafrost.

Noad, N. C. (2021). *Spatial and temporal trends of surface-based temperature inversion impact on permafrost distribution.*MSc. Thesis. University of Lethbridge (Canada)

Noad, N. C., & Bonnaventure, P. P. Surface temperature inversion characteristics in dissimilar valleys, Yukon Canada. *Arctic Science.* 2022;8(4); 1320-1339.

Noad, N. C., & Bonnaventure, P. P. (Submitted). Examining the influence of microclimatic conditions on the life cycle of surface-based temperature inversions in two proximally dissimilar Yukon valleys. Submitted to The Canadian Geographer. January 23, 2023.

Noh, M.-J., & Howat, I. M. The Surface Extraction from TIN based Search-space Minimization (SETSM) algorithm. *ISPRS Journal of Photogrammetry and Remote Sensing.* 2017;129; 55-76. doi:https://doi.org/10.1016/j.isprsjprs.2017.04.019

O'Donnell, J. A., Romanovsky, V. E., Harden, J. W., & McGuire, A. D. (2009). The Effect of Moisture Content on the Thermal Conductivity of Moss and Organic Soil Horizons From Black Spruce Ecosystems in Interior Alaska. Soil Science, 174(12), 646-651. doi:10.1097/SS.0b013e3181c4a7f8

O'Neill, H. B., & Burn, C. R. (2017a). Impacts of variations in snow cover on permafrost stability, including simulated snow management, Dempster Highway, Peel Plateau, Northwest Territories. Arctic Science, 3(2), 150-178.

O'Neill, H. B., & Burn, C. R. (2017b). Talik formation at a snow fence in continuous permafrost, Western Arctic Canada. Permafrost and periglacial processes, 28(3), 558-565.

O'Neill, H.B., Smith, S.L. & Duchesne, C., 2019b. Long-term permafrost degradation and thermokarst subsidence in the Mackenzie Delta area indicated by thaw tube measurements. In: J.-P. Bilodeau, D.F. Nadeau, D. Fortier and D. Conciatori (Editors), Cold Regions Engineering 2019, Proceedings of the 18th International Conference on Cold Regions Engineering and the 8th Canadian Permafrost Conference. American Society of Civil Engineers, Quebec, Quebec, Canada, pp. 643-651.

O'Neill, H. B., Wolfe, S. A., & Duchesne, C. New ground ice maps for Canada using a paleogeographic modelling approach. *The Cryosphere.* 2019a;13(3); 753-773. doi:10.5194/tc-13-753-2019

Oblogov, G. E., Vasiliev, A. A., Streletskiy, D. A., Shiklomanov, N. I., & Nyland, K. E. Localized Vegetation, Soil Moisture, and Ice Content Offset Permafrost Degradation under Climate Warming. *Geosciences.* 2023;13(5); 129.

Obu, J., Westermann, S., Bartsch, A., Berdnikov, N., Christiansen, H. H., Dashtseren, A., . . . Zou, D. Northern Hemisphere permafrost map based on TTOP modelling for 2000–2016 at 1 km2 scale. *Earth-Science Reviews.* 2019;193; 299-316. doi:https://doi.org/10.1016/j.earscirev.2019.04.023

Oelke, C., Zhang, T., Serreze, M. C., & Armstrong, R. L. Regional-scale modeling of soil freeze/thaw over the Arctic drainage basin. *Journal of Geophysical Research: Atmospheres (1984–2012).* 2003;108(D10). doi:10.1029/2002JD002722

Palazzi, E., Mortarini, L., Terzago, S., & Von Hardenberg, J. Elevation-dependent warming in global climate model simulations at high spatial resolution. *Climate Dynamics.* 2019;52(5); 2685-2702.

Palmer, M., Burn, C., & Kokelj, S. Factors influencing permafrost temperatures across tree line in the uplands east of the Mackenzie Delta, 2004–2010 1, 2 1 This article is one of a series of papers published in this CJES Special Issue on the theme of Fundamental and applied research on permafrost in Canada. 2 Polar Continental Shelf Contribution 03611. *Canadian Journal of Earth Sciences.* 2012;49(8); 877-894.

Pastick, N. J., Rigge, M., Wylie, B. K., Jorgenson, M. T., Rose, J. R., Johnson, K. D., & Ji, L. Distribution and landscape controls of organic layer thickness and carbon within the Alaskan Yukon River Basin. *Geoderma.* 2014;230-231; 79-94. doi:https://doi.org/10.1016/j.geoderma.2014.04.008

Patton, A. I., Rathburn, S. L., & Capps, D. M. Landslide response to climate change in permafrost regions. *Geomorphology.* 2019;340; 116-128. doi:https://doi.org/10.1016/j.geomorph.2019.04.029

Pendergrass, D. C., Zhai, S., Kim, J., Koo, J. H., Lee, S., Bae, M., . . . Jacob, D. J. Continuous mapping of fine particulate matter (PM2.5) air quality in East Asia at daily 6  ×  6 km2 resolution by application of a random forest algorithm to 2011–2019 GOCI geostationary satellite data. *Atmos. Meas. Tech.* 2022;15(4); 1075-1091. doi:10.5194/amt-15-1075-2022

Pepin, N., Bradley, R., Diaz, H., Baraër, M., Caceres, E., Forsythe, N., . . . Liu, X. Elevation-dependent warming in mountain regions of the world. *Nature Climate Change.* 2015a;5(5); 424-430.

Pepin, N., Bradley, R. S., Diaz, H. F., Baraer, M., Caceres, E. B., Forsythe, N., . . . Mountain Research Initiative, E. D. W. W. G. Elevation-dependent warming in mountain regions of the world. *Nature Climate Change.* 2015b;5(5); 424-430. doi:10.1038/nclimate2563

Pichugina, Y. L., Banta, R. M., Bonin, T., Brewer, W. A., Choukulkar, A., McCarty, B. J., ... & Stoelinga, M. (2019). Spatial variability of winds and HRRR–NCEP model error statistics at three Doppler-lidar sites in the wind-energy generation region of the Columbia River Basin. Journal of Applied Meteorology and Climatology, 58(8), 1633-1656.

Ran, Y., Jorgenson, M. T., Li, X., Jin, H., Wu, T., Li, R., & Cheng, G. Biophysical permafrost map indicates ecosystem processes dominate permafrost stability in the Northern Hemisphere. *Environmental Research Letters.* 2021;16(9); 095010. doi:10.1088/1748-9326/ac20f3

Rangecroft, S., Suggitt, A. J., Anderson, K., & Harrison, S. Future climate warming and changes to mountain permafrost in the Bolivian Andes. *Climatic Change.* 2016;137(1); 231-243. doi:10.1007/s10584-016-1655-8

Rangwala, I., & Miller, J. R. Twentieth Century Temperature Trends in Colorado's San Juan Mountains. *Arctic, Antarctic, and Alpine Research.* 2010;42(1); 89-97. doi:10.1657/1938-4246-42.1.89

Rangwala, I., & Miller, J. R. Climate change in mountains: a review of elevation-dependent warming and its possible causes. *Climatic Change.* 2012;114(3); 527-547. doi:10.1007/s10584-012-0419-3

Riseborough, D. The effect of transient conditions on an equilibrium permafrost-climate model. *Permafrost and Periglacial Processes.* 2007;18(1); 21-32. doi:10.1002/ppp.579

Riseborough, D., Shiklomanov, N., Etzelmüller, B., Gruber, S., & Marchenko, S. Recent advances in permafrost modelling. *Permafrost and Periglacial Processes.* 2008;19(2); 137-156. doi:10.1002/ppp.615

Riseborough, D., & Smith, M. (1998). *Exploring the limits of permafrost.* Paper presented at the Proceedings Permafrost: 7th International Conference. Yellowknife, Canada. Edited by Lewkowicz, AG, and Allard, M. Nordicana, Quebec.

Riseborough, D. W. The mean annual temperature at the top of permafrost, the TTOP model, and the effect of unfrozen water. *Permafrost and Periglacial Processes.* 2002;13(2); 137-143. doi:10.1002/ppp.418

Roberts, K. E., Lamoureux, S. F., Kyser, T. K., Muir, D. C. G., Lafrenière, M. J., Iqaluk, D., . . . Normandeau, A. Climate and permafrost effects on the chemistry and ecosystems of High Arctic Lakes. *Scientific Reports.* 2017;7(1); 13292. doi:10.1038/s41598-017-13658-9

Romanovsky, V. E., & Osterkamp, T. E. Interannual variations of the thermal regime of the active layer and near-surface permafrost in northern Alaska. *Permafrost and Periglacial Processes.* 1995;6(4); 313-335. doi:10.1002/ppp.3430060404

Ruman, C. J., Monahan, A. H., & Sushama, L. Climatology of Arctic temperature inversions in current and future climates. *Theoretical and Applied Climatology.* 2022;150(1); 121-134. doi:10.1007/s00704-022-04147-9

Sazonova, T. S., & Romanovsky, V. E. A model for regional-scale estimation of temporal and spatial variability of active layer thickness and mean annual ground temperatures. *Permafrost and Periglacial Processes.* 2003;14(2); 125-139. doi:10.1002/ppp.449

Schuur, E. A. G., Bockheim, J., Canadell, J. G., Euskirchen, E., Field, C. B., Goryachkin, S. V., . . . Zimov, S. A. Vulnerability of Permafrost Carbon to Climate Change: Implications for the Global Carbon Cycle. *BioScience.* 2008;58(8); 701-714. doi:10.1641/B580807

Screen, J. A., Simmonds, I., Deser, C., & Tomas, R. The Atmospheric Response to Three Decades of Observed Arctic Sea Ice Loss. *Journal of Climate.* 2013;26(4); 1230-1248. doi:https://doi.org/10.1175/JCLI-D-12-00063.1

Seppälä, M. (1982). *An experimental study of the formation of palsas.* Paper presented at the Proceedings of the Fourth Canadian Permafrost Conference. Ottawa, Canada: National Research Council of Canada.

Serreze, M. C., & Barry, R. G. Processes and impacts of Arctic amplification: A research synthesis. *Global and Planetary Change.* 2011;77(1); 85-96. doi:https://doi.org/10.1016/j.gloplacha.2011.03.004

Shiklomanov NI & Nelson FE (2002) Active-layer mapping at regional scales: A 13-year spatial time series for the Kuparuk region, north-central Alaska. Permafrost and Periglacial Processes 13: 219–230. https://doi.org/10.1002/ppp.425

Shiklomanov, N. I., Streletskiy, D. A., Nelson, F. E., Hollister, R. D., Romanovsky, V. E., Tweedie, C. E., Bockheim, J.G., Brown, J. (2010). Decadal variations of active-layer thickness in moisture-controlled landscapes, Barrow, Alaska. Journal of Geophysical Research: Biogeosciences, 115(G4), n/a-n/a. doi:10.1029/2009JG001248

Shiozawa, S., & Campbell, G. S. Soil thermal conductivity. *Remote Sensing Reviews.* 1990;5(1); 301-310. doi:10.1080/02757259009532137

Shur, Y., Hinkel, K. M., & Nelson, F. E. The transient layer: implications for geocryology and climate-change science. *Permafrost and Periglacial Processes.* 2005;16(1); 5-17.

Shur, Y. L., & Jorgenson, M. T. Patterns of permafrost formation and degradation in relation to climate and ecosystems. *Permafrost and Periglacial Processes.* 2007;18(1); 7-19. doi:10.1002/ppp.582

Smith, M. W. Microclimatic Influences on Ground Temperatures and Permafrost Distribution, Mackenzie Delta, Northwest Territories. *Canadian Journal of Earth Sciences.* 1975;12(8); 1421-1438. doi:10.1139/e75-129

Smith, M. W., & Riseborough, D. W. Permafrost monitoring and detection of climate change. *Permafrost and Periglacial Processes.* 1996;7(4); 301-309. doi:10.1002/(sici)1099-1530(199610)7:4<301::aid-ppp231>3.0.co;2-r

Smith, M. W., & Riseborough, D. W. Climate and the limits of permafrost: a zonal analysis. *Permafrost and Periglacial Processes.* 2002;13(1); 1-15. doi:10.1002/ppp.410

Smith, S., Burgess, M., & Nixon, F. (2001). Response of active-layer and permafrost temperatures to warming during 1998 in the Mackenzie Delta, Northwest Territories and at Canadian Forces Station Alert and Baker Lake, Nunavut: Natural Resources Canada, Geological Survey of Canada. https://doi.org/10.4095/212685

Smith, S. L., Riseborough, D. W., & Bonnaventure, P. P. Eighteen Year Record of Forest Fire Effects on Ground Thermal Regimes and Permafrost in the Central Mackenzie Valley, NWT, Canada. *Permafrost and Periglacial Processes.* 2015;26(4); 289-303. doi:10.1002/ppp.1849

Smith, S. L., Riseborough, D. W., Bonnaventure, P. P., & Duchesne, C. (2016). An ecoregional assessment of freezing season air and ground surface temperature in the Mackenzie Valley corridor, NWT, Canada. Cold Regions Science and Technology, 125(Supplement C), 152-161. doi:https://doi.org/10.1016/j.coldregions.2016.02.007

Smith, S. L., Wolfe, S. A., Riseborough, D. W., & Nixon, F. M. Active-layer characteristics and summer climatic indices, Mackenzie Valley, Northwest Territories, Canada. *Permafrost and Periglacial Processes.* 2009a;20(2); 201-220. doi:https://doi.org/10.1002/ppp.651

Smith, S. L., Wolfe, S. A., Riseborough, D. W., & Nixon, F. M. Active-layer characteristics and summer climatic indices, Mackenzie Valley, Northwest Territories, Canada. *Permafrost and Periglacial Processes.* 2009b;20(2); 201-220. doi:10.1002/ppp.651

Soong, J. L., Phillips, C. L., Ledna, C., Koven, C. D., & Torn, M. S. CMIP5 Models Predict Rapid and Deep Soil Warming Over the 21st Century. *Journal of Geophysical Research: Biogeosciences.* 2020;125(2); e2019JG005266. doi:https://doi.org/10.1029/2019JG005266

Stanek, W., Alexander, K., & Simmons, C. S. Reconnaissance of vegetation and soils along the Dempster Highway, Yukon Territory: 1. Vegetation types. *Report Pacific Forest Research Centre (Canada). no. BC-X-217.* 1980.

Strobl, C., Boulesteix, A.-L., Kneib, T., Augustin, T., & Zeileis, A. Conditional variable importance for random forests. *BMC Bioinformatics.* 2008;9(1); 307. doi:10.1186/1471-2105-9-307

Strobl, C., & Zeileis, A. Danger: High power!–exploring the statistical properties of a test for random forest variable importance. 2008.

Sturm, M., Holmgren, J., McFadden, J. P., Liston, G. E., Chapin III, F. S., & Racine, C. H. (2001). Snow–shrub interactions in Arctic tundra: a hypothesis with climatic implications. Journal of Climate, 14(3), 336-344. https://doi.org/10.1175/1520-0442(2001)014<0336:SSIIAT>2.0.CO;2

Tarnocai, C., Mark Nixon, F., & Kutny, L. Circumpolar-Active-Layer-Monitoring (CALM) sites in the Mackenzie Valley, northwestern Canada. *Permafrost and Periglacial Processes.* 2004;15(2); 141-153. doi:https://doi.org/10.1002/ppp.490

Tolosi, L., & Lengauer, T. Classification with correlated features: unreliability of feature ranking and solutions. *Bioinformatics.* 2011;27(14); 1986-1994. doi:10.1093/bioinformatics/btr300

Uhlemann, S., Dafflon, B., Peterson, J., Ulrich, C., Shirley, I., Michail, S., & Hubbard, S. S. (2021). Geophysical monitoring shows that spatial heterogeneity in thermohydrological dynamics reshapes a transitional permafrost system. Geophysical Research Letters, 48(6), e2020GL091149.

Vegter, S. E. (2023). *A TTOP model of permafrost distribution in the boreal wetland environment of Whatì, NT, Canada.* Lethbridge, Alta.: University of Lethbridge, Dept. of Geography,

Viereck, L. A. Forest Succession and Soil Development Adjacent to the Chena River in Interior Alaska. *Arctic and Alpine Research.* 1970;2(1); 1-26. doi:10.1080/00040851.1970.12003558

Vivoni, E. R., Gebremichael, M., Watts, C. J., Bindlish, R., & Jackson, T. J. Comparison of ground-based and remotely-sensed surface soil moisture estimates over complex terrain during SMEX04. *Remote sensing of Environment.* 2008;112(2); 314-325. doi:https://doi.org/10.1016/j.rse.2006.10.028

Walker, D. A., Gould, W. A., Maier, H. A., & Raynolds, M. K. The Circumpolar Arctic Vegetation Map: AVHRR-derived base maps, environmental controls, and integrated mapping procedures. *International Journal of Remote Sensing.* 2002;23(21); 4551-4570. doi:10.1080/01431160110113854

Walvoord, M. A., & Kurylyk, B. L. Hydrologic Impacts of Thawing Permafrost—A Review. *Vadose Zone Journal.* 2016;15(6). doi:10.2136/vzj2016.01.0010

Wang, T., Hamann, A., Spittlehouse, D., & Carroll, C. Locally Downscaled and Spatially Customizable Climate Data for Historical and Future Periods for North America. *PLOS ONE.* 2016;11(6); e0156720. doi:10.1371/journal.pone.0156720

Way, R.G. & Lapalme, C.M., 2021. Does tall vegetation warm or cool the ground surface? Constraining the ground thermal impacts of upright vegetation in northern environments. Environmental Research Letters, 16(5): 054077. https://doi.org/10.1088/1748-9326/abef31

Way, R. G., & Lewkowicz, A. G. Modelling the spatial distribution of permafrost in Labrador–Ungava using the temperature at the top of permafrost. *Canadian Journal of Earth Sciences.* 2016;53(10); 1010-1028. doi:10.1139/cjes-2016-0034

Way, R. G., & Lewkowicz, A. G. Environmental controls on ground temperature and permafrost in Labrador, northeast Canada. *Permafrost and Periglacial Processes.* 2018;29(2); 73-85. doi:doi:10.1002/ppp.1972

Westermann, S., Østby, T. I., Gisnås, K., Schuler, T. V., & Etzelmüller, B. A ground temperature map of the North Atlantic permafrost region based on remote sensing and reanalysis data. *The Cryosphere.* 2015;9(3); 1303-1319. doi:10.5194/tc-9-1303-2015

Wilcox, E. J.; Keim, D.; de Jong, T.; Walker, B.; Sonnentag, O.; Sniderhan, A. E.; Mann, P. & Marsh, P.; Tundra shrub expansion may amplify permafrost thaw by advancing snowmelt timing; Arctic Science, 2019, 5, 202-217 https://doi.org/10.1139/as-2018-0028

Williams, P. J., & Smith, M. W. (1989). *The Frozen Earth: Fundamentals of Geocryology*: Cambridge University Press.

Williams, T. J., Pomeroy, J. W., Janowicz, J. R., Carey, S. K., Rasouli, K., & Quinton, W. L. (2015). A radiative–conductive–convective approach to calculate thaw season ground surface temperatures for modelling frost table dynamics. Hydrological Processes, 29(18), 3954-3965.

Williamson, S. N., Zdanowicz, C., Anslow, F. S., Clarke, G. K., Copland, L., Danby, R. K., . . . Hik, D. S. Evidence for elevation-dependent warming in the St. Elias Mountains, Yukon, Canada. *Journal of Climate.* 2020;33(8); 3253-3269.

Wilson, G., Green, M., Brown, J., Campbell, J., Groffman, P., Durán, J., & Morse, J. (2020). Snowpack affects soil microclimate throughout the year. Climatic Change, 163, 705-722.

Woo, M.-k., Mollinga, M., & Smith, S. L. Climate warming and active layer thaw in the boreal and tundra environments of the Mackenzie Valley. *Canadian Journal of Earth Sciences.* 2007;44(6); 733-743. doi:10.1139/e06-121

Woo, M. k. Permafrost hydrology in North America. *Atmosphere-Ocean.* 1986;24(3); 201-234. doi:10.1080/07055900.1986.9649248

Woo, M. K., Kane, D. L., Carey, S. K., & Yang, D. Progress in permafrost hydrology in the new millennium. *Permafrost and Periglacial Processes.* 2008;19(2); 237-254. doi:10.1002/ppp.613

Wright, J., Duchesne, C., & Côté, M. (2003). *Regional-scale permafrost mapping using the TTOP ground temperature model.* Paper presented at the Proceedings of the Eighth International Conference on Permafrost, Zurich, Switzerland, Phillips M, Springman SM, Arenson LU (eds). AA Balkema: Lisse.

Yang, D., & Woo, M. K. Representativeness of local snow data for large scale hydrologic investigations. *Hydrological Processes.* 1999;13(12-13); 1977-1988. doi:10.1002/(SICI)1099-1085(199909)13:12/13<1977::AID-HYP894>3.0.CO;2-B

Yi, Y., Kimball, J. S., Chen, R. H., Moghaddam, M., Reichle, R. H., Mishra, U., Zona, D., and Oechel, W. C.: Characterizing permafrost active layer dynamics and sensitivity to landscape spatial heterogeneity in Alaska, The Cryosphere, 12, 145–161, https://doi.org/10.5194/tc-12-145-2018, 2018.

Yin, G.-a., Niu, F.-j., Lin, Z.-j., Luo, J., & Liu, M.-h. Performance comparison of permafrost models in Wudaoliang Basin, Qinghai-Tibet Plateau, China. *Journal of Mountain Science.* 2016;13(7); 1162-1173. doi:10.1007/s11629-015-3745-x

You, Q., Kang, S., Pepin, N., Flügel, W.-A., Yan, Y., Behrawan, H., & Huang, J. Relationship between temperature trend magnitude, elevation and mean temperature in the Tibetan Plateau from homogenized surface stations and reanalysis data. *Global and Planetary Change.* 2010;71(1-2); 124-133.

Young, K. L., Woo, M.-k., & Edlund, S. A. Influence of Local Topography, Soils, and Vegetation on Microclimate and Hydrology at a High Arctic Site, Ellesmere Island, Canada. *Arctic and Alpine Research.* 1997;29(3); 270-284. doi:10.2307/1552141

Yu, R., Yang, Y., Yang, L., Han, G., & Move, O. A. RAQ–A Random Forest Approach for Predicting Air Quality in Urban Sensing Systems. *Sensors.* 2016;16(1); 86.

Yukon Ecoregions Working Group, 2004. Yukon Coastal Plain. In: Ecoregions of the Yukon Territory: Biophysical properties of Yukon landscapes, C.A.S. Smith, J.C. Meikle and C.F. Roots (eds.), Agriculture and Agri-Food Canada, PARC Technical Bulletin No. 04-01, Summerland, British Columbia, p. 63-72.

Yukon. (2020). *Dempster Fibre Project.* https://yukon.ca/dempsterfibreproject#current-project-status

Zhang, T. Influence of the seasonal snow cover on the ground thermal regime: An overview. *Reviews of Geophysics.* 2005;43(4); n/a-n/a. doi:10.1029/2004RG000157

Zhang, T., Osterkamp, T. E., & Stamnes, K. Effects of Climate on the Active Layer and Permafrost on the North Slope of Alaska, U.S.A. *Permafrost and Periglacial Processes.* 1997;8(1); 45-67. doi:10.1002/(SICI)1099-1530(199701)8:1<45::AID-PPP240>3.0.CO;2-K

Zhang, Y., Chen, W., & Cihlar, J. A process-based model for quantifying the impact of climate change on permafrost thermal regimes. *Journal of Geophysical Research: Atmospheres.* 2003;108(D22); n/a-n/a. doi:10.1029/2002jd003354

Zou, D., Zhao, L., Sheng, Y., Chen, J., Hu, G., Wu, T., . . . Cheng, G. A new map of permafrost distribution on the Tibetan Plateau. *The Cryosphere.* 2017;11(6); 2527-2542. doi:10.5194/tc-11-2527-2017

## S. Supplemental Data and Information

## S.3 Chapter 3 Supplemental

**Table S3-1.** Active layer monitoring site names and ecoregion in the Mackenzie Valley transect (Smith et al., 2009a). For the ecoregion name "P" stands for "Plains".

| GSC Site Code | Site Name | Ecoregion | Lat (°N) | Long (°E) | Elevation (m) | Closest EC Station | Distance to EC Station (km) | Record Length (yrs) | Substrate |
|---|---|---|---|---|---|---|---|---|---|
| **90-TT-01** | North Head ridge | Tundra P LA*n* | 69.708 | -134.486 | 17 | Tuktoyaktuk A | 66.2 | 13 | Silt |
| **90-TT-02** | North Point summit | Tundra P LA*n* | 69.657 | -134.387 | 29 | Tuktoyaktuk A | 58.5 | 22 | Clay till |
| **90-TT-03** | YaYa Lake high | Tundra P LA*n* | 69.145 | -134.717 | 40 | Tuktoyaktuk A | 73.5 | 23 | Sand |
| **90-TT-04** | YaYa Lake low | Tundra P LA*n* | 69.139 | -134.702 | 10 | Tuktoyaktuk A | 73 | 23 | Silt |
| **90-TT-05** | Lousy Point ridge | Tundra P LA*n* | 69.219 | -134.291 | 39 | Tuktoyaktuk A | 54.7 | 23 | Silt |
| **90-TT-06** | Lousy Point low terrace | Tundra P LA*n* | 69.219 | -134.291 | 9 | Tuktoyaktuk A | 54.5 | 22 | Organic sand |
| **90-TT-07** | Lousy Point flood plain | Tundra P LA*n* | 69.218 | -134.273 | 2 | Tuktoyaktuk A | 54.3 | 16 | Silt |
| **90-TT-08** | Mason Bay high | Tundra P LA*n* | 69.524 | -134.021 | 14 | Tuktoyaktuk A | 39.8 | 21 | Silt till |
| **90-TT-09** | Mason Bay shore | Tundra P LA*n* | 69.525 | -134.008 | 4 | Tuktoyaktuk A | 39.5 | 21 | Organic sand |
| **90-TT-10** | Mason Bay inlet | Tundra P LA*n* | 69.522 | -134.041 | 14 | Tuktoyaktuk A | 40.6 | 18 | Silt sand |
| **90-TT-11** | North Point mid-slope | Tundra P LA*n* | 69.655 | -134.383 | 16 | Tuktoyaktuk A | 58 | 19 | Silt clay |
| **90-TT-12** | North Point shore | Tundra P LA*n* | 69.653 | -134.387 | 3 | Tuktoyaktuk A | 57.4 | 20 | Organic silt |
| **90-TT-13** | North Head shore | Tundra P LA*n* | 69.721 | -134.461 | 3 | Tuktoyaktuk A | 63.4 | 14 | Silt |
| **90-TT-14** | North Head high | Tundra P LA*n* | 69.719 | -134.441 | 15 | Tuktoyaktuk A | 64.9 | 5 | Organic silt |
| **91-TT-01** | Swimming Point slope | Tundra P LA*n* | 69.108 | -134.402 | 8 | Tuktoyaktuk A | 66.5 | 22 | Organic sand |
| **91-TT-02** | Swimming Point shore | Tundra P LA*n* | 69.108 | -134.385 | 3 | Tuktoyaktuk A | 65.8 | 14 | Clay silt |
| **91-TT-03** | Swimming Point Holmes | Tundra P LA*n* | 69.108 | -134.351 | 11 | Tuktoyaktuk A | 64.8 | 18 | Organic sand |
| **91-TT-05** | Wolf Lake | Tundra P LA*n* | 69.241 | -134.433 | 53 | Tuktoyaktuk A | 60.8 | 12 | Organic sand |
| **91-TT-06** | Wolf Lake hollow | Tundra P LA*n* | 69.241 | -134.419 | 23 | Tuktoyaktuk A | 60.3 | 12 | Organic silt |

| | | | | | | | | | |
|---|---|---|---|---|---|---|---|---|---|
| **91-TT-07** | Wolf Lake Hill | Tundra P LA*n* | 69.241 | -134.403 | 37 | Tuktoyaktuk A | 59.8 | 12 | Organic sand |
| **91-TT-08** | Lousy Point inland | Tundra P LA*n* | 69.404 | -134.339 | 50 | Tuktoyaktuk A | 58.3 | 6 | Organic clay till |
| **91-TT-09** | Lousy Point hollow | Tundra P LA*n* | 69.217 | -134.3 | 16 | Tuktoyaktuk A | 56.9 | 20 | Organic silt |
| **91-TT-11** | Trail Valley Creek | Tundra P LA*n* | 68.737 | -133.487 | 53 | Inuvik A | 48.6 | 19 | Clay |
| **91-TT-A** | Harry Channel mouth | Tundra P LA*n* | 69.475 | -134.824 | 2 | Tuktoyaktuk A | 70.3 | 19 | Organic silt |
| **91-TT-B** | Big Horn Point | Tundra P LA*n* | 69.478 | -134.843 | 2 | Tuktoyaktuk A | 72.8 | 10 | Organic silt |
| **91-TT-C** | Taglu | Tundra P LA*n* | 69.369 | -134.948 | 2 | Tuktoyaktuk A | 75.4 | 17 | Sand silt |
| **91-TT-F** | Kendall Meadow | Tundra P LA*n* | 69.44 | -135.338 | 2 | Tuktoyaktuk A | 90.2 | 14 | Silt |
| **92-TT-02** | Involuted Hill flat | Tundra P LA*n* | 69.474 | -132.637 | 4 | Tuktoyaktuk A | 16.2 | 15 | Silt clay |
| **94-TT-01** | Illasarvik | Tundra P LA*n* | 69.483 | -134.565 | 5 | Tuktoyaktuk A | 59.5 | 17 | Clay organic |
| **90-TT-17** | Navy Channel | Taiga P HS | 68.424 | -133.786 | 5 | Inuvik A | 18.0 | 15 | Silt |
| **91-TT-12** | Reindeer station plateau | Taiga P HS | 68.689 | -134.106 | 152 | Inuvik A | 50.3 | 21 | Silt clay |
| **91-TT-13** | William's Island (Williams Island) | Taiga P HS | 68.685 | -134.145 | 5 | Inuvik A | 50.5 | 23 | Silt |
| **91-TT-14** | Rengleng River Mouth | Taiga P HS | 67.795 | -134.126 | 8 | Inuvik A | 61.9 | 17 | Sand |
| **91-TT-15** | Rengleng Lake | Taiga P HS | 67.758 | -134.075 | 8 | Inuvik A | 64.4 | 11 | Silt clay |
| **91-TT-16** | Tsiigehchic | Taiga P HS | 67.476 | -133.770 | 14 | Inuvik A | 91.6 | 16 | Silt |
| **91-TT-17** | Grand View mouth | Taiga P HS | 66.786 | -130.120 | 22 | Fort Good Hope A | 135.9 | 4 | Silt |
| **91-TT-18** | Grand View inland | Taiga P HS | 66.786 | -130.118 | 24 | Fort Good Hope | 135.7 | 8 | Organic |
| **92-TT-03** | Arctic Red | Taiga P HS | 67.496 | -133.759 | 30 | Inuvik A | 103.7 | 14 | Silt clay till |
| **93-TT-01** | Caribou Creek | Taiga P HS | 68.111 | -133.476 | 30 | Inuvik A | 22.3 | 21 | Clay silt till |
| **93-TT-02** | Havikpak Creek | Taiga P HS | 68.319 | -133.513 | 80 | Inuvik A | 3.0 | 20 | Organic clay silt till |
| **91-TT-19** | Sans-sault | Taiga P LS | 65.657 | -128.774 | 38 | Norman Wells A | 101.7 | 13 | Organic silt |
| **91-TT-20** | Mountain River | Taiga P LS | 65.674 | -128.829 | 39 | Norman Wells A | 104.6 | 14 | Gravel |
| **91-TT-21** | Francis Creek mouth | Taiga P LS | 65.188 | -126.468 | 54 | Norman Wells A | 65.188 | 10 | Silt till |

| | | | | | | | | | |
|---|---|---|---|---|---|---|---|---|---|
| **91-TT-22** | Francis Creek | Taiga P LS | 65.193 | -126.469 | 51 | Norman Wells A | 17 | 14 | Silt till |
| **92-TT-12** | Tulita | Taiga P LS | 64.912 | -125.576 | 93 | Norman Wells A | 45.0 | 10 | Peat organic silt clay |
| **94-TT-05** | NW ROW (kp 2) off | Taiga P LS | 65.298 | -126.846 | 65 | Norman Wells A | 4.1 | 12 | Organic silt clay |
| **92-TT-04** | Manners Creek mouth | Taiga P MB | 61.770 | -121.193 | 126 | Fort Simpson A | 3.1 | 17 | Organic silt |
| **92-TT-05** | Manners Creek upper | Taiga P MB | 61.766 | -121.186 | 142 | Fort Simpson A | 3.1 | 14 | Silt |
| **92-TT-06** | Martin River | Taiga P MB | 61.888 | -121.601 | 166 | Fort Simpson A | 24.6 | 10 | Sand |
| **92-TT-07** | Willowlake River | Taiga P MB | 62.697 | -123.065 | 103 | Fort Simpson A | 141.8 | 18 | Silt |
| **92-TT-08** | River between two mountains | B & T Cordillera | 62.955 | -123.204 | 99 | Fort Simpson A | 169.1 | 16 | Organic silt |
| **92-TT-09** | Ochre River | B &T Cordillera | 63.462 | -123.689 | 97 | Fort Simpson A | 228.4 | 17 | Peat |
| **92-TT-10** | Ochre River cabin | B &T Cordillera | 63.466 | -123.690 | 97 | Fort Simpson A | 229 | 17 | Silt |
| **96-TT-01** | Mio Lake | B &T Cordillera | 64.467 | -124.792 | 132 | Norman Wells A | 131.1 | 7 | Organic silt gravel |

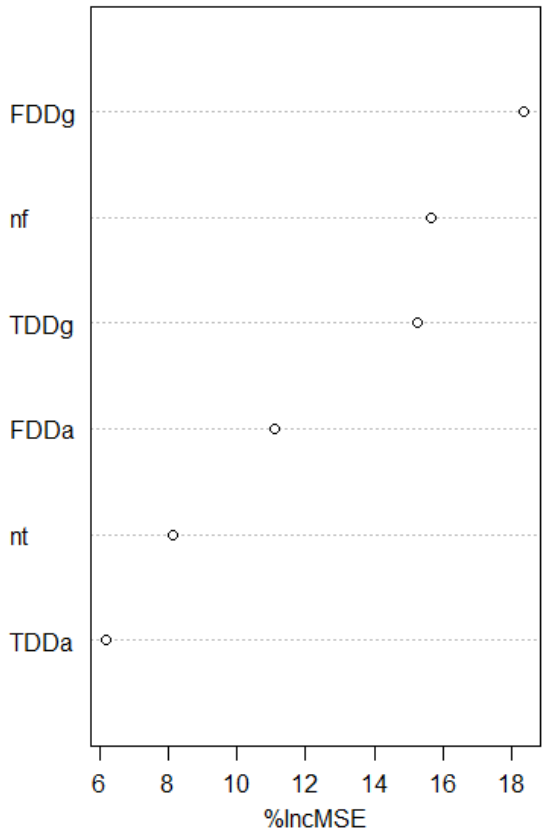


**Figure S3-1.** Random forest variable importance rankings for active layer thickness.

## S.4 Chapter 4 Supplemental

### *S.4.1 TTOP Model Sensitivity Percentile Substitution*

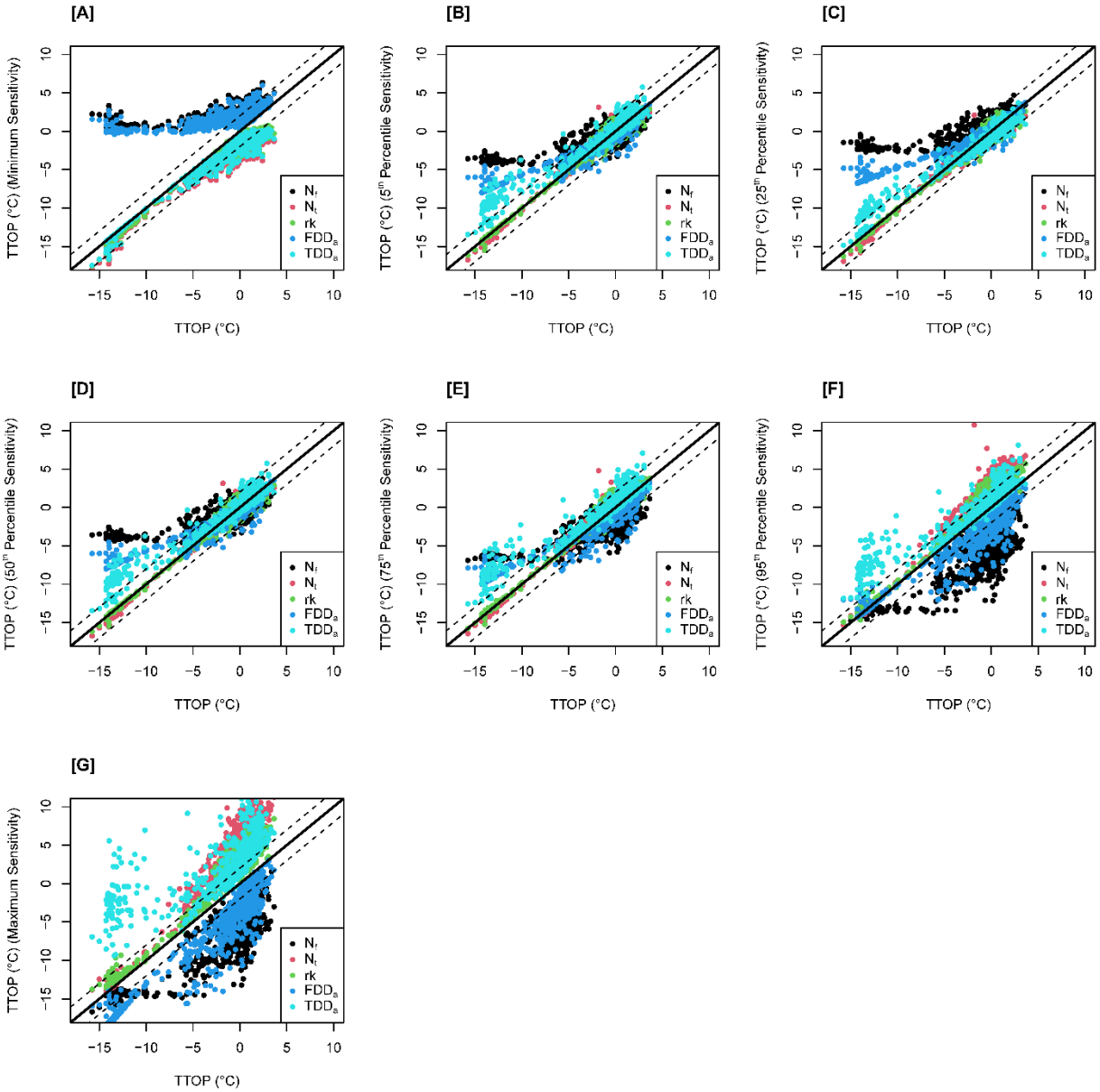


**Figure S4-1.** Reference temperature at top of permafrost (TTOP) compared to perturbed TTOP resulting from the substitution of the [A] minimum, [B] 5$^{th}$ percentile, [C] 25$^{th}$ percentile, [D] 50$^{th}$, [E] 75$^{th}$ percentile, [F] 95$^{th}$ percentile, and [G] maximum value for each parameter. The solid line indicates no (0 °C) difference between the two TTOP values while the dashed line shows ± 2 °C difference.

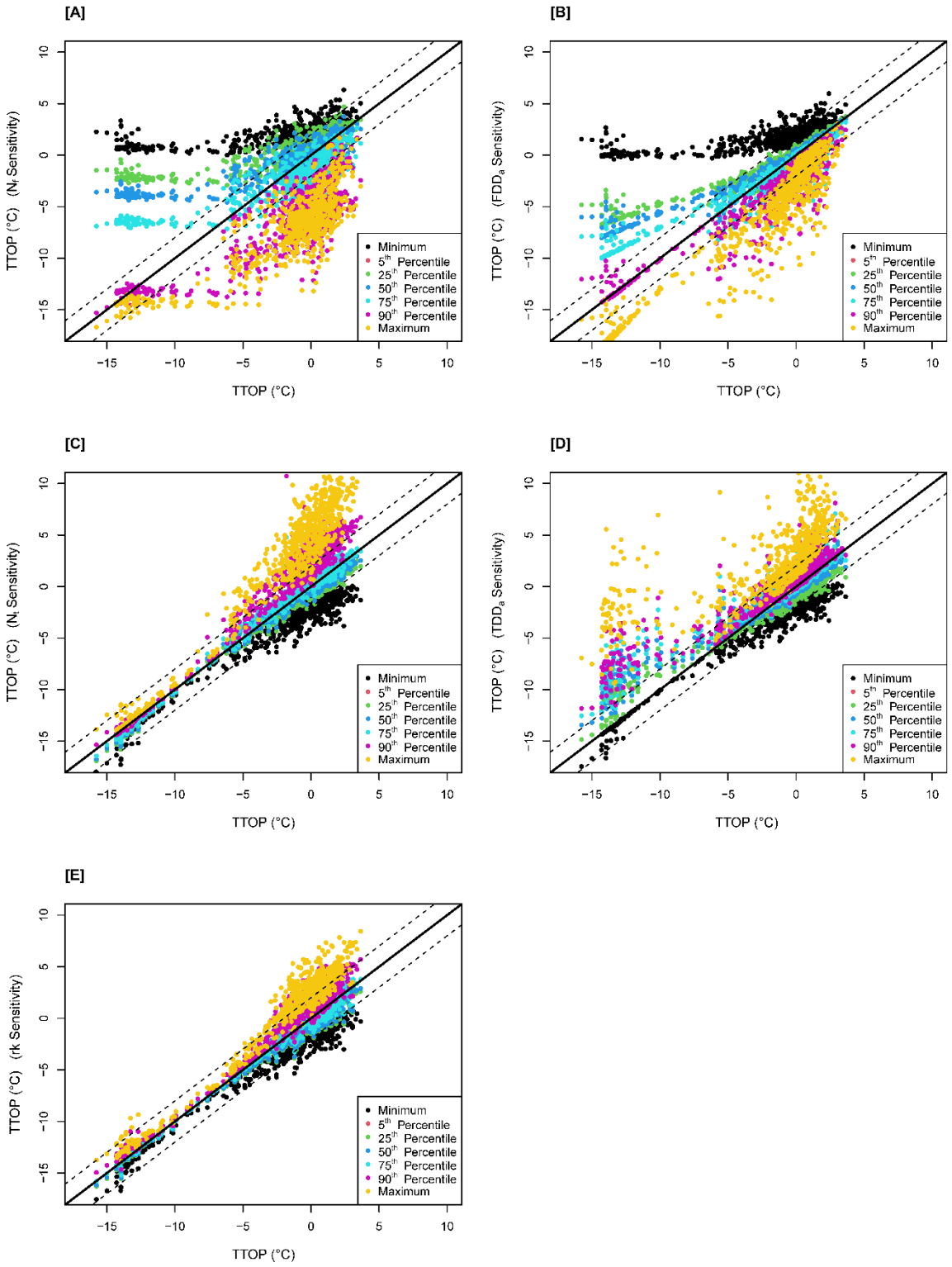


**Figure S4-2.** Reference temperature at top of permafrost (TTOP) compared perturbed TTOP for each direct substitution each iteration's percentile value for [A] $n_f$, [B] $FDD_a$, [C] $n_t$, [D] $TDD_a$, and [E] rk. The solid line indicates no (0 °C) difference between the two TTOP values while the dashed line shows ± 2 °C difference.

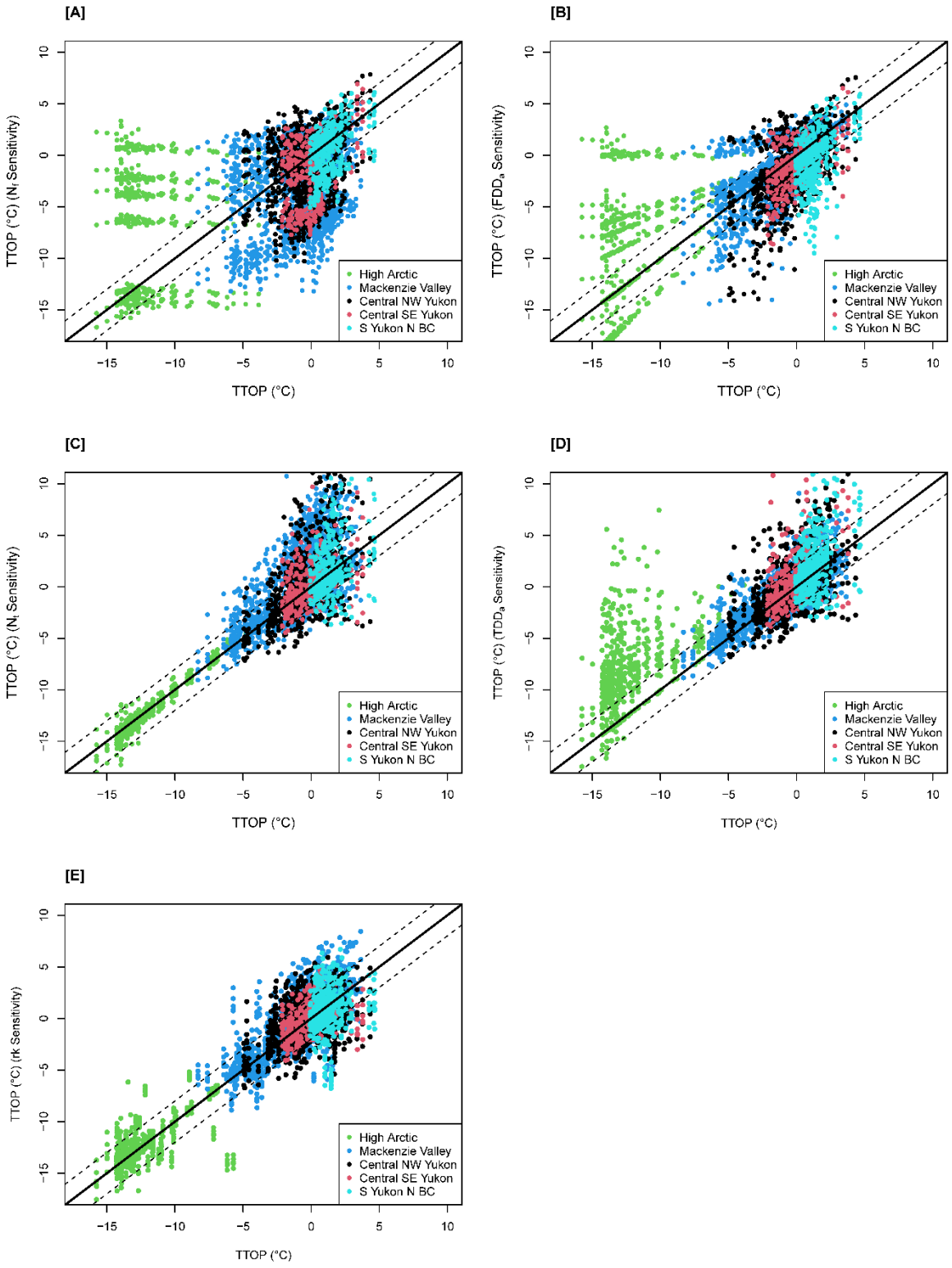


**Figure S4-3.** Regional temperature at top of permafrost (TTOP) model sensitivity to changes in [A] $n_f$, [B] $FDD_a$, [C] $n_t$, [D] $TDD_a$, and [E] rk for the direct substitution of a percentile value. The solid line indicates no (0 °C) difference between the reference and perturbed TTOP values while the dashed line shows ± 2 °C difference.

*S.4.2 TTOP Model Sensitivity ± Percentage*

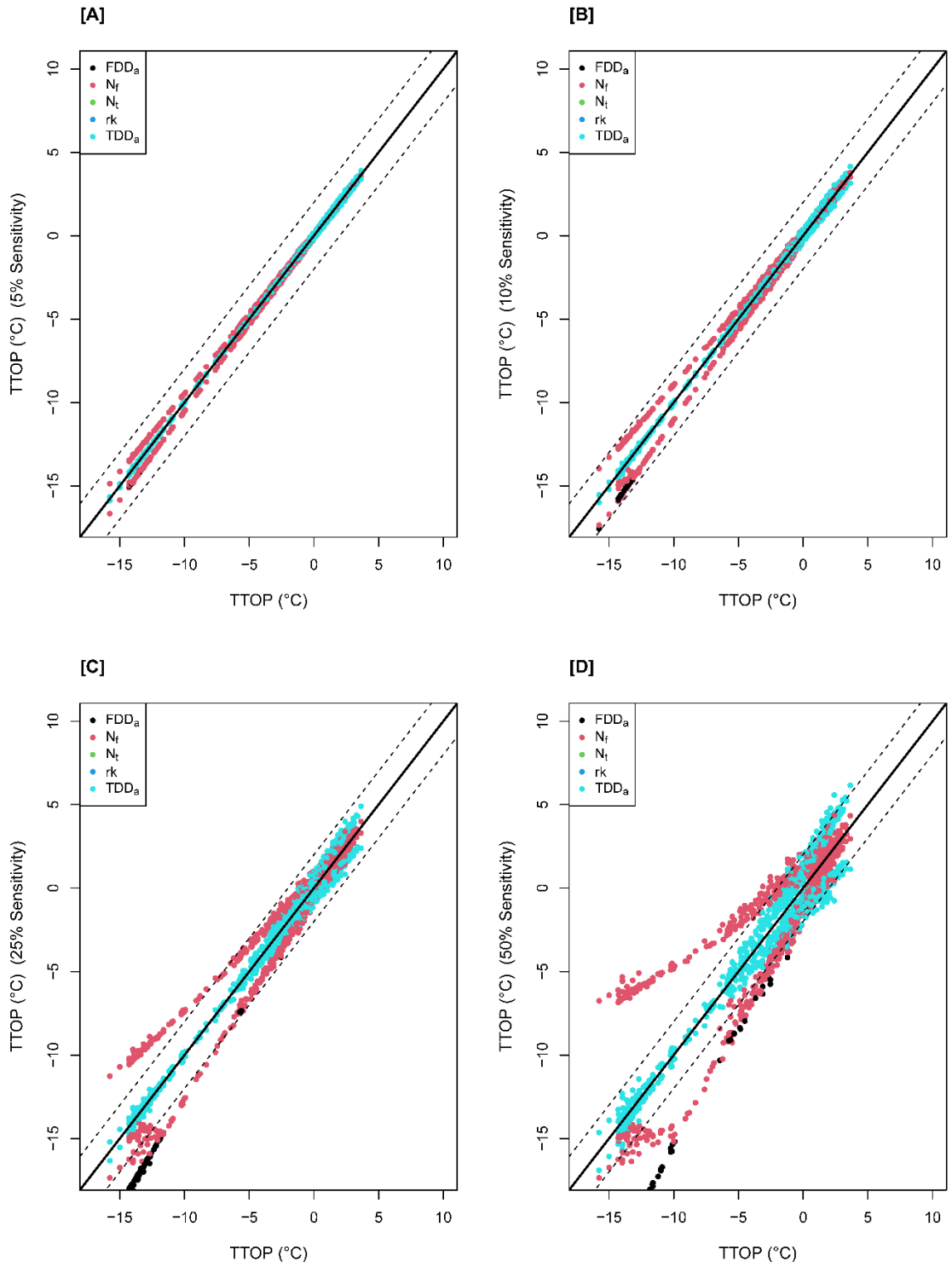


**Figure S4-4.** Reference temperature at top of permafrost (TTOP) compared to perturbed TTOP resulting from the addition or subtraction of [A] 5 % [B] 10 %, [C] 25 %, and [D] 50% of the measured value for each parameter. The solid line indicates no (0 °C) difference between the two TTOP values while the dashed line shows ± 2 °C difference.

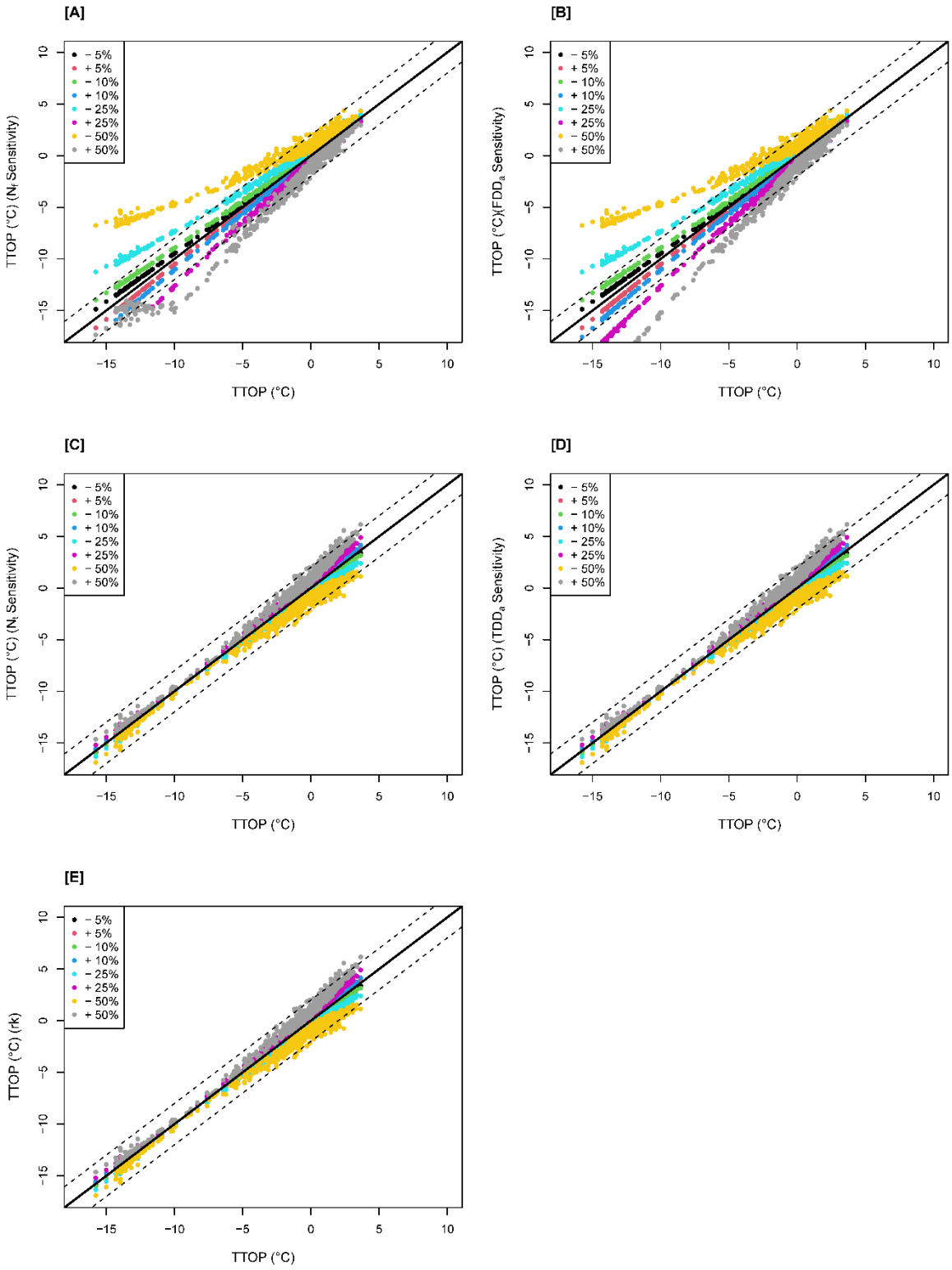


**Figure S4-5.** Reference temperature at top of permafrost (TTOP) compared perturbed TTOP for each percentage change for [A] $n_f$, [B] $FDD_a$, [C] $n_t$, [D] $TDD_a$, and [E] rk. The solid line indicates no (0 °C) difference between the two TTOP values while the dashed line shows ± 2 °C difference.

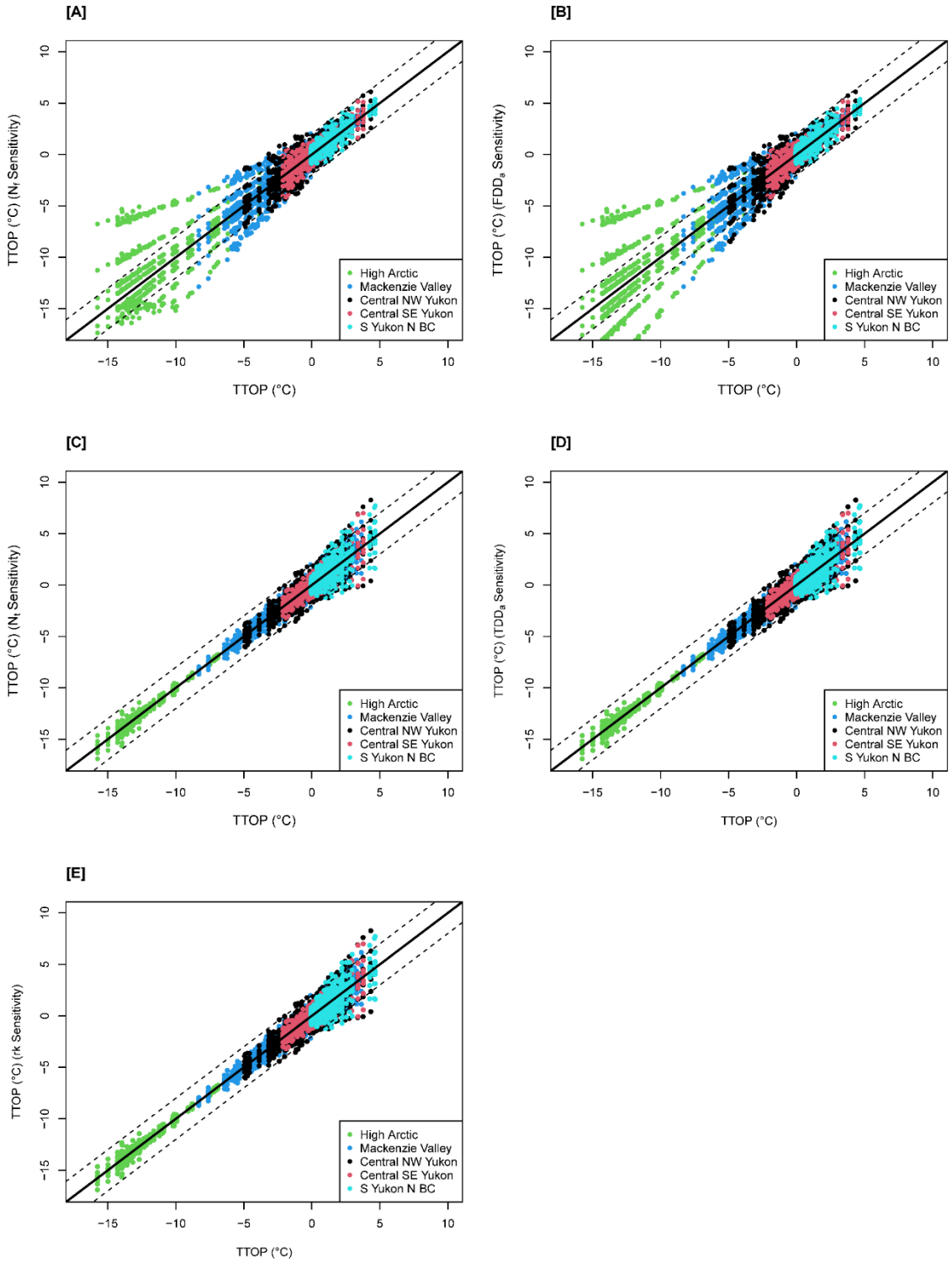


**Figure S4-6.** Regional temperature at top of permafrost (TTOP) model sensitivity to changes in [A] $n_f$, [B] $FDD_a$, [C] $n_t$, [D] $TDD_a$, and [E] rk by a percentage. The solid line indicates no (0 °C) difference between the reference and perturbed TTOP values while the dashed line shows ± 2 °C difference.

*S.4.3 TTOP Model Sensitivity Fixed Change Assigned*

S.4.3.1 Fixed Change Assigned Results

The third TTOP sensitivity trial involved changing each individual observation by a fixed amount. This method involved capping of $n_f$ and rk values to less than one and three, respectively and all parameters to be greater than zero. For this method, since the fixed values are not proportional across the different types of parameters (ratio compared to degree-days) the discrepancies for $n_f$, $n_t$ and rk are not directly comparable to those for $FDD_a$ and $TDD_a$. Similar to the previous two methods, there was overall greater sensitivity to changes in $n_f$ than $n_t$ and rk. However, there was greater sensitivity to $TDD_a$ than $FDD_a$ for every iteration for all observations (Figure S4-7). Overall, the changes in $n_f$ and $TDD_a$ resulted in the smallest number of observations (46 and 76 %) within 1 °C of the original TTOP value, while changes in $n_t$, rk, and $FDD_a$ had the greatest number of observations (77, 79 and 88 %, respectively). Unsurprisingly, the greatest magnitude of change resulted in the greatest difference in predicted TTOP resulting in the largest percentage of observations with a difference of at least 1 °C from the reference value for all parameters.

Locations with the coldest permafrost showed a greater response to changes in winter parameters ($n_f$ and $FDD_a$) and minimal response to changes in summer parameters ($n_t$) and the thermal conductivity (rk) with most sample points remaining within 1 °C of the reference value despite changes in these parameters by up to 0.50 and 1000 °C days. However, the overall response to changes in $FDD_a$ was minimal compared to the other parameters.

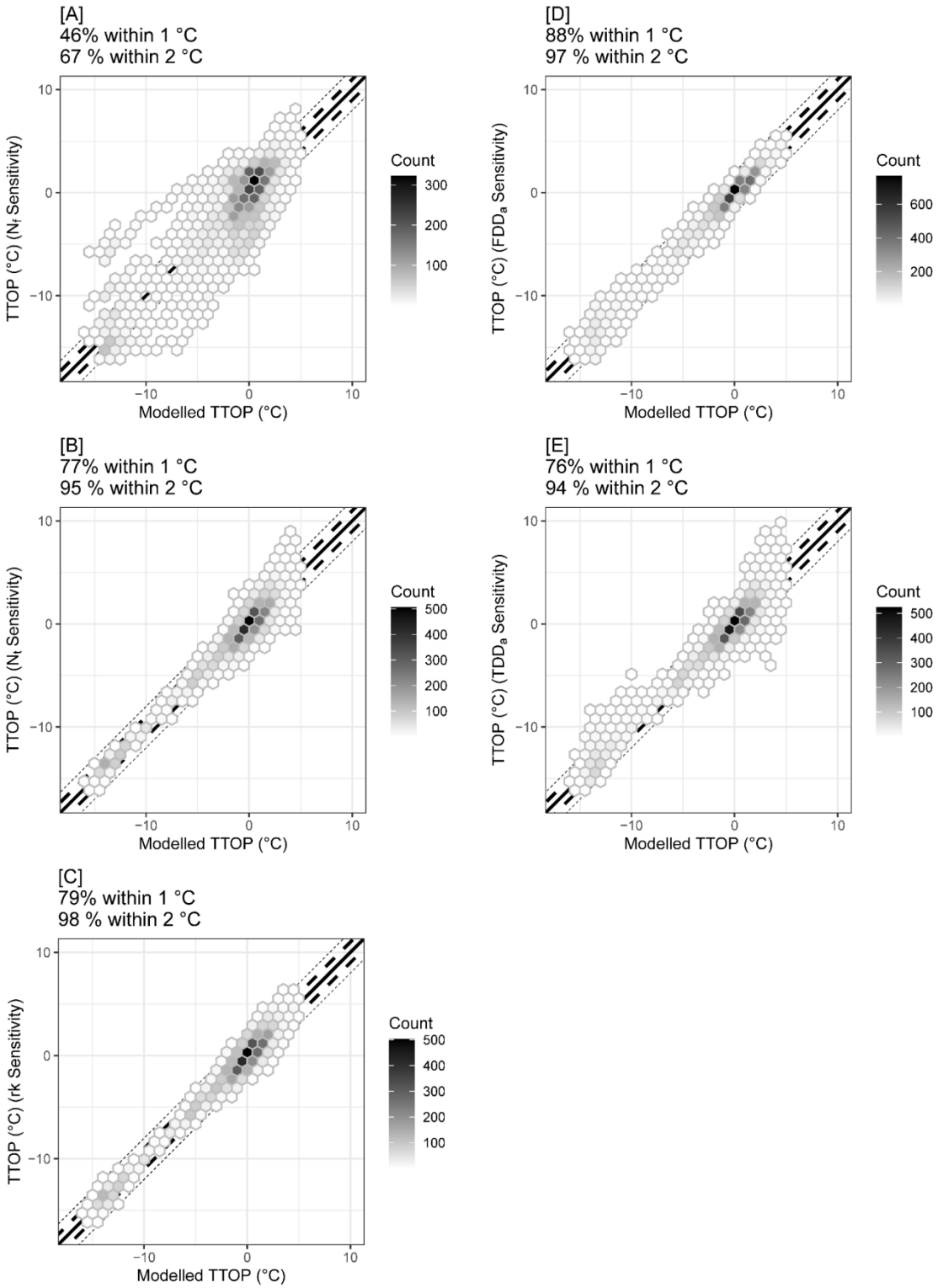


**Figure S4-7.** Reference temperature at top of permafrost (TTOP) model values compared to perturbed TTOP model values for the addition and subtraction of 0.05, 0.10, 0.25, and 0.50 for [A] $n_f$, [C] $n_t$, and [E] rk and 100, 250, 500, and 1000 °C days for [B] $FDD_a$, and [D] TDDa. Large dashes indicate a ± 1 °C difference while small dashes indicated a ± 2 °C difference.

The sensitivity at individual sites also differed by region and parameter with the maximum and minimum discrepancies found in the High Arctic, Mackenzie Valley, and Central Southeast Yukon. The largest difference between the reference and perturbed TTOP for $n_f$ and $FDD_a$ (9.9 and 2.6 °C) was found in the High Arctic after altering the measured values by ± 0.5 and ± 1000 °C days, respectively. For $n_t$ and rk, the greatest difference was observed in the Mackenzie Valley (5.0 and 2.9 °C) again altering the measured values by ± 0.5. Lastly, the largest difference caused by changes in $TDD_a$ was in the Central Southeast Yukon (8.3 °C) for ± 1000 °C days. The smallest difference for changes in $n_t$, rk and $TDD_a$ was observed in the High Arctic (0 °C) across all subtractive iterations for $n_t$ (the initial value was close to 0), all iterations for rk and ± 100, ±250 and ± 500 °C days for $TDD_a$. Similarly, the smallest difference for $n_f$ and $FDD_a$ (0 °C) was observed in the Mackenzie Valley for all subtractive iterations for $n_f$ (initially value was 0) and ± 100 and ± 250 °C days for $FDD_a$.

Regionally, there was a trend in the most sensitive parameters by latitude with the High Arctic showing the greatest sensitivity to changes in the winter parameters, $n_f$ and $FDD_a$ (2.8 and 1.1 °C, respectively) while the southernmost region, Southern Yukon Northern BC showed the least sensitivity to changes in $n_f$ (0.9 °C) (Figure S4-8). There is more variability in the region with the greatest and least sensitivity to the other parameters, differing from the previous two methods. The High Arctic had the smallest response to changes in $n_t$ and rk (0.2 and 0.4 °C), while Central Northwest Yukon and Southern Yukon Northern BC had the greatest response to $n_t$ and rk (0.7 °C), respectively. Southern Yukon Northern BC had the greatest response to changes in $TDD_a$ (1.1 °C) while the Mackenzie Valley had the smallest response (0.5 °C). Lastly, Central Southeast Yukon had the smallest response (0.3 °C) to changes in $FDD_a$.

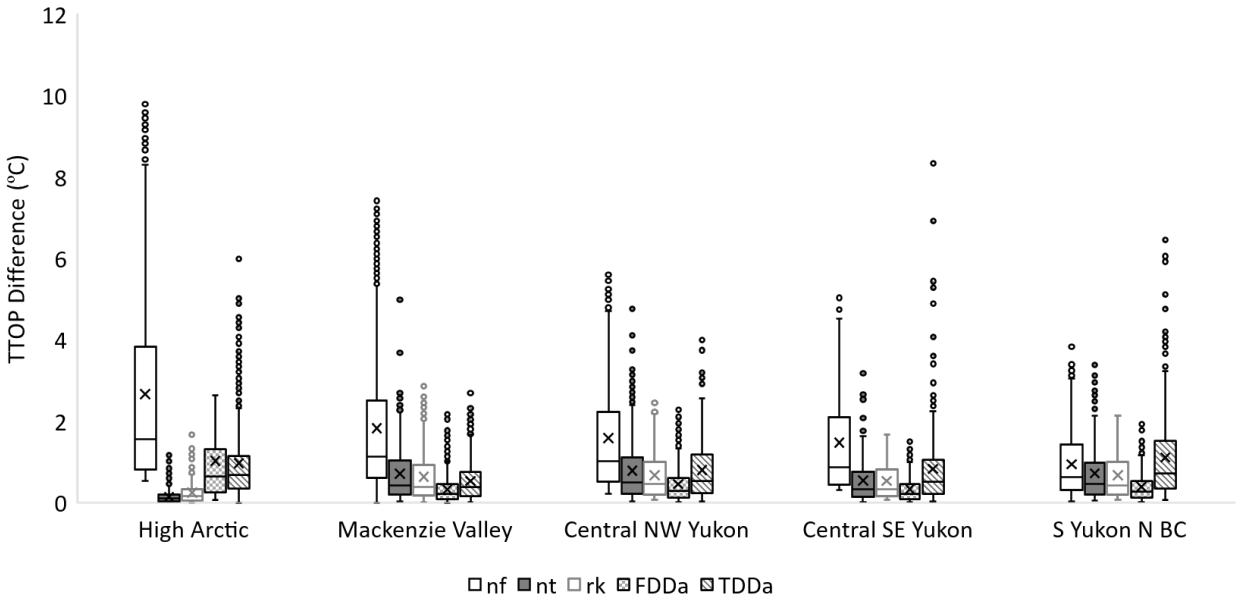


**Figure S4-8.** Boxplots for the regional absolute difference between the reference TTOP and the TTOP calculated when parameters were directly substituted to a percentile value.

Looking at each region individually, the High Arctic showed the greatest sensitivity to changes in $n_f$ with 68 % of perturbed TTOP having a greater than 1 °C difference from the reference value. The High Arctic also showed the least sensitivity to changes in $n_t$ with only 2 % of observations changing by more than 1 °C. Moving southward, all the remaining regions showed the least sensitivity to changes in $FDD_a$, 8, 17, 5, and 11 % of observations changing by more than 1 °C for the Mackenzie Valley, Central Northwest Yukon, Central Southeast Yukon and Southern Yukon Northern BC, respectively. The parameter with the greatest response in the Mackenzie Valley, Central Northwest Yukon and Central Southeast Yukon was $n_f$ with 56, 50, and 46 % of observations changing by more than 1 °C, while for the Southern Yukon Northern BC region changes in $TDD_a$ elicited the greatest response (49 % of observations changed by more than 1 °C).

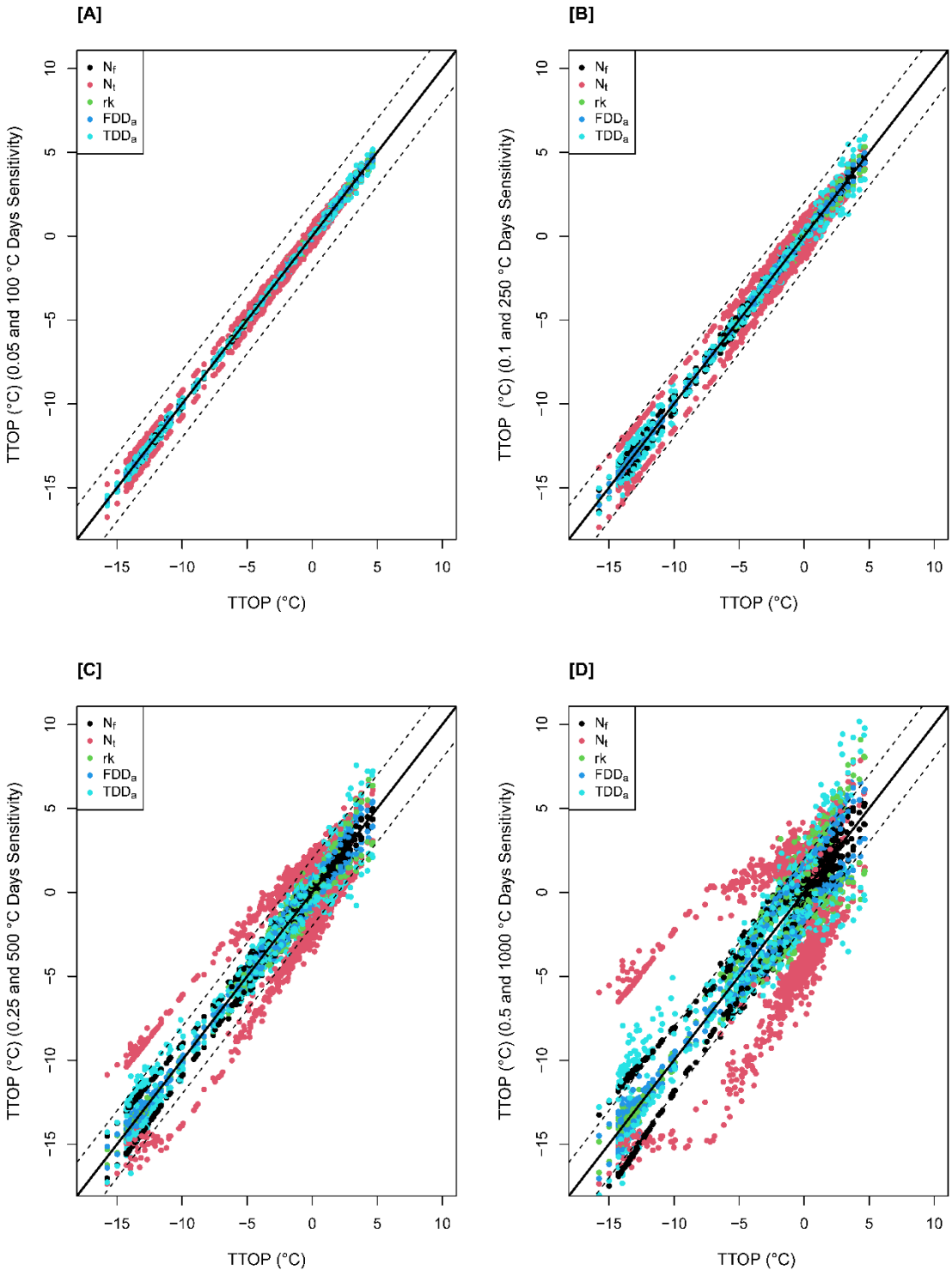


**Figure S4-9.** Reference temperature at top of permafrost (TTOP) compared to perturbed TTOP resulting from the addition or subtraction of [A] 0.05 or 100 °C days [B] 0.10 or 250 °C days, [C] 0.25 or 500 °C days, and [D] 0.5 or 1000 °C days of the measured value for the offset and degree day parameters, respectively. The solid line indicates no (0 °C) difference between the two TTOP values while the dashed line shows ± 2 °C difference.

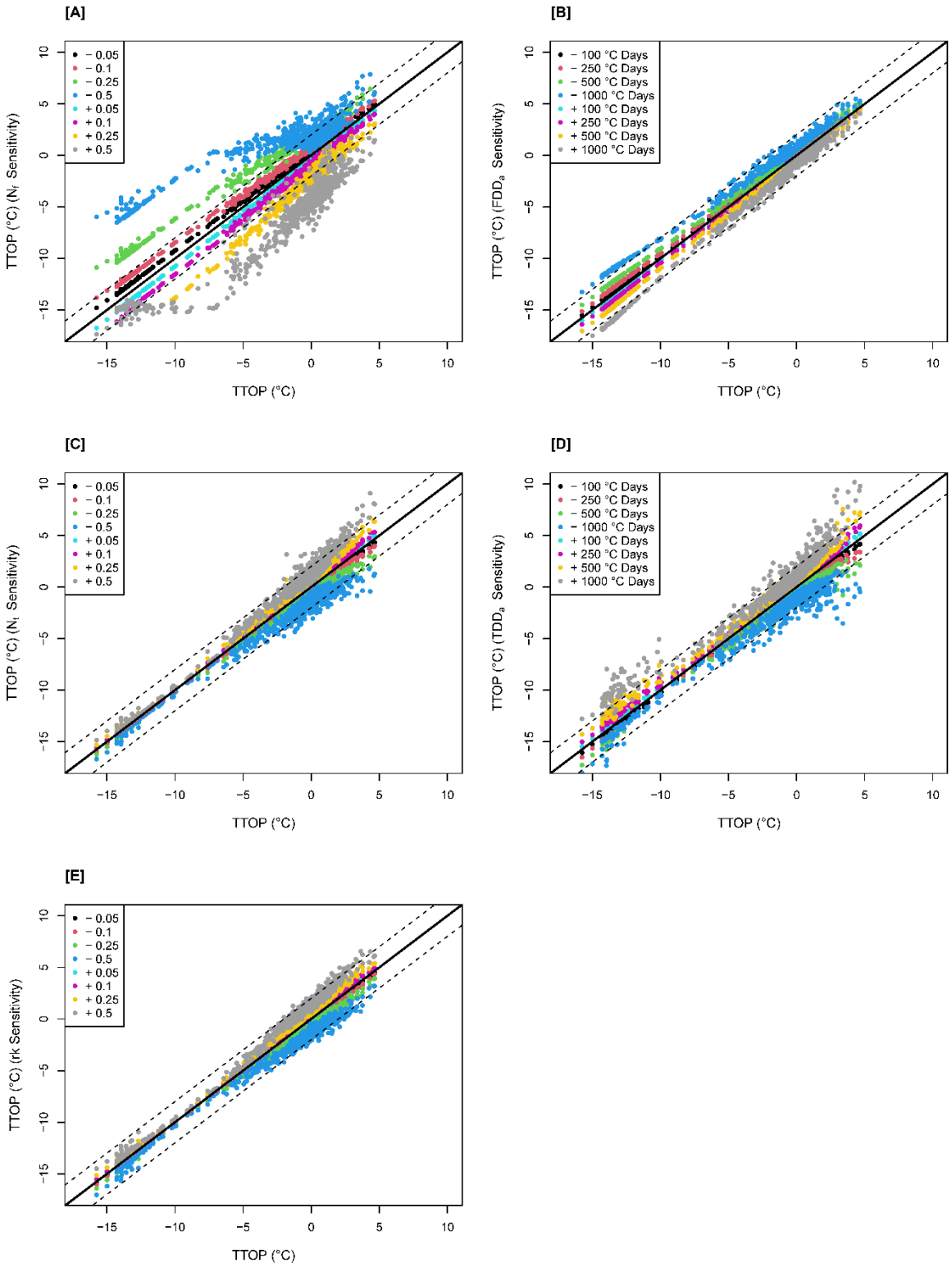


**Figure S4-10.** Reference temperature at top of permafrost (TTOP) compared perturbed TTOP for each assigned change in [A] $n_f$, [B] $FDD_a$, [C] $n_t$, [D] $TDD_a$, and [E] rk. The solid line indicates no (0 °C) difference between the two TTOP values while the dashed line shows ± 2 °C difference.

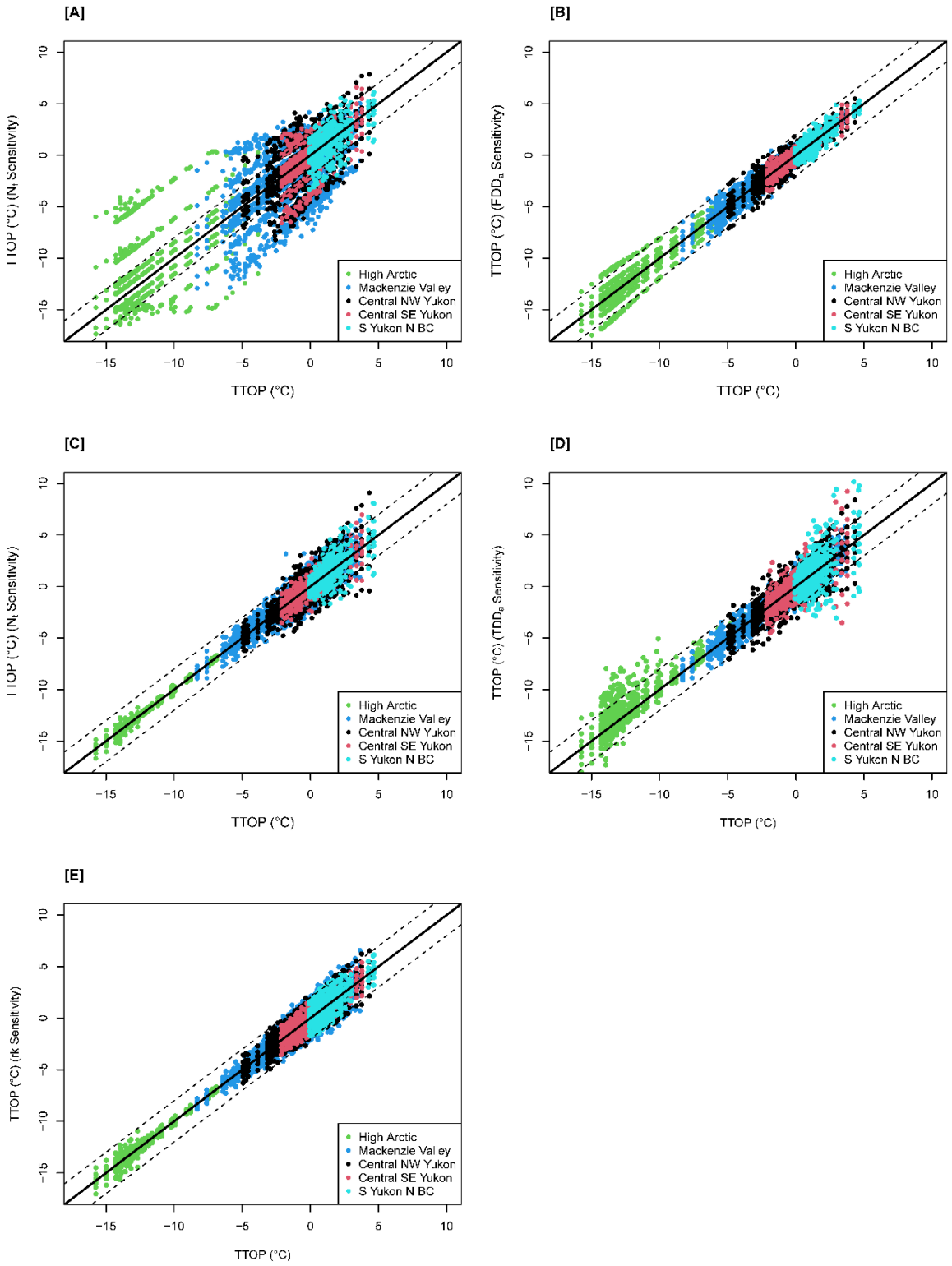


**Figure S4-11.** Regional temperature at top of permafrost (TTOP) model sensitivity to changes in [A] $n_f$, [B] $FDD_a$, [C] $n_t$, [D] $TDD_a$, and [E] rk by an assigned value. The solid line indicates no (0 °C) difference between the reference and perturbed TTOP values while the dashed line shows ± 2 °C difference.

4.5.1.5 Fixed Change Assigned Discussion

For the third trial (increase or decrease by a fixed amount), the main advantage is the ability to make a direct comparison of the impact for the same magnitude of change in the offset parameters and the degree-day parameters. For example, the impact of a 0.1 magnitude of change in $n_f$ can be directly compared to the impact of the same magnitude of change in $n_t$. However, assigning the magnitude of perturbation can also cause some problems as the change in magnitude for the two types of parameters, offsets ($n_f$, $n_t$ and rk) and degree days ($FDD_a$ and $TDD_a$) may not be equivalent as the magnitude of the initial values are substantially different (0-3 compared to 200-6000). Additionally, the assigned values are not proportional to the initial parameter values, which can lead to an underestimation of sensitivity for parameters with high initial values. For example, this is the only trial for which the TTOP model was least sensitive to changes in $FDD_a$. This likely results from the magnitude of assigned values not being high enough relative to the initial values to illicit a response. Lastly, all parameters using this method also need to be capped to keep parameter values realistic. While each perturbation method has advantages and disadvantages, which may influence the resulting sensitivity, together they give a complete representation of TTOP model sensitivity to each parameter, which can guide future modelling.

*S.4.4 TTOP Model Sensitivity Fixed Change Percentile*

S.4.4.1 Fixed Change Percentiles Results

The fourth and final TTOP sensitivity trial was conducted by changing the measured parameter values by the percentiles (Table S4-1). This method also required capping of $n_f$ and rk values to less than one and three, respectively and all parameters to be greater than zero.

**Table S4-1.** Percentile values added to and subtracted from the measured parameter for each iteration of this trial method.

| | Minimum | 5th Percentile | 10th Percentile | 25th Percentile | 50th Percentile |
|---|---|---|---|---|---|
| **$N_f$** | 0 | 0.08 | 0.11 | 0.19 | 0.29 |
| **$N_t$** | 0.01 | 0.38 | 0.48 | 0.60 | 0.70 |
| **rk** | 0.15 | 0.35 | 0.49 | 0.62 | 0.73 |
| **$FDD_a$** | 274.3 | 1789.9 | 2330.1 | 2813.5 | 3284.0 |
| **$TDD_a$** | 189.6 | 226.3 | 244.7 | 1072.0 | 1542.1 |

This method showed different sensitivity results compared to the others, with overall sensitivity greatest for $FDD_a$ followed by $n_t$ and rk, while changes to $n_f$ and $TDD_a$ resulted in the least sensitivity (Figure S4-12). Overall, the changes in $FDD_a$, $n_t$, and rk resulted in the smallest number of observations (35 and 44 %) within 1 °C of the original TTOP value, while changes in $n_f$, and $TDD_a$ had the greatest number of observations (52 and 67 %, respectively). Unsurprisingly, the greatest magnitude of change (± 50th percentile) resulted in the greatest difference in predicted TTOP resulting the largest percentage of observations with a difference of at least 1 °C from the reference value for all parameters.

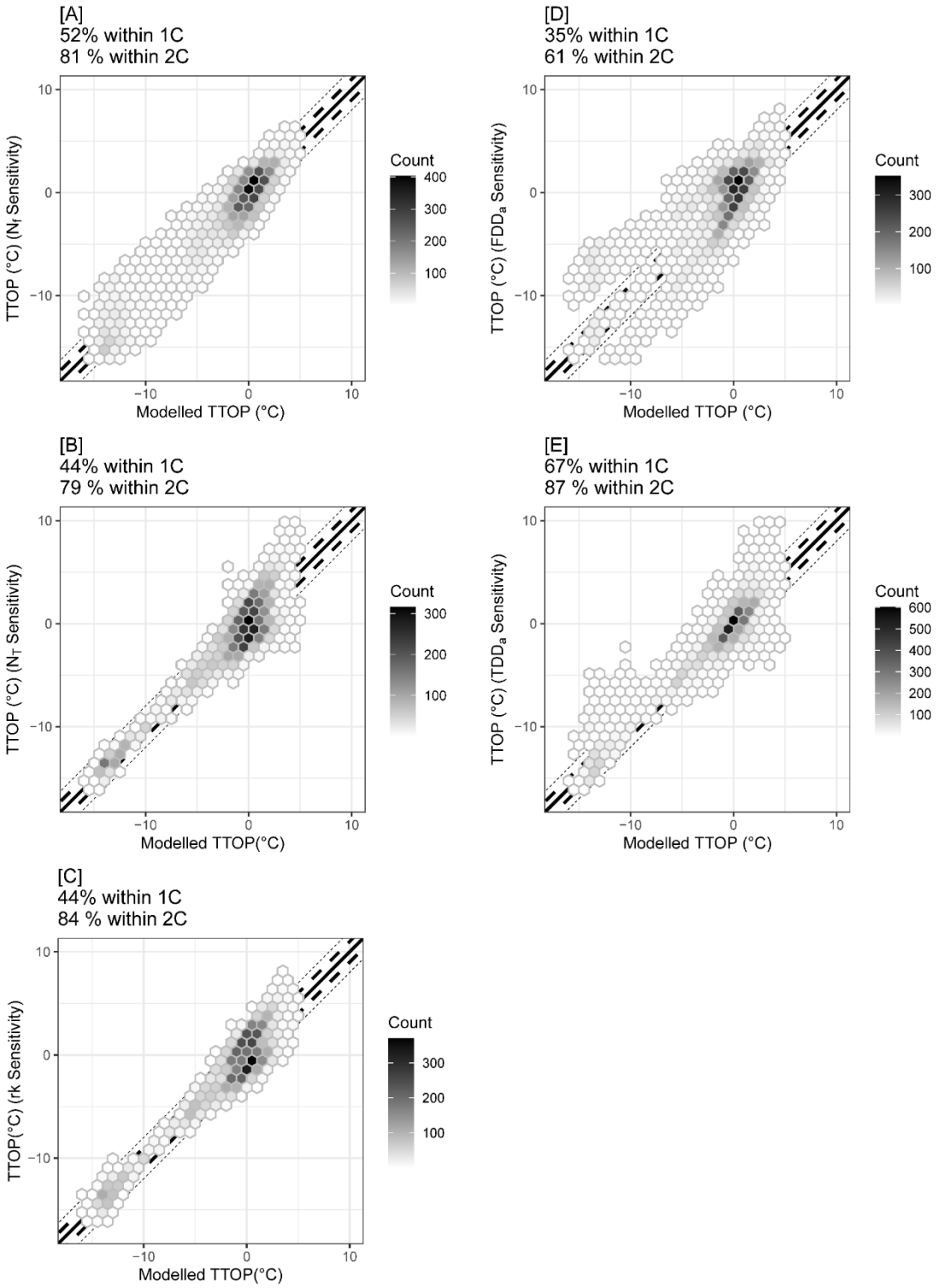


**Figure S4-12.** Reference temperature at top of permafrost (TTOP) model values compared to perturbed TTOP model values for the addition and subtraction of the minimum, 5$^{th}$ percentile, 10$^{th}$ percentile, 25$^{th}$ percentile, and 50$^{th}$ percentile value for [A] $n_f$, [B] $FDD_a$, [C] $n_t$, [D] $TDD_a$, and [E] rk. Large dashes indicate a ± 1 °C difference while small dashes indicated a ± 2 °C difference.

Locations with the coldest permafrost showed a greater response to changes in winter parameters ($n_f$ and $FDD_a$) and minimal response to changes in summer parameters ($n_t$) and the thermal conductivity (rk) with most sample points remaining within 1 °C of the reference value despite changes in these parameters by up to 0.70. However, for this trial the sites with the coldest modelled permafrost were much less responsive to changes in $n_f$ than $FDD_a$ differing from the previous trial results. The maximum and minimum response to changes in each parameter at individual sites differed by region with the maximum discrepancies found in the High Arctic, Mackenzie Valley, and Central Southeast Yukon. The largest difference between the reference and perturbed TTOP for $n_f$ and $FDD_a$ (5.8 and 8.7 °C) was found in the High Arctic altering the measured values ± 50$^{th}$ percentile. For $n_t$ and rk, the greatest difference was observed in the Mackenzie Valley (7.0 and 4.3 °C) again altering the measured values by ± 0.5. Lastly, the largest difference caused by changes in $TDD_a$ was in Central Southeast Yukon (12.9 °C) for + 50$^{th}$ percentile. The smallest difference for changes in $n_t$, rk and $TDD_a$ was observed in the High Arctic (0 °C) for adding the minimum $n_t$, and $TDD_a$ and ± the minimum for rk. Similarly, the smallest difference for $n_f$ (0 °C) was observed in the Central Southeast Yukon for ± the minimum value. Lastly the smallest difference for changes in $FDD_a$ (0 °C) was observed in the Mackenzie Valley for all changes in $FDD_a$ ($n_f$ at this location is 0).

Looking at the average sensitivity for each region, there was a trend in the most sensitive parameters by latitude, with the High Arctic showing the greatest sensitivity to changes in the winter parameters, $n_f$ and $FDD_a$ (2.3 and 5.9 °C, respectively), while the southernmost region, Southern Yukon Northern BC, showed the least sensitivity to changes in $n_f$ (0.8 °C) (Figure S4-13).

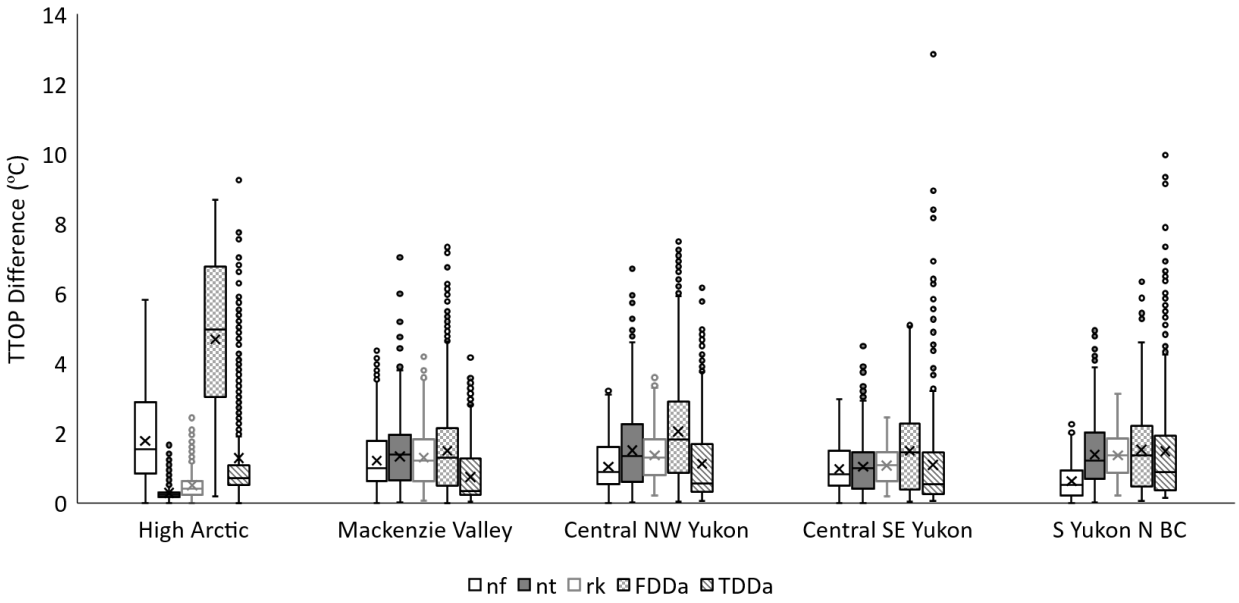


**Figure S4-13**. Boxplots for the regional absolute difference between the reference TTOP and the TTOP calculated when parameters were increased or decreased by a percentile value.

Similar to the other fixed change method there is variability in the regions with the greatest and least sensitivity to the other parameters, differing from the percentile substitution and percentage change methods. The High Arctic had the smallest response to changes in $n_t$, rk, and $TDD_a$ (0.5, 0.9 and 0.8 °C) while the Central Northwest Yukon and Southern Yukon Northern BC had the greatest response to $n_t$ and rk (1.7 and 1.6 °C), respectively. The Central Southeast Yukon had the greatest response to changes in $TDD_a$ (1.4 °C) while the Mackenzie Valley had the smallest response to changes in $FDD_a$ (1.8 °C).

Unlike the previous methods, there was less uniformity between the most and least sensitive parameter for each region. The High Arctic showed the greatest sensitivity to changes in $n_f$ and $FDD_a$ with 72 and 80 % of perturbed TTOP having a greater than 1 °C difference from the reference value. The High Arctic also showed the least sensitivity to changes in $n_t$ and rk with only 4 and 10 % of observations changing by more than 1 °C. Moving southward, the Mackenzie Valley was most sensitive to changes in $n_t$ with 67 % of perturbed TTOP different by

more than 1 °C from the reference TTOP. Both Central Northwest and Southeast Yukon showed the greatest response to changes in $FDD_a$ (71 and 63 % of perturbed observations were more than 1 °C different) while Southern Yukon Northern BC was most sensitive to changes in rk (70 % > 1 °C difference). Changes in $TDD_a$ resulted in the smallest changes in TTOP for the Mackenzie Valley, Central Northwest, and Central Southeast Yukon with 33, 34, and 28 % of observations changing by more than 1 °C. Finally, Southern Yukon Northern BC was least sensitive to changes in $n_f$ (23 % of observations > 1 °C difference).

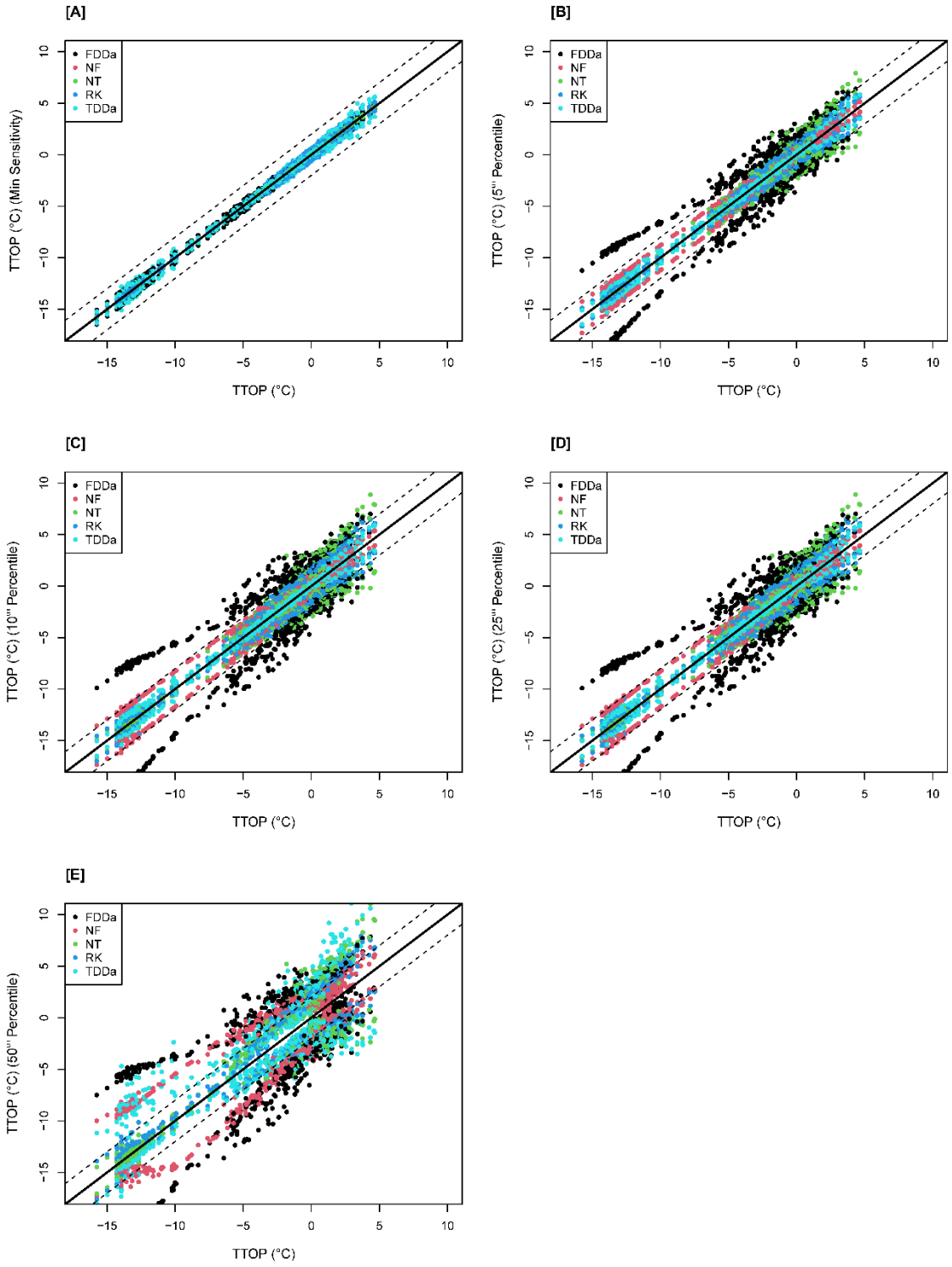


**Figure S4-14.** Reference temperature at top of permafrost (TTOP) compared to perturbed TTOP resulting from the addition or subtraction of the [A] minimum [B] 5$^{th}$ percentile, [C] 10$^{th}$ percentile, [D] 25$^{th}$ percentile, and [E] 50$^{th}$ percentile of the measured value for each parameter. The solid line indicates no (0 °C) difference between the two TTOP values while the dashed line shows ± 2 °C difference.

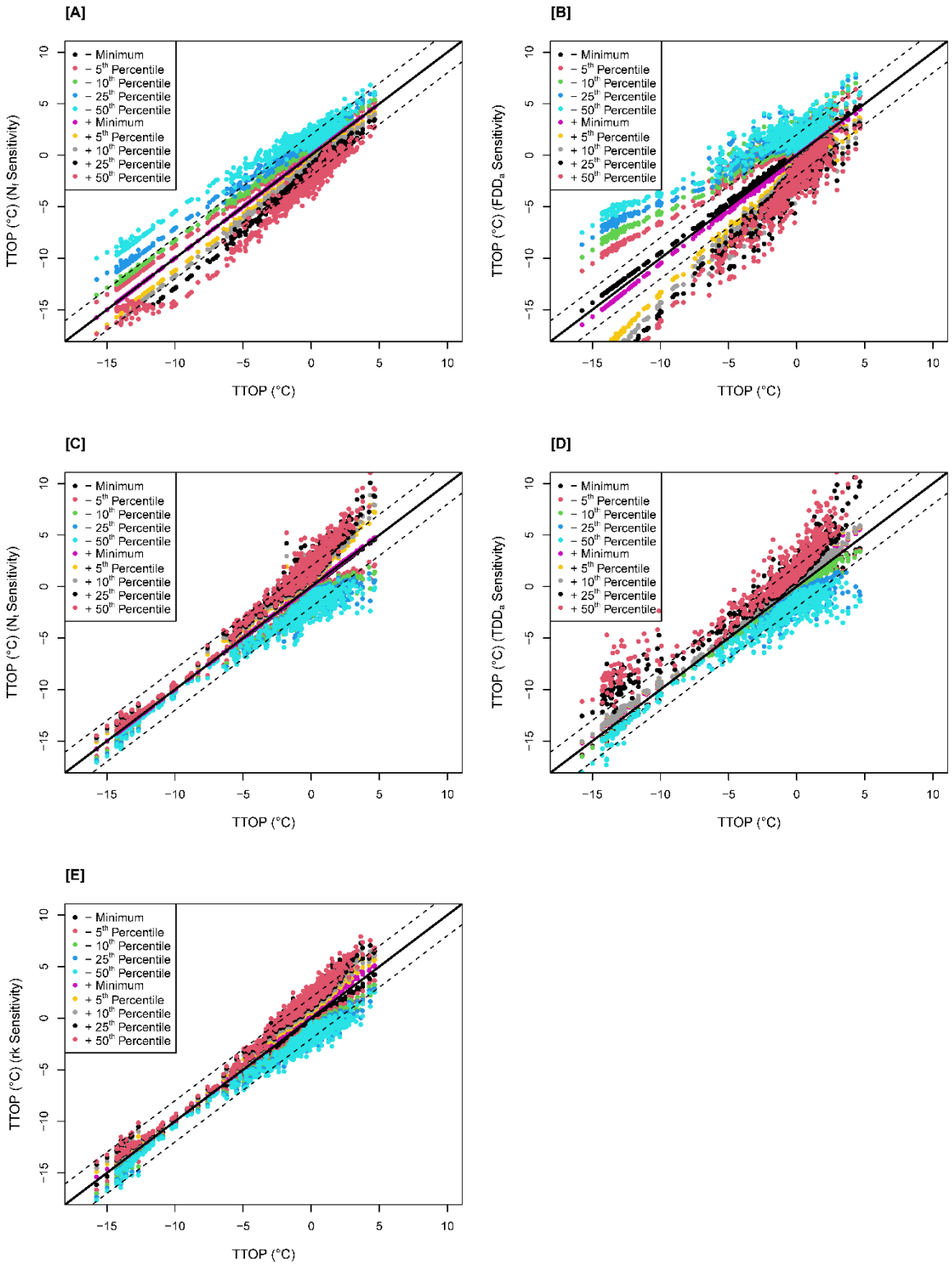


**Figure S4-15.** Reference temperature at top of permafrost (TTOP) compared perturbed TTOP for each addition or subtraction of the various percentile values of [A] $n_f$, [B] $FDD_a$, [C] $n_t$, [D] $TDD_a$, and [E] rk. The solid line indicates no (0 °C) difference between the two TTOP values while the dashed line shows ± 2 °C difference.

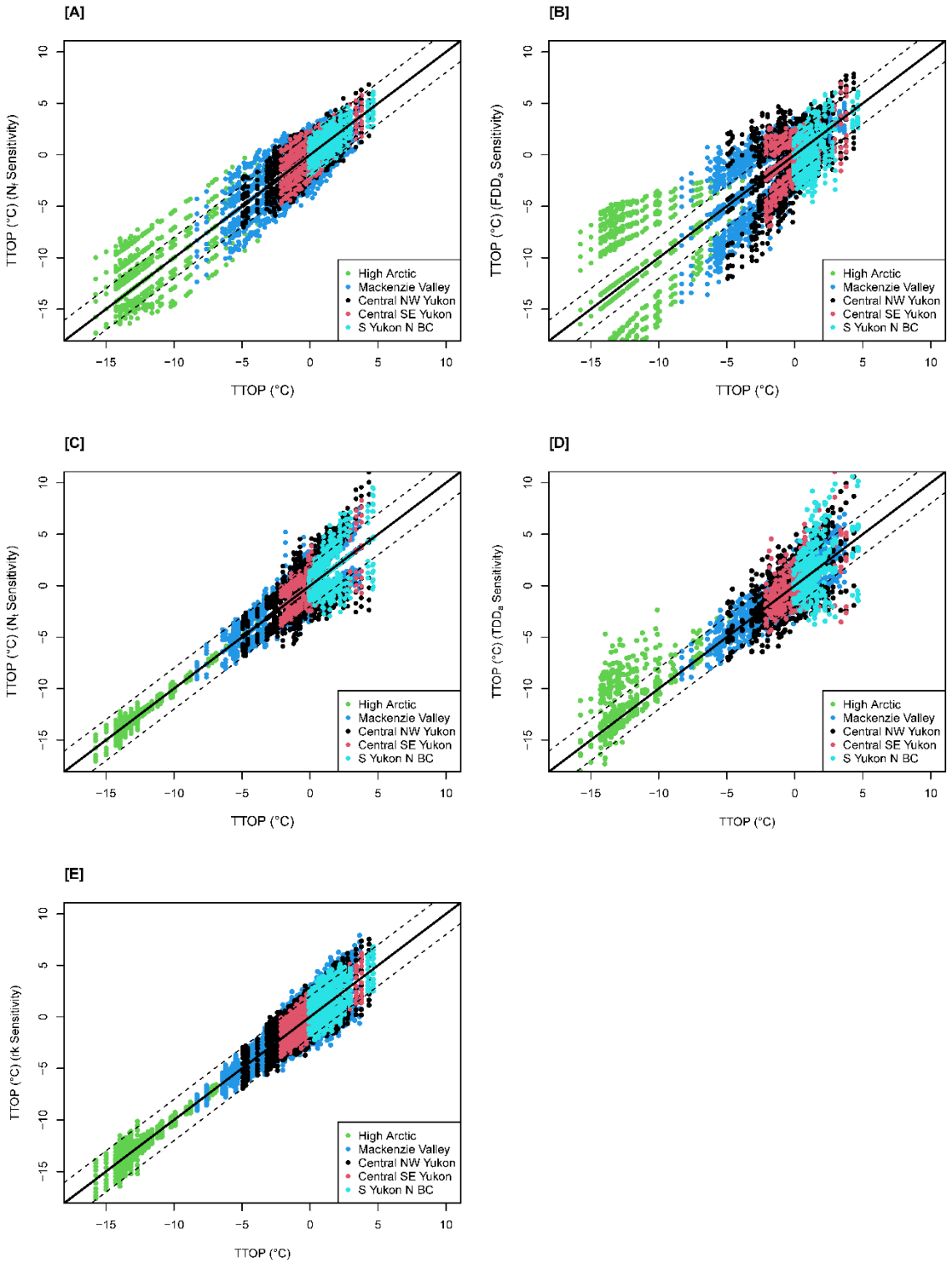


**Figure S4-16.** Regional temperature at top of permafrost (TTOP) model sensitivity to changes in [A] $n_f$, [B] $FDD_a$, [C] $n_t$, [D] $TDD_a$, and [E] rk by addition or subtraction of the various percentile value. The solid line indicates no (0 °C) difference between the reference and perturbed TTOP values while the dashed line shows ± 2 °C difference.

S.4.4.2 Fixed Change Percentiles Discussion

For the third trial (increase or decrease by a percentile value), one major advantage is this method allows for the direct comparison between regions for each individual parameter change, unlike Trial 1, as the magnitude of change will be the same. Additionally, using percentiles to determine the increments the perturbation is generally proportional to the initial values for each parameter. However, for this method, capping is required for every parameter, which may lead to artificial lowering of model response. Additionally, much like Trial 1, the magnitude of the perturbation for each parameter is determined by the range and values of the parameter, which may limit direct comparison between parameters

## S.5 Chapter 5 Supplemental

### *S.5.1 Methodology*

S.5.1.1 Site Selection

To reduce the area analyzed for site selection, the rasters were clipped using a 15 km buffer around the lowest air station for Valley WS01, Valley WS02, and Valley MTS or 15 km from an ATV trail for Valley M222. Each raster was then classified into three classes, using natural breaks, except for aspect, which was classified into four classes based on degrees for cardinal directions. The new classes were changed to be 1-3 with three being the highest values and one being the lowest. To simplify the selection process, aspect and slope were eliminated, as aspect and slope are related to PISR and TPI, respectively. Finally, a raster for each study area with a unique code for each class of the three variables was created using Raster Calculator. First, the three variables were individually multiplied by a constant, TPI by 100, PISR by 10 and elevation by 1. These new rasters were then added together creating a unique 3-digit code for

each pixel of the landscape (Table S5-1). The final rasters for each valley were then smoothed to eliminate individual or small groups of pixels of one class within a larger surrounding class. This was accomplished using the focal statistics tool. Finally, the percentage of each valley within each class was calculated using the focal statistics tool and classes less than 1 % were eliminated. Some classes were also eliminated if they were too far away to reasonably access.

**Table S5-1.** Breakdown of area for each valley by each classification code used during site selection

| Classification Code | % Weather Station Valley 1 | % Weather Station Valley 2 | % Mile 222 Valley | % Valley MTS | Description |
|---|---|---|---|---|---|
| **111** | 1.2 | 1.1 | 0.2 | 0.2 | Low TPI, low PISR, low elevation |
| **112** | 2.4 | 3.6 | 1.8 | 2.0 | Low TPI, low PISR, mid elevation |
| **113** | 1.5 | 1.8 | 0.9 | 2.0 | Low TPI, low PISR, high elevation |
| **121** | 4.8 | 7.3 | 3.4 | 4.1 | Low TPI, mid PISR, low elevation |
| **122** | 3.1 | 3.4 | 3.1 | 3.3 | Low TPI, mid PISR, mid elevation |
| **123** | 0.9 | 0.8 | 1.5 | 1.0 | Low TPI, mid PISR, high elevation |
| **131** | 3.0 | 2.9 | 0.9 | 2.0 | Low TPI, high PISR, low elevation |
| **132** | 2.97 | 4.3 | 3.8 | 3.7 | Low TPI, high PISR, mid elevation |
| **133** | 1.79 | 2.0 | 2.8 | 1.8 | Low TPI, high PISR, high elevation |
| **211** | 0.9 | 0.7 | 0.2 | 0.3 | Mid TPI, low PISR, low elevation |
| **212** | 2.9 | 4.7 | 0.9 | 1.1 | Mid TPI, low PISR, mid elevation |
| **213** | 1.74 | 2.9 | 0.5 | 1.2 | Mid TPI, low PISR, high elevation |
| **221** | 18.7 | 16.4 | 35.0 | 45.2 | Mid TPI, mid PISR, low elevation |
| **222** | 8.7 | 5.7 | 5.3 | 2.4 | Mid TPI, mid PISR, mid elevation |

| | | | | | |
|---|---|---|---|---|---|
| **223** | 1.4 | 0.6 | 1.6 | 1.0 | Mid TPI, mid PISR, high elevation |
| **231** | 12.7 | 3.0 | 4.3 | 8.9 | Mid TPI, high PISR, low elevation |
| **232** | 8.43 | 7.0 | 8.0 | 5.8 | Mid TPI, high PISR, mid elevation |
| **233** | 1.6 | 2.6 | 4.2 | 1.6 | Mid TPI, high PISR, high elevation |
| **311** | 0.3 | 0.2 | 0.1 | 0.2 | High TPI, low PISR, low elevation |
| **312** | 1.9 | 2.3 | 0.8 | 0.5 | High TPI, low PISR, mid elevation |
| **313** | 2.9 | 4.6 | 1.5 | 2.2 | High TPI, low PISR, high elevation |
| **321** | 0.4 | 1.2 | 3.2 | 0.7 | High TPI, mid PISR, low elevation |
| **322** | 2.9 | 5.0 | 2.4 | 1.1 | High TPI, mid PISR, mid elevation |
| **323** | 3.3 | 3.0 | 2.7 | 2.03 | High TPI, mid PISR, high elevation |
| **331** | 0.4 | 0.8 | 1.0 | 0.2 | High TPI, mid PISR, low elevation |
| **332** | 4.1 | 5.41 | 3.8 | 2.0 | High TPI, high PISR, mid elevation |
| **333** | 4.9 | 7.3 | 6.6 | 3.6 | High TPI, high PISR, high elevation |

When it came time to deploy the sensors some proposed sites needed to be moved due to physical limitations and some additional sites were added based on unique conditions observed in the field. However, even with these changes the site locations are still representative of each of the valleys (Figures S5-1 to S5-4).

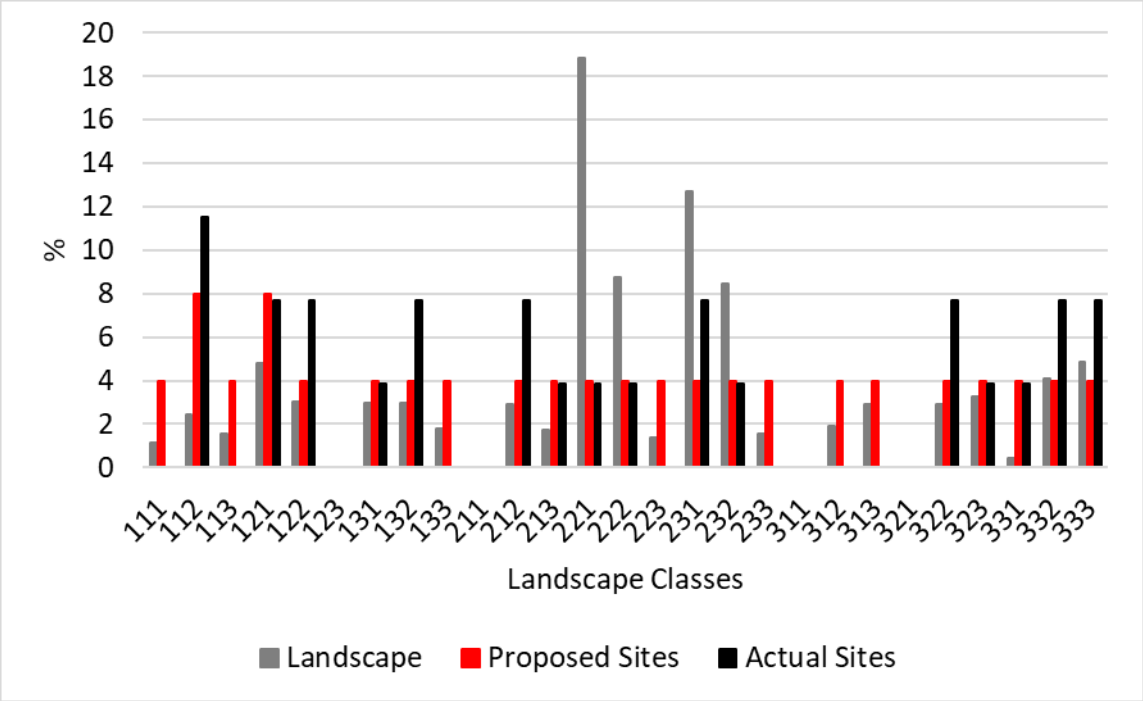


**Figure S5-1.** Breakdown of percentages for each landscape class and proposed and actual sites for Weather Station Valley 1 (Valley WS01). Landscape refers the percentage of the class in the delineated area for site selection.

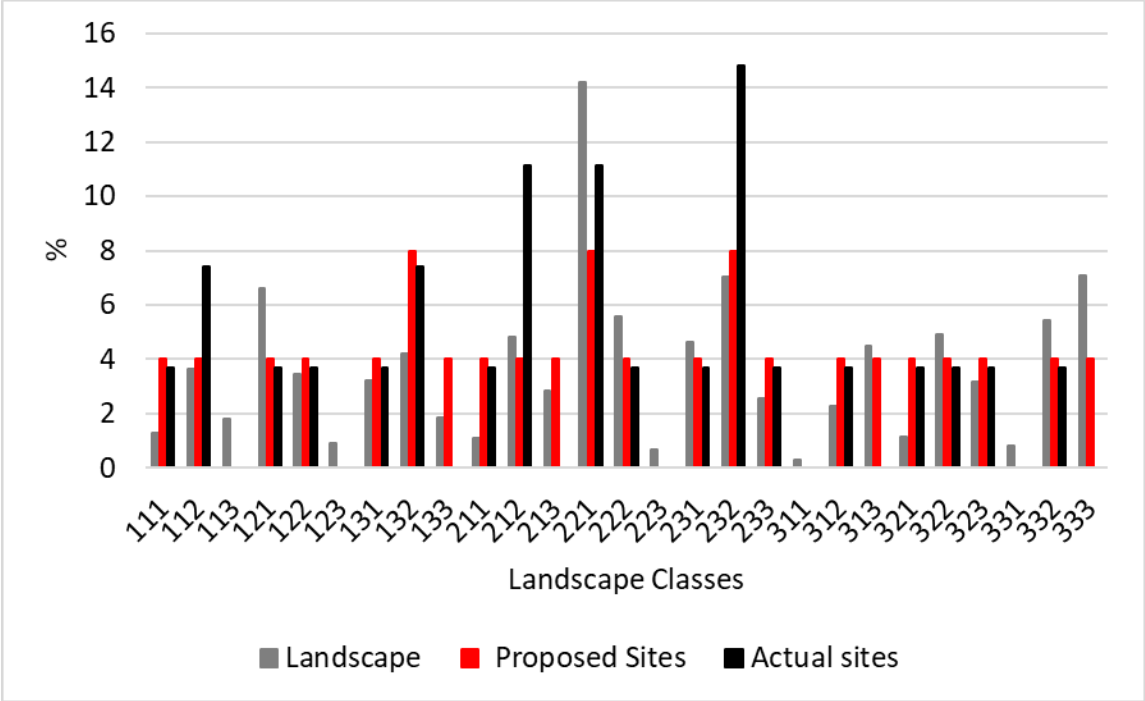


**Figure S5-2.** Breakdown of percentages for each landscape class and proposed and actual sites for Weather Station Valley 2 (Valley WS02). Landscape refers the percentage of the class in the delineated area for site selection.

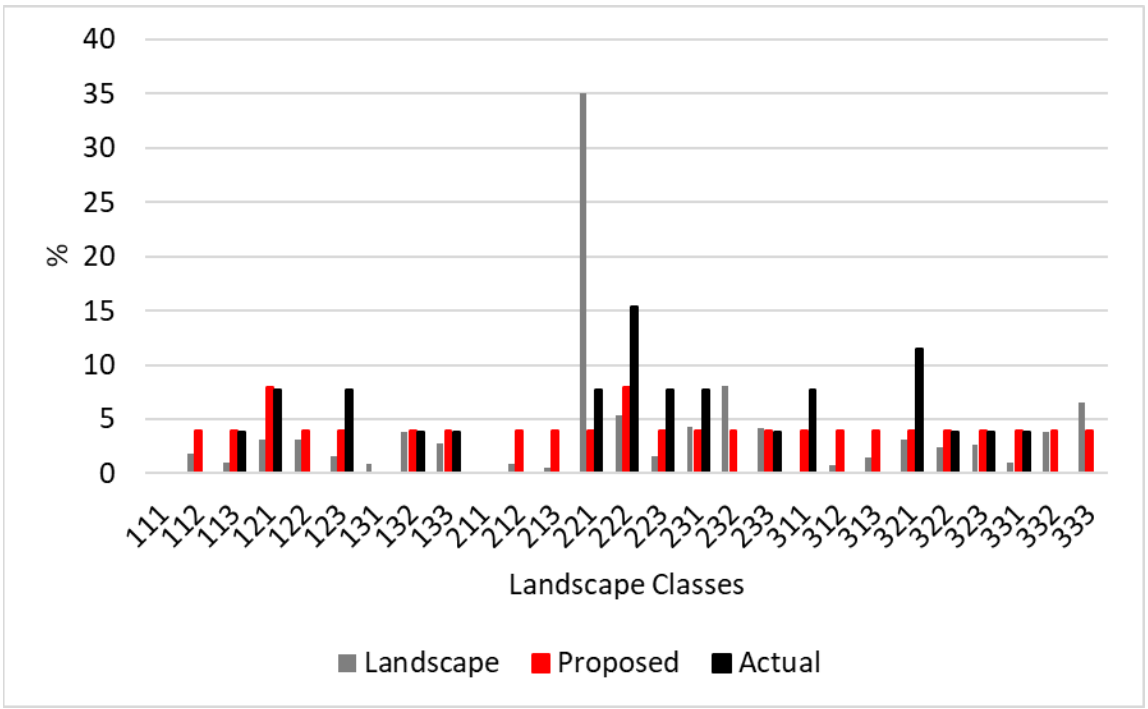


**Figure S5-3.** Breakdown of landscape classes and proposed and actual sites for Mile 222 Valley (Valley M222). Landscape refers the percentage of the class in the delineated area for site selection.

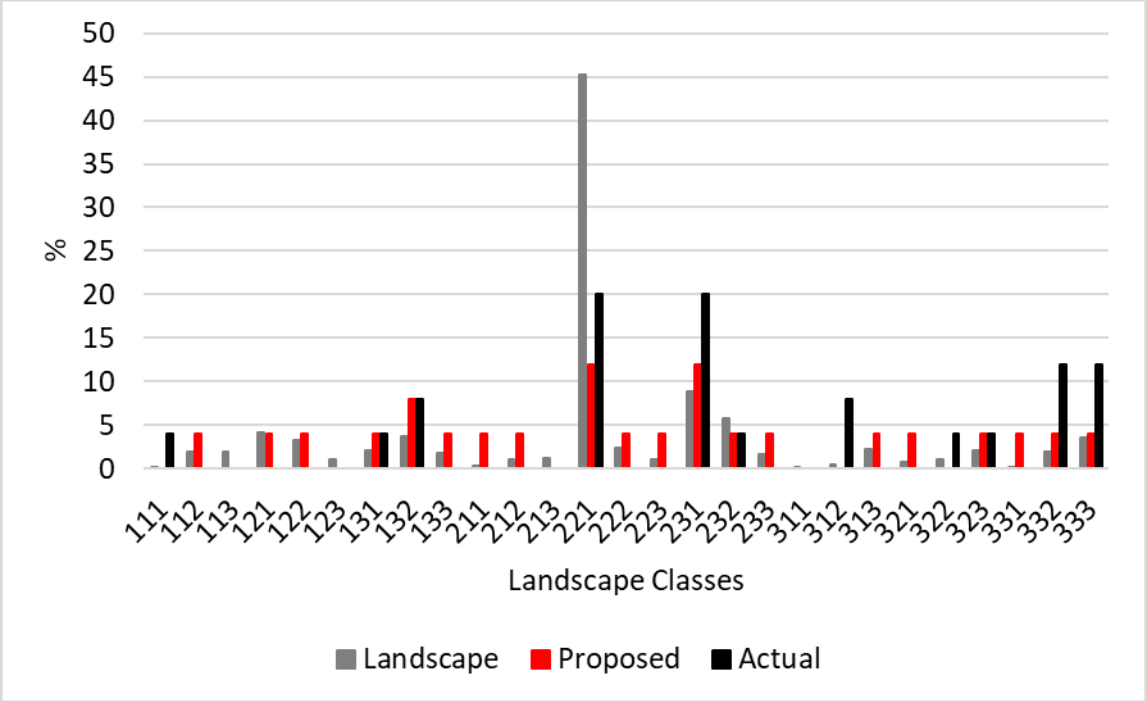


**Figure S5-4.** Breakdown of landscape classes and proposed and actual sites for Mac T South Valley (Valley MTS). Landscape refers the percentage of the class in the delineated area for site selection.

Additionally, although vegetation was not directly used to select the preliminary site locations, when deploying the sensors care was taken to ensure a variety of vegetation conditions were sampled. Loggers were deployed August 2019 with the intent to be revisited in August of 2020 for data collection and battery change before being deployed for another year. However due to the COVID-19 pandemic and restricted access to Yukon, sites were not revisited until August 2021.

S.5.1.2 Data Analysis Ground Temperature Nodes

The statistical differences between AMGST for each valley both landform and landcover classifications were also determined through an analysis of variance (ANOVA) for valleys with a normal distribution of AMGST (n=3) and a permutations ANOVA for valleys with a non-normal distribution (n =1). Landcover classifications were derived from a 30 m vegetation inventory

feature layer (Government of Canada, 2015), while landform classifications were derived from the 2m DEM and the Jenness landform classification tool in ArcGIS Pro (Jenness, 2006).

S.5.1.3 Area Delineation for Spatial Modelling

The modelling area for each valley was delineated to maximize the number of sample points within the study area, keep all of the area about the same size while also minimizing errors for unsampled aspects and topographic positions (Figures 3-6). For Valley WS01, Valley WS02, and Valley MTS watershed tools in ArcGIS Pro were used to define the modelling extent while for Valley M222 a 7.5 km buffer around an existing ATV trail was used. Ultimately, the modelled area for each valley were similar ranging from 7.7 $km^2$ for Valley MTS to 9.3 $km^2$ for Valley M222. The modelled area for two valleys on the Dempster were 8.2 and 9.1 $km^2$ for Valley WS01 and Valley WS02, respectively.

S.5.1.4 Missing Data

As the 2020 field season was cancelled due to travel restrictions, several stations failed due to low battery. This was the case in Valley WS02 were one of the mid slope stations failed in December 2021. To fill this data gap, the difference in SLR for each side of the valley were calculated for each year with data on both slopes (2 year 2018-2020). The difference between the two lapse rates was then applied to the SLR on the slope with data to calculate the SLR for the opposite slope for the 2020-2021 SLR. For Valley M222, the middle station in the transect failed for 2020-2021 and with limited capacity to fill the missing data, the lapse rate measured in 2019-2020 was used for both years. Again, due to battery failure, the second lowest station in the Valley MTS valley failed for the entire monitoring period and as such, the lapse rates were

calculated using only three stations. The SLRs were then used to create a spatial model of air temperature for each valley in ArcGIS Pro.

S.5.1.5 Ground Temperature Spatially Modelling

Three methods utilizing these variables were tested to spatially model $n_f$ and $n_t$. Spatial models for each n-factor for each year of monitoring were created using three different methods, multivariable linear regression (MVLR), random forest and Empirical Bayesian Kriging (EBK). MVLR was run in Excel, while the random forest and EBK surfaces were generated in ArcGIS Pro. N-factors at sites used in the spatial model creation (training), in addition to the calculated N-factors at each air station (testing) were used to determine the best method. For all four valleys, EBK resulted in the lowest error for both training and testing data points (Table S5-2).

**Table S5-2.** Standard errors for each parameter for each of the three methods used for spatial modelling of ground surface temperature

| Valley | Parameter | EBK | Random Forest | MVLR |
|---|---|---|---|---|
| **Valley WS01** | $n_f$ | 0.03 | 0.25 | 0.19 |
| | $n_t$ | 0.14 | 0.18 | 0.14 |
| | AMGST | 0.3 | 0.2 | 1.5 |
| **Valley WS02** | $n_f$ | 0.13 | 0.12 | 0.14 |
| | $n_t$ | 0.14 | 0.08 | 0.20 |
| | AMGST | 0.2 | 0.1 | 1.0 |
| **Valley M222** | $n_f$ | 0.10 | 0.12 | 0.17 |
| | $n_t$ | 0.15 | 0.12 | 0.20 |
| | AMGST | 1.0 | 0.2 | 1.2 |
| **Valley MTS** | $n_f$ | 0.08 | 0.16 | 0.13 |
| | $n_t$ | 0.09 | 0.21 | 0.18 |
| | AMGST | 0.5 | 0.2 | 1.1 |

For individual valleys and N-factors, differing combinations of input variables produced the lowest error, likely due to the difference in valley topography and vegetation regimes (Table S5-3).

**Table S5-3.** Topographic and vegetation variables used in the EBK regression model for the n-factor parameters for each valley. The percentage indicated the amount of the valley area, which was capped between 0 and 1.0 for $n_f$ and between 0 and 2.0 for $n_t$.

| Valley | Parameter | Input Variables | Parameter | Input Variables |
|---|---|---|---|---|
| **Valley WS01** | $n_f$ (9.1 %) | Aspect/PISR<br>TPI<br>Vegetation | $n_t$ (0.4 %) | Aspect/PISR<br>TPI<br>Vegetation |
| **Valley WS02** | $n_f$ (2.6 %) | Aspect/PISR<br>TPI | $n_t$ (0.5 %) | Aspect/PISR<br>TPI |
| **Valley M222** | $n_f$ (2.0%) | Aspect/PISR<br>TPI<br>Vegetation | $n_t$ (0 %) | Aspect/PISR<br>TPI<br>Vegetation |
| **Valley MTS** | $n_f$ (0 %) | Aspect<br>TPI<br>Vegetation | $n_t$ (0 %) | Aspect<br>TPI<br>Vegetation |

**Table S5-4.** Vegetation and topographic variables used to assign rk values in each valley

| Valley | Assigned rk | Vegetation | Elevation (m) | Slope (º) | TWI |
|---|---|---|---|---|---|
| **Valley WS01** | 0.61 | Coniferous Forest | All | All | NA |
| | 0.61 | Herbaceous | < 1000 | < 20 | |
| | 1 | Herbaceous | > 1000 | All | |
| | 0.61 | Bare ground | < 958 | All | |
| | 1 | Bare ground | > 958 | All | |
| **Valley WS02** | 0.78 | Shrubs | All | All | NA |
| | 0.64 | Herbaceous | < 1160 | < 11 | |
| | 0.91 | Herbaceous | > 1160 | All | |
| | 0.93 | Bare ground | All | All | |
| **Valley M222** | 0.73 | NA | < 1274 | NA | All |
| | 0.73 | | > 1274, < 1480 | | > 5.1 |
| | 1 | | > 1274, < 1480 | | < 5.1 |
| | 1 | | > 1480 | | All |
| **Valley MTS** | 0.18 | Shrub<br>Coniferous Forest | < 1085 | NA | NA |
| | 0.4 | Wetland<br>Coniferous Forest | > 1085, < 1140 | | |
| | 0.58 | Coniferous Forest<br>Shrub | > 1140 | | |
| | 0.8 | Mixed Wooded<br>Herbaceous | >1085 | | |
| | 0.85 | Bare ground | > 1085 | | |

*S.5.2 Results*

S.5.2.1 Measured Air Temperature

**Table S5-5.** Change in freezing degree days and thawing degree days in the air ($FDD_a$ and $TDD_a$) with elevation for each valley.

| Valley | Lower change in $FDD_a$ (ºC days $km^{-1}$) | Upper Change in $FDD_a$ (ºC days $km^{-1}$) | Lower Change in $TDD_a$ (ºC days $km^{-1}$) | Upper Change in $TDD_a$ (ºC days $km^{-1}$) |
|---|---|---|---|---|
| **Valley WS01** | -3816 (DMP04)<br>-3252 (DMP05) | -521 (DMP10)<br>-485 (DMP11) | 379 (DMP04)<br>-253 (DMP05) | -863 (DMP10)<br>-485 (DMP11) |
| **Valley WS02** | -2190 (DMP09)<br>-2735 (DMP06) | -789 (DMP16)<br>-1144 (DMP17) | -664 (DMP09)<br>-87 (DMP06) | -835 (DMP16)<br>-686 (DMP17) |
| **Valley M222** | -1035 | 104 | -890 | -535 |
| **Valley MTS** | -2575 | 918 | 767 | -930 |

S.5.2.2 Measured Ground Surface Temperature

Each valley showed a different range of spatial variability in AMGST, and surface offsets based on measured values (Table S5-6). Some valleys showed significant differences in AMGST and $FDD_s$ based on either landform or landcover classes; however, the significant classes for each valley differed. Additionally, the rates and timing of freezing in the ground were observed to differ both between and within valleys depending on landcover or landform class. The results for each individual valley will be presented.

**Table S5-6**. Ground surface temperature metrics for the four valleys. Intra-annual amplitude is the difference between the warmest and coldest daily average ground surface temperature while the interannual difference is the difference in AMGST for the two years sampled.

| Valley | Average AMGST (ºC) | Max AMGST (ºC) | Min AMGST (ºC) | Average Intra-annual Amplitude (ºC) | Max Intra-annual Amplitude (ºC) | Min Intra-annual Amplitude (ºC) | Average Interannual Difference (ºC) | Max Interannual Difference (ºC) | Min Interannual Difference (ºC) |
|---|---|---|---|---|---|---|---|---|---|
| **Valley WS01** | 0.0 | 2.5<br>G03 | -3.7<br>G01 | 24.2 | 45.4<br>G15 | 12.2<br>G16 | 0.7 | 2.1<br>G10 | 0.0<br>G20 |
| **Valley WS02** | -1.6 | 1.1<br>G13 | -4.5<br>G20 | 30.1 | 51.0<br>G09 | 11.1<br>G04 | 0.5 | 1.6<br>G07 | 0.0<br>G21 |
| **Valley M222** | 0.1 | 1.7<br>G07 | -4.0<br>G10 | 17.7 | 35.7<br>G10 | 10.1<br>G25 | 0.5 | 2.9<br>G20 | 0.0<br>G08 |
| **Valley MTS** | 1.1 | 3.4<br>G24 | -1.8<br>G09 | 20.0 | 30.0<br>G12 | 11.0<br>G10 | 0.2 | 0.6<br>G01 | 0.0<br>G02 |

S.5.2.2.1 Valley WS01

Valley WS01 had the second coldest overall AMGST of the four valleys, with considerable differences in annual amplitudes between sites and yearly differences. In addition to the large annual amplitudes and interannual variability, Valley WS01 also had the largest overall range in AMGST (6.2 ºC). In this valley, annual amplitude showed an inverse relation ($R^2$ = 0.64) with AMGST, as colder sites had larger annual amplitudes (Figure S5-5A). The opposite of this relation was shown between annual amplitude and $FDD_s$ and $TDD_s$, as sites with larger annual amplitudes had higher $FDD_s$ and $TDD_s$ (Figure S5-5B). $FDD_s$ showed a stronger relation with annual amplitude than $TDD_s$ with $R^2$ of 0.88 and 0.51, respectively. There was no relation between annual amplitude, AMGST and $FDD_s$ and elevation ($R^2$ of 0.03, 0.01 and 0.0, respectively) (Figure S5-5C and D). $TDD_s$ showed a very weak relation with elevation ($R^2$ = 0.20).

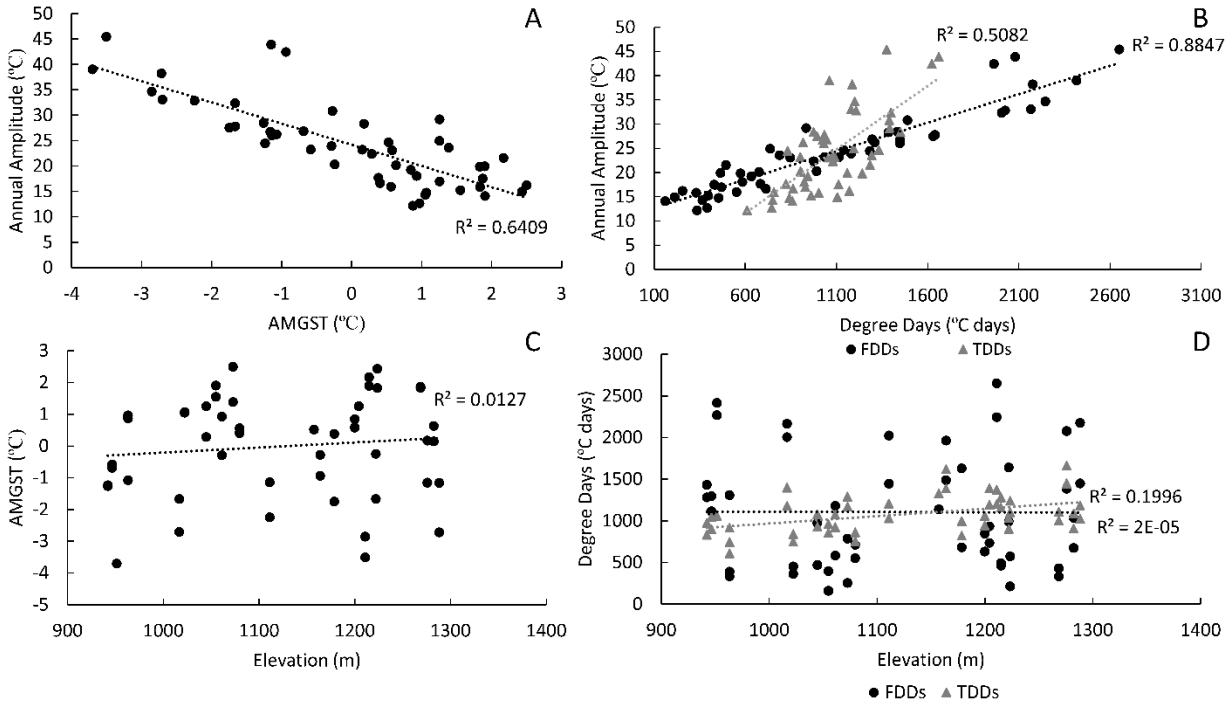


**Figure S5-5.** Plot of Valley WS01 ground temperature metrics. A) the annual range in daily average temperature (annual amplitude) compared to the annual mean ground surface temperature (AMGST), B) Annual amplitude at each site compared to freezing degree days (FDD) and thawing degree days (TDD) in the ground surface (s), C) AMGST compared to elevation for each site, and D) measured FDDs and TDDs for each site compared to elevation.

Cumulative $FDD_s$ showed substantial difference from $FDD_a$ across the valley, indicating fairly large surface offsets (Figure S5-6). There was also a substantial range in cumulative $FDD_s$, with G06 located in the valley bottom accumulating the lowest (161 ºC days) and G01, G15, and G23 having the highest (2416, 2246, and 2166 ºC days, respectively). G01 was located in the valley bottom, G15 was located at high to mid elevation, and G23 was on an exposed slope near the valley bottom. Generally, the cumulative $FDD_s$ for this valley clustered on the lower end compared to $FDD_a$. The presence of persistent winter inversions can also be seen in the cumulative $FDD_a$ record, with the valley bottom air station (DMP WS01) having the highest number of $FDD_a$ while the two mid slope stations have the lowest. There was also a noticeable

difference between the $FDD_a$ for the two mid-slope air stations, with the station in the trees DMP04 having lower recorded cumulative $FDD_a$ than the station on the treeless slope (DMP05).

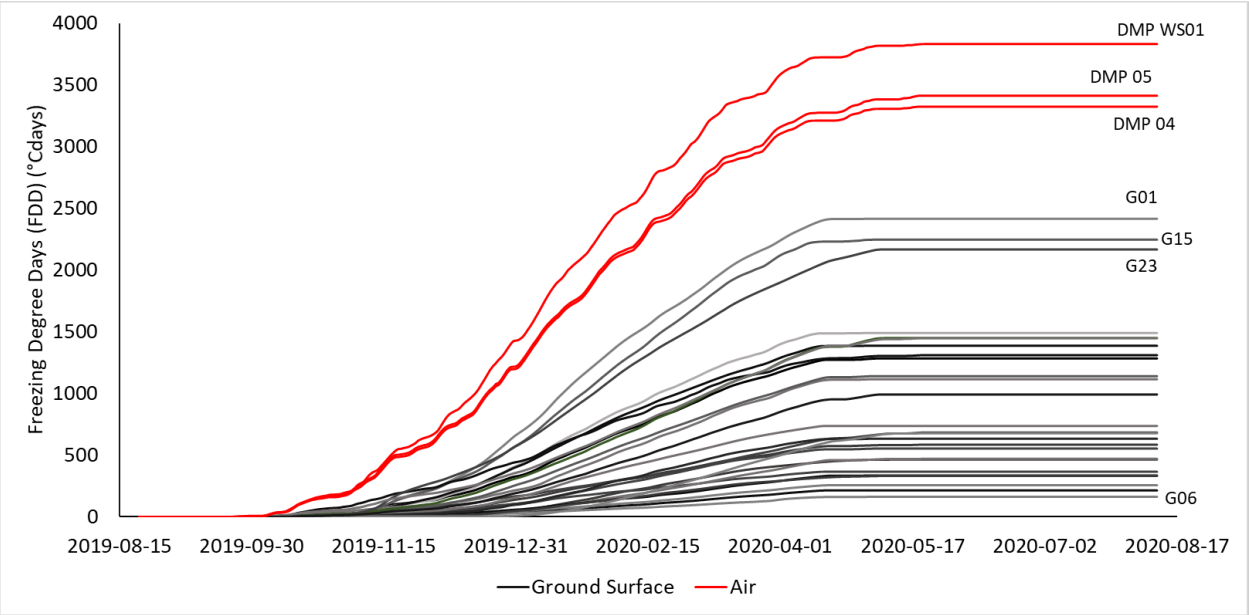


**Figure S5-6.** Cumulative freezing degree days (FDD) for air and ground surface stations in Valley WS01.

There was no significant difference in AMGST or $FDD_s$ between vegetation (landcover) or topographic (landform) classes, however general trends were still present (Figure S5-7). Generally, AMGST increased with increasing incision for landforms with ridges having the coldest average AMGST and valleys having the warmest. However, there was substantial variability within both classes, with about a 6 ºC range in AMGST for ridges and about a 7 ºC range for valleys. Based on landcover class, coniferous forest had the warmest average AMGST, while herbaceous had the coldest. Additionally, herbaceous and rock sites showed the largest range in measured AMGST, while coniferous forest had the smallest range. Similar to the general differences in AMGST per landform class, $FDD_s$ increased with increasing exposure, meaning more exposed classes such as ridges became colder during the freezing season than the more incised classes, slopes and valleys. However, one main difference is that the slope class had

on average fewer $FDD_s$ than sites in the valley bottom. The valley bottom class also had the largest range in $FDD_s$, while the slope class had the lowest. Average $FDD_s$ based on landcover class was different from that of AMGST, with coniferous forest having the lowest number of $FDD_s$ while rock sites had the highest. Again, similar to AMGST and landcover, herbaceous and rock landcover classes showed the highest range in $FDD_s$.

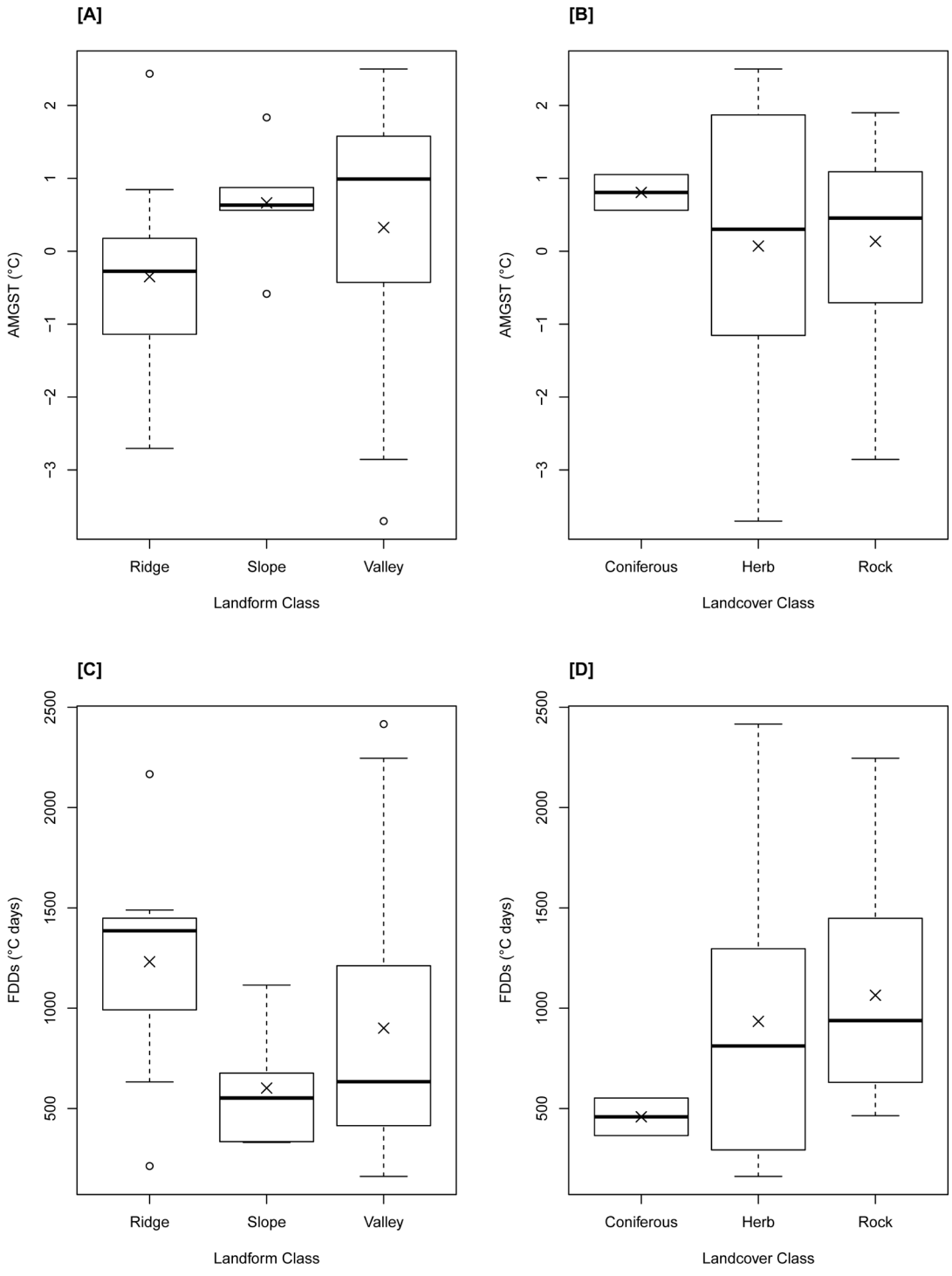


**Figure S5-7.** Box and whiskers plots for Valley WS01 showing A) annual mean ground surface temperature (AMGST) for landform class, B) AMGST and vegetation classes (landcover), C) $FDD_s$ and landform class, and D) $FDD_s$ and vegetation class.

Although there was no significant difference between the average AMGST for each landform and landcover class, general patterns the timing of freezing and thawing as well as temperature fluctuations can be discerned (Figure S5-8). First, the slope landform sites remained warmer in the freezing season than both ridges and valley bottoms. Additionally, the slope and valley classes lagged behind the ridge class during temperature fluctuations especially during spring and autumn. During the thawing season, AMGSTs in the valley were cooler than those on the slope and ridges, and the AMGST for the slope and ridge classes were more similar than during the freezing season. Looking at the average daily pattern of AMGST for landcover classes, the rock class showed the coldest AMGST during the freezing and thawing season and the most rapid temporal variability closely followed by the herbaceous class. The rock landcover was also the warmest in summer followed by the herbaceous class. Finally, coniferous forest was the warmest class during the winter and the coldest during the summer. The coniferous forest class also lagged slightly behind the other classes during temporal swings in temperature.

Overall, the ground surface temperatures in Valley WS01 showed substantial annual and temporal variability. Although the pattern of ground surface temperature distribution was not directly related to elevation, topography or vegetation individually, they in combination and in addition to the strong winter inversions, likely contributed to the variability in AMGST in this valley.

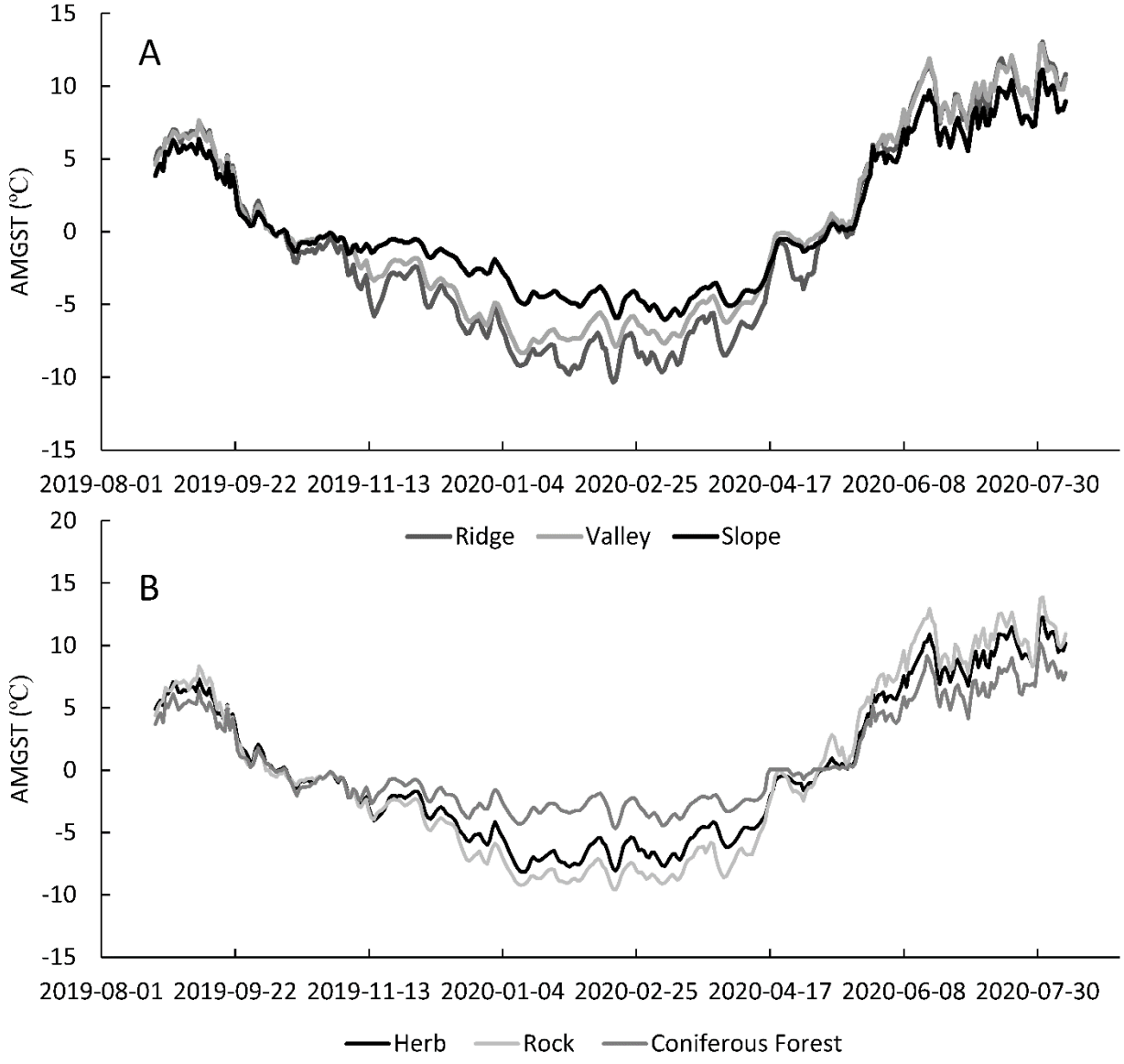


**Figure S5-8.** Average daily ground surface temperature in Valley WS01 for A) Landform classes and B) Landcover classes.

S.5.2.2.2 Valley WS02

Valley WS02 had the overall coldest AMGST and the largest average annual amplitude. However, sites in this valley had one of the lower interannual differences in AMGST and a smaller range (5.6 ºC) making the ground thermal regime more homogeneous in this valley than

others. The annual amplitude at the sites in this valley showed an inverse relation with AMGST ($R^2 = 0.59$), indicating that colder sites had larger changes in temperature between the summer and winter (Figure S5-9A). $FDD_s$ and $TDD_s$ showed a normal relation to annual amplitude, with $FDD_s$ and $TDD_s$ increasing with larger seasonal temperature changes (Figure S5-9B). Of these two metrics, $FDD_s$ had a stronger linear relation with amplitude ($R^2 = 0.89$) compared to $TDD_s$ ($R^2 = 0.64$). There are weak relations between AMGST, annual amplitude, and $FDD_s$ and elevation with $R^2$ of 0.25, 0.17 and 0.22, respectively. In this valley, there was no relation between $TDD_s$ and elevation ($R^2 = 0.04$).

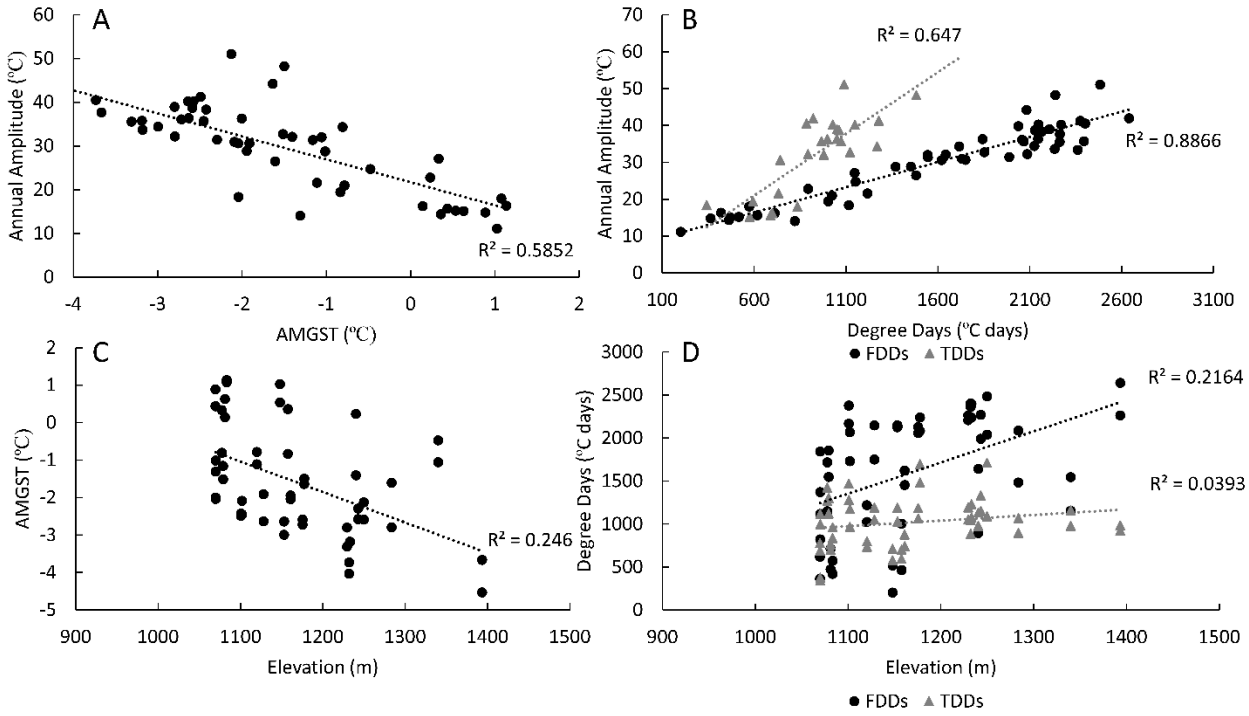


**Figure S5-9.** Plot of Valley WS02 ground temperature metrics. A) the annual range in daily average temperature (annual amplitude) compared to the annual mean ground surface temperature (AMGST), B) Annual amplitude at each site compared to freezing degree days (FDD) and thawing degree days (TDD) in the ground surface (s), C) AMGST compared to elevation for each site, and D) measured $FDD_s$ and $TDD_s$ for each site compared to elevation.

Cumulative FDD in this valley also showed a large degree of variability both between sites and between the ground surface and the air (Figure S5-10). In Valley WS02 there was a

smaller difference in FDD between the coldest ground surface site and the warmest air station than Valley WS01 (754 ºC days difference compared to 908 ºC days) indicating smaller surface offsets in this valley Additionally, most of the sites in this valley have fairly large cumulative $FDD_s$ compared to the cumulative $FDD_a$. Sites G10, G20 and G21 had the greatest number of $FDD_s$ (2362, 2210, and 2236 ºC days) while sites G04, G11, and G13 had the least (202, 364, and 364 ºC days, respectively). Site G10 was located near the valley bottom on a slope; while site G20 was located on the ridge, and site G21 was located near the ridge on a slope. G04, G11 and G13 were all located in the valley bottom. The presence of persistent winter inversions was also apparent, with the valley bottom air station (DMP WS02) having a greater number of $FDD_a$ than the two mid slope stations. However, in this valley the two mid slope stations have similar $FDD_a$, indicating more similar SLRs on both slopes compared to Valley WS01.

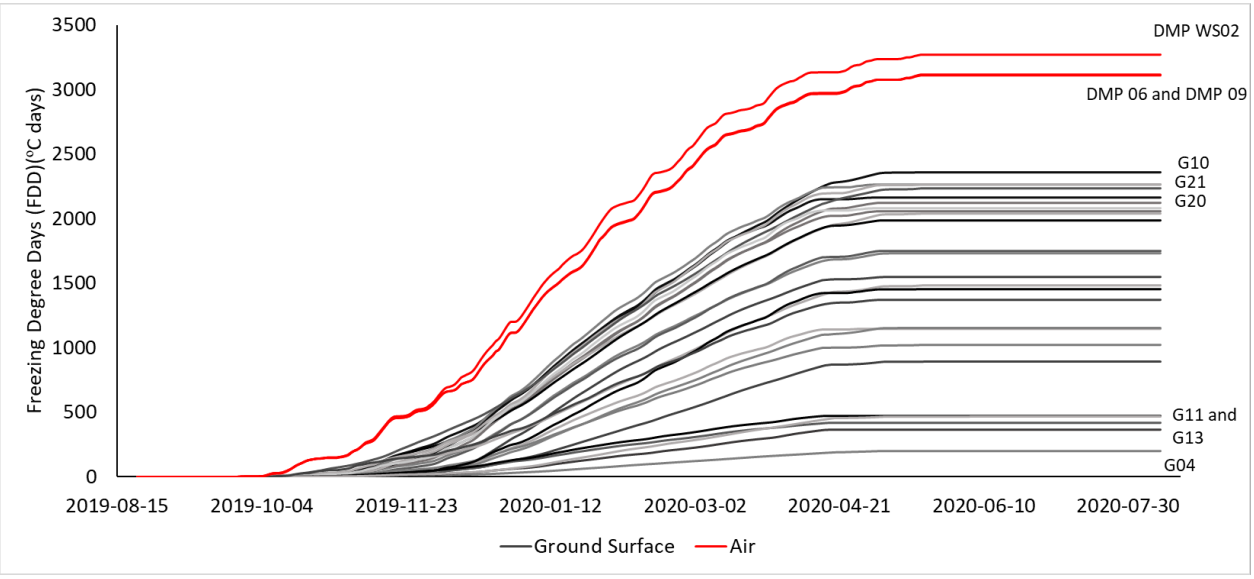


**Figure S5-10.** Cumulative freezing degree days (FDD) for air and ground surface station in Valley WS02.

There were significant differences between landcover and landform classes for both AMGST and $FDD_s$ (Figure S5-11). Average AMGST was significantly different for the rock and shrub landcover classes ($p = 0.03$). Generally, AGMST were lowest and $FDD_s$ were highest at

sites on the ridges and lower in the more incised landform classes. However, slope sites had on average lower $FDD_s$ and warmer MAGST than the valley sites. There were substantial ranges in AMGST and $FDD_s$ for the slope and valley landform classes (about 4 ºC and about 1800 ºC days). The ridge landform class had the smallest variability in both AMGST and $FDD_s$ across sites. For landcover, the slope and ridge classes and valley and ridge classes had significantly different averages for both AMGST and $FDD_s$ ($p = 0.01$ and $p = 0.05$, respectively). The rock class had the lowest average AMGST and highest $FDD_s$, while the shrub class had the warmest average AMGST and the lowest number of $FDD_s$. However, there were only two sites classified as shrub. Both the herbaceous and rock classes showed large ranges in both AMGST and $FDD_s$, while the shrub class had minimal variability, possibly due to only two sites.

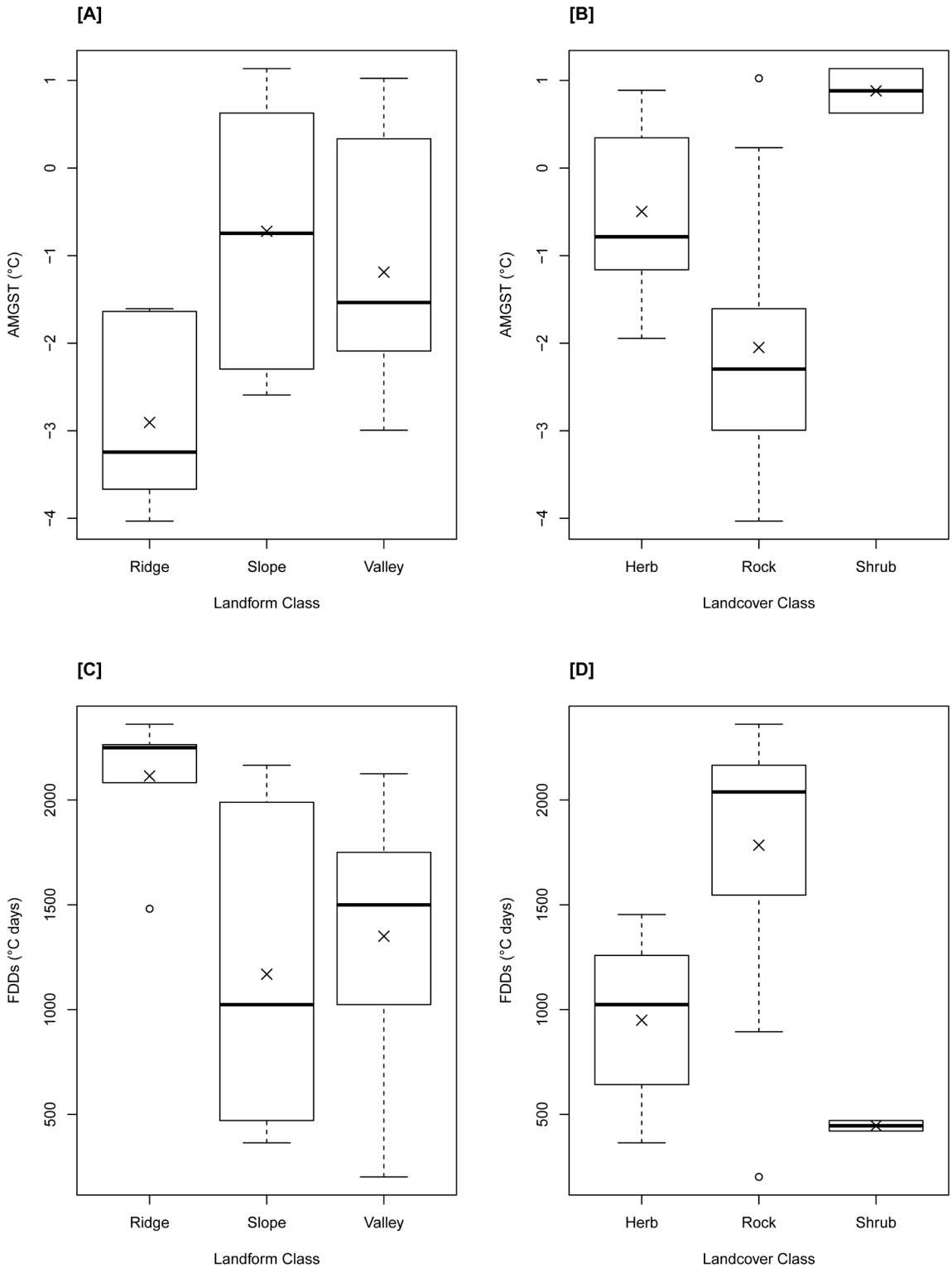


**Figure S5-11.** Box and whiskers plots for Valley WS02 showing A) annual mean ground surface temperature (AMGST) for landform class, B) AMGST and vegetation classes (landcover), C) $FDD_s$ and landform class, and D) $FDD_s$ and vegetation class.

Over a year, the daily average ground surface temperature for each landform and landcover class varied more during the freezing season than the thawing season (Figure S5-12). First, on average the slope landform sites remained warmer in the freezing season than both ridges and valley bottoms. Additionally, the slope and valley classes lagged behind the ridge class during temperature fluctuations and showed a longer zero curtain period during freezing. During the thawing season, AMGSTs on the slopes were cooler on average than those in the valley and on ridges. Looking at the average daily pattern of AMGST for landcover classes, the shrub class (n = 2) showed the warmest AMGST during the freezing and thawing season and the slowest temporal response. The rock landcover class was both the coldest in winter and the warmest in summer followed by the herbaceous class, with the rock class showing the most rapid temporal variability, especially during spring and autumn.

Overall, the ground surface temperatures in Valley WS02 showed substantial annual and temporal variability. The variability in ground surface temperature metrics stemmed largely from topography, vegetation, and their impact on the magnitude of the surface offset, affecting how the AMAT can influence the site.

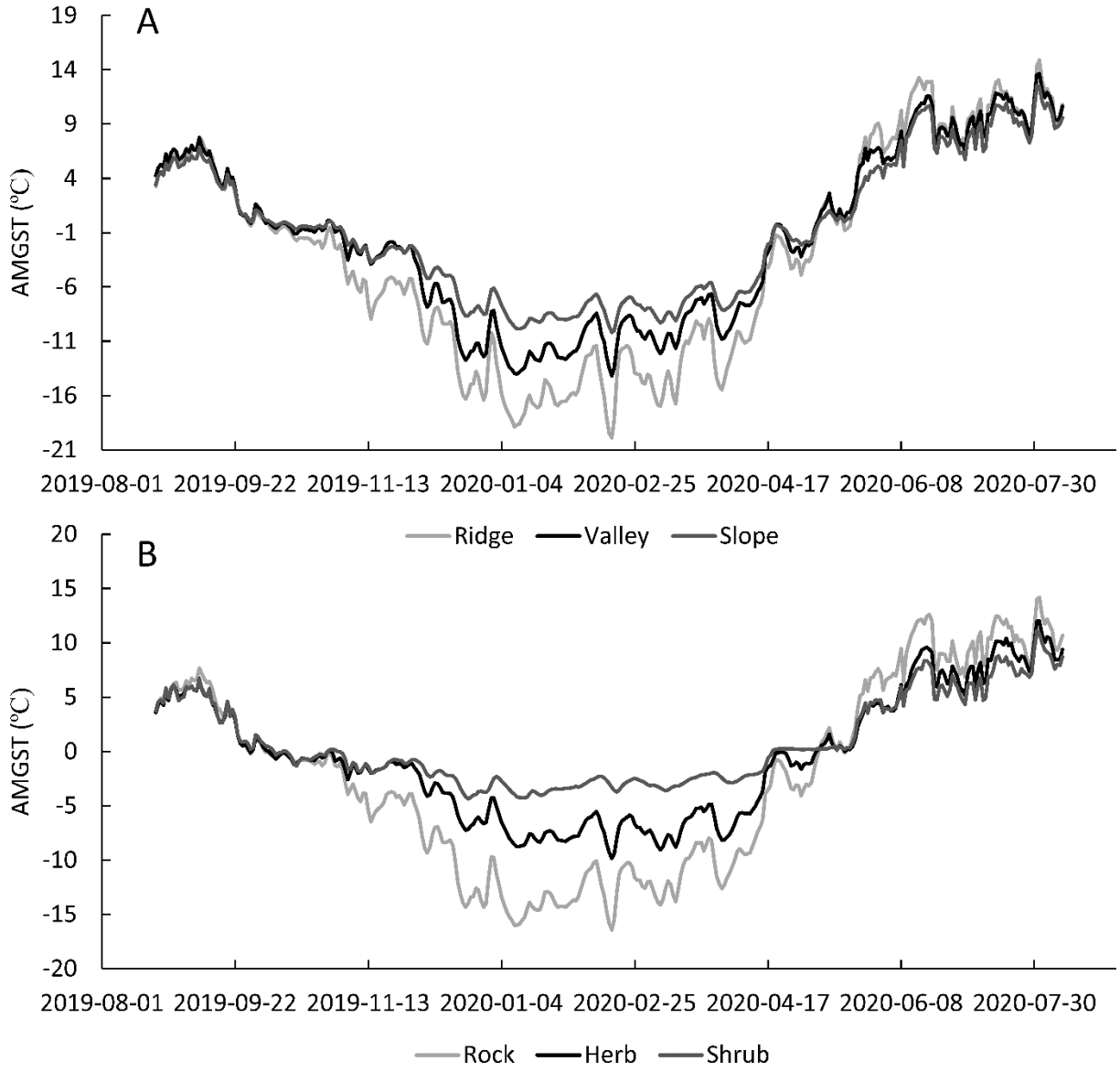


**Figure S5-12.** Average daily ground surface temperature in Valley WS02 for A) Landform classes and B) Landcover classes.

S.5.2.2.3 Valley M222

Mile 222 Valley was one of the warmer valleys, with an overall average of 0.1 ºC. This valley also had the lowest average annual amplitude, showing a more limited seasonal difference in ground surface temperatures. Despite the limited annual amplitude overall, Mile 222 Valley

had the second highest range in AMGST (5.7 ºC). As with the previous valleys, there was an inverse relation between annual amplitude and AMGST with higher seasonal variability at colder sites ($R^2 = 0.52$) (Figure S5-13A). The opposite of this relation was shown between annual amplitude and $FDD_s$, with larger annual amplitudes having higher $FDD_s$ ($R^2 = 0.76$) (Figure S5-13B). There was a much weaker relation between $TDD_s$ and annual amplitude in this valley than the previous ones ($R^2 = 0.22$). There was minimal relation between annual amplitude, AMGST and $FDD_s$ and elevation ($R^2$ of 0.28, 0.27 and 0.23, respectively) (Figure S5-13C and D). $TDD_s$ showed no weak relation with elevation ($R^2 = 0.02$).

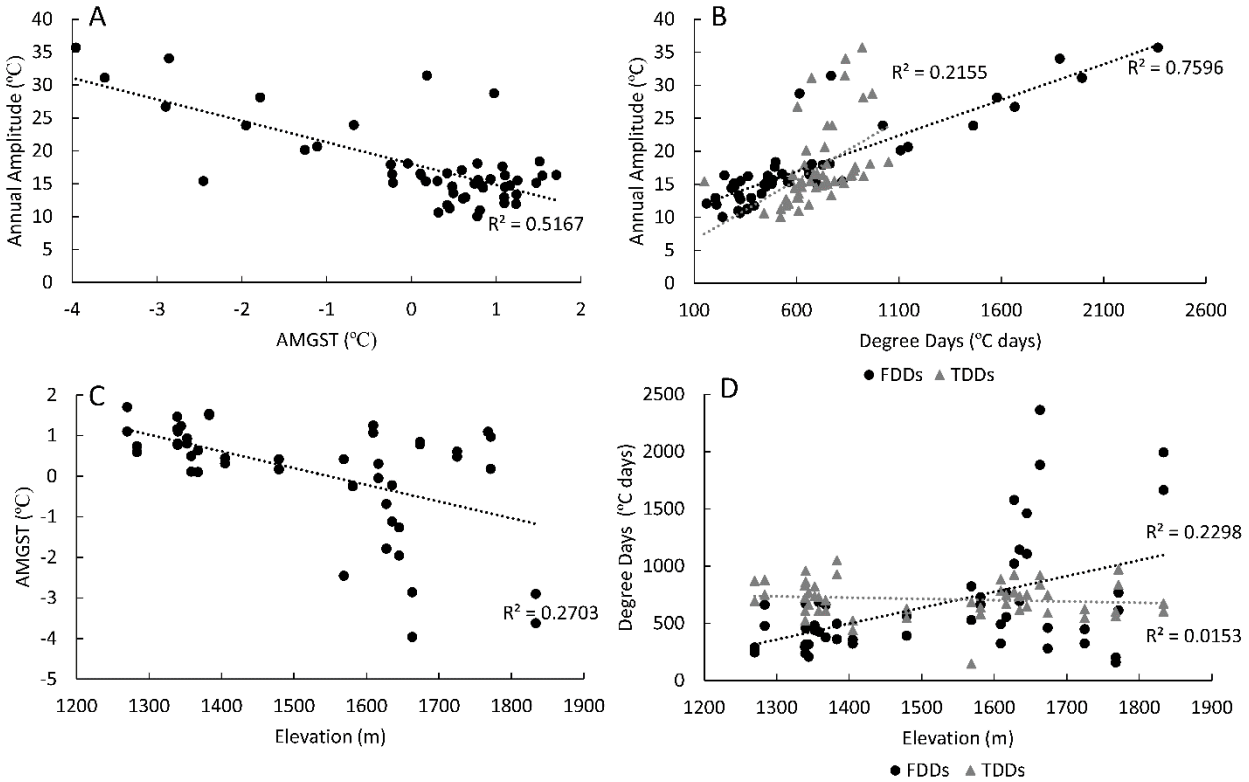


**Figure S5-13.** Plot of Valley M222 ground temperature metrics. A) the annual range in daily average temperature (annual amplitude) compared to the annual mean ground surface temperature (AMGST), B) Annual amplitude at each site compared to freezing degree days (FDD) and thawing degree days (TDD) in the ground surface (s), C) AMGST compared to elevation for each site, and D) measured $FDD_s$ and $TDD_s$ for each site compared to elevation.

Cumulative $FDD_s$ in this valley were grouped toward the lower end of the measured range, with only a few sites having a relatively high number (Figure S5-14). The difference in

cumulative FDD between the warmest air station and the coldest ground surface site were much higher in this valley than the previous two (1257 ºC days compared to 754 and 908 ºC days), indicating higher surface offsets in this valley. Sites G10 and G24 had the greatest number of $FDD_s$ (1886, and 1666 ºC days) while sites G08 had the least (160 ºC days, respectively). Site G10 and G24 were located at higher elevations and in exposed topography, while G08 was also located at higher elevations but in a less exposed area. The presence of persistent winter inversions was also apparent, with the valley bottom air station (M22 01) having a greater number of $FDD_a$ than the two upper stations. However, in this valley, the inversion ended at the mid-slope station (M222 02) and a normal SLR resumed above this elevation, as the cumulative $FDD_a$ for the highest station (M222 03) was greater than those recorded at M222 02. This resulted in the warmest winter conditions at the mid elevations.

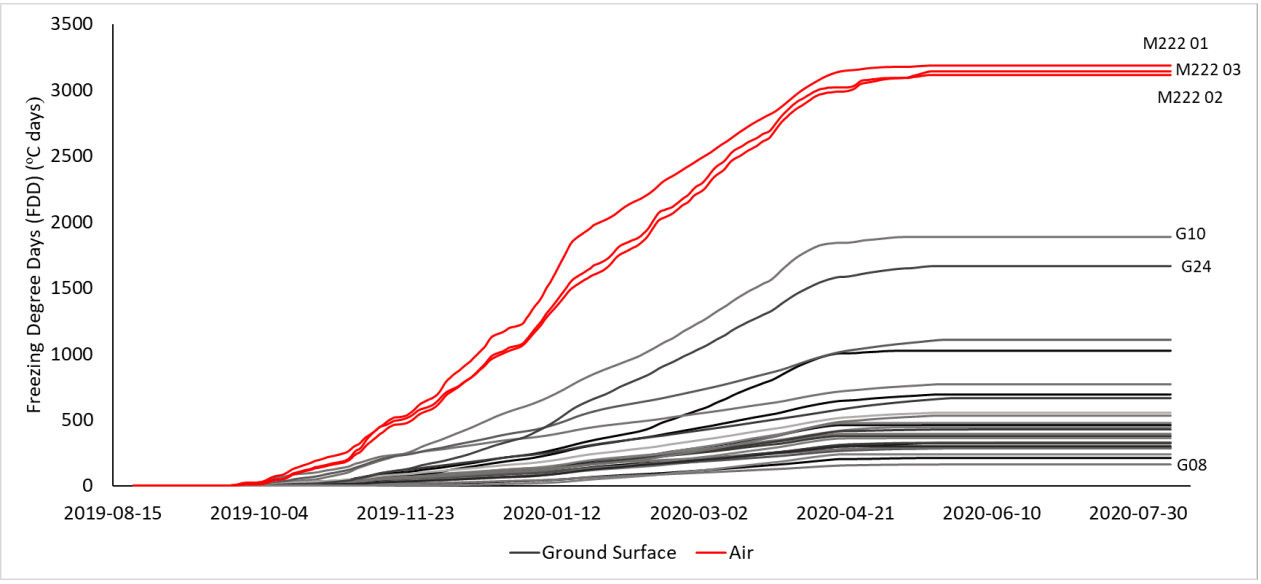


**Figure S5-14.** Cumulative freezing degree days (FDD) for air and ground surface stations in Valley M222.

There was no significant difference in the average $FDD_s$ for landcover and landform classes. Although there was no significant difference, some trends were still present. $FDD_s$ was highest for the least incised classes (slopes and ridges) and lowest for the most incised (flatland

and valleys) (Figure S5-15). The ridge class had the largest range in $FDD_s$, while flatland had the smallest; however, there were only two sites in this class. For landcover, the rock class had the highest average $FDD_s$, while herbaceous and shrubs had the lowest. Additionally, the herbaceous class showed the largest range in $FDD_s$, while the shrub class showed the least. There was a significant difference in average AMGST between the rock and herb ($p = 0.04$) and the rock and shrub ($p = 0.04$) landcover classes. The rock class had the lowest average AMGST, while shrubs and herbaceous had similar average AMGSTs that were warmer. The rock class also showed the largest range in AMGST. Finally, there was no significant difference in average AMGST between the landform classes. The trend in AMGST by landform matched that of $FDD_s$, with slopes and ridges having the highest average AMGST and valleys and flatlands having the least. Additionally, the ridge class had the largest range in AMGST.

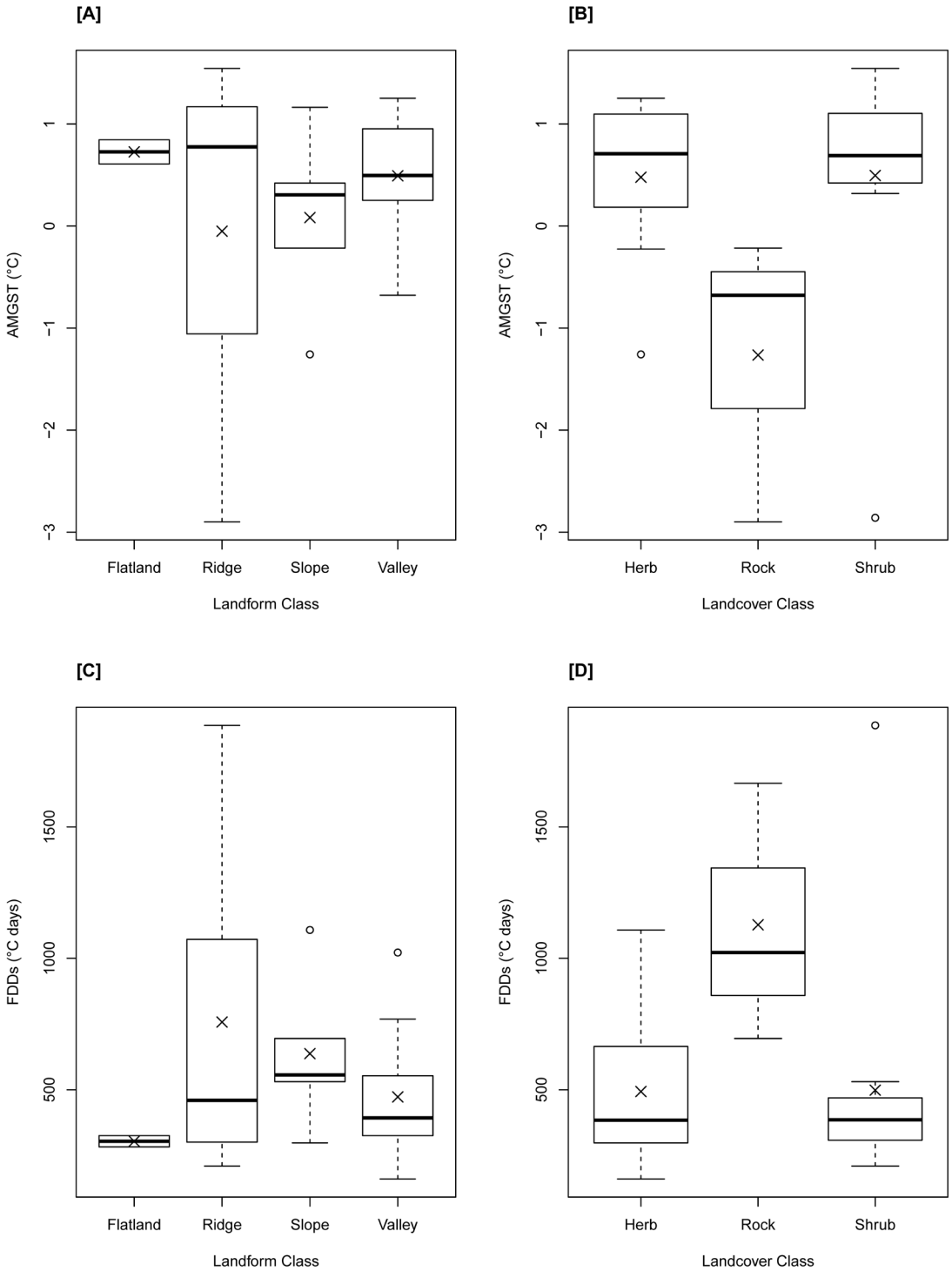


**Figure S5-15.** Box and whiskers plots for Valley M222 showing A) annual mean ground surface temperature (AMGST) for landform class, B) AMGST and vegetation classes (landcover), C) FDDs and landform class, and D) FDDs and vegetation class.

Temporally, the average daily ground surface temperature for each landform and landcover class varied more during the freezing season than the thawing season, although this difference was less than in the previous valleys (Figure S5-16). On average, the ridge landform sites remained colder in the freezing season, followed closely by the slope and valley classes. In this valley, flatland sites remained the warmest during winter; however, there were only two sites in this class. During the thawing season, the ridge class warms much faster than the other three and remains the warmest, if only slightly, during the summer months. The flatland sites remain the coldest during summer. Additionally, the flatland sites show limited daily variability compared to the other classes. Average ground surface temperature in the rock landcover class became much colder during the freezing season than those in the other two classes. Average temperatures in the shrub and herbaceous classes remain relatively similar throughout the year except from February to June, when the average temperature for the herbaceous class is warmer from February to April and then colder from April to June than the shrub class. The shrub and herbaceous classes were much less variable on an annual and daily scale than the rock class.

Overall, the ground surface temperatures in Valley M222 showed a more limited annual and temporal variability compared to the other valleys. The variability in ground surface temperature metrics stemmed partially from vegetation differences but also likely from topographic influences and the presence of strong winter inversions, even if these were not directly apparent or statistically significant.

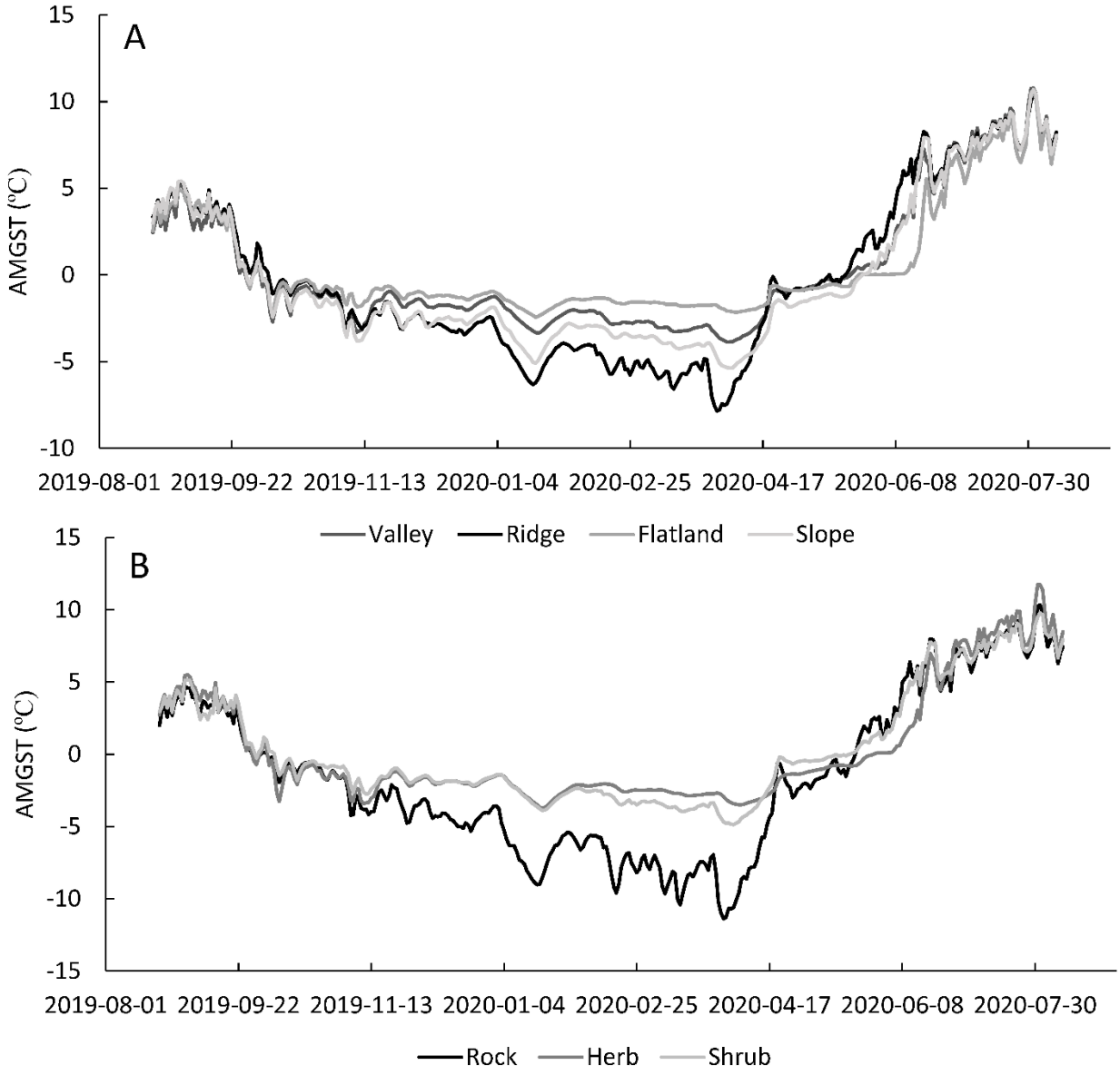


**Figure S5-16.** Average daily ground surface temperature in Valley M222 for A) Landform classes and B) Landcover classes.

S.5.2.2.4 Valley MTS

Valley MTS had the overall lowest range in AMGST (5.2 ºC) and the lowest average interannual variability. As a result, this valley was relatively homogeneous both spatially and temporally compared to the other valleys. The sites in this valley also had relatively low annual amplitudes. Once again, there was an inverse relation between AMGST and the annual

amplitude; however, it was slightly weaker in this valley than the others ($R^2$ = 0.43) (Figure S5-17A). As with the other valleys, there was also a strong relation between $FDD_s$ and the annual amplitude, with higher $FDD_s$ corresponding with a higher seasonal temperature change ($R^2$ = 0.76) (Figure S5-17B). However, there was only a weak relation between $TDD_s$ and annual amplitude, similar to Valley M222 but differing from Valley WS01 and Valley WS02 ($R^2$ = 0.22). There was also a weak relation between annual amplitude, AMGST, and $FDD_s$ and elevation ($R^2$ of 0.28, 0.27 and 0.23, respectively) (Figure S5-17C and D). Lastly, there was no relation between $TDD_s$ and elevation ($R^2$ = 0.02).

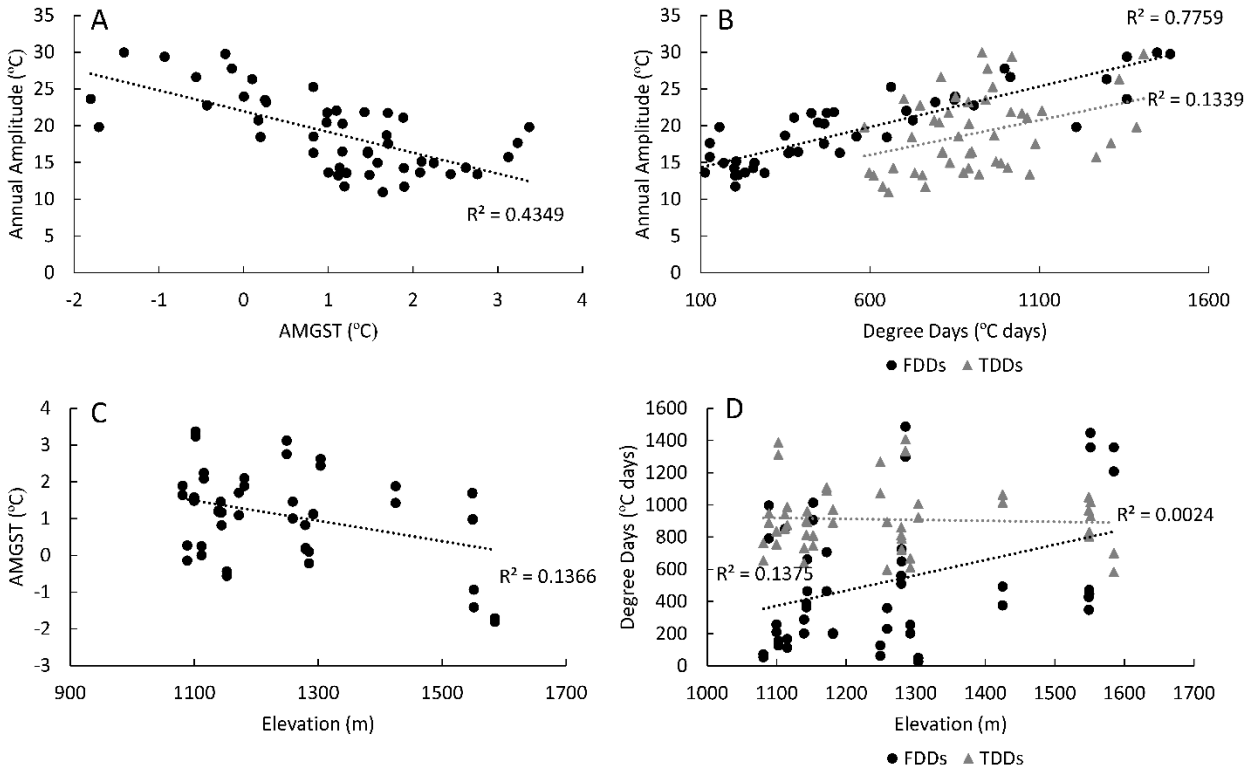


**Figure S5-17.** Plot of Valley MTS ground temperature metrics. A) the annual range in daily average temperature (annual amplitude) compared to the annual mean ground surface temperature (AMGST), B) Annual amplitude at each site compared to freezing degree days (FDD) and thawing degree days (TDD) in the ground surface (s), C) AMGST compared to elevation for each site, and D) measured $FDD_s$ and $TDD_s$ for each site compared to elevation.

Sites in Valley MTS were considerably warmer compared to those in other valleys, as some GTNs accumulated less than 50 FDDs over the year (Figure S5-18). The difference in cumulative FDD between the warmest air station and the coldest ground surface site was much less than Valley M222 and Valley WS01 but more than Valley WS02 (829 ºC days), indicating smaller surface offsets than Valley M222 and Valley WS01 but greater than in Valley WS02. Sites G12, G23 and G09 had the greatest number of $FDD_s$ (1448, 1299, and 1209 ºC days) while sites G17 had the least (28 ºC days, respectively). Sites G12, G23 and G09 were located at high elevations and in exposed topography, while G17 was also located at mid elevations in shrubs. The presence of persistent winter inversions was also apparent, with the valley bottom air station (MTS Lower) having a greater number of $FDD_a$ than the two upper stations. The strong persistent winter inversion can be seen in the cumulative $FDD_a$ record, with the lower most station (MTS Lower) having the highest number of FDD. As with Valley M222, the inverted SLR reverts to normal above the mid elevation air station (MTS Mid) cooling with elevation to the top station (MTS Ridge). This resulted in the warmest winter conditions at the mid elevations.

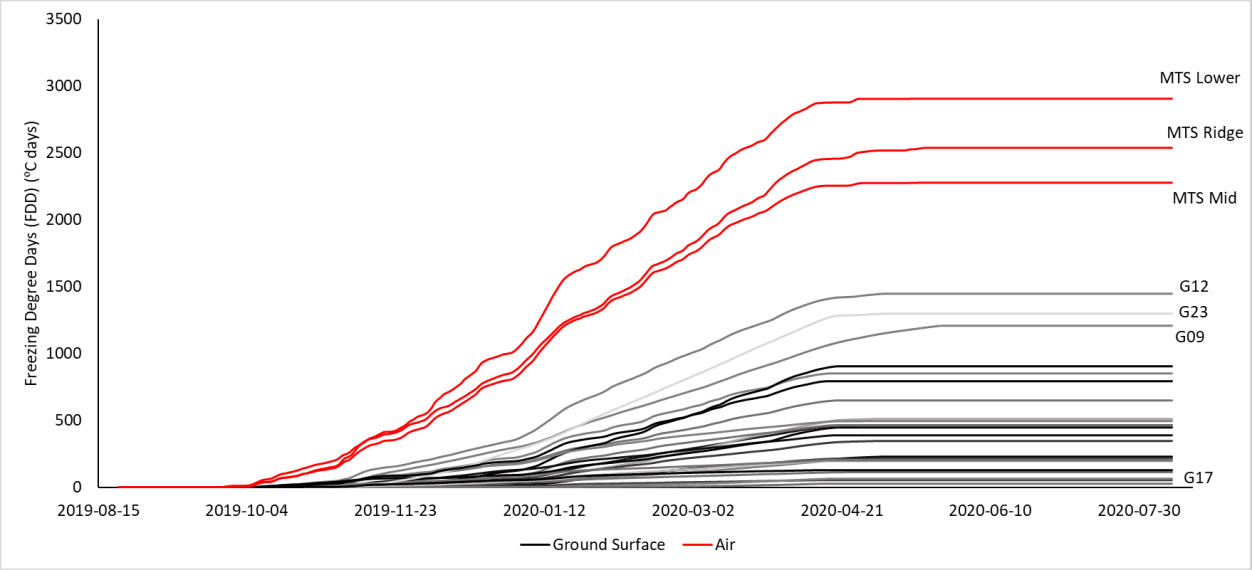


**Figure S5-18.** Cumulative freezing degree days (FDD) for air and ground surface stations in Valley MTS.

There was no significant difference between the means of AMGST or $FDD_s$ for landform classes; however, there were some visible differences (Figure S5-19). Average $FDD_s$ was highest for the ridge landform class and lowest for the valley, indicating that $FDD_s$ decreased with increasing incision. The slope class showed the largest range in $FDD_s$. The difference in average AMGST amongst the landform classes was minimal, with the ridge class slightly colder and the valley class slightly warmer. Similar to $FDD_s$, the slope class had the largest range in AMGST. There was also no significant difference in average AMGST for the landcover classes; however, the rock class had the coldest average AMGST while the shrub class had the warmest. The rock and coniferous forest classes had the largest range in AMGST; however, the large range in the coniferous forest may be attributed to one burned site that was still classified as forested in the landcover classification file. This site had the warmest AMGST in this class (3.2 °C). Finally, there was a significant difference in the average $FDD_s$ for the rock and coniferous forest ($p = 0.03$) and the rock and shrub ($p = 0.02$) landcover classes. The average $FDD_s$ in the rock class

was significantly higher than both the coniferous forest and shrub classes. Shrubs had the lowest average $FDD_s$ of the sampled landcovers.

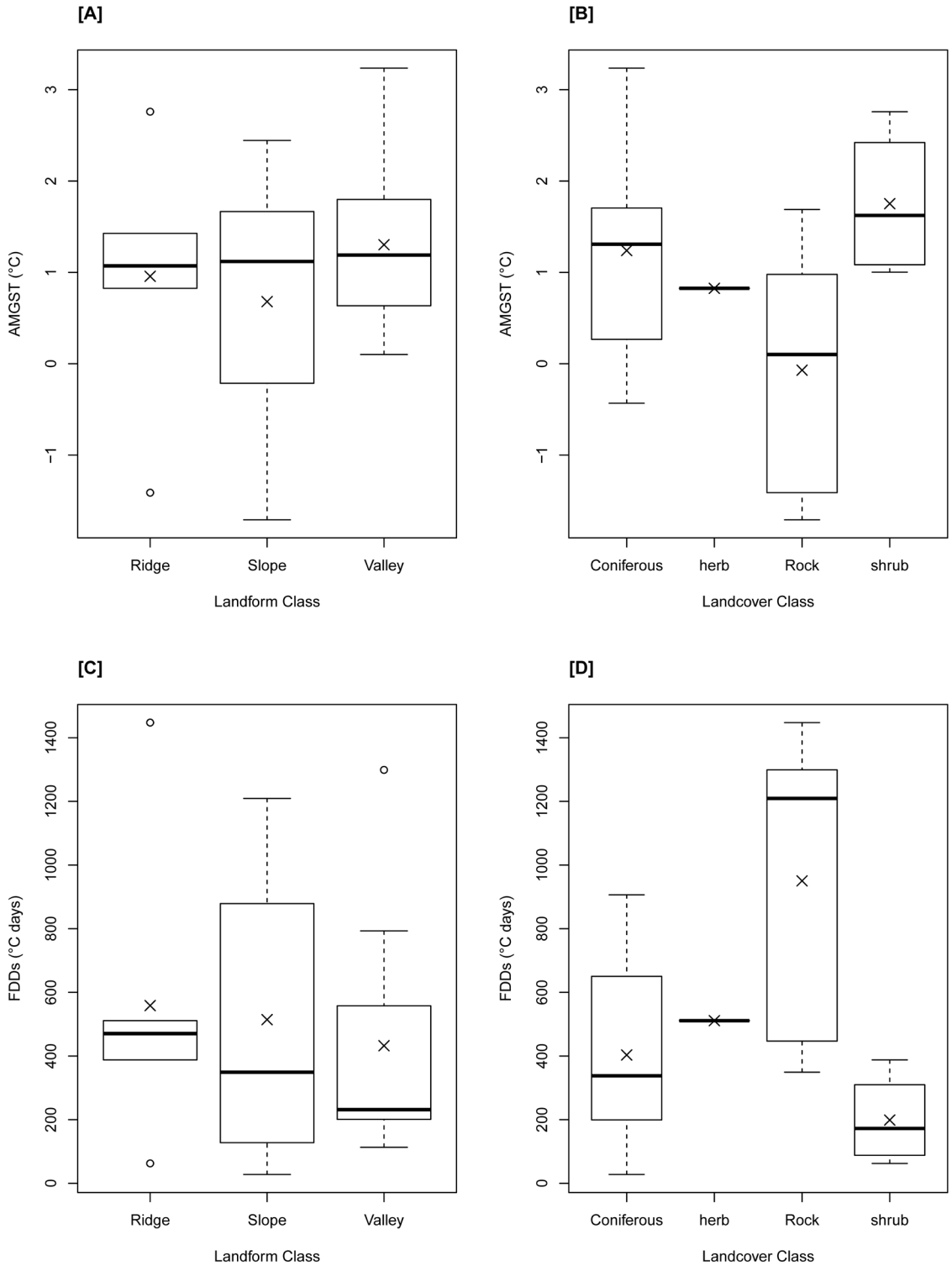


**Figure S5-19.** Box and whiskers plots for Valley MTS showing A) annual mean ground surface temperature (AMGST) for landform class, B) AMGST and vegetation classes (landcover), C) $FDD_s$ and landform class, and D) $FDD_s$ and vegetation class.

There was minimal difference temporally in average AMGST for each landform class over a year (Figure S5-20). The average AMGST for the ridge class was slightly colder than the other classes and showed a bit more temporal variability. The ridge average AMGST was also the warmest class during summer. The valley remained the warmest during winter, while the slope class was coldest during summer. There was more temporal variability between the average AMGST for the landcover classes, with the rock classes becoming substantially colder than the others during winter and slightly warmer during summer. The coniferous forest class was the next coldest and also remained the coldest during the summer. This class also showed a large zero curtain, especially during spring. The shrub class remained the warmest during winter and also had much smaller variations in temperature during this season compared to the other classes. The shrub class also remained colder than the other classes farther into the summer, only becoming warmer than the forest around mid-June. Finally, there was only one site in the herbaceous class, so the temporal variability and trends in AMGST cannot be reliably compared to the other classes. Overall, the variability both spatially and temporally for this valley was less than the other valleys, making Valley MTS relatively homogenous in ground surface temperature in comparison. Valley MTS also had substantially warmer ground surface temperatures, with some sites barely freezing during winter.

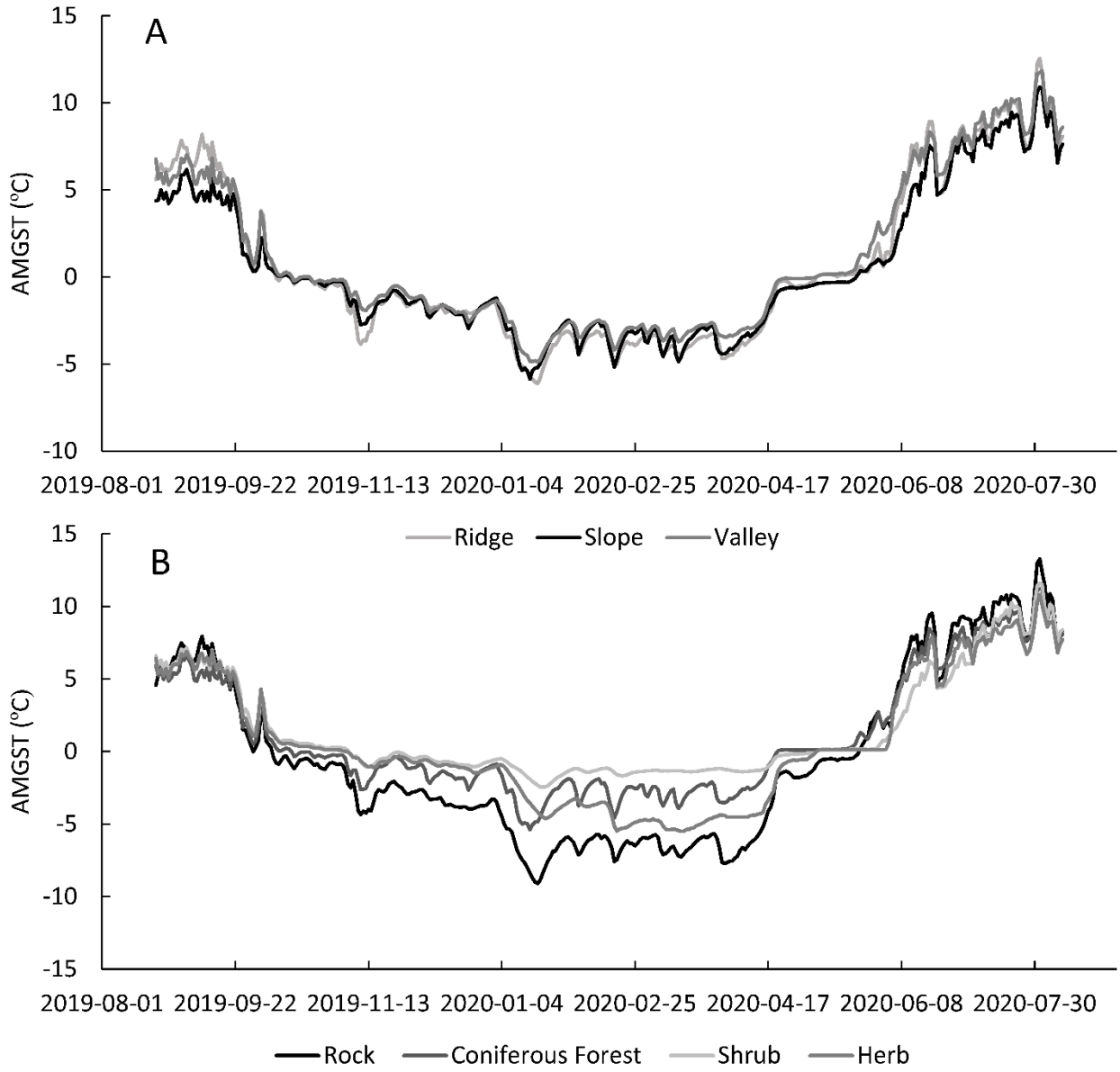


**Figure S5-20.** Average daily ground surface temperature in Valley MTS for A) Landform classes and B) Landcover classes.

S.5.2.3 Additional Models for TTOP Model Parameters

S.5.2.3.1 Valley WS01

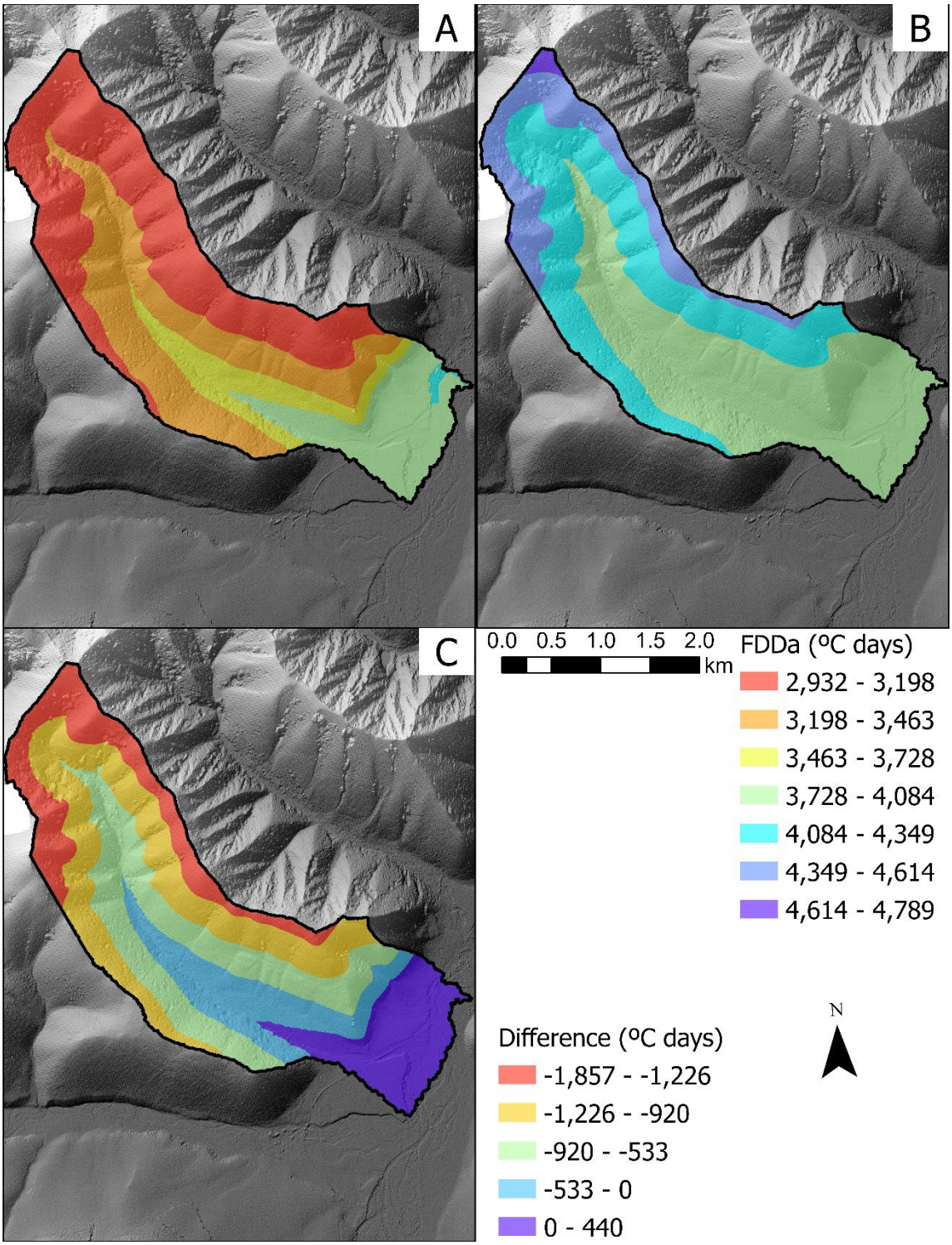


**Figure S5-21**. Freezing degree days air ($FDD_a$) models for Valley WS01 A) calculated change in $FDD_a$ with elevation, B) a -6.5 °C $km^{-1}$ change for every day with annual mean air temperature (AMAT) below 0 °C, and C) the difference between the two where negative values indicate actual $FDD_a$ (measured change with elevation) is lower than expected following the normal environmental SLR and positive values indicate actual $FDD_a$ is higher than expected.

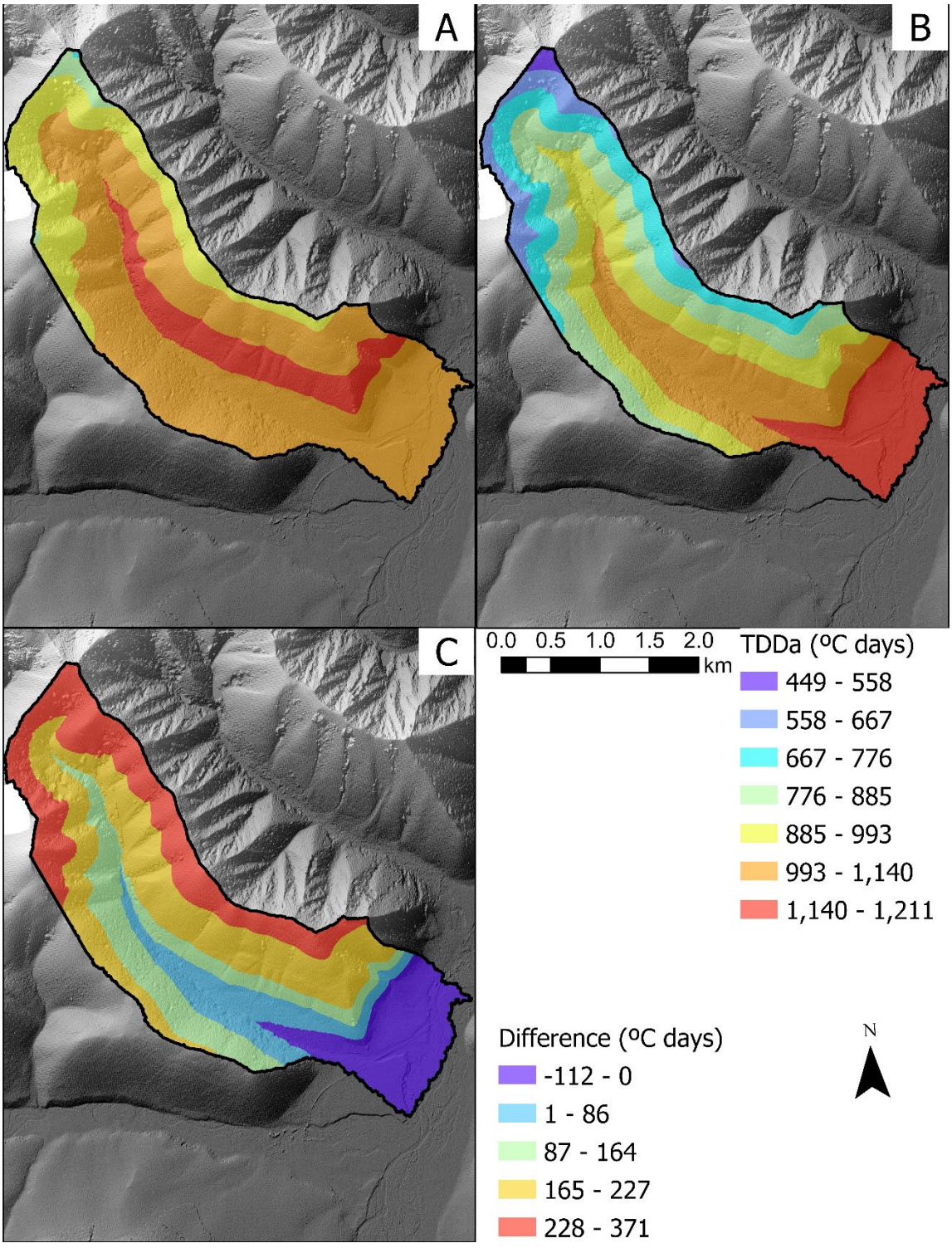


**Figure S5-22.** Thawing degree days air ($TDD_a$) models for Valley WS01 A) calculated change in $TDD_a$ with elevation, B) a -6.5 °C $km^{-1}$ change for every day with annual mean air temperature (AMAT) above 0 °C, and C) the difference between the two where negative values indicate actual $TDD_a$ (measured change with elevation) is lower than expected following the normal environmental SLR and positive values indicate actual $TDD_a$ is higher than expected.

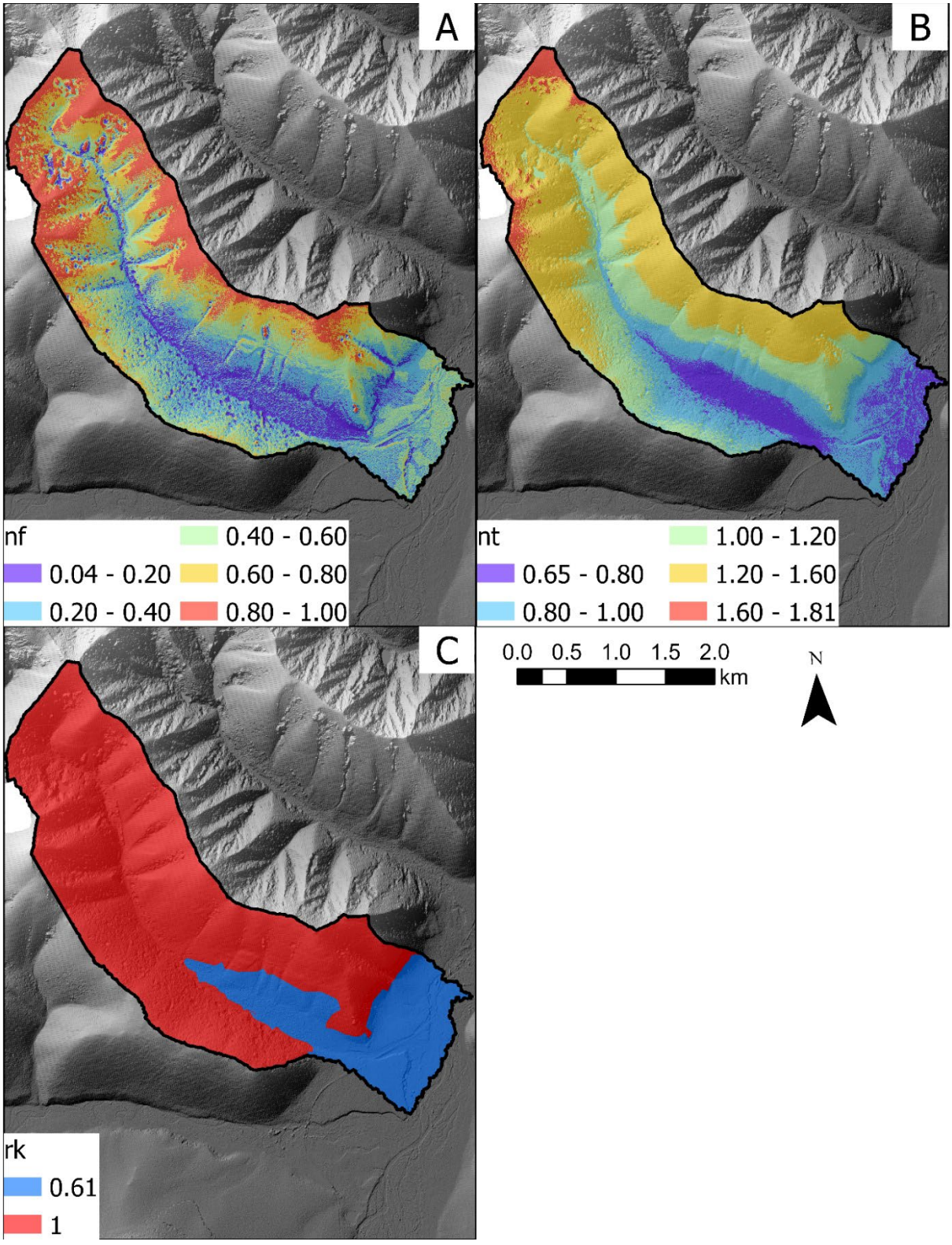


**Figure S5-23.** Current Valley WS01 models for A) $n_f$, B) $n_t$, and C) rk.

S.5.2.3.2 Valley WS02

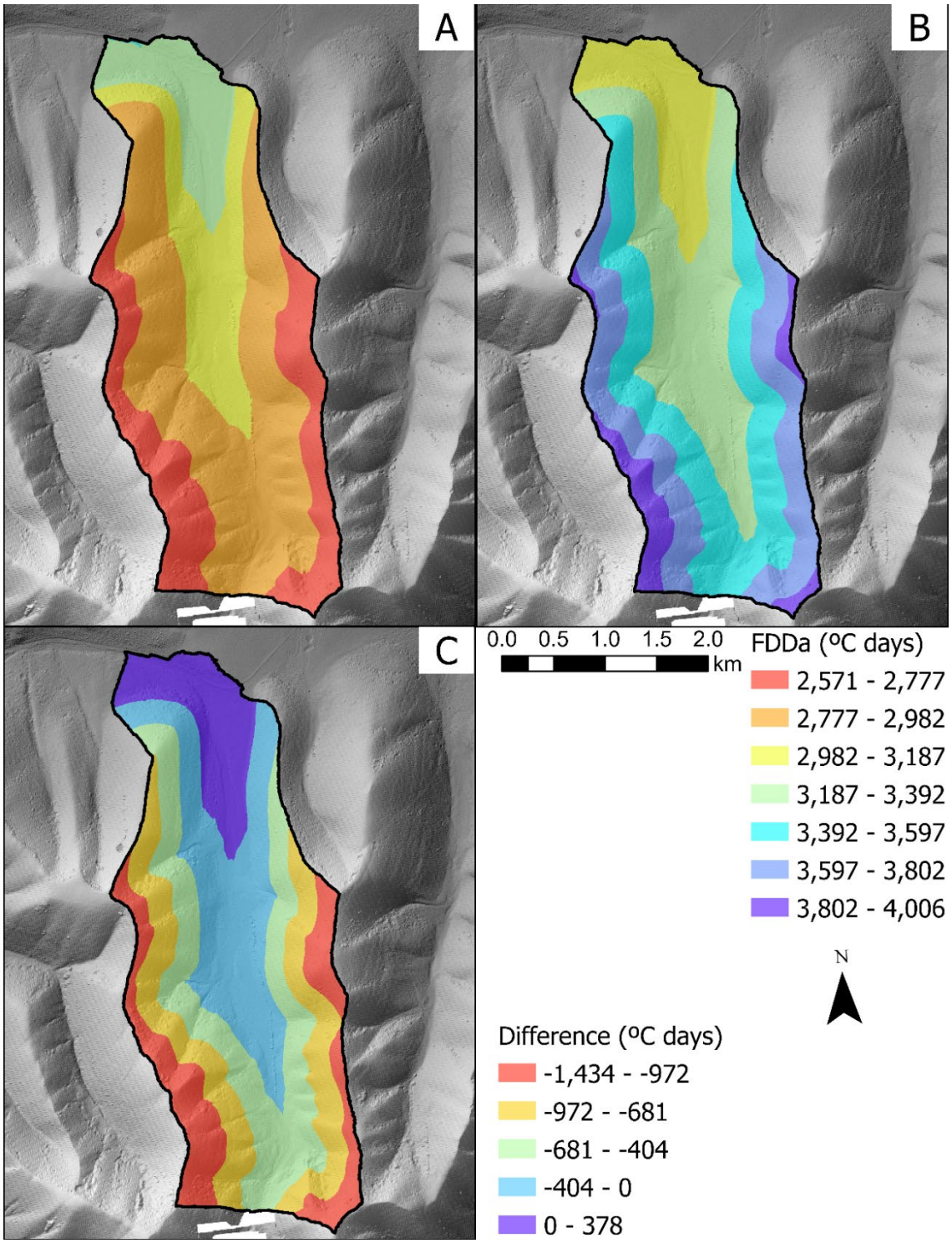


**Figure S5-24.** Freezing degree days air ($FDD_a$) models for Valley WS02 A) calculated change in $FDD_a$ with elevation, B) a -6.5 °C $km^{-1}$ change for every day with annual mean air temperature (AMAT) below 0 °C, and C) the difference between the two where negative values indicate actual $FDD_a$ (measured change with elevation) is lower than expected following the normal environmental SLR and positive values indicate actual $FDD_a$ is higher than expected.

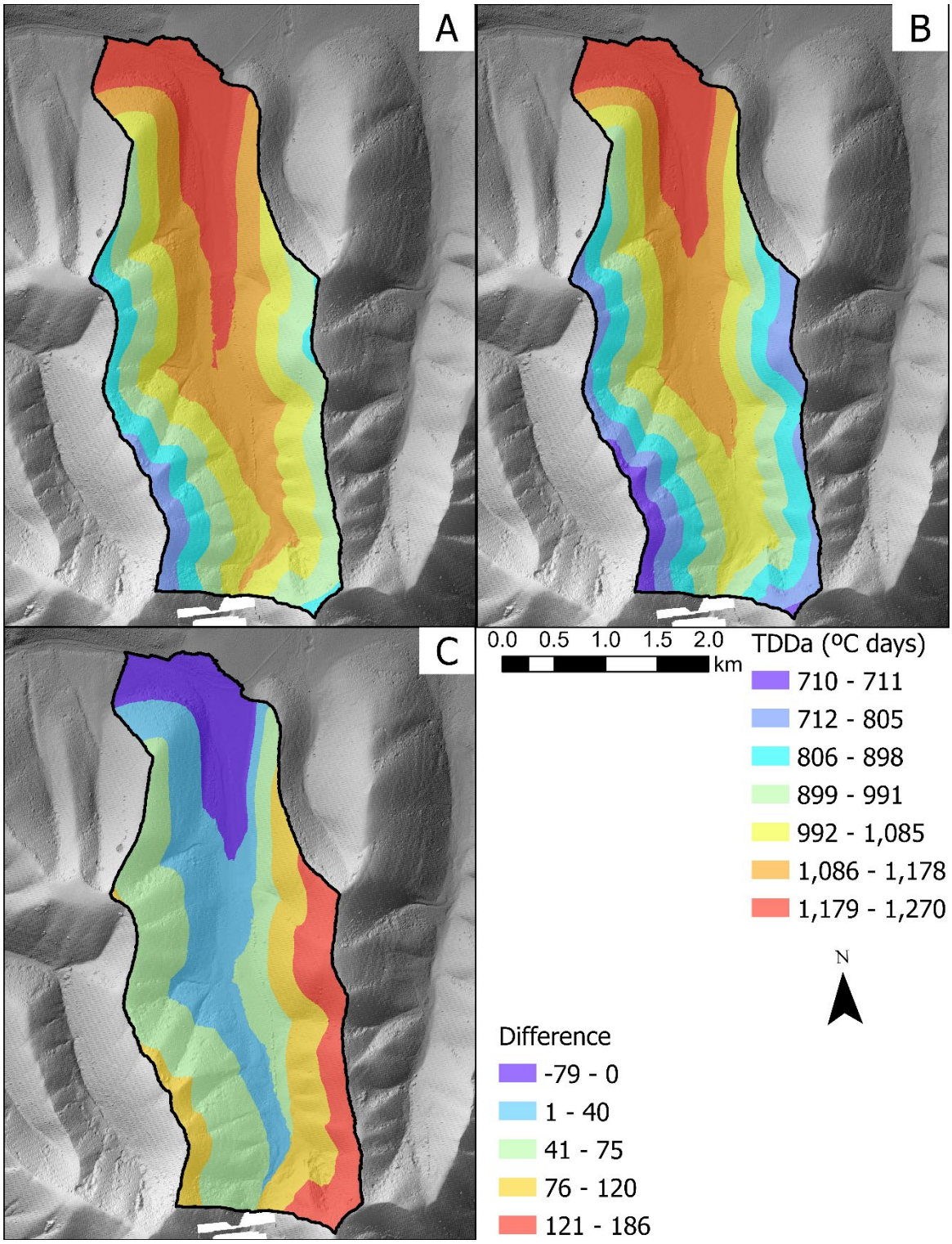


**Figure S5-25.** Thawing degree days air ($TDD_a$) models for Valley WS02 A) calculated change in $TDD_a$ with elevation, B) a -6.5 °C $km^{-1}$ change for every day with annual mean air temperature (AMAT) above 0 °C, and C) the difference between the two where negative values indicate actual $TDD_a$ (measured change with elevation) is lower than expected following the normal environmental SLR and positive values indicate actual $TDD_a$ is higher than expected.

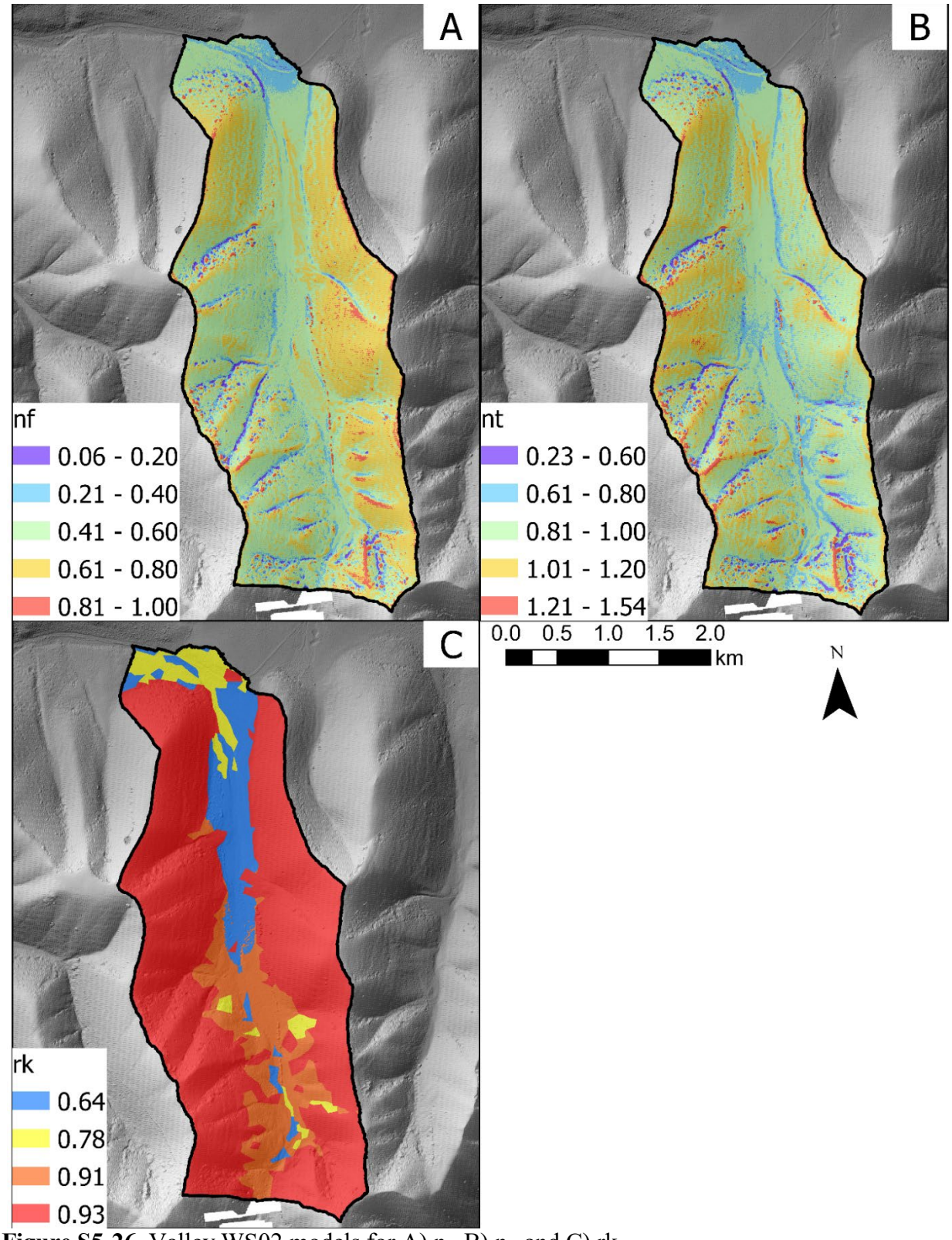


**Figure S5-26.** Valley WS02 models for A) $n_f$, B) $n_t$, and C) rk.

S.5.2.3.3 Valley M222

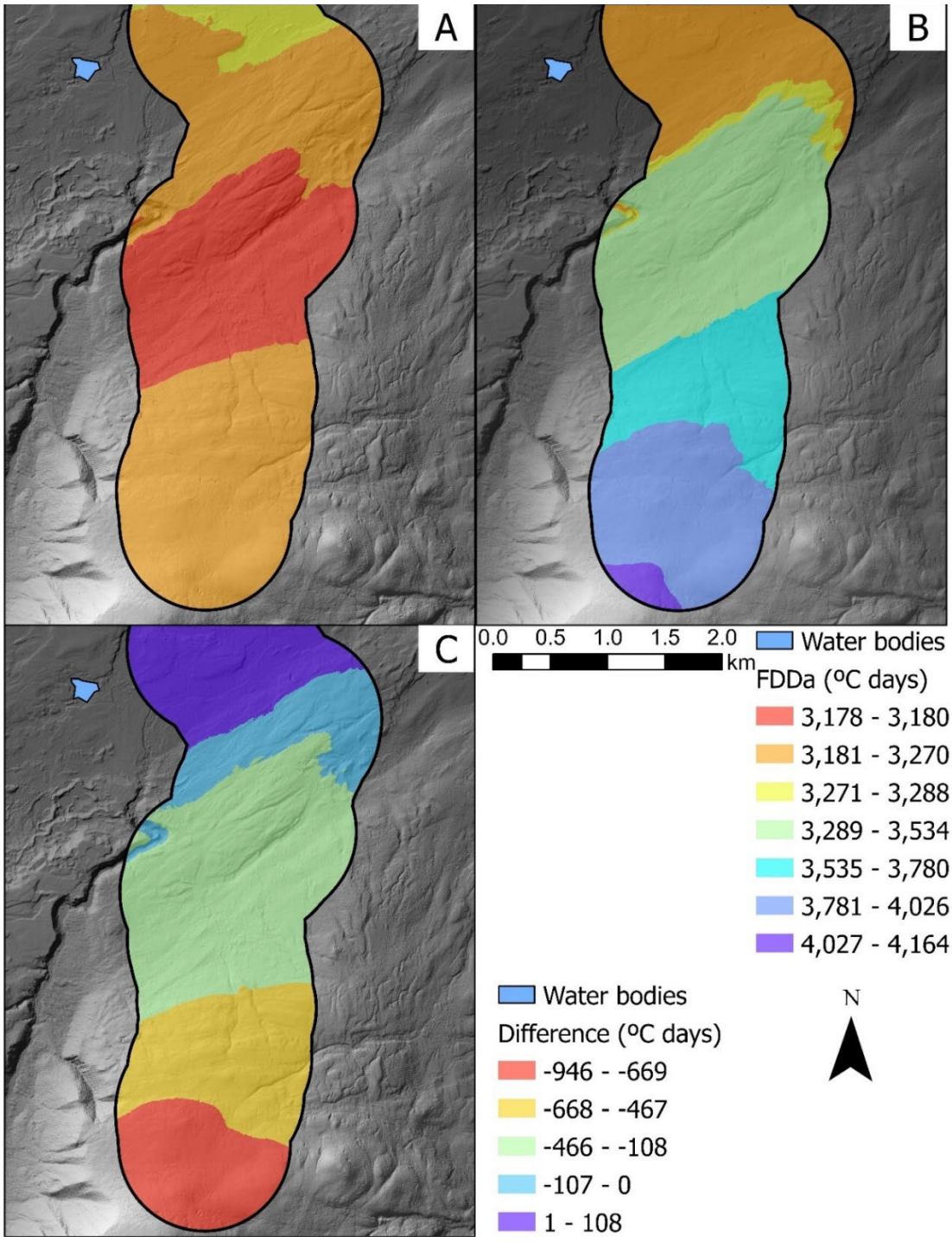


**Figure S5-27.** Freezing degree days air ($FDD_a$) models for Valley M222 A) calculated change in $FDD_a$ with elevation, B) a -6.5 °C $km^{-1}$ change for every day with annual mean air temperature (AMAT) below 0 °C, and C) the difference between the two where negative values indicate actual $FDD_a$ (measured change with elevation) is lower than expected following the normal environmental SLR and positive values indicate actual $FDD_a$ is higher than expected.

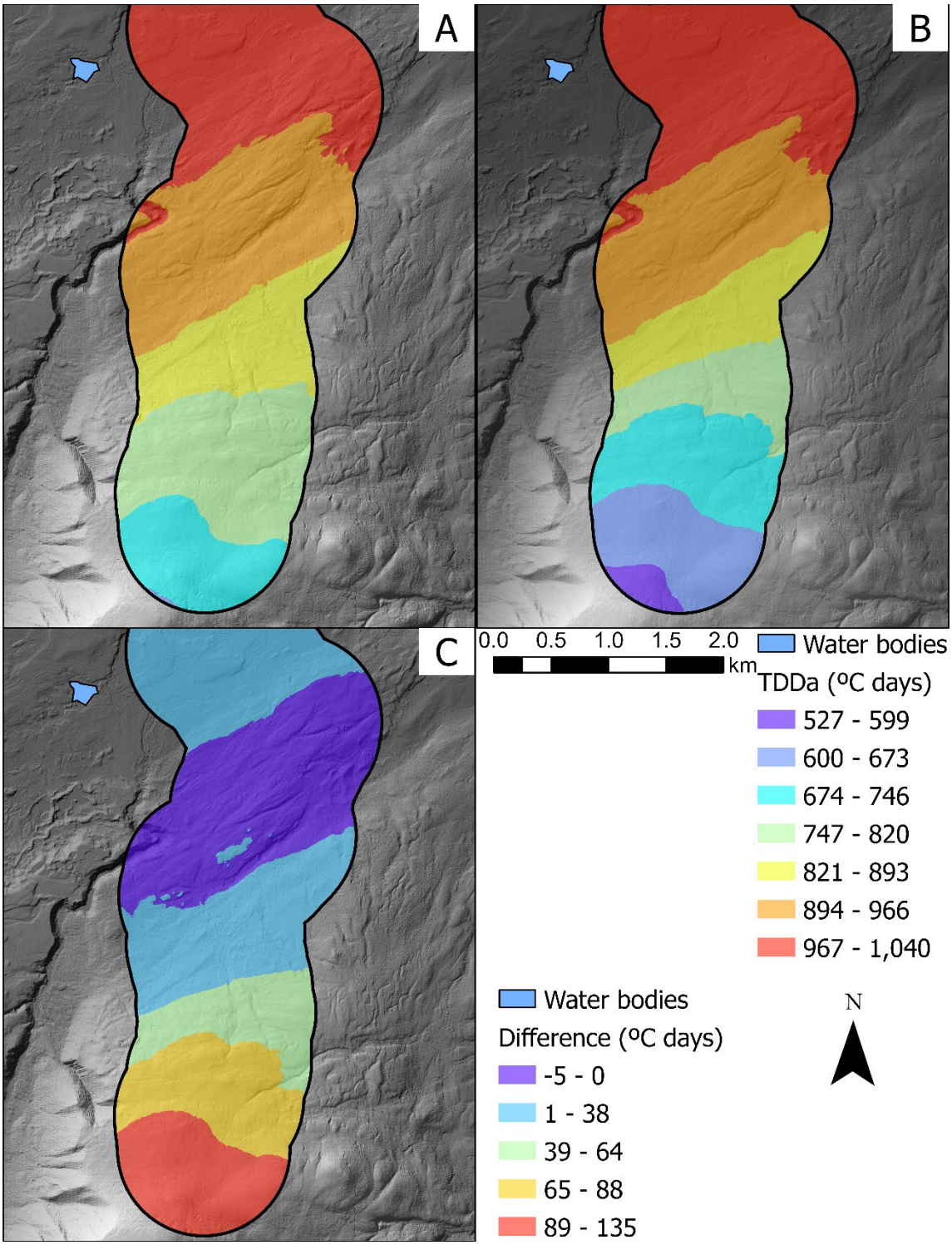


**Figure S5-28.** Thawing degree days air ($TDD_a$) models for Valley M222 A) calculated change in $TDD_a$ with elevation, B) a -6.5 °C $km^{-1}$ change for every day with annual mean air temperature (AMAT) above 0 °C, and C) the difference between the two where negative values indicate actual $TDD_a$ (measured change with elevation) is lower than expected following the normal environmental SLR and positive values indicate actual $TDD_a$ is higher than expected.

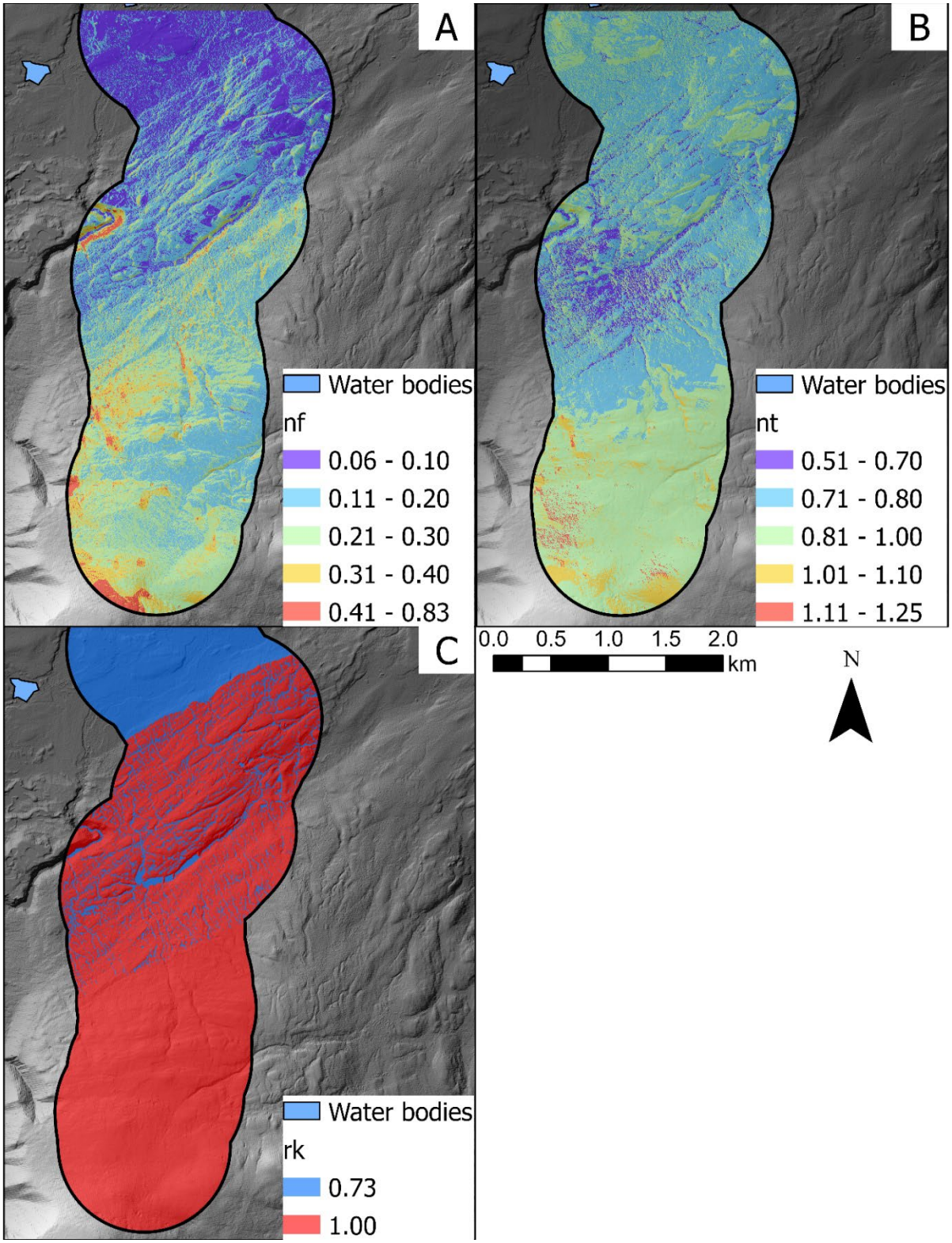


**Figure S5-29.** Valley M222 models for A) $n_f$, B) $n_t$, and C) rk.

S.5.2.3.4 Valley MTS

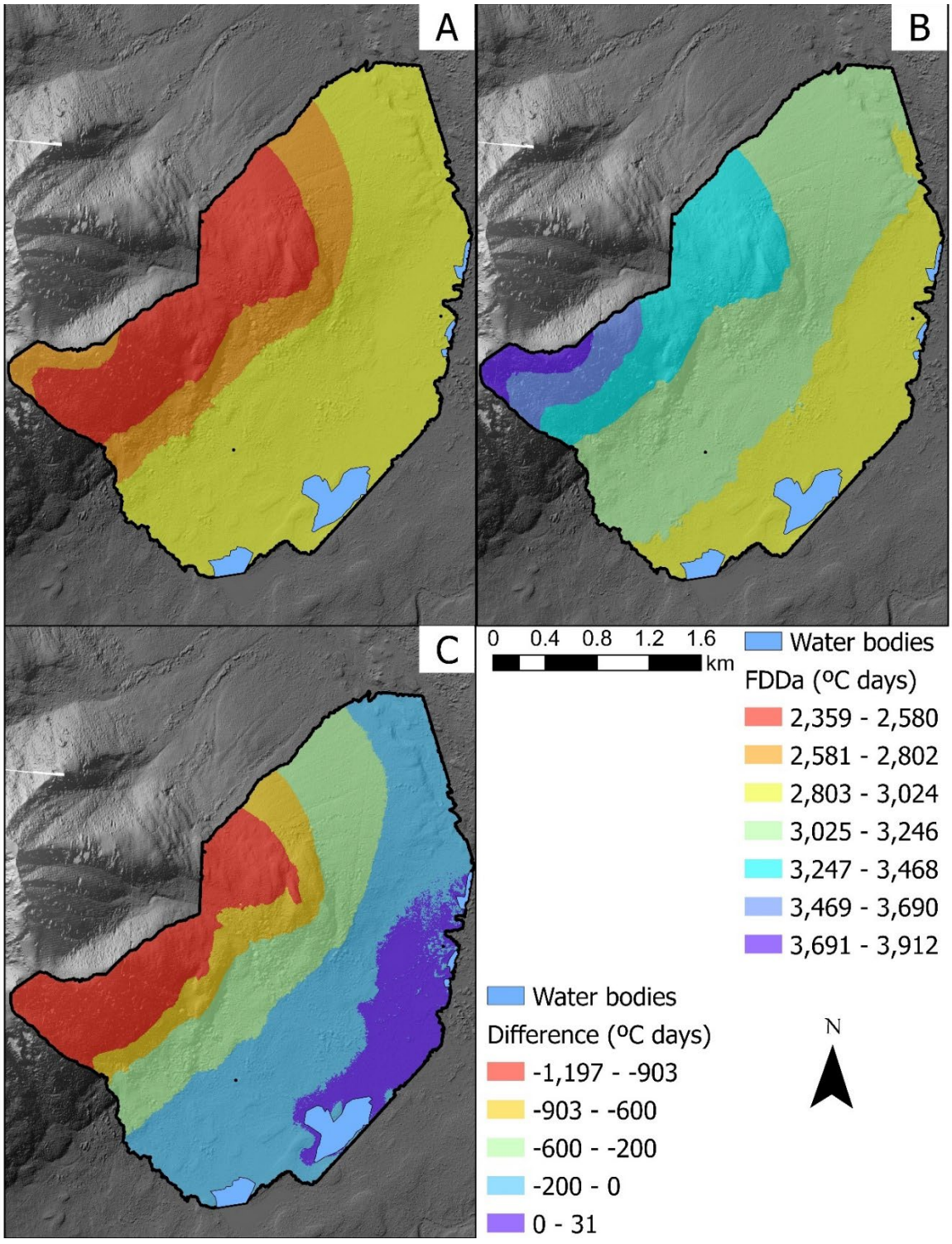


**Figure S5-30.** Freezing degree days air ($FDD_a$) models for Valley MTS A) calculated change in $FDD_a$ with elevation, B) a -6.5 °C $km^{-1}$ change for every day with annual mean air temperature (AMAT) below 0 °C, and C) the difference between the two where negative values indicate actual $FDD_a$ (measured change with elevation) is lower than expected following the normal environmental SLR and positive values indicate actual $FDD_a$ is higher than expected.

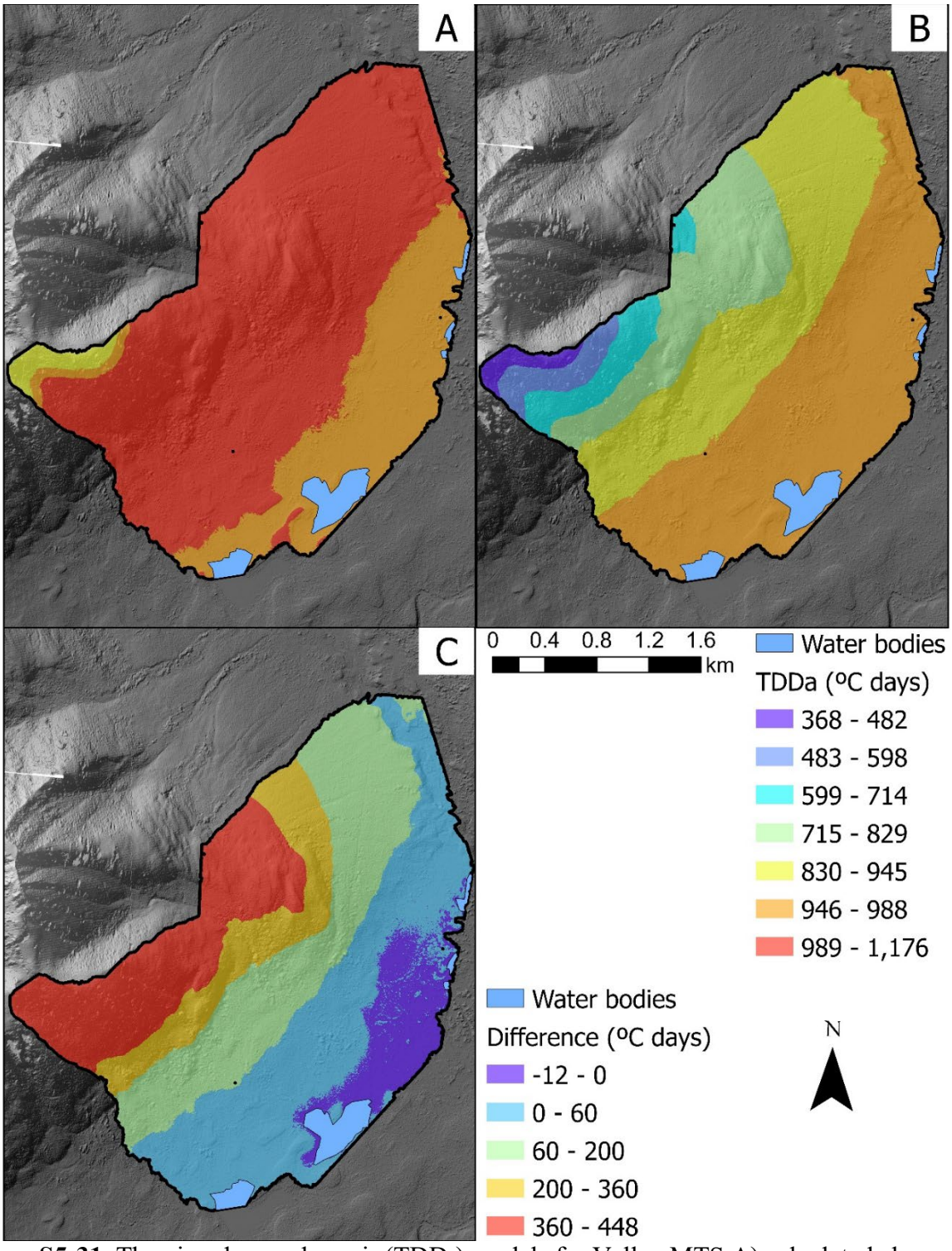


**Figure S5-31.** Thawing degree days air ($TDD_a$) models for Valley MTS A) calculated change in $TDD_a$ with elevation, B) a -6.5 °C $km^{-1}$ change for every day with annual mean air temperature (AMAT) above 0 °C, and C) the difference between the two where negative values indicate actual $TDD_a$ (measured change with elevation) is lower than expected following the normal environmental SLR and positive values indicate actual $TDD_a$ is higher than expected.

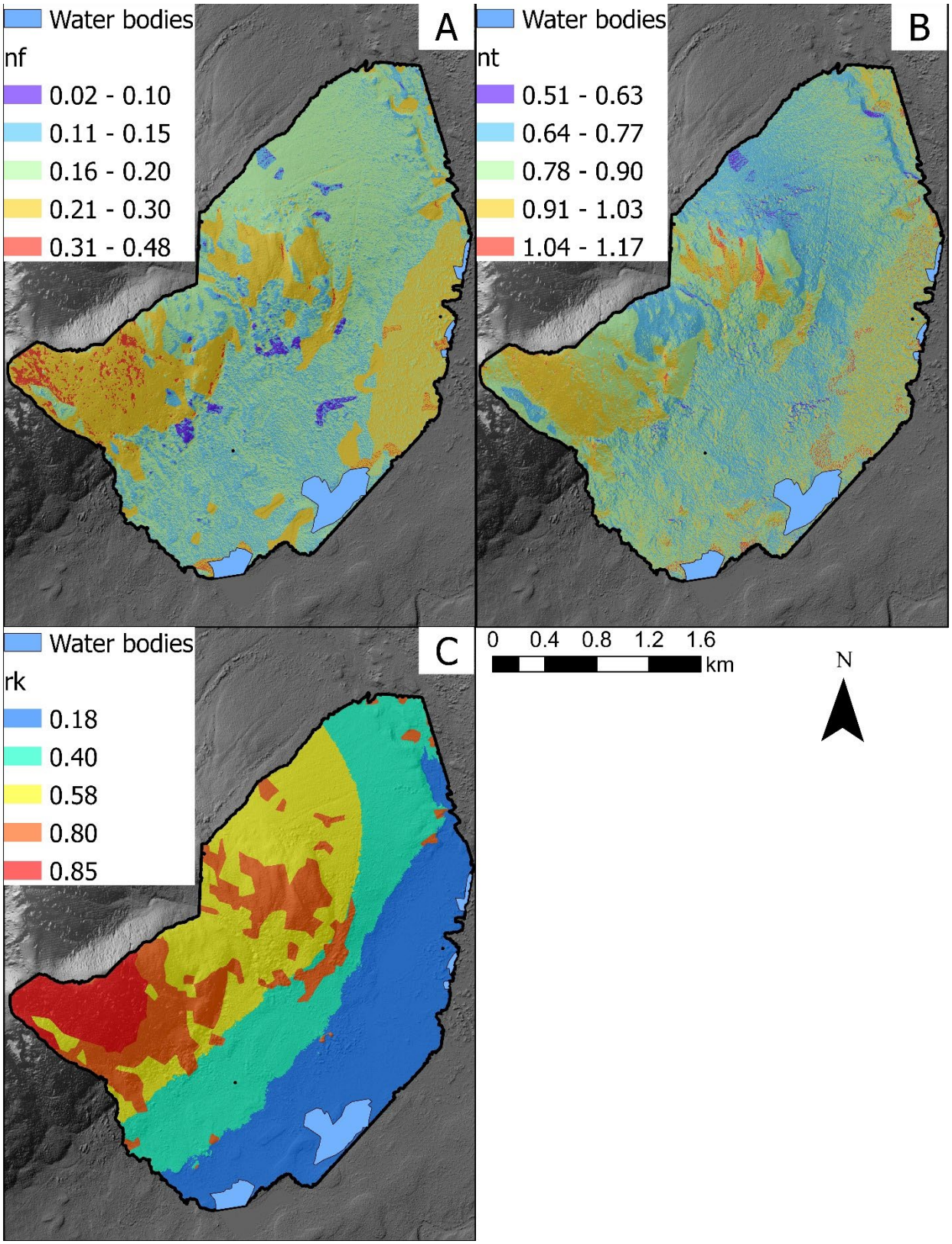


**Figure S5-32.** Valley MTS models for A) $n_f$, B) $n_t$, and C) rk.

*S.5.3 Discussion*

S.5.3.1 Influences on Measured AMGST Between Valleys

In all four valleys, the impact of the winter inversions on AMGST and $FDD_s$ was directly moderated by topographic position and vegetation, which influence snow retention and shading (Zhang, 2005). The impact of topographic position and vegetation moderating the influence of winter air temperatures was shown in all four valleys, with the lowest $FDD_s$ measured in the valley bottom despite the cold air pooling during winter. This is due to the increased surface offsets (lower $n_f$) in the valley bottom resulting from increased snow retention (compared to exposed upper elevation slopes) based on topography (flat and incised) and increased vegetation cover (Lewkowicz et al., 2012; Bevington & Lewkowicz, 2015; Freudiger et al., 2017). Additionally, the valley bottom likely has higher soil moisture content, which can delay sensible heat changes in the ground surface (Famiglietti et al., 1998; Karunaratne & Burn, 2004; Vivoni et al., 2008). In Valley M222 and Valley MTS, the highest $FDD_s$ were measured at high elevations on exposed slopes where the winter air temperatures have a more direct influence on the ground thermal regime due to limited vegetation cover and convex topography allowing for snow to be readily removed. This results in higher $n_f$ (lower surface offsets). However, the influence of the SLRs may also have contributed to these colder temperatures, as the higher elevations in these valleys are subjected to normal winter SLRs. To support, this the highest $FDD_s$ in both Valley WS01 and Valley WS02 were not measured at the highest, most exposed locations, as the air temperatures were warmest during winter at the high elevations due to the inverted SLR. Instead, they were measured at exposed locations on slopes near the valley bottom where the air temperatures were colder relative to the higher elevations, indicating the impact of

the inversion on AMGST. The impact of the inverted SLRs and the influence of landform and vegetation can also be observed in difference in average AMGST for each class.

In Valley WS01, there was no significant difference between landform and landcover classes for AMGST and $FDD_s$. This likely results from the complex interactions of topography and vegetation, with different vegetation regimes on either side of the valley at similar elevations and topographic positions. As a result, a site classified as slope may be either bare ground or forested, which would result in different ground thermal regimes in the same landform class. However, the impact of the inverted SLRs in this valley can be observed through the average AMGST and $FDD_s$ for each class as well as in the temporal changes in ground surface temperature. For Valley WS01, the slope class had lower $FDD_s$ on average than both the ridge and valley classes. As the slope class is mainly comprised of herbaceous and rock landcover and located at mid to upper elevations, it is likely that this is a result of the inverted winter SLRs producing lowest amount of $FDD_a$ at mid to high elevations. Similarly, this can also be observed in the temporal record, as the slope class remained warmer during the freezing season than the ridge and valley classes. However, despite having the least amount of $FDD_a$ at the highest elevations, the ridge class accumulated more $FDD_s$ on average than the other classes and was the coldest class during the freezing season. This discrepancy between the ridge and slope classes may result from higher $n_f$ values (less accumulation of snow) in the ridge class, allowing for greater numbers of $FDD_s$ in the ground surface despite the warmer air temperatures.

In Valley WS02, the impact of the inversion on the distribution of ground surface temperatures was more apparent than in the other valleys due to the limited vegetation cover on the slopes. Additionally, this lack of vegetation cover also resulted in the largest average annual amplitude, as the slopes mainly comprised of bare ground, were able to warm and cool

substantially over the year. Slope sites had on average lower $FDD_s$, higher AMGST and temporally remained warmer in the winter than the valley or ridge sites, which may be a product of the inversion. However, the shrubs sites were classified as slope landforms, which may have contributed to the warmer conditions in this class, not necessarily the winter inversions. Additionally, the ridge class remained the coldest despite having the warmest air temperatures, likely resulting from the increased exposure and lack of vegetation in this class. Looking at the slope and valley classes, if only bare ground sites were considered, average ground surface thermal conditions in the slope class would still be warmer than in the valley, indicating that at least some of this ground surface temperature distribution is due to the winter inversions.

In Valley M222, average ground surface conditions were warmer for the ridge class than the valley; however, this is not likely a product of the winter inversions as the ridge class was colder in winter. More likely, this is a result of vegetation cover during summer, as the ridge class became substantially warmer than sites in the valley. Additionally, since this valley is farther south than the two Dempster valleys, conditions during the thawing season begin to increase in importance to the ground surface thermal regime (Karjalainen et al., 2019; Garibaldi et al., 2022). Valley MTS showed the lowest interannual difference, likely due to the presence of well-developed vegetation over most of the valley, limiting the ground surface response to changes in air temperature (Viereck, 1970; Shur & Jorgenson, 2007; Dashtseren et al., 2014; Ran et al., 2021). Similar to Valley WS01, the complex interactions between landcover and landform prevent significant differences in AMGST and $FDD_s$ between the classes. For example, both shrub and treed sites were classified as a valley site and both shrubs and rock landcovers were grouped into the ridge class. This likely resulted in the similar averages for AMGST and $FDD_s$ for all three landform classes. However, the landcover classes showed more variability resulting

from increased snow retention by certain vegetation types (Yang & Woo, 1999; Zhang, 2005; Palmer et al., 2012). Rock and herbaceous sites had the coldest average conditions both annually and during the freezing season, resulting from the limited snow retention due to the lack of vegetation and the increased topographic exposure (these vegetation classes were generally found at high elevations on exposed slopes). Contrastingly, the shrub class had the warmest ground surface conditions due to the increased snow accumulation (Yang & Woo, 1999; Zhang, 2005; Palmer et al., 2012). The relatively high amounts of snow at shrub-covered sites may also be apparent through the temporal temperature trends, with this class warming slowest during spring and the minimum daily average temperature for this class remaining close to 0 ºC throughout the winter. Overall, the impact of the inverted SLRs was most apparent at sites with limited vegetation cover and exposed topography, allowing for a more direct connection between the air and the ground surface during winter. Despite the cold air pooling at low elevation, the vegetation and snow buffer limited the impact of these colder conditions, keeping the valley bottoms relatively warm when compared to the higher elevation slopes. These spatial temporal patterns were replicated in the spatial models of AMGST and AMGT.

## S.6 Chapter 6 Supplemental

### *S.6.1 Difference in MAAT*

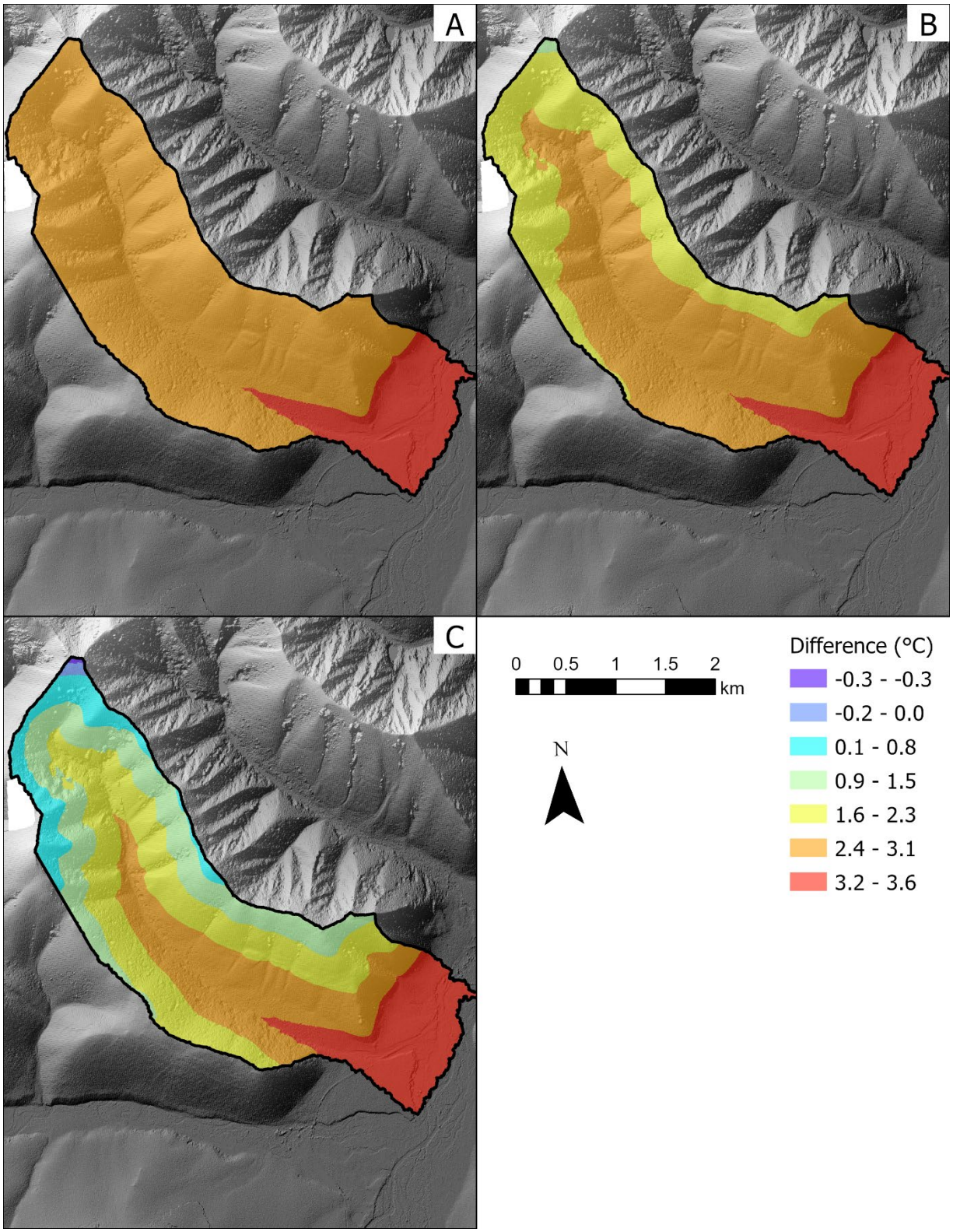


**Figure S6-1.** Difference in mean annual air temperature (MAAT) for Valley WS01 between current climate conditions and a baseline warming (SSP2-4.5 2071-2011) with A) a 1 ºC $km^{-1}$ decrease in inverted surface lapse rate (SLR), B) a 2.5 ºC $km^{-1}$ decrease in inverted SLR, and C) a 5 ºC $km^{-1}$ decrease in inverted SLR.

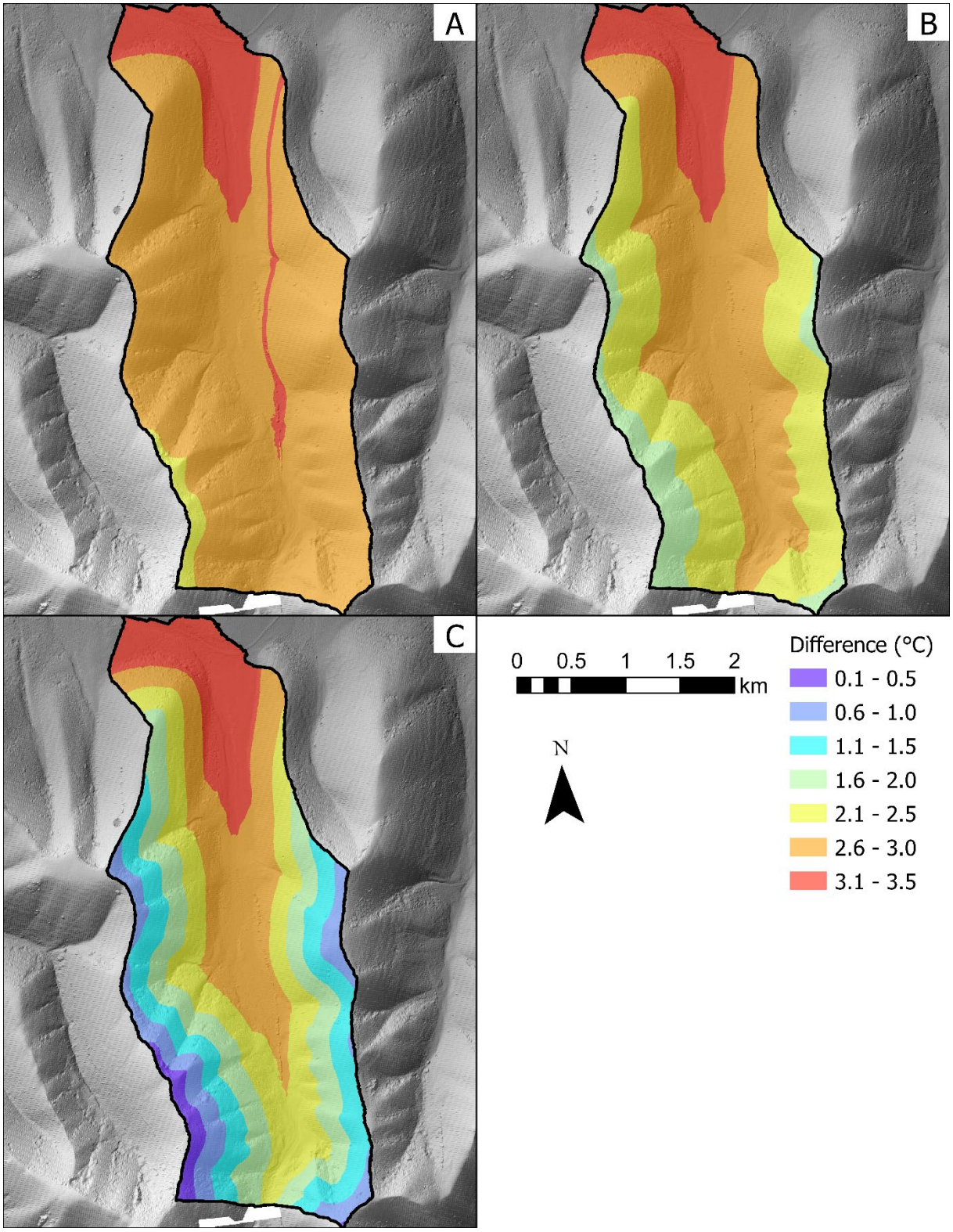


**Figure S6-2.** Difference in mean annual air temperature (MAAT) for Valley WS02 between current climate conditions and a baseline warming (SSP2-4.5 2071-2100) with A) a 1 ºC km-1 decrease in inverted surface lapse rate (SLR), B) a 2.5 ºC km-1 decrease in inverted SLR, and C) a 5 ºC km-1 decrease in inverted SLR.

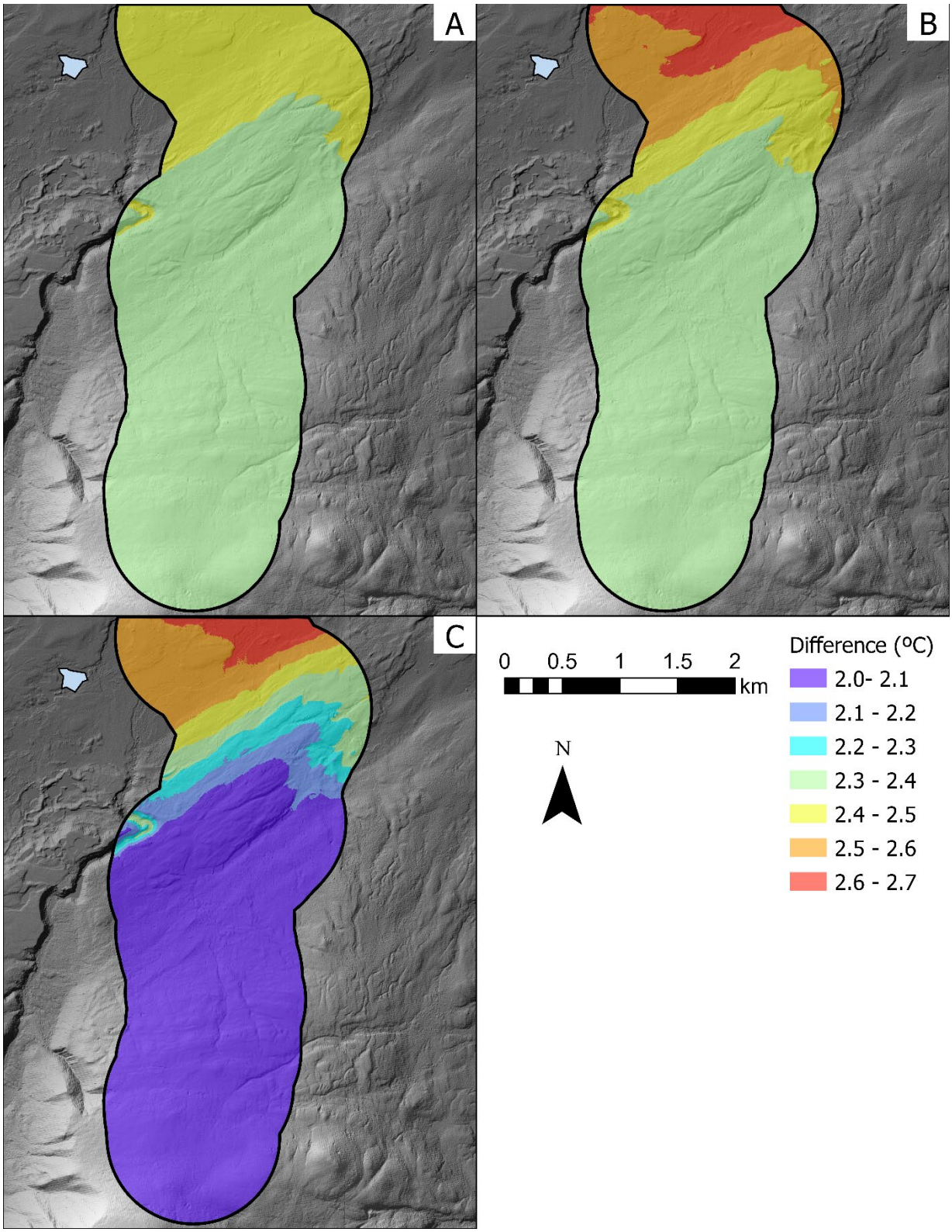


**Figure S6-3.** Difference in mean annual air temperature (MAAT) for Valley M222 between current climate conditions and a baseline warming (SSP2-4.5 2071-2100) with A) a 1 ºC $km^{-1}$ decrease in inverted surface lapse rate (SLR), B) a 2.5 ºC $km^{-1}$ decrease in inverted SLR, and C) a 5 ºC $km^{-1}$ decrease in inverted SLR.

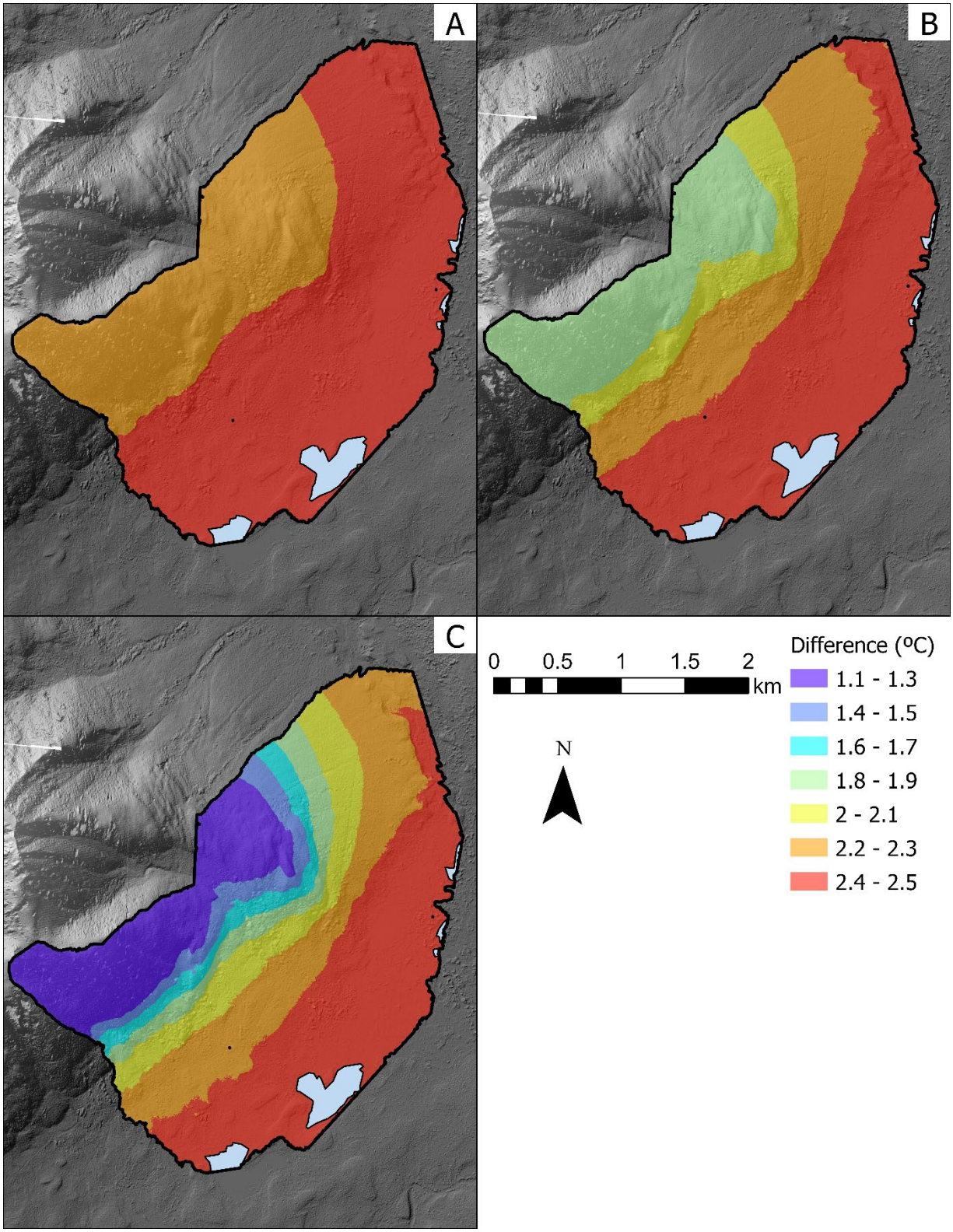


**Figure S6-4.** Difference in mean annual air temperature (MAAT) for Valley MTS between current climate conditions and a baseline warming (SSP2-4.5 2071-2100) with A) a 1 ºC $km^{-1}$ decrease in inverted surface lapse rate (SLR), B) a 2.5 ºC $km^{-1}$ decrease in inverted SLR, and C) a 5 ºC $km^{-1}$ decrease in inverted SLR.

*S.6.2 Difference in MAGST*

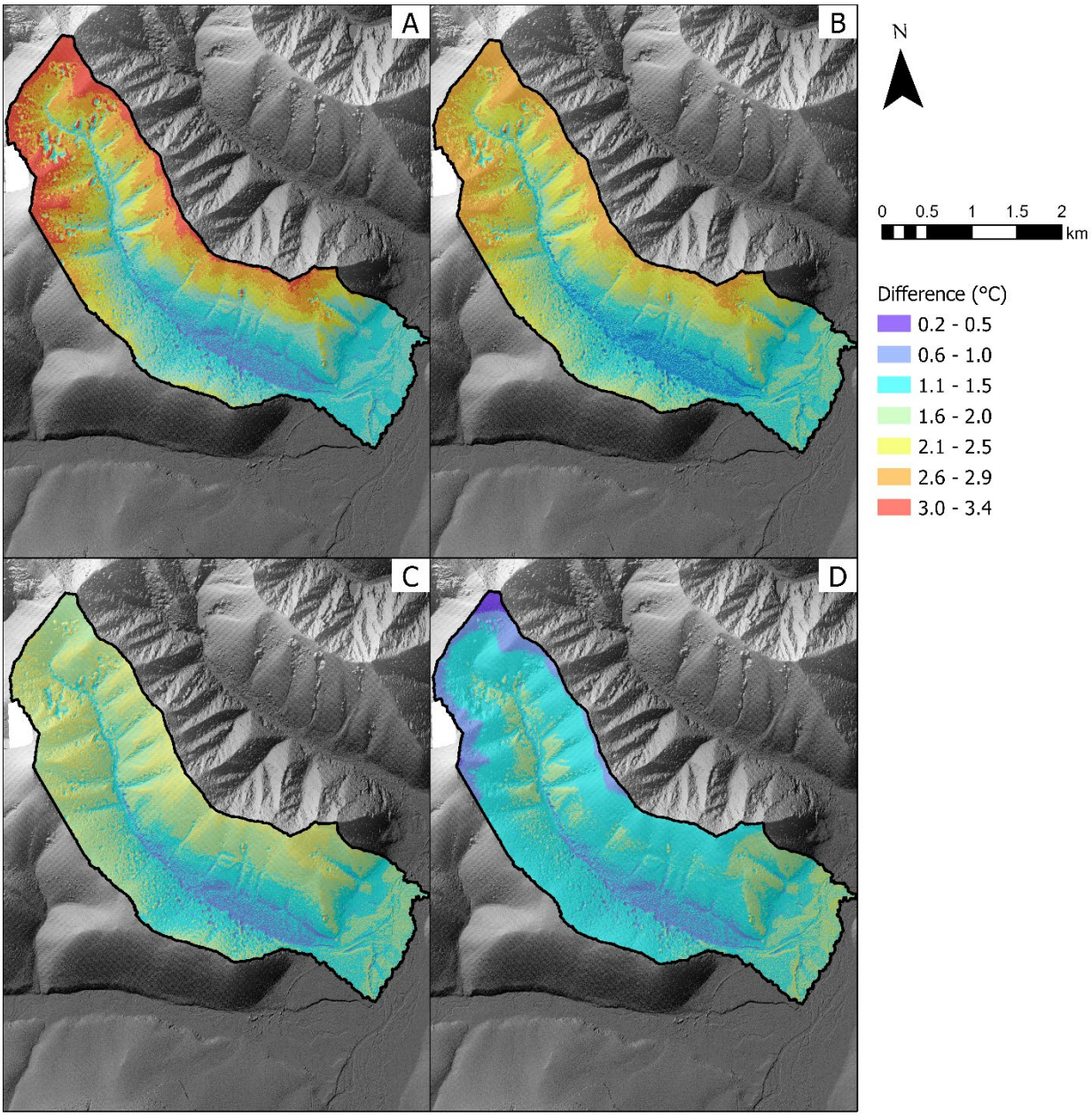


**Figure S6-5.** Difference in mean annual ground surface temperature (MAGST) for Valley WS01 between current climate conditions and a baseline warming (SSP2-4.5 2071-2100) with A) no change to surface lapse rate (SLR) B) a 1 ºC $km^{-1}$ decrease in SLR, C) a 2.5 ºC $km^{-1}$ decrease in inverted SLR, and D) a 5 ºC $km^{-1}$ decrease in inverted SLR.

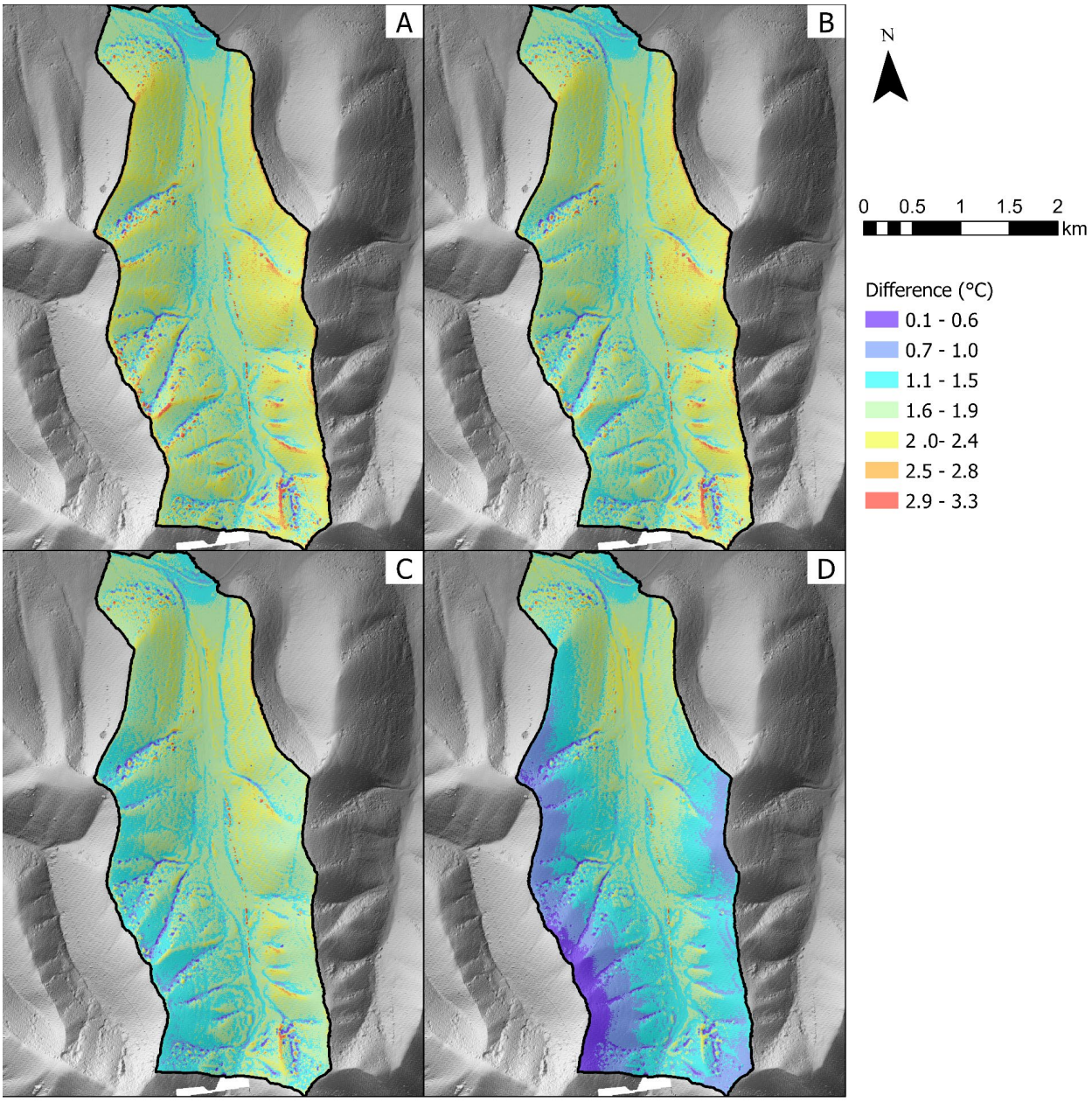


**Figure S6-6.** Difference in mean annual ground surface temperature (MAGST) for Valley WS02 between current climate conditions and a baseline warming (SSP2-4.5 2071-2100) with A) no change to surface lapse rate (SLR) B) a 1 ºC $km^{-1}$ decrease in SLR, C) a 2.5 ºC $km^{-1}$ decrease in inverted SLR, and D) a 5 ºC $km^{-1}$ decrease in inverted SLR.

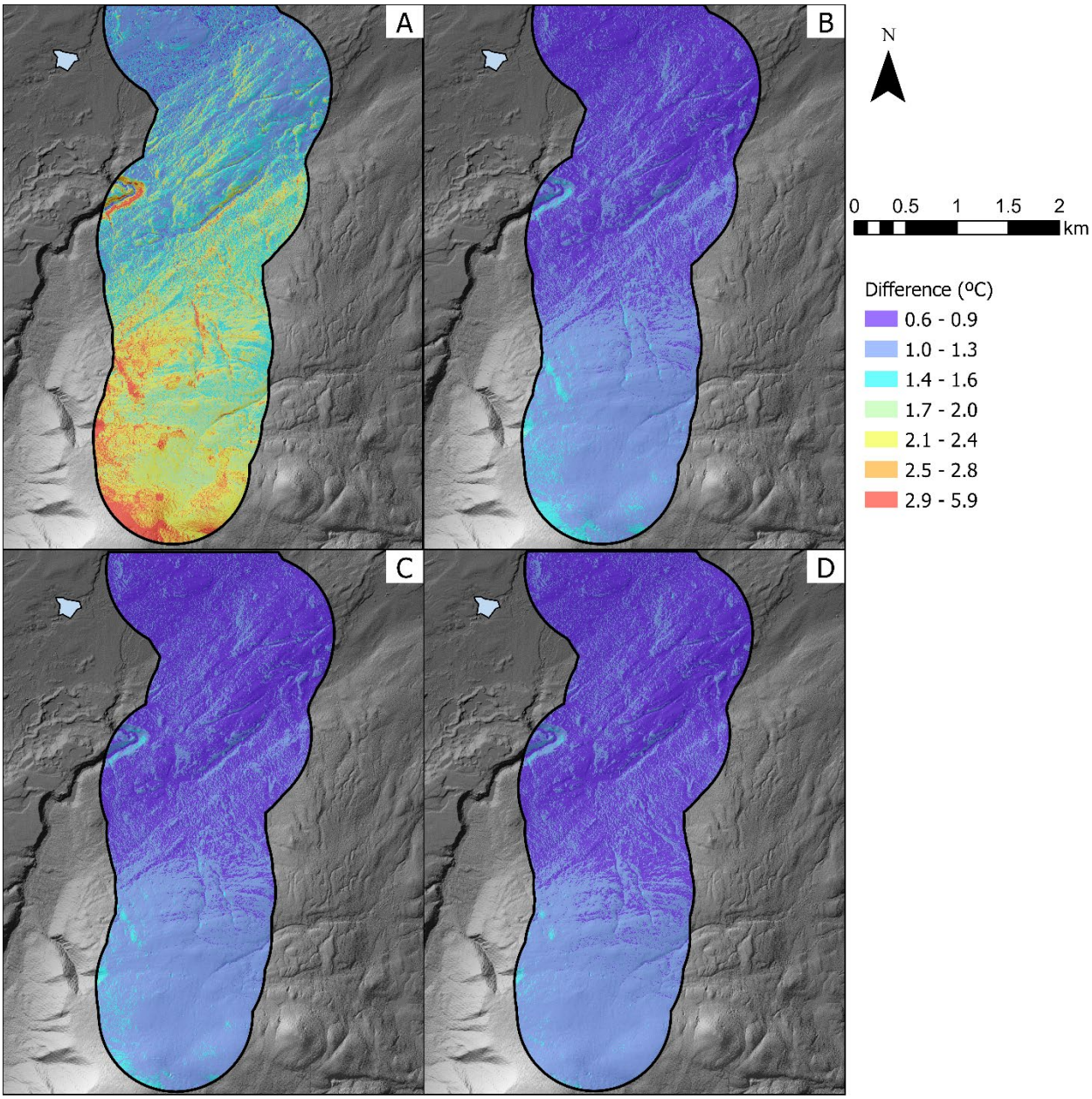


**Figure S6-7.** Difference in mean annual ground surface temperature (MAGST) for Valley M222 between current climate conditions and a baseline warming (SSP2-4.5 2071-2100) with A) no change to surface lapse rate (SLR) B) a 1 ºC $km^{-1}$ decrease in SLR, C) a 2.5 ºC $km^{-1}$ decrease in inverted SLR, and D) a 5 ºC $km^{-1}$ decrease in inverted SLR.

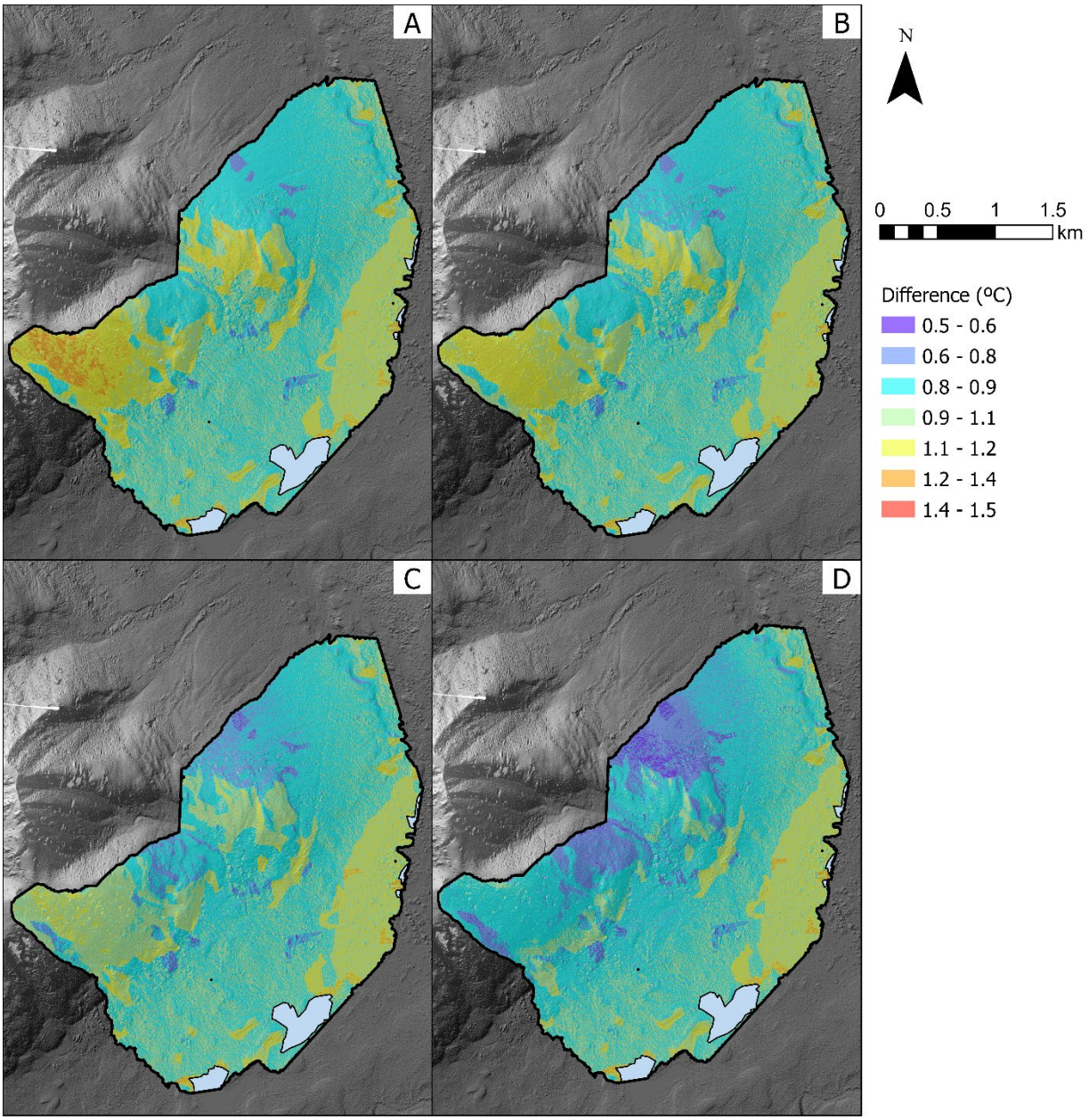


**Figure S6-8.** Difference in mean annual ground surface temperature (MAGST) for Valley MTS between current climate conditions and a baseline warming (SSP2-4.5 2071-2100) with A) no change to surface lapse rate (SLR) B) a 1 ºC $km^{-1}$ decrease in SLR, C) a 2.5 ºC $km^{-1}$ decrease in inverted SLR, and D) a 5 ºC $km^{-1}$ decrease in inverted SLR.

*S.6.3 Difference in MAGT*

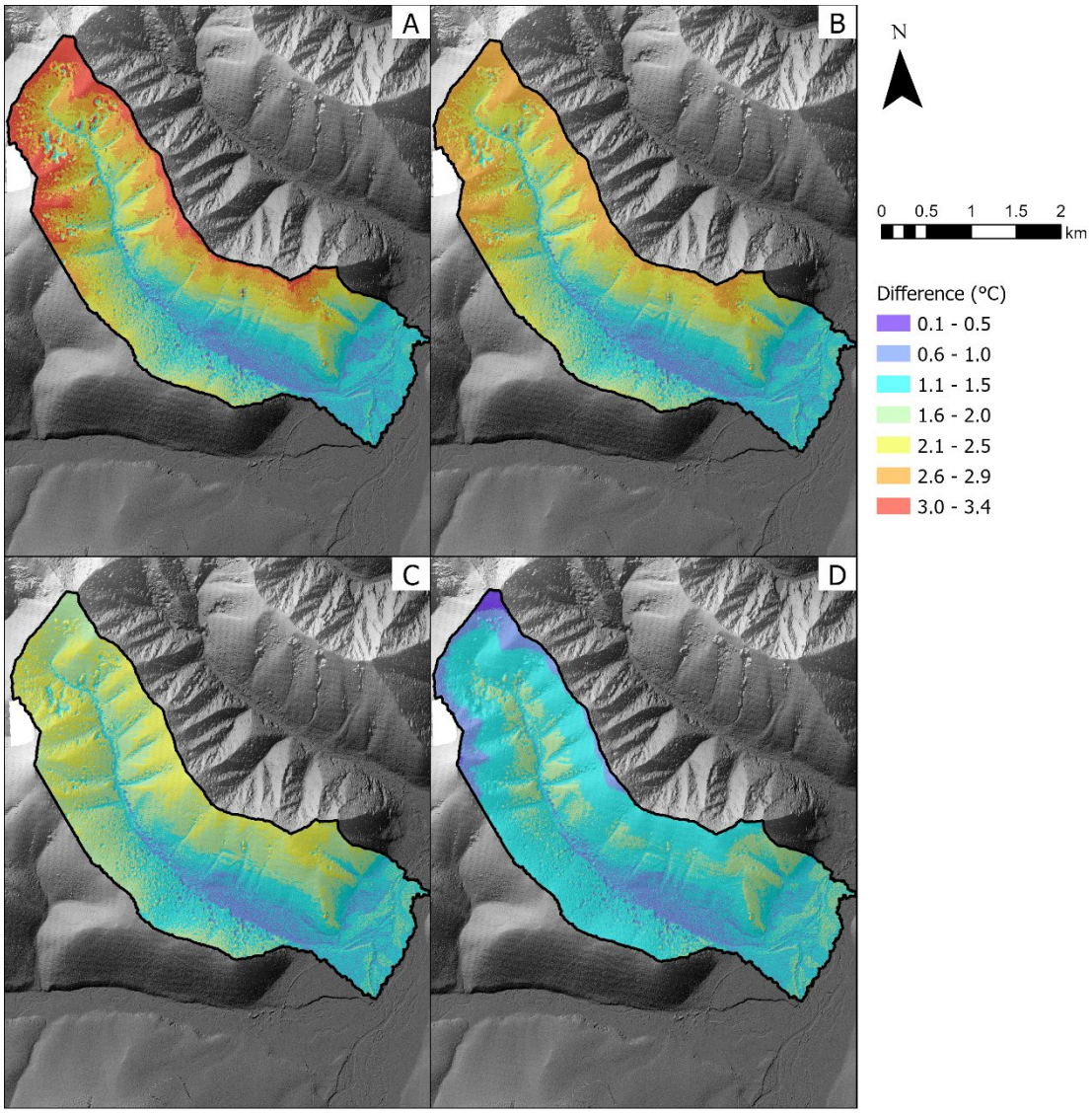


**Figure S6-9.** Difference in mean annual ground temperature (MAGT) for Valley WS01 between current climate conditions and a baseline warming (SSP2-4.5 2071-2100) with A) no change to surface lapse rate (SLR) B) a 1 ºC $km^{-1}$ decrease in SLR, C) a 2.5 ºC $km^{-1}$ decrease in inverted SLR, and D) a 5 ºC $km^{-1}$ decrease in inverted SLR.

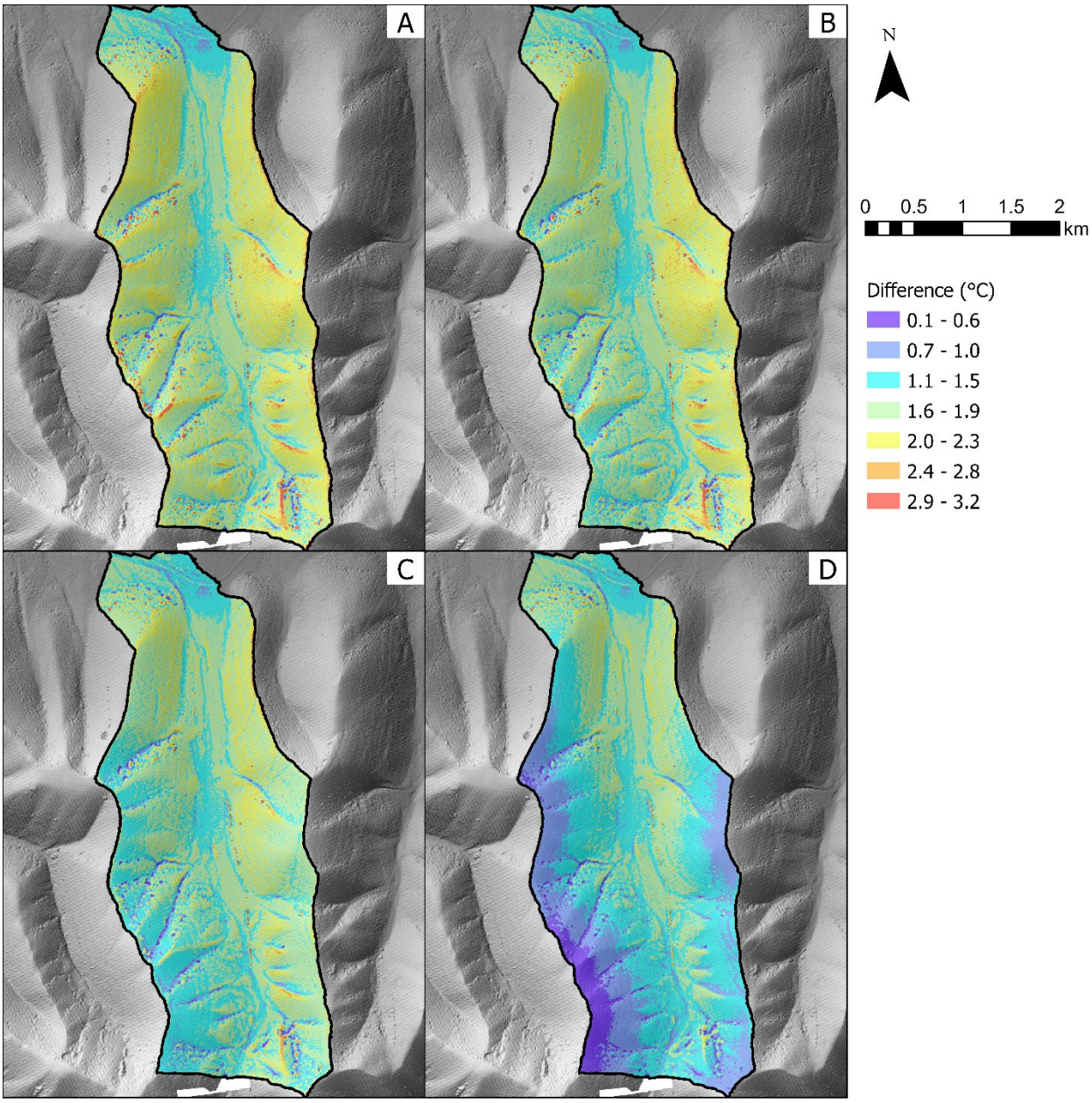


**Figure S6-10.** Difference in mean annual ground temperature (MAGT) for Valley WS02 between current climate conditions and a baseline warming (SSP2-4.5 2071-2100) with A) no change to surface lapse rate (SLR) B) a 1 ºC $km^{-1}$ decrease in SLR, C) a 2.5 ºC $km^{-1}$ decrease in inverted SLR, and D) a 5 ºC $km^{-1}$ decrease in inverted SLR.

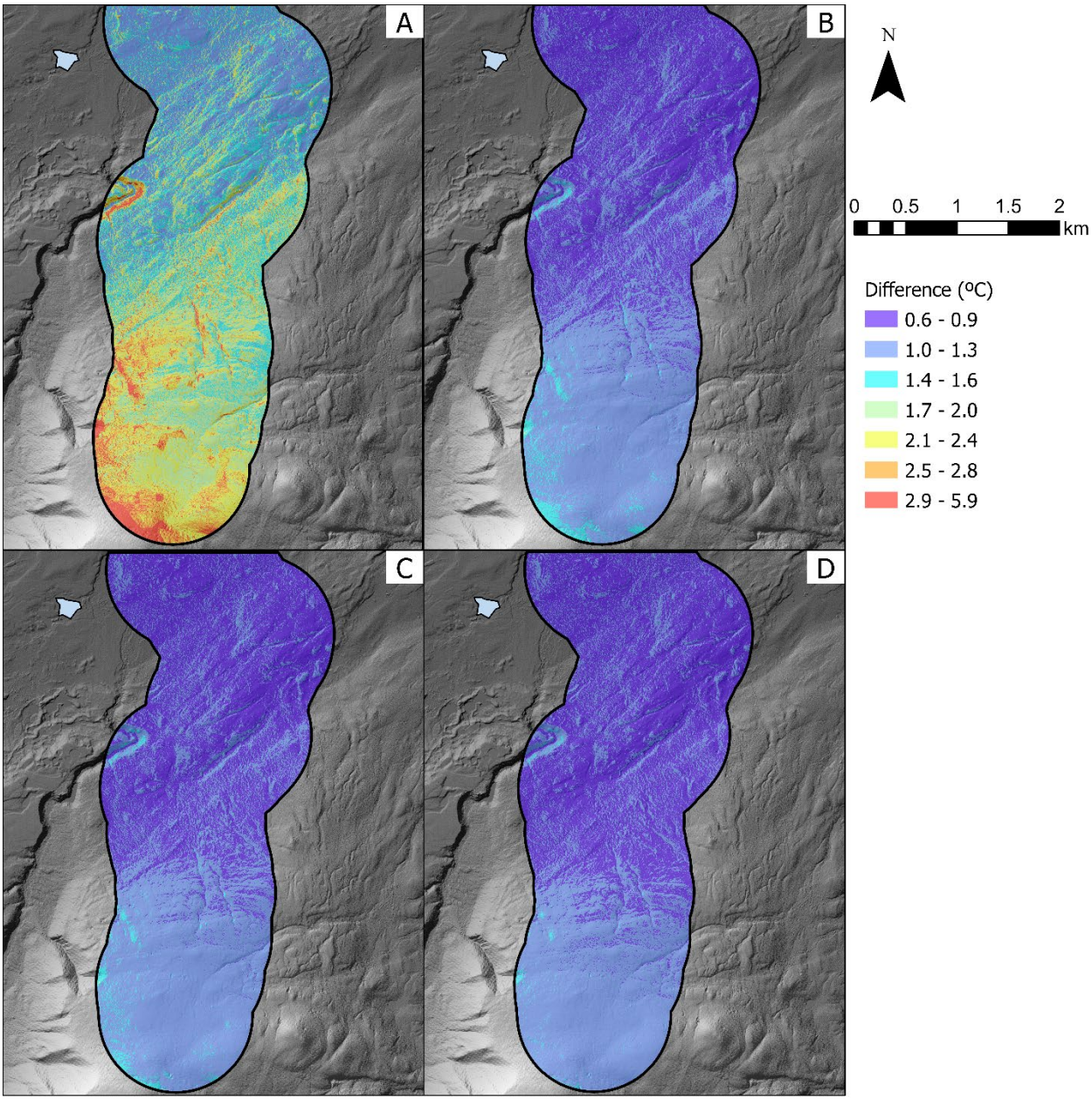


**Figure S6-11.** Difference in mean annual ground temperature (MAGT) for Valley M222 between current climate conditions and a baseline warming (SSP2-4.5 2071-2100) with A) no change to surface lapse rate (SLR) B) a 1 ºC $km^{-1}$ decrease in SLR, C) a 2.5 ºC $km^{-1}$ decrease in inverted SLR, and D) a 5 ºC $km^{-1}$ decrease in inverted SLR.

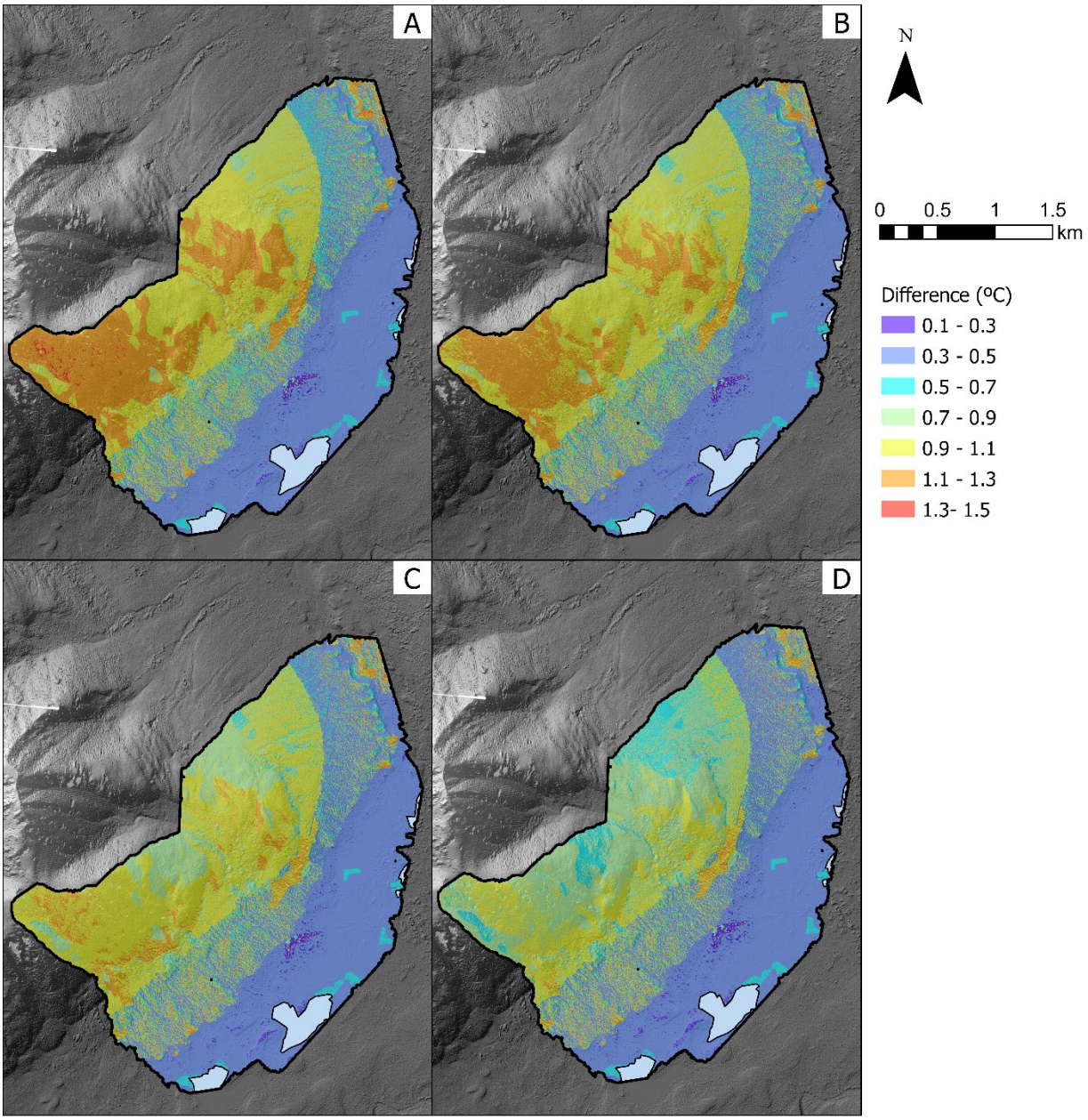


**Figure S6-12.** Difference in mean annual ground temperature (MAGT) for Valley WS01 between current climate conditions and a baseline warming (SSP2-4.5 2071-2100) with A) no change to surface lapse rate (SLR) B) a 1 ºC $km^{-1}$ decrease in SLR, C) a 2.5 ºC $km^{-1}$ decrease in inverted SLR, and D) a 5 ºC $km^{-1}$ decrease in inverted SLR.